Erzincan Üniversitesi
Fen Bilimleri Enstitüsü Dergisi
2024,17(1), 174-195
ISSN: 1307-9085, e-ISSN: 2149-4584
Araştırma Makalesi

Erzincan University
Journal of Science and Technology
2024,17(1), 174-195
DOI: 10.18185/erzifbed.1196037
Research Article

Evaluation of Different Strengthening Projects of Yenice Kalaycılar Primary School According to 2007 and 2019 Turkish Earthquake Regulations

Şenol GÜRSOY[2*], Mustafa Esat COŞKUN[1], Zehra Şule GARİP[2]

[1]Karabük University, Faculty of Engineering, Department of Civil Engineering, 78050, Karabük

[2]Graduate Education Institute, Department of Civil Engineering, 78050, Karabük

Received: 28/10/2023, **Revised:** 28/10/2023, **Accepted:** 05/11/2023, **Published:** 28/03/2024

Abstract

Earthquakes that frequently occur in Turkey may cause structural damage in structures, and/or existing structures cannot provide the new earthquake code requirements. This matter requires us to check the static suitability of existing structures and strengthen them when necessary. In this article, a comparative evaluation of two different strengthening projects, which are considered to be implemented in Kalaycılar primary school in Yenice district of Karabük province, according to 2007 and 2019 Turkish earthquake regulations, is made. For this purpose, the survey projects of the said school building were first prepared, and laboratory experiments were carried out according to the level of comprehensive knowledge. Then, according to the findings obtained from the laboratory experiments, the performance analyses of the school building in question were made according to the 2007 and 2019 Turkish earthquake regulations. According to carried out the performance analyses, two different strengthening projects prepared for the school building have presented some results and suggestions by comparing the 2007 and 2019 Turkish earthquake regulations. The findings obtained reveal that there is more than one option for strengthening a reinforced concrete structure, and all parameters should be evaluated together when deciding to strengthen the structure in question.

Keywords: Reinforced concrete buildings, repair-strengthening, performance analysis

2007 ve 2019 Türk Deprem Yönetmeliklerine Göre Yenice Kalaycılar İlkokulunun Farklı Güçlendirme Projesinin Değerlendirilmesi

Öz

Türkiye'de sıklıkla meydana gelen depremler yapılarda yapısal hasarlara neden olabilmekte ve/veya mevcut yapılar yeni deprem yönetmeliği gerekliliklerini sağlayamamaktadır. Bu husus mevcut yapıların statik açıdan uygunluğunu kontrol etmemizi ve gerekli durumlarda güçlendirilmesini gerektirmektedir. Bu makalede Karabük ili Yenice ilçesindeki Kalaycılar ilkokulunda uygulanması düşünülen iki farklı güçlendirme projesinin 2007 ve 2019 Türk deprem yönetmeliklerine göre karşılaştırmalı değerlendirilmesi yapılmaktadır. Bu amaçla önce söz konusu okul binasının rölöve projeleri hazırlanmış ve kapsamlı bilgi düzeyine göre laboratuvar deneyleri gerçekleştirilmiştir. Daha sonra laboratuvar deneylerinden elde edilen bulgulara göre söz konusu okul binasının 2007 ve 2019 Türk deprem yönetmeliklerine göre performans analizleri yapılmıştır. Yapılan performans analizlerine göre okul binası için hazırlanan iki farklı güçlendirme projesi 2007 ve 2019 Türk deprem yönetmeliklerine göre karşılaştırılarak bazı sonuçlar ve öneriler sunulmaktadır. Elde edilen bulgular betonarme bir yapının güçlendirilmesinde birden fazla seçeneğin olduğu ve söz konusu yapının güçlendirilmesine karar verilirken tüm parametrelerin birlikte değerlendirilmesi gerektiğini ortaya koymaktadır.

Anahtar Kelimeler: Betonarme binalar, onarım-güçlendirme, performans analizi

*Corresponding Author: sgursoy@karabuk.edu.tr
Şenol GÜRSOY, https://orcid.org/ 0000-0001-8133-0906
Mustafa Esat COŞKUN, https://orcid.org/ 0000-0001-6616-7311
Zehra Şule GARİP, https://orcid.org/ 0000-0001-9268-3985

1. Introduction

Due to its location, Turkey is a critical region in terms of seismicity. Therefore, earthquake-resistant building design is very important for civil engineers in Turkey [1, 2, 3, 4]. On the other hand, it is compulsory to evaluate the existing buildings, with economic factors being the main effect. For this reason, the number of buildings whose performance analysis has been carried out has been increasing recently. The earthquake codes used for this purpose allow the application of many methods for performance analysis and strengthening existing buildings.

After the recent earthquakes in Turkey, it has been seen that many reinforced concrete structures need to be repaired and strengthened. As a result of the observations and performance analyses made in reinforced concrete structures, it has been understood that the lateral stiffness of most of them is insufficient [5]. Cast-in-situ shear walls are the most preferred and applied strengthened methods that will provide lateral rigidity to the structure in question in reinforced concrete structures. However, applying this strengthening method is a disadvantage as the structure in question is emptied and cannot be used for a long time. For this reason, many researchers have turned to developing structurally effective, easy-to-apply, and economical strengthening methods [6-12]. In addition, in some references, design principles related to the evaluation and strengthening of existing buildings according to Specification for Buildings to be Built in Seismic Zones (SBBSZ) and Turkish Building Earthquake Code (TBEC) were given comparatively [5, 13].

After the last earthquakes in our country, administrations demand performance states of public buildings hence performance analyses. The performance status of public buildings for which performance analysis is requested (especially in buildings designed according to the 2007 earthquake regulation but not completed) is evaluated according to the regulations of the year they were built. When this is the case, it is aimed to reveal the performance differences between earthquake codes in this article. On the other hand, both the administration's requested issues and the cost of the retrofitting processes to be made by the owner reveal different results according to the regulations.

Since Karabük province is a critical region in terms of seismicity, it is very important to examine the school buildings that have completed their economic life according to the current regulations. In this article, a reinforced concrete school building was chosen as an example to obtain information about the static sufficiency of school buildings. Laboratory studies were performed first according to the comprehensive knowledge level specified in the TBEC. Then in the light of the data obtained from the experiments, the school building in question performed performance analyses by modeling in the Sta4-CAD program [14]. The findings obtained from the structural analyses were evaluated according to the SBBSZ and TBEC, and strengthening methods were proposed [15, 16].

2. Gathering Information About Kalaycılar Primary School

This study examined Kalaycılar primary school, located in the Yenice district of Karabük province. Kalaycılar primary school was chosen as the sample school building because the cost of strengthening is rational compared to the cost of rebuilding, and it has not completed its economic life. Kalaycılar primary school structural system consists of a 3-story reinforced concrete frame and shear wall, and the construction year was 2005. Accordingly, the school building consisting of ground, 1st and 2nd normal storeys is 1051,02 m² in total (see Figure 1). The ground storey of Kalaycılar primary school is 3,55 m high, and the 1st and 2nd typical storeys are 3,15 m high. Since no project exists for the mentioned school building, static and architectural survey projects were prepared [13]. On the other hand, the performance results of the said school building are more likely to be sufficient according to today's regulations. Experimental studies were carried out according to the comprehensive knowledge level of the school building whose projects were prepared. Accordingly, 4 core sampling were taken from each storey (see Table 1). From this table as a TBEC condition, when the bigger *average-standard deviation* or *0,85*average* values is considered as the existing concrete compressive strength, 20 MPa on the ground storey, 13 MPa on the 1st storey, and 12 MPa on the 2nd storey are considered. In addition, the detection of destructive reinforcement (peel test) was carried out with 4 structural elements on the ground storey and 3 structural elements on the other storeys. In addition, the non-destructive reinforcement detection method (X-ray) was performed on 40 structural elements throughout the building (see Figure 2~Figure 4). The studies performed on detecting destructive reinforcement in the said school building are shown in Figure 5 and Figure 6.

Figure 1. A view of the Kalaycılar primary school building

Table 1. Obtaining the average pressure values for the existing drilling core results of Kalaycılar primary school

Storeys	Compressive Strength (N/mm²)	Evaluation of the lowest value	Standard deviation values (SD)	Average SD	Average*0,85
Ground storey	15,89	21,38*0,75=16,04 16,04 > 15,89	0,85	20,53	18,17
	20,88				
	22,37				
	20,90				
1st storey	10,03	16,14*0,75=12,105 12,105 > 10,03	4,46	11,68	13,71
	15,96				
	20,69				
	11,77				
2nd storey	19,39	15,73*0,75=11,8	3,1	11,78	12,64

	12,32	11,8 < 12,32			
	13,71				
	14,11				

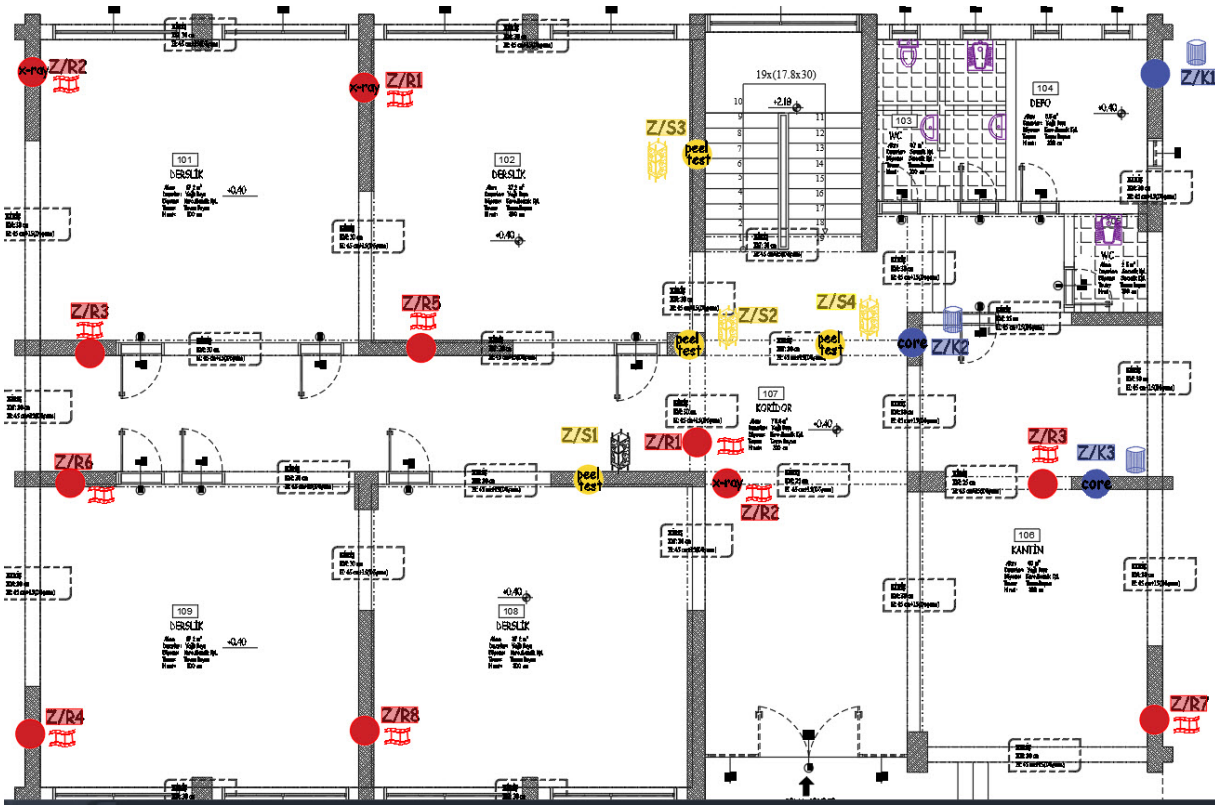

Figure 2. Structural elements where experiments are performed on the ground storey

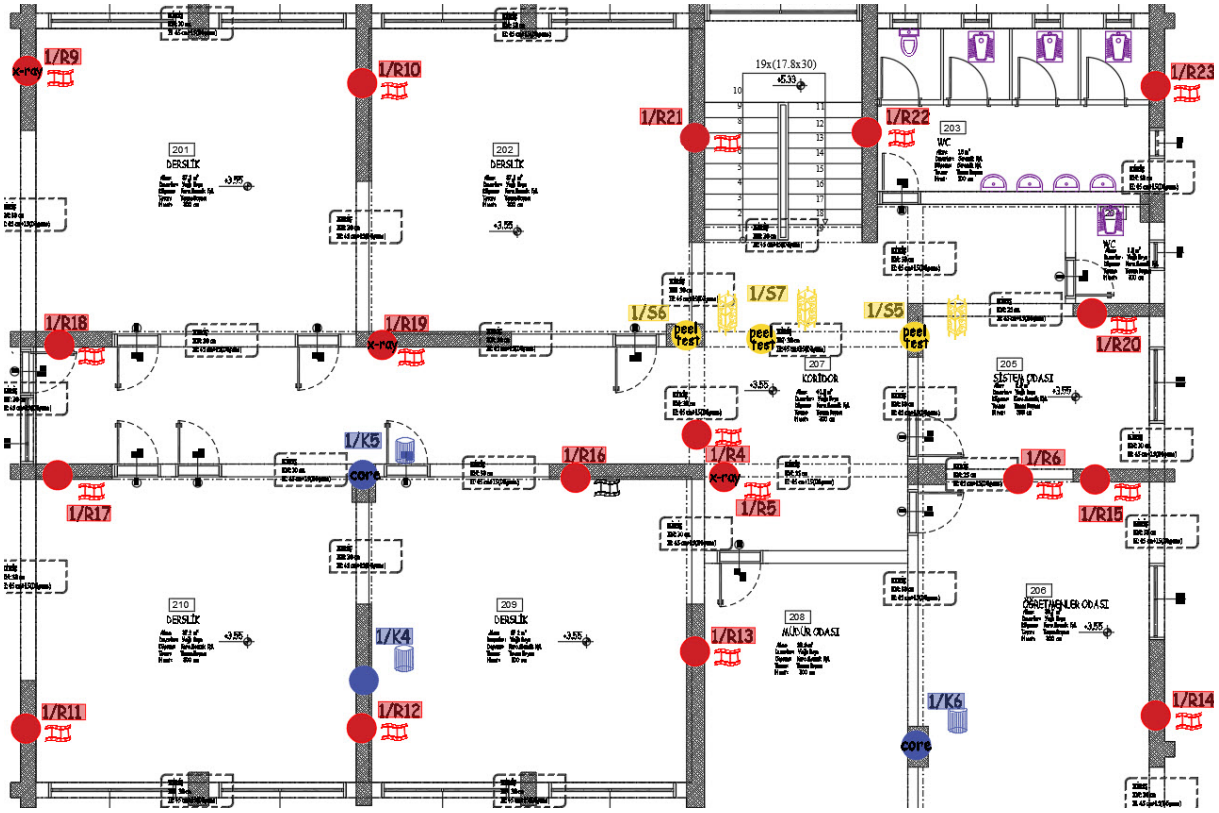

Figure 3. Structural elements where experiments are performed on the 1st storey

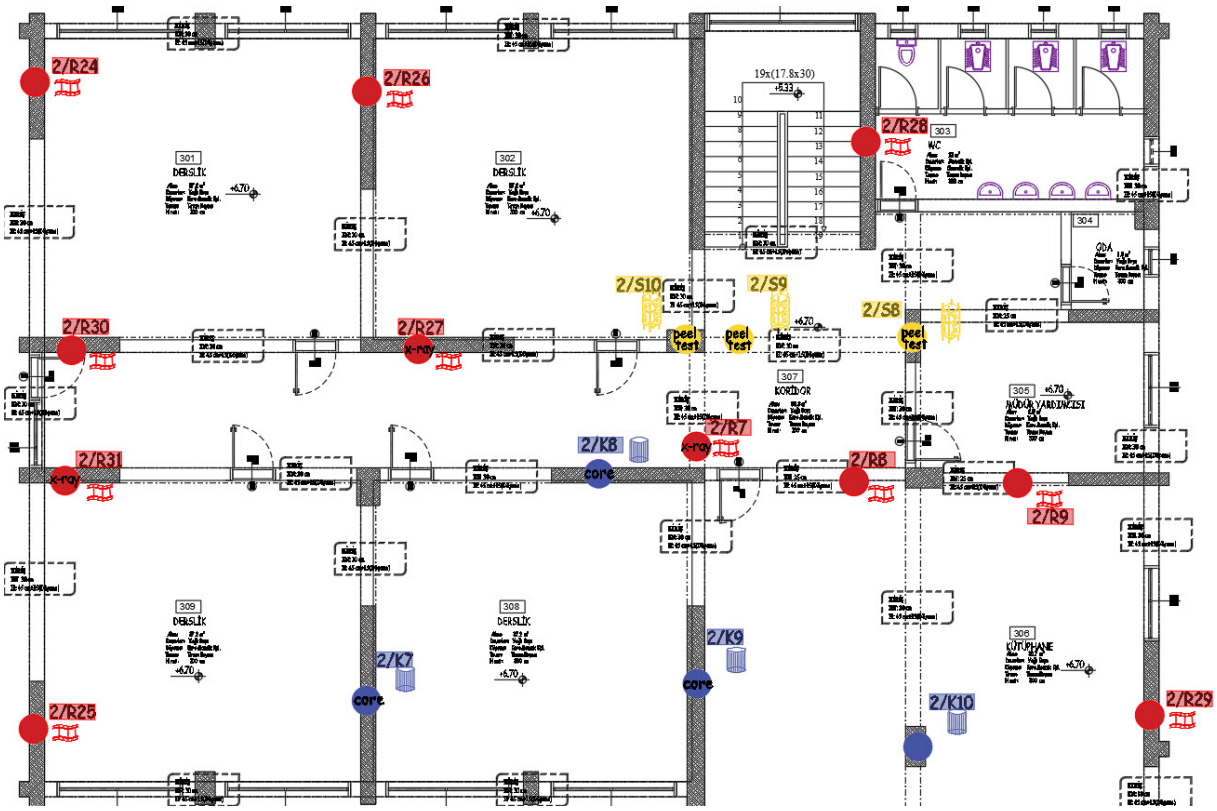

Figure 4. Structural elements where experiments are performed on the 2nd storey

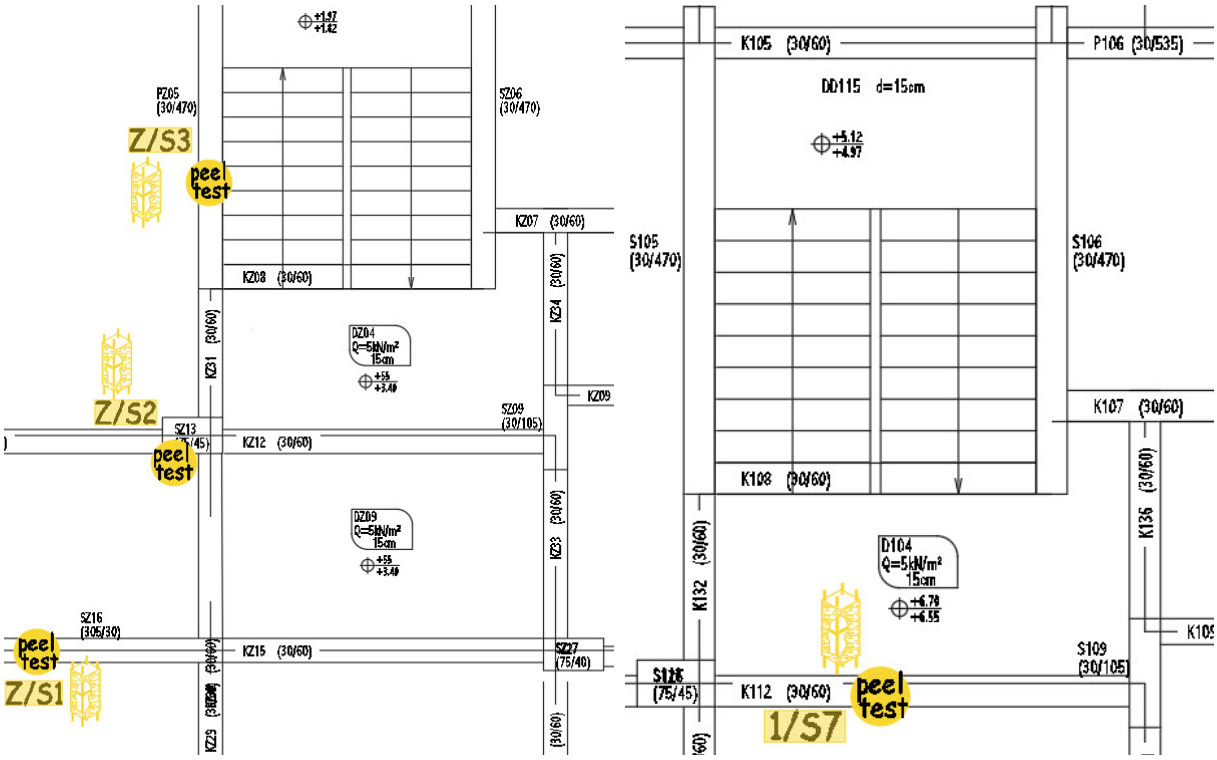

Ground storey 1st storey

Figure 5. Locations of the peel test structural elements on the ground storey of Kalaycılar primary school

Ground SZ13 column Ground-storey SZ16 column Ground storey PZ05 shear wall Ground K112 beamGround SZ27 beam

Figure 6. Views from the scraping process applied to some structural elements of Kalaycılar primary school

3. Structural Analyses of Kalaycılar Primary School

The performance results were obtained by performing a pushover analysis in the Sta4-Cad program of the Kalaycılar primary school building. In the Sta4-Cad program, plastic hinge properties are automatically assigned to structural elements. In this article, the lumped plastic hinge model is preferred in the analyses. In addition, pushover analyses of Kalaycılar primary school can be performed as single-mode and multi-modal. For the single-mode pushover analysis to be valid, the building height class, torsion coefficient, and mass participation rates in TBEC are considered. Accordingly, since the mass participation rates in the x and y directions of the school building are less than 70%, the results of the unimodal pushover analysis cannot be verified. For this reason, the multi-modal pushover analysis method was applied as the calculation method. On the other hand, the processes of the panel elements and the columns sheathing used for strengthening in the Sta4-Cad program are modeled by considering the regulations.

For structural analyses, the model of Kalaycılar primary school was created as in Figure 7 with the Sta4-Cad program, considering the TS498 and TS500 codes [17, 18]. An earthquake-free analysis was made, and cross-section adequacy was checked when the school building did not have application projects. As a result of the earthquake-free analyses, it was seen that there were no insufficient structural elements and that the school building had sufficient strength under service loads. Then, the existing concrete compressive strengths and rebars are defined separately for each storey. Accordingly, 20 MPa concrete strength on the ground storey, 13 MPa on the 1st storey, and 12 MPa on the 2nd storey, and existing S420 rebar information determined on-site were entered into the school building model (see Table 1). In addition, the parameters in Table 2 were considered for the structural analyses. First, performance analysis was made according to SBBSZ of the school building model in that information was entered. Accordingly, performance levels should be provided *Life Safety* (LS) for earthquake effects with a 2% probability of being exceeded in 50 years and *Immediate Use* (IU) for earthquake effects with a 10% probability of being exceeded in 50 years [15]. From structural analyses, the

school building failed to provide the target performance levels (see Figure 12 and Figure 15). As a result of the performance analyses made according to TBEC, while Kalaycılar primary school provided the target performance level at the DD1 earthquake level, it could not provide the target performance level at the DD3 earthquake level (see Figure 16 and Figure 19). In other words, this result shows that the target performance *Limited Damage* (LD) level could not be achieved at the DD3 earthquake level. In contrast, the target performance *Controlled Damage* (CD) performance level was achieved in the DD1 earthquake.

Here, it would be useful to state that the S420 type rebar is detected in the structural elements where made the peel test, that the tensile test is not performed to breaking. Because re-be adding the rebars will affect their mechanical properties, the rebar detection methods in the 2007 and 2019 Turkish earthquake codes are considered in determining the said rebars.

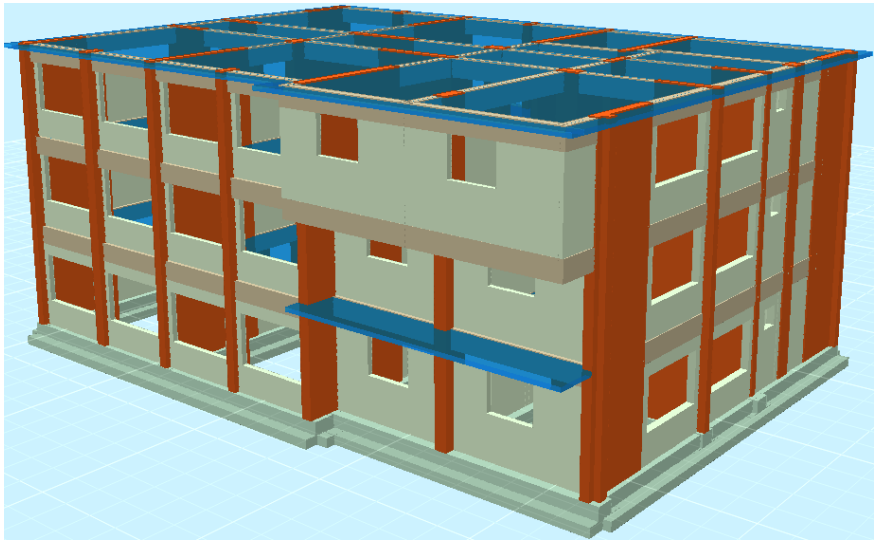

Figure 7. A view from the created model of Kalaycılar primary school

Table 2. Project parameters used in structural analyses

Parameters	SBBSZ	TBEC
Building importance coefficient (School)	1,5	
Building behaviour coefficient (R)	4	
Live load participation coefficient (n)	0,6	
Short-period spectral acceleration coefficient (S_s)	-	0,599
Spectral acceleration coefficient for 1s period (S_1)	-	0,203
Short-period design spectral acceleration coefficient (S_{ds})	-	0,791
Design spectral acceleration coefficient for 1s period (S_{d1})	-	0,445
Earthquake levels	-	DD1 / DD3
Earthquake Design Class (EDC)	-	1a
Building Height Class (BHC)	-	7
Coefficients of strength excess (D)	-	2,5
Soil bearing capacity (t/m²)	51,46	
Soil bedding coefficient (t/m³)	2882	
Earthquake zone coefficient (A_o)	0,4	-
Spectrum characteristic period (Ta/Tb)	0,2 / 0,9	-
DD1: Earthquake level with a 2% probability of exceeding in 50 years (recurrence period of 2475 years) DD3: Earthquake level with 50% probability of exceedance in 50 years (recurrence period of 72 years)		

4. Preparing the Strengthening Projects of the Kalaycılar Primary School

For this purpose firstly, studies in the technical literature on the strengthening of the school building and the location and effects of the shear wall were examined [19-31]. Later, two different strengthening projects were prepared when the existing school building could not provide the target performance levels. All storeys to the structural system in the model 1 strengthening were added to two shear walls in the y direction. In model 2 strengthening, shear walls were added in the x and y directions, and some columns were sheathed.

4.1. Model 1 strengthening project

While deciding on the strengthening process, the structural irregularities in the school building were considered, and intervention methods were preferred in a way that would not cause torsion problems and would affect the architectural plan the least. In addition, the cost of strengthening the school building was also considered. Accordingly, in model 1 strengthening, The axle, which did not provide the current performance condition and where the most structural damage occurred, was intervened. Because there is *Advanced Damage Region* (ADR) condition to the beams and columns on this axis, for this reason, by adding reinforcement bulkheads to the axis in question, both structural damage situations are reduced, and TBEC conditions are met.

While preparing the strengthening project of Kalaycılar primary school, torsional irregularities and structural elements damaged at the DD3 earthquake level were considered. Accordingly, a shear wall was added to the polygonal columns in case of *Marked Damage* (MD) in the y-direction on the ground story (see Figure 8). Performance analyses of the strengthened school building (model 1) were made according to SBBSZ and TBEC. As a result of the analyses, while the model 1 strengthening did not provide the target performance level according to SBBSZ, it provided the target performance level according to TBEC (see Figure 12~19). In addition, it was observed that there were no brittle structural elements with the model 1 strengthening.

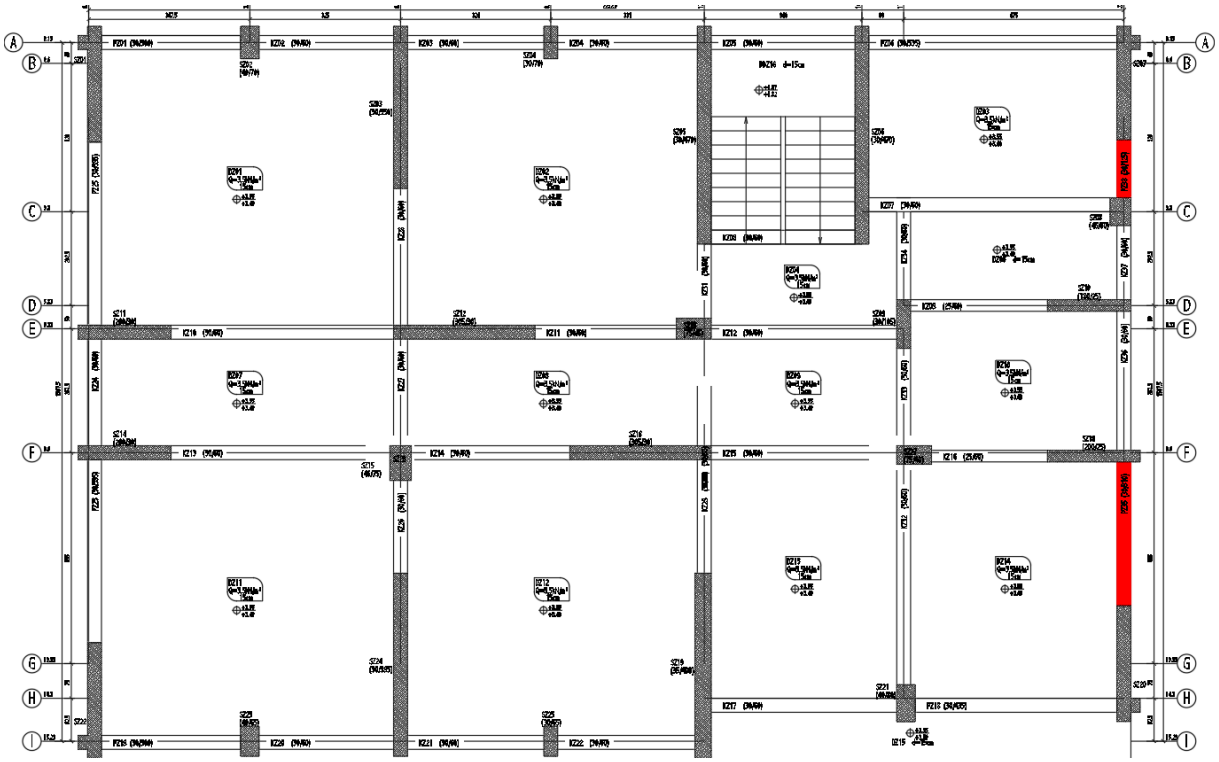

Figure 8. Locations of shear walls added to Kalaycılar primary school for strengthening purposes (model 1).

4.2. Model 2 strengthening project

Since the strengthening project prepared as model 1 did not provide the target performance level according to SBBSZ, the strengthening project defined as model 2 was prepared. Accordingly, the views of the structural elements to which strengthening is applied are seen in Figure 9~Figure 11, respectively. As a result of the analyses of the school building (model 2) strengthened according to SBBSZ and TBEC regulations, it is seen that the model 2 strengthening provides all target performance levels according to both SBBSZ and TBEC (see Figure 12~Figure 19).

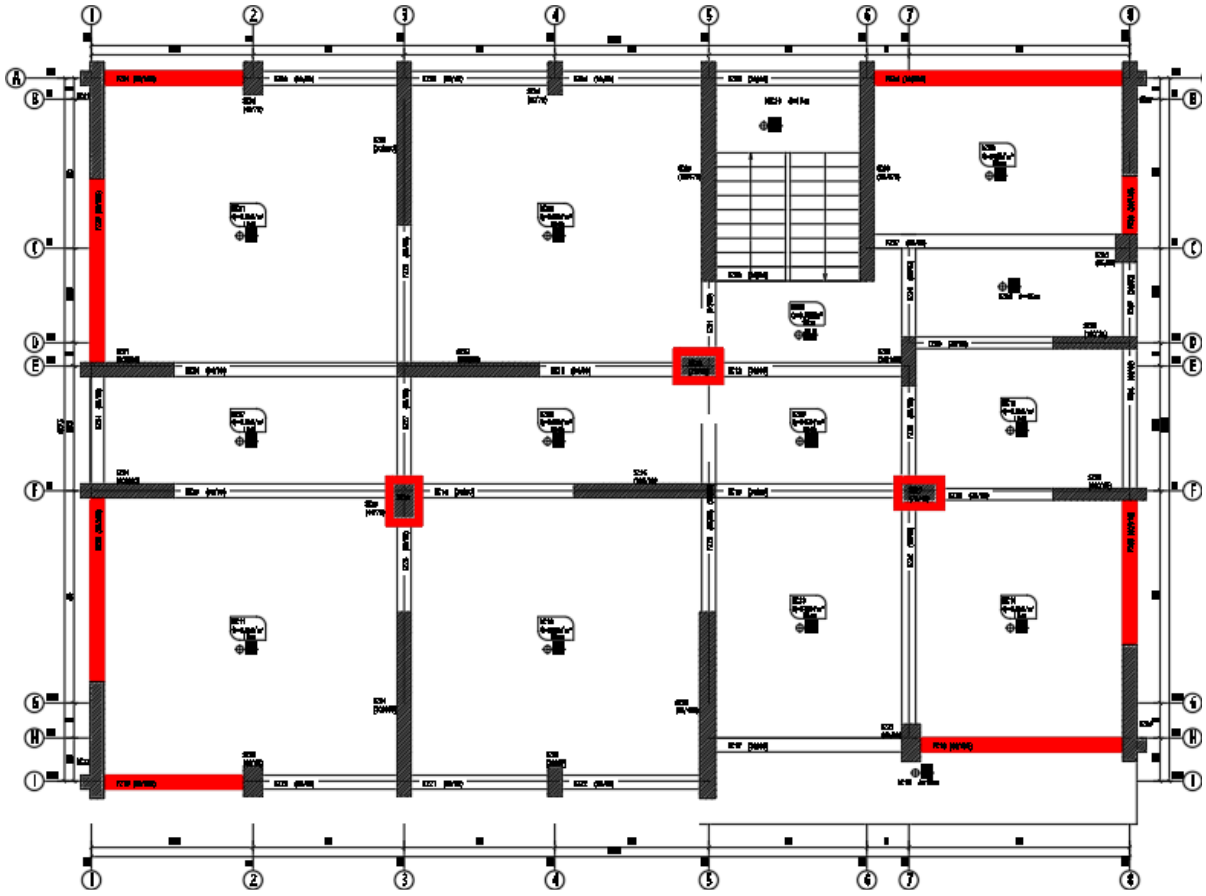

Figure 9. Strengthening applied to the ground-storey structural elements of Kalaycılar primary school (model 2).

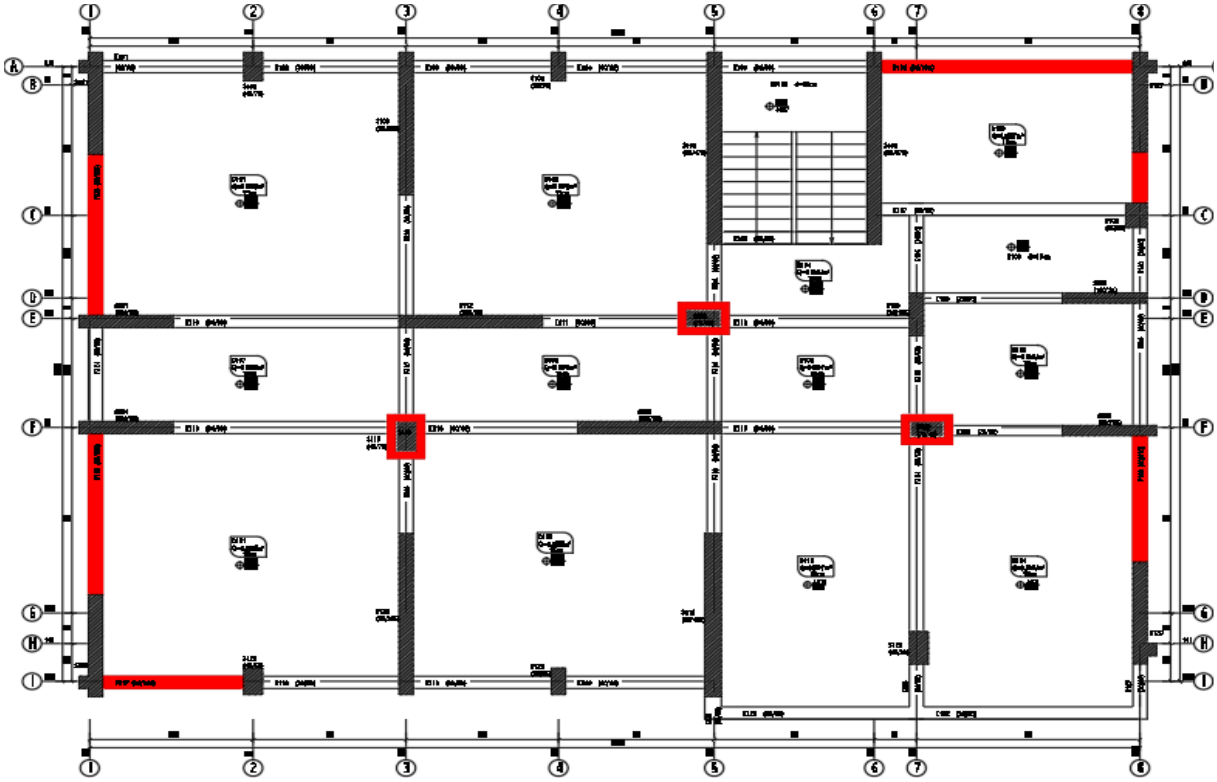

Figure 10. Strengthening applied to the 1st storey structural elements of Kalaycılar primary school (model 2).

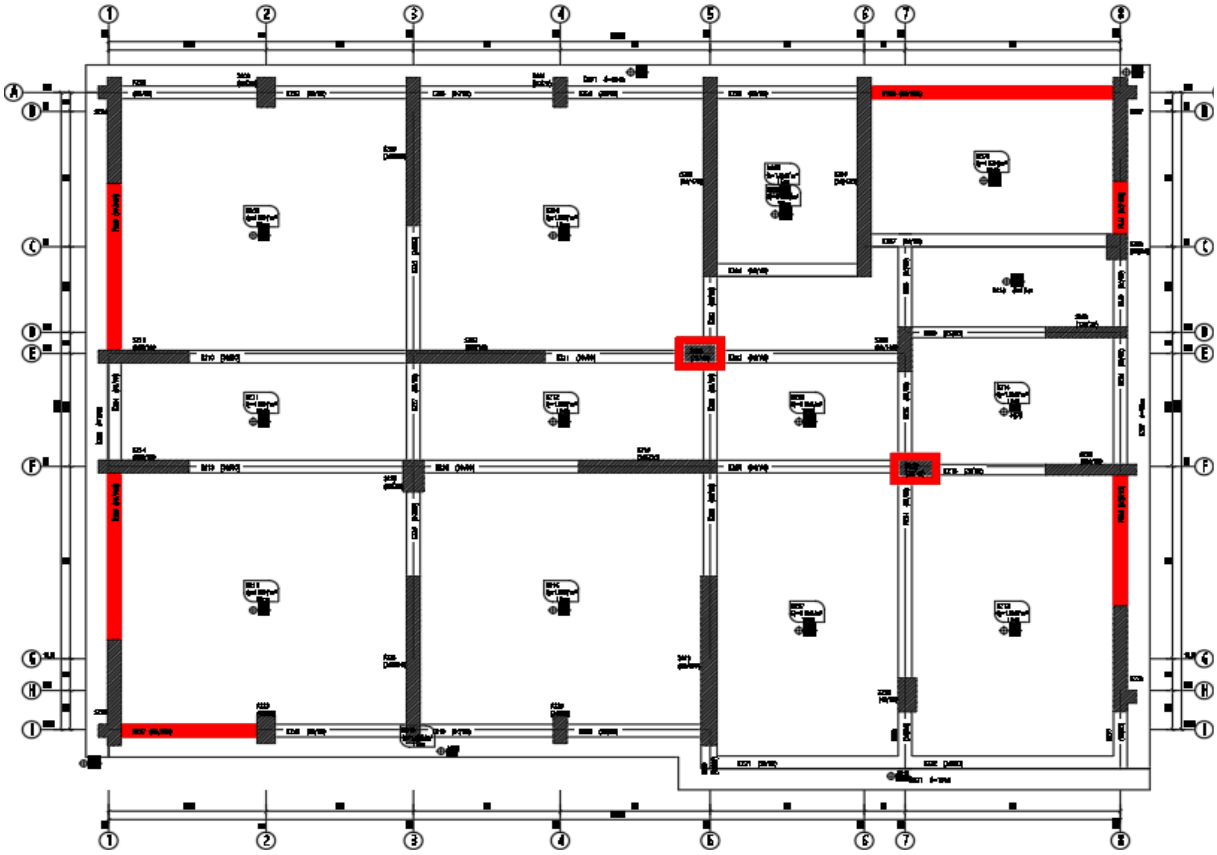

Figure 11. Strengthening applied to the 2nd storey structural elements of Kalaycılar primary school (model 2).

5. Findings And Assessments

From the analyses of the current and strengthened models (models 1 and 2) of Kalaycılar primary school according to SBBSZ, their performance status is given in Figure 12~Figure 15, respectively. These figures show that the required performance target could not be provided when the current and the strengthened school building, according to model 1, is evaluated according to the LS and IU performance levels. Since the Kalaycılar primary school cannot be provided, target performance levels of the situation strengthened according to existing and model 1, and a better performance level is obtained when the strengthened school building according to model 2 is evaluated according to the LS and IU. In other words, the target performance level is provided when the strengthened school building, according to model 2, is evaluated according to the LS and IU performance levels.

From the analyses of the current and strengthened models of Kalaycılar primary school according to TBEC, their performance status is given in Figure 16~Figure 19, respectively. According to this, it is seen that the required performance target is provided when the current and strengthened school-building models are evaluated according to the CD performance level. When the current and the strengthened school building according to model 1 is evaluated according to the LD performance level, the target performance level according to the DD3

earthquake level does not provide. By contrast, it is seen that the school building strengthened with the model 2 method provides all target performance levels.

When the Sa and Sd values in the x and y directions are examined for the earthquake levels recommended in the 2007 and 2019 Turkish earthquake codes, it is seen that model 2 strengthening has more spectral acceleration than the current situation and model 1 strengthening. In contrast, the model 2 strengthening has less spectral displacement value. This situation shows that the rigidity of the structural system in question increases due to the large number of shear walls added to the structural system in the model 2 strengthening. In addition, it is seen from these figures that the energy absorption capacity of the strengthened school models is higher than the current situation for all earthquake levels.

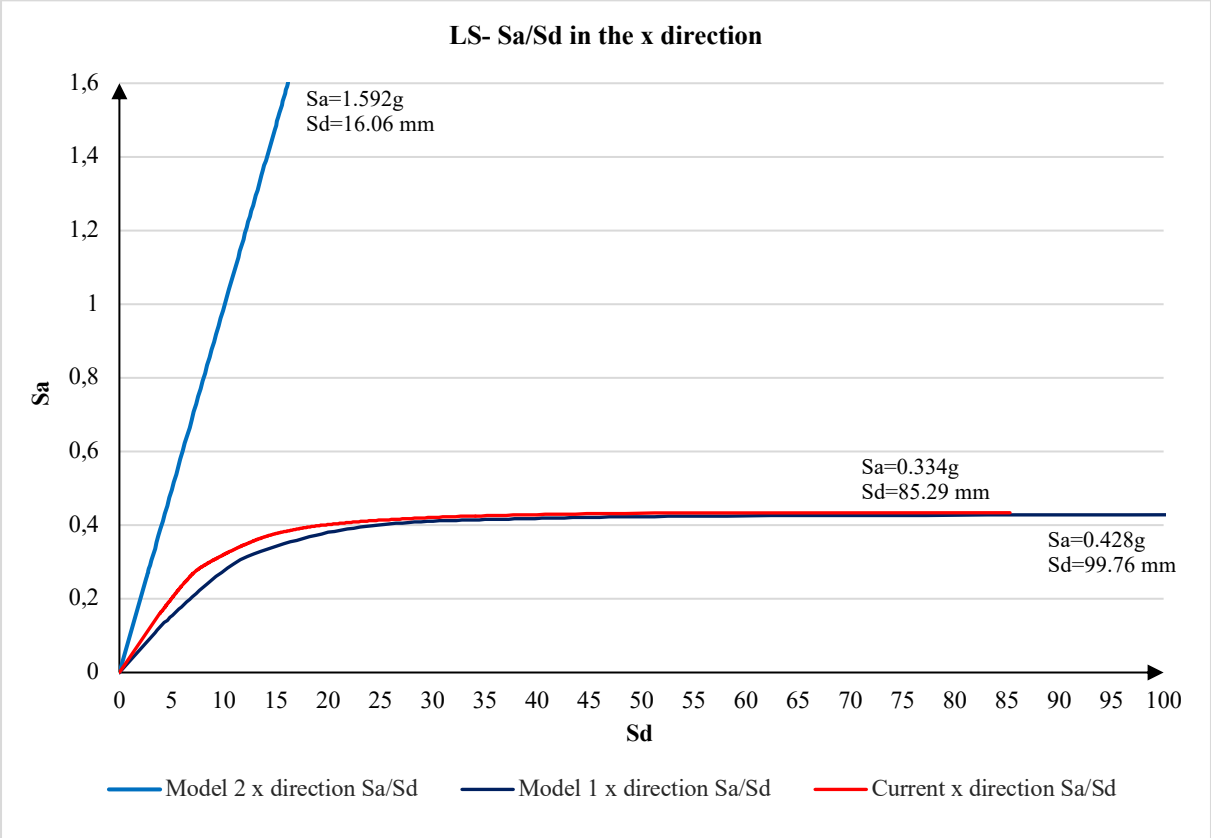

Figure 12. Performance results in LS earthquake of Kalaycılar primary school with the current situation, the model 1 and model 2 strengthening's in the x direction

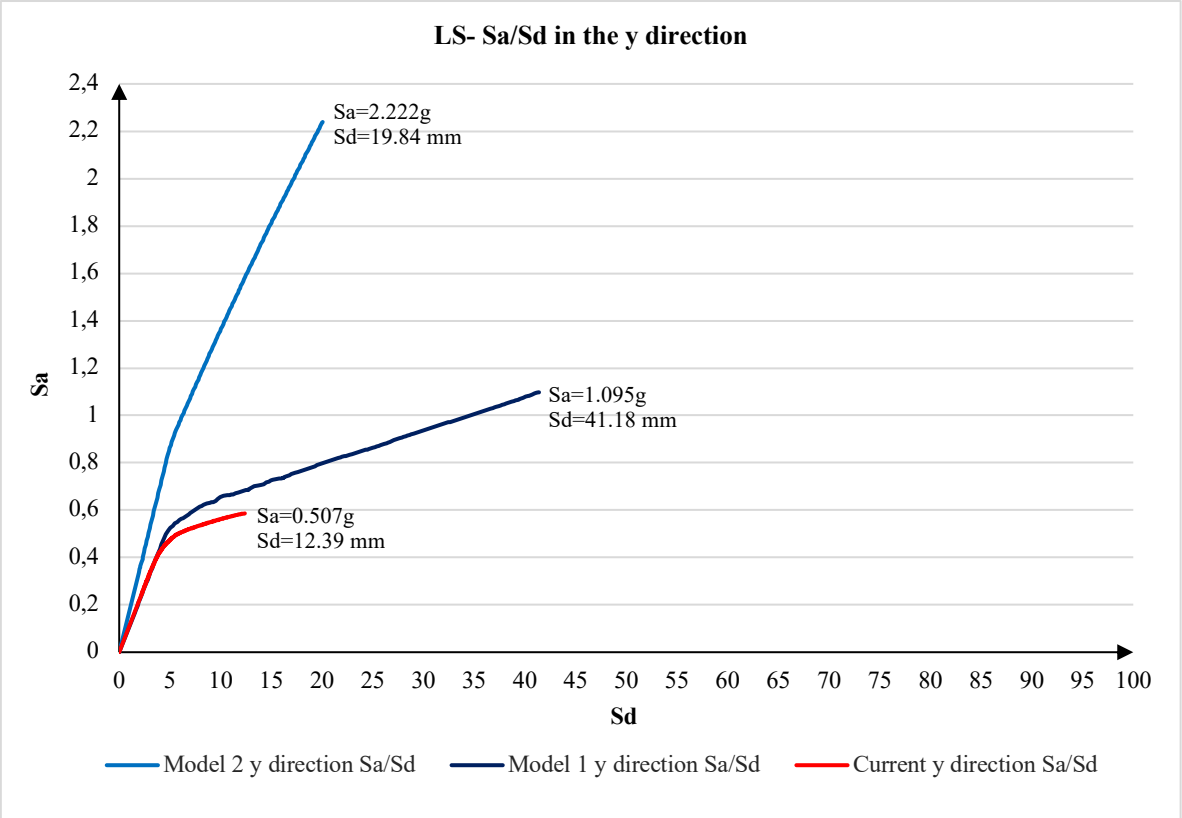

Figure 13. Performance results in LS earthquake of Kalaycılar primary school with the current situation, the model 1 and model 2 strengthening's in the y direction

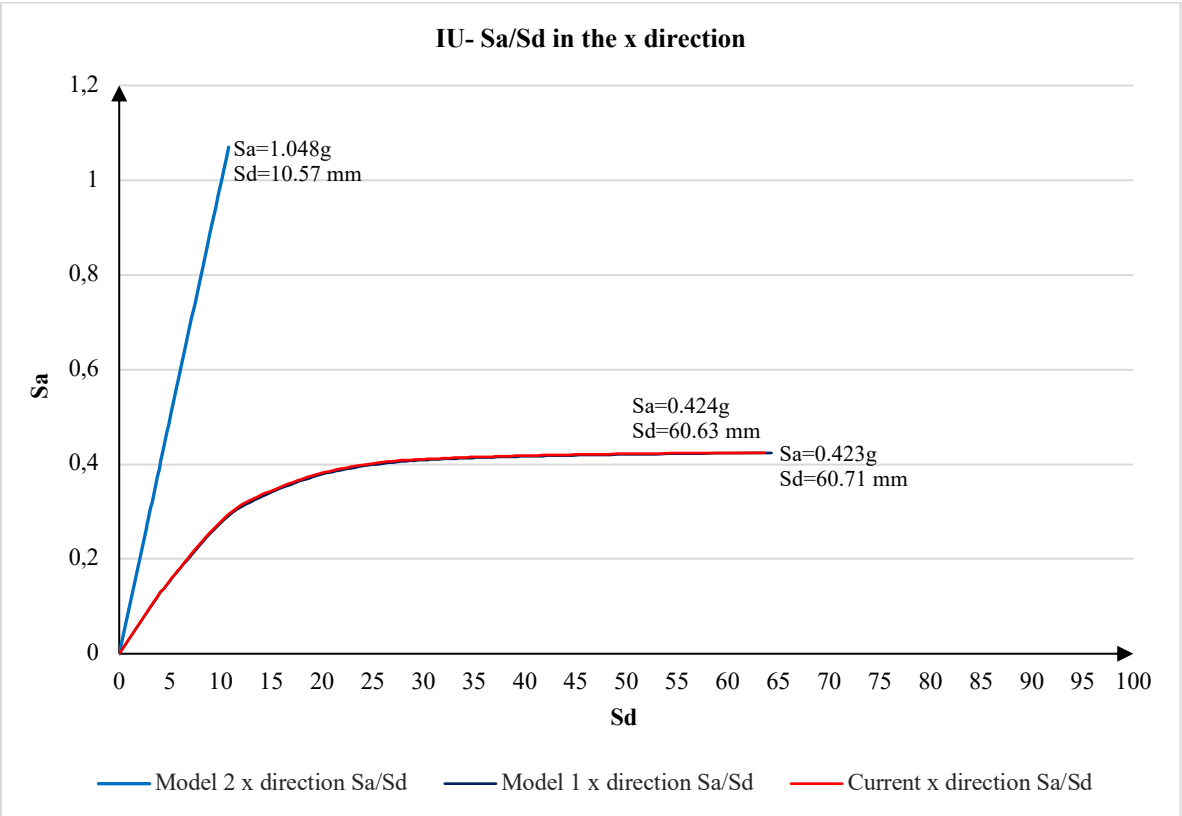

Figure 14. Performance results in IU earthquake of Kalaycılar primary school with the current situation, the model 1 and model 2 strengthening's in the x direction

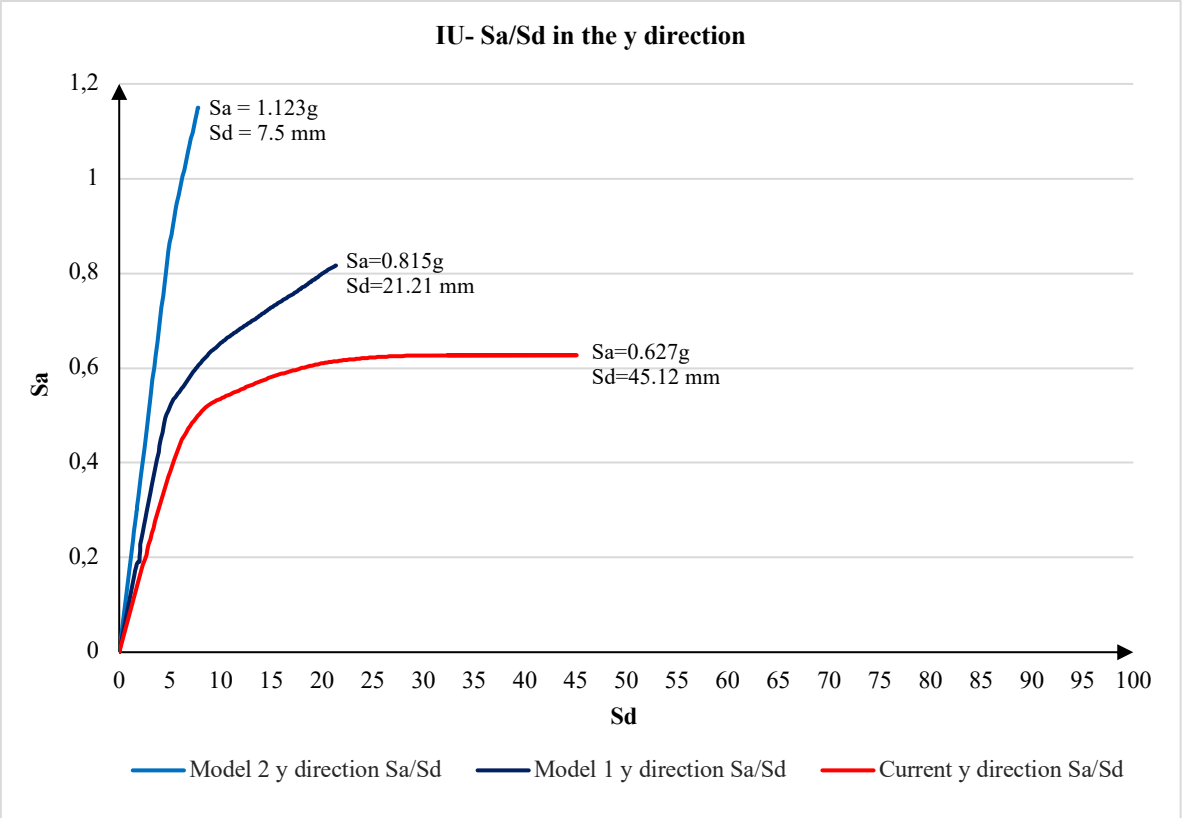

Figure 15. Performance results in IU earthquake of Kalaycılar primary school with the current situation, the model 1 and model 2 strengthening's in the y direction

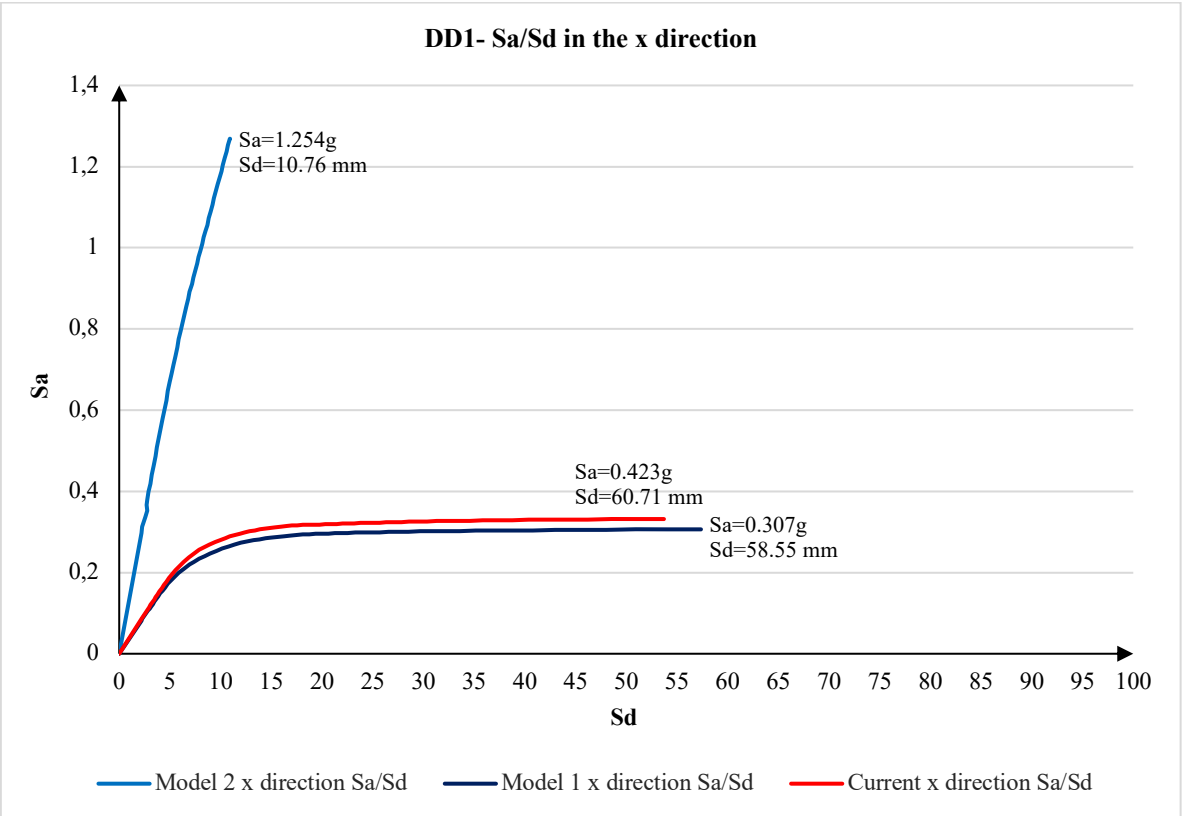

Figure 16. Performance results in DD1 earthquake of Kalaycılar primary school with the current situation, the model 1 and model 2 strengthening in the x direction

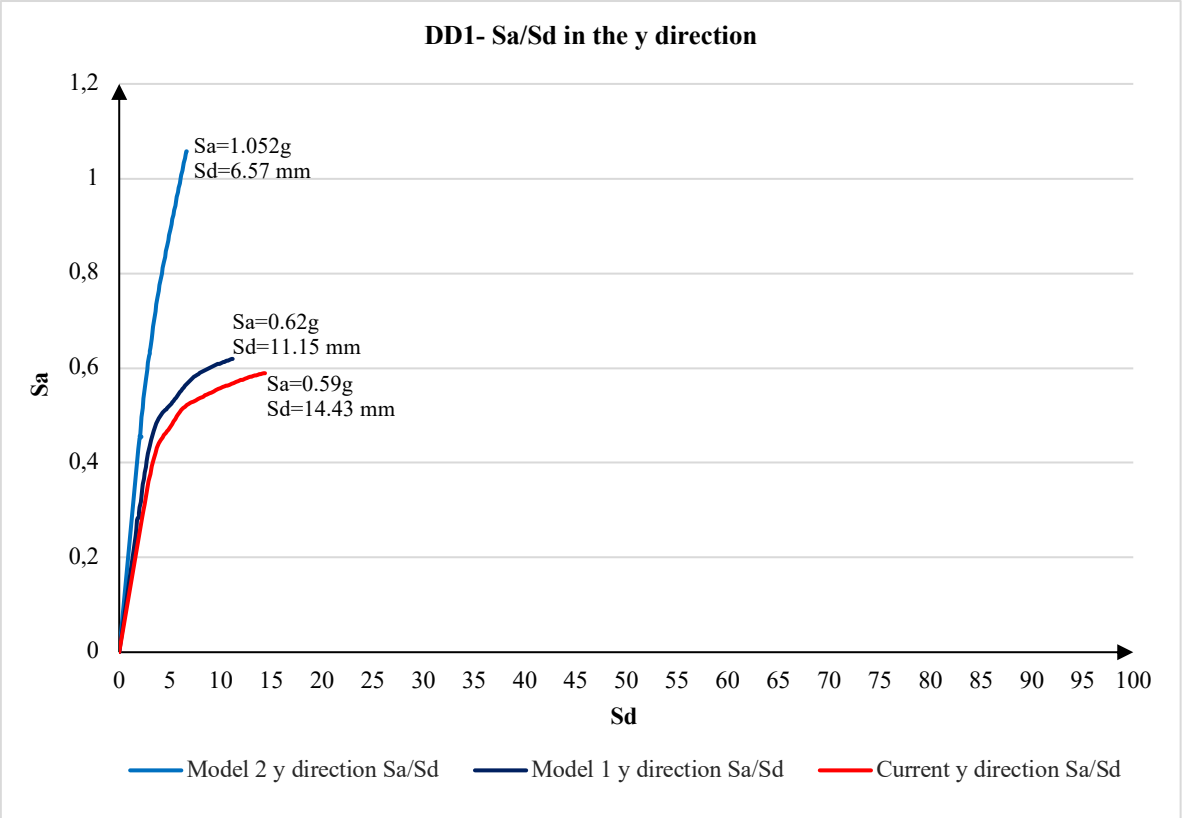

Figure 17. Performance results in DD1 earthquake of Kalaycılar primary school with the current situation, the model 1 and model 2 strengthening in the y direction

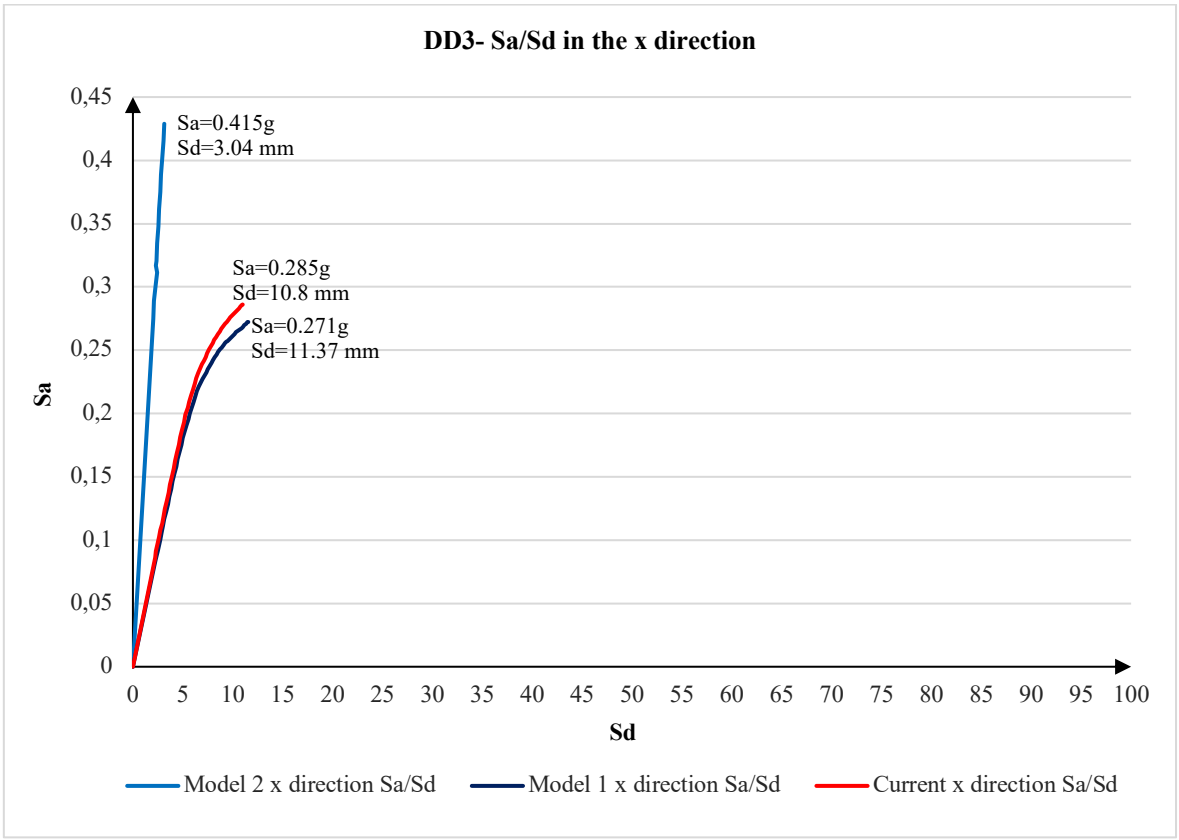

Figure 18. Performance results in DD3 earthquake of Kalaycılar primary school with the current situation, the model 1 and model 2 strengthening in the x direction

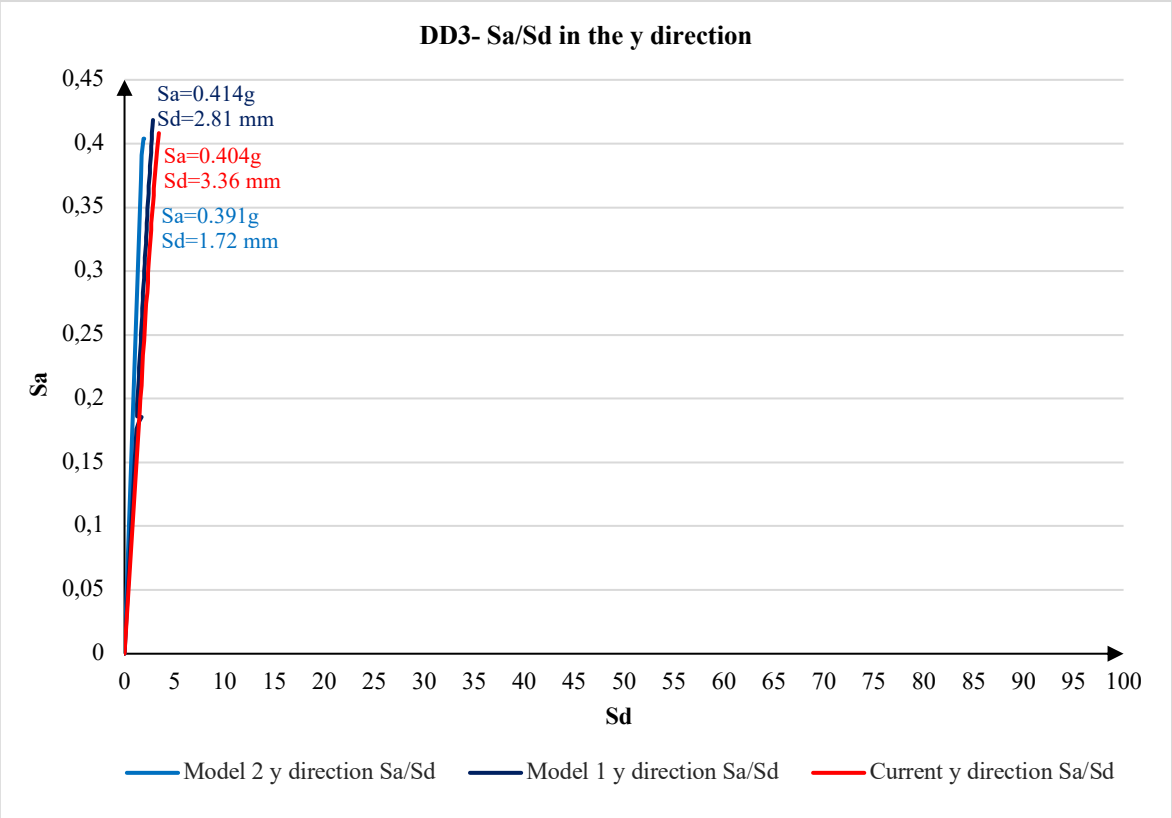

Figure 19. Performance results in DD3 earthquake of Kalaycılar primary school with the current situation, the model 1 and model 2 strengthening in the y direction

The comparison of model 1 and model 2 strengthening methods and costs applied to Kalaycılar primary school, considering the 2021-unit price year with the OSKA program, is given in Table 3. From this table, it is seen that the model 2 strengthening gives better performance than the model 1 strengthening, but the cost of the model 2 strengthening is 2 times more than the model 1 strengthening.

Table 3. Kalaycılar primary school model 1 and model 2 performance levels and strengthening costs for 2021year

Strengthening Method	Performance Levels				Strengthening Cost	Strengthening Cost / Structure Approximate Cost	Structure Approximate Cost
	LS	IU	DD1	DD3			
Model 1	Collapsing	Collapsing	CD	LD	302.628,03 ₺	%21	1.429.360 ₺
Model 2	IU	IU	LD	LD	663.163,83 ₺	%46	

The total number of plastic hinges formed in the columns and beams according to the earthquake levels recommended in SBBSZ and TBEC for the current and strengthened conditions of Misakı Milli primary school is given in Figures 20~22, respectively. These figures show that the number of plastic hinges formed in the strengthened state according to model 2 has decreased significantly compared to the current situation. Also, for the limited knowledge level, it has been observed that there is a general increase in the total number of plastic hinges formed in the columns and beams compared to the comprehensive knowledge level.

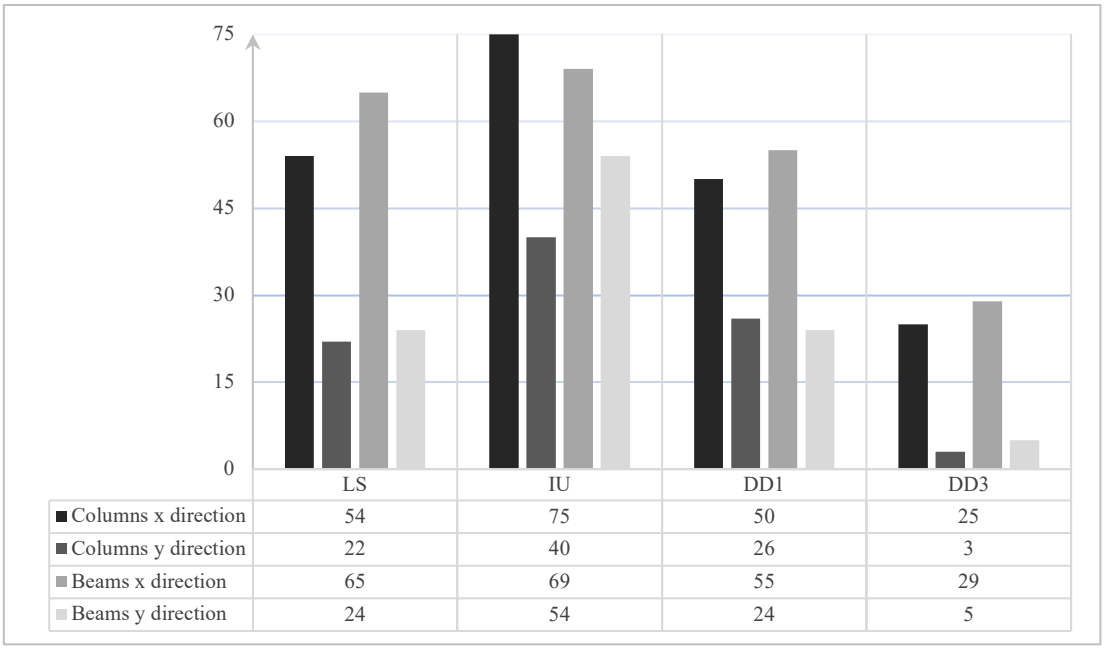

	LS	IU	DD1	DD3
Columns x direction	54	75	50	25
Columns y direction	22	40	26	3
Beams x direction	65	69	55	29
Beams y direction	24	54	24	5

Figure 20. Number of structural elements plasticized in x and y earthquake directions of the current situation of Kalaycılar primary school

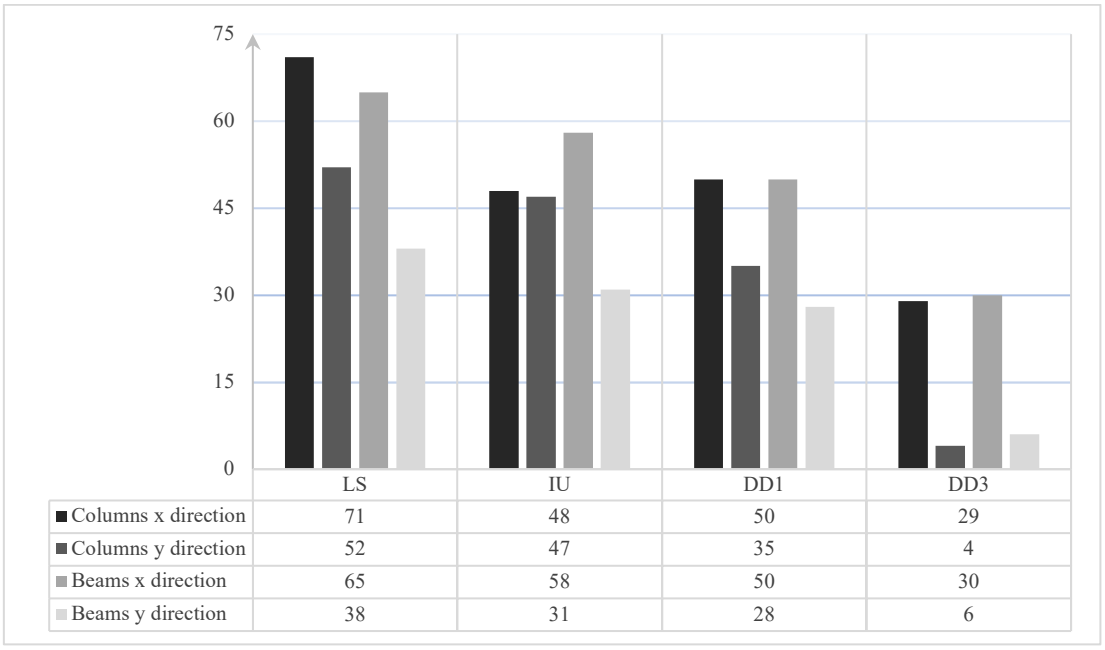

	LS	IU	DD1	DD3
Columns x direction	71	48	50	29
Columns y direction	52	47	35	4
Beams x direction	65	58	50	30
Beams y direction	38	31	28	6

Figure 21. Number of structural elements plasticized in the x and y earthquake directions of Kalaycılar primary school model 1 strengthening

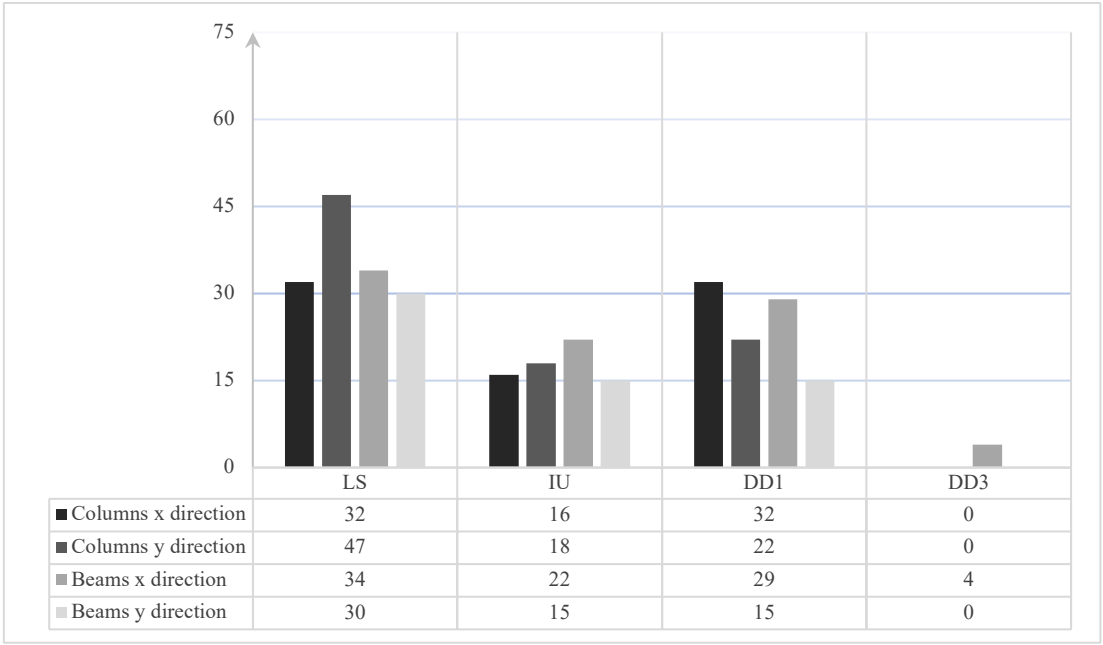

	LS	IU	DD1	DD3
Columns x direction	32	16	32	0
Columns y direction	47	18	22	0
Beams x direction	34	22	29	4
Beams y direction	30	15	15	0

Figure 22. Number of structural elements plasticized in the x and y earthquake directions of Kalaycılar primary school model 2 strengthening

In this article, the strengthening method has been chosen in a way that will minimum interfere with the architecture of the school building in question, will not create structural irregularities, and be economical. Accordingly, while the model 1 strengthening method, which is the most optimal method, provided the TBEC target performance levels, the target performance level could not be achieved in the SBBSZ regulation. When this is the case, the model 2 strengthening method has been applied to the school building that will meet the TBEC and SBBSZ earthquake regulations. It reveals that the chosen strengthening method (due to the added structural elements) significantly affects the rigidity and ductility of the building in question. In addition, the cost of strengthening is also effective in selecting the strengthening method. On the other hand, there are many strengthening methods other than the selected strengthening method in this study. Still, the design criteria recommended in the regulations of the selected strengthening method should be considered.

6. Conclusions and Recommendations

It is possible to summarize the results and recommendations obtained from this study as follows.

• Kalaycılar school building, analysed without earthquakes with the Sta4-Cad program, has sufficient stability. However, from the performance analyses made according to SBBSZ, while the required performance target could not be achieved at the earthquake level, which has a 2% probability of exceeding in 50 years, the LS performance target was achieved at the earthquake level which has a 10% probability of exceeding in 50 years. From the performance analyses made according to TBEC, a sufficient performance target was also reached at the DD1 earthquake level. By contrast, it is seen that the target performance level could not be provided at the DD3 earthquake level.

- The target performance is provided at the DD1 and DD3 earthquake levels suggested in TBEC from the structural analyses of Kalaycılar primary school, which was strengthened according to model 1. In contrast, LS and IU earthquake levels recommended in SBBSZ are in the CR.

- From the structural analyses of Kalaycılar primary school that was strengthened according to model 2, it gives a *Limited Damage* performance level at DD1 and DD3 earthquake levels while giving *Immediate Use* performance level at LS and IU earthquake levels. This result shows that for earthquake levels with a 2% probability of exceeding 50 years, a better performance level than the target performance level recommended in the regulations considered in this study is obtained.

- According to model 2 of Kalaycılar primary school, structural analyses of the strengthened situation showed that brittle structural elements are formed in some newly added strengthening elements, except for the DD3 earthquake level. This matter can be eliminated by increasing the distribution rebars' diameter and/or spacing.

- From the structural analyses, the strengthened state of Kalaycılar primary school, according to model 2, outperforms the strengthened state according to model 1.

- The approximate cost of the Kalaycılar primary school, built in 2005, is 1.429.360 ₺. To propose the demolition of Kalaycılar primary school from an economic point of view, the cost of strengthening should exceed 56% of the approximate cost of the building [13, 32]. Today, evaluating the economic life of the 17-year-old school building, the ratio of the cost of model 1 strengthening to the approximate cost of the building is 21%, and that of model 2 strengthening is 46%. Since these calculated rates are lower than 56%, it seems that it would be rational to strengthen the Kalaycılar primary school.

- From the results of this article, it can be seen that there is more than one option for strengthening a reinforced concrete structure. The authors suggest that all parameters should be evaluated together while strengthening a reinforced concrete structure, and the cost/performance optimum of one of the strengthening options should be considered.

Ethics in Publishing

There are no ethical issues regarding the publication of this study.

Author Contributions

This article is part of Mustafa Esat COŞKUN's Master's thesis titled "*Comparison of Reinforcement Principles in Reinforced Concrete School Buildings According to 2007 and 2019 Turkish Earthquake Regulations*" under the supervisor of Prof. Dr. Şenol GÜRSOY. One of the researchers, Assist. Prof. Dr. Zehra Şule GARİP is a jury member of Mustafa Esat COŞKUN's master's thesis defense and contributed to developing the thesis and writing this article.

References

[1] Gürsoy, Ş., Öz, R. & Baş, S. (2015). Investigation of the Effect of Weak-Story on Earthquake Behavior and Rough Construction Costs of RC Buildings, *Computers and Concrete*, 16 (1), 141-161.

[2] Gürsoy, Ş. (2013). Farklı Rijitleştirici Elemanlara Sahip Binaların Depreme Göre Maliyetlerinin Karşılaştırılması, *Journal of the Faculty of Engineering and Architecture of Gazi University*, 28 (3), 533-544.

[3] Garip, Z.Ş. & Erhan, E. (2022). Perde Duvarlı ve Çerçeveli Betonarme Binalarda Deprem Tasarım Sınıflarının Bina Maliyetine Etkisi, *Düzce Üniversitesi Bilim ve Teknoloji Dergisi*, 10 (2): 700-715.

[4] Tunç, G. & Tanfener, T. (2021). Reinforced Concrete Design of Tall Buildings According to the Turkish Earthquake Code, *Erzincan University Journal of Science and Technology*, 14 (1), 27-40.

[5] Coşkun, M.E., Gürsoy, Ş. & Garip, Z.Ş. (2023). Betonarme Bir Okul Binasında Güçlendirme İlkelerinin 2007 ve 2019 Türk Deprem Yönetmeliklerine Göre Karşılaştırılması, *Gümüşhane Üniversitesi Fen Bilimleri Enstitüsü Dergisi (GÜFBED/GUSTIJ),* 13 (1), 127-144.

[6] Erdem, İ., Akyüz, U., Ersoy, U. & Özcebe, G. (2006). An Experimental Study on Two Different Strengthening Techniques for RC Frames, *Engineering Structures*, 28 (13), 1843-1851.

[7] Altın, S., Anıl, Ö., Kara, M. E. & Kaya, M. (2008). An Experimental Study on Strengthening of Masonry Infilled RC Frames Using Diagonal CFRP Strips, *Composites: Part B*, 39 (4), 680-693.

[8] Kalkan, İ., Aykaç, B., Baran, M., Babayani, R. & Aykaç, S. (2013). Delikli Çelik Levhalarla Güçlendirilmiş Dolgu Duvarların Deprem Davranışı, *TMMOB İnşaat Mühendisleri odası 5. Çelik Yapılar Sempozyumu*, 13-15 Kasım, İstanbul, Türkiye.

[9] Baran, M., Aktaş, M. & Aykaç, S. (2014). Sıvanmış Tuğla Dolgu Duvarların Şerit Beton/Betonarme Panellerle Güçlendirilmesi, *Gazi Üniversitesi Mühendislik Mimarlık Fakültesi Dergisi*, 29 (1), 23-33.

[10] Aksoylu, C. & Sezer, R. (2018). Investigation of Precast New Diagonal Concrete Panels in Strengthened the Infilled Reinforced Concrete Frames, *KSCE Journal of Civil Engineering*, 22 (1), 236-246.

[11] Aksoylu, C. & Kara, N. (2020). Strengthening of RC Frames by Using High Strength Diagonal Precast Panels, *Journal of Building Engineering*, 31, 101338.

[12] Baran, M. (2020). Comparison of Seismic Performances of Reinforced Concrete Frames Strengthened by Different Techniques, *Latin American Journal of Solids and Structures*, 18(2), 1-22.

[13] Coşkun, M.E. (2022). Betonarme Okul Binalarında Güçlendirme İlkelerinin 2007 ve 2019 Türk Deprem Yönetmeliklerine Göre Karşılaştırılması, *Yüksek Lisans Tezi, Karabük Üniversitesi Lisansüstü Eğitim Enstitüsü*, Karabük.

[14] Sta4-CAD, (2021). Structural Analysis for Computer Aided Design, ver.14.1. STA Bilgisayar Mühendislik ve Müşavirlik San. ve Tic. Ltd. Şti, www.sta.com.tr

[15] SBBSZ, (2007). Specification for Buildings to be Built in Seismic Zones, *Ministry of Public Works and Settlement Government of Republic of Turkey*, Ankara, Turkey.

[16] TBEC, (2019), Turkish Building Earthquake Regulation, *Disaster and Emergency Management Presidency*, Ankara, Turkey.

[17] TS-498, (1997). Calculation Values of Loads to be Taken in the Dimensioning of Structural Elements, *Turkish Standards Institute*, Ankara, Turkey. (in Turkish).

[18] TS500, (2000). Requirements for Design and Construction of Reinforced Concrete *Structures, Turkish Standards Institute*, Ankara, Turkey. (in Turkish).

[19] Anil, Ö. & Altın, S. (2007). An Experimental Study on Reinforced Concrete Partially Infilled Frames, *Engineering Structures*, 29 (3):449-460.

[20] Chuang, M.C., Liao, E., Lai, V.P., Yu, Y.J. & Tsai, K.C. (2011). Development of PISA4SB for Applications in the Taiwan School Building Seismic Retrofit Program, *Procedia Engineering*, 14, 965-973.

[21] Chrysostomou, C.Z., Kyriakides, N., Papanikolaou, V.K., Kappos, A.J., Dimitrakopoulos, E.G. & Giouvanidis, A.I. (2015). Vulnerability Assessment and Feasibility Analysis of Seismic Strengthening of School Buildings, *Bulletin of Earthquake Engineering*, 13, 3809-3840.

[22] Erdem, I., Akyuz, U., Ersoy, U. & Ozcebe, G. (2006). An Experimental Study on Two Different Strengthening Techniques for RC Frames, *Engineering Structures*, 28 (13):1843-1851.

[23] Gur, T., Pay, A.C., Ramirez, J.A., Sozen, M.A., Johnson, A.M., Irfanoglu, A. & Bobet, A. (2009). Performance of School Buildings in Turkey During the 1999 Düzce and the 2003 Bingöl Earthquakes, *Earthquake Spectra*, 25 (2): 239-256.

[24] Hadzima-Nyarko, M., Ademović N. & Krajnović M. (2021). Architectural Characteristics and Determination of Load-Bearing Capacity as a Key Indicator for a Strengthening of the Primary School Buildings: Case Study Osijek, *Structures*, 34, 3996-4011.

[25] Hancilar, U., Çaktı, E., Erdik, M., Franco, G.E. & Deodatis, G. (2014). Earthquake Vulnerability of School Buildings: Probabilistic Structural Fragility Analyses, *Soil Dynamics and Earthquake Engineering*, 67, 169-178.

[26] Kaltakci, M.Y., Arslan, M.H., Yilmaz, U.S. & Arslan, H.D. (2008). A New Approach on the Strengthening of Primary School Buildings in Turkey: An Application of External Shear Wall, *Building and Environment*, 43 (6), 983-990.

[27] Kaltakci, M.Y., Arslan, M.H. & Yavuz, G. (2010). Effect of Internal and External Shear Wall Location on Strengthening Weak RC Frames, *Scientia Iranica*, 17 (4): 312-323.

[28] Kaltakci, M.Y., Arslan, M.H. & Özturk, M. (2010). An Experimental Investigation for External RC Shear Wall Applications. *Natural Hazards and Earth System Sciences*, 10: 1941-1950.

[29] Karadogan, H.F, Pala, S., Ilki, A., Yüksel, E., Mowrtage, W., Teymur, P., Erol, G., Taskin, K. & Çömlek, R. (2009). Improved Infill Walls and Rehabilitation of Existing Low Rise Buildings, *Seismic Risk Assess Retrofit*, 387-426.

[30] Oyguc, R. (2016). Seismic Performance of RC School Buildings after 2011 Van Earthquakes, *Bulletin of Earthquake Engineering*, 14, 821-847.

[31] Samadian, D., Ghafory-Ashtiany, M., Naderpour, H. & Eghbali M. (2019). Seismic Resilience Evaluation Based on Vulnerability Curves for Existing and Retrofitted Typical RC School Buildings, *Soil Dynamics and Earthquake Engineering*, 127, 105844.

[32] Mutlu, A.H. (2015). Mevcut Yapıların Güçlendirilmesi ya da Yıkılmasına Karar Verilmesi Aşamasında Göz Önüne Alınması Gereken Kriterler, *3. Türkiye Deprem Mühendisliği ve Sismoloji Konferansı*, 14-16 Ekim, İzmir, 1-5.

Erzincan Üniversitesi
Fen Bilimleri Enstitüsü Dergisi
2024,17(1), 1-15
ISSN: 1307-9085, e-ISSN: 2149-4584
Araştırma Makalesi

Erzincan University
Journal of Science and Technology
2024,17(1), 1-15
DOI: 10.18185/erzifbed.1196965
Research Article

Prediction of Radio Signal Failures of Communication Based Train Operating Systems by Machine Learning Methods

Burak ARSLAN[1], Hasan TİRYAKİ[1*]

[1] Department of Electrical and Elektronics Engineering, Faculty of Engineering, Istanbul University-Cerrahpasa, Istanbul, Türkiye

Received: 31/10/2022, **Revised:** 26/12/2023, **Accepted:** 26/02/2023, **Published:** 28/03/2024

Abstract

The use of rail systems in urban public transportation has become a necessity for reasons such as time saving, travel comfort and operating costs, especially in cities with high population and road traffic. Communication based train operating systems (CBTC) are used for the safe use of urban rail systems and the maximum capacity of the railway line. In this study, in line with the data collected from the trains on a railway line operated with CBTC, the status of the radio signals that enable the wireless communication of the trains with the trackside signaling equipment was evaluated by machine learning methods, and the situations that may have negative effects on the train operations of the problems at the signal level were evaluate. The problems on the antennas which receives signals from trackside above trains, the poor connection related with fiber optical and LAN cables, the trackside transmitter antenna orientation problems causes decrease on signal levels. It is aimed that to take actions about the problematic signal levels without any negative impact on the passenger comfort and the operation yet. The radio signal losses cause unexpected trains stops and delays. A decision support model has been developed that will offer early solution suggestions to system maintainers in order to intervene first. In conclusion, since it is the first study related with failure prediction by using radio signal levels data on railway signaling system, this study presents an important innovation in terms of literature.

Keywords: Railway transportation, communication based train operating systems, machine learning methods, failure prediction, maintenance management

Makine Öğrenmesi Yöntemleri ile Haberleşme Tabanlı Tren İşletim Sistemlerinin Radyo Sinyal Hatalarının Tahmini

Öz

Kentsel toplu taşımada raylı sistemlerin kullanılması, özellikle nüfus ve karayolu trafiğinin yoğun olduğu şehirlerde zaman tasarrufu, seyahat konforu ve işletme maliyetleri gibi nedenlerle bir zorunluluk haline gelmiştir. Kent içi raylı sistemlerin güvenli kullanımı ve demiryolu hattının maksimum kapasiteyle kullanımı için haberleşme tabanlı tren işletim sistemleri (CBTC) kullanılmaktadır. Bu çalışmada, CBTC ile işletilen bir demiryolu hattındaki trenlerden toplanan veriler doğrultusunda, trenlerin yol kenarı sinyalizasyon ekipmanları ile kablosuz iletişimini sağlayan sinyallerinin durumu makine öğrenmesi yöntemleri ile değerlendirilmiş ve durumlar değerlendirilmiştir. Tren üzerinde radyo sinyallerini yakalayan antenlerin bağlantılarında, hat boyu verici radioların fiber optic ve LAN kablo sonlandırmalarında, hat boyu verici antenlerin oryantasyonlarındaki problemler sinyal seviyelerinde düşmelere sebep olmaktadır. Sinyal seviyesindeki problemlerin tren işletmesini olumsuz etkileyebileceği durumlar değerlendirilmiş, yolcu konforuna ve operasyonuna henüz olumsuz bir etkisi olmadan müdahale edilmesi amaçlanmıştır. Radyo sinyal seviyelerindeki kayıplar beklenmedik tren duruşlarına ve tehirlere sebep olmaktadır. Sistem yöneticilerine önceden müdahale etmeleri için erken çözüm önerileri sunacak bir karar destek modeli geliştirilmiştir. Sonuç olarak, demiryolu sinyalizasyon sistemindeki radio sinyal seviyeleri verileri kullanılarak arıza tahmini ile ilgili ilk çalışma olması nedeniyle bu çalışma literatür açısından önemli bir yenilik sunmaktadır.

Anahtar Kelimeler: Demiryolu ulaşımı, haberleşme tabanlı tren işletim sistemleri, makine öğrenmesi yöntemleri, hata tahmini, bakım yönetimi

*Corresponding Author: hasan.tiryaki@istanbul.edu.tr
Burak ARSLAN, https://orcid.org/0000-0001-8658-2109
Hasan TİRYAKİ, https://orcid.org/0000-0001-9175-0269

1. Introduction

Transportation and social life styles are significantly impacted by technological advancements. Due to improved connectivity and ties between far-flung places, the importance and speed of long-distance passenger and freight transportation is growing every day. Additionally, it has become crucial for logistics and transport to compete on the basis of moving people and goods as swiftly, safely, affordably, and sustainably as feasible. In recent years, rail transit has gained popularity in urban and intercity freight and passenger transportation because to its affordability, safety, and environmental friendliness.

The unexpected breakdowns of numerous pieces of railroad equipment, however, pose the biggest threat to the continuous and secure operation of rail transit. If appropriate action is not taken, these failures result in a loss of time, money, and confidence. To avoid breakdowns from happening in the first place, railway lines must undergo planned maintenance.

As it is known, CBTC are used for the safe use of urban rail systems and the maximum capacity of the railway line. Examining the failures of the aforementioned railway equipment reveals that CBTC radio signal failures have a direct impact on the railway operates [1]. By identifying and fixing the issue without interfering with train movement, continuous operation can be achieved. When a failure has already happened, the time it takes to fix it can be cut in half by learning what caused it, and the operation of the railway can resume normally with the least amount of disruption. Statistical analysis, classification, model-based methods are used in the literature to evaluate data related to failures and make predictions [2-4]. Particularly, for the detection of railway failures used classification methods [2].

Machine learning methods such as artificial neural networks (ANN) are widely used in the solution of many engineering and biomedical engineering problems by classification and prediction [5]. In recent years, a maintenance decision model has been established and successfully implemented in many areas. Grobellar S. and Visser J. K have combined a renewal theory and a decision analysis model to develop a model that predicts the frequency of equipment change [6]. O.F. Eker et al. have used the SVM method for detecting misalignment failures in the actuators connected to the railway switch motors [7]. J. Lee et al. have used sound sensors for the detection of switch motor failures and classified the data with the support vector machines (SVM) and performed a fault prediction study [1]. L.F. Molina et al. have used image processing to detect wear failures on railway tracks [8]. Arslan and Tiryaki have used various artificial intelligence methods for predicting switch point failures [9]. Cinus et al. have used ANN methods for production plan optimization through preventive maintenance management [10]. Amruthnath and Gupta have used vibration data which is collected from an exhoust fan and classified the data with machine learning methods to minimize maintenance costs [11]. Krenek et al. have used ANN methods for early fault detection and predictive maintance suggestions [12]. Sun et al. have used self-organizing map (SOM) For failure prediction and information interaction problems of multi-equipment health management, fault prediction technology of multi-equipment and multi-parameter was proposed based on the system network [13]. Jancikova et al. have used artificial neural networks for prediction of steel atmospheric

corrosion by using various factors such as local temperature, relative humidity, amount of precipitation, pH of rainfall, concentration of main pollutants and exposition time [14].

In this study, in line with the data collected from the trains on a railway line operated with CBTC, the status of the radio signals that enable the wireless communication of the trains with the roadside signaling equipment was evaluated by machine learning methods, and the situations that may have negative effects on the train management of the problems at the signal level were evaluated, without any negative impact on the passenger comfort and the operation yet. A decision support model has been developed that will offer early solution suggestions to system maintainers in order to intervene first. A decision support model was created that can both forecast potential failures and provide details on the underlying causes of failures that have already happened. By ensuring that the data acquired about changes in radio signals is processed and that the maintenance staff is informed of the required corrective and preventive actions, this model seeks to ensure that failures are eliminated before they impair railway operations and that the time it takes to solve existing failures is shortened. In supervised learning, the intended and actual outputs were compared, error calculations were performed, and the process for producing predictions with higher accuracy was looked at. In conclusion, since it is the first study related with failure prediction by using radio signal levels data on railway signaling system, this study presents an important innovation in terms of literature.

In the second section of this study, the materials employed in the system - the radio signals of CBTC - as well as the parameters used as model inputs were initially explained. The model outputs that were produced as a consequence of the interpretations that were formed using these inputs were provided. An explanation was given of the machine learning techniques applied to the data processing. The established model's performance was assessed using specified criteria, which were explained. In the third section, tables containing the outcomes of the data processing using MATLAB Classification Learner Application were displayed, and it was discussed which machine learning techniques produce the best results in comparison. The results were interpreted in the fourth section.

2. Materials and Method

2.1. Communication based train operating systems

According to IEEE 1474.1, CBTC is a continuous and automatic train control system based on high-precision train positioning and high-capacity train-to-track communication [15]. In general, the CBTC system instantly receives information such as rail circuit occupancy, switch position, safe stopping distance, and allowed speed limits of the conventional trackside signaling system via the wireless communication equipment on the train. In line with this information, the train proceeds safely through the automatic train supervision (ATS) system. Likewise, the train sends information such as its instant precise location and speed to the center. Thus, it is ensured that the block processor in the center gives safe movement authorization to each train according to the situation of other trains in the region. Thanks to the block processor, which instantly monitors all trains in the region, the line is operated with maximum frequency and safety. All this communication flow is provided by 2.4 GHz wireless radio signals. In case

of any interruption in this communication, the train that cuts off its communication is stopped by ATS with an emergency brake. Evaluating that there is an unsafe situation, and proceeds with a maximum speed of 25 km/h which is a safe and limited speed, by the driver, until it provides CBTC communication again. All trains in the operating cycle will be affected by this delay and there will be serious disruptions in train operation. In addition, emergency braking of the train will cause wear on the train wheels and rails, thus shortening their useful life. In this direction, it is of great importance that there is no loss in the CBTC signal when evaluated in terms of both passenger comfort, operational continuity and equipment life.

Figure 1 shows the communication structure of CBTC operation with classical signaling systems, traffic management center, line length radios and block processor.

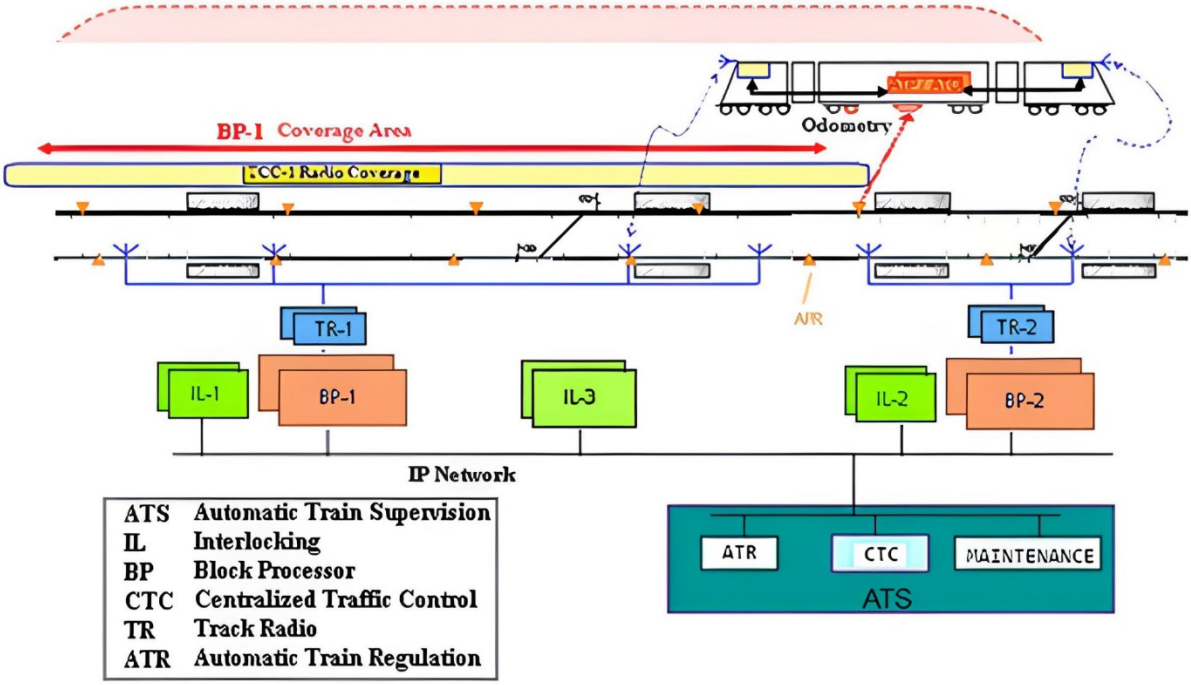

Figure 1. CBTC train communication general concept [15]

As it can be seen from the Figure 1, ATS monitorize the track conditions and train positions continously. Interlocking (IL) tells to BP track conitions (point machine position, next signal status etc), Block processor (BP) gives movement authority to trains accordingly. The communication between ATS, IL, BP and track radios provided by optical fiber and ethernet cables. The communication between trains and track hub radios is provided by wireless radio signals. In this study, the wireless signal values which are received by trains were evaluated.

2.2. Proposed method

In this study, it is aimed to evaluate the instant wireless communication signals during the course of the trains on a railway line operated by CBTC, to detect possible problems at the signal level and to determine solutions. It is aimed to eliminate these negativities in signal levels by warning the system maintainers before they reach the level that will affect the train operation.

In this context, the signal levels received by the trains from the radios along the line during the journey were interpreted with the industry experience and system requirements, and the problems were determined and solution suggestions were put forward. Considering the technical features of the system in which the study is carried out, the ideal working conditions are that the train receives a signal higher than -85db from at least one trackside radio and the packet loss rate is less than 1%. According to these conditions, the signals received instantly were evaluated and 6 different results/ recommendations in Table 1 were presented.

Table 1. Maintenance recommendations provided as system output

Recommendations	Maintenance Proposal
R1	Signal Level normal Level normal
R2	Low Packet Loss, F/O and LAN connections should be checked
R3	High Packet Loss, F/O and LAN connections should be checked
R4	Signal level is low, radio and antenna should be checked
R5	Zone without CBTC Signal
R6	Signals are received from more than one radio at the same level, radio output powers should be checked

Based on the results of this study, the Artificial Neural Networks structure, which was decided as the best method for all outputs, is explained in detail in below.

Artificial neural networks (ANNs) are the systems that can learn from samples by simulating the human brain's nerves, and then use that knowledge to make judgements about samples they have never seen [16]. The engineering equivalent of a biological neuron is an artificial neuron [17]. Inputs, weights, addition, activation, and output are the five elements that make up an ANN [18]. The artificial neuron is depicted in Figure 2.

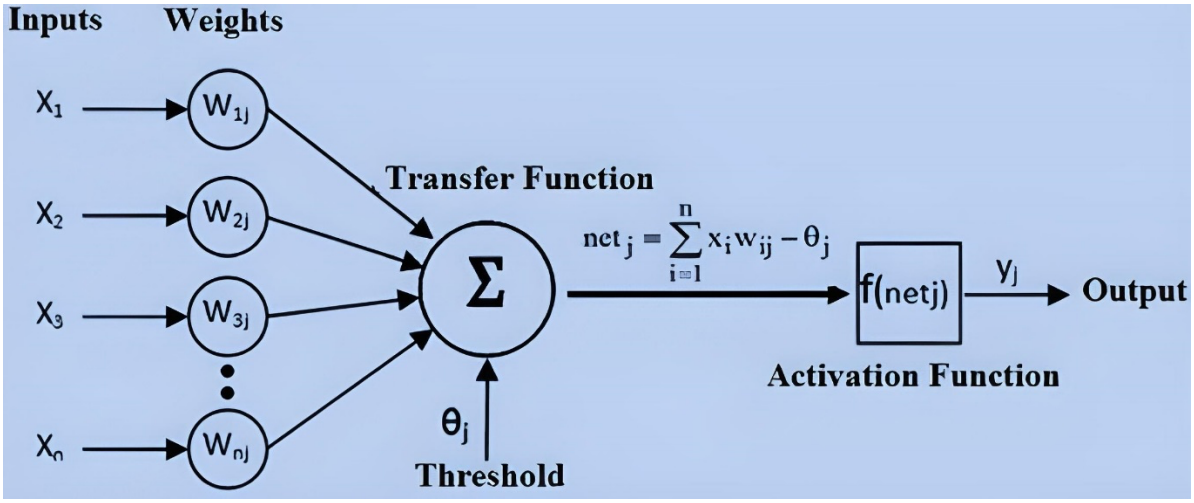

Figure 2. Artificial neuron [9]

The network incorporates the data from the input layer. These inputs are handled in the middle layers before being sent to the top layer. Each input is converted to an output using the network weight values in the intermediary layers. To get the right outputs, weight values must also be computed accurately. By correctly training the network, the correct weights can be found. At first, these weight values are assigned at random. The weights are then modified in accordance with the network's learning rule during training, when each sample is submitted to the network [19]. The network is then given a new sample, the weights are changed once more, and the best weight values are sought for. Until the right results are produced for each sample in the training set, these actions are repeated. The test set samples are presented to the network once all weights have been determined. The network is considered to have been effectively trained if it responds correctly to the test set samples [9].

$$V = \sum_{i=0}^{i=n} W_i x X_i \tag{1}$$

$$y = \varphi(V) \tag{2}$$

Here; W shows the weights matrix of the cell, X shows the input vector of the cell, V shows the net input of the cell, y shows the output of the cell and φ shows the activation function of the cell.

3. Results and Discussion

First of all, with the training data of the radio signals of CBTC training was carried out using 29 machine learning methods and the most successful method was determined.

3.1. Training and validation

During the training phase, 29 machine learning methods Decision Trees (Coarse Tree, Medium Tree, Fine Tree), Discriminant Analysis (Linear Discriminant), Naive Bayes (Kernel Naive Bayes), Support Vector Machines (Linear SVM, Quadratic SVM, Cubic SVM, Fine Gaussian SVM, Medium Gaussian SVM, Coarse Gaussian SVM), Nearest Neighbor (Fine KNN, Medium KNN, Coarse KNN, Cosine KNN, Cubic KNN, Weighted KNN), Kernel Approximation (SVM Kernel, Logistic Regression Kernel), Ensembles (Boosted Trees, Bagged Trees, Subspace Discriminant, Subspace KNN, RUSBoost Trees) and Neural Networks (Narrow Neural Network, Medium Neural Network, Wide Neural Network, Bilayered Neural Network, Trilayered Neural Network) in the MATLAB R2022a Classification Learner application were used for 502 training data and the most successful method was determined.

In order to make an objective evaluation, all 502 training data were applied and compared with 10-k fold cross validation for the different machine learning methods mentioned above. In order for the match to be carried out in a healthy way, the Correlation Coefficient (R^2), Root Mean Square Error (RMSE) and Mean Absolute Error (MAE) values were calculated as performance criteria. The formulae of these criteria are given below.

$$R^2 = 1 - \frac{\sum_{l=1}^{n}(y_i - \hat{y}_l)^2}{\sum_{l=1}^{n}\left(y_i - \widehat{y_{avg}}\right)^2} \quad (3)$$

$$RMSE = \sqrt{\frac{1}{n}\sum_{i=1}^{n}(y_i - \hat{y}_l)^2} \quad (4)$$

$$MAE = \frac{1}{n}\sum_{i=1}^{n}|(y_i - \hat{y}_l)| \quad (5)$$

Here, y_i, $\hat{y}_l$, and $\widehat{y_{avg}}$ are the desired output *i*, the predicted output, and the average of the desired output, respectively. *n* represents each sample in the dataset [20, 21].

In Table 2, the training results of the most successful of the method families applied for the machine learning model are presented comparatively.

Table 2. Training results

Classification Methods Families	R^2 (Squared Correlation coefficient)	RMSE (Root Mean Squared Error)	MAE (Mean Absolute Error)
Neural Networks (Bilayered Neural Network)	0.972	0.0333	0.0238
Nearest Neighbor	0.960	0.0713	0.0437
Decision Trees	0.960	0.0738	0.0449
Support Vector Machines	0.958	0.0899	0.0644
Ensembles	0.954	0.1203	0.0795
Naive Bayes	0.916	0.1293	0.0879
Discriminant Analysis	0.871	0.1331	0.1008
Kernel Approximation	0.867	0.2308	0.1588

As can be seen in Table 2, the most successful machine learning method is the Bilayered Neural Network method for training. For this method, the actual training data and the prediction data obtained as a result of the training are presented in Figure 3 comparatively.

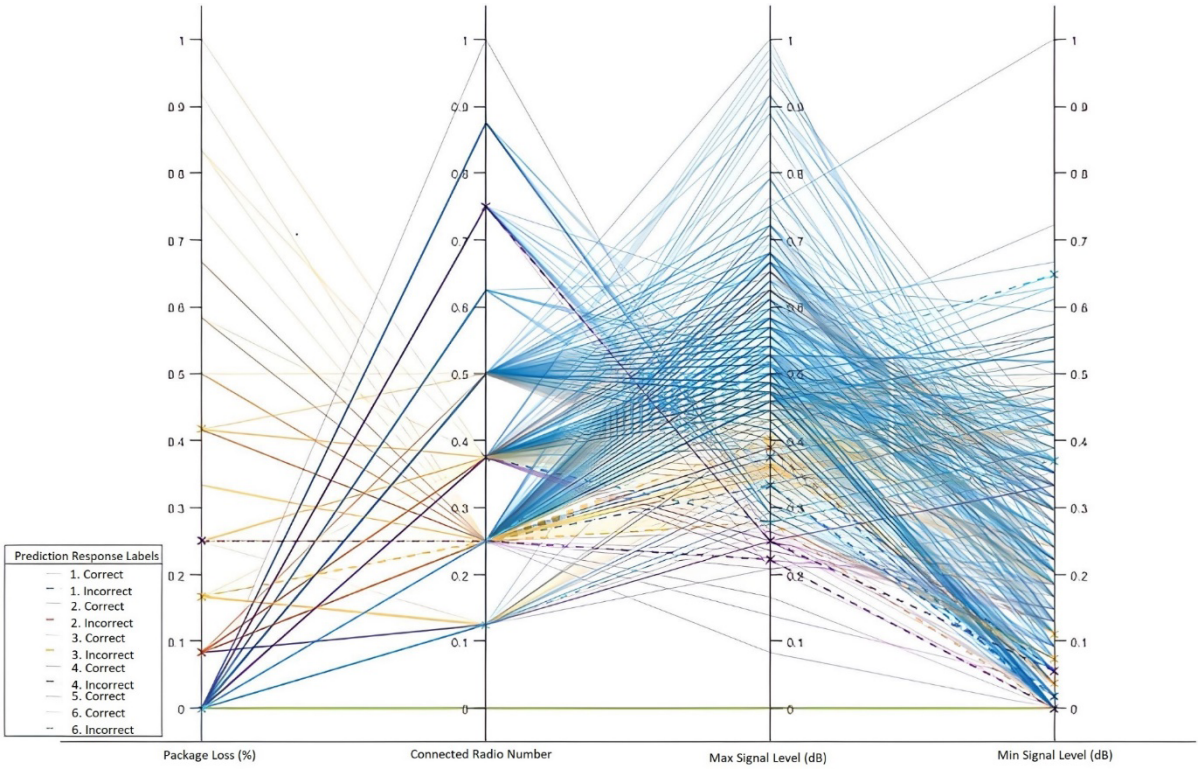

Figure 3. Real and predicted training data

As seen in Figure 3, the prediction data obtained as a result of the training is very close to the real training data. This situation demonstrates that the established decision support model is successful. Figure 4 shows the confusion matrix of validation for the Bilayered Neural Network method.

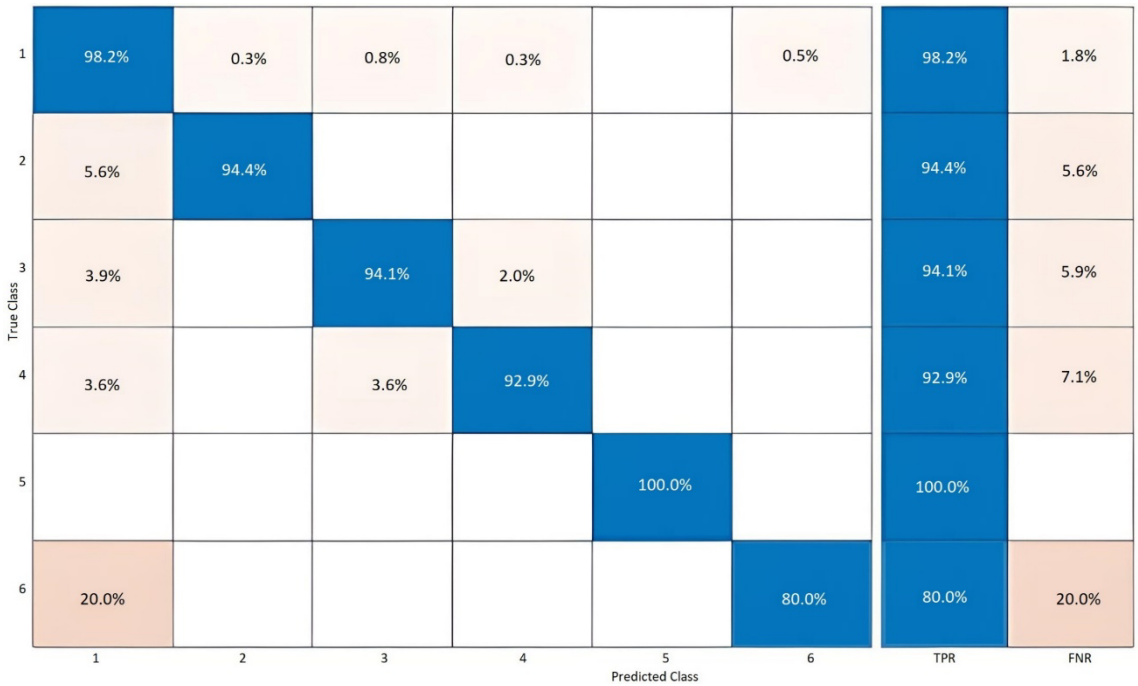

Figure 4. Confusion matrix of validation

As can be seen in Figure 4, True Positive Rates (TPR) higher than False Negative Rates (FNR). This situation shows that the Bilayered Neural Network method is successful for the CBTC system. Figure 5 shows the ROC curve of validation for the Bilayered Neural Network method.

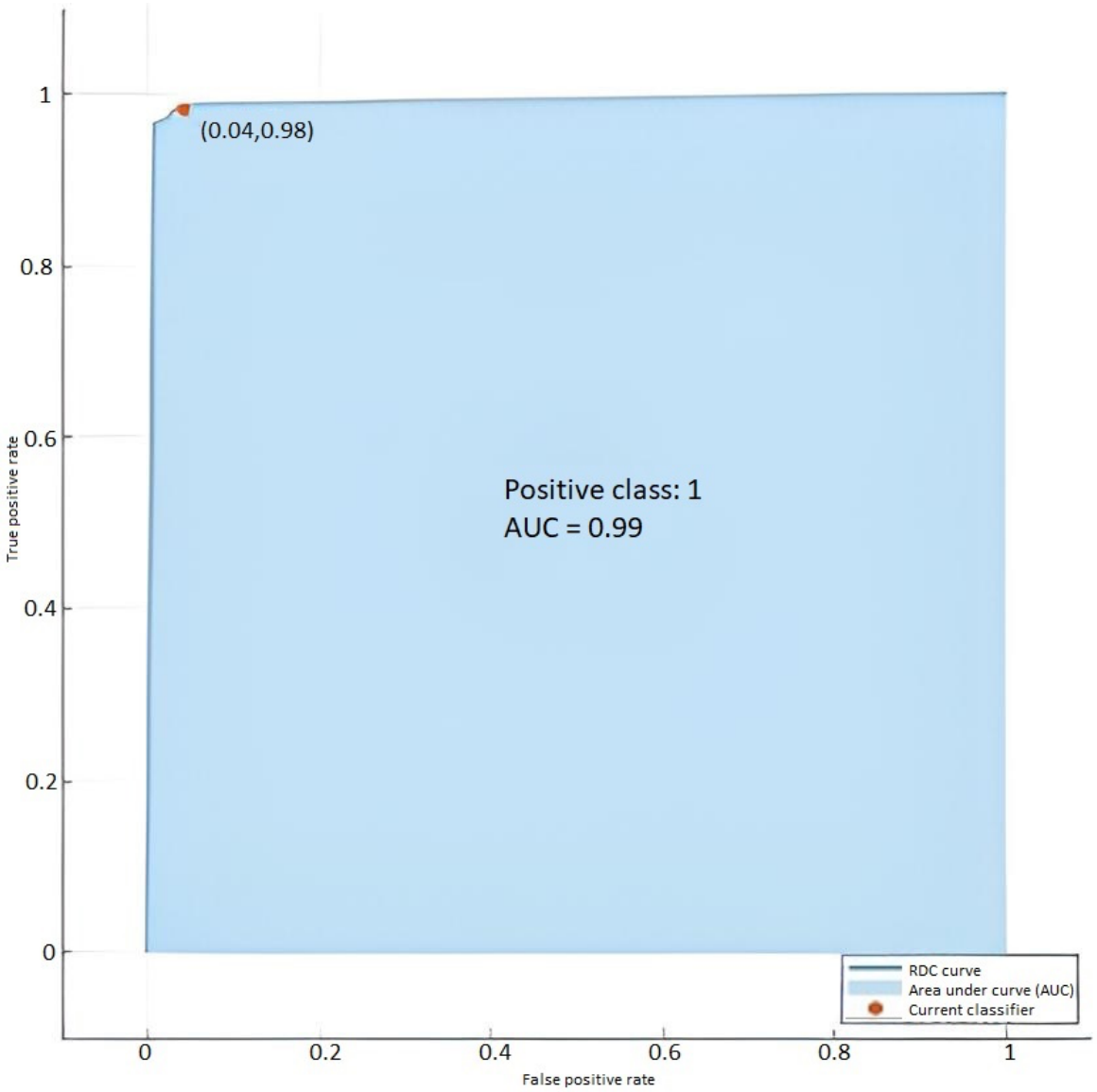

Figure 5. ROC curve of validation

As can be seen in Figure 5, area under curve (AUC) is very close to the 1. As known, this value is expected to be 1 is the most perfect result. Since the value obtained from the Bilayered Neural Network method used for the CBTC system is 0.99, it is quite successful.

3.2. Test

During the test phase, 29 machine learning methods mentioned training phase in the MATLAB R2022a Classification Learner application were used for 101 test data and the most successful method was determined. The Multi Layer Perceptron method, which is the equivalent of the Artificial Neural Networks method in WEKA 3.8.5 program, which was decided as the best method for all outputs based on the training results in the MATLAB R2022A Classification

Learner application, was used for show the artificial neural network architecture. Figure 6 show artificial neural network architecture for CBTC data.

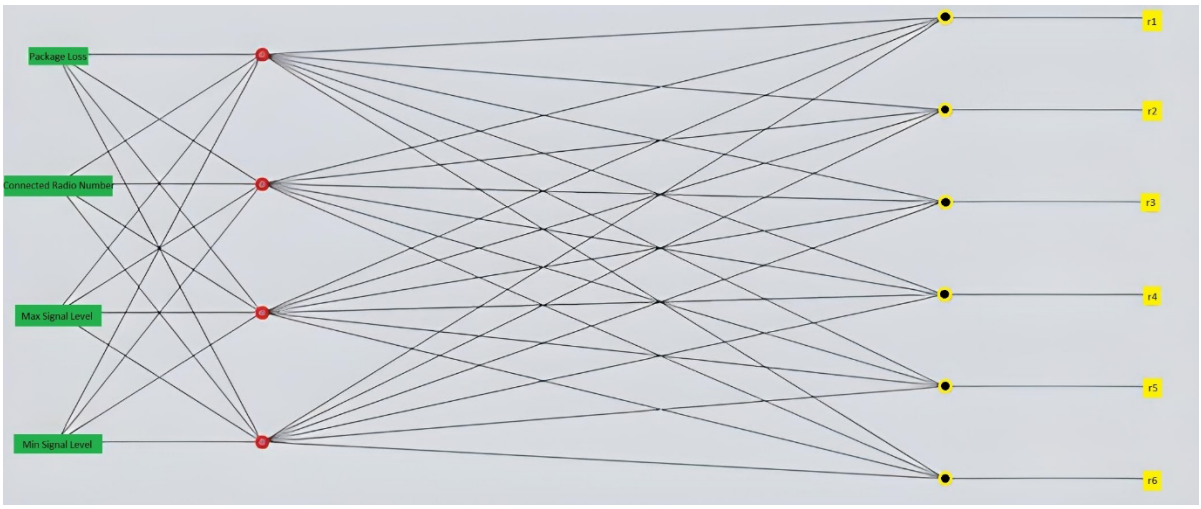

Figure 6. Neural network architecture for CBTC data

In this architecture, 4 neurons in a single hidden layer are used for inputs and 6 (for each recommendations) neuron is used for outputs. In Table 3, the test results of the most successful of the method families applied for the machine learning model are presented comparatively.

Table 3. Test results

Classification Methods Families	R^2 (Squared Correlation coefficient)	RMSE (Root Mean Squared Error)	MAE (Mean Absolute Error)
Neural Networks (Bilayered Neural Network)	0.980	0.0232	0.0137
Ensembles	0.970	0.0612	0.0336
Nearest Neighbor	0.950	0.0637	0.0348
Support Vector Machines	0.941	0.0798	0.0543
Decision Trees	0.931	0.1102	0.0694
Kernel Approximation	0.861	0.1192	0.0778
Naive Bayes	0.842	0.1230	0.0907
Discriminant Analysis	0.792	0.1307	0.1487

As can be seen in Table 3, the most successful machine learning method is the Bilayered Neural Network method for test. Figure 7 shows the confusion matrix of test for this method.

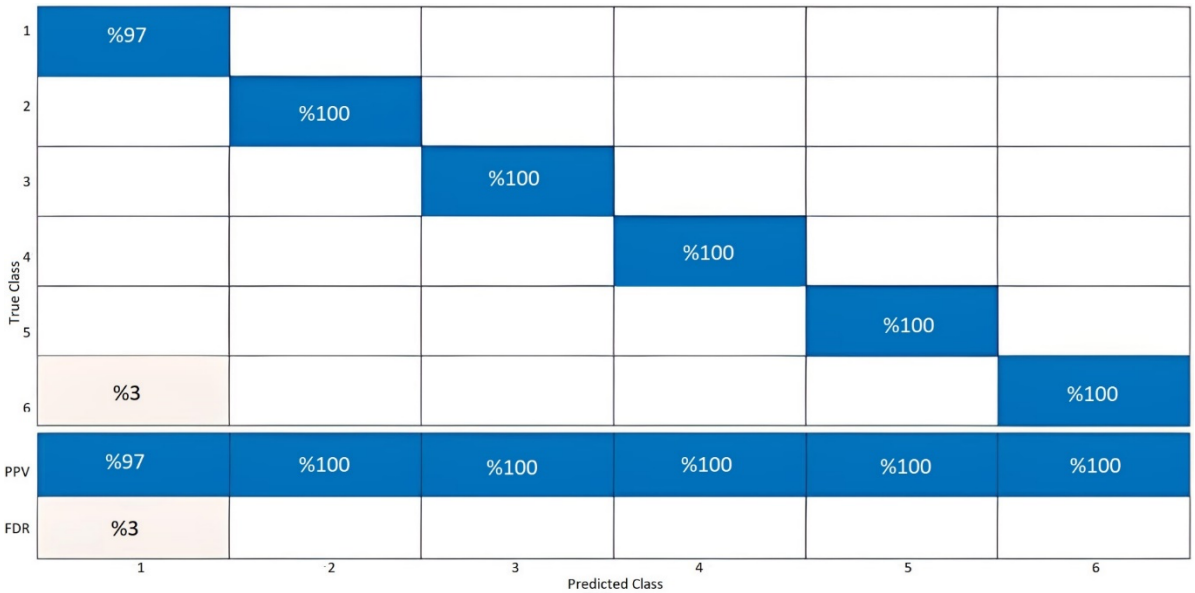

Figure 7. Confusion matrix of test

As can be seen in Figure 7, Positive Predictive Values (PPV) higher than False Discovery Rates (FDR). This situation shows that the Bilayered Neural Network method is successful for the CBTC system. Figure 8 shows the ROC curve of validation for the Bilayered Neural Network method.

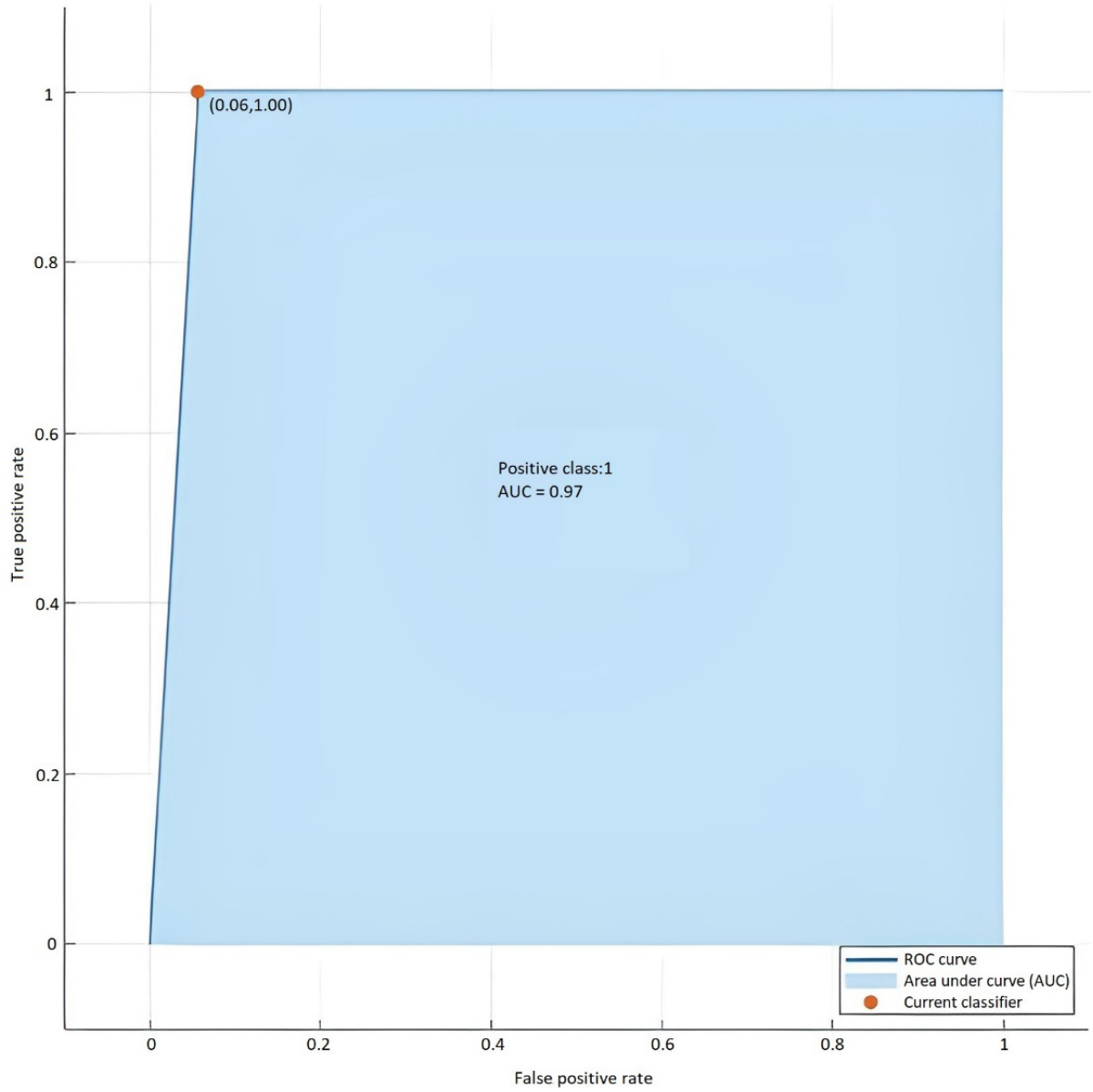

Figure 8. ROC curve of test

As can be seen in Figure 8, area under curve (AUC) is very close to the 1. As previously stated, this value is expected to be 1 is the most perfect result. Since the value obtained from the Bilayered Neural Network method used for the CBTC system is 0.97, it is quite successful.

4. Conclusion

This study aims to contribute to the planned maintenance operations on trains by using machine learning techniques to address radio signal failures of CBTC. Classification and failure prediction studies were conducted and the findings evaluated using the model that was built to expedite the process of resolving radio signal problems and to fix the faults before they grew big enough to affect operation.

Using MATLAB software, the data set was processed using different machine learning methods, and the outcomes were assessed. The assessments showed that the outcomes of the cross-validation model performance were quite similar to the conclusions drawn from the

training and testing phases. These findings indicate that, as a result of the significantly optimal computation of the R-Squared, RMSE, and MAE values, the employment of artificial neural networks will be more effective in the implementation of the failure prediction model developed.

High success rates for machine learning methods demonstrate that the model was developed using relevant industry knowledge and the right strategy. Due to the established model's success, even if the system's inputs vary, the system will still accurately predict failures and decide its outputs.

In this approach, radio signal failures will be prevented, unscheduled train stops will be avoided, the resolution procedure for problems will be sped up, and the continuity of railway traffic will be guaranteed. Similar apps that help scheduled maintenance would enable high-level railway maintenance management, preventing the loss of time, money, energy, and manpower.

The aforementioned study will be expanded upon in the future to produce interface software that may be actively utilized in preventative maintenance operations and function as a failure operator decision support model.

Ethics in Publishing

There are no ethical issues regarding the publication of this study

Author Contributions

ARSLAN, B.: conceived and designed the study, scanned the literature, collected the material, determined and interpreted the results.

TIRYAKİ, H.: organized the study, implemented the method and wrote the study, analyzed and interpreted the study, evaluated and interpreted the results.

References

[1] Lee, J., *et al.*, (2016), “Fault detection and diagnosis of railway point machines by sound analysis”, *Sensors*, vol. 16, no. 4, pp. 549-561. doi: 10.3390/s16040549

[2] Vileniskis, M., Remenyte Prescott, R., Rama, D., (2015), “A fault detection method for railway point systems”, *Proceedings of IMechE Part F: J Rail and Rapid Transit* vol. 230, no. 3, pp. 852-865. doi: 10.1177/0954409714567487

[3] Arakani, H., *et al.*, (2012), “PHM for railway system- a case study on health assessment of the point machines”, in *IEEE Conference on Prognostics and Health Management (PHM)*, Denver CO, USA, pp. 1-5.

[4] Bemment, S.D., Goodall, R.M., Dixon, R., Ward, C.P., (2017), "Improving the reliability and availability of railway track switching by analysing historical failure data and introducing functionally redundant subsystems", *Proceedings of IMechE Part F: J Rail and Rapid Transit*, vol. 232, no. 5, pp. 1407-1424. doi: 10.1177/0954409717727879

[5] Vapnik, V., Izmailov, R., (2017), "Knowledge transfer in SVM and neural networks", *Annals of Mathematics and Artificial Intelligence*, vol. 81, no. 2017, pp. 3-19. doi: 10.1007/s10472-017-9538-x

[6] Grobbelaar, S., Visser, J.K., (2015), "Determining the cost of predictive component replacement in order to assist with maintenance decision-making", *South African Journal of Industrial Engineering*, vol. 26, no. 1, pp. 150-162. doi: 10.7166/26-1-713

[7] Eker, O.F., Camci, F., Kumar, U., (2012), "SVM based diagnostics on railway turnouts", *International Journal of Performability Engineering*, vol. 8, no. 3, pp. 289-298. doi: 10.23940/ijpe.12.3.p289.mag

[8] Molina, L., *et al.*, (2011), "Condition monitoring of railway turnouts and other track components using machine vision", in *Transportation Research Board 90th Annual Meeting,* Washington DC, USA, pp. 1-17.

[9] Arslan, B., Tiryaki, H., (2020), "Prediction of railway switch point failures by artificial intelligence methods", *Turkish Journal of Electrical Engineering and Computer Science*, vol. 28, no. 2, pp. 1044-1058. doi: 10.3906/elk-1906-66

[10] Cinus, M., Confalonieri, M., Barni, A., Valente, A., (2016), "An ANN based decision support system fostering production plan optimization through preventive maintenance management", in *Advances in neural networks*, Springer, Cham.

[11] Amruthnath, N., Gupta, T., (2018), "A research study on unsupervised machine learning algorithms for early fault detection in predictive maintenance", in *5th International Conference on Industrial Engineering and Applications (ICIEA),* Singapore, pp. 355-361.

[12] Krenek, J., Kuca, K., Blazek, P., Krejcar, O., Jun, D., (2016), "Application of artificial neural networks in condition based predictive maintenance", in *Recent developments in intelligent information and database systems. Studies in computational intelligence*, Springer, Cham.

[13] Sun, F., Gao, L., Zou, J., Wu, T., Li, J., (2013), "Study on multi-equipment failure prediction based on system network", *Sensors & Transducers*, vol. 158, no. 11, pp. 427-435.

[14] Jančíková, Z., Zimný, O., Koštial, P., (2013), "Prediction of metal corrosion by neural networks", *Metalurgija*, vol. 52, no. 3, pp. 379-381.

[15] Xu, J.K., Chen, L.J., Gao, W.M., Zhao, M.J., (2015), "CBTC simulation platform design and study", *Journal of Computer and Communications*, vol. 3, no. 2015, pp. 61-67. doi: 10.4236/jcc.2015.39007

[16] Oztemel, E., (2012), *Artificial neural networks*, Papatya Publishing, Türkiye.

[17] Sharma, V., Rai, S., Dev, A., (2012), "A comprehensive study of artificial neural networks", *International Journal of Advanced Research in Computer Science and Software Search*, vol. 2, no. 10, pp. 278-284. doi: 10.1.1.468.9353

[18] Cuhadar, M., (2006), "Use of artificial neural networks for demand forecasting in tourism sector and comparative analysis with other methods", Ph.D. dissertation, Social Sciences Institute, Suleyman Demirel Univ., Isparta, Türkiye.

[19] Maind, S.B., Wankar, P., (2014), "Research paper on basic of artificial neural network", *International Journal on Recent and Innovation Trends in Computing and Communication*, vol. 2, no. 1, pp. 96-100.

[20] Akcay, M.T., Akgundogdu, A., Tiryaki, H., (2021), "Estimation of the average speed for a railway signaling system by using gaussian process regression methods with bayesian optimization", *Railway Engineering*, no. 14, pp. 274-286. doi: 10.47072/demiryolu.942730

[21] Akcay, M.T., Akgundogdu, A., Tiryaki, H., (2022), "Prediction of travel time for railway traffic management by using the adaboost algorithm," *Journal of Balikesir University Institute of Natural and Applied Sciences*, vol. 24, no. 1, pp. 300-312. doi: 10.25092/baunfbed.937333

Erzincan Üniversitesi
Fen Bilimleri Enstitüsü Dergisi
2024, 17(1), 16-36
ISSN: 1307-9085, e-ISSN: 2149-4584
Araştırma Makalesi

Erzincan University
Journal of Science and Technology
2024, 17(1), 16-36
DOI: 10.18185/erzifbed.1229541
Research Article

Risk Prioritization in A Manufacturing Project with Fuzzy SWARA and Fuzzy MOORA Methods

Tülay KORKUSUZ POLAT[1]*, Gülsüm SALTAN YAŞLI[2]

[1]Sakarya Üniversitesi, Mühendislik Fakültesi, Endüstri Mühendisliği Bölümü

[2]Sakarya Üniversitesi, Fen Bilimleri Enstitüsü

Received: 04/01/2023, **Revised:** 01/11/2023, **Accepted:** 01/11/2023, **Published:** 28/03/2024

Abstract

Businesses must constantly change and develop to keep up with customer needs and changes in the market. Being unable to adapt to change or being unprepared can bring risks. These changes and risks can affect both the process and the outputs of the process. It is essential to be prepared for the possible risks experienced in the operations, especially in project-based, production-to-order enterprises, to meet the customer's demands and to comply with the delivery date. Businesses must implement an effective risk assessment process to achieve this. This study implemented a risk prioritization for a new business project that produces energy storage systems by having to order. Changes must be made in the production process for an additional feature to be added to the product per the customer's request. The risks posed by the change and the short deadline were analyzed and prioritized. A new model was developed by developing the classical Decision Matrix Risk Assessment (DMRA) method, one of the risk assessment methods to evaluate the ten identified risks. The "severity" component of the classical DMRA method is divided into three sub-components (the severity of delivery time, the severity of cost, and the severity of quality) to be evaluated more specifically. Moreover, since the weights of these sub-components on the risks are different, the components are weighted with the Fuzzy SWARA method. The weights obtained from the Fuzzy SWARA method are used in the Fuzzy MOORA method, and the risks are prioritized. Thus, the effectiveness of the classical risk assessment approach has increased by detailing the "severity" component of the risk assessment components and weighting and prioritizing the components using multi-criteria decision-making (MCDM) techniques. With the fuzzy SWARA method, the weights of the risk components (severity of delivery time (C_1), severity of cost (C_2), severity of quality (C_3) and likelihood (C_4)) to be used in risk assessment were determined. BNP (best non-fuzzy performance) values for risks were calculated according to C_1, C_2, C_3 and C_4 values with the fuzzy MOORA method. As a result of the study, the most priority risk was determined as the risk of going to the customer with the QR code written in incorrect or non-desired quality of the product (Risk 8).

Keywords: Risk Analysis, Risk Prioritization, Matrix Risk Assessment Method, Fuzzy SWARA, Fuzzy MOORA

Bir Üretim Projesinde Bulanık SWARA ve Bulanık MOORA Yöntemleri ile Risk Önceliklendirme

Öz

İşletmeler müşteri ihtiyaçları ve pazardaki değişime ayak uydurabilmek için sürekli değişmek ve gelişmek zorundadırlar. Değişime uyum sağlayamamak veya yeterince hazır olamamak beraberinde riskleri getirebilmektedir. Bu değişiklikler ve riskler hem süreci hem de sürecin çıktılarını etkileyebilmektedir. Özellikle proje bazlı, siparişe göre üretim yapan işletmelerde süreçlerde yaşanabilecek olası risklere hazırlıklı olmak müşterinin isteklerini karşılayabilmek ve teslim tarihine uyabilmek için oldukça önemlidir. Bunu sağlayabilmek için de etkili bir risk değerlendirme sürecinin uygulanması gerekmektedir. Bu çalışmada siparişe göre üretim yaparak enerji depolama sistemleri üreten bir işletmenin yeni bir projesi için risk önceliklendirmesi çalışması yapılmıştır. Müşterinin talebi doğrultusunda ürüne eklenecek ek bir özellik için üretim sürecinde değişiklik yapılması gerekmektedir. Değişikliğin ve termin süresinin kısa olmasının getireceği riskler analiz edilerek önceliklendirilmiştir. Belirlenen on adet riskin değerlendirilmesi için risk değerlendirme yöntemlerinden klasik karar matrisi risk değerlendirme yöntemi geliştirilerek yeni bir model geliştirilmiştir. Klasik karar matrisi risk değerlendirme yönteminin "etki" bileşeni daha spesifik halde değerlendirilebilmek için üç alt bileşene ayrılmıştır (teslim süresine etki, maliyete etki ve kaliteye etki). Ve bu alt bileşenlerin riskler üzerindeki ağırlıkları farklı olduğu için çok kriterli karar verme tekniklerinden Bulanık SWARA yöntemi ile bileşenler ağırlıklandırılmıştır. Bulanık SWARA yönteminden elde edilen ağırlıklar, çok kriterli karar verme tekniklerinden Bulanık MOORA yönteminde kullanılarak riskler önceliklendirilmiştir. Böylece hem risk değerlendirme bileşenlerinden "etki" bileşeninin detaylandırılması hem de çok kriterli karar verme teknikleri kullanılarak bileşenlerin ağırlıklandırılması ve önceliklendirilmesi ile klasik risk değerlendirme yaklaşımının etkinliği arttırılmıştır. Bulanık SWARA yöntemi ile risk değerlendirmesinde kullanılacak risk bileşenlerinin ağırlıkları (teslim süresinin etkisi (C_1), maliyetin etkisi (C_2), kalitenin etkisi (C_3) ve olasılık (C_4)) belirlenmiştir. Risk bileşenlerinin ağırlıkları kullanılarak risklere ilişkin öncelik durumlarını gösteren BNP (Best non-fuzzy performance-bulanık olmayan en iyi performans) değerleri Bulanık MOORA yöntemi ile hesaplanmıştır. Çalışma sonucunda en öncelikli riskin, ürünün yanlış veya istenmeyen kalitede yazılmış QR kod ile müşteriye gitme riski olduğu ortaya çıkmıştır (Risk 8).

Anahtar Kelimeler: Risk Analizi, Risk Önceliklendirme, Matris Risk Değerlendirme Yöntemi, Bulanık SWARA, Bulanık MOORA

1. Introduction

In businesses where the general structure of the product is known and the details are shaped according to customer requests, production is made according to the order. Customer satisfaction is critical in ensuring the continuity of sales and production in businesses that make order production [1]. One of the essential criteria for ensuring customer satisfaction is the timely delivery of products. In make-to-order production, each new order is considered a new project. Production and process planning is done according to the customer order, the workloads to be undertaken by the machines are determined, and the production line is rearranged if necessary. Effective project management must know the risks that will delay production, reduce customer satisfaction, and take precautions accordingly. Risk management is very effective in the project's success, especially for new projects requiring changes in production processes. Risk management determines, analyzes, and evaluates risks and takes necessary precautions before they occur.

*Corresponding Author: korkusuz@sakarya.edu.tr
Tülay KORKUSUZ POLAT, https://orcid.org/0000-0001-6693-7873
Gülsüm SALTAN YAŞLI, https://orcid.org/0000-0001-6412-5951

Risks are uncertain events that can affect the time-cost-performance objectives of the relevant process/department/project [2]. Businesses must protect themselves against risks that may have consequences such as financial difficulties, failure to meet customer deadlines, loss of image, production disruptions, and loss of critical personnel. Businesses manage risk by helping decision-making processes and providing a sustainable competitive advantage [3]. Risks that are unknown and necessary precautions are not taken can deviate projects from their targets. Therefore, effective risk management is essential for successful projects [4].

Especially in engineering and manufacturing processes, it is possible to encounter risks due to the diversity and complexity of machines and techniques, the frequency of unexpected and uncertain events, and the intense human factor. There are many techniques used to prevent failures/delays/accidents from occurring or reoccurring by assessing the risks: Such as the DMRA (Decision Matrix Risk Analysis) Method, HAZOP (Hazard and Operability), Fine-Kinney, FMEA (Fault Mode and Effects Analysis) [5]. MCDM techniques and fuzzy set theory are generally used in integration with risk assessment techniques to manage risks more effectively by increasing the applicability and effectiveness of the techniques. The function of the MCDM methods used is usually to prioritize risks. The risk prioritization activity can be considered an MCDM problem in which many criteria must be evaluated.

In the literature, there are studies in which MCDM techniques are used in risk assessment and prioritization. Tomak and Korkusuz Polat [6] used the AHP (Analytical Hierarchy Process) technique to determine the criterion weights in their models developed for success factor-triggered risk prioritization. Becker et al. [7] used the TOPSIS (Technique for Order Preference by Similarity to Ideal Solution) method to rank the micropollutants they identified by conducting a risk assessment. Bid and Siddique [8] used TOPSIS and WASPAS (Weighted Aggregated Sum Product Assessment) techniques, which are MCDM techniques, to prioritize the risks posed by dams on humans. Jena et al. [9] used AHP and VIKOR (VIseKriterijumska Optimizacija I Kompromisno Resenjemethods) to assess the risks that increase vulnerability to earthquakes in urban areas. Senthill et al. [10] conducted a study in which they integrated TOPSIS, PROMETHEE (Preference Ranking Organization METHOD for Enrichment Evaluations), and AHP methods to prioritize the risks that may arise in reverse logistics activities. Sivageerthi et al. [11] used the SWARA (Stepwise Weight Assessment Ratio Analysis) method to prioritize risks in the coal supply chain.

Risks contain uncertainty due to their structural characteristics. There are studies in which the Fuzzy Logic approach, which has the feature of processing uncertain information, is used to increase the effectiveness of risk assessment techniques. Tian et al. [12] developed a new model for the oil industry, in which experts added their risk attitudes to the assessment as fuzzy while assessing risks. Korkusuz Polat [13] used fuzzy logic approach while prioritizing the risks in the textile factory. Moreno-Cabezali and Fernandez-Crehuet [14] applied a fuzzy logic-based model to evaluate risks in R&D projects developed for additive manufacturing. Lin et al. [15] used fuzzy set theory and machine learning techniques to assess the risks in the construction excavation system.

There are also studies in which MCDM techniques are used together with the Fuzzy Logic approach to eliminate the disadvantages of evaluating uncertain information. Yazdani et al. [16] developed a model that integrated Triangular Fuzzy Hesitant Sets, FMEA, and Combined Compromise Solution methods to assess outsourcing risks. Xu et al. [17] identified the risk factors that threaten the reliability of integrated energy systems. They developed a new model to evaluate the risks with integrated HFS (Hesitant Fuzzy Sets), DEMATEL (Decision Making Trial and Evaluation Laboratory), and CPT (Cumulative Prospect Theory). In their study, Shannazi and Alimohammadlou [18] determined the risks in renewable energy sources and prioritized them using MCDM techniques based on type-2 fuzzy sets. Singer and Över Özçelik [19] used Fuzzy AHP, Fuzzy EDAS (Evaluation based on Distance from Average Solution), and Fuzzy FMEA methods in an integrated way to evaluate the risks in metallic biomaterials. Gölcük et al. [20] proposed a new model by combining the whole consistency method and graph theory matrix approach in a fuzzy environment to overcome the disadvantages of the classical FMEA risk assessment method in prioritizing occupational health and safety risks. Ali et al. [21] used the Fuzzy VIKOR method to evaluate the risks that may occur in the China-Pakistan Fiber Optic Project. Jokar et al. [22] evaluated and prioritized the risks in highway projects carried out with public-private cooperation in Iran with Fuzzy AHP and Fuzzy TOPSIS. Severi et al. [23] developed the classical HAZOP risk assessment technique with MCDM. Researchers combined Fuzzy AHP and Fuzzy TOPSIS, which are MCDM techniques, with classical HAZOP and proposed the Fuzzy Multi-Attribute HAZOP technique, in which the weight risk factors and rank risks. Yücenur and Şenol [24] used SWARA and Fuzzy VIKOR methods to determine the most appropriate lean technique to eliminate waste in construction processes. Dehshiri [25] used Fuzzy SWARA and Fuzzy WASPAS (Weighted Aggregated Sum Product Assessment) methods in an integrated way to prioritize risks in offshore wind farms. Arabsheybani and Khasmeh [26] developed a mathematical model for the coordinated operation of production planning-supplier selection-order-distribution activities for a food factory in Iran. Researchers wanted to determine resilience factors to reveal risks and uncertainties, and they used Fuzzy AHP and Fuzzy MOORA (Multi-Objective Optimization based on Ratio Analysis) methods for this. Arabsheybani et al. [27] used FMEA supported by the Fuzzy MOORA method to evaluate supplier performance.

Although there are frequent risk assessment and prioritization studies in the literature in which MCDM techniques are integrated with the fuzzy logic approach, there are very few applications where the "severity" component used in risk assessment is detailed. In this study, the risks that may occur in the new project of an enterprise producing energy storage systems are predetermined and evaluated, and the risks that may arise are prioritized by using MCDM techniques. In the study, first of all, the risks that may occur were determined by taking support from the past experiences of the experts in the business. While evaluating risks, a new risk assessment model has been developed since the meaning of the "severity" component of the classical DMRA method on risks may differ. In the new model, the "severity" component is evaluated as three different sub-components: "severity on delivery time," "severity on cost," and "severity on quality." The new model differs from the classical DMRA method in the literature because it provides a more detailed analysis of the "severity" component. In addition, the weight of the three different "severity sub-components" on the risks is also additional.

Considering this situation, in the third stage of the study: "severity sub-components" in the proposed new model and the "likelihood" component, which is the other component of the classical DMRA model, were weighted using the Fuzzy SWARA method, which is one of the MCDM techniques. In the fourth stage of the study: The risks were prioritized with the Fuzzy MOORA method using the weights obtained from the Fuzzy SWARA method. Finally, risk strategies were determined for priority risks. The contribution of this article is threefold: firstly, it is to fill the deficiency of the classical DMRA method in assessing the severity of risks in different areas. Secondly, since the weight of the newly determined sub-components of the "severity" component on the risks was not equal, the "severity sub-components" were weighted in this study. Third, in the risk prioritization applications in the literature, there has yet to be an application in which Fuzzy SWARA and Fuzzy MOORA methods are integrated. This study is expected to contribute to the literature in this respect significantly. In the second part of the study, Decision Matrix Risk Assessment, Fuzzy Logic, Fuzzy SWARA and Fuzzy MOORA methods are explained respectively. In the third section, the risk assessment practice carried out in a company that produces energy storage systems is explained. In practice, the Fuzzy SWARA method was used when determining the weights of risk criteria, and the Fuzzy MOORA method was used when prioritizing risks. In the last section, Conclusion, it is given in detail which risk emerged as a priority as a result of the application.

2. Material and Methods

The methodological approach of the study is presented in this section. First, the DMRA method, a classical risk assessment approach, is included. Then, Fuzzy SWARA and Fuzzy MOORA methods are explained by defining the essential functions of Fuzzy Logic.

2.1. Decision Matrix Risk Assessment Method

Activities in all processes of a manufacturing or service business may involve risk. So, it is necessary to risk assessment in all companies, especially in new and critical processes. The DMRA (Decision Matrix Risk Assessment Method - Also known as the Risk Matrix method), developed in the 1990s, can be analyzed in which the probability of occurrence of risks and their after-effects are used to assess risks [28].

DMRA is a very convenient and frequently encountered method in practical applications to evaluate and prioritize risks according to the determined risk sizes while considering possible hazards. The Risk Matrix is commonly used to assist in setting priorities and assigning resources and is recommended by national/international standards [29].

There are two components in the risk matrix method (severity and likelihood), and the combination of the "severity" and "likelihood" values (Equation (1)) gives the size of the risk [30-31].

$$Risk\ Size\ (RS) = Severity\ (S)\ x\ Likelihood\ (L) \quad (1)$$

In the DMRA method, the expected risks are determined first. The likelihood of occurrence for the identified risks and the severity of the exposed person/process/department, if the risk occurs,

is determined. Relevant experts and old records should be used to determine the risks' likelihood and severity [6].

2.2. Fuzzy Logic

Fuzzy Logic is an approach developed by Lotfi Zadeh in 1965 to solve problems where information cannot be accurately measured in cases of uncertainty and insufficiency [32]. Fuzzy Logic is a method that uses approximate thinking rather than definite values. The Fuzzy Logic approach provides subjective evaluation for the evaluation process in complex and uncertain decision problems [33].

Fuzzy numbers are defined as a fuzzy subset of real numbers expressing linguistic uncertainty. The membership function establishes the degree of fuzziness in the subset to which any element belongs [34]. Triangle Fuzzy numbers (l, m, u) were used in this study. The numbers represent the lowest, best, and highest possible values. The membership function is shown in Equation (2) (adapted from Alvand et al. [35]):

$$\mu_{\tilde{A}}(x; l, m, u) = \begin{cases} l \le x \le m & ; \quad \frac{x-1}{m-1} \\ m \le x \le u & ; \quad \frac{u-x}{u-m} \\ x > u \; or \; x < l & ; \quad 0 \end{cases} \tag{2}$$

The basic algebraic operations of any two positive fuzzy numbers are as shown in Equation (3)-(4)-(5) (adapted from Alvand et al. [35]):

- Fuzzy Sum:

$$M_1 + M_2 = (l_1 + l_2, m_1 + m_2, u_1 + u_2); \tag{3}$$

- Fuzzy Subtraction:

$$M_1 - M_2 = (l_1 - l_2, m_1 - m_2, u_1 - u_2); \tag{4}$$

- Fuzzy Multiplication:

$$M_1 \times M_2 = (l_1 \times l_2, m_1 \times m_2, u_1 \times u_2) \tag{5}$$

2.3. Fuzzy SWARA

The SWARA method is an approach developed by Kersuliene et al. [36], and the technique has been developed for weight criteria in decision-making processes. It is an uncomplicated MCDM technique in which experts can incorporate their tacit knowledge and experience into decision-making [37-38]. One of the advantages of the method is that it provides tools for assessing the accuracy of expert opinions about the weights determined for the decision-making process [39]. The SWARA technique is a technique that can also be used in cases where expert opinions are not compatible and the degree of consistency values are not within limits [40]. The method provides the opportunity to evaluate the experts' opinions and determine the relative importance weights of each criterion accordingly [41]. There are also studies in which the SWARA method

is used together with the Fuzzy Logic approach to eliminate the method's weaknesses in evaluating uncertain information.

The fuzzy SWARA method consists of six steps [40, 42-44]:
Step 1: Ranking the criteria from most important to least important by each decision-making expert, considering the decision-making purpose of the problem. Table 1 shows the fuzzy scales used for this step.

Table 1: Fuzzy Member Function Values

	Fuzzy Number		
Equal importance	0.75	1.00	1.00
Relatively low importance	0.50	0.75	1.00
Low importance	0.25	0.50	0.75
Very low importance	0.00	0.25	0.50
Extremely little importance	0.00	0.00	0.25

Step 2: From the second criterion, decision-makers will compare each criterion (j) with the previous one (j-1).
Step 3: Determination of k_j coefficient according to Equation (6).

$$k_j^{\sim} = \begin{cases} 1^{\sim} & ; \quad j = 1 \\ s_j^{\sim} + 1^{\sim} & ; \quad j > 1 \end{cases} \tag{6}$$

(where s_j represents the comparative significance of the mean value)

Step 4: Determining the importance vector q_j according to Equation (7).

$$q_j^{\sim} = \begin{cases} 1^{\sim} & ; \quad j = 1 \\ \frac{(x_{j-1}^{\sim})}{k_j^{\sim}} & ; \quad j > 1 \end{cases} \tag{7}$$

(where the notation x_{j-1} refers to q_{j-1}).

Step 5: Calculation of fuzzy weight values (w_j) (Equation (8)).

$$w_j^{\sim} = \frac{q_j^{\sim}}{\sum_{k=1}^{n} q_k^{\sim}} \tag{8}$$

Step 6: Performing the defuzzification (Equation (9)).

$$w_j = \frac{\left(w_j^u - w_j^l\right) + \left(w_j^m - w_j^l\right)}{3} + w_j^l \tag{9}$$

2.4. Fuzzy MOORA

The MOORA method was first developed in 2006 [45]. There are some reasons for applying MOORA instead of other well-known MCDM methods in the recent literature. The MOORA method is the proposed MCDM technique to overcome the weaknesses of the old methods, and MOORA is easy to implement and has a stable structure [46].

The Fuzzy MOORA method, which is used to process the uncertain information of decision-makers, consists of six steps [44, 46-48]:

Step 1: Evaluation of m alternatives by each of the k decision makers (using the Triangular Fuzzy Numbers shown in Table 2)

Table 2: Linguistic Variables and Fuzzy Numbers

Linguistic Variables	Fuzzy Number		
Very Low (VL)	0.0	0.0	0.1
Low (L)	0.0	0.1	0.3
Medium Low (ML)	0.1	0.3	0.5
Medium (M)	0.3	0.5	0.7
Medium High (MH)	0.5	0.7	0.9
High (H)	0.7	0.9	1.0
Very High	0.9	1.0	1.0

Step 2: Combining the fuzzy evaluations made by the decision makers for the alternatives according to Table 2 (Equation (10)) and the formation of the fuzzy decision matrix (the decision matrix in which *p* decision makers evaluate *n* alternatives as fuzzy for *m* criteria).

$$X = \begin{bmatrix} [x_{11}^l, x_{11}^m, x_{11}^u] & [x_{12}^l, x_{12}^m, x_{12}^u] & \dots & [x_{1n}^l, x_{1n}^m, x_{1n}^u] \\ [x_{21}^l, x_{21}^m, x_{21}^u] & [x_{22}^l, x_{22}^m, x_{22}^u] & \dots & [x_{2n}^l, x_{2n}^m, x_{2n}^u] \\ \dots & \dots & \dots & \dots \\ [x_{m1}^l, x_{m1}^m, x_{m1}^u] & [x_{m2}^l, x_{m2}^m, x_{m2}^u] & \dots & [x_{mn}^l, x_{mn}^m, x_{mn}^u] \end{bmatrix} \quad (10)$$

Step 3: Normalize the fuzzy decision matrix using Equation (11)-(12)-(13).

$$r_{ij}^l = \frac{x_{ij}^l}{\sqrt{\sum_{i=1}^m \left[\left(x_{ij}^l\right)^2 + \left(x_{ij}^m\right)^2 + \left(x_{ij}^u\right)^2\right]}} \quad (11)$$

$$r_{ij}^m = \frac{x_{ij}^m}{\sqrt{\sum_{i=1}^m \left[\left(x_{ij}^l\right)^2 + \left(x_{ij}^m\right)^2 + \left(x_{ij}^u\right)^2\right]}} \quad (12)$$

$$r_{ij}^u = \frac{x_{ij}^u}{\sqrt{\sum_{i=1}^m \left[\left(x_{ij}^l\right)^2 + \left(x_{ij}^m\right)^2 + \left(x_{ij}^u\right)^2\right]}} \quad (13)$$

Step 4: Weighting of the normalized decision matrix using Equation (14)-(15)-(16).

(In this study, the weights obtained by the Fuzzy SWARA method were used).

$$v_{ij}^l = w_j r_{ij}^l \quad (14)$$

$$v_{ij}^m = w_j r_{ij}^m \quad (15)$$

$$v_{ij}^u = w_j r_{ij}^u \quad (16)$$

Step 5: Ranking of alternatives in terms of benefit and cost criteria.

For benefit criteria (Equation (17)-(18)-(19)):

$$s_i^{+l} = \sum_{j=1}^{n} \; v_{ij}^{l} \big| \; j \in j^{max} \tag{17}$$

$$s_i^{+m} = \sum_{j=1}^{n} \; v_{ij}^{m} \big| \; j \in j^{max} \tag{18}$$

$$s_i^{+n} = \sum_{j=1}^{n} \; v_{ij}^{n} \big| \; j \in j^{max} \tag{19}$$

For cost criteria (Equation (20), (21) and (22)):

$$s_i^{-l} = \sum_{j=1}^{n} \; v_{ij}^{l} \big| \; j \in j^{min} \tag{20}$$

$$s_i^{-m} = \sum_{j=1}^{n} \; v_{ij}^{m} \big| \; j \in j^{min} \tag{21}$$

$$s_i^{-n} = \sum_{j=1}^{n} \; v_{ij}^{n} \big| \; j \in j^{min} \tag{22}$$

Step 6: Establishing the performance index value of each alternative. Defuzzification of the fuzzy utility and cost values calculated for the alternatives (Equation (23)). Thus, each alternative calculates the best non-fuzzy performance (BNP) value. Moreover, ranking the alternatives according to their performance values (by BNPs) from highest to lowest.

$$S_i(s_i^{+}, s_i^{-}) = \sqrt{\frac{1}{3}\Big[\left(s_i^{+l} - s_i^{-l}\right)^2 + (s_i^{+m} - s_i^{-m})^2 + (s_i^{+u} - s_i^{-u})^2 \Big]} \tag{23}$$

3. Results and Discussion

The business that produces energy storage systems has made-to-order. The company makes changes to its production lines for each new project. Changes to be made in production lines and risks that may occur before the project starts are presented to the management. Changes are made after management approval. In the sample implementation determined for this study: a new activity should be added to the production process due to an additional feature requested by the customer for their products. The customer wants to add traceability to their products.

For this reason, it switches to QR (Quick Response) code application in its products and requests a QR code application from its suppliers in the raw materials it sends. The business writes the QR code the customer wants with a laser printer. However, since no laser printer can write a QR code on top of the product's cover on the production lines, the laser printer should

also be included in the production process. When the project started, a deadline was given by the customer company. All evaluations were made considering the closeness of the deadline and the short duration. Risks may arise due to this new demand and the short deadline. Considering the past project experiences, ten possible risks were determined with an expert team from the business (sales and marketing specialist, logistics specialist, production team leader, and project management specialist).

- **Risk 1: The risk that the laser printer will not fit on the line:** A laser printer and its components should be placed on the production line at the customer's request. However, since the supplier company and laser printer have not been decided yet, it is unclear whether all the equipment will fit on the line. There is a risk that the areas positioned on the lines of the laser printer devices are insufficient.
- **Risk 2: The risk that production stops due to a malfunction and the order is not fulfilled:** In case of a sudden breakdown or failure of the purchased laser printer, production may stop. Since the deadline is also short, this may cause problems in the timely delivery of the product.
- **Risk 3: The risk of not growing new QR code products due to being unable to find a budget for two devices:** The customer's products are currently produced on two separate production lines. For this reason, the laser printer will need to be positioned for two different lines. Laser printers cost much more than label devices. If the business is still looking for a budget for two new laser printers to be purchased, there is a risk that the new products with QR codes cannot be delivered within the customer's deadline.
- **Risk 4: Due to the long purchasing process, the risk of delaying the installation of the laser printer and failing to comply with the customer deadline:** Due to the purchasing process in the enterprise, offers from three companies are required. During the collection of bids, technical details are explained to the supplier companies in the field, and it may take a long time to determine the companies' qualifications. For this reason, there is a risk that the commissioning of laser printers will fail to meet the customer deadline.
- **Risk 5: The risk that the installation does not reach the customer deadline due to the contract process:** Due to the long duration of the contract sub-process within the purchasing process of the enterprise, there is a risk that the laser printer installation will not reach the customer deadline (Contract sub-process takes approximately one month).
- **Risk 6: Risk of product not reaching customer deadline due to installation delays caused by laser printer company:** Supplier companies that bid for laser printers bring laser printers from abroad (The supply time can take up to eight weeks). If there is no laser printer in the stock of the supplier company that can meet the needs of the business, the supplier company will order the laser printer from abroad. A problem during the order may cause the risk of delay in the customer delivery time.
- **Risk 7: Risk of injury to workers from laser beams:** It is planned to place laser printers in a cabinet on the production line, considering occupational health and safety conditions. However, if the cover of the cabinet used for machine adjustment is opened while the laser printer is operating, the workers may be harmed by the light beams.
- **Risk 8: The risk of the product going to the customer with the QR code written with the wrong content or not of the desired quality.** The customer company requires a unique

code that contains different parts codes for the QR code, written with a laser printer, and will be different in each product. Therefore, there is a risk that the content of the QR code needs to be of the correct or desired quality.

- **Risk 9: Risk of writing the QR code in the wrong place on the product and sending it to the customer in this way:** If the laser printer located on the production line is moved from its position, there may be a risk that the QR code will be written in the wrong place.
- **Risk 10: Risk of sending a product without a QR code to the customer:** A QR code may not be written on the product for any reason that may occur during production. The company can send the customer a product without a QR code if the error is not noticed.

According to the classical DMRA method, one of the most used methods for risk assessment, two risk components are used in the evaluation: The probability of risk and the effect of the formation. The impacts of risks (severity) after they occur may occur differently in many different areas. Therefore, more than measuring the impact with a single component will be required to assess it objectively. This study proposes a new risk assessment model detailing the "severity" component in the classical matrix risk assessment method, including different areas, to increase objectivity. According to the recommended model, risk size (*RS*) is calculated as shown in Equation (24).

$$RS = the\ severity\ of\ delivery\ time\ (C_1) \times the\ severity\ of\ cost\ (C_2) \times the\ severity\ of\ quality\ (C_3) \times likelihood\ (C_4) \quad (24)$$

The flow chart of the implementation is shown in Figure 1.

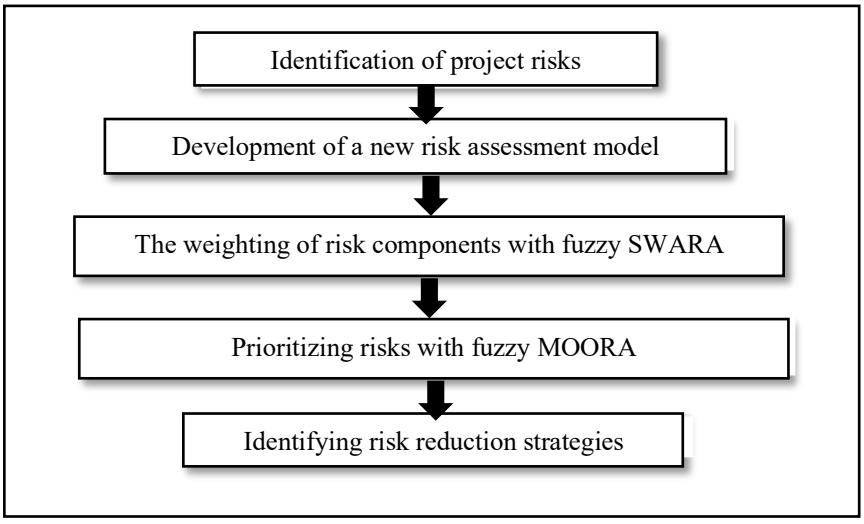

Figure 1: Flow chart for implementation

Fuzzy Swara Results

Since the importance of the four components in determining the risk size is different, the components are weighted using the Fuzzy SWARA method. The fuzzy SWARA method is used to solve problems with different decision-makers. The opinions of four experts were utilized in this study. The first decision maker (KV_1) is the sales and marketing specialist, the second decision maker (KV_2) is the logistics specialist, the third decision maker (KV_3) is the production team leader, and the fourth decision maker (KV_4) is the project management specialist. According to the first step of the fuzzy SWARA method, the ranking of the decision makers' criteria in order of importance is shown in Table 3.

Table 3: Criteria ranking according to decision-makers

Criteria	KV_1	KV_2	KV_3	KV_4
C_1 (The severity of delivery time)	3	1	1	1
C_2 (The severity of cost)	1	4	3	2
C_3 (The severity of quality)	2	2	4	3
C_4 (Likelihood)	4	3	2	4

The decision makers' comparison of criteria (s_j) with each other according to the fuzzy number transformations given in Table 1, k_j values calculated according to Equation (6), q_j importance vectors calculated according to Equation (7), and w_j fuzzy weight values calculated according to Equation (8) are shown in table 4.

Table 4: Fuzzy Weight Values

KV_1	**s_{jl}**	**s_{jm}**	**s_{ju}**	**k_{jl}**	**k_{jm}**	**k_{ju}**	**q_{jl}**	**q_{jm}**	**q_{ju}**	**w_{jl}**	**w_{jm}**	**w_{ju}**
C_2	0.75	1.00	1.00	0.75	1.00	1.00	0.75	1.00	1.00	0.38	0.52	0.58
C_3	0.50	0.75	1.00	1.25	1.75	2.00	0.60	0.57	0.50	0.31	0.30	0.29
C_1	0.25	0.50	0.75	1.50	2.25	2.75	0.40	0.25	0.18	0.21	0.13	0.11
C_4	0.50	0.75	1.00	2.00	3.00	3.75	0.20	0.08	0.05	0.10	0.04	0.03
KV_2	**s_{jl}**	**s_{jm}**	**s_{ju}**	**k_{jl}**	**k_{jm}**	**k_{ju}**	**q_{jl}**	**q_{jm}**	**q_{ju}**	**w_{jl}**	**w_{jm}**	**w_{ju}**
C_1	0.75	1.00	1.00	0.75	1.00	1.00	0.75	1.00	1.00	0.27	0.45	0.53
C_4	0.25	0.50	0.75	1.00	1.50	1.75	0.75	0.67	0.57	0.27	0.30	0.30
C_3	0.00	0.25	0.50	1.00	1.75	2.25	0.75	0.38	0.25	0.27	0.17	0.13
C_2	0.50	0.75	1.00	1.50	2.50	3.25	0.50	0.15	0.08	0.18	0.07	0.04
KV_3	**s_{jl}**	**s_{jm}**	**s_{ju}**	**k_{jl}**	**k_{jm}**	**k_{ju}**	**q_{jl}**	**q_{jm}**	**q_{ju}**	**w_{jl}**	**w_{jm}**	**w_{ju}**
C_1	0.75	1.00	1.00	0.75	1.00	1.00	0.75	1.00	1.00	0.22	0.41	0.49
C_4	0.00	0.25	0.50	0.75	1.25	1.50	1.00	0.80	0.67	0.29	0.33	0.32
C_2	0.25	0.50	0.75	1.00	1.75	2.25	1.00	0.46	0.30	0.29	0.19	0.14
C_3	0.50	0.75	1.00	1.50	2.50	3.25	0.67	0.18	0.09	0.20	0.07	0.04
KV_4	**s_{jl}**	**s_{jm}**	**s_{ju}**	**k_{jl}**	**k_{jm}**	**k_{ju}**	**q_{jl}**	**q_{jm}**	**q_{ju}**	**w_{jl}**	**w_{jm}**	**w_{ju}**
C_1	0.75	1.00	1.00	0.75	1.00	1.00	0.75	1.00	1.00	0.41	0.53	0.59
C_2	0.50	0.75	1.00	1.25	1.75	2.00	0.60	0.57	0.50	0.33	0.31	0.29
C_3	0.50	0.75	1.00	1.75	2.50	3.00	0.34	0.23	0.17	0.19	0.12	0.10
C_4	0.50	0.75	1.00	2.25	3.25	4.00	0.15	0.07	0.04	0.08	0.04	0.02

The fuzzy weights calculated separately for the four decision makers (shown in Table 4) are combined and given in Table 5.

Table 5: Combined fuzzy weights

	KV_1			KV_2			KV_3			KV_4			Criterion weight		
	w_{jl}	w_{jm}	w_{ju}	w_{jl}	w_{jm}	w_{ju}	w_{jl}	w_{jm}	w_{ju}	w_{jl}	w_{jm}	w_{ju}	p_{jl}	p_{jm}	p_{ju}
C_1	0.21	0.13	0.11	0.27	0.45	0.53	0.22	0.41	0.49	0.41	0.53	0.59	0.28	0.38	0.43
C_2	0.38	0.52	0.58	0.18	0.07	0.04	0.29	0.19	0.14	0.33	0.31	0.29	0.30	0.27	0.26
C_3	0.31	0.30	0.29	0.27	0.17	0.13	0.20	0.07	0.04	0.19	0.12	0.10	0.24	0.17	0.14
C_4	0.10	0.04	0.03	0.27	0.30	0.30	0.29	0.33	0.32	0.08	0.04	0.02	0.19	0.18	0.17
													1.00	1.00	1.00

The combined fuzzy weights of the criteria (shown in Table 5) and defuzzification according to Equation (9) are given in Table 6.

Table 6: Defuzzification criterion weights

	p_{jl}	p_{jm}	p_{ju}	
C_1	0.28	0.38	0.43	0.36
C_2	0.30	0.27	0.26	0.28
C_3	0.24	0.17	0.14	0.18
C_4	0.19	0.18	0.17	0.18

After determining the weight of each criterion with the Fuzzy SWARA method, the weights obtained were used in the Fuzzy MOORA method to prioritize the risks.

Fuzzy Moora Results

The prioritization of project risks by the Fuzzy Moora method was performed in six steps.

Step 1: The decision-makers evaluate the risks (alternatives) affecting the customer's deadline. Linguistic variables in Table 2 were used for evaluation. Table 7 shows risk assessments made by decision-makers.

Table 7: Fuzzy assessment of risks by decision-makers

KV_1	C_1			C_2			C_3			C_4		
R_1	0.50	0.70	0.90	0.10	0.30	0.50	0.10	0.30	0.50	0.00	0.10	0.30
R_2	0.70	0.90	1.00	0.10	0.30	0.50	0.30	0.50	0.70	0.00	0.10	0.30
R_3	0.70	0.90	1.00	0.00	0.10	0.30	0.00	0.10	0.30	0.00	0.10	0.30
R_4	0.70	0.90	1.00	0.00	0.10	0.30	0.10	0.30	0.50	0.90	1.00	1.00
R_5	0.70	0.90	1.00	0.00	0.10	0.30	0.10	0.30	0.50	0.90	1.00	1.00
R_6	0.70	0.90	1.00	0.00	0.10	0.30	0.10	0.30	0.50	0.70	0.90	1.00
R_7	0.70	0.90	1.00	0.10	0.30	0.50	0.30	0.50	0.70	0.70	0.90	1.00
R_8	0.50	0.70	0.90	0.50	0.70	0.90	0.70	0.90	1.00	0.50	0.70	0.90
R_9	0.50	0.70	0.90	0.50	0.70	0.90	0.50	0.70	0.90	0.10	0.30	0.50
R_{10}	0.00	0.10	0.30	0.50	0.70	0.90	0.70	0.90	1.00	0.00	0.10	0.30
KV_2	C_1			C_2			C_3			C_4		
R_1	0.70	0.90	1.00	0.30	0.50	0.70	0.10	0.30	0.50	0.10	0.30	0.50
R_2	0.70	0.90	1.00	0.30	0.50	0.70	0.30	0.50	0.70	0.10	0.30	0.50
R_3	0.70	0.90	1.00	0.00	0.10	0.30	0.00	0.10	0.30	0.00	0.10	0.30
R_4	0.70	0.90	1.00	0.00	0.10	0.30	0.30	0.50	0.70	0.90	1.00	1.00
R_5	0.70	0.90	1.00	0.00	0.10	0.30	0.30	0.50	0.70	0.90	1.00	1.00
R_6	0.70	0.90	1.00	0.10	0.30	0.50	0.30	0.50	0.70	0.70	0.90	1.00
R_7	0.70	0.90	1.00	0.30	0.50	0.70	0.50	0.70	0.90	0.70	0.90	1.00
R_8	0.70	0.90	1.00	0.70	0.90	1.00	0.70	0.90	1.00	0.50	0.70	0.90
R_9	0.70	0.90	1.00	0.70	0.90	1.00	0.70	0.90	1.00	0.30	0.50	0.70
R_{10}	0.10	0.30	0.50	0.70	0.90	1.00	0.70	0.90	1.00	0.10	0.30	0.50
KV_3	C_1			C_2			C_3			C_4		
R_1	0.70	0.90	1.00	0.10	0.30	0.50	0.10	0.30	0.50	0.00	0.10	0.30
R_2	0.50	0.70	0.90	0.30	0.50	0.70	0.10	0.30	0.50	0.00	0.10	0.30
R_3	0.70	0.90	1.00	0.10	0.30	0.50	0.10	0.30	0.50	0.10	0.30	0.50
R_4	0.50	0.70	0.90	0.00	0.10	0.30	0.10	0.30	0.50	0.70	0.90	1.00
R_5	0.70	0.90	1.00	0.10	0.30	0.50	0.10	0.30	0.50	0.90	1.00	1.00
R_6	0.70	0.90	1.00	0.10	0.30	0.50	0.10	0.30	0.50	0.70	0.90	1.00
R_7	0.70	0.90	1.00	0.10	0.30	0.50	0.10	0.30	0.50	0.70	0.90	1.00
R_8	0.50	0.70	0.90	0.50	0.70	0.90	0.50	0.70	0.90	0.50	0.70	0.90
R_9	0.50	0.70	0.90	0.50	0.70	0.90	0.50	0.70	0.90	0.10	0.30	0.50
R_{10}	0.10	0.30	0.50	0.70	0.90	1.00	0.70	0.90	1.00	0.10	0.30	0.50
KV_4	C_1			C_2			C_3			C_4		
R_1	0.50	0.70	0.90	0.10	0.30	0.50	0.10	0.30	0.50	0.00	0.10	0.30
R_2	0.50	0.70	0.90	0.10	0.30	0.50	0.30	0.50	0.70	0.00	0.10	0.30
R_3	0.50	0.70	0.90	0.00	0.10	0.30	0.00	0.10	0.30	0.00	0.10	0.30
R_4	0.50	0.70	0.90	0.00	0.10	0.30	0.00	0.10	0.30	0.50	0.70	0.90
R_5	0.50	0.70	0.90	0.00	0.10	0.30	0.00	0.10	0.30	0.70	0.90	1.00
R_6	0.50	0.70	0.90	0.00	0.10	0.30	0.10	0.30	0.50	0.50	0.70	0.90
R_7	0.50	0.70	0.90	0.10	0.30	0.50	0.10	0.30	0.50	0.50	0.70	0.90
R_8	0.50	0.70	0.90	0.50	0.70	0.90	0.50	0.70	0.90	0.50	0.70	0.90
R_9	0.50	0.70	0.90	0.50	0.70	0.90	0.50	0.70	0.90	0.10	0.30	0.50
R_{10}	0.00	0.10	0.30	0.50	0.70	0.90	0.50	0.70	0.90	0.00	0.10	0.30

Step 2: The decision makers' risk evaluations were combined using Equation (10). The combined fuzzy decision matrix created is given in Table 8.

Table 8: Combined fuzzy decision matrix

	C_1			C_2			C_3			C_4		
R_1	0.60	0.80	0.95	0.15	0.35	0.55	0.10	0.30	0.50	0.03	0.15	0.35
R_2	0.60	0.80	0.95	0.20	0.40	0.60	0.25	0.45	0.65	0.03	0.15	0.35
R_3	0.65	0.85	0.98	0.03	0.15	0.35	0.03	0.15	0.35	0.03	0.15	0.35
R_4	0.60	0.80	0.95	0.00	0.10	0.30	0.13	0.30	0.50	0.75	0.90	0.98
R_5	0.65	0.85	0.98	0.03	0.15	0.35	0.13	0.30	0.50	0.85	0.98	1.00
R_6	0.65	0.85	0.98	0.05	0.20	0.40	0.15	0.35	0.55	0.65	0.85	0.98
R_7	0.65	0.85	0.98	0.15	0.35	0.55	0.25	0.45	0.65	0.65	0.85	0.98
R_8	0.55	0.75	0.93	0.55	0.75	0.93	0.60	0.80	0.95	0.50	0.70	0.90
R_9	0.55	0.75	0.93	0.55	0.75	0.93	0.55	0.75	0.93	0.15	0.35	0.55
R_{10}	0.05	0.20	0.40	0.60	0.80	0.95	0.65	0.85	0.98	0.05	0.20	0.40

Step 3: By using Equation (11)-(12)-(13), normalization is done for the combined fuzzy decision matrix. The normalized fuzzy decision matrix is shown in Table 9.

Table 9: Normalized fuzzy decision matrix

	C_1			C_2			C_3			C_4		
R_1	0.09	0.15	0.21	0.01	0.05	0.11	0.00	0.03	0.08	0.00	0.01	0.04
R_2	0.09	0.15	0.21	0.01	0.06	0.13	0.02	0.07	0.14	0.00	0.01	0.04
R_3	0.10	0.17	0.23	0.00	0.01	0.05	0.00	0.01	0.04	0.00	0.01	0.04
R_4	0.09	0.15	0.21	0.00	0.00	0.03	0.01	0.03	0.08	0.16	0.24	0.28
R_5	0.10	0.17	0.23	0.00	0.01	0.05	0.01	0.03	0.08	0.21	0.28	0.29
R_6	0.10	0.17	0.23	0.00	0.01	0.06	0.01	0.04	0.10	0.12	0.21	0.28
R_7	0.10	0.17	0.23	0.01	0.05	0.11	0.02	0.07	0.14	0.12	0.21	0.28
R_8	0.07	0.13	0.20	0.11	0.21	0.31	0.12	0.22	0.31	0.07	0.14	0.24
R_9	0.07	0.13	0.20	0.11	0.21	0.31	0.10	0.19	0.29	0.01	0.04	0.09
R_{10}	0.00	0.01	0.04	0.13	0.24	0.33	0.14	0.24	0.32	0.00	0.01	0.05

Step 4: Equation (14)-(15)-(16) weighted normalized fuzzy decision matrix. The weighted fuzzy normalized decision matrix obtained is shown in Table 10.

Table 10: Weighted fuzzy decision matrix

	C_1			C_2			C_3			C_4		
R_1	0.03	0.05	0.08	0.00	0.01	0.03	0.00	0.01	0.02	0.00	0.00	0.01
R_2	0.03	0.05	0.08	0.00	0.02	0.04	0.00	0.01	0.03	0.00	0.00	0.01
R_3	0.04	0.06	0.08	0.00	0.00	0.01	0.00	0.00	0.01	0.00	0.00	0.01
R_4	0.03	0.05	0.08	0.00	0.00	0.01	0.00	0.01	0.02	0.03	0.04	0.05
R_5	0.04	0.06	0.08	0.00	0.00	0.01	0.00	0.01	0.02	0.04	0.05	0.05
R_6	0.04	0.06	0.08	0.00	0.00	0.02	0.00	0.01	0.02	0.02	0.04	0.05
R_7	0.04	0.06	0.08	0.00	0.01	0.03	0.00	0.01	0.03	0.02	0.04	0.05
R_8	0.03	0.05	0.07	0.03	0.06	0.09	0.02	0.04	0.06	0.01	0.03	0.04
R_9	0.03	0.05	0.07	0.03	0.06	0.09	0.02	0.03	0.05	0.00	0.01	0.02
R_{10}	0.00	0.00	0.01	0.04	0.07	0.09	0.03	0.04	0.06	0.00	0.00	0.01

Step 5-6: In this implementation, since all alternatives (risks) are about cost, not benefit, risks are listed using Equation (20)-(21)-(22). With the fuzzy SWARA method, the weights of the risk components (severity of delivery time (C_1), severity of cost (C_2), severity of quality (C_3) and likelihood (C_4)) to be used in risk assessment were determined. BNP values for risks were calculated according to C_1, C_2, C_3 and C_4 values with the fuzzy MOORA method. Fuzzy performance index values were defuzzification using Equation (23). The highest BNP value is 0.17, which belongs to risk 8. When the BNP values of the risks are ranked from the highest to the lowest, the order of priority is as follows: Risk 8 > Risk 9 > Risk 7 > Risk 5 > Risk 10 > Risk 4 > Risk 6 > Risk 2 > Risk 1 > Risk 3

4. Conclusion

Anticipating risks and making the necessary action plans are essential for businesses to prevent or reduce undesirable situations (not complying with customer deadlines, malfunctions, delays in production, etc.).

This study discusses the risks of a business producing energy storage systems and starting a new project. It aims to develop a risk assessment model different from the classical matrix risk assessment approach to identify and prioritize the risks that may occur before the start of the project. For this reason, the "severity" component in the classical matrix method is divided into three sub-components due to the different areas that the risk can affect and the different weights in these areas. Therefore, the risk size is not composed of the multiple of two components, "Severity" and "Likelihood," but the multiple of four components of the risk as "The severity of delivery time (C_1)," "The severity of cost (C_2)," and "The severity of quality (C_3)," and "Likelihood (C_4)". The SWARA method was used to calculate the weights of the four risk components. The criteria weights calculated with the Fuzzy SWARA method were used in the Fuzzy MOORA method, and the ten risks identified were prioritized according to these weight values.

As a result of the study, the most priority risk was determined as the risk of going to the customer with the QR code written in incorrect or non-desired quality of the product (Risk 8). Three action plans have been determined to reduce this risk. The first action plan is to add a barcode reader to the laser printer's output on the production line and to verify the accuracy of

the written QR code by comparing it with the coding algorithm. Thus, it is aimed to identify and reject the non-conforming product. This way, the risk of going to the customer will be reduced even if a faulty product occurs on the production line. However, the cost of this action plan is high. The second action plan is to control the alphanumeric code under the written QR code with the camera control unit at the end of the production line. Since the serial number cannot be checked with the camera, only the alphanumeric code can be checked, and this plan is not a suitable plan to reduce the risk. The third action plan: A screen where product selection can be made is to be placed next to the laser printer unit in the production line not to write the wrong QR code. The QR code will be written in the correct algorithm by selecting the relevant product from this screen. This way, it will be sufficient for the personnel to select the product's name from the screen without having to design the relevant QR code at the beginning of the process. Thus, the wrong QR code design can be prevented and reduced risk. The business has decided to implement the third action plan.

In the study, Fuzzy SWARA and Fuzzy MOORA techniques were used to take into account the uncertainties in the risks and the evaluations of the decision-makers. Different MCDM techniques can be used and integrated into subsequent studies. In addition, new risk assessment models can be developed by dividing the severity component used in the classical risk assessment method into subcomponents in different ways for different sectors and different problems.

Ethics in Publishing

There are no ethical issues regarding the publication of this study

Author Contributions

Conceptualization, G.S.Y.; methodology, G.S.Y. and T.K.P.; validation, G.S.Y. and T.K.P.; formal analysis, G.S.Y. and T.K.P.; investigation, G.S.Y.; resources, G.S.Y. and T.K.P.; data curation, G.S.Y.; writing – original draft preparation, G.S.Y.; writing – review and editing, T.K.P.; visualization, G.S.Y. and T.K.P.; supervision, T.K.P.; project administration, T.K.P.

References

[1]Calapoğlu A., Şişeci Çeşmeli M., Pençe İ., Çetinkaya Bozkurt Ö. (2021) Siparişe göre üretim yapan firmalarda sipariş sıralaması ve teslim tarihi problemi için bir karar modeli, Acta Infologica, 5(2), pp 341-357.

[2]Oehmen, J., Olechowski, A., Kenley, C.R., Ben-Daya, M., (2014) Analysis of the effect of risk management practices on the performance of new product development, Technovation, 34, pp 441-453.

[3]De Oliveira, U.R., Neto, L.A., Abreu, P.A.F., Fernandes, V.A., (2021) Risk Management applied to the reverse logistics of solid waste, Journal of Cleaner Production, 296, 126517.

[4]Okudan, O., Budayan, C., Dikmen, I., (2021) A knowledge-based risk management tool for construction projects using case-based reasoning, Expert Systems With Applications, 173, 114776.

[5]Yılmaz N., Şenol M.B. (2017) İş sağlığı ve güvenliği risk değerlendirme süreci için bulanık çok kriterli bir model ve uygulaması, Journal of the Faculty of Engineering and Architecture of Gazi University, 32(1), pp 77-87.

[6]Tomak, N., Korkusuz Polat, T., (2022) Risk prioritization model driven by success factor in the light of multi-criteria decision making, Open Chemistry, vol 20, no 1, pp 759-776. https://doi.org/10.1515/chem-2022-0188.

[7]Becker, R.W., Jachstet, L.A., Dallegrave, A., Ruiz-Padillo, A., Zanello, R., Sirtori, C., (2021) Multi-criteria decision-making techniques associated with (Q) SAR risk assessment for ranking surface water microcontaminants identified using LC-QTOF MS, Science of the Total Environment, 797, 149002.

[8]Bid, S., Siddique, G., (2019) Humans risk assessment of Panchet Dam in India using TOPSIS and WASPAS multi-criteria decision-making (MCDM) methods, Helion, 5, e01956.

[9]Jena, R., Pradhan, B., Beydoun, G., (2020), Earthquake vulnerability assessment in Northern Sumatra province by using a multi-criteria decision-making model, International Journal of Disaster Risk Reduction, vol 46, 101518, ISSN 2212-4209, https://doi.org/10.1016/j.ijdrr.2020.101518 .

[10] Senthill, S., Murugananthan, K., Ramesh, A., (2018) Analysis and prioritisation of risks in reverse logistics network using hybrid multi-criteria decision making methods, Journal of Cleaner Production, 179, pp 716-730.

[11] Sivageerthi, T., Bathrinath, S., Uthayakumar, M., Bhalaji, R.K.A., (2022) A SWARA method to analyze the risks in coal supply chain management, Materials Today: Proceedings, 50, pp 935-940.

[12] Tian, D., Chen, J., Wu, X., (2022) A two stage risk assessment model based on interval-valued fuzzy numbers and risk attitudes, Engineering Applications of Artificial Intelligence, 114, 105086.

[13] Korkusuz Polat, T., (2019) Risk priority with fuzzy Logic: Application of a textile factory, Sakarya University Journal of Science, 23(2), 203-212, DOI: 10.16984/saufenbilder.458807.

[14] Moreno Cabezali, M.M., Fernandez-Crehuet, J.M., (2020) Application of a fuzzy-logic based model for risk assessment in additive manufacturing R&D projects, Computers & Industrial Engineering, 145, 106529.

[15] Lin, S-S., Shen, S-L., Zhou, A., Xu, Y-S., (2021) Risk assessment and management of excavation system based on fuzzy set theory and machine learning methods, Automation in Construction, 122, 103490.

[16] Yazdani, M., Mohammed, A., Bai, C., Labib, A., (2021) A novel hesitant-fuzzy-based group decision approach for outsourcing risk, Expert Systems With Applications, 184, 115517.

[17] Xu, F., Gao, K., Xiao, B., Liu, J., Wu, Z., (2022) Risk assessment for the integrated energy system using a hesitant fuzzy multi-criteria decision-making framework, Energy Reports, 8, pp 7892-7907.

[18] Shannazi, R., Alimohammadlou, M., (2022) Investigating risks in renewable energy in oil-producing countries through multi-criteria decision-making methods based on interval type-2 fuzzy sets: A case study of Iran, Renewable Energy, 191, pp 1009-1027.

[19] Singer, H., Över Özçelik, T., (2022) Bir risk temelli karar verme yaklaşımı ile metalik biyomalzeme değerlendirme, Gazi Üniversitesi Mühendislik Mimarlık Fakültesi Dergisi, 37(2), pp 641-654.

[20] Gölcük, İ., Durmaz, E.D., Şahin, R., (2023) Bulanık FUCOM ve bulanık çizge teorisi-matris yaklaşımı ile iş güvenliği risklerinin önceliklendirilmesi, Gazi Üniversitesi Mühendislik Mimarlık Fakültesi Dergisi, 38(1), pp 57-69.

[21] Ali, Y., Awan, M.A., Bilal, M., Khan, J., Petrillo, A., (2019) Risk assessment of China-Pakistan Fiber Optic Project (CPFOP) in the light of multi-criteria decision making (MCDM), Advanced Engineering Informatics, 40, pp 36-45.

[22] Jokar, E., Aminnejad, B., Lork, A., (2021) Assessing and prioritizing risks in public-private partnership (PPP) projects using the integration of fuzzy multi-criteria decision-making methods, Operations Research Perspective, 8, 100190.

[23] Severi, C.A., Pérez, Ví., Pascual, C., Muñoz, Raú., Lebrero, R., (2022) Identification of critical operational hazards in a biogas upgrading pilot plant through a multi-criteria decision making and FTOPSIS-HAZOP approach, Chemosphere, DOI: https://doi.org/10.1016/j.chemosphere.2022.135845 .

[24] Yücenur, G.N., Şenol, K., (2021) Sequential SWARA and fuzzy VIKOR methods in elimination of waste and creation of lean construction processes, Journal of Building Engineering, 44, 103196

[25] Dehshiri, S.S.H., (2022) New hybrid multi-criteria decision making method for offshore windfarm site location in Persian Gulf, Iran, Ocean Engineering, 256, 111498

[26] Arabsheybani, A., Khasmeh, A.A., (2021) Robust and resilient supply chain network design considering risks in food industry: flavour industry in Iran, International Journal of Management Science and Engineering Management, 16(3), pp 197-208, DOI: 10.1080/17509653.2021.1907811.

[27] Arabsheybani, A., Paydar, M.M., Safaei, A.S., (2018) An integrated fuzzy MOORA method and FMEA technique for sustainable supplier selection considering quantity discounts and supplier's risk, Journal of Cleaner Production, 190, pp 577-591.

[28] Wu, C., Zhou, L., Jin, J., Ning, S., Zhang, Z., Bai, L., (2020) Regional water resource carrying capacity evaluation based on multi-dimensional precondition cloud and risk matrix coupling model, Science of the Total Environment, 710, 136324.

[29] Wu, K.F., Sasidharan, L., Thor, C.P., Chen, S.Y., (2018) Crash sequence based risk matrix for motorcycle crashes, Accident Analysis and Prevention, 117, pp 21-31.

[30] Marhavilas, P.K., Koulouriotis, D., Gemeni, V., (2011) Risk analysis and assessment methodologies in the work sites: On a review, classification and comparative study of the scientific literature of the period 2000-2009, Journal of Loss Prevention in the Process Industries, 24, pp 477-523.

[31] Jusoh, Z., Shattar, N.A., Majid, HAMA, Adenan, N.D., (2016) Determination of hazard in captive hotel laundry using semi quantitative risk assessment matrix, Procedia – Social and Behavioral Sciences, 222, pp 915-922.

[32] Zadeh, L.A., (1996) Fuzzy Control: Issues, contentions and perspectives, IFAC, 13th Triennial World Congress, San Francisco, USA.

[33] Ayyıldız, E., (2022) Fermatean fuzzy step-wise weight assessment ratio analysis (SWARA) and its application to prioritizing indicators to achieve sustainable development goal-7, Renewable Energy, 193, pp 136-148.

[34] Mufazzal, S., Khan, N.Z., Muzakkir, S.M., Siddiquee, A.N., Khan, Z.A., (2022) A new fuzzy multi-criteria decision-making method based on proximity index value, Journal of Industrial and Production Engineering, 39(1), pp 42-58, DOI: 10.1080/21681015.2021.1958935

[35] Alvand, A., Mirhosseini, S.M., Ehsanifar, M., Zeighami, E., Mohammadi, A., (2021) Identification and assessment of risk in construction projects using the integrated FMEA-SWARA-WASPAS model under fuzzy environment: a case study of a construction project in Iran, International Journal of Construction Management, DOI: 10.1080/15623599.2021.1877875

[36] Keršulienė, V., Zavadskas, E. K., Turskis, Z., (2010) Selection of rational dispute resolution method by applying new step-wise weight assessment ratio analysis (SWARA), Journal of Business Economics and Management, 11(2), pp 243-258. https://doi.org/10.3846/jbem.2010.12

[37] Mardani, A., Nilashi, M., Zakuan, N., Loganathan, N., Soheilirad, S., Saman, M.Z.M., Ibrahim, O., (2017) A systematic review and meta analysis of SWARA and WASPAS methods: Theory and applications with recent fuzzy developments, Applied Soft Computing, 57, pp 265-292.

[38] Erol, I., Ar, I.M., Peker, I., (2022), Scrutinizing blockchain applicability in sustainable supply chains through an integrated fuzzy multi-criteria decision making framework, Applied Soft Computing, 116, 108331, https://doi.org/10.1016/j.asoc.2021.108331.

[39] Dahooie, J.H., Mohammadi, N., Daim, T., Vanaki, A.S., (2021) Matching of technological forecasting technique to a technology using fuzzy multi-attribute decision-making methods: Case study from the aerospace industry, Technology in Society, 67, 101707.

[40] Ansari, Z.N., Kant, R., Shankar, R., (2020) Evaluation and ranking of solutions to mitigate sustainable remanufacturing supply chain risks: a hybrid fuzzy SWARA fuzzy COPRAS framework approach, International Journal of Sustainable Engineering, 13(6), pp 473-494, DOI: 10.1080/19397038.2020.1758973

[41] Agarwal, S., Kant, R., Shankar, R., (2020) Evaluating solutions to overcome humanitarian supply chain management barriers: A hybrid fuzzy SWARA-fuzzy WASPAS approach, International Journal of Disaster Risk Reduction, 51, 101838.

[42] Zarbakhshnia, N., Soleimani, H., Ghaderi, H., (2018) Sustainable third-party reverse logistics provider evaluation and selection using fuzzy SWARA and developed fuzzy COPRAS in the presence of risk criteria, Applied Soft Computing, 65, pp 307-319.

[43] Şengül, D., Çağıl, G., Ardalı, Z., (2021) Bulanık SWARA ve Aralık Değerli Sezgisel Bulanık AHP Yöntemi ile İş Değerlemesi, Yönetim ve Ekonomi Dergisi, 28(2), pp 243-263. https://dergipark.org.tr/en/pub/yonveek/issue/63117/731727

[44] Savaş, H., Yacan, İ., (2022) Dış kaynak kullanım stratejisi kapsamında alt yüklenicilerin Bulanık SWARA ve Bulanık MOORA yöntemleriyle değerlendirilmesi, Gümüşhane Üniversitesi Sosyal Bilimler Dergisi, 13(2), pp 504-522.

[45] Brauers, W.K.M., Zavadskas, E.K., (2006) The MOORA method and its application to privatization in a transition economy, Control and Cybernetics, vol 35, no 2, pp 445-469.

[46] Paydar, M.M., Arabsheybani, A. Safaei, AA, (2017) Sustainable supplier selection and order allocation problem using FMEA and fuzzy MOORA, International Journal of Industrial Engineering & Production Research, March, vol 28, no 1, pp 47-59.

[47] Vatansever, K., Uluköy, M., (2013) Kurumsal Kaynak Planlaması Sistemlerinin Bulanık AHP ve Bulanık MOORA yöntemleriyle seçimi: Üretim sektöründe bir uygulama, Celal Bayar Üniversitesi Sosyal Bilimler Dergisi, vol 11, no 2.

[48] Uygurtürk, H., (2015) Bankaların internet şubelerinin Bulanık MOORA yöntemi ile değerlendirilmesi, Uluslararası Yönetim İktisat ve İşletme Dergisi, vol 11, no 25.

Erzincan Üniversitesi
Fen Bilimleri Enstitüsü Dergisi
2024, 17(1), 37-43
ISSN: 1307-9085, e-ISSN: 2149-4584
Araştırma Makalesi

Erzincan University
Journal of Science and Technology
2024, 17(1), 37-43
DOI: 10.18185/erzifbed.1251658
Research Article

On τ-Discrete Modules

Burcu NİŞANCI TÜRKMEN [1*] and Ergül TÜRKMEN [2]

[1, 2]Departments of Mathematics, Faculty of Science and Arts, Amasya University, Amasya, Turkey

Received: 15/02/2023, **Revised:** 12/01/2024, **Accepted:** 12/01/2024, **Published:** 28/03/2024

Abstract

An R-module M is said to be *(quasi) τ-discrete* if M is τ-lifting and has the property (D_2) (respectively, has the property (D_3)), where τ is a preradical in $R-mod$. It is shown that: (1) direct summands of a (quasi) τ-discrete module are (quasi) τ-discrete; (2) a projective module M is τ-discrete if and only if $\frac{M}{\tau(M)}$ is semisimple and $\tau(M)$ is QSL; (3) if a projective module M is *Soc-lifting,* then $\frac{M}{Soc(M)}$ is *Soc-discrete* and $Rad(\frac{M}{Soc(M)})$ is semisimple.

Keywords: preradical, τ-lifting module, (quasi) τ-discrete module.

τ-Ayrık Modüller Üzerine

Öz

τ tüm sol R-modüllerin kategorisinde öncül radikal olmak üzere τ-yükseltilebilir ve (D_2) özelliğini sağlayan (sırasıyla, (D_3) özelliğini sağlayan) bir R-modülü M'e *(ayrık) τ-ayrık* denir. Şu gösterilmiştir: (1) Bir (quasi) τ-ayrık modülün her direkt toplam terimi (quasi) τ-ayrıktır; (2) bir projektif M modülünün τ-ayrık olması için gerek ve yeter koşul $\frac{M}{\tau(M)}$ nin yarıbasit ve $\tau(M)$ nin QSL olmasıdır; (3) bir projektif M modülü Soc-yükseltilebilirse, $\frac{M}{Soc(M)}$ Soc-ayrıktır ve $Rad(\frac{M}{Soc(M)})$ yarıbasittir.

Anahtar Kelimeler: öncül radikal, τ-yükseltilebilir modül, (yarı) τ-ayrık modül.

*Corresponding Author: burcu.turkmen@amasya.edu.tr
Burcu NİŞANCI TÜRKMEN, https://orcid.org/0000-0001-7900-0529
Ergül TÜRKMEN, https://orcid.org/0000-0002-7082-1176

1. Introduction

In our article, all rings are associative with identity and all modules are unity left modules over these rings. For a ring R, $R-mod$ denotes the category of all left R-modules. A submodule N of a module M will be denoted by $N \leq M$. A nonzero $E \leq M$ is called *essential* in M and written by $E \trianglelefteq M$ if $E \cap F \neq 0$ for every nonzero submodule F of M. We call a module M *extending* if it satisfies (C_1), that is, its submodules are essential in a direct summand of M as in [5].

We call an extending module M *continuous* if it satisfies (C_2), that is, every submodule isomorphic to a direct summand of M is a direct summand as in [5].

We call an extending module M *quasi continuous* if it satisfies (C_3), that is, whenever $M = A \oplus B = C \oplus D$ and $A \cap C = 0$, M has a decomposition $M = (A \oplus C) \oplus E$ as in [5] Since a module M with (C_2) has the property (C_3) every continuous module is quasi continuous. Injective modules are an example of a continuous module.

As a dual notation of an essential submodule of A, one call a proper submodule S of A *small* in M and denoted by $S \ll M$ if $S+X$ is not M for every proper submodule $X<M$. With the notation of immediately extending modules, lifting modules are defined as: M is *lifting* if it satisfies

(D_1) For any $A \leq M$, we can write $M = A_1 \oplus L$, $A_1 \leq A$ and $A \cap L \ll L$ for submodules A_1, L of M.

We call a lifting module M *quasi-discrete* if it satisfies

(D_2) If $A \leq M$ with $\frac{M}{A} \cong B$ and $M = B \oplus C$, we can write $M = A \oplus A'$.

We call a lifting module M *discrete* if it satisfies

(D_3) Whenever $M = A \oplus B$, $M = C \oplus D$ and $M = A + C$, M has a decomposition $M = (A \cap C) \oplus E$.

The modules that provide quasi-projective and the property (D_2) are coincide. Since a module M with (D_2) provides (D_3), quasi-discrete modules are a generalization of discrete modules. It is obvious that (quasi) discrete modules are a dual notion of (quasi) continuous modules. Although injective modules are continuous, a projective module usually does not have to be discrete. Hollow modules (that is, its proper submodules are small) are quasi-discrete. The family of (quasi-) discrete modules are extensively studied by researchers. A module M has the property P^* if for every submodule A of M M has the decomposition $M = A' \oplus B$ such that $A' \leq A$ and $\frac{A}{A'} \leq Rad(\frac{M}{A'})$ for some submodules A' and B of M. Every lifting module has the property P^*. Also, a finitely generated module with the property P^* is lifting. In general, a module with the property P^* need not be lifting. For example, consider the left $\mathbb{Z}$-module $M = {}_{\mathbb{Z}}\mathbb{Q}$. Since radical modules have the property P^*, M has the property P^*. On the other hand, M is not lifting.

In recent years, types of lifting modules have been defined and studied in $R-mod$ with the help of preradicals. A functor τ from the category $R-mod$ to itself is said to be *preradical* if it provides the following properties:

(1) $\tau(M) \leq M$, where $M \in R-mod$;
(2) If $f: M \longrightarrow M'$ is homomorphism, then $f(\tau(M)) \subseteq \tau(M)$ and $\tau(f)$ is the restriction of to $\tau(M')$.

A preradical τ for $R-mod$ is called *exact* if for $N \leq M$ $\tau(N) = N \cap \tau(M)$, and it is called *radical* if $\tau\left(\frac{M}{\tau(M)}\right) = 0$.

Rad(M) and *Soc(M)* denote the radical, socle of a module *M*, respectively. *Rad* and δ are radical in $R-mod$, and *Soc* is an exact preradical in $R-mod$.

Let τ be a preradical in $R-mod$. Following [1, 2.8 and 2.9], we call *M* τ*-lifting* if for any $N \leq M$, we can write $M = A \oplus B$ with $A \subseteq N$ and $N \cap B \leq \tau(B)$ for *A, B* $\leq M$. In [1], for $\tau = Rad$, *M* is Rad-lifting if and only if *M* has the property P^*. Lifting modules are an example of *Rad*-lifting modules. It is shown in [1, 2.10 (2)] that whenever $M = A \oplus B$ is a τ-lifting module, so does *A*.

2. Preliminaries

Let *R* be a ring and τ be a preradical in $R-mod$. In our study, we introduce the concept of (quasi) τ-discrete modules. We obtain some properties of such modules. In particular, we show that direct summands of a (quasi) τ-discrete module are (quasi) τ-discrete. Moreover, we prove that a projective module *M* is τ-discrete if and only if $\frac{M}{\tau(M)}$ is semisimple and $\tau(M)$ is QSL. Also, we show that if a projective module *M* is *Soc-lifting,* $\frac{M}{Soc(M)}$ is *Soc-discrete* and $Rad(\frac{M}{Soc(M)})$ is semisimple.

3. Main Theorem and Proof

In this section, we study on (quasi) τ-discrete modules.

Definition 3.1 A module *M* is called τ*-discrete* (respectively, *quasi* τ*-discrete*) if *M* is τ-lifting with (D_2) (respectively, (D_3)).

Theorem 3.2 Given a (quasi) τ-discrete module $M = N \oplus N'$. Then *N* is (quasi) discrete.

Proof. By [9, 2.10.(2)], we obtain that *N* is τ-lifting. Hence *N* is (quasi) τ-discrete by [5, Lemma 4.6].

Given modules $U \leq X$. In [6], *U* is said to be *strongly lifting* in *X* provided whenever $\frac{X}{U} = \frac{A+U}{U} \oplus \frac{B+U}{U}$, we can write $M = Z \oplus T$ where $Z \subseteq A$, $\frac{A+U}{U} = \frac{Z+U}{U}$ and $\frac{B+U}{U} = \frac{T+U}{U}$. Alkan [3] generalizes the definition; *U* is called *quasi strongly lifting (QSL)* in *X* if whenever $\frac{X}{U} = \frac{A+U}{U} \oplus \frac{C}{U}$, we can write $X = Z \oplus T$, $Z \subseteq A$ and $Z + U = A + U$. Observe from [3, Lemma 3.5] that if a

module M is τ-lifting, then $\tau(M)$ is *QSL*. Using this fact we obtain that a characterization of (quasi) τ-discrete modules.

Proposition 3.3 Let M be a module with (D_2) (respectively, (D_3)). Then the following statements are equivalent:

(1) it is (quasi) τ-discrete,
(2) it is τ-supplemented and $\tau(M)$ is QSL.
(3) $\frac{M}{\tau(M)}$ is semisimple with *QSL* $\tau(M)$.

Proof. By Lemma 3.5 and Proposition 3.6 in [3].

Corollary 3.4 A projective module M is τ-discrete if and only if $\frac{M}{\tau(M)}$ is semisimple and τ(M) is QSL.

Proof. Since projective modules are (D_2), it follows from Proposition 3.3.

Given a module E. We call *E (quasi) Rad-discrete* if E has the property P^* and (D_2) (respectively, has the property P^* and (D_3)) as in [7].

Lemma 3.5 A projective M is Rad-discrete if and only if M is semilocal and $Rad(M)$ is QSL.

Proof. The proof follows from Corollary 3.4.

Theorem 3.6 The following statements are equivalent for a ring R:

(1) R is semiperfect;
(2) R is Rad-discrete;
(3) R has the property (P^*);
(4) R is Rad-⊕-supplemented;
(5) R is semilocal and $Rad(R)$ is QSL.

Proof. (1)⇒(2)⇒(3)⇒(4)⇒(1) By [7, Corollary 2.10].

(1)⇔(5) It follows from Corollary 3.4.

Follows from [6, Theorem 10], the socle Soc($_RR$) of a ring R is strongly lifting. Using this fact we characterize Soc-discrete rings in the following.

Proposition 3.7 A ring R is Soc-discrete if and only if $\frac{R}{Soc(_RR)}$ is semisimple.

Proof. By Corollary 3.4 and [6, Theorem 10].

Given a module E. We call *E τ-torsion free* if $\tau(E) = 0$.

Proposition 3.8 Let M be a τ-torsion free module. If it is quasi τ-discrete, it is semisimple.

Proof. Let $N \leq M$. By assumption, we can write $M = A \oplus B$ with $A \leq N$ and $N \cap B \subseteq \tau(B)$. Since M is τ-torsion free, we can write $N \cap B \subseteq \tau(B) \subseteq \tau(M) = 0$ and so $N = N \cap B = A \oplus (N \cap B) = A$, as required.

Recall from [2] that a submodule Z of a module E is *a τ–supplement* of some submodule $T \leq M$ provided $Z+T$ is M and $Z \cap T \subseteq \tau(Z)$.

Theorem 3.9 Let τ be an exact preradical and let M be a τ-lifting module and V be τ-supplement in M. Then V is τ-lifting.

Proof. Let $N \leq V$. Since M is τ-lifting, we can write $M = A \oplus B$, $A \leq N$ and $N \cap B \subseteq \tau(B)$. By the modularity, we can write V *is* $A \oplus (V \cap B)$, and clearly, $N \cap (V \cap B) = N \cap B \subseteq \tau(B)$. Since τ is an exact preradical in R-Mod, we can write $\tau(V \cap B)$ is $V \cap \tau(B)$. Now $N \cap B \subseteq V \cap \tau(B)$ is $\tau(V \cap B)$. It means that V is τ-lifting.

Corollary 3.10 Let τ be an exact preradical in $R - Mod$ and M be a uniform R-module. If M is τ-lifting, then every τ-supplement submodule V of M is quasi τ-discrete.

Proof. By Theorem 3.9, we obtain that V is τ-lifting. Since uniform modules have the property (D_3), we get that V is quasi τ-discrete.

Proposition 3.10 Let τ be a radical in $R - Mod$ and M be a (quasi) τ-discrete module with small $\tau(M)$. Then $\tau(M) = Rad(M)$ and it is (quasi) discrete.

Proof. By [2, 2.10 (1)], we obtain that $Rad(M) \subseteq \tau(M)$. Since $\tau(M) \ll M$, $\tau(M) = Rad(M)$ is small in M. So M is lifting. Hence it is (quasi) discrete.

A module E is called *τ-torsion* if $E=\tau(E)$. For example, semisimple modules are Soc-torsion, radical modules are Rad-torsion, and projective semisimple modules are δ-torsion.

Lemma 3.11 Suppose that M is a τ-lifting module. If $N \leq M$ is τ-torsion, $\frac{M}{N}$ is τ-lifting.

Proof. Let $N \leq A \leq M$. Then we can write $M = A' \oplus B$, $A' \leq A$ and $A \cap B \subseteq \tau(B)$ for submodules $A', B \leq M$. It follows that $\frac{M}{N} = \frac{A'+N}{N} + \frac{B+N}{N}$ and $\frac{A \cap B+N}{N} \subseteq \tau(\frac{B+N}{N})$. Since N is τ-torsion, we can write $\left(\frac{A'+N}{N}\right) \cap \left(\frac{B+N}{N}\right) = 0$. Thus $\frac{M}{N}$ is τ-lifting.

Theorem 3.12 Suppose that N is a τ-torsion submodule of a projective module M. If M is τ-lifting, $\frac{M}{N}$ is τ-discrete.

Proof. Since M is a projective module and N is τ-torsion, $\frac{M}{N}$ has the property (D_2). Applying Lemma 3.11, we deduce that $\frac{M}{N}$ is τ-discrete.

Corollary 3.13 If M is a projective and Soc-lifting module, then $\frac{M}{Soc(M)}$ is Soc-discrete and its radical is semisimple.

Proof. Following Theorem 3.12, we get that $\frac{M}{Soc(M)}$ is Soc-discrete. Also, applying [2, 2.10 (1)], $Rad(\frac{M}{Soc(M)})$ is semisimple. This completes the proof.

4. Conclusion

In this article, we introduce the concept of (quasi) τ-discrete modules and investigate the basic properties of these modules by preradicals in $R-mod$, where R is an associative ring with identity. We characterize projective τ-discrete modules. We show that if a module is τ-lifting, then its factor modules by τ-torsion submodules are τ-lifting. We prove that if a projective module M is *Soc*-lifting, then $\frac{M}{Soc(M)}$ is Soc-discrete and its radical is semisimple

Ethics in Publishing

There are no ethical issues regarding the publication of this study.

Author Contributions

All authors have investigated and studied no the published version of the manuscript.

Acknowledgments

We would like to thank the referees for the valuable suggestions and comments which improved the revision of the paper.

References

[1] Al-Khazzi, I., and Smith, P.F., (1991) Modules with chain conditions on superfluous submodules, Communications in Algebra, Vol. 19(8), pp. 2331-2351.

[2] Al-Takhman, K., Lomp, C. and Wisbauer, R. (2006) τ-complement and τ-supplement submodules, Algebra and Discrete Mathematics, 3, 1-15.

[3] Alkan, M. (2009) On τ-lifting modules and τ-semiperfect modules, Turkish Journal of Mathematics, 33(2), 117-130.

[4] Büyükaşık, E., Mermut, E. and Özdemir, S. (2010) Rad-supplemented modules, Rendiconti del Seminario Matematico della Universita di Padova, 124, 157-177.

[5] Mohamed S.H. and Müller, B.J. (1990) Continuous and Discrete Modules", London Mathematical Society, LNS 147 Cambridge University Press, Cambridge.

[6] Nicholson, W.K. and Zhou, Y. (2005) Strongly lifting, Journal of Algebra, 285, 795-818.

[7] Nişancı Türkmen, B., Ökten, H.H. and Türkmen, E. (2021) Rad-discrete Modules, Bulletin of the Iranian Mathematical Society, 47, 91-100.

[8] Türkmen, E. (2013) Rad-⊕-supplemented modules", Analele Stiintifice ale Universitatii Ovidius Constanta Seria Mathematica, 21 (1), 225-238.

[9] Wisbauer, R. (1991) Foundations of Module and Ring Theory (A handbook for study and research)", Gordon and Breach Science Publishers.

Erzincan Üniversitesi
Fen Bilimleri Enstitüsü Dergisi
2024, 17(1), 44-54
ISSN: 1307-9085, e-ISSN: 2149-4584
Araştırma Makalesi

Erzincan University
Journal of Science and Technology
2024, 17(1), 44-54
DOI: 10.18185/erzifbed.1261211
Research Article

Investigation of the Effect of Zoning Peace on Construction in Plateau and Rangeland

Alper AKAR[1*], Özlem AKAR[1], H. Ferit BAYATA[2]

[1]Department of Architecture and Urban Planning, Vocational School, Erzincan Binali Yıldırım University, Yalnızbağ Campus, 24002 Erzincan, Turkey

[2]Department of Civil Engineering, Faculty of Engineering and Architecture, Erzincan Binali Yıldırım University, Yalnızbağ Campus, 24002 Erzincan, Turkey

Received: 06/03/2023, **Revised:** 11/09/2023, **Accepted:** 11/09/2023, **Published:** 28/03/2024

Abstract

Rangelands and plateaus typically have naturally occurring plant groups. The estimates reveal that rangeland ecosystems cover approximately 50% of the planet's land and provide most of the forage requirements of the world's animal population. In this study, we aim to investigate the impact of Law No. 7143, also known as the Zoning Peace among the People, which entered into force in 2018, on potential illegal buildings in rangeland and plateau areas. As the study area, we chose the plateau and rangeland areas of the Akçaabat district of Trabzon province. We identified illegal buildings in the study areas using Google Earth Pro software satellite images and Triplesat satellite images. We examined 16 plateaus, and as a result of our determinations, we observed that a total of 83 new buildings were constructed during this time, with 33 in the first study area and 50 in the second. The results showed that illegal construction continues in some places, the inspection process is inefficient, and the Zoning Peace Law encourages this.

Keywords: Rangeland, Plateaus, Illegal building, Triplesat, Zoning Peace

İmar Barışının Mera ve Yayla Alanlarındaki Yapılaşmaya Etkisinin İncelenmesi

Öz

Yayla ve meralar genellikle doğal yollarla oluşan bitki topluluklarıdır. Yapılan tahmini hesaplamalara göre, mera ekosistemleri dünya topraklarının yaklaşık %50' sini kapsamakta ve dünyadaki hayvanların yem ihtiyacının büyük bir kısmını karşılamaktadır. Yapılan çalışma ile, 2018 yılında yürürlüğe giren ve halk arasında imar barışı olarak adlandırılın 7143 sayılı yasanın, mera ve yayla alanlarında oluşabilecek kaçak yapılaşmaya olan etkisi araştırılmıştır. Çalışma alanı olarak Trabzon ili Akçaabat ilçesi sınırları içerisinde yer alan mera ve yaylalar seçilmiştir. Çalışmada Google Earth Pro programından elde edilen uydu görüntüleri ile Triplesat uydu görüntüleri kullanılarak zaman içerisinde meydana gelen kontrolsüz yapılaşma tespit edilmiştir. 1. çalışma bölgesinde 33 ve 2. çalışma bölgesinde 50 olmak üzere toplam 83 yeni yapının bu süre içerisinde yapıldığı belirlenmiştir. Elde edilen sonuçlar halen bu alanlarda kaçak yapılaşmanın devam ettiğini, denetlenme sürecinin hızlı ve etkili bir suretle yapılamadığını ve çıkarılan bu af niteliğindeki yasaların kaçak yapılaşmayı teşvik ettiğini göstermektedir.

Anahtar Kelimeler: Mera, Yayla, Kaçak Yapılaşma, Triplesat, İmar Barışı

*Corresponding Author: alperakar24@gmail.com
Alper AKAR, https://orcid.org/0000-0003-4284-5928
Özlem AKAR, https://orcid.org/0000-0001-6381-4907
Halim Ferit BAYATA, https://orcid.org/0000-0001-8274-8888

1. Introduction

Perennial herbaceous plant communities that are generally formed naturally are called rangeland and plateaus [1]. According to estimated calculations, rangeland ecosystems constitute approximately 50% of the world's land [2], and meet 70% of the forage requirements of in the world [3]. In our country, rangeland ecosystems meet 30% of the forage need used in animal nutrition [4]. The Rangeland Law (No. 4342 enacted on 28.02.1998) defines plateaus as a place allocated for farmers to spend the summer with their animals, graze their animals, and benefit from grass [5]. Plateaus in mountainous areas are areas where nomadic and semi-nomadic, and villagers do animal husbandry [6]. Those who dealt with animal husbandry in the past mostly used plateaus and rangeland. However, because of the decline in the population who depend on livestock for a living and the rising demand for tourism in these areas, these locations are now also used for temporary or seasonal settlements for recreational activities in addition to animal husbandry [6, 7, 8]. In recent years, it has been observed that there are many illegal buildings used as housing and tourism facilities in the plateaus [9].

The first development that is thought to affect the change in rangeland and plateau areas is the Green Road Tourism Project. In order to meet the increasing tourism demands, the Green Road Tourism Project, which connects the plateaus of eight provinces in the Eastern Black Sea Region, was implemented in 2013. With this project, transportation to the plateau and rangeland areas has become easier, and the use of these areas has increased [10].

Another development that is thought to have impacted the plateau areas is law no.7143, which is known as the Zoning Peace and entered into force in 2018. This law covers illegal structures created before December 2017. Taking the statement of those who want to benefit from the law as a basis has encouraged illegal construction. Especially in the plateaus of the Black Sea Region, it has been seen that illegal building for housing and commercial use is more common, and the people who cause this illegal construction apply to obtain a building registration certificate [11, 12]. As a result, it is thought that illegal construction in the plateaus has increased significantly with the law enacted.

In this study, we aimed to determine the change in illegal buildings in the plateau and rangeland areas between the enactment of Law No. 7143 and the end of the process. As the study area, we selected 16 plateaus located within the borders of the Akçaabat district of Trabzon province. In the study, we detected the change over time using Triplesat satellite images and satellite images in the Google Earth Pro software. As a result of this change detection, we examined the effect of this law on the uncontrolled building.

1.1. Legal regulations about plateaus and the effects of these regulations

The use of plateaus for tourism purposes in Turkey started in 1990 with the encouragement of the state. In this sense, 12 plateaus in the Eastern Black Sea Region have been declared as tourism centers by the Ministry of Tourism to attract investors to the plateaus. Giresun-Bektaş, Çaykara-Uzungol, Akçaabat-Karadağ, and Tonya-Erikbeli plateaus are the plateaus declared as

tourism centers [13]. Within the scope of the Tourism Encouragement Law, the number of plateaus declared as tourism centers increased to 21 as of 2019, 18 of which are located in the Black Sea Region [14].

The "Green Road" Project carried out by the Eastern Black Sea Regional Development Administration started in 2013. The project aims to connect the important plateaus and tourism centers of 8 provinces (Artvin, Bayburt, Giresun, Gümüşhane, Ordu, Rize, Samsun, Trabzon) in the Black Sea Region [15]. In addition, the project aimed to expand the tourism demand in the plateaus over a wider period of time, to offer more alternatives to the tourists coming to the region by connecting the plateaus to each other, to facilitate the transportation opportunities of the local people who are engaged in transhumance, and to increase their income levels with the newly created road networks [10].

Today, more than 50% of the country in general consists of structures that are against zoning, which corresponds to approximately 13 million independent sections. This situation leads to many legal disputes between the citizen and the state [16]. It is seen that legalization policies are continuing in our country to find a solution to the problem of informal construction [17, 18, 19]. It is seen that the laws that came into force in our country from 1948 to 2018 include provisions to register illegal structures on urban and rural lands [10]. Unfortunately, a definite solution to urbanization problems has not been produced yet. Over time, various amnesties have been issued to solve the problem of unplanned urbanization. It has been observed that these amnesties have not had the desired effect and have instead encouraged unauthorized construction [20].

The law, which was accepted on 11.05.2018 and called "zoning peace" by the public, entered into force [21]. The implementation of Zoning Peace can be defined as the registration of buildings that are unlicensed, contrary to the license and its annexes, or that do not comply with the zoning legislation, by issuing a building registration document [22]. The implementation of the zoning peace included the buildings built before 31.12.2017. Applications were made to the Ministry of Environment and Urbanization and institutions and organizations authorized by this ministry until 31.10.2018. Building registration documents of those who paid the registration fee until 31.12.2018 were issued and the buildings were registered in the land registry [10, 21, 23].

Moreover, with the Building Registration Certificate, it has become possible to carry out the registration procedures in the land registry. In addition, unauthorized structures on treasury lands have gained the right to apply for a Building Registration Certificate. The Building Registration Certificate provides the owners of unauthorized buildings with the opportunity to stop the previous demolition decisions for their buildings, cancel the fines, benefit from infrastructure services such as electricity and natural gas, and provide property assurance through registration to the land registry [10, 21]. The deadline for obtaining the Building Registration Certificate, which was determined as 31.10.2018, has been extended twice and updated to 15.06.2019 [21]. Finally, it was announced that 10.250.000 citizens applied to benefit from zoning peace until 15.06.2019 [23]. The last payment date of the fee to be paid to

obtain the building registration certificate has been extended until 31.12.2019. Building Registration Certificate applications were made based on the declarations of the unauthorized building owners through the e-Government application. After the payment of the Building Registration Certificate price calculated during the application, the Building Registration Certificate was prepared and given to the beneficiaries.

The main purpose of the enacted law has been described as registering and legalizing illegal uses. In addition, one of the main goals has been to produce the economic resource needed for urban transformation projects [22]. According to the official data of the Ministry of Environment and Urbanization, as of 16.11.2020, 7.280.457 Building Registration Certificates have been received throughout Turkey within the scope of the Zoning Peace. Since the updating and cancellation processes of the building registration documents continue, there are changes in the specified number [21]. As can be understood from the number of building registration certificates received, many unregistered buildings have become legal by obtaining a building registration certificate. The Reconstruction Peace arrangement, which came into force, created a new construction opportunity and caused real people to perceive this arrangement as if it would produce more buildings [11]. We may deduce that the inhabitants of the plateau who construct houses surround the areas where their structures are located and have expectations from potential future legislation from the analysis of satellite images obtained by remote sensing technology and from field observations [9].

2. Material and Methods

In the study, the effect of the law, which is called "zoning peace" in the public, on the illegal construction in the rangelands and plateaus areas within the borders of the Akçaabat district of Trabzon province was investigated. In the study, the examination of the changes in rangelands and plateaus on satellite images covering an area of approximately 9000 hectares was considered as 2 separate study areas.. In the first study area, Balıklı, Hıdırnebi, Karadağ, Kuruçam and Livera plateaus are located, while in the second study area, Bela, Büyükhanzar, Büyükoba, Enginoba, İskobel, İskotinoz, Karaağaç, Kurtkayası, Limanoba, Ortahanzar, and Simba plateaus are located (Figure 1).

Because they are frequently used by residents of the city center and other provinces in the summer, these plateaus were chosen as the site for the study. Triplesat-2 satellite images (multispectral (MS) and panchromatic (PAN)) from July 2017 and RGB satellite images from July 2019 in Google Earth Pro were used in the study. The MS band of Triplesat-2 with 3.2m spatial resolution has 4 bands (red, green, blue, near infrared), while the PAN band has a spatial resolution of 0.8 m. Radiometric and atmospheric of the Triplesat-2 (MS and PAN) images were carried out by the NIK Construction Trade Ltd – NIK System from which the images were provided. The geometric correction of the images (MS and PAN) images was performed with sub-pixel accuracy using 42 Ground Control Points (GCPs) selected to be homogeneously distributed over the image coordinated Continuously Operating Reference Stations- Türkiye (CORS-TR) GPS method in the field. Other RGB images were then registered with the Triplesat-2 PAN image.

In the next stage, structures of different years were manually digitized in ArcGIS software using Triplesat (MS and PAN) images and RGB images. As a result, vector building layers were produced. Following this, the areas and numbers of the structures built in different years were calculated in the ArcGIS software. Finally, using the data, the changes in the plateau areas over time were determined.

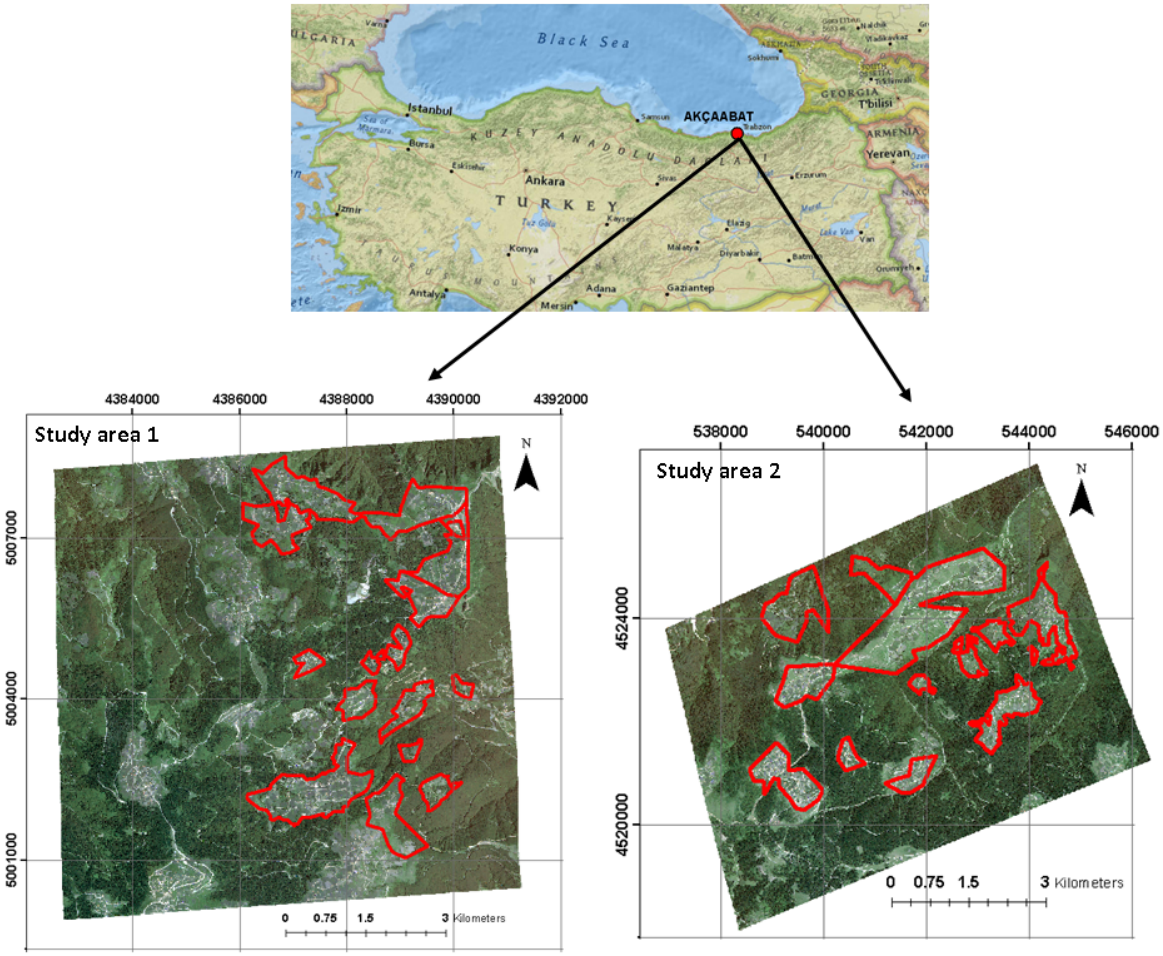

Figure 1. Study areas

3. Results and Discussion

In the study, the effect of the law, which was accepted on 11.05.2018 and called "zoning peace" in the public, on the change in the plateau and plateau areas was examined. As per the law, the building registration certificate is given to the buildings constructed before 31.12.2017. For this reason, the change made between this date and the deadline of 15.06.2019 to benefit from the zoning peace has been determined. The variation was determined using Triplesat satellite images from 2017 and satellite images from the Google Earth Pro program.

3.1. Change Detection Analysis for Study Area 1

According to the results of the change analysis shown in Table 1 for study area 1, it was observed that the number of buildings in Balıklı Plateau increased by 307 in 2017 and increased by 10 in 2019 to 317. The average building area for these years was 102 m^2 (Table 1). Hıdırnebi Plateau is a highly preferred plateau in the region for both animal husbandry and tourism purposes. When the data is analyzed, the number of buildings in this plateau was determined as 239 in 2017 and 244 in 2019. It was observed that the average building area was 103 m^2. The results of the change in Karadağ Plateau show that the number of buildings was 275 in 2017 and 289 in 2019. The average building area was calculated as 118 m^2. When the change in the Kuruçam plateau was examined, it has seen that this plateau is one of the preferred plateaus for settlement purposes. The number of buildings was determined as 238 in 2017 and 242 in 2019. When the building areas average was examined, it has been determined that the average of the building areas in 2017 and 2019 was 106m^2. Finally, the analyses on the Livera plateau led to the conclusion that the number of structures will stay at 15 in both 2017 and 2019. The building areas average was estimated to be 94 m^2.

Table 1. Change in the number of buildings and building areas average for the Study Area 1

Plateau	Plateau Areas (m^2)	Building Areas (m^2)		Number of Buildings		Building Areas Average (m^2)	
		2017	2019	2017	2019	2017	2019
Balıklı	529854	31428	32483	307	317	102	102
Hıdırnebi	517458	24867	25242	239	244	104	103
Karadağ	1946883	32337	33462	275	289	118	116
Kuruçam	539658	25268	25612	238	242	106	106
Livera	54019	1417	1417	15	15	94	94

3.2. Change Detection Analysis for Study Area 2

According to the results of the change analysis shown in Table 2 for study area 2, it was seen that the Bela plateau was not a region that was used as a residential area more than the other plateaus in the region. According to the analysis, it was determined that the number of buildings, which was 13 in 2017, was 19 in 2019. It was also possible to say that the building area average on the plateau was 75 m^2. Büyükhanzar plateau is similar to the Bela plateau in terms of usage as a residential area. The number of buildings was determined as 33 in 2017 and 34 in 2019. It has been observed that the building area average in the plateau was 82 m^2 and generally similar buildings were built. In 2017, 196 buildings were found to be present on the Büyükoba plateau. By 2019, there were 206 buildings, an increase of 10. The building area

average was estimated to be 101 m^2. The average building area has demonstrated to us that the homes constructed on the plateau are not intended for short-term habitation but rather for long-term habitation. The Enginoba plateau is one of the most popular plateaus for the construction of permanent buildings, according to the data. In 2017, there were estimated to be 217 buildings, with a building area average of 103 m^2. There were 223 buildings in existence in 2019, and it was noted that the building area average over the previous time period remained unchanged. Considering the number of buildings, it is understood that the İskobel plateau is one of the most preferred plateaus in terms of settlement. The number of buildings, which was determined as 346 in 2017, became 354 in 2019, and it was observed that there was no change in the average building's areas and which was approximately 109 m^2. When the change analysis made in the İskotinoz plateau was examined, the number of buildings was determined as 69 in 2017, and 76 in 2019. The building area average was detected as 91 m^2. According to the results of the change analysis in the Karaağaç plateau, the number of buildings has been determined as 203 in 2017, and 207 in 2019 with an increase of 4 units. However, when the building areas were examined, it has been seen that the building area average was 91 m^2 and it was built as a permanent building. In the Kurtkayası plateau, it was determined that the number of buildings in 2017 and 2019 was 28. It has been determined that the building area average was 113 m^2. The Limanoba plateau was found to be less frequently settled than other plateaus when the evaluation of the results was done. In 2017, there were 103 buildings, and in 2019, there will be 107 structures, according to calculations. The building areas average between 2017 and 2019 was 93 m^2, according to the analysis of the building areas. The examination conducted on the Ortahanzar plateau led to the conclusion that the number of buildings remained constant between 2017 and 2019 at 40. The building areas average was found to be 108 m^2, and they were constructed as permanent buildings, even though the total number of buildings remained constant. Finally, 131 buildings were there on Simba Plateau in 2017; 135 were there in 2019. Between 2017 and 2019, the building's areas average was determined to be 136 m^2.

Change analyzes were made in ArcGIS software for 16 plateaus, and the structuring over the years was determined in this way. As an illustration, Figure 2 shows the construction of the Büyükoba plateau in 2017 and 2019.

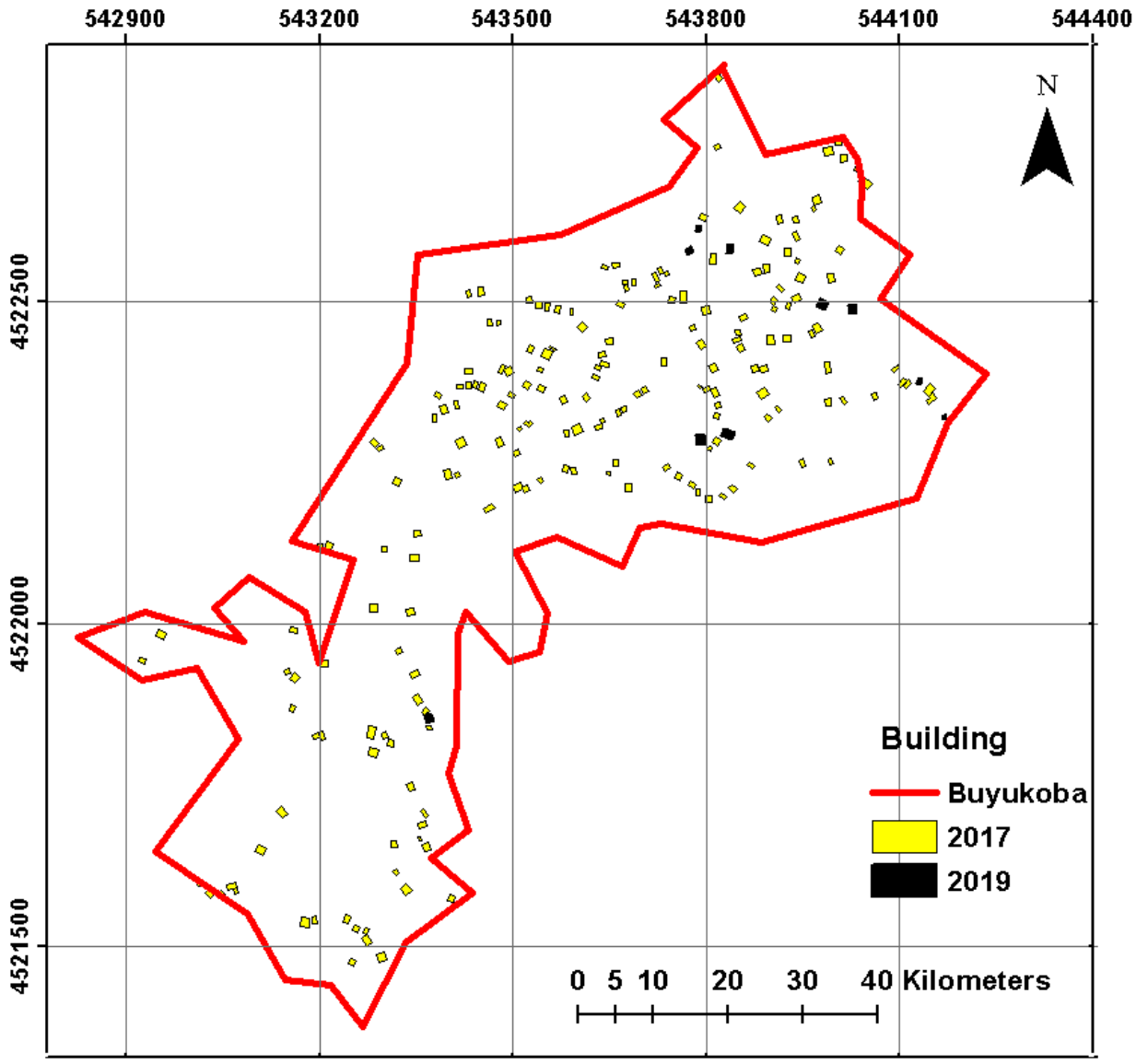

Figure 2. Change analysis for Büyükoba plateaus

Change analysis results for study area 2 are shown in Table 2.

Table 2. Change in the number of buildings and building areas average for the Study Area 2

Plateau	Plateau Areas (m^2)	Building Areas (m^2)		Number of Buildings		Building Areas Average (m^2)	
		2017	2019	2017	2019	2017	2019
Bela	480643	976	1446	13	19	75	76
Büyükhanzar	101892	2721	2769	33	34	82	81
Büyükoba	719644	19844	21047	196	206	101	102
Enginoba	622300	22268	23033	217	223	103	103
İskobel	821134	37704	38755	346	354	109	109
İskotinoz	310129	6255	6811	69	76	91	90
Karaağaç	3147997	18383	18806	203	207	91	91
Kurtkayası	220965	3154	3154	28	28	113	113
Limanoba	174083	9589	9904	103	107	93	93
Ortahanzar	234007	4302	4302	40	40	108	108
Simba	978302	17786	18294	131	135	136	136

4. Conclusion

In Turkey, in the past, rangeland and plateau areas were known as spaces used by individuals engaged in livestock farming to provide feed for their animals. However, nowadays, it is observed that these areas are predominantly utilized for tourism and recreation purposes, with unauthorized permanent buildings being constructed in these regions. The study examined the state of construction in these plateau areas between the start date of the zoning peace law and the expiration of extension periods. The results indicate that construction activity continued from the inception of the law until the conclusion of the extension period. During this timeframe, a total of 83 new buildings were identified in the study areas, with 33 buildings in the first study area and 50 in the second study area. These findings reveal that construction activities continue in these areas, the inspection process is not carried out quickly and effectively, and amnesty laws encourage further construction.

Ethics in Publishing

There are no ethical issues regarding the publication of this study.

Author Contributions

All the authors were involved in designing the study, collecting data; evaluation of results and in the writing of the article.

Acknowledgements

Triplesat satellite images have been provided by Erzincan Binali Yıldırım University Scientific Research Project [NumberFBA-2019-637] research grant.

References

[1] Altın, M., Gökkuş, A., Koç, A., (2011) Çayır ve mera yönetimi. 1st ed, (pp 376). Onur Grafik, Ankara

[2] Wang, J., Brown, D. G., Bai, Y. (2014) Investigating the spectral and ecological characteristics of grassland communities across an ecological gradient of the Inner Mongolian grasslands with in situ hyperspectral data. International Journal of Remote Sensing., 35(20), 7179– 7198.

[3] Brown, J. R., Thorpe, J. (2008) Climate change and rangelands: responding rationally to uncertainty. Rangelands., *30*(3), 3-6.

[4] Ok, H., Çaçan, E. (2023) Övündüler Köyü (Diyarbakır-Türkiye) merasının verim, botanik kompozisyonu ve otlatma kapasitesinin belirlenmesi. Artvin Çoruh Üniversitesi Orman Fakültesi Dergisi., *24*(1), 148-154.

[5] Akar, A. (2014) Mera Ve Yayla Alanlarındaki Değişimin Tespiti Ve Yeni Bir Mera Yönetim Modeli Yaklaşımı: Trabzon İli Akçaabat İlçesi Örneği. PhD Thesis. Karadeniz Technical University Graduate Institute of Natural and Applied Sciences.

[6] Somuncu, M. (2007) Kırsal ve Kentsel Alanlardaki Sosyoekonomik Değisime Bağlı Olarak Türkiye Yaylalarının Fonksiyonlarındaki Farklılasma. Paper presented at the 38 th International Congress of Asian and North African Studies.

[7] Başer, V. (2019) Yaylalardaki Arazi Kullanım Değişiminin Coğrafi Bilgi Sistemi İle Analizi: Giresun Örneği. BEÜ Fen Bilimleri Dergisi., *8*(1), 167-175.

[8] Somuncu, M. (2010) The Dilemma in Turkish highlands: preservation of natural and cultural heritage and tourism development – A case study of the Eastern Black Sea Region. Paper presented at the 2nd International Conference on Heritage and Sustainable Development, 1, 431-440.

[9] İban, M. C., Kılıç, M. E. (2022) Yayla Alanlarında Yapılaşmanın İncelenmesi: Bolu Atyaylası Örneği. Kahramanmaras Sutcu Imam University Journal of Engineering Sciences, *25*(3), 249-258.

[10] Döner, F. (2021) Yayla alanlarındaki yapılaşma değişiminin incelenmesi: Gümüşhane örneği. Gümüşhane Üniversitesi Fen Bilimleri Enstitüsü Dergisi., *11*(3), 721-728.

[11] İban, M. C. (2020) Lessons from approaches to informal housing and non-compliant development in Turkey: An in-depth policy analysis with a historical framework. Land Use Policy., 99, 105104. https://doi.org/10.1016/j.landusepol.2020.105104

[12] Özkaya Özlüer, I. 2018 İmar barışı düzenlemesine hukuki bir yaklaşım. İnönü Üniversitesi Hukuk Fakültesi Dergisi., *9*(2), 313–340. https://doi.org/10.21492/inuhfd.467904

[13] Bay, A. (2014) Uludağ yöresinde (Bursa) alternatif turizm türü olarak yayla turizmi. Master Thesis. Çanakkale Onsekiz Mart Üniversitesi Social Sciences Institute.

[14] https://yigm.ktb.gov. https://yigm.ktb.gov.tr/TR-11533/yayla-turizm-merkezleri.html, (20 Mayıs 2022)

[15] https://www.dokap.gov.tr/projeler/yesil-yol-projesi/1/Detay, (20 Mayıs 2022)

[16] Uşak, B., Yalçın, G. (2019) İmar Barışı Düzenlemesi Üzerine Bir İçerik Analizi. Türkiye Arazi Yönetimi Dergisi, *1*(1), 1-10.

[17] Cengiz, S., Atmiş, E., Görmüş, S. (2019) The impact of economic growth oriented development policies on landscape changes in İstanbul province in Turkey. Land Use Policy., 87, 1-12. https://doi.org/10.1016/j.landusepol.2019.104086

[18] Arslanoğlu, U. (2019) The role of spatial designer in the prestigious housing projects: the case of Ankara. Master Thesis. Middle East Technical University Graduate Institute of Natural and Applied Sciences.

[19] Gürbüztürk, A. (2017) Social housing policy and the welfare regime in Turkey: a comparative perspective. Master Thesis. Boğaziçi Üniversitesi Social Sciences Institute.

[20] Polat, Z. A., (2019) Analysis of the Regulation of "Zoning Reconciliation" in Local Governments. Planlama Dergisi, *29*(3), 202-209. DOI: 10.14744/planlama.2019.04796

[21] Çay, T., Kandemir, E. S. (2022) Türkiye'de imar uygulama mevzuatındaki gelişim süreci. Journal of Geomatics., *7*(1), 26-40.

[22] Özelmacıklı, M. H., Baz, İ. (2018) İmar Barışı'nın Getirdikleri ve Yaşanabilecek Aksaklıklar. İstanbul Ticaret Üniversitesi Teknoloji ve Uygulamalı Bilimler Dergisi., *1*(1), 65-72.

[23] Zengin, A. A., (2023) Türkiye'de Devletin Olağanüstü Taşınmaz Yönetimi ve Değerlendirmesi. Fiscaoeconomia., *7*(2), 1402-1428.

Erzincan Üniversitesi
Fen Bilimleri Enstitüsü Dergisi
2024, 17(1), 55-68
ISSN: 1307-9085, e-ISSN: 2149-4584
Araştırma Makalesi

Erzincan University
Journal of Science and Technology
2024, 17(1), 55-68
DOI: 10.18185/erzifbed.1302579
Research Article

Photocatalytic Performances of ZnS/g-C_3N_4 Nanocomposites with Different Mass Ratios

Bilge Doğan[1], Agah Oktay Özdemir[2], Bülent Çağlar[3*], Eda Keleş Güner[4]

[1] Department of Chemistry, Institute of Science and Technology, Erzincan Binali Yıldırım University, Erzincan, Türkiye
[2]Department of Design, Vocational School, Erzincan Binali Yıldırım University, Erzincan, Türkiye
[3]Department of Chemistry, Faculty of Arts and Sciences, Erzincan Binali Yıldırım University, Erzincan, Türkiye
[4]Department of Property Protection and Security, Uzumlu Vocational School, Erzincan Binali Yıldırım University, 24150 Erzincan, Türkiye

Received: 25/05/2023, **Revised:** 07/07/2023, **Accepted:** 07/07/2023, **Published:** 28/03/2024

Abstract

In this study, we prepared a series of ZnS/graphitic-C_3N_4 nanocomposites in various mass percentages and morphological properties of all the nanocomposites were examined by utilizing SEM/EDX technique. The photocatalytic performances of ZnS/graphitic-C_3N_4 nanocomposites were evaluated by degradation of Rhodamine B molecules under visible light. The photocatalytic performances of all nanocomposites under various photocatalyst dosages and initial Rhodamine B concentrations were further investigated for determination of optimal conditions. The obtained results indicated that ZnS/graphitic-C_3N_4 nanocomposites show almost 2 times higher photocatalaytic performances than pure graphitic-C_3N_4 and ZnS nanoparticles. The scavenger studies indicated that the superoxide radicals had a major role in the photodegradation and the photodegradation of Rhodamine B follows the pseudo-first-order kinetic.

Keywords: g-C_3N_4, mechanism, photocatalysis, ZnS nanoparticles

Farklı Kütle Oranlarına Sahip ZnS/g-C_3N_4 Nanokompozitlerin Fotokatalitik Performansları

Öz

Bu çalışmada, çeşitli kütle yüzdelerinde bir seri ZnS/grafit-C_3N_4 nanokompozitler hazırladık ve bütün bu nanokompozitlerin morfolojik özellikleri SEM/EDX tekniği kullanılarak incelendi. ZnS/grafitik-C_3N_4 nanokompozitlerinin fotokatalitik performansları, Rhodamine B moleküllerinin görünür ışık altında parçalanmasıyla değerlendirildi. Optimum koşulların belirlenmesi için tüm nanokompozitlerin fotokatalitik performansları çeşitli fotokatalizör miktarları ve başlangıç Rhodamine B derişimleri için incelendi. Elde edilen sonuçlar, ZnS/grafitik-C_3N_4 nanokompozitlerin saf grafitik-C_3N_4 ve ZnS nanoparçacıklarına nispeten yaklaşık 2 kat daha yüksek fotokatalitik performans gösterdiğini ortaya koymuştur. Süpürücü çalışmaları, süperoksit radikallerinin fotobozunmada önemli bir role sahip olduğunu ve Rhodamine B'nin fotobozunmasının yalancı birinci dereceden kinetiği takip ettiğini göstermiştir.

Anahtar Kelimeler: g-C_3N_4, mekanizma, fotokataliz, ZnS nanoparçacıklar

*Corresponding Author: bcaglar@erzincan.edu.tr
Bilge DOĞAN, https://orcid.org/0000-0001-7552-3461
Agah Oktay ÖZDEMİR, https://orcid.org/0000-0003-4488-746X
Bülent ÇAĞLAR, https://orcid.org/0000-0002-6087-3685
Eda KELEŞ GÜNER, https://orcid.org/0000-0002-4421-1315

1. Introduction

Increase in the utilization of hazardous dyes in industrial areas such as rubber, plastic, textile, paint, printing, pharmaceutical, leather have caused the accumulation of these toxic dye molecules in water resources, effecting aquatic life, human health and ecosystem [1-3]. Therefore, improving some influential techniques for removal of these pollutants in wastewater is important sense to the ecosystem, aquatic life and human health [4-5]. Hence, various biological, physical and chemical techniques such as filtration, adsorption, precipitation, chemical reduction and oxidation, flocculation, microbial treatment and photocatalysis have used to the wastewater purifications [6-10]. Among them, photocatalysis has been widespreadly used for the degradation of permanent dye pollutants from wastewater due to its effectively, high performance rate, simplicity, operational simplicity, low cost, stability, good reusibilty as well as being green technology [11]. To degrade dye pollutants from wastewater, reactive oxygen species like hole-electron pairs, hydroxyl and superoxide radicals are produced by irradiation of photocatalysts in photocatalysis [12]. Thereafter, generated these species degrade pollutants into nontoxic products as well as carbon dioxide, water and oxygen molecules [13]. Diverse photocatalysts such as ZnO, TiO_2, CuO and CdS semiconductors have been extensively conducted for degradation of dye molecules in [14-17]. However, these mentioned photocatalysts can be used in existence of UV irradiation because of wide band gap values, which restricted their practical photocatalysis processes under presence of visible light. Therefore, numerous research groups have improved new photocatalytic materials for the influential utilizationin photocatalysis under visible light [4,5,12,13]. Among these photocatalytic materials, graphitic carbon nitride (g-C_3N_4) has been widely attracted for the degradation of dye pollutants because of narrow band gap value, low cost, thermal stability and ability to absorb visible light [18-20]. Nevertheless, the fast electron-hole pairs recombination property of g-C_3N_4 limits photocatalytic activity [18-20]. To prevent the electron-hole pairs recombination and develop the photocatalytic performance of g-C_3N_4, coupling with proper semiconductor materials to produce heterostructure materials and nanocomposites [18-20].

In the present study, we synthesized ZnS/g-C_3N_4 nanocomposites at diffrenet mass ratios and morphological properties of these nanocomposites were examined by SEM/EDX technique. The photocatalytic performaces of the synthesized nanocomposites were investigated for degradation of RhB under visible light irradiation. The effects of initial RhB concentaration and photocatalysts dosages and kinetic of photodegration were also examined for the defination of optimal conditions. The mechanism of photocatalysis process was proposed by using various scavengers such as tert-butyl alcohol (TBA), L-ascorbic acid (LA), ethylenediaminetetraacetic acid disodium salt (EDTA) and $AgNO_3$.

2. Material and Methods

2.1. Materials

Zinc nitrate hexahydrate ($Zn(NO_3)_2.6H_2O$), melamine, thioacetamide, ethylene glycol, 2,6-Di-tert-butyl-4-methylphenol bic acid, ethylenediaminetetraacetic acid disodium salt and $AgNO_3$ were purchased from Sigma-Aldrich.

2.2. Synthesis of ZnS Nanoparticles

0.004 mol $Zn(NO_3)_2.6H_2O$ and 0.012 mol thioacetamide were separately dissolved in ethylene glycol (30 mL). Then dissolved thioacetamide solution was slowly added dropwise into the dissolved $Zn(NO_3)_2.6H_2O$ solution and stirring for 1 hour at room temperature. Then, the obtained homogeneous solution was transferred to a Teflon-coated stainless steel autoclave. The autoclave heated up 170 °C and it was kept at 170 °C for 14 hours and then naturally cooled to room temperature. The obtained solid product was filtered and washed with distilled water and ethanol three times. Then solid sample was dried at 80 °C for 12 hours and obtained an off-white powder (ZnS nanoparticles).

2.3. Synthesis of g-C_3N_4

The muffle furnace was purged with Ar gas for 10 min and then the heating rate is programmed to increase from 25 °C to 580 °C in 3 hours, to wait at 580 °C for 30 minutes and to cool in 30 minutes. After, 5 g melamine was placed in a crucible and melamine was annealed under these programmed conditions in the muffle furnace and obtained yellow powder (g-C_3N_4) was grinded in a morter.

2.4. Synthesis of ZnS/g-C_3N_4 Nanocomposites

0.004 mol $Zn(NO_3)_2.6H_2O$ was dissolved in ethylene glycol (25 mL). 390 mg of g-C_3N_4 was well dispersed in ethylene glycol (10 mL) in other beaker. The g-C_3N_4 dispersion was added into the dissolved $Zn(NO_3)_2.6H_2O$ solution and mixture was stirred under these conditions for 30 min. Then, dissolved thioacetamide in ethylene glycol (25 mL) was slowly added dropwise to the prepared mixture. After the addition was completed, the mixture was stirred at room temperature at high speed for 1 hour. The mixture was transferred to a Teflon coated stainless steel autoclave and it was kept in an autoclave at 170 °C for 14 hours and then rapidly cooled to room temperature. The obtained solid powder was filtered and washied with distilled water and ethanol three times separately. The solid sample was dried at 80 °C for 12 hours and the ZnS/g-C_3N_4 nanocomposite was obtained in a 1:1 ratio and labelled as ZnS/g-C_3N_4 1:1. ZnS/g-C_3N_4 2:1 and ZnS/g-C_3N_4 1:2 nanocomposites were synthesized by using a similar synthesis method.

2.5. Measurement of Photocatalytic Activities of Samples

The studies of photocatalytic activities of g-C_3N_4, ZnS, ZnS/g-C_3N_4 1:2, ZnS/g-C_3N_4 1:1 and ZnS/g-C_3N_4 2:1 samples were examined via photodegradation of RhB dyestuff under visible light in photoreactor (Luzchem, LZC-4X). The photocatalyts (2gL-1) and dyestuff solution (5mgL-1) were stirred without irradiation (in the dark) for 60 min to attain the adsorption/desorption equilibrium between dyestuff molecules and photocatalyts. After the adsorption/desorption equilibrium, 2mL was taken from suspension, centifureged and measured the absorbance value at 554nm for determination of initial concentration (C_0) of RhB dyestuff. Then, the mixtures were exposed to visible-light irradiation for an extented irridation time under

stirring. At determined time intervals, 2mL suspensions was extrated and centrifuged to remove the solid photocatalysts. Then dye concentration (C_t) at given time in centrifuged solution was determined via measuring the absorbance value at maximum wavelenght (554nm) by utilizing UV-vis spectrometer. Finally, the photodegradation activities were calculated according to Eq.(1) given below.

$$\text{Photodegradation (\%)} = \frac{C_0 - C_t}{C_0} x100 \quad (1)$$

The influence of catalyst dosage (1-3gL^{-1}) and initial RhB dye concentration (5-15mgL^{-1}) on photodegradation activities of photocatalysts were examined under same experimental procedure at determined pH value.

2.6. Instruments

The SEM-EDX analysis to obtained morphological features and elemental composition of samples were taken on a Field Emission Scanning Electron Microscope (Quanta FEG 450-FEI). PG Instrument T80+ model UV-Vis spectrophotometer was used in photocatalytic activity studies of samples.

3. Results and Discussion

3.1. SEM-EDX analysis of samples

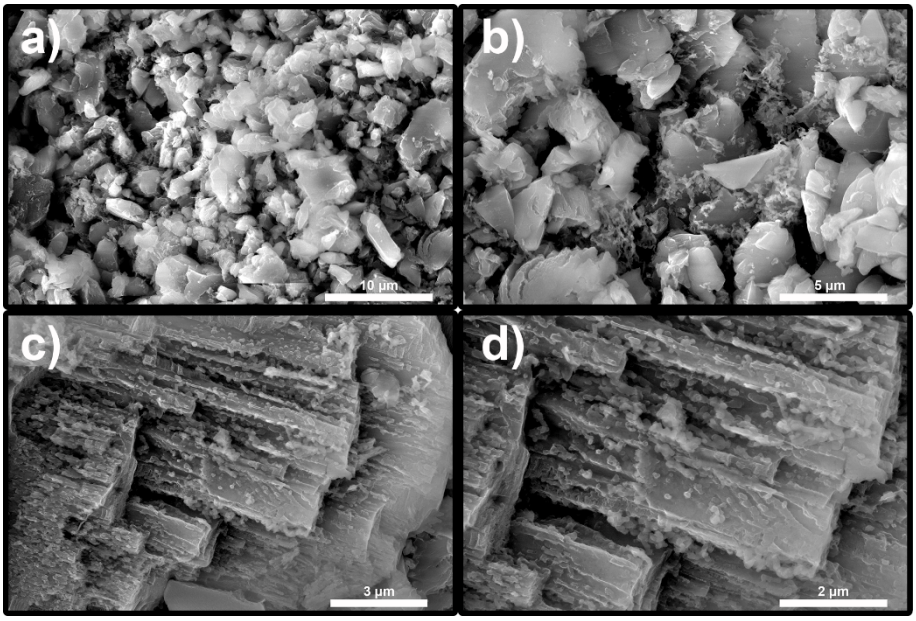

Figure 1. SEM images of g-C_3N_4 at different magnifications

The morphological features of g-C_3N_4, ZnS, ZnS/g-C_3N_4 1:2, ZnS/g-C_3N_4 1:1 and ZnS/g-C_3N_4 2:1 samples were investigated by SEM analysis. As illustrated as **Fig. 1a-d**, pure g-C_3N_4 showed a layered stacking morphology with roughness surface which provide an advantage for

decoration of ZnS nanoparticles on its surface. ZnS have mostly exhibited the nano-sphere structure together with considerable aggregation **(Fig. 2a-d)**. The SEM images of ZnS/g-C_3N_4 1:2, ZnS/g-C_3N_4 1:1 and ZnS/g-C_3N_4 2:1 nanocomposites evidently showed that ZnS nano-spheres covered on g-C_3N_4 sheets with well dispersion, which supplied direct proof for the successful synthesis of ZnS/g-C_3N_4 nanocomposites **(Fig. 3-5 a-d)**. As it is known, the decrease in aggregation of ZnS nanoparticles on g-C_3N_4 sheets increases the photocatalytic performances of nanocomposites via providing more active sites [21]. However, the appropriate quantity ratios of materials are also significant parameter to improve the photocatalytic performances of nanocomposites [18-21]. The SEM images of ZnS/g-C_3N_4 nanocomposites demonstrated that the aggregation of ZnS nano-spheres on g-C_3N_4 surface decreased with the amount of ZnS loaded.

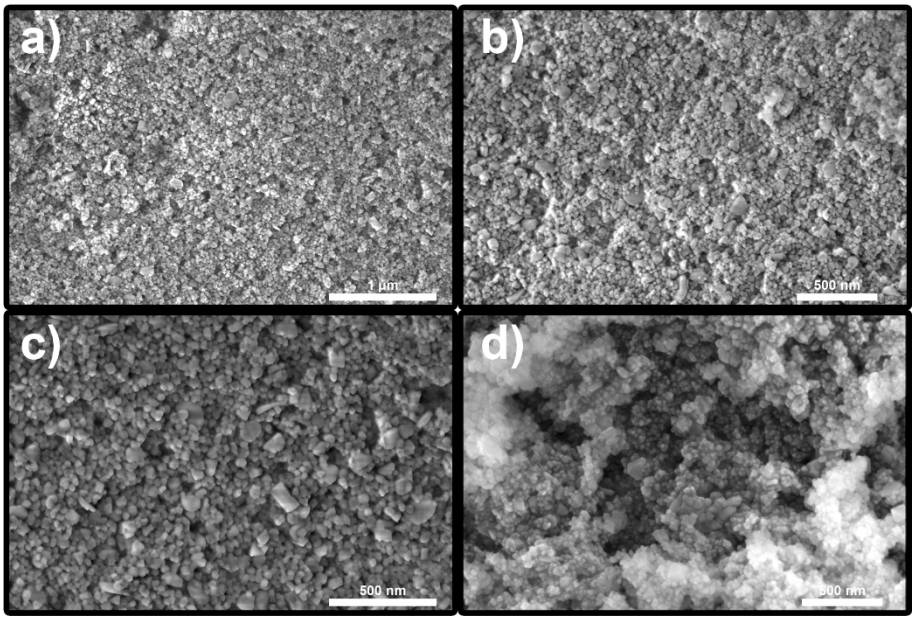

Figure 2. SEM images of ZnS nanoparticles at different magnifications

The elemental composition of g-C_3N_4, ZnS, ZnS/g-C_3N_4 1:2, ZnS/g-C_3N_4 1:1 and g- ZnS/g-C_3N_4 2:1 samples were performed by using EDX analysis and EDX spectra of samples were given in **(Fig. 6)**. The atomic % of elements on the samples were also given in the inset of **(Fig. 6)**. The pure g-C_3N_4 have only C and N atoms while pure ZnS contains Zn and S atoms, which are in well agreement with stoichiometric ratio of their formula's components. The EDX data of ZnS/g-C_3N_4 nanocomposites indicate the existence of C, N, Zn and S elements which confirmed the successful formation of ZnS/g-C_3N_4 nanocomposites with good purities. The tight connection between ZnS and g-C_3N_4 provides prevention of recombination of holes and electrons, which increases the catalytic activities of nanocomposites [21].

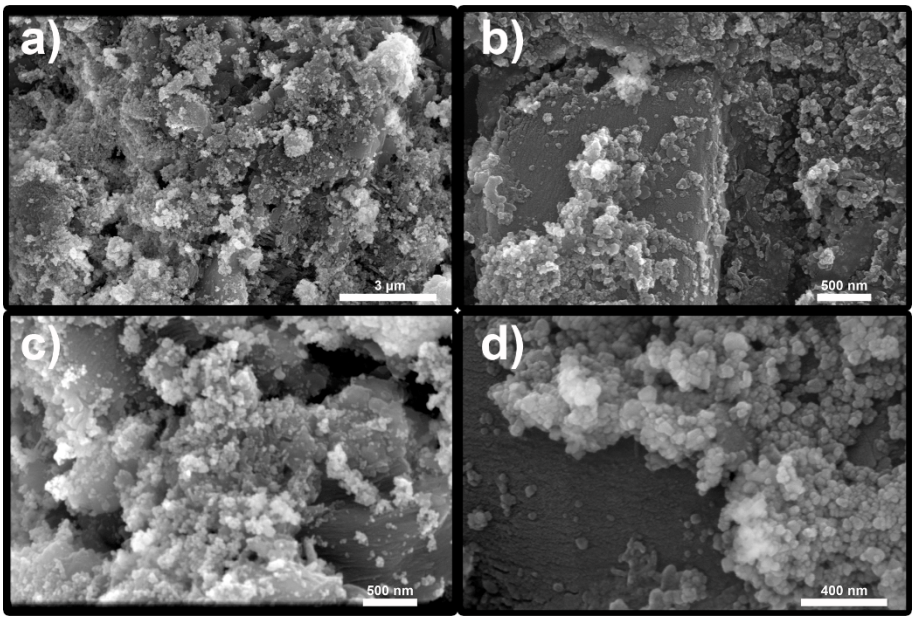

Figure 3. SEM images of ZnS/g-C_3N_4 1:2 nanocomposite at different magnifications

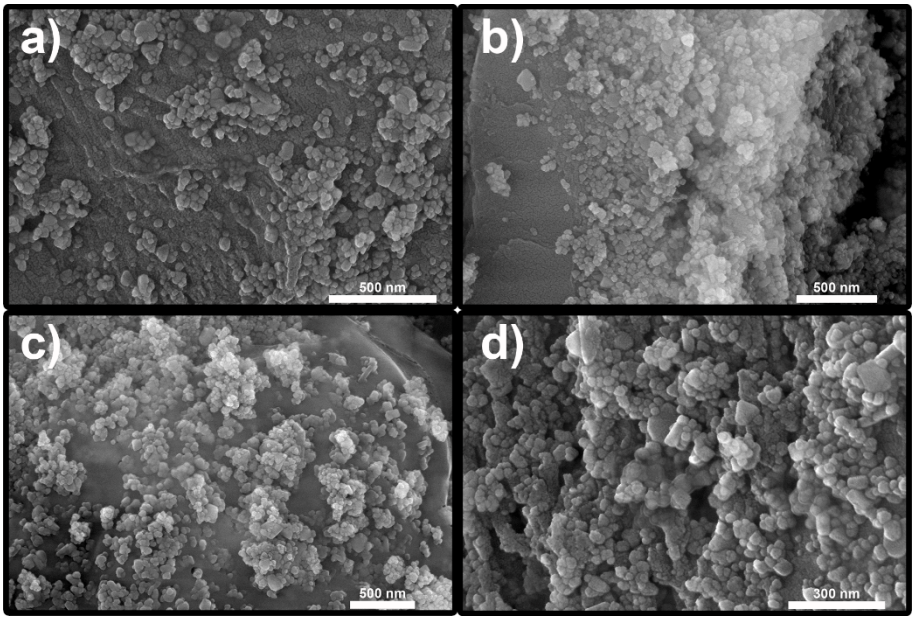

Figure 4. SEM images of ZnS/g-C_3N_4 1:1 nanocomposite at different magnifications

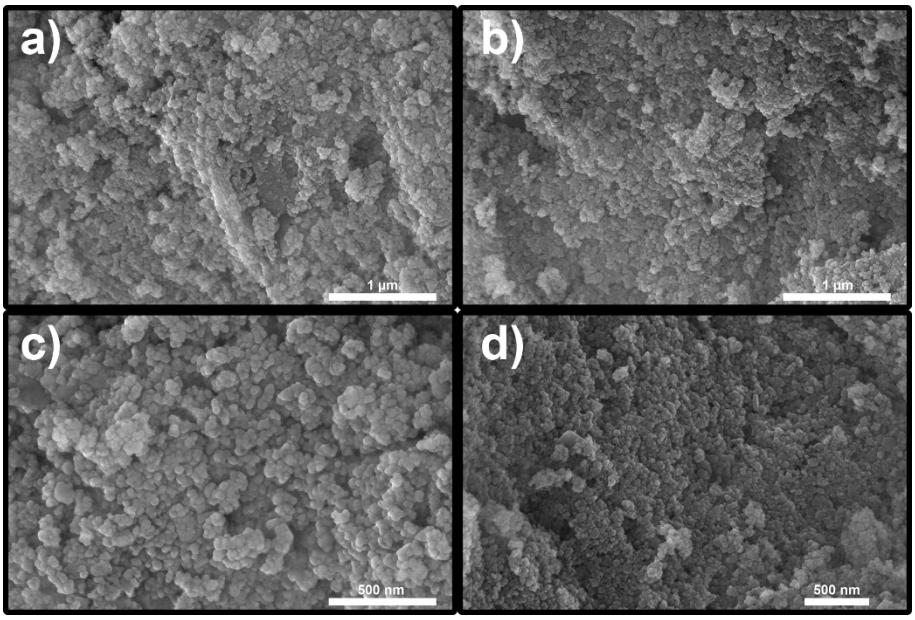

Figure 5. SEM images of ZnS/g-C_3N_4 2:1 nanocomposite at different magnifications

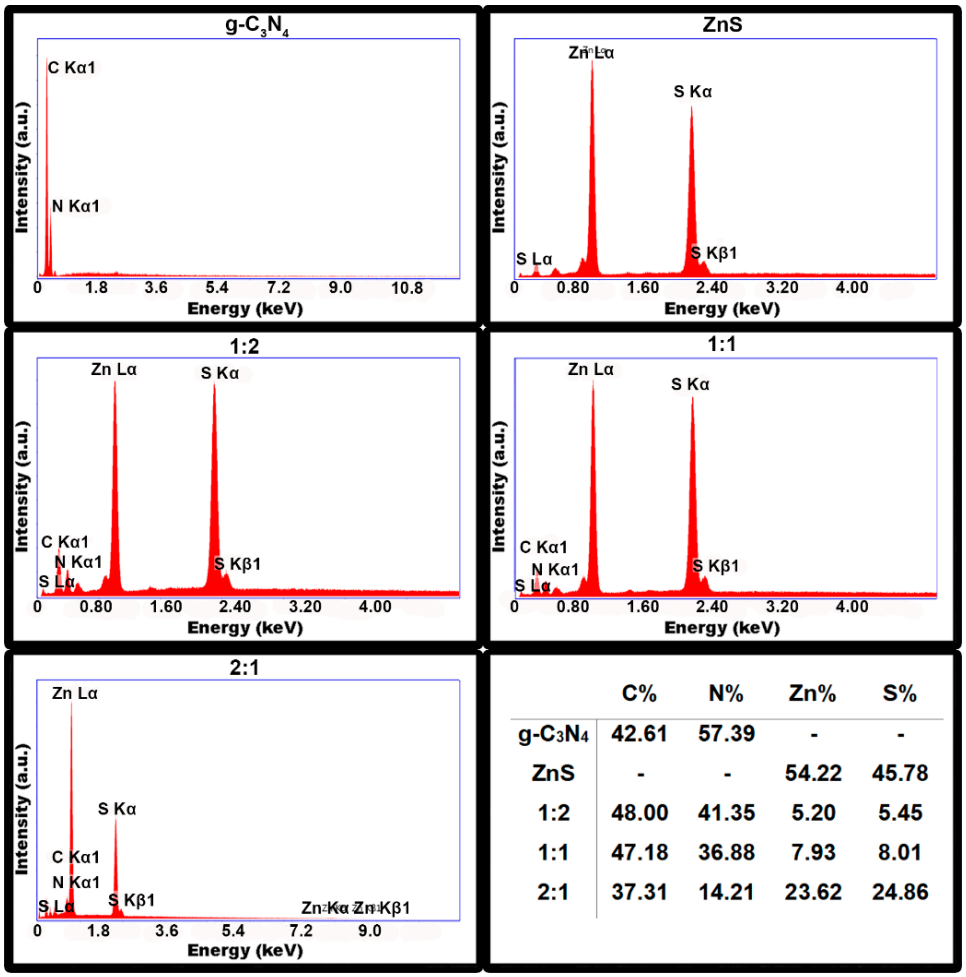

	C%	N%	Zn%	S%
g-C_3N_4	42.61	57.39	-	-
ZnS	-	-	54.22	45.78
1:2	48.00	41.35	5.20	5.45
1:1	47.18	36.88	7.93	8.01
2:1	37.31	14.21	23.62	24.86

Figure 6. EDX spectra and atomic mass ratio of samples

3.2. Photocatalytic degradation of Rhodamine B

The photocatalyst dosage, initial solution pH and initial dye concentration are important parameters affecting photocatalytic activity in addition to the surface area, particle size and aggregation of the photocatalyst. Therefore, the effect of catalyst dosage and initial dye concentration on the photodegradation of RhB dyestuff under visible light were investigated in the presence of ZnS/g-C_3N_4 1:2, ZnS/g-C_3N_4 1:1 and ZnS/g-C_3N_4 2:1 catalyst. In order to examine the effect of the photocatalyst dosage on the photodegradation of RhB, the photocatalyst dosages were taken as 1, 2 and 3 g/L at pH 6,36 for an initial dyestuff concentration of 5 mg/L. When the catalyst dosages are taken as 1, 2 and 3 g/L, the photodegradation of RhB molecules were determined as 87%, 92% and 95% for the ZnS/g-C_3N_4 1:2 catalysts, 68%, 98% and 91% for ZnS/g-C_3N_4 1:1 catalyst, and also 68%, 79% and 75% for ZnS/g-C_3N_4 2:1 catalyst, respectively **(Fig.7a-c)**. It was found that the photodegradation efficiencies of all catalysts towards RhB increased when catalyst dosage was increased from 1g/L to 2g/L whereas the photodegradation efficiencies decreased after the catalyst dosage was increased to 3g/L. The increases in photodegradation efficiencies is associated with an increase in the amount of active centers on the catalyst surface responsible for the adsorption of dye molecules, depending on the amount of catalyst [12,13,22]. On the other hand, while an increase in the photodegradation of RhB was expected due to the increase in the catalyst dosage, but it was found to a decrease [22]. This situation is explained by the scattering of light by suspension due to the increase in the opacity of the suspension with the increasing amount of catalyst and thus preventing the light from reaching the active centers on the catalyst surface [12,13,22]. According to the catalyst dosage studies, the best catalyst dosage was determined as 2g/L for all catalysts.

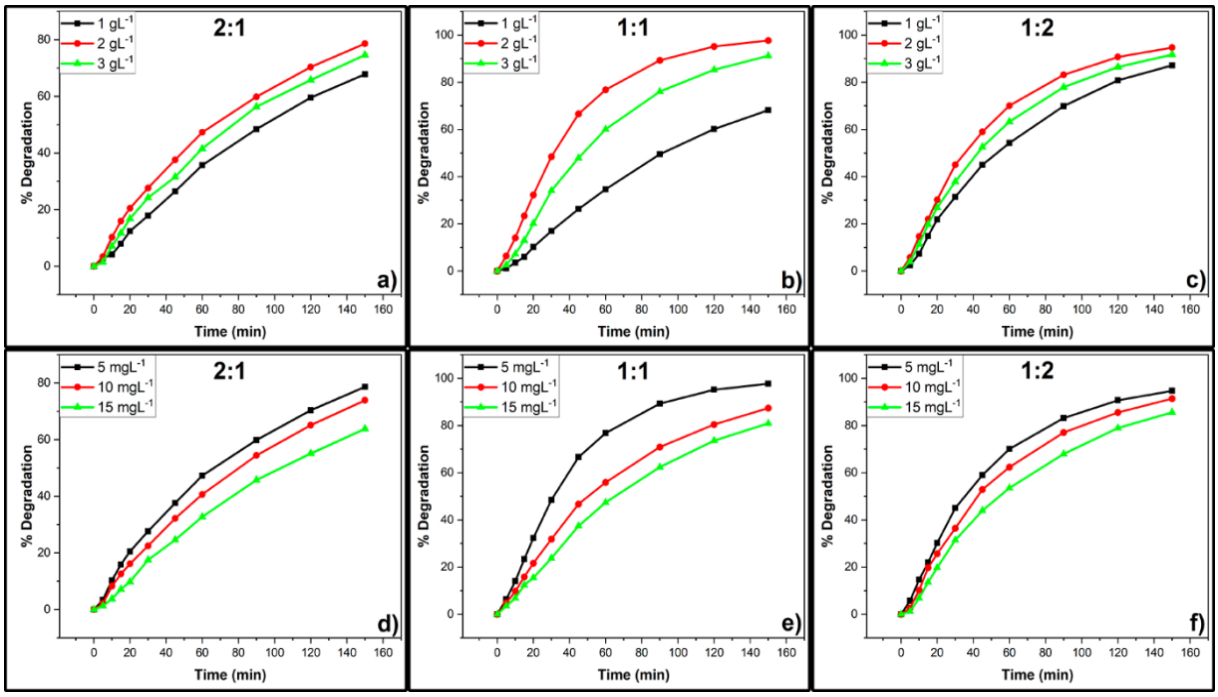

Figure 7. The influence of the photocatalyst dosage (a,b,c) and initial dye concentartion (d,e,f) on the photodegradation of RhB

To investigate the influence of the initial dye concentration on the photodegradation of RhB, the initial dye concentrations were taken as 5, 10 and 15 mg/L at pH 6,36 using 2g/L catalyst dosage. When the initial dye concentrations were taken as 5, 10 and 15 mg/L, the photodegradation of RhB molecules were detected as 95%, 91% and 85% for the ZnS/g-C_3N_4 1:2 catalysts, 98%, 87% and 81% for ZnS/g-C_3N_4 1:1 catalyst, and also 79%, 74% and 64% for ZnS/g-C_3N_4 2:1 catalyst, respectively **(Fig. 7d-f)**. As seen from Fig. 7d-f, it was observed that the photodegradation efficiencies of all catalysts were decreased by increasing the initial dye concentration. This situation is associated with the fact that increasing dye concentration causes an increase in the amount of non-adsorbed dye molecules [12,13,23]. These non-adsorbed dye molecules cause both a decrease in the light transmittance and a prevent the penetration of the light used on the catalyst surface due to the characteristic light absorption ability of the dye molecules [12,13,23]. These events induce a decrease in the amount of photodegradation. According to the initial dye concentration studies, the most appropriate initial dye amount was found as 5mg/L.

We further investigated the photocatalytic activities of pure g-C_3N_4, pure ZnS and ZnS/g-C_3N_4 nanocomposites by examining photodegradation of RhB molecules under visible light in the determined optimum conditions (5mg/L initial dye concentration, 1g/L catalyst dosage, and pH=6.36) and the obtained results are showed in **(Fig. 8a)**. Photolysis of RhB was detected as 10 % under visible light within 150 minutes without the presence of any catalyst. In the presence of ZnS and g-C_3N_4 catalysts, the photodegradation of RhB under the same conditions was found to be 43% and 70%, respectively. The photocatalytic performances of ZnS/g-C_3N_4 heterostructures significantly increased compared to pure g-C_3N_4 and ZnS. The photocatalytic performances of ZnS/g-C_3N_4 1:2; ZnS/g-C_3N_4 1:1 and ZnS/g-C_3N_4 2:1 photocatalysts were detected as 95%, 98% and 79%, respectively, which showed that ZnS/g-C_3N_4 heterostructures have satisfactory photocatalytic performances. The production of heterojunction structure between the g-C_3N_4 and ZnS facilitated the electron transition from g-C_3N_4 to ZnS and thus resulted in preventing of the recombination of hole-electron pairs, which increases the photocatalytic performance of nanocomposites. The ZnS/g-C_3N_4 1:1 nanocomposite indicated the best photocatalytic performance which degraded 98 % of RhB molecules after visible light irradiation for 150 minutes.

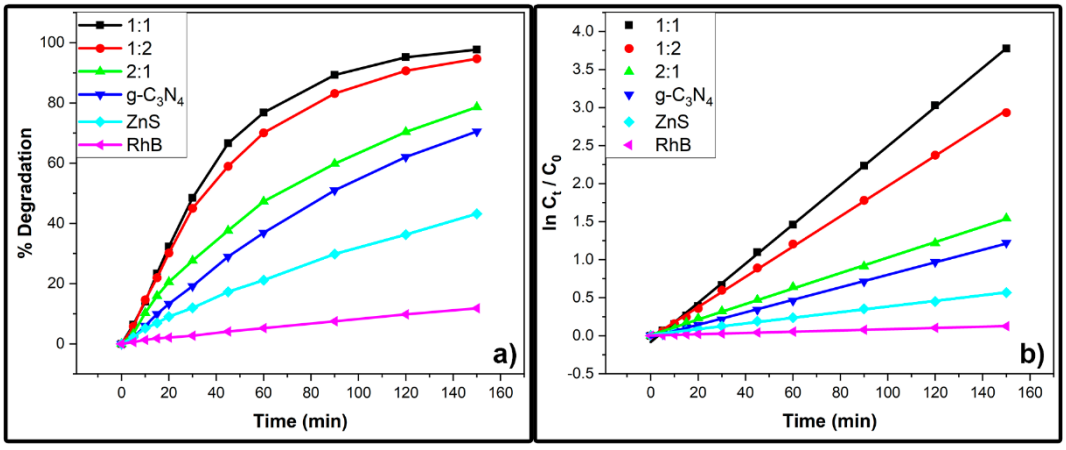

Figure 8. The photocatalytic performances of samples under optimum conditions

To determine the kinetic parameters, the pseudo-first-order kinetic model was performed according to equation is given below. **Fig. 8b** showed that a plot of $\ln(C_0/C_t)$ versus time have straight lines for all samples, proving degradation reaction of RhB in the presence of all samples follow the pseudo-first-order kinetic.

$$\ln \frac{C_0}{C_t} = k_{app}.t \quad (2)$$

The C_0, C_t and t are the initial concentration of dye molecules, the concentration of dye molecules at the relevant irradiation time and time (minute), respectively. The kapp is the apparent rate constant (min^{-1}) which obtained from the slope of the plot of $\ln(C_0/C_t)$ versus time. In addition, the calculated k_{app} constants and correlation coefficients (R^2) values are offered in **Table 1**. The kapp and R^2 values of ZnS/g-C_3N_4 1:1 nanocomposite are highly higher than those of g-C_3N_4, ZnS and other ZnS/g-C_3N_4 nanocomposites. Therefore, these data showed that the photodegradation of RhB in the existence of ZnS/g-C_3N_4 1:1 nanocomposite fits the pseudo-first-order kinetic very well and it has the supreme photocatalytic performance.

Table 1. The calculated k_{app} constants and correlation coefficients (R^2)

Samples	**k_{app} (dak^{-1})**	**R^2**
g-C_3N_4	0.00822	0.99944
ZnS	0.00371	0.99844
1:1	0.02574	0.99925
1:2	0.01685	0.99961
2:1	0.01018	0.99920

In order to find the influences of reactive species to photodegradation of RhB on ZnS/g-C_3N_4 catalyts and to evaluate the catalytic mechanism, the trapping studies were carried out the same experimental conditions as photocatalysis studies. Tert-butyl alcohol (TBA), L-ascorbic acid (LA), ethylenediaminetetraacetic acid disodium salt (EDTA) and $AgNO_3$ were utilized as the scavengers to evaluate the effect of hydroxyls radicals, superoxide radicals, holes and electrons, respectively. **Fig. 9** shows the photocatalytic performances of ZnS/g-C_3N_4 catalyts for the RhB photodegradation under visible light the existence of the scavengers and except of the addition of them. The scavenger results indicate that the roles of scavengers in the order of superoxide radicals > holes > electrons and hydroxyls radicals. The superoxide radicals and holes have primary and secondary roles in the photodegradation of RhB, respectively, whereas electrons and hydroxyls radicals have minor roles in the photodegradation of RhB.

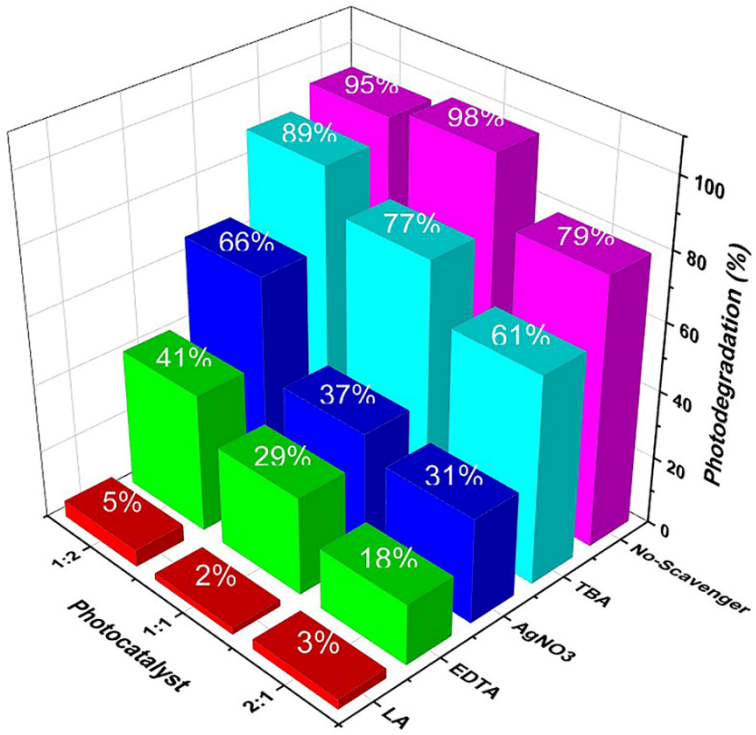

Figure 9. The effects of scavengers on the photodegradation of RhB

According to the literature, the band gap values of g-C_3N_4 and ZnS are approximately 2.5 and 3.9 eV. [19]. Therefore, the g-C_3N_4 can be photoexcited by visible light whereas ZnS cannot be photoexcited by visible light. Based on the band gap values and scavenger studies, the plausible mechanism for degradation of RhB under visible light in presence of all ZnS/g-C_3N_4 catalyts was given in following equations [3-7].

$$g - C_3N_4 + hv \rightarrow h^+_{VB} + e^-_{CB}(g - C_3N_4) \quad (3)$$

$$h^+_{VB} + e^-_{CB}(g - C_3N_4) \rightarrow h^+_{VB}(g - C_3N_4) + e^-_{CB}(ZnS) \quad (4)$$

$$e^-_{CB}(ZnS) + O_2 \rightarrow \cdot O_2^- \quad (5)$$

$$\cdot O_2^- + RhB \rightarrow degraded\ products \quad (6)$$

$$h^+_{VB}(g - C_3N_4) + RhB \rightarrow degraded\ products \quad (7)$$

4. Conclusion

ZnS/g-C_3N_4 nanocomposites with various mass percentages were synthesized and characterizd by SEM/EDX analysis. The ZnS/g-C_3N_4 1:1 nanocomposite showed excellent visible-light-driven photocatalytic performance. The obtained results indicated that the photocatalytic performances of the synthesized materials against RhB molecules in order of ZnS/g-C_3N_4 1:1, ZnS/g-C_3N_4 1:2, ZnS/g-C_3N_4 2:1, g-C_3N_4 and ZnS. The superoxide radicals have principle roles while other species play minor effects in the photodegradation of RhB. The degradation of RhB molecules existence of all photocatalysts was determined to follow the pseudo-first-order kinetic. This present work provides novel approach for improving ZnS/g-C_3N_4 nanocomposites for photodegradation of various pollutants.

Ethics in Publishing

There are no ethical issues regarding the publication of this study.

Author Contributions

All authors contributed equally to the writing of this manuscript

Acknowledgements

This study was produced from Bilge Doğan's PhD thesis. Bilge Doğan was supported by YÖK as a 100/2000 scholar in the priority field (micro and nanotechnology) during her PhD thesis.

.

References

[1] Ren, Z., Zhu, B., Xia, J., Ming, M., Zhang, S., Zhi, X., Chen, S., Zhang, W., (2023) High quality factor infrared notch filter with compact electromagnetically induced transparency metamaterial structure, Materials Letters, 343, 134349.

[2] Wang, P., Zhong, S., Lin, M., Lin, C., Lin, T., Gao, M., Zhao, C., Li, X., Wu, X., (2022) Signally enhanced piezo-photocatalysis of $Bi_{0.5}Na_{0.5}TiO_3$/MWCNTs composite for degradation of rhodamine B, Chemosphere, 308, 136596.

[3] Xu, D., Ma, H., (2021) Degradation of rhodamine B in water by ultrasound-assisted TiO_2 photocatalysis, Journal of Cleaner Production, 313, 127758.

[4] Kong, H., Li, H., Wang, H., Li, S., Lu, B., Zhao, J., Cai, Q., (2023) Fe-Mo-O doping g-C_3N_4 exfoliated composite for removal of rhodamine B by advanced oxidation and photocatalysis, Applied Surface Science, 610, 155544.

[5] Ashok, B., Ramesh, K., Madhu, D., Nagesh, T., Vijaya Kumar, B., Upender, G., (2023) Characterization and photocatalysis of visible light driven Z-scheme Bi_2WO_6/Bi_2MoO_6

heterojunction for Rhodamine B degradation, Inorganic Chemistry Communications, 150, 110495.

[6] Mittal, H., Al Alili, A., Morajkar, P. P., Alhassan, S. M., (2021) Graphene oxide crosslinked hydrogel nanocomposites of xanthan gum for the adsorption of crystal violet dye, Journal of Molecular Liquids, 323, 115034.

[7] Khumalo, N. P., Nthunya, L. N., De Canck, E., Derese, S., Verliefde, A. R., Kuvarega, A. T., Mamba, B. B., Mhlanga, S. D. Dlamini, D. S., (2019) Congo red dye removal by direct membrane distillation using PVDF/PTFE membrane, Separation and Purification Technology, 211, 578- 586.

[8] Menon, P., Anantha Singh, T. S., Pani, N., Nidheesh, P. V., (2021) Electro-Fenton assisted sonication for removal of ammoniacal nitrogen and organic matter from dye intermediate industrial wastewater, Chemosphere, 269, 128739.

[9] Tekin, D., Tekin, T., Kiziltas, H., (2020) Synthesis and characterization of TiO_2 and Ag/TiO_2 thin-film photocatalysts and their efficiency in the photocatalytic degradation kinetics of Orange G dyestuff, 198, 376- 385.

[10] Giwa, A., Yusuf, A., Balogun, H. A., Sambudi, N. S., Bilad, M. R., Adeyemi, I., Chakraborty, S., Curcio, S., (2021) Recent advances in advanced oxidation processes for removal of contaminants from water: A comprehensive review, Process Safety and Environmental Protection, 146, 220- 256.

[11] Pera-Titus, M., García-Molina, V., Baños, M. A., Giménez, J., Esplugas, S., (2004) Degradation of chlorophenols by means of advanced oxidation processes: a general review, Applied Catalysis B: Environmental, 47(4), 219- 256.

[12] Caglar, B., Keles Guner, E., Ersoy, S., Caglar, S., Özdemir, A. O., Özdokur, K. V., Doğan, B., İçer, F., Çırak, Ç., (2021) Bi_2S_3 nanorods decorated on bentonite nanocomposite for enhanced visible-light-driven photocatalytic performance towards degradation of organic dyes, Journal of Alloys and Compounds, 885, 160964.

[13] Caglar, B., Keles Guner, E., Özdokur, K. V., Özdemir, A. O. İçer, F., Caglar, S., Doğan, B., Beşer, B. M. Çırak, Ç., Tabak, A., Ersoy, S., (2021) Application of $BiFeO_3$ and $Au/BiFeO_3$ decorated kaolinite nanocomposites as efficient photocatalyst for degradation of dye and electrocatalyst for oxygen reduction reaction, Journal of Photochemistry and Photobiology A: Chemistry, 418, 113400.

[14] Chen, X., Wu, Z., Liu, D., Gao, Z., (2017) Preparation of ZnO Photocatalyst for the Efficient and Rapid Photocatalytic Degradation of Azo Dyes, Nanoscale Research Letters, 12(1), 1-10.

[15] Tao, C., Jia, Q., Han, B., Ma, Z., (2020) Tunable selectivity of radical generation over TiO_2 for photocatalysis, Chemical Engineering Science, 214, 115438.

[16] Sahu, K., Choudhary, S., Khan, S. A., Pandey, A., Mohapatra, S., (2019) Thermal evolution of morphological, structural, optical and photocatalytic properties of CuO thin films, Nano-Structures & Nano-Objects, 17, 92- 102.

[17] Dey, P. C., Das, R., (2020) Enhanced photocatalytic degradation of methyl orange dye on interaction with synthesized ligand free CdS nanocrystals under visible light illumination, Spectrochimica Acta Part A: Molecular and Biomolecular Spectroscopy, 231, 118122.

[18] Ma, Y., Li, J., Cai, J., Zhong, L., Lang, Y., Ma, Q., (2022) Z-scheme g-C_3N_4/ZnS heterojunction photocatalyst: One-pot synthesis, interfacial structure regulation, and improved photocatalysis activity for bisphenol A, Colloids and Surfaces A: Physicochemical and Engineering Aspects, 653, 130027.

[19] Palanisamy, G., Al-Shaalan, N. H., Bhuvaneswari, K., Bharathi, G., Bharath, G., Pazhanivel, T., Sathishkumar, V. E., Arumugam, M. K., Pasha, S. K. K., Habila, M. A., El-Marghany, A., (2021) An efficient and magnetically recoverable g-C_3N_4/ZnS/$CoFe_2O_4$ nanocomposite for sustainable photodegradation of organic dye under UV–visible light illumination, Environmental Research, 201, 111429.

[20] Danish, M., Muneer, M., (2021) Excellent visible-light-driven Ni-ZnS/g-C_3N_4 photocatalyst for enhanced pollutants degradation performance: Insight into the photocatalytic mechanism and adsorption isotherm, Applied Surface Science, 563, 150262.

[21] Yan, Y., Yang, M., Wang, C., Liu, E., Hu, X., Fan, J., (2019) Defected ZnS/bulk g–C_3N_4 heterojunction with enhanced photocatalytic activity for dyes oxidation and Cr (VI) reduction, Colloids and Surfaces A: Physicochemical and Engineering Aspects, 582, 123861.

[22] Liu, Y., Ding, S., Xu, J., Zhang, H., Yang, S., Duan, X., Sun, H., Wang, S., (2017) Preparation of a p-n heterojunction $BiFeO_3$@TiO_2 photocatalyst with a core–shell structure for visible-light photocatalytic degradation, Chinese Journal of Catalysis, 38(6), 1052- 1062.

[23] Chakrabarti, S., Dutta, B. K., (2004) Photocatalytic degradation of model textile dyes in wastewater using ZnO as semiconductor catalyst, Journal of Hazardous Materials, 112(3), 269-278.

Erzincan Üniversitesi
Fen Bilimleri Enstitüsü Dergisi
2024, 17(1), 69-79
ISSN: 1307-9085, e-ISSN: 2149-4584
Araştırma Makalesi

Erzincan University
Journal of Science and Technology
2024, 17(1), 69-79
DOI: 10.18185/erzifbed.1315542
Research Article

Investigation and Improvement of Thermal and Mechanical Properties of Recycled Polypropylene / Oxidized Polyethylene Composites

Erhan DEMİRCAN[1], Betül GÜLGEÇ[1], Hakan AKAT*[1]

[1]Ege University, Faculty of Science, Department of Chemistry, 35100 Bornova, Izmir, Turkey

Received: 16/06/2023, **Revised:** 21/02/2024, **Accepted:** 21/02/2024, **Published:** 28/03/2024

Abstract

In this study, different composites were prepared from oxidized polyolefin (OxPO) and synthetic waste (recycled polyolefin) to enhance the mechanical and thermal properties of recycled polyolefin, and the results of experimental studies on the mechanical (elongation, elasticity, tensile strength, etc.) and thermal properties of these composites were discussed. The composites were prepared in a laboratory-scale twin-screw extruder by grafting an oxidized polyolefin/styrene (St) blend onto recycled polypropylene (rPP) using the melt-free radical polymerization method. The prepared composites' mechanical properties (elongation and tensile strength) were determined according to the ISO 527-2 standard method. It was observed that the modulus of elasticity of (OxPO/St/rPP) composites increased by 24% compared to the modulus of elasticity of rPP and the tensile strength increased by 45% compared to the tensile strength of rPP. The composites were characterized by Thermogravimetric analysis and Fourier Transform Infrared (FTIR) spectroscopy. Thermogravimetric analysis (TGA) results showed that the thermal stability of the composites 36 °C increased compared to the thermal stability of rPP. Melt Flow Index (MFI) tests showed a 15% decrease in the Melt Flow Index value of the composites.

Keywords: recycled polypropylene; oxidized polyethylene; composite; styrene; maleic anhydride

Geri Dönüştürülmüş Polipropilen / Oksitlenmiş Polietilen Kompozitlerin Termal ve Mekanik Özelliklerinin Araştırılması ve İyileştirilmesi

Öz

Bu çalışmada, geri dönüştürülmüş poliolefinlerin mekanik ve termal özelliklerini geliştirmek amacıyla oksitlenmiş poliolefin (OxPO) ve sentetik atıklardan (geri dönüştürülmüş poliolefin) farklı kompozitler hazırlanmış ve bu kompozitlerin mekanik (uzama, elastikiyet, çekme mukavemeti vb.) ve termal özellikleri üzerine yapılan deneysel çalışmaların sonuçları tartışıldı. Kompozitler, laboratuvar ölçekli çift vidalı ekstrüderde, oksitlenmiş poliolefin/stiren (St) karışımının geri dönüştürülmüş polipropilen (rPP) üzerine eriyik serbest radikal polimerizasyon yöntemi kullanılarak aşılanmasıyla hazırlandı. Hazırlanan kompozitlerin mekanik özellikleri (uzama ve çekme mukavemeti) ISO 527-2 standart yöntemine göre belirlendi. (OxPO/St/rPP) kompozitlerinin elastisite modülünün, rPP'nin elastisite modülüne kıyasla %24, kompozitlerin çekme mukavemetinin ise rPP'nin çekme mukavemetine kıyasla %45 oranında arttığı gözlemlendi. Kompozitler Fourier Transform Infrared (FTIR) spektroskopisi, Termogravimetrik analiz ile karakterize edildi. Termogravimetrik analiz (TGA) sonuçları, kompozitlerin termal stabilitesinin, rPP'nin termal stabilitesine kıyasla 36 °C arttığını gösterdi. Eriyik Akış İndeksi (MFI) testleri, kompozitlerin eriyik akış indeksi değerinde %15 düşüş olduğunu göstermiştir.

Anahtar Kelimeler: geri dönüştürülmüş polipropilen; oksitlenmiş polietilen; kompozit; stiren; maleik anhidrit

*Corresponding Author: hakan.akat@ege.edu.tr

Erhan DEMİRCAN, https://orcid.org/0000-0002-5363-3835
Betül GÜLGEÇ, https://orcid.org/0009-0002-4922-0795
Hakan AKAT, https://orcid.org/0000-0003-4002-5352

1. Introduction

Big bags are a versatile type of packaging that protects the products they contain from moisture, contamination, and UV light during transportation and storage. They are easy to fill and empty, offer high security, and can be tailored to the customer's exact requirements. Depending on requirements, big bags can be supplied with or without an inner liner, come with single or multiple carry handles, and are available in a range of sizes, colors, styles, and specifications. Big bags are industrial packaging with a load capacity of 500 kg to 2000 kg. The main elements of big bags consist of a main body, lifting handles, top and bottom closures, and filling and emptying spouts. These components are made exclusively from polyolefin (PO) raw materials. The cost of raw materials is the most important cost factor in the manufacture of these products. In Turkey, standard plastics (PE, PP, PVC, PS) account for the majority of plastic raw material consumption. The domestic supplier PETKIM covers around 35% of the demand for polypropylene (PP) and polyethylene (PE), thermoplastics derived from crude oil, which are mainly used for the production of large bags. Imports cover the rest of the demand. The current situation in the commodities market has led to fluctuations in oil prices and exchange rates. These external factors pose a threat to the competitiveness of the synthetic textiles sector, particularly due to lower labor costs in China and India, which have their oil resources. Recipe design and confidentiality, waste reduction, and improving raw material efficiency are key components to improving competitiveness. Thermoplastics increasing consumption, the fact that they are petroleum derivatives, the creation of uncontrollable waste mountains, and their environmental impact make the recycling of products made from polyolefins unsustainable. Disposal of plastic waste in the environment is considered to be a big problem due to its very low biodegradability and presence in large quantities [1,2]. Although recycling and reuse are sustainable methods to overcome these obstacles, the mechanical properties of polyolefins decrease during the recycling process.

Polyolefins are thermoplastic polymers with a wide range of applications, from automotive parts to textile and food packaging. Due to its low cost, thermal stability, and corrosion resistance [3-5], polypropylene is widely used for various applications such as packaging, technical automotive parts, and composites. Polypropylene which is produced by polymerizing the monomer propylene, is generally very resistant to chemical solvents. It is difficult for microorganisms in the environment to break down commercially produced plastics [6]. Despite numerous commercial applications, a major disadvantage of polyolefins (PP, PE) is their weak interaction with other materials. In addition, attempts to blend these types of polyolefins with other polymers have been unsuccessful for the reasons mentioned above. For example, if we want to overcome the incompatibility of polypropylene, we need to add polar groups to it. Like many other materials, PP forms only weakly interacting blends [7] because it lacks the chemical groups necessary for these interactions. It is a challenge to produce compatible blends or composites with PP without specific interactions [8]. The modification of polypropylene, i.e. the introduction of functional groups, makes it compatible with other materials. It has been found that PP modified with maleic anhydride significantly improves the impact strength and tensile strength of PP and LCP blends [9]. Many approaches, such as incorporating elastomers,

inorganic fillers, or blending with other polymers, can improve the thermal and mechanical properties of recycled PP [10-12].

Oxidized polypropylene is an oxidized polymer that contains peroxides and peracids in its structure in the presence of a strong oxidizing agent (H_2O_2 or $KMnO_4$) [13-15]. The presence of peracid-like groups in the polymer structure gives oxidized polypropylene certain properties (functionality, compatibility, solubility, etc.). It can therefore be used to create blends, compatibilized nanocomposites or to hold materials together. Due to their high strength and lightness, composite materials have a wide range of applications (defense industry, aerospace, automotive, transport, etc.) [16-18].

In this study, to improve the mechanical and thermal properties of recycled polypropylene, which are crucial for environmental waste reduction and sustainable production, composites were prepared by melt grafting into the polymer chain using monomers containing maleic anhydride (MAH) or styrene (St) with oxidized polyethylene (OxPE). To improve the overall performance of recycled PP, the methods developed by many researchers to produce long-chain branched PP were used and the branched structure was introduced into the recycled PP by reactive extrusion. The resulting composites were characterized and tested for their thermal properties. Test specimens were produced from dog bones and the composites were subjected to the ISO 527-2 standard test for fracture and elongation. The improvement in tensile strength of the composites compared to recycled polypropylene indicates the formation of a branched structure in the composites.

2. Material and Methods

2.1 Materials

Virgin polypropylene with MFI 4.3 g/10 min. (230 °C/2.16 kg) (PP, Sibur Sibex H043 FF/3). Oxidized polyethylene (OxPE, TRX K-90 Akdeniz Chemson). Benzoyl peroxide (BPO, 98% Merck). Maleic Anhydride (MAH, 99% BDH). Styrene (St, 99% Merck).

2.2 Calculations of the peroxide concentration of the oxidized polyolefin

Calculations of the peroxide concentration of the oxidized polyolefin were determined by titration method. The following formula was used to calculate the acid number.

Definitions of the variables in the formula:

a: amount of thiosulfate consumed for the sample in the titration, ml

b: the amount of thiosulfate consumed for the blank in the titration, ml

N: normality of thiosulfate, N

m: amount of sample taken, g

$$The\ acidity\ number\ = \left\{\frac{(a-b)\ x\ N\ x\ 1000}{m}\right\}$$

2.3 Preparation of synthetic waste

To simulate synthetic waste, virgin polypropylene with an MFI of 4.3 g/10 min (230 °C/2.16 kg) was thermally degraded at 260 °C with an L/D of 40 in a twin-screw extruder.

2.4 Preparation of mixtures

In reactive extrusion, depending on the solubility of the monomer in the polyolefin melt and monomer stability and volatility, the monomer can be added together with the polyolefin, added directly to the molten polyolefin, adsorbed onto another polymer or dissolved in a suitable solvent [19]. The recipes given as examples in Table 1 and Table 2 were prepared by mixing the monomer in oxidized polyethylene at a temperature of 70 °C for 15 minutes.

Table 1. Compositions prepared for blending with MAH and OxPE

Sample Name	**OxPE** *(%)*	**MAH** *(%)*
OX100	100	-
OX90MAH10	90	10
OX50MAH50	50	50
OX10MAH90	10	90
MAH100	-	100

Table 2. Compositions prepared for blending with St and OxPE

Sample Name	**OxPE** *(%)*	**St** *(%)*
OX50ST50	50	50

2.5 Preparation of the Composites

To prolong the polypropylene chains exposed to high temperatures and subjected to chain fragmentation by thermal degradation and/or to increase the molecular weight of the polymer, mixtures prepared according to the recipes given in Table 1 and Table 2 were added to the degraded polypropylene and passed through an extruder at 180 °C.

2.6 MFI Tests of the Composites

The MFI tests of the prepared composites were performed on the Davenport MFI-10 apparatus according to ASTM 1238 B to monitor the changes in chain length and molecular weight of the prepared composites. The densities of the composites were measured using the AND GR-200 instrument. MFI and density measurements of composites are shown in Table 3 and Table 4.

2.7 Characterization of the composites

The formation of functional groups on composites by thermal degradation was investigated using the PerkinElmer FTIR spectrometer. Figure 1 shows the FTIR analysis of the samples.

2.8 Tensile strength tests of composites

To investigate the mechanical properties of composite OxPE/St/rPP, PP, and rPP samples in Table 4, dog bone-shaped specimens were prepared by injection molding and tested on WDW series universal testing machine (Hensgrand testing machine factory, China) by ISO 527-2 tensile test standard at (23 ± 2) °C test atmosphere and (50 ± 10) % relative humidity. Stress-strain curves are shown in Figure 2.

2.9 Termal analysis of the composites

Thermogravimetric analysis (TGA) and differential thermal analysis (DTG) measurements were carried out using a Perkin-Elmer thermal analyzer. The mass of the samples was between 9 to 10 mg. The composite samples were heated in the range of 30-1000 °C with a flow heating rate of 10 °C/min under a nitrogen atmosphere. Thermal analysis thermograms are shown in Figure 2.

3. Results and Discussion

An important disadvantage of polyolefins is their poor interaction with other materials. In this study, polypropylene, a polyolefin, was degraded through thermal degradation, and functional groups were created on its chains and mixed with other materials (such as monomers and other polymers, etc.) interaction has been increased. The acid number of the polymer was determined to find the number of functional groups formed during oxidation. for this purpose, an acid number of the oxidized polyethylene, which was used in this study to prepare composites for increasing the chain length of recycled polypropylene, was determined to be 40.80.

Table 3. Density and MFI values for rPP/OxPE/MAH composites, unmodified rPP, and virgin PP

Sample Name	**rPP** *(%)*	**OxPE** *(%)*	**MAH** *(%)*	**MFI** *(g/10min)*	**Density** *(g/cm^3)*
1VPP	0	0	0	4.37	0.9024
2VPP	100	0	0	4.81	0.8846
$2VPP_{OX100}$	98	2.0	0	5.11	0,8940
$2VPP_{OX90MAH10}$	98	1.8	0.2	5.29	0,8995
$2VPP_{OX50MAH50}$	98	1.0	1.0	5.67	0,8910
$2VPP_{OX10MAH90}$	98	0.2	1.8	6.03	0,8876
$2VPP_{MAH100}$	98	0	2.0	6.28	0,8890

The MFI values of the experiments prepared with styrene monomer decreased compared to the MFI values of rPP. The decrease in MFI value suggests that recycled PP, forming the composite matrix, intermingles with oxidized polyethylene and styrene monomer to elongate its chain.

Table 4. Density and MFI values for rPP/OxPE/St composites, unmodified rPP, and virgin PP

Sample Name	**rPP (%)**	**OxPE** *(%)*	**St** *(%)*	**MFI** *(g/10min)*	**Density** *(g/cm^3)*
1VPP	**0**	0	0	4.45	0.9024
3VPP	**0**	0	0	5.98	0.8846
$3VPP_{OX50ST50}$	**99**	0.5	0.5	5.10	0.8912

3.1 FTIR spectral analysis

The formation of functional groups by thermal degradation was studied using the FTIR method. Figure 1 shows the FTIR analysis of the samples. The carbonyl C=O peak around 1700 cm^{-1} and the C-O ester peak around 1100 cm^{-1} indicate the formation of functional groups. In addition, the overtone transitions observed around 2000 cm^{-1} indicate the presence of a benzene ring structure.

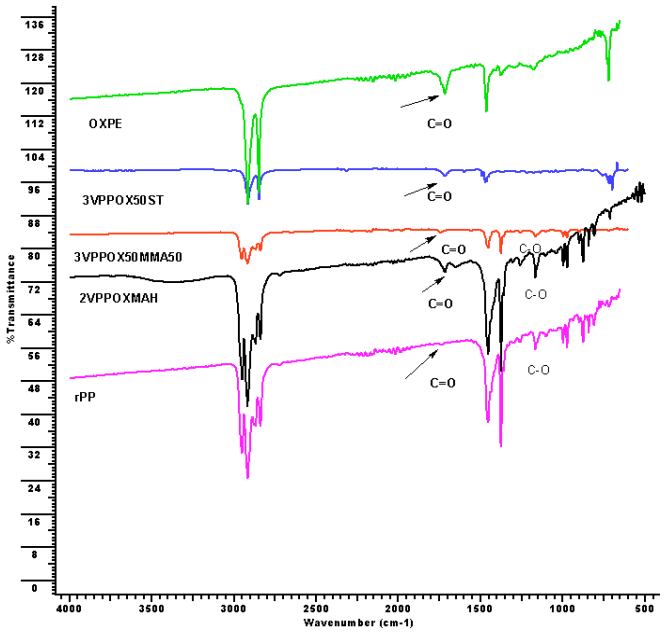

Figure 1. FTIR analysis of rPP/OxPE/St composites and rPP

3.2 Termal analysis (TGA/DTG)

The TGA and DTG analyses are shown in Figure 2. It was found that all samples were degraded in a single step. The degradation temperature of PP, rPP, and composite starts at about 310°C and ends at 511°C. The degradation temperature (Td, 5% mass loss temperature and Td, 50% mass loss temperature) was also analyzed and it was found that the thermal stability of rPP was lower than that of the composites. It was found that the thermal stability of the composite of 1 wt% OxPE/St and rPP was about 36 °C higher than the thermal stability of rPP. When comparing the composite sample with the rPP sample, it was found that the temperature at which thermal degradation began (T_{onset}) was 325°C and 343°C, respectively, and the temperature at which the samples were fully degraded (T_{offset}) was 325°C and 343°C, respectively.

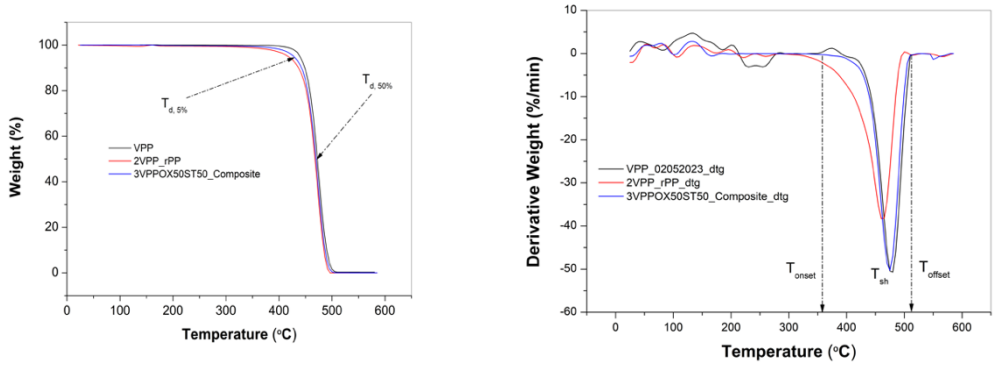

Figure 2. TGA and DTG analysis of rPP/OxPE/St composites, unmodified rPP, and virgin PP

Table 5. TGA results of rPP/OxPE/St composites, unmodified rPP, and virgin PP

Sample Code	rPP *(%)*	OxPE *(%)*	St *(%)*	Consent *(±0.5°C)*	T_5 *(±0.5°C)*	T_{50} *(±0.5°C)*	T_{offset} *(±0.5°C)*
1VPP	0	0	0	353	440	471	511
3VPP	100	0	0	310	418	467	492
$3VPP_{OX50ST50}$	99	0.5	0.5	346	427	469	506

3.3 Mechanical properties of the composites

In the current study, the composites extracted from synthetic waste were treated with oxidized polyolefin (OxPO). Oxidized polyolefin/styrene (St) was grafted onto recycled polypropylene (rPP) by the radical polymerization method. Thus, a homogenous composite was obtained. The mechanical properties of the composites prepared with recycled PP and the recycled PP and virgin PP samples were tested with a tensile testing machine. In Table 3, a summary of the tensile tests for both PP and composites is presented. As a result, an increase in the tensile strength and elongation at the break of the composites prepared with recycled PP was observed. The stress-strain curves of PP, rPP, and the composites are shown in Figure 3.

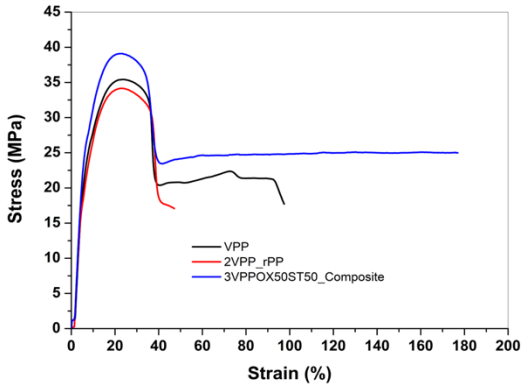

Figure 3. Stress-strain graphs for PP, rPP, and the composites

Table 6. Mechanical properties of PP, rPP, and the composites

Sample Code	rPP *(%)*	OxPE *(%)*	St *(%)*	Ultimate tensile strength *(MPa)*	Young's modulus *(MPa)*	Elongation *(%)*
1VPP	0	0	0	36	1.1851	95
3VPP	100	0	0	34	0.8765	43
$3VPP_{OX50ST50}$	99	0.5	0.5	39	1.0879	170

4. Conclusion

In this study, to improve the mechanical and thermal properties of recycled polypropylene, composites of oxidized polyolefin (OxPO) and synthetic waste (recycled polyolefin) were produced and their mechanical (elongation, elasticity, tensile strength, etc.) and thermal properties were investigated. The test results show that the MFI values of the samples produced with styrene decreased or remained almost constant. The fact that the MFI values of the composite prepared with styrene and oxidized polyethylene and rPP remain constant may indicate an increase in molecular weight or the presence of cross-linking. The peak observed at 1730 cm^{-1} in the FTIR spectrum indicates the formation of C=O and C-O - bonds leading to long chains. Experimental results on dog bone samples prepared with styrene formulations show a 45% increase in tensile strength and a 295% increase in elongation of recycled PP. A comparison of the modulus of elasticity of the composite and the rPP showed a 24% improvement in the modulus of elasticity of the composite.

Ethics in Publishing

There are no ethical issues regarding the publication of this study.

Acknowledgements

This study is being carried out with the support of TÜBİTAK's 2244 Industry University Project, numbered 119C140, and we would like to thank TÜBİTAK for their contributions.

This study is being carried out with the support of Ege University Scientific Research Projects Directorate, numbered FDK-2012-23124, and we would like to thank Ege University Scientific Research Projects Directorate for their contributions.

Due to the financial and laboratory support it provides to the project within the scope of the 2244-Industry Doctoral Program conducted by TÜBİTAK Scientist Support Programs Directorate (BIDEB), we would like to thank İşbir Sentetik Dokuma Sanayi A.Ş.

References

[1] Tapkire G., Parihar S., Patil P., and Kumavat H. R., (2014) Recycling plastic used in concrete paver, International Journal of Research in Engineering and Technology, 3(9), 33-35.

[2] Jassim A. K., (2017) Recycling of polyethylene waste to produce plastic cement, Elsevier, Procedia Manufacturing, 8, 635-642.

[3] Hegde, R. R., Bhat, G. S., (2010) Nanoparticle Effects on the Morphology and Mechanical Properties of Polypropylene Spunbond Webs, Journal of Applied Polymer Science, 118 (6), 3141-3155.

[4] Asl, D. H., Abdouss, M., Angaji, T. M., Haji, A., (2013) Chem. Ind. Chem. Eng., 19 (3), 441-448.

[5] Awad, S., Khalaf, E., (2017) Improvement, the Performance of Polyurethane (PUR), Y-290 Resin as Coating of Oil Pipeline by Using Multi-Walled Carbon Nanotubes (MWCNTs), Engineering and Technology Journal, 35, 845- 848.

[6] Arcana, I M., Bundjali, B., Yudistira, I., Jariah, B., and Sukria, L., (2007) Study on Properties of Polymer Blends from Polypropylene with Polycaprolactone and Their Biodegradability, Polymer Journal, Vol.39, No.12., 1337-1344.

[7] Chung, T.C., and Rhubright, D., (1993) Functionalization of polypropylene by hydroboration, Polym. Sci., Part A: Polym. Chem., 31 (11), 2759-2763.

[8] Chung, T.C., and Rhubright, D., (1994) Polypropylene-graft-Polycaprolactone: Synthesis and Applications in Polymer Blends, Macromolecules 27, 1313-1319.

[9] Bataille, P., Boisse, S., and Schreiber, H., (1987) Mechanical properties and permeability of polypropylene and poly(ethylene terephthalate) mixtures, Polym. Eng. Sci., 27(9), 622-626.

[10] Harris, M., Potgieter, J., Ray, S., Archer, R., and Arif, K. M., (2019) Acrylonitrile Butadiene Styrene and Polypropylene Blend with Enhanced Thermal and Mechanical Properties for Fused Filament Fabrication, MDPI, 12(24), 4167.

[11] Li, Y., Jia, S., Du, S., Wang, Y., Lv, L., Zhang, J., (2018) Improved properties of recycled polypropylene by introducing the long chain branched structure through reactive extrusion, Elsevier, Waste Management, 76, 172-179.

[12] Srivabut, C., Ratanawilai, T., Hiziroglu, S., (2017) Effect of nanoclay, talcum, and calcium carbonate as filler on properties of composites manufactured from recycled polypropylene and rubberwood fiber, Elsevier, Construction and Building Materials, 162, 450-458.

[13] Gijsman, P., Hennekens, J., (1993) The mechanism of the low-temperature oxidation of polypropylene, Polymer Degradation and Stability, 42, 95-105.

[14] Seven, M. K., Wheeler, M. R., (2009) Method for preparing oxidized polyolefin waxes, US Patent No. US 7.622,031 B2.

[15] Seven, K., (2007) Method for preparing oxidized polyolefin waxes, WO Patents.

[16] Qu, J., (1993) The effect of slightly weakened interfaces on the overall elastic properties of composite materials, Elsevier, Mechanics of Materials, 14(4), 269-281.

[17] Rosato, D. V., (1997) Designing with reinforced composites, Hanser Gardner Publications, New York.

[18] Vasiliev, V. V., Morozov, E. V., (2001) Mechanics and analysis of composite materials, Elsevier Pub.

[19] Moad, G., (1999) The synthesis of polyolefin graft copolymers by reactive extrusion, Progress in Polymer Science, 24, 81–142.

Erzincan Üniversitesi
Fen Bilimleri Enstitüsü Dergisi
2024, 17(1), 80-90
ISSN: 1307-9085, e-ISSN: 2149-4584
Araştırma Makalesi

Erzincan University
Journal of Science and Technology
2024, 17(1), 80-90
DOI: 10.18185/erzifbed.1323490
Research Article

Investigation of Genetic Diversity in Lentil Genotypes Obtain from Different Countries Using SDS-PAGE Methodology

Mehmet Zahit YEKEN[1*], Faheem Shehzad BALOCH[2],
Muhammad Azhar NADEEM[2], Muhammad SAMEEULLAH[1], Ekrem GÜREL[3]

[1]Department of Field Crops, Faculty of Agriculture, Bolu Abant Izzet Baysal University, Bolu, Türkiye
[2]Department of Plant Production and Technologies, Faculty of Agricultural Sciences and Technologies, Sivas University of Science and Technology, Sivas, Türkiye
[3]Department of Biology, Faculty of Science and Literature, Bolu Abant Izzet Baysal University, Bolu, Türkiye

Received: 06/07/2023, **Revised:** 12/12/2023, **Accepted:** 12/12/2023, **Published:** 28/03/2024

Abstract
In the current study, the characterization of 44 lentil genotypes was performed using SDS-PAGE (Sodium dodecyl sulfate-polyacrylamide gel electrophoresis) technique. The protein bands were scored according to a binary system as the present (1) or absent (0) that ranged 12-20 bands in lentil genotypes. The Jaccard's coefficient of genetic dissimilarity (GD) was measured, and the mean GD was 0.216. Maximum genetic distance was found as 0.526 between Syria2 with Iraq3 and these genotypes might be recommended for future lentil breeding. AMOVA explored the presence of higher genetic variety within genotypes (83%) than among genotypes (17% variations). STRUCTURE algorithm separated lentil genotypes into two groups mainly on the basis of their geographic. The UPGMA clustering separated lentil genotypes into two main clusters A and B. The PCoA was also conducted to confirm the results of structure and UPGMA analyses. Findings from the PCoA and structure analyses were in full agreement with those obtained by UPGMA. The results might be useful for researchers worldwide who are interested in lentil breeding.

Keywords: Genetic diversity, germplasm characterization, population structure, protein

Farklı Ülkelerden Elde Edilen Mercimek Genotiplerinde Genetik Çeşitliliğinin SDS-PAGE Yöntemi ile Araştırılması

Öz
Bu çalışmada, 44 mercimek genotipinin karakterizasyonu, SDS-PAGE kullanılarak gerçekleştirilmiştir. Protein bantları, var (1) veya yok (0) şeklinde puanlanmış ve mercimek genotiplerinin bant aralığının 12-20 bant arasında olduğu belirlenmiştir. Jaccard'ın genetik benzerlik katsayısı (GD), ortalama 0.216 olarak tespit edilmiştir. Suriye2 ile Irak3 genotipleri arasında maksimum genetik uzaklık 0.526 olarak bulunmuş ve gelecekteki mercimek ıslahı çalışmalarında kullanılabileceği belirlenmiştir. AMOVA mercimek genotiplerindeki yüksek genetik çeşitliliğini varlığını araştırmış ve popülasyon içindeki (%83) varyasyonun popülasyonlar arasındaki (%17) varyasyona kıyasla yüksek olduğunu göstermiştir. STRUCTURE algoritması, mercimek genotiplerini coğrafi bölgelerine göre iki gruba ayırmıştır. UPGMA kümelemesi, mercimek genotiplerini iki ana kümeye (A ve B) ayırmıştır. STRUCTURE ve UPGMA analizlerinin sonuçlarını doğrulamak için PCoA gerçekleştirilmiş ve sonuçların uyum içerisinde olduğu belirlenmiştir. Araştırma sonuçları dünyanın farklı yerlerinde mercimek ıslahı ile ilgilenen araştırmacılara önemli katkılar sağlayacaktır.

Anahtar Kelimeler: Genetik çeşitlilik, germplazm karakterizasyonu, popülasyon yapısı, protein.

*Corresponding Author: yekenmehmetzahit@gmail.com
Mehmet Zahit YEKEN, https://orcid.org/0000-0003-0490-371X
Faheem Shehzad BALOCH, https://orcid.org/0000-0002-7470-0080
Muhammad Azhar NADEEM, https://orcid.org/0000-0002-0637-9619
Muhammad SAMEEULLAH, https://orcid.org/0000-0001-6767-2539
Ekrem GÜREL, https://orcid.org/0000-0001-6262-2866

1. Introduction

Pulses are considered the best source of plant-based protein and other essential nutrients like zinc, iron and vitamins required for the development and growth of the human body [1]. Besides their importance for human health, pulses are also a valuable resource employed for fodder or pasture [2]. Among the pulse crops, lentil (*Lens culinaris* Medik.) is a self-pollinating plant with diploid (2n = 2x = 14) chromosomes [3]. It existed around 7000–10,000 years ago in the Eastern Mediterranean region [4]. This crop is produced in more than 58 countries worldwide, and its seeds are high in protein content, vitamins, and essential nutrients [5,6]. As a legume crop, lentil contributes significantly to a sustainable agriculture production system through nitrogen fixation capacity and lowers the application of fertilizer in cereal-based cropping system [7]. According to FAO [8], lentil was grown in a 5.58 million ha area having a production of 5.61 million tons in 2021.

Germplasm characterization is crucial because it provides a source of variations that can be employed for breeding purposes [9]. Similarly, investigation of the relationship among the genotypes is very important for efficient breeding activities to develop modern varieties having high yield, high nutritional value and resistance to biotic and abiotic stress [10]. In the last two decades, genetic diversity has gained great attention and importance [11,12]. It is critical for successful plant breeding studies to discover and characterize novel genes/alleles [13,14].

Numerous research have been undertaken to investigate genetic diversity in various lentil germplasm using DNA-based markers such as RFLP (Restriction fragment length polymorphism) [15], RAPD (Random amplified polymorphic DNA) [16], AFLP (Amplified fragment length polymorphism) [17], ISSR (Inter-simple sequence repeat [18], SSR (Simple sequence repeat) [19], DArT (Diversity Array Technology) [20], SNP (Single Nucleotide Polymorphism technique [13,21,22]. To investigate genetic differences among plant species/subspecies, biochemical markers or seed protein patterns are widely performed [23]. SDS-PAGE technique has mainly been applied for the differentiation of seed protein [24,25]. This technique was used previously to determine genetic diversity in various crop species such as common bean [26,27], coriander [28] and lentil [5,29,30]. In this study, genetic diversity among forty-four lentil genotypes originating from thirteen counties was investigated using seed storage protein pattern. The outputs of this study would contribute an influential source for lentil genetic programs in the future, and support lentil breeders to make successful selections in the near future.

2. Material and Methods

2.1. Plant material

As plant material, the 44 genotypes of lentils from 13 different countries were employed (Table 1). These genotypes were supplied by the USDA (United States Department of Agriculture).

Table 1. The passport information of the lentil genotypes employed in this study.

No	ID	Plant Name	Taxon	Collected Place
1	PI 320946	ILL 513	*Lens culinaris* subsp. *culinaris*	Ancient Palestine
2	PI 193550	ILL 207	*Lens culinaris* subsp. *culinaris*	Ethiopia
3	PI 193549	ILL 206	*Lens culinaris* subsp. *culinaris*	Ethiopia
4	PI 193817	ILL 208	*Lens culinaris* subsp. *culinaris*	Ethiopia
5	PI 193548	ILL 205	*Lens culinaris* subsp. *culinaris*	Ethiopia
6	PI 273664	ILL 247	*Lens culinaris* subsp. *culinaris*	Ethiopia
7	PI 297772	ILL 304	*Lens culinaris* subsp. *culinaris*	Greece
8	PI 297773	ILL 305	*Lens culinaris* subsp. *culinaris*	Greece
9	PI 297765	ILL 297	*Lens culinaris* subsp. *culinaris*	Greece
10	PI 297770	ILL 302	*Lens culinaris* subsp. *culinaris*	Greece
11	PI 297774	ILL 306	*Lens culinaris* subsp. *culinaris*	Greece
12	PI 472365	33-069-00299	*Lens culinaris* subsp. *culinaris*	India
13	PI 472360	33-069-00294	*Lens culinaris* subsp. *culinaris*	India
14	PI 472355	33-069-00288	*Lens culinaris* subsp. *culinaris*	India
15	PI 472370	33-069-00304	*Lens culinaris* subsp. *culinaris*	India
16	PI 472600	33-071-10647	*Lens culinaris* subsp. *culinaris*	Iran
17	PI 472605	33-071-10792	*Lens culinaris* subsp. *culinaris*	Iran
18	PI 472630	33-071-11104	*Lens culinaris* subsp. *culinaris*	Iran
19	PI 472620	33-071-11053	*Lens culinaris* subsp. *culinaris*	Iran
20	PI 472580	33-071-10475	*Lens culinaris* subsp. *culinaris*	Iran
21	PI 577163	W6 8376	*Lens culinaris* subsp. *culinaris*	Iraq
22	PI 577162	W6 8375	*Lens culinaris* subsp. *culinaris*	Iraq
23	PI 577161	W6 8374	*Lens culinaris* subsp. *culinaris*	Iraq
24	PI 577160	W6 8372	*Lens culinaris* subsp. *culinaris*	Iraq
25	PI 577159	W6 8371	*Lens culinaris* subsp. *culinaris*	Iraq
26	PI 612301	Jordan 3	*Lens culinaris* subsp. *culinaris*	Jordan
27	PI 612302	Jordan 1	*Lens culinaris* subsp. *culinaris*	Jordan
28	PI 612303	Jordan 2	*Lens culinaris* subsp. *culinaris*	Jordan
29	PI 302398	ILL 486	*Lens culinaris* subsp. *culinaris*	Jordan
30	PI 420926	11	*Lens culinaris* subsp. *culinaris*	Jordan
31	PI 300559	ILL 479	*Lens culinaris* subsp. *culinaris*	Lebanon
32	PI 300561	ILL 481	*Lens culinaris* subsp. *culinaris*	Lebanon
33	PI 300560	ILL 480	*Lens culinaris* subsp. *culinaris*	Lebanon
34	PI 432253	RPIP 33-085-10610	*Lens culinaris* subsp. *culinaris*	Lebanon
35	PI 432251	RPIP 33-085-10607	*Lens culinaris* subsp. *culinaris*	Lebanon
36	PI 577147	2340	*Lens culinaris* subsp. *culinaris*	Nepal
37	PI 477290	-	*Lens culinaris* subsp. *culinaris*	Pakistan
38	PI 606650	Spanish Brown	*Lens culinaris* subsp. *culinaris*	Spain
39	PI 643449	HALA	*Lens culinaris* subsp. *culinaris*	Syria
40	PI 643450	RACHAYYA	*Lens culinaris* subsp. *culinaris*	Syria
41	PI 643448	KEF	*Lens culinaris* subsp. *culinaris*	Syria
42	PI 644221	TESHALE	*Lens culinaris* subsp. *culinaris*	Syria
43	PI 635040	OZBEK	*Lens culinaris* subsp. *culinaris*	Syria
44	PI 176604	ILL 142	*Lens culinaris* subsp. *culinaris*	Türkiye

2.2. Buffers and reagents

The analysis was carried out in the Biotechnology lab., Department of Biology, Bolu Abant İzzet Baysal University, Bolu, Türkiye. The chemicals used in the study were obtained from Merck. with some modifications of Ghafoor et al. [31], the extraction buffer was arranged using Tris-Hydrochloride 62.5 mM (pH 6.8), SDS 2%, Dithiothreitol (DTT) 10 mM, glycerol 10%, and urea 5M. To obtain seed flour of lentil and extraction of proteins, sterilized microcentrifuge tubes were employed in the study.

2.3. Lentil protein extraction and SDS-PAGE analysis

Twenty seeds were selected for each genotype and bulked. Then, the seeds were grounded using mortar and pestle, and 10 mg powder was weighed in 1.5 ml micro-centrifuge tubes. The proteins were extracted from finely ground lentil seed flour (10 mg) using 400 µL extraction buffer. Following complete mixing by vortex, the micro-centrifuge tubes were heated on a heat block at 40°C for one hour. Following that, homogenates were vortexed for a brief period. The mixtures were centrifuged at 13.000 rpm for 5 minutes. After the centrifuge process, soluble proteins as supernatant were carried to new sterile micro-centrifuge tubes. Total protein concentration was determined as described earlier [32]. Then, the tubes were stored at 4ºC in the fridge. The following day, 20 µg protein of each genotype was mixed with 2X bromophenol blue loading dye and heated at 95 ºC for five minutes. A total of 20 µL denatured protein was loaded into the wells of the polyacrylamide-based discontinuous gel. SDS-PAGE was carried out using the method previously reported by Laemmli [33]. SDS-PAGE was arranged with 4.5% stacking gel and 15% resolving gel. Using the P9DS electrophoresis apparatus (Thermo Scientific, USA), the proteins were electrophoresed at 230 voltage for 4 hours at 4ºC. The gels were then stained using Bio-Safe Coomassie stain (Bio-Rad, Hercules, California, USA) in accordance with the manufacturer's instructions.

2.4. Data analysis

The clear, strong, unambiguous bands were selected for analysis. We scored the strong, clear, and unambiguous protein bands according to a binary system as the present (1) or absent (0). A pairwise genetic distance (GDj) matrix between lentil genotypes was performed according to Jaccard's coefficient [34]. The UPGMA (Unweighted Pair-group Method with Arithmetic Means) clustering analysis and PCoA (Principal Coordinate Analysis) were performed to visualize the pattern of genetic diversity among the lentil genotypes. The UPGMA clustering was constructed via the Jaccard coefficient among the lentil genotypes with Pop Gene v.1.32 software. According to Evanno et al. [35], the number of clusters was found using STRUCTURE software. AMOVA (Analysis of molecular variance) was performed with the vegan library Ver. 2.4.4 in R statistical software.

3. Results and Disscussion

Composed of acidic and basic subunits linked by disulfide bonds, 7S (vicilins and convicilins) and 11S (legumins) globulins represent important storage proteins in lentil seeds [29,36]. The amount of protein bands in the electropherogram was determined to range from 12 to 20 bands in 44 lentil genotypes in SDS. The protein bands obtained from different genotypes were

presented in Figure 1. Using R statistical software, a pairwise genetic distance (GD) matrix among forty-four lentil genotypes was determined, and the maximum GD was found as 0.526 between Syria2 and Iraq3, while the mean GD was 0.216. AMOVA explored the existence of higher genetic diversity within genotypes (83%) compared to among genotypes accounting 0.166% variations (Table 2). The STRUCTURE algorithm separated 44 lentil genotypes into two groups (Figure 2 and Figure 3).

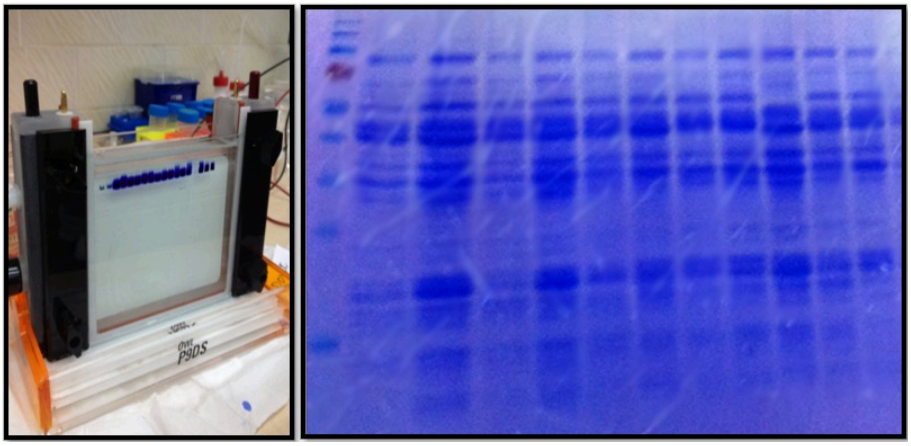

Figure 1. P9DS device used in the study, and some protein bands from different genotypes.

Table 2. Results for AMOVA among lentil genotypes from the different countries as grouped by the clustering algorithm.

Source	df	SS	MS	Estimated Variance	% Variation
Among Population	7	11.305	1.615	0.166	17
Within Population	31	24.952	0.805	0.805	83
Total	38	36.257		0.971	100

MS: Mean square, SS: Sum of squares, df: degrees of freedom,

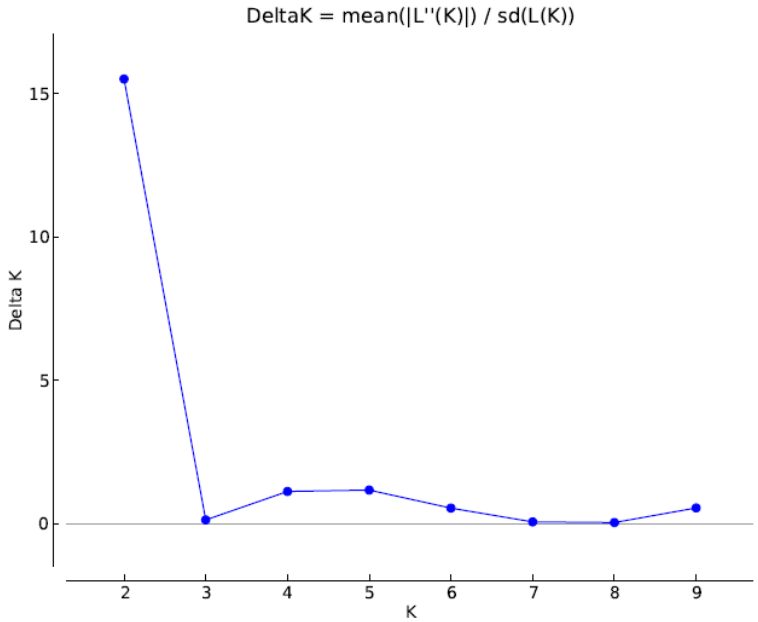

Figure 2. Valued amount of K for the lentil genotypes structure analysis.

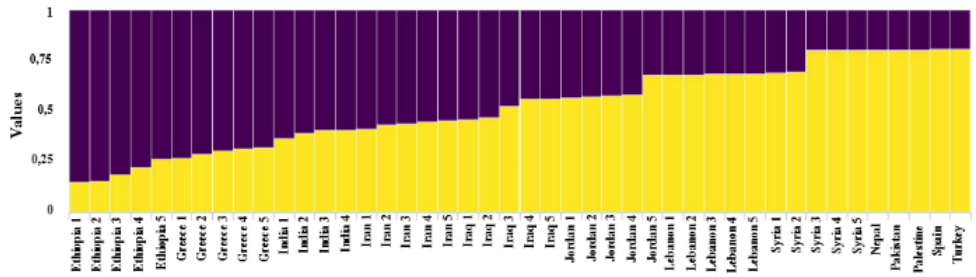

Figure 3. Structure based clustering of lentil genotypes using SDS-PAGE analysis.

The UPGMA clustering was carried out to reveal the pattern of differences among the 44 lentil genotypes. Using the Jaccard genetic distance coefficient, the UPGMA tree was constructed (Figure 4). The studied lentil genotypes were separated into two main clusters A and B. The Cluster A was further grouped in to A1 and A2 by clustering Syria2 and Syria1; Ethiopia5 genotypes, respectively. Cluster B was determined larger than A by clustering a total of 41 lentil genotypes. The main group B cluster was further divided into B1 and B2 subgroups. Subgroup B1 included Iran1, Pakistan and Türkiye lentil genotypes. Results of the UPGMA analysis and principal coordinate analysis, all lentil genotypes were not separated on the basis of their provenance. Interestingly, geographically near genotypes were found genetically distant. For instance, the genotypes from Syria1 and Ethiopia5 which are geographically located in different regions were in group A1. On the other hand, subgroup B2 contained 38 lentil genotypes. The PCoA was also conducted to confirm the results of structure and UPGMA analyses (Figure 5). Results from the PCoA and Structure analyses were in full agreement with those obtained by UPGMA.

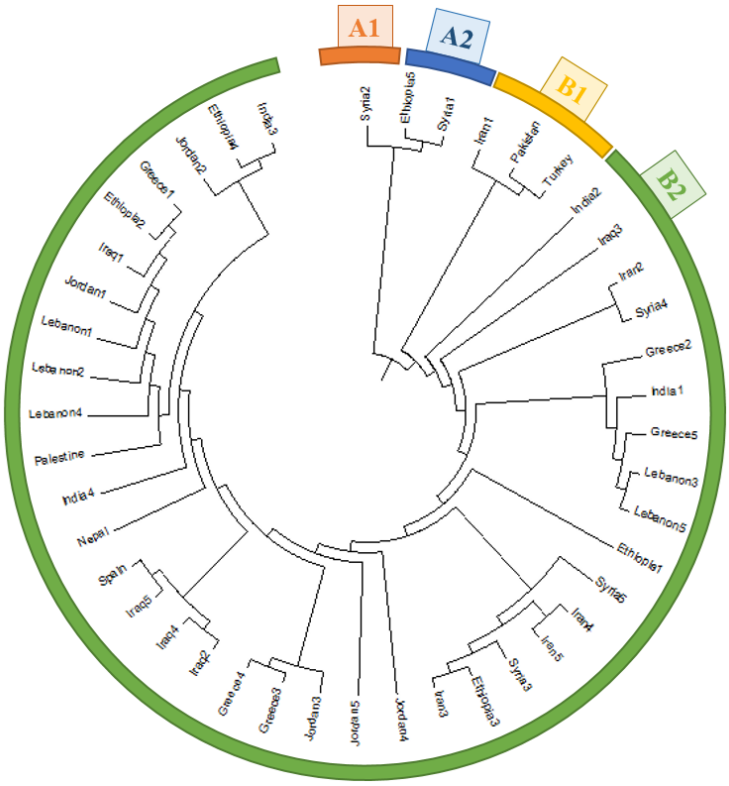

Figure 4. UPGMA clustering analysis of lentil genotypes.

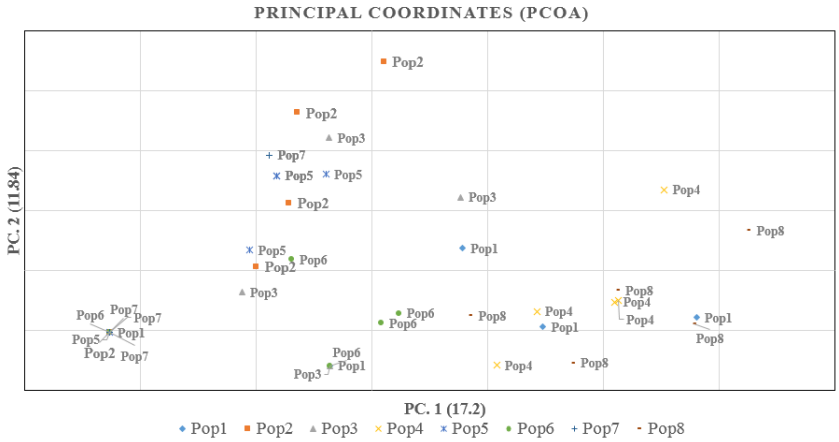

Figure 5. Principal coordinates analysis result of lentil genotypes.

Genetic resources showing the highest level of genetic distance are very important and should be conserved and utilized for future breeding activities. The results of UPGMA, PCoA, and STRUCTURE methods revealed a clear separation of all the lentil genotypes. Various studies were previously performed to explore the genetic variation of different lentil germplasms. For instance, using ISSR markers, Fikiru et al. [37] explored the genetic diversity and population structure of 70 Ethiopian landraces. They reported the presence of higher (56.28%) with the genotypes. In another study, Yüzbaşıoğlu et al. [38] separated 14 lentil cultivars into two main cluster groups using SDS-PAGE analysis. Toklu et al. [39] investigated genetic diversity using molecular markers (AFLP, ISSR, combined AFLP/ISSR) data. They determined that Turkish lentil landraces were separated into two main clusters. Kushwaha et al. [40] determined the highest level of genetic distance in lentil germplasm as 0.027273 using SSR markers. Khazaei et al. [13] used to characterize a total of 352 lentil genotypes with SNP markers and reported that higher genetic variations in their studied material are due to differences within groups (86%). Tahir and Omer [41] explored the genetic variations in lentil genotypes using RAPD markers and morpho-agronomic traits. They reported the existence of higher variation (60%) within lentil genotypes. Lombardi et al. [21], Khazaei et al. [13] and Dissanayake et al. [6] found a weak correlation between clusters and geographical origins in lentil germplasm. Throughout history, the Mediterranean region has been a junction of cultures. It is thought that immigrants and traders played a significant role in the distribution of lentil resources. The genetically different groups determined herein can be evaluated to develop parental lines to initiate lentil breeding programs.

4. Conclusion

A high level of diversity was determined in a panel of 44 lentil genotypes obtained from different countries using SDS-PAGE analysis. The findings have increased the knowledge of the literature on the SDS-PAGE technique in lentil. The results might be useful for breeders/researchers in various parts of the world who are interested in the lentil.

Ethics in Publishing

There are no ethical issues regarding the publication of this study.

Author Contributions

Resources: FSB, Investigation: MZY and MS, Formal analysis: MAN and MZY, Writing-original draft: MZY, MAN, MS, Writing- review & editing: FSB and EG, Supervision: FSB and EG.

References

[1] Maphosa, Y., Jideani, V.A., (2017) Functional Food. María Chávarri Hueda, The Role of Legumes in Human Nutrition (pp: 1-13) IntechOpen: London, UK.

[2] Atnaf, M., Tesfaye, K., Dagne, K., (2015) The importance of legumes in the Ethiopian farming system and overall economy: An overview, American J. Exp. Agric., 7, 347-358.

[3] Singh, M., Sharma, S. K., Singh, B., Malhotra, N., Chandora, R., Sarker, A., Singh, K., Gupta, D., (2018) Widening the genetic base of cultivated gene pool following introgression from wild *Lens* taxa, Plant Breed., 137, 470-485.

[4] Ford-Lloyd, B., (2011) Wild Crop Relatives. Genomic and Breeding Resources. Legume Crops and Forages. *Experimental Agriculture*, 48(1), 152-153. Springer, Heidelberg, Dordrecht, London, New York.

[5] Pal, T., Ghosh, S., Mondal, A., De, K. K., (2016) Evaluation of genetic diversity in some promising varieties of lentil using karyological characters and protein profiling, J. Genetic Eng. Biotechnol., 14, 39-48.

[6] Dissanayake, R., Braich, S., Cogan, N. O., Smith, K., Kaur, S., (2020) Characterization of genetic and allelic diversity amongst cultivated and wild lentil accessions for germplasm enhancement, Front. Gen., 11, 546.

[7] Shah, Z., Shah, S., Peoples, M., Schwenke, G., Herridge, D., (2003) Crop residue and fertiliser N effects on nitrogen fixation and yields of legume–cereal rotations and soil organic fertility, Field Crops Res., 83, 1-11.

[8] FAO (2023). Food and Agriculture Statistics. Retrieved October 06, 2023 from: https:// www.fao.org/faostat/en/#home

[9] Nadeem, M. A., Yeken, M. Z., Shahid, M. Q., Habyarimana, E., Yılmaz, H., Alsaleh, A., Hatipoğlu, R., Çilesiz, Y., Khawar, K.M., Ludidi, N., (2021) Common bean as a potential crop for future food security: an overview of past, current and future contributions in genomics, transcriptomics, transgenics and proteomics, Biotechnol. Biotechnol. Equip., 35, 759-787.

[10] Yeken, M. Z., Emiralioğlu, O., Çiftçi, V., Bayraktar, H., Palacioğlu, G., Özer, G. (2022). Analysis of genetic diversity among common bean germplasm by start codon targeted (SCoT) markers. Mol.Biol. Rep., 49(5), 3839-3847.

[11] Shah, M. A., Khan, A. I., Awan, F. S., Sadaqat, H. A., Bahadur, S., Baloch, F. S., (2015) Genetic diversity of some tomato cultivars and breeding lines commonly used in Pakistani breeding program, Turk J Agric For., 3, 126-132.

[12] Nadeem, M. A., Karaköy, T., Yeken, M. Z., Habyarimana, E., Hatipoğlu, R., Çiftçi, V., Nawaz, M. A., Sönmez, F., Shahid, M. Q., Yang, S. H., (2020) Phenotypic characterization of 183 Turkish common bean accessions for agronomic, trading, and consumer-preferred plant characteristics for breeding purposes, Agronomy., 10, 272.

[13] Khazaei, H., Caron, C. T., Fedoruk, M., Diapari, M., Vandenberg, A., Coyne, C.J. McGee, R. Bett, K.E. (2016) Genetic diversity of cultivated lentil (*Lens culinaris* Medik.) and its relation to the world's agro-ecological zones, Front. Plant Sci., 7, 1093.

[14] Ali, A. Altaf, M. T., Nadeem, M. A., Karaköy, T., Shah, A. N., Azeem, H., Baloch, F. S. Baran, N., Hussain, T., (2022) Duangpan, S. Recent advancement in OMICS approaches to enhance abiotic stress tolerance in legumes, Front. Plant Sci., 13, 952759.

[15] Havey, M., Muehlbauer, F., (1989) Variability for restriction fragment lengths and phylogenies in lentil, Theo. Appl. Genet., 77, 839-843.

[16] Yüzbaşıoğlu, E., Özcan, S., Açık, L., (2006) Analysis of genetic relationships among Turkish cultivars and breeding lines of *Lens culinatis* Mestile using RAPD markers, Genet. Resou. Crop Evo., 53, 507-514.

[17] Alghamdi, S. S., Khan, A. M., Ammar, M. H., El-Harty, E. H., Migdadi, H. M., Abd El-Khalik, S. M., Al-Shameri, A. M., Javed, M. M., Al-Faifi, S. A., (2013) Phenological, nutritional and molecular diversity assessment among 35 introduced lentil (*Lens culinaris* Medik.) genotypes grown in Saudi Arabia, Inter. J. Mol Sci., 15, 277-295.

[18] Seyedimoradi, H., Talebi, R., (2014) Detecting DNA polymorphism and genetic diversity in Lentil (*Lens culinaris* Medik.) germplasm: comparison of ISSR and DAMD marker, Physiol. Mol. Biol. Plant., 20, 495-500.

[19] Tsanakas, G. F., Mylona, P. V., Koura, K., Gleridou, A., Polidoros, A. N., (2018) Genetic diversity analysis of the Greek lentil (*Lens culinaris*) landrace 'Eglouvis' using morphological and molecular markers, Plant Gen. Res., 16, 469-477.

[20] Duygu, A., (2019) Genetic diversity in lentil landraces revealed by diversity array technology (DArT), Turkish J. Field Crop., 24, 252-260.

[21] Lombardi, M., Materne, M., Cogan, N. O., Rodda, M., Daetwyler, H. D., Slater, A. T., Forster, J. W., Kaur, S., (2014) Assessment of genetic variation within a global collection of lentil (*Lens culinaris* Medik.) cultivars and landraces using SNP markers, BMC Gen., 15, 1-10.

[22] Wong, M. M., Gujaria-Verma, N., Ramsay, L., Yuan, H. Y., Caron, C., Diapari, M., Vandenberg, A., Bett, K. E., (2015) Classification and characterization of species within the genus Lens using genotyping-by-sequencing (GBS), PLoS One*.,* 10, e0122025.

[23] Jan, S. A., Shinwari, Z. K., Rabbani, M. A., Shah, S. H., Ibrahim, M. I., Ilyas, M., (2016) Optimization of an efficient SDS-PAGE protocol for rapid protein analysis of *Brassica rapa*., J. Bio. Env. Sci*.,* 9, 17-24.

[24] Kakaei, M., Kahrizi, D., (2011) Study of seed proteins pattern of *Brassica napus* varieties via sodium dodecyl sulfate polyacrylamid gel electrophoresis, Inter. Res. J. Biotech*., 2,* 026-028.

[25] Javaid, A., Ghafoor, A., Anwar, R., (2004) Seed storage protein electrophoresis in groundnut for evaluating genetic diversity, Pak. J. Bot., 36, 25-30.

[26] Berber, İ., Yaşar, F., (2011) Characterization of Bean (*Phaseolus vulgaris* L.) cultivars grown in Turkey by SDS-PAGE of seed proteins, Pak. J. Bot*.,* 43, 1085-1090.

[27] Sher, K., Nisar, M., Subhan, M., Hazrat, A., Muhammad, A., Hancı, F., Fazal, Z., (2020) Protein Profiling of Indegnous Common Bean Through SDS-PAGE, Biosci. Res*.,* 17, 688-898.

[28] Yaldiz, G., Sameeullah, M., Çamlıca, M., Baloch, F. S., (2016) Lack of population structure in coriander populations based on SDS (Seed Storage Protein) page analysis, Turkish J.Agric. Food Sci.Tech*.,* 4, 656-661.

[29] Zaccardelli, M., Lupo, F., Piergiovanni, A. R., Laghetti, G., Sonnante, G., Daminati, M. G., Sparvoli, F., Lioi, L., (2012) Characterization of Italian lentil (*Lens culinaris* Medik.) germplasm by agronomic traits, biochemical and molecular markers, Genet. Resou. Crop Evo., 59, 727-738.

[30] Kumar, P., Trivedi, A., Adarsh, A., Verma, R., Kumar, R., Vyas, R., Yadav, M., (2018) Genetic characterization of lentil genotypes based on SDS-PAGE, J. Pharm. Phytochem*.,* 7, 274-278.

[31] Ghafoor, A., Ahmad, Z., Qureshi, A. S., Bashir, M., (2002) Genetic relationship in *Vigna mungo* (L.) Hepper and *V. radiata* (L.) R. Wilczek based on morphological traits and SDS-PAGE, Euphytica*.,* 123, 367-388.

[32] Sameeullah, M., Sasaki, T., Yamamoto, Y., (2013) Sucrose transporter NtSUT1 confers aluminum tolerance on cultured cells of tobacco (*Nicotiana tabacum* L.), Soil Sci. Plant Nut*.,* 59, 756-770.

[33] Laemmli, U. K., (1970) Cleavage of structural proteins during the assembly of the head of bacteriophage T4, Nature., 227, 680-685.

[34] Jaccard, P., (1908) Nouvelles recherches sur la distribution florale, Bull. Soc. Vaud. Sci. Nat*.,* 44, 223-270.

[35] Evanno, G., Regnaut, S., Goudet, J., (2005) Detecting the number of clusters of individuals using the software STRUCTURE: a simulation study, Mol. Ecol., 14, 2611-2620.

[36] Scippa, G. S., Rocco, M., Ialicicco, M., Trupiano, D., Viscosi, V., Di Michele, M., Arena, S., Chiatante, D., Scaloni, A., (2010) The proteome of lentil (*Lens culinaris* Medik.) seeds: discriminating between landraces, Electrophoresis., 31, 497-506.

[37] Fikiru, E., Tesfaye, K., Bekele, E., (2007) Genetic diversity and population structure of Ethiopian lentil (*Lens culinaris* Medikus) landraces as revealed by ISSR marker, African J. Biotechnol., 6, 1460-1468.

[38] Yüzbaşioğlu, E., Acik, L., Özcan, S., (2008) Seed protein diversity among lentil cultivars, Biologia Plantarum**.,** 52, 126-128.

[39] Toklu, F., Karaköy, T., Haklı, E., Bicer, T., Brandolini, A., Kilian, B., Özkan, H., (2009) Genetic variation among lentil *(Lens culinaris* Medik) landraces from Southeast Turkey, Plant Breed., 128, 178-186.

[40] Kushwaha, U., Ghimire, S., Yadav, N., Ojha, B., (2013) Genetic relatedness of lentil (*Lens culinaris* L.) germplasm by using SSR markers, Int. J. Appl. Sci. Biotechnol., 1, 132-136.

[41] Tahir, N. A. R., Omer, D., (2017) Genetic variation in lentil genotypes by morpho-agronomic traits and RAPD-PCR, J Anim. Plant Sci. 27, 468-480.

Erzincan Üniversitesi
Fen Bilimleri Enstitüsü Dergisi
2024,17(1), 91-99
ISSN: 1307-9085, e-ISSN: 2149-4584
Araştırma Makalesi

Erzincan University
Journal of Science and Technology
2024,17(1), 91-99
DOI: 10.18185/erzifbed.1329880
Research Article

Evaluation of Antimicrobial Effects of Some Plant Species Growing in Turkiye: *Verbascum lydium* Boiss. var. *lydium* Boiss., *Euphorbia anacampseros* Boiss. var. *tmolea* M.S. Khan., *Rosa pisiformis* subsp. *pisiformis* (Christ) D. Sosn., *Stachys tmolea* Boiss. subsp. *tmolea* and *Aronia melanocarpa* (Michx.) Elliott

Çiğdem BİLGİ[1*], Hatice DEMİRAY[2], Engin KAPLAN[3]

[1]Department of Pharmacognosy, Faculty of Pharmacy, Istanbul University-Cerrahpasa, Istanbul, Turkiye.
[2] Department of Biology, Section of Botany, Faculty of Science, Ege University, Izmir, Turkiye.
[3] Department of Pharmaceutical Microbiology, Faculty of Pharmacy, Istanbul University-Cerrahpasa, Istanbul, Turkiye.

Received: 19/07/2023, **Revised:** 19/02/2024, **Accepted:** 19/02/2024, **Published:** 28/03/2024

Abstract
The increasing prevalence of antibiotic-resistant bacteria has emerged as a critical global public health issue, necessitating the exploration of alternative measures to combat infectious diseases. Traditional medicinal plants have been long recognized for their potential in providing natural compounds with antimicrobial properties for various therapeutic purposes. The diverse plant biodiversity in Turkiye offers a promising potential for the discovery of novel antimicrobial compounds. Therefore, this study aimed to investigate the antimicrobial activities of extracts from several endemic and non-endemic plant species against various microorganisms. The endemic species included *Verbascum lydium* Boiss. var. *lydium* Boiss. (stem), *Euphorbia anacampseros* Boiss. var. *tmolea* M. S. Khan. (root), *Stachys tmolea* Boiss. subsp. *tmolea* (leaves and stem), *Rosa pisiformis* subsp. *pisiformis* (Christ) D. Sosn. (fruit, petiole, root, leaves), while non-endemic species were represented by cultivated *Aronia melanocarpa* (Michx.) Elliott (fruit). In this research, the effectiveness of *V. lydium* var. *lydium* (stem), *E. anacampseros* var. *tmolea* (root), *R. pisiformis* subsp. *pisiformis* (all tested parts) and *A. melanocarpa* (fruit) were demonstrated against *Staphylococcus aureus* and *Escherichia coli*. Methanolic extracts of the roots and leaves of *R. pisiformis* subsp. *pisiformis* showed the most promising bioactivity with a MIC value of 62.5 µg mL^{-1} on *Pseudomonas aeruginosa* among all tested extracts. In addition, the results showed that antimicrobial activities were observed for *V. lydium*; *S. tmolea* and *R. pisiformis* against *Candida parapsilosis*, *Candida glabrata* and *Klebsiella pneumoniae* with MIC values of 31.5 µg mL^{-1} per each. The findings of this study could provide valuable information for future research into the use of Turkish plants for pharmacological purposes, public health and traditional medicine applications.
Keywords: *Verbascum lydium*, *Euphorbia anacampseros*, *Rosa pisiformis*, *Aronia melanocarpa*, *Stachys tmolea*, antimicrobial.

*Corresponding Author: cigdem.karakoyun@iuc.edu.tr
Çiğdem BILGI, https://orcid.org/0000-0003-1150-7061
Hatice DEMIRAY, https://orcid.org/0000-0002-4400-237X
Engin KAPLAN, https://orcid.org/0000-0001-5705-717X

Türkiyede yetişen bazı bitki türlerinin antimikrobiyal etkilerinin değerlendirilmesi: *Verbascum lydium* Boiss. var. *lydium* Boiss., *Euphorbia anacampseros* Boiss. var. *tmolea* M.S. Khan., *Rosa pisiformis* subsp. *pisiformis* (Christ) D. Sosn., *Stachys tmolea* Boiss. subsp. *tmolea* ve *Aronia melanocarpa* (Michx.) Elliott

Antibiyotiklere dirençli bakterilerin yaygınlığının artması sebebiyle, bulaşıcı hastalıklarla mücadele etmek için alternatif yöntemlerin araştırılması, halk sağlığı açısından kritik öneme sahip bir durum haline gelmiştir. Geleneksel tıbbi bitkiler, çeşitli terapötik amaçlar için kullanılabilecek doğal antimikrobiyal özelliklere sahip bileşikler içermesi ile bilinmektedir. Türkiye'deki bitki çeşitliliği, yeni antimikrobiyal bileşiklerin keşfi için umut verici bir potansiyel sunmaktadır. Bu araştırma, bazı bitki türlerinin ekstrelerinin antimikrobiyal aktivitelerini araştırmayı amaçlamıştır. Endemik türler arasında *Verbascum lydium* var. *lydium* Boiss. (sap), *Euphorbia anacampseros* var. *tmolea* Boiss. (kök), *Stachys tmolea* Boiss. subsp. *tmolea* (yapraklar ve sap), *Rosa pisiformis* subsp. *pisiformis* (Christ) D. Sosn. (meyve, sap, kök, yaprak) bulunurken, endemik olmayan tür *Aronia melanocarpa* (Michx.) Elliott (meyve) ile temsil edilmiştir. *V. lydium* var. *lydium*, *E. anacampseros* var. *tmolea* (kök), *Rosa pisiformis* subsp. *pisiformis* (test edilen tüm kısımları) ve *A. melanocarpa* (meyve) örneklerinin antibakteriyel etkinlikleri *Staphylococcus aureus* ve *Escherichia coli*'ye karşı gösterilmiştir. *Rosa pisiformis*'in kökleri ve yapraklarından elde edilen metanolik ekstreler, tüm test edilen ekstreler arasında *Pseudomonas aeruginosa* üzerinde 62.5 µg mL^{-1} MIC değeriyle en umut verici biyoaktiviteyi göstermiştir. Ayrıca, *Verbascum lydium* var. *lydium*; Stachys tmolea subsp. tmolea ve *Rosa pisiformis* subsp. *pisiformis* için *Candida parapsilosis*, *Candida glabrata* ve *Klebsiella pneumoniae* için antimikrobiyal aktivitelerin gözlendiği sonuçlar, her biri için 31.5 µg mL^{-1} MIC değeriyle gösterilmiştir. Bu çalışmanın bulguları, Türkiye bitkileri üzerinde gelecekte yapılacak olan farmakolojik araştırmalar ile, halk sağlığı ve geleneksel tıp uygulamaları için değerli bilgiler sağlama potansiyeline sahiptir.

Anahtar Kelimeler: *Verbascum lydium*, *Euphorbia anacampseros*, *Rosa pisiformis*, *Aronia melanocarpa*, *Stachys tmolea*, antimikrobiyal.

1. Introduction

Antibiotics have been widely used as the main therapeutic agents against bacterial and fungal infections since their discovery and were believed to lead to the eradication of infectious diseases [1]. However, the overuse or misuse of antibiotics have resulted in the emergence and spread of multi-drug resistant strains of various microorganisms, such as *Escherichia coli*, *Klebsiella pneumoniae*, and *Candida albicans* causing an increase in the cost of medicines and patient mortality. Consequently, the search for new antimicrobial agents has become imperative, and attention has turned towards natural products as potential sources [2].

Many traditional medicinal plants have been used for centuries to treat infectious diseases, with some plants having demonstrated remarkable efficacy in treating infections [3]. Researchers have found that plants contain a wide variety of secondary metabolites such as tannins, alkaloids, terpenoids, saponins and flavonoids, which exhibit *in vitro* antimicrobial properties [4]. Numerous medicinal plants are used as phytotherapeutics for treating infectious diseases due to their availability, fewer side effects, and reduced toxicity.

In this research a comprehensive screening of antimicrobial activity was performed for some plants growing in Turkiye including *Verbascum lydium* Boiss. var. *lydium* Boiss., *Euphorbia anacampseros* Boiss. var. *tmolea* M. S. Khan., *Stachys tmolea* Boiss. subsp. *tmolea*, *Rosa pisiformis* subsp. *pisiformis* (Christ) D. Sosn., and *Aronia melanocarpa* (Michx.) Elliott.

Verbascum is a genus of flowering plants, in the family Scrophulariaceae, being represented with approximately 360 species [5]. *V. lydium* var. *lydium*, is a subspecies of the *V. lydium* being endemic to Turkiye. In traditional medicine, various parts of the plants belonging to *Verbascum* genus have been used to treat various ailments [6]. For instance, the leaves and flowers have been used to relieve coughs, sore throat, and bronchitis [7]. The plant has also been used to treat ear infections and hemorrhoids. In addition, the seeds of the plant have been used to treat skin diseases [8]. The flowers of *V. lydium* var. *lydium* are edible and mainly consumed by children [9]. However studies on *V. lydium* var. *lydium* is quite limited. Although morphological and taxonomic studies have been conducted on this species, no study evaluating its antimicrobial effect has been found.

E. anacampseros var. *anacampseros* is an endemic plant of Turkiye belonging to the family Euphorbiaceae. This family is represented by approximately 240 genera and 6000 species worldwide. *Euphorbia* L. is the most well-known genus of the family and represented by approximately 2150 taxa worldwide, including 120 taxa in Turkiye, 18 of which are endemic to Turkiye. Studies on the bioactivity of *E. anacampseros* var. *anacampseros* are very limited, with more emphasis on botanical, morphological, and taxonomic studies [10,11]. Some phytochemical analysis was performed on the plant. According to the literature, the Fourier-transform infrared (FTIR) spectroscopic data obtained from *E. anacampseros* indicated the presence of hydrocarbons, particularly terpenoids, alkanes, and olefin structures, in the plant's composition. The efficacy of extracts with different polarities obtained from a plant against *Mycobacterium tuberculosis* has been investigated [12]. Research on bioactivity and medicinal properties of this endemic plant is very limited.

S. tmolea subsp. *tmolea* is a perennial herbaceous plant belonging to the Lamiaceae family, which is widely distributed in the Mediterranean region. The genus *Stachys* comprises over 300 species, and is known for its diverse medicinal and culinary uses. *S. tmolea* subsp. *tmolea* has a great importance for Turkiye being an endemic plant for this region. In traditional medicine, *Stachys* species has been used as a natural remedy for various ailments such as digestive problems, respiratory tract infections, and skin disorders [13]. The plant is also known for its antimicrobial, anti-inflammatory, and antioxidant properties.

In addition to its traditional use, *S. tmolea* subsp. *tmolea* has been the subject of scientific research due to its potential therapeutic benefits. Studies have shown that the plant contains

various bioactive compounds such as flavonoids, phenolic acids, and terpenes, which are responsible for its medicinal properties [14]. It has been reported that the ethanol extract of *S. tmolea* leaves exhibited strong effects against *S. aureus*, a Gram-positive strain [15]. In another research, plants were collected from the Kütahya-Eskişehir region and aerial parts were extracted using methanol and water. These extracts were analysed to determine phenolic constituents and antioxidant activities were evaluated [14].
R. pisiformis subsp. *psiformis* (Christ) D. Sosn. is a shrub species belonging to the family Rosaceae, which is widely distributed in the eastern Mediterranean region, including Turkiye, Lebanon, and Syria. In recent years, the genus has gained attention from researchers due to its potential pharmacological activities, particularly its antioxidant, antimicrobial, and anti-inflammatory properties [16]. Despite being a relatively unknown species, *R. pisiformis* has been traditionally used in local medicine for the treatment of various ailments, including gastrointestinal disorders, hemorrhoides and diabetes [17]. Ercisli et al., investigated the fatty acid composition of the seeds of the plant [18]. Also total phenolic content, ascorbic acid, total soluble solids, total dry weight, total fat, fatty acids, pH, acidity, moisture, fruit color and macro- and micro-element profiles were investigated in the fruits of *R. pisiformis* comparatively with some other *Rosa* species [19]. Yılmaz and Ercisli reported antimicrobial activity of fruits of *R. pisiformis* which was collected from the Eastern Anatolia region in Turkiye [20]. Further studies are required to fully understand the pharmacological potential of *R. pisiformis* subsp, *pisiformis* and its possible applications in modern medicine.

The present study aimed to investigate the antibacterial and antifungal activity of the extracts of endemic species *Verbascum lydium* Boiss. var. *Lydium* (stem), *Euphorbia anacampseros* Boiss. var. *tmolea* M.S. Khan (root), *Stachys tmolea* Boiss. subsp. *tmolea* (leaves and stem), *Rosa pisiformis* subsp. *pisiformis* (Christ) D. Sosn. (fruit, petiole, root, leaves) and a non-endemic species *Aronia melanocarpa* (Michx.) Elliott (fruit) against various microorganisms: *E. coli*, *Klebsiella pneumoniae*, *Staphylococcus aureus, Acetobacter baumannii, Pseudomonas aeruginosa, Candida albicans*, *Candida parapsilosis* and *Candida glabrata.*
This study highlights the importance of screening plants for their antibacterial and antimycotic activities. The exploration of natural products could offer a promising and sustainable approach towards the development of novel drugs. Further studies are required to determine the active compounds responsible for the observed antimicrobial activity, and to elucidate their mechanisms of action. Ultimately, the discovery of new antimicrobial agents from natural sources could have a significant impact on public health and the global fight against infectious diseases.

2. Material and Methods

2.1 Plant material

The plant materials were carefully examined to ensure their accurate identification, including their anatomical structures and physical features. The names of the species, local names, collection dates, locations, and herbarium codes are all listed in Table 1. The identification of plant species and taxa was conducted by Prof. Dr. Hatice Demiray from Ege University, Izmir, Turkiye.

Table 1. Botanical and Depositional Characteristics of Tested Plant Species

Extract Code	Botanical Name of plant	Part used	Collection date	Location	Herbarium Code
1	*Verbascum lydium* Boiss. var. *lydium* Boiss.	Stem	07/2017	Ödemiş-İzmir	25095
2	*Euphorbia anacampseros* Boiss. var. *tmolea* M.S. Khan	Root	07/2017	Ödemiş-İzmir	42191
3 4	*Stachys tmolea* Boiss. subsp. *tmolea*	Leaves Stem	07/2019	Ödemiş-İzmir	19578
5 6 7 8	*Rosa pisiformis* subsp. *psiformis* (Christ) D. Sosn.	Fruit Stem Root Leaves	08/2020	Akçakale-Gümüşhane	44010
9	*Aronia melanocarpa* (Michx.) Elliott	Fruit	09/2022	Büyükçekmece-İstanbul	220901

Fruits of *A. melanocarpa* (Michx.) Elliott (commonly known as chokeberries) were collected from a producer's field, in the Kamiloba region in Büyükçekmece, Istanbul during the flowering season. These fruits were cultivated and deposited at the Istanbul University-Cerrahpaşa, Faculty of Pharmacy Herbarium, with a voucher number of 220901.
The other plants tested in this study were *R. pisiformis* subsp. *psiformis* samples collected from Akçakale district of Gümüşhane province (Eastern Black Sea Region, Turkiye); *V. lydium* var. *lydium*, *E. anacampseros* var. *tmolea* and *S. tmolea* subsp. *tmolea* collected from Ödemiş-Bozdağ/İzmir and voucher specimens deposited at Ege University Herbarium Center in Izmir, Turkiye, as listed in Table 1. After collection, these plants were air-dried, ground into a fine powder, and stored in light-proof glass bottles at room temperature until extraction step.

1.2 Preparation of Herbal Extracts

Extract code 1-8: Powdered samples were macerated with methanol (10g/100mL; Fisher Scientific, analytical grade) using an ultrasonic bath for 30 minutes. Extractions were performed triplicate and then collected. The crude extracts were obtained by evaporating the organic solvents in vacuum (Heidolph Laborata, Germany).

Extract code 9: The fruits of *A. melanocarpa* were homogenized and centrifuged 3000 rpm for 3 min. Supernatant was freeze dried and stored at -20 °C until experiment.

2.3 Antimicrobial Bioactivity Test

The microbroth dilution method was utilized to determine the minimum inhibitory concentration (MIC) values of the extracts in antimicrobial activity studies following the Clinical and Laboratory Standards Institute M27-A and M27-A3 documents against *E. coli* (ATCC 25922), *P. aeruginosa* (ATCC 27853), *S. aureus* (ATCC 29213), *A. baumannii* (ATCC 02026), *C. albicans* (ATCC 14053), *C. parapsilosis* (ATCC 22019), and *C. glabrata* (ATCC 15126) [21,22]. Stock solutions of the plant extracts were prepared at 1000 µg mL^{-1}. Density of the cells was adjusted to Mc Farland 0.5 in sterilized saline solution. Two-fold dilutions were prepared in 100 µL of Mueller-Hinton broth (Sigma-Aldrich, St. Louis, MO) and RPMI 1640

medium (Sigma-Aldrich, St. Louis, MO) for 18 hours for bacteria and yeasts. Then, 10 µL microorganisms suspensions were added for each species. The MIC values were determined visually and by spectrophotometric evaluation at 450 nm after 18 hours incubation at 37 °C. The ciprofloxacin and the fluconazole were used as reference drugs.

3. Results and Disscussion

Antimicrobial activities of nine herbal extracts (single or combine) were evaluated against *E. coli*, *P. aeruginosa*, *S. aureus*, *A. baumannii*, *C. albicans*, *C. parapsilosis* and *C. glabrata* (Table 1). In this study, the effectiveness of *V. lydium* var. *lydium*, *E. anacampseros* var. *tmolea*, *R. pisiformis* subsp. *pisiformis* and *A. melanocarpa* (fruits) were demonstrated against *S. aureus* and *E. coli* at a concentration of 62.5 µg mL^{-1} when used individually. However, *S. tmolea* subsp. *tmolea* did not exhibit any antimicrobial activity on these two species up to 125 µg mL^{-1}. Methanolic extracts of the roots and leaves of *R. pisiformis* (roots and leaves) showed the most promising bioactivity with a MIC value of 62.5 µg mL^{-1} on *P. aeruginosa* among all tested extracts (Table 2).

Table 2. *Antimicrobial activities of herbal extracts collected from Turkiye. MICs are given in µg mL^{-1}.*

Extract No	Sa	Ec	Pa	Ab	Kp	Ca	Cp	Cg
1	62.5	62.5	125	62.5	31.25	31.25	31.25	31.25
2	62.5	62.5	125	62.5	62.5	62.5	31.25	31.25
3	125	125	125	62.5	31.25	62.5	31.25	31.25
4	125	125	125	62.5	62.5	62.5	31.25	31.25
5	62.5	62.5	125	62.5	31.25	62.5	31.25	31.25
6	62.5	62.5	125	62.5	31.25	62.5	31.25	31.25
7	62.5	62.5	62.5	62.5	31.25	62.5	31.25	31.25
8	62.5	62.5	62.5	62.5	31.25	62.5	31.25	31.25
9	62.5	62.5	125	125	62.5	62.5	500	Nt
C*(5+9)	250	125	Nt	Nt	Nt	125	Nt	Nt
C*(1+2)	250	125	Nt	Nt	Nt	62.5	Nt	Nt
Ciprofloxacin	3.90	3.90	7.81	3.90	3.90	–	–	–
Fluconazole	–	–	–	–	–	1.95	3.90	7.81

1, *Verbascum lydium* var. *lydium* (stem); 2, *Euphorbia anacampseros* var. *tmolea* (stem); 3,4, *Stachys tmolea* subsp. *tmolea* (leaves and stem); 5-8, *Rosa pisiformis* subsp. *pisiformis* (fruit, petiole, root, leaves); 9, *Aronia melanocarpa* (fruit). Ec, *Escherichia coli*; Pa, *Pseudomonas aeruginosa*; Sa, *Staphylococcus aureus*; Ab, *Acetobacter baumannii*; Ca, *Candida albicans*; Cp, *C. parapsilosis*; Cg, *C. glabrata*. Nt: not tested; C*: combination formulations. Tested concentration range: 500 – 0.48 µg/mL.

All single extract treatments exhibited similar antibacterial effects at 62.5 µg mL^{-1} concentration against *A. baumannii* except for *A. melanocarpa* fruit juice for which MIC was calculated as 125 µg mL^{-1}. Striking bioactivities were observed for *V. lydium* var. *lydium; S. tmolea* subsp. *tmolea. and R. pisiformis* subsp. *psiformis* (with MIC value of 31.5 µg mL^{-1} per each) against *C. parapsilosis*, *C. glabrata* and *K. penemanue*.

The combination prepared using *E. anacampseros* var. *tmolea* roots with *V. lydium* var. *lydium* Stems displayed superior antimycotic activity on *C. albicans* compared to DMSO, the solvent control. Also, all extracts except for fruit juice of *A. melanocarpa* inhibited *Acetobacter* sp.

compared to DMSO. Methanol extract of *V. lydium* var. *lydium* stems was the most prominent preparation against *C. albicans* while only *V. lydium* var. *lydium* stem extract and *Rosa pisiformis* leaf extracts showed antimycotic activity against *C. parapsilosis.*

To our knowledge this is the first report on the antimicrobial acitivity evaluations of endemic species tested in this study. However, antibacterial effects of *A. melanocarpa* extracts against *S. aureus*, *E. coli* and *B. subtilis* were reported in the literautre [23,24]. Tanagardi investigated differential effects of commercial, liquid and dry extracts of *A. melanocarpa* on various microbial strains such as *Saccharomyces cerevisiae*, *S. aureus*, *E. coli* O157:H7, and *Salmonella typhimurium* [24]. Notably, the results demonstrated that the liquid and dry extracts of *A. melanocarpa* exhibited distinct effects on Gram (+) bacteria, Gram (-) bacteria, and the *S. cerevisiae* yeast strain. The antifungal activity of the liquid and dry extracts at a concentration of 180 µg/mL against *S. cerevisiae* resulted in a remarkable 99% reduction in fungal growth. Furthermore, the liquid extract showed significant antibacterial activity at a concentration of 180 µg/mL against *E. coli*, leading to a 99% reduction in bacterial population. In the case of *S. typhimurium*, the liquid extract at a concentration of 180 µg/mL exhibited a 100% inhibition of bacterial growth, while the dry extract did not display significant antibacterial effects. The evaluation of *S. aureus* bacterial strains further highlighted the differential antibacterial activities of the liquid and dry extracts at varying concentrations, with the liquid extract at 180 µg/mL and 90 µg/mL concentrations resulting in 100% and 99.9% bacterial reduction, respectively. The dry extract also demonstrated strong antibacterial effects, with a 99.9% inhibition of bacterial growth at a concentration of 180 µg/mL. These findings align with the result obtained in our study, where the MIC of *A. melanocarpa* was 62.5 µg/mL against both *S. aureus* and *E. coli*.

4. Conclusion

In conclusion, this study has shed light on the bioactivities of some valuable plant species in Turkiye. This provides significant contributions towards the evaluation of plants growing in Turkiye for pharmaceutical approaches, public health, traditional medicine applications, and pharmacological purposes.

Based on the findings, significant bioactivities were observed for *V. lydium* var. *lydium*, *S. tmolea* subsp. *tmolea*, and *R. pisiformis* subsp. *psiformis* (each with a MIC value of 31.5 µg mL-1) against *C. parapsilosis, C. glabrata*, and *K. penemanue*. This highlights the research value of these plants which are growing in Turkiye, emphasising their potential in exhibiting antimicrobial activity. *A. melanocarpa* also displayed antibacterial and antifungal activities consistent with finding in the literature. The obtained findings involve preliminary evaluations of tested plant species in relation to their antimicrobial potential against diverse bacterial and fungal strains. However, further research is needed to understand the mechanism of antimicrobial action of these plant extracts. The information obtained from this study serves as a starting point for future investigations, which can aid in the discovery of new drug leads and the development of novel therapeutics.

Ethics in Publishing

There are no ethical issues regarding the publication of this study. Approval from any committee is not required for collection of plant material.

Author Contributions

Authors declares the contribution of the authors is equal. Conceptualization: ÇB; Investigation: HD; Methodology: EK; Writing: ÇB and EK; Review-editing: HD.

Acknowledgements

We wish to acknowledge Feridun Bakır for kindly providing aronia fruits for this research.

References

[1].Khan, Rosina, Barira Islam, Mohd Akram, Shazi Shakil, Anis Ahmad, S Manazir Ali, Mashiatullah Siddiqui, and Asad U Khan. 2009. "Antimicrobial Activity of Five Herbal Extracts against Multi Drug Resistant (MDR) Strains of Bacteria and Fungus of Clinical Origin." *Molecules* 14 (2): 586–97.

[2].Cragg, Gordon M, and David J Newman. 2013. "Natural Products: A Continuing Source of Novel Drug Leads." *Biochimica et Biophysica Acta (BBA)-General Subjects* 1830 (6): 3670–95.

[3].Mahady, Gail B. 2005. "Medicinal Plants for the Prevention and Treatment of Bacterial Infections." *Current Pharmaceutical Design* 11 (19): 2405–27.

[4].Arif, Tasleem, J D Bhosale, Naresh Kumar, T K Mandal, R S Bendre, G S Lavekar, and Rajesh Dabur. 2009. "Natural Products–Antifungal Agents Derived from Plants." *Journal of Asian Natural Products Research* 11 (7): 621–38.

[5]Shakeri, A R, and A Farokh. 2015. "Phytochemical Evaluation and Antioxidant Activity of Verbascum Sublobatum Murb. Leaves." *Research Journal of Pharmacognosy* 2 (3): 43–47.

[6].Panchal, Mayank A, Krishna Murti, and Vijay Lambole. 2010. "Pharmacological Properties of Verbascum Thapsus—A Review." *Int J Pharm Sci Rev Res* 5 (2): 73–77.

[7].Jamshidi-Kia, Fatemeh, Zahra Lorigooini, Sedigheh Asgari, and Karamatollah Saeidi. 2018. "Iranian Species of Verbascum: A Review of Botany, Phytochemistry, and Pharmacological Effects." *Toxin Reviews*.

[8].Tatli, I Irem, and Zeliha Fi Akdemir. 2006. "Traditional Uses and Biological Activities of Verbascum Species." *FABAD Journal of Pharmaceutical Sciences* 31 (2): 85.
[9].Ertuğ, Füsun. 2004. "Wild Edible Plants of the Bodrum Area (Muğla, Turkey)." *Turkish Journal of Botany* 28 (1): 161–74.

[10].Gokcen, Ümmüşen, Onur Koyunvu, and Okan Sezer. 2018. "Euphorbia Anacampseros Boiss. Var. Anacampseros Üzerinde Morfo-Anatomik Araştırmalar." *Biyoloji Bilimleri Araştırma Dergisi* 11 (2): 11–13.

[11]Tutgun, Gizem, and Ahmet Gönüz. 2020. "An Endemic Plant Growing In Kazdağı Importance And Usage Areas Of Euphorbia Anacampseros Boiss. Var. Anacampseros taxon." *Journal of Scientific Perspectives* 4 (4): 281–88.

[12].Askun, Tülin, Emmanuel Mouafo Tekwu, Fatih Satil, Seyma Modanlioglu, and Hatice Aydeniz. 2013. "Preliminary Antimycobacterial Study on Selected Turkish Plants (Lamiaceae) against Mycobacterium Tuberculosis and Search for Some Phenolic Constituents." *BMC Complementary and Alternative Medicine* 13 (1): 1–11.

[13].Demiray, Hatice, Nurhayat Tabanca, Alden S Estep, James J Becnel, and Betül Demirci. 2019. "Chemical Composition of the Essential Oil and N-Hexane Extract of Stachys Tmolea Subsp. Tmolea Boiss., an Endemic Species of Turkey, and Their Mosquitocidal Activity against Dengue Vector Aesdes Aegypti." *Saudi Pharmaceutical Journal* 27 (6): 877–81.

[14].Elfalleh, Walid, Bulent Kirkan, and Cengiz Sarikurkcu. 2019. "Antioxidant Potential and Phenolic Composition of Extracts from Stachys Tmolea: An Endemic Plant from Turkey." *Industrial Crops and Products* 127: 212–16.

[15].Leblebici, Sema, Özge Kaygusuz, Tülin Korkmaz, and Cihan Darcan. 2016. "The Antimicrobial Activities of the Leaves of Some Endemic Stachys Species Spreading in West Anatolia, Turkey." *Mitteilungen Klosterneuburg*.

[16].Selahvarzian, Amin, Abuzar Alizadeh, Peyman Amanolahi Baharvand, Omayma A Eldahshan, and Bahram Rasoulian. 2018. "Medicinal Properties of Rosa Canina L." *Herbal Medicines Journal (Herb Med J)*, 77–84.

[17].Dalar, Abdullah, Muzaffer Mukemre, Murat Unal, and Fevzi Ozgokce. 2018. "Traditional Medicinal Plants of Ağrı Province, Turkey." *Journal of Ethnopharmacology* 226: 56–72.
[18].Ercisli, S, E Orhan, and A Esitken. 2007. "Fatty Acid Composition of Rosa Species Seeds in Turkey." *Chemistry of Natural Compounds* 43: 605–6.

[19].Ercisli, Sezai. 2007. "Chemical Composition of Fruits in Some Rose (Rosa Spp.) Species." *Food Chemistry* 104 (4): 1379–84.

[20].Yilmaz, Suzan Ozturk, and SEZAI Ercisli. 2011. "Antibacterial and Antioxidant Activity of Fruits of Some Rose Species from Turkey." *Romanian Biotechnological Letters* 16 (4): 6407–11

[21]. Institute, Clinical and Laboratory Standards. 2006. "Methods for Dilution Antimicrobial Susceptibility Tests for Bacteria That Grow Aerobically." *Approved Standard M7-A7*. Clinical and Laboratory Standards Institute Wayne, PA.

[22].Wayne, P A. 2002. "Reference Method for Broth Dilution Antifungal Susceptibility Testing of Yeasts, Approved Standard." *CLSI Document M27-A2*.

[23].Zhang, X., Song, M., Xu, W., & Xu, W. (2023). Polyphenols extracted from Aronia melanocarpa by combined enzymatic and ultrasonication and their antioxidant potential and antimicrobial activity. *多酚*, *5*(1), 35-47.

[24].Tanağardı, D. (2023). *Antimicrobial, antioxidant, antiproliferative and cytotoxic activities of aronia fruit extract* (Master's thesis, 01. Izmir Institute of Technology).

Erzincan Üniversitesi
Fen Bilimleri Enstitüsü Dergisi
2024,17(1), 100-112
ISSN: 1307-9085, e-ISSN: 2149-4584
Araştırma Makalesi

Erzincan University
Journal of Science and Technology
2024,17(1), 100-112
DOI: 10.18185/erzifbed.1331065
Research Article

Determination of the Relationship Between the Number of Clusters and Primary Bud Size in *Vitis vinifera* and *Vitis labrusca* Grapevines by Histological Sectioning Method

Muhammed KÜPE[1*]

[1]Atatürk University, Faculty of Agriculture, Department of Horticulture, 254240, Erzurum, Turkey

Received: 21/07/2023, **Revised:** 26/10/2023, **Accepted:** 26/10/2023, **Published:** 28/03/2024

Abstract

This study was conducted to reveal the relationship between the number of clusters and primary buds size in dormant grapevine winter buds. In addition, it has been tried to determine how the size of the primary bud and the cluster primordials in it change according to the position on one-year-old shoots. In this study, *Vitis vinifera* L. cv. 'Karaerik' and *Vitis labrusca* L. cv. 'Ülkemiz' varieties was used. Primary buds are separated from other shoot beds (secondary and tertiary buds) with scalpel, fixation, vacuuming, paraffin impregnation, paraffin embedding, freezing, sectioning and tissue staining were performed, respectively. The stained samples were examined microscopically, images were taken and these images were transferred to the computer and histological analyzes was made. In the study, it was determined that bud sizes including three clusters were statistically different ($p < 0.05$) from other bud sizes (without clusters, one cluster and two clusters of buds). It was determined that there were statistical differences between cultivars in terms of both bud size and the number of cluster. In addition, it was determined that the middle (0.77) buds of the 'Karaerik' variety contained more clusters than the basal (0.66) and apical (0.59) buds, whereas the apical (1.19) buds of 'Ülkemiz' variety contained more clusters than the basal (0.88) and middle (0.98) buds. It is very important to know the structural features of the buds in order to make the right pruning application suitable for the variety.

Keywords: Bud histology, grapevine, primary bud, cluster number

Asmalarda Salkım Sayısı ile Primer Tomurcuk Büyüklüğü Arasındaki İlişkinin Histolojik Kesit Alma Yöntemiyle Belirlenmesi

Öz

Bu çalışma dormant haldeki asma kış gözü içerisindeki primer tomurcukların büyüklüğü ve salkım sayıları arasındaki ilişkiyi açıklamak için yapılmıştır. Ayrıca primer tomurcuk büyüklüğü ve salkım taslaklarının bir yaşlı sürgün üzerindeki pozisyonlarına göre nasıl değiştiği belirlenmeye çalışılmıştır. Çalışmada *Vitis vinifera* L. cv. 'Karaerik' ve *Vitis labrusca* L. cv. 'Ülkemiz' çeşitleri kullanılmıştır. Primer tomurcuklar diğer sürgün yataklarından (sekonder ve tersiyer tomurcuklar) bir bistüri yardımı ile ayrılarak sırasıyla fiksasyon, vakumlama, parafin emdirme, parafine gömme, dondurma, kesit alma ve doku boyama işlemleri yapılmıştır. Boyanmış örnekler mikroskobik olarak incelenip görüntüleri alınmış ve bu görüntüler bilgisayara aktarılarak histolojik incelemeler yapılmıştır. Çalışmada, üç salkım içeren tomurcuk boyutlarının diğer tomurcuklardan (salkımsız, bir salkımlı ve iki salkımlı) istatistiksel olarak farklı olduğu ($p < 0.05$) belirlenmiştir. Çeşitler arasında hem tomurcuk büyüklüğü hem de salkım sayısı bakımından istatistiksel olarak farklılıklar olduğu belirlenmiştir. Ayrıca Karaerik üzüm çeşidinin orta (0.77) tomurcuklarının dip (0.66) ve uç (0.59) tomurcuklara göre daha fazla salkım içerdiği, Ülkemiz üzüm çeşidinin ise uç (1.19) tomurcuklarının dip (0.88) ve orta (0.98) tomurcuklara göre daha fazla salkım içerdiği belirlenmiştir. Çeşide uygun doğru budama uygulamasının yapılabilmesi için, tomurcukların yapısal özelliklerinin bilinmesi oldukça önemlidir.

Anahtar Kelimeler: Tomurcuk histolojisi, asma, primer tomurcuk, salkım sayısı

*Corresponding Author: muhammed.kupe@atauni.edu.tr
Muhammed KÜPE, https://orcid.org/0000-0002-7225-8065

1. Introduction

Horticultural crops include a diverse array of crops comprising fruits, grapes, vegetables, nuts, flowers, aromatic and medicinal plants. They provide nutritional, medicinal, and aesthetic benefits to mankind for centuries [1-5]. They are genetically very diverse group and including cultivars, accessions, genotypes, types etc. [6-10].

Grapevine dormant buds are quite complex due to their anatomical and morphological structure [11, 12]. Dormant buds various shapes and appearances, but they are generally large and angular [13]. They contain leaf scales, shoots and clusters and take their final shape in autumn [14]. Dormant buds on the shoots are closely related to the yield of vine [15, 16]. Dormant buds occur in leaf apical on summer shoots. The dormant buds that complete their development in the spring and spend the winter resting usually consist of more than one bud [17]. These are called the primary, secondary and tertiary buds. The primary bud is the main fruiting bud for the following year [18].

One of the shoot apical is in the middle and the other two are on the sides. The scales of the middle shoot apical (primary buds) are larger and the organs are better developed. With the beginning of the vegetation period, the shoot apical in the middle develops and forms the summer shoot. In the shoot apical called the secondary bud, the organs are weaker than the primary buds and in some cases they may form clusters. The growth cone, which is called the tertiary bud and located on the upper part of the middle shoot apical, is more primitive than the other two shoot axillaries and does not contain clusters. The growth of the dormant buds (shooting) is seen in March-April in temperate climates and usually as the growth of the primary bud, which is the apical middle shoot that has completed its development [16, 18]. If this primary bud is damaged due to late spring frosts, diseases and pests or mechanical impacts, the secondary bud development, and if secondary bud is damaged, the tertiary bud it begins to develop. However, the most important bud in terms of grape yield in viticulture is the primary buds [19, 20]. In the grapevine, 0-4 cluster primordium can occur in the primary buds. Many studies have shown that the total number of clusters in a shoot apical varies according to the age of the grapevine, the nutritional status, genetic structure and the position of the dormant buds on a year old shoot [21-23].

It is stated that the number of cluster is high in the basal and middle buds in the seeded varieties and in the apical buds in the seedless varieties. In addition, it has been observed that the number of cluster in the middle node is higher than the other nodes in most of the table grape varieties [18, 24]. Bud productivity for grapes is closely related to the growth, development and performance of the vine during the vegetation period one year ago. The main purpose of this study is to reveal the relationship between the size of the primary buds and their productivity. In addition, it has been tried to determine how the size of the primary bud and the cluster primordiums in it change according to the position on a year old shoot. In this study conducted on two grape cultivars, (*Vitis vinifera* L. cv. ‘Karaerik’ and *Vitis labrusca* L. cv. 'Ülkemiz') the

*Corresponding Author: muhammed.kupe@atauni.edu.tr
Muhammed KÜPE, https://orcid.org/0000-0002-7225-8065

size of the primary buds and the number of cluster primordiums within the buds were determined by histological examinations. By determining the cluster primordium in the primary buds, it will be possible to make an accurate yield estimation in the early period in the vineyards. Depending on the relationship between the structure of the primary buds and their productivity, the traditional pruning method may need to be updated.

2. Materials and Methods

It is known that there are structural differences between grapevine specie, varieties and cultivars [25-28]. In the study, two different cultivars with high economic value, which differ in terms of genetic, morphological, physiological characteristics and adaptability, were preferred. Samples of the 'Karaerik' grape cultivar of *V. vinifera* with large berries consumed for table (fresh) are taken from within the borders of Üzümlü District of Erzincan Province. In Erzincan, a 25-year-old vineyard at 1190 m altitude in Baran trained system was used. Examples of genotype 'Ülkemiz' belonging to V. labrusca specie, which stands out with its resistance to high humidity and low temperatures [29-31]. It was obtained from Samsun Ondokuz Mayıs University. 'Ülkemiz' grape cultivar were formed with a wired training system at 195 m altitude, shaped like a cord, and were obtained from 15 aged vineyards.

During the winter of 2016-2017 samples taken from Erzincan and from Samsun were transported to the laboratory in polyethylene protection bags for histological testing. In the study carried out on two different cultivars, dormant buds in three different positions (basal nodes, middle nodes and apical nodes) were examined. The study was planned as three repetitions for each position and three samples for each repetition. In the study, 1st, 2nd and 3rd nodes are considered basal buds, 4th, 5th and 6th nodes are considered as middle buds, and 7th, 8th and 9th nodes are considered as apical buds. Efficiency values in different buds in grapevine can be determined using different methods such as binocular microscopy, sectioning from dormant buds with microtome, shooting test, counting the somacs by forcing single-bud cuttings, or determining the somacs on the long pruned annual shoots [32, 33]. In this study, we used the microtome sectioning method for histalogical examination.

2.1. Histological studies

Since the number of cluster primordiums in the buds changes according to the position of dormant buds on one year old shoot [15, 34], primary buds were taken from different positions. Histological examination of the cluster primordiums on the primary buds was made according to Odabas [15] (Figure 1).

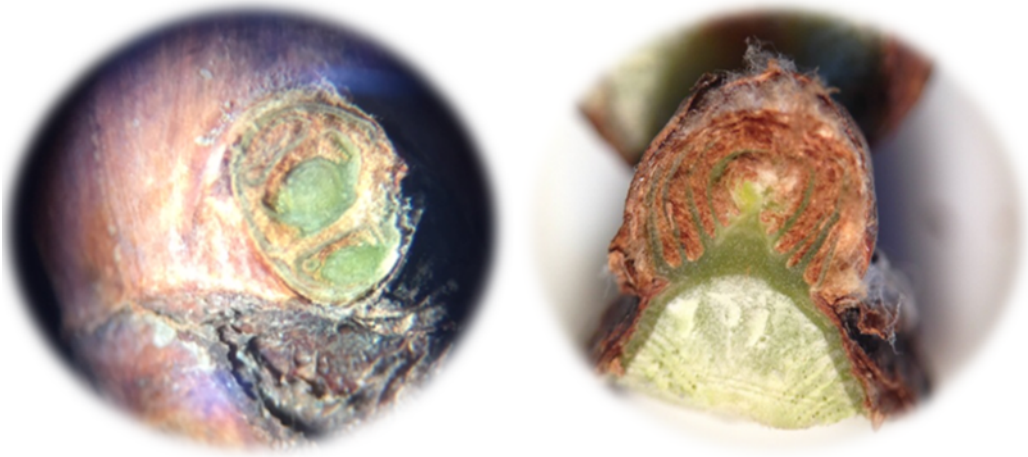

Figure 1. Cross-sectional view of the primary bud (original).

Primary buds separated from secondary and tertiary buds in the dormant buds with the help of a scalpel were placed in separate bottles. In order to soften the primary bud tissue, 2 mL of fixation liquid consisting of 5 mL formaldehyde, 5 mL glacial acetic acid, 90 mL 70% alcohol was added on each sample and placed in the desiccator and vacuuming was performed at certain intervals. According to Odabas (1976) samples was kept in a solution consisting of 50 mL of water + 40 mL of ethyl alcohol (95%) + 10 mL of tertiary butyl alcohol for two hours. After the fixation process was completed, paraffin was added to completely cover the samples taken into the empty bottles, and paraffin impregnation was performed by keeping them in the oven at 60 °C for 24 hours. Samples removed from the oven at the end of 24 hours (through liquid paraffin) were embedded in paraffin. The paraffin blocks in which the samples are embedded were kept in the freezer at -20 ºC for 24 hours. Samples taken out of the freezer are stored at room temperature (22-24 ºC) for 5 minutes. After waiting for a period of time, longitudinal sections were taken with the help of a rotary microtome in thicknesses varying between 8-12 microns depending on the fragmentation of the tissues. Since the buds are at different depths in the buds, care has been taken to take sections from different depths. The sections taken were laid in a gelatin-poured hot water bath (30 ºC).

Intact tissues were selected, placed on a slide and labeled. The samples taken on the slide were heat treated in the oven at 60-70 ºC for 1 h, and then the paraffin on them was melted. To remove the melted paraffin from the tissue in the samples taken from the oven, it was kept in xylol, ethyl alcohol and distilled water for 5 minutes, respectively.

After waiting for the water on the slide to dry, a drop of Toluidine blue was dropped on each section sample and after waiting for 5 minutes, the sections were washed with water and allowed to dry. The coverslip was adhered by dropping 1 drop-holding gel on each of the dried sections and the sections were conduct ready for examination under a light microscope.

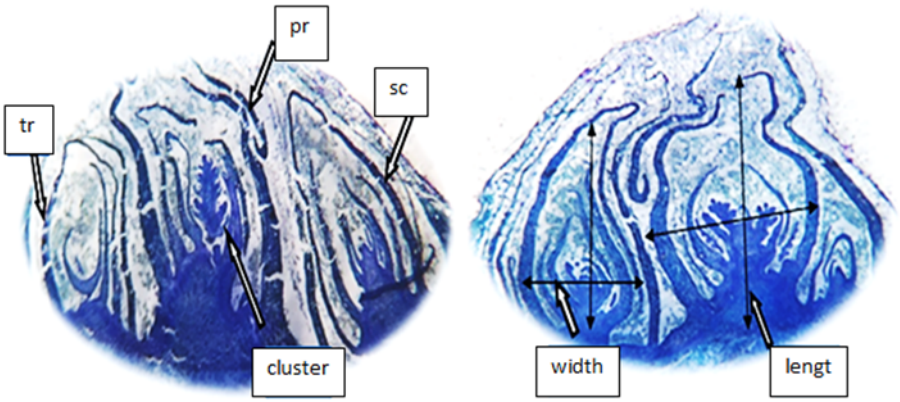

Figure 2. Method of determining the position, width and length of buds in histological observations (pr: primary bud, sc: secondary bud, tr: tertiary bud).

Histological examinations, computer transferred to be imaged with the help of a camera (moticam 480) integrated into the microscope. With the help of the program installed on the computer (motic images 2010), the examinations of the tissues were made. To make examinations, the number of cluster primordial in the primary bud and the size of the buds (width x height). Firstly bud width and length were measured and by using these two values is expressed as the size of the bud in mm^2. While observing the bud and its size, attention has been paid to make these measurements from the widest points of the buds (Figure 2).

2.2. Statistical Analysis

Duncan test was conducted to reveal the relationship between the size and productivity of primary buds in dormant buds. In the study, the number of clusters was divided into four different groups as buds with no cluster and one, two and three clusters in the bud, and whether there was a difference between the sizes of these buds was determined on a variety basis. In addition, the change of bud size and cluster number according to the positions of the genotypes was demonstrated by [35]. In the study, each group was planned to have three repetitions and 20 samples per repetition.

3. Results and Discussion

Many different studies have been carried out to determine the productivity of grape varieties. While determining the productivity of grapevines, methods of maintaining in the greenhouse, maintaining in the vineyard and examining under microscope conditions are applied [36-39]. In this study, these cross-section images were examined under a binocular microscope after the primary buds were sectioned on the microtome.

The Duncan test results, that revealed the relationship between the size of the primary buds and their productivity (number of clusters) in dormant buds is presented in Table 1. when the genotypes are evaluated together, it was determined that there is a statistically significant difference ($p < 0.05$) between the size of the buds that include three clusters and include two clusters, one cluster or without clusters. When Table 1 is examined, it is understood that the

buds without clusters are the smallest, while the buds with three clusters have the largest structure.

It was determined that there is a statistically significant difference ($p < 0.05$) between genotypes in terms of the size of the primary buds. In the 'Karaerik' grape variety, the buds containing two and three clusters were placed statistically in the same group ($p > 0.05$) and they were differed from the buds without clusters and one cluster in terms of bud size. 'Karaerik' grape variety, it has been determined that there are buds without clusters, buds with one cluster, buds with two clusters and buds with three clusters in order from the smallest to the largest in terms of the size of the buds. It was determined that there is a statistically significant difference ($p < 0.05$) between the buds with three clusters in the 'Ülkemiz' grape variety and the buds without clusters, one cluster and two clusters. Similar to the 'Ülkemiz' grape variety, it was determined that there are buds without clusters, buds with one cluster, buds with two clusters and buds with three clusters in order from the smallest to the largest in bud size (Table 1).

Table 1. The number of clusters and bud size in the grape varieties.

Cluster Number	Primary bud size (mm^2)		General Mean
	'Karaerik'	'Ülkemiz'	
	*	*	***
Without cluster	0.065±0.028 ^{b}	0.073±0.031^{b}	0.069±0.029 ^{B}
One cluster	0.070±0.028 ^{b}	0.078±0.030 ^{b}	0.074±0.029 ^{B}
Two clusters	0.078±0.028 ^{ab}	0.084±0.037 ^{b}	0.081±0.034 ^{B}
Three clusters	0.095±0.014 ^{a}	0.114±0.034 ^{a}	0.105±0.026 ^{A}

a, b: Mean values of cultivars with different superscripts are significantly different;
A, B: General mean values with different superscripts are significantly different;
*: $p < 0.05$, ***: $p < 0.001$

The Duncan Test, which was made to determine whether the number of clusters changes according to the position of the primary buds in dormant buds, is presented in Table 2. When the genotypes were evaluated together, no statistically significant difference was found between the basal, middle and apical buds in terms of cluster number. It was determined that there is a statistically significant ($p < 0.05$) difference between the genotypes in terms of the number of clusters according to the position. The average number of clusters per bud in the 'Ülkemiz' grape variety is higher than the 'Karaerik' grape variety.

In 'Karaerik' grape variety, it was determined that the basal and middle buds are statistically in the same group in terms of the number of clusters and they are differed from the apical buds. It was determined that the highest number of clusters in the 'Karaerik' grape variety was in the middle buds and the least number of clusters in the apical buds. In the 'Ülkemiz' grape variety, it was determined that the apical buds and middle buds were statistically in the same group in terms of the number of clusters and they were different from the basal buds. It was revealed that in the 'Ülkemiz' grape variety, the highest number of clusters was in the apical buds and the least number of clusters was in the basal buds.

Table 2. The position of the primary buds and the number of clusters in grape varieties

Position	Cluster numbers		General Mean
	'Karaerik'	'Ülkemiz'	
	*	*	ns
Basal buds	0.660±0. 668 ^{ab}	0.876±0.804 ^{b}	0.823±0.761
Middle buds	0.765±0.720 ^{a}	0.981 ±0.759 ^{ab}	0.848±0.742
Apical buds	0.588±0.698 ^{b}	1.192±0.768 ^{a}	0.893±0.791

a, b: Mean values of cultivars with different superscripts are significantly different;
ns: non-significant, *: $p < 0.05$

In order to determine whether there is a relationship between the position of primary buds and their size in dormant buds, Duncan test was conducted in Table 3. When the genotypes were evaluated together, it was determined that the primary buds in the apical buds were statistically different from the primary buds in the basal and middle buds in terms of bud size. It was understood that the largest primary bud in terms of bud size was in the middle buds and the smallest primary bud in the basal buds. It was determined that there is a statistically significant difference between the genotypes in terms of the size of the primary buds. When Table 3 is examined, it has been determined that the primary buds of the 'Ülkemiz' grape variety are larger than the primary buds of the 'Karaerik' grape variety.

Table 3. The position and size of the primary buds in grape varieties

Position	Primary bud size		General Mean
	'Karaerik'	'Ülkemiz'	
	**	***	***
Basal buds	0.062±0.021 ^{b}	0.080±0.027 ^{a}	0.071±0.026 ^{A}
Middle buds	0.073±0.031 ^{a}	0.083±0.036 ^{a}	0.078±0.034 ^{A}
Apical buds	0.059±0.020 ^{b}	0.061±0.016 ^{b}	0.060±0.018 ^{B}

a, b: Mean values of cultivars with different superscripts are significantly different;
A, B: General mean values with different superscripts are significantly different;
**: $p < 0.01$, ***: $p < 0.05$

It was determined that the bud size of 'Karaerik' grape variety at the middle buds was statistically different from basal and apical buds. It has been revealed that the largest primary buds in the 'Karaerik' grape variety are in the middle buds and the smallest primary buds are in the apical buds. In the 'Ülkemiz' grape variety, it was determined that the bud size in apical buds was statistically different from the basal and middle buds. In the 'Ülkemiz' grape variety, it was determined that the largest buds were in the middle buds and the smallest buds in the apical buds, as in the 'Karaerik' grape variety.

The results showed relationship between the bud size and dormant bud productivity on the genotype of 'Karaerik' grape variety (*V. vinifera)* and 'Ülkemiz' (*V. labrusca*). [40], also stated that the growth power is one of the most important factors affecting the cluster and flower formation. The results also clearly indicated that the buds included 3 clusters were different than buds include one cluster, two clusters or without cluster. In terms of size of primer buds, there were statistically differences among genotypes. The biggest and the smallest buds were obtained from buds included 3 clusters and buds without cluster in both genotypes, respectively. [41], reported that very strong growth reduced bud productivity in grapevine. In general, it is known that the yield of one year later is negatively affected when the vegetative and generative development of the grapevine is not in balance [42]. [17], stated that very strong vegetative growth delay the formation of cluster primordium in dormant buds and decrease the number of clusters / bud ratio, and the growth power is one of the most important factors affecting the cluster and flower formation in grapevine. On the other hand, [43] reported that the relationship between shoot diameter and cluster number/bud was statistically insignificant in Kalecik Karası variety. In addition, [44] stated that one of the factors that show the strength of shoot development is the carbohydrate level in the bud tissues differ according to varieties, climatic conditions and cultural practices. There was no study that directly correlated the bud size with the number of cluster primordiums.

Since the grape yield obtained from the vineyards can vary depending on the position of the dormant buds on the 1-year-old shoot, it is of great importance to be able to determine the dormant bud productivity in different positions (node) [33, 45]. It was determined that the number of clusters was high in the middle buds of the 'Karaerik' grape variety and in the middle and apical buds in the 'Ülkemiz' grape variety. There is a statistically significant ($p < 0.05$) difference between the genotypes in terms of the number of clusters according to the position, and the average number of clusters per bud in the 'Ülkemiz' grape variety is higher than the 'Karaerik' grape variety. As a matter of fact, [24] investigated the maximum productivity of the buds in five different wine grape varieties and found that the maximum productivity was obtained at 4th, 5th and 6th buds in the Hasandede grape variety, the 5th and 6th buds in the Papazkarası grape variety, the 1st and the 7th in the Kalecik grape variety, 6th buds in the Öküzgözü grape variety and 5th buds in the Furmint grape variety, respectively. In addition, [23] in their study, in which they determined the productivity of 37 grape varieties grown in Tokat region according to the positions of the first 10 internodes, reported that the maximum productivity varied between the 3rd and 10th nodes, and the first nodes were inefficient in some varieties. [17], stated that the number of buds and clusters in an bud varies according to the position of the buds, and although it varies according to the varieties, generally, the buds at the base and apical buds contain less buds than the middle part. The results obtained in terms of the average number of clusters per dormant buds are similar to the findings of some researchers regarding the differences between grape varieties [16, 22, 24]. Considering the averages obtained, the difference seen in the primary bud productivity values on the 1-year old shoot on the basis of genotypes, mainly affected by genetic structure, yearly cultivation treatments, number of buds left in pruning, training method and climate factors, etc.

It was determined that the highest number of clusters in the ‘Karaerik grape variety was in the middle buds and the least number of clusters in the apical buds. Because, in a study conducted on grape varieties known to be suitable for short pruning, the productivity values in the dormant buds were found higher in the second buds of Hamburg Muscat and Balbal grape varieties; In Hafızali, Razaki and Çavuş grape varieties, it is 3rd-4th buds [46]. [32], determined that table grape varieties such as Ata Sarısı and Cardinal should be pruned short over 2 buds, Yalova Incisi, Amasya and Italia grape varieties should be pruned short over 2-3 buds, and Uslu grape varieties should be pruned in medium length over 3-5 buds. It was revealed that in the ‘Ülkemiz’ grape variety, the highest number of clusters was in the apical buds and the least number of clusters was in the basal buds. As a matter of fact, [34], conducted their study to determine the variation of bud fruitfulness in Samsun ecological conditions of four different grape types belongs to foxy grape and the productivity in the buds located in the first node of Pazar 3 and Güneysu 3 types was less than 1. These findings are in accordance with the findings determined by different researchers that the productivity increases towards the middle buds but decreases again towards the apical buds [15, 16].

When the genotypes were evaluated together in terms of bud size according to their position, it was found that the primary buds in the base (basal) buds were statistically different from the primary buds in the basal and middle buds. It was found that the largest primary bud is in the middle buds and the smallest primary bud is in the basal buds. It was determined that there is a statistically significant difference between the genotypes in terms of the size of the primary buds. It was determined that the primary buds of the ‘Ülkemiz’ grape variety has larger than the primary buds of the ‘Karaerik’ grape variety. It has been revealed that the largest primary buds are in the middle buds and the smallest primary buds are in the basal buds of the ‘Karaerik’ grape variety. In the ‘Ülkemiz’ grape variety, it was determined that the largest buds were in the middle buds and the smallest buds in the basal buds, as in the ‘Karaerik’ grape variety. We believe that this situation may be related to the aging of an old shoot and related nutrient delivery. As a matter of fact, it is known that an old shoot in the grapevine begins to lignify from the basal to the apical, and accordingly it is known that it is more wooded in the basal nodes and less in the apical nodes compared to the middle nodes [18]. As a matter of fact, [24] reported that the primary buds form structures containing 1-4 bunches, 6-12 nodes and/or leaves, and a few leech drafts in the 7-8 month period from the beginning of the development period to the enter rest. After this date, [47] stated that the buds entered winter dormancy until March of the following year, and then the development of the buds started again, but new organs could not be formed, but the structures that were formed developed. In addition, [48] reported that shoots developed better due to the long vegetation in hot regions and there was a positive correlation between shoot development and bud development.

4. Conclusion

In this study, it was determined that the number of clusters in the primary buds in the vines affects the bud sizes. In the study, it was observed that the size of the bud increased as the number of primordium of clusters in the bud increased in both ‘Karaerik’ and ‘Ulkemiz’ grape varieties (It was determined that buds containing 1 cluster were larger than buds without

clusters, buds containing 2 clusters were larger than buds with 1 cluster, and buds containing 3 clusters were larger than buds with 2 clusters). As a result of the study, it was understood that the basal and middle buds of 'Karaerik' grape variety were larger than the apical buds and the number of cluster primordium of these buds was higher. In 'Ulkemiz' grape variety, although the apical buds are smaller than the basal and middle buds, it has been determined that the number of clusters is higher. It was determined that the base and middle buds of Karaerik grape variety were more productive, so the buds could be left up to the 6th node in pruning. Since the apical buds of 'Ulkemiz' grape variety are more productive, it has been seen that long pruning would be more appropriate. According to the results obtained from this study, in addition to the growth forces of the one-year-old shoots to be preferred in winter pruning, bud structures/sizes should also be taken into account.

Ethics in Publishing

There are no ethical issues regarding the publication of this study.

Author Contributions

Conceptualization, data curation, formal analysis, methodology, visualization, writing-original draft, writing-review and editing

References

[1] Nadeem, M. A., Habyarimana, E., Çiftçi, V., Nawaz, M. A., Karaköy, T., Comertpay, G., Shahid, M. Q., Hatipoglu, R., Yeken, M. Z., Ali, F., Ercisli, S., Chung, G., Baloch, F. S., (2018) Characterization of genetic diversity in Turkish common bean gene pool using phenotypic and whole-genome DArTseq-generated silicoDArT marker information. PLoS ONE 13(10):e0205363.

[2] Colak, A. M., Kupe, M., Bozhuyuk, R. M., Ercisli, S., Gundogdu, M., (2019) Identification of some fruit characteristics in wild bilberry (*Vaccinium myrtillus* L.) accessions from Eastern Anatolia. Gesunde Pflanzen 70: 31-38.

[3] Grygorieva, Oç, Klymenko, Sç, Kuklina, A., Vinogradova, Y., Vergun, O., Sedlackova, V. H., Brindza, J., (2021) Evaluation of *Lonicera caerulea* L. genotypes based on morphological characteristics of fruits germplasm collection. Turk J Agric For 45: 850-860.

[4] Juric, S., Vlahovicek-Kahlina, K., Duralija, B., Maslov Bandic, L., Nekic, P., Vincekovic, M., (2021) Stimulation of plant secondary metabolites synthesis in soilless cultivated strawberries (Fragaria × ananassa Duchesne) using zinc-alginate microparticles. Turk J Agric For 45: 324-334.

[5] Ozdemir, B., Okay, F. Y., Sarikamis, G., Ozmen, C. Y., Kibar, U., Ergul, A., (2021) Crosstalk between flowering and cold tolerance genes in almonds (*Amygdalus* spp.). Turk J Agric For 45(4): 484-494.

[6] Ercisli, S., Esitken, A., Turkkal, C., Orhan, E., (2005) The allelopathic effects of juglone and walnut leaf extracts on yield, growth, chemical and PNE composition of strawberry cv. Fern. Plant Soil Environ 51: 283-387.

[7] Erturk, Y., Ercisli, S., Cakmakci, R., (2012) Yield and growth response of strawberry to plant growth-promoting rhizobacteria inoculation. J Plant Nutr 35(6): 817-826.

[8] Doğan, H., Ercişli, S., Jurıkova, T., Temim, E., Leto, A., Hadziabulic, A., Zia-Ul-Haq, M., (2014) Physicochemical and antioxidant characteristics of fruits of cape gooseberry (*Physalis peruviana* L.) from Turkey. Oxidation Communications, 37(4).

[9] Kupe, M., Karatas, N., Unal, M. S., Ercisli, S., Baron, M., Sochor, J., (2021) Phenolic composition and antioxidant activity of peel, pulp and seed extracts of different clones of the Turkish grape cultivar 'Karaerik'. Plants 10: 2154.

[10] Taskesenlioglu, M.Y., Ercisli , S., Kupe, M., Ercisli, N., (2022) History of grape in Anatolia and historical sustainable grape production in Erzincan agroecological conditions in Turkey. Sustainability 14: 1496.

[11] Mullins, M. G., Bouqueti A., Williamsi L. E., (1992) Biology of the grapevine. Cambridge University Press. England.

[12] Carmona, M. J., Chaïb, J., Martínez-Zapater, J.M., Thomas, M. R., (2008) A molecular genetic perspective of reproductive development in grapevine. J Exp Bot 59: 2579-2596.

[13] Morrison, J. C., Lodi, M., (1990) The development of primary bud necrosis in Thompson Seedless and Flame Seedless grapevines. Vitis 29: 133-144.

[14] Sabir, A., Tangolar, S., Buyukalaca, S., Kafkas, S., (2009) Ampelographic and molecular diversity among grapevine (*Vitis* spp.) cultivars. Czech J Genet Plant Breed 45: 160-168.

[15] Odabas, F., (1976) Determination of efficiency according to where the buds are located by examining the floral development periods of some important grape varieties grown in Erzincan. Atatürk Univ Pub 466: 130-141.

[16] Kismali, I., (1984) Research on winter bud yield of some table grape varieties. Turkey 2nd Symposium on Viticulture and Winemaking, Manisa, pp 35-48.

[17] Agaoglu, Y. S., (1999) Scientific and applied viticulture (grapevine biology). Ankara Univ Agric Fac Vol I. (pp 205-209). Kavaklıdere Educ Pub1, Ankara.

[18] Celik, H., Agaoglu, Y. S., Marasalı, B., Soylemezoglu, G., Fidan, Y., (1998) General viticulture. (1: 253-260). Sun Fidan Aş. Prof Books Series Ankara.

[19] Oraman, M. N., (1959) New viticulture. Ankara Univ Fac of Agric Publications 78: 298.

[20] Kupe, M., Ercisli, S., (2021) Determınatıon of the productivity and development status of the secondary buds in the Karaerik grape variety. XII International Scientific Agriculture Symposium, pp 401. Book of Agrosym, Serbia.

[21] Alleweldt, G., Hofacker, W., (1975) Influence of environmental factors on bud burst flowering fertility and shoot growth of vines. Vitis 14: 103-115.

[22] Ilter, E., (1980) Studies on the effect of some chemical substances applied to leaves on winter bud efficiency. Ege Üniv Agric Pub 372: 132-133.

[23] Agaoglu, Y. S., Kara, Z., (1993) Research on determination of bud efficiency of some grape varieties grown in Tokat region. Turk J Agric For 17: 451-458.

[24] Agaoglu, Y. S., (1969) Comparative studies on the bud structures, floral growth periods of table grape varieties of Hasandede, Kalecik Karası, Papaz Karası, Öküzgözü and Furmint and the determination of pruning methods suitable for these varieties Ankara Univ Agric Fac Doctoral Thesis, Ankara.

[25] Zhang, J., Wu, X., Niu, R., Liu, Y., Liu, N., Xu, W., Wang, Y., (2012) Cold-resistance evaluation in 25 wild grape species. Vitis 51: 153-160.

[26] Carvalho, D. C. D., Silva, A. L. L. D., Schuck, M. R., Purcino, M., Tanno, G. N., Biasi, L. A., (2013) Fox grape cv. Bordô (*Vitis labrusca* L.) and grapevine cv. Chardonnay (*Vitis vinifera* L.) cultivated in vitro under different carbohydrates, amino acids and 6-Benzylaminopurine levels. Braz Arch Biol Technol 56: 191-201.

[27] Abe, L. T., Mota, R. V. D., Lajolo, F. M., Genovese, M. I., (2007). Phenolic compounds and antioxidant activity of *Vitis labrusca* and Vitis vinifera cultivars. Food Sci Tech 27: 394-400.

[28] Köse, B., (2014) Phenology and ripening of *Vitis vinifera* L. and *Vitis labrusca* L. varieties in the maritime climate of Samsun in Turkey's Black Sea Region. South African J Enol Vitic 35: 90-102.

[29] Gökdemir, N., (2016).- The effect of different doses of Boron application on yield, quality and leaf nutrient content of Isabella (*V. Labrusca* L.) grape variety. Ordu Üniv Inst of Sci Master's Thesis, Ordu.

[30] Kupe, M., (2021). Determination of freezing points of secondary buds in *Vitis vinifera* and *Vitis labrusca*. Int. J Agric Wildlife Sci 7: 217-221.

[31] Ferreira, G. M., Moreira, R.R., Jarek, T.M., Nesi, C.N, Biasi, L.A., May De Mio, L. L. (2022) Alternative control of downy mildew and grapevine leaf spot on *Vitis labrusca*. Australasian Plant Path 51: 193-201.

[32] Dardeniz, A., Kismali, I., (2005) Researchs on determining the bud fertility and obtaining optimum pruning levels in some table grape varieties, Ege Univ Fac Agric J 42: 1-10.

[33] Kupe, M, Kose, C., (2020) The relationship between bud size and exotherm formation in dormant buds of grapevine. Atatürk Univ J of Agric Fac 51: 243-248.

[34] Celik, H., Kose, B., Ates, S., Karabulut, B., (2015) Determination of bud fertility of foxy grape (Vitis labrusca L.) genotypes selected from Rize. Selçuk Univ Agric Food Sci J Special Issue 27: 238-245.

[35] Duncan, D. B., (1957) Multiple range tests for correlated and heteroscedastic means. Biometrics 13: 164-174.

[36] Balasubrahmanyam, V. R., Khanduja, S.D., (1977) Effect of the varying cane lengths on the fruiting potantial of Thompson Seedless vines. Indian J Hortic 34: 113-116.

[37] Kırdar, T., Odabas, F., (1992). A research on the determination of productivity status and yield potential estimation according to bud positions in some important grape varieties grown in Amasya. Ondokuzmayıs Univ J Fac Agric 7: 19-28

[38] Kara, Z., Beyoglu, N., (1995) A research on the determination of bud productivity of grape varieties grown in Konya province Beyşehir region. Turkey II. National Horticultural Congress, Cilt: II, (pp 524-528). Konya.

[39] Celik, H., (1999) Researches on the fruitfulness of some grape varieties grown in Amasya. Turk J Agric For 23: 685-690.

[40] Huglin, P., (1958) Recherches sur les Bourgeons de la vigne. initiation florale et developpement vegetatif. Ann Am él Plantes 8: 113-272.

[41] Sartorıus, O., (1968) Die Blütenknospen der reben. Weinwissenschaft 23: 309-338.

[42] Kupe, M., Kose, C., (2015) Determining suitable pruning level after winter frost damage in Karaerik grape cultivar. Atatürk Univ J Agric Fac 46: 21–28.

[43] Basaran, C., (2006). Relationships between grapevine performance and bud fertility, yield and berry qulity on Kalecik karası clones. Ankara Üniv Inst of Sci Master's Thesis, Ankara.

[44] Morrison, J. C., Lodi, M., (1990) The development of primary bud necrosis in Thompson Seedless and Flame Seedless grapevines. Vitis 29: 133-144.

[45] Karatas, H, Agaoglu, Y. S., (2005) Bud efficiency in grapevines. Alatarım 4: 13-22.

[46] Fidan, Y., (1966) Research on bud structures and crop status of table grape varieties.

[47] Oraman, M. N., Agaoglu, Y. S., (1969) A research on the relationship between morphological distinction and floral development phases, blossoming and ripening of grapes in some wine grape varieties grown in Ankara. Ankara Univ Fac Agric 19: 503-519.

[48] Lavee, S., (2000) Grapevine (Vitis vinifera) growth and performance in warm climates. In: Temperate Fruit Crops in Warm Climates Boston, (pp 343-366). London, England.

Erzincan Üniversitesi
Fen Bilimleri Enstitüsü Dergisi
2024,17(1), 113-128
ISSN: 1307-9085, e-ISSN: 2149-4584
Araştırma Makalesi

Erzincan University
Journal of Science and Technology
2024,17(1), 113-128
DOI: 10.18185/erzifbed.1347386
Research Article

A new Turkish pharmacokinetics software program for therapeutic drug monitoring of theophylline

Gülbeyaz YILDIZ TÜRKYILMAZ[1,2,3], Mehmet Ali EGE[1,2], A.Levent ALPARSLAN[4], Ercüment KARASULU[1,2,3], Levent KIRILMAZ[2,3]

[1]Center for Drug Research & Development and Pharmacokinetic Applications (ARGEFAR), Ege University, Izmir-Türkiye

[2]Department of Pharmaceutical Technology, Faculty of Pharmacy, Ege University, İzmir-Türkiye

[3]Department of Biopharmaceutics and Pharmacokinetics, Faculty of Pharmacy, Ege University, İzmir-Türkiye

[4]Department of Pharmaceutical Technology, Faculty of Pharmacy, Istinye University, 34010, İstanbul, Türkiye

Received: 21/08/2023, **Revised:** 02/11/2023, **Accepted:** 02/11/2023, **Published:** 28/03/2024

Abstract

In this study, it was aimed to develop a Turkish software with pharmacokinetic (PK) data for therapeutic drug monitoring and IV dose adjustment of narrow therapeutic index theophylline.

The study involved three groups, each comprising two rabbits. The dose required for the target concentration (15µg/mL) was calculated with the developed program according to the weight of the rabbits in the first group. Blood samples taken at certain times were analyzed by validated HPLC method to calculate the elimination rate constant (ke) after IV bolus administration. The r^2 values for ke were found to be 0.86 and 0.95. The second dose calculated according to revised PK findings was administered and blood samples were taken. When the analyzed results and theoretical results were compared, the deviation was found to be 5.53% and 8.795%. The findings were taken as the population PK for other applications.

IV multiple dose bolus and IV fast-slow combined infusion were administered to the second group and the third group, respectively. The results obtained from the analysis of blood samples taken at the times determined according to the application were compared with the theoretical results.

As a result, although there is a high difference between theory and practice at low concentrations, there is very little variation at high concentrations. By using this program, it has been achieved to keep theophylline at the desired level without reaching the minimum toxic concentration and without falling below the minimum effective concentration. It is thought that deviations will be reduced with larger samples.

Keywords: TDM, theophylline, software pharmacokinetic programme

*Corresponding Author: ercument.karasulu@ege.edu.tr
Gülbeyaz YILDIZ TÜRKYILMAZ, https://orcid.org/0000-0002-8601-0263
Mehmet Ali EGE, https://orcid.org/0000-0002-4953-2812
A.Levent ALPARSLAN, https://orcid.org/0000-0003-0113-6850
Ercüment KARASULU, https://orcid.org/0000-0002-3992-6201
Levent KIRILMAZ, https://orcid.org/0000-0003-2554-0823

Teofilinin terapötik ilaç izlemi için yeni bir Türkçe farmakokinetik yazılım programı

Öz

Terapötik ilaç izlemi için farmakokinetik (FK) veriler ile Türkçe bir yazılım geliştirilmesi hedeflendi ve dar terapötik indeksli teofilinin iv doz ayarlaması yapılması amaçlandı.

Her grupta 2 tavşan olacak şekilde 3 grup oluşturuldu. İlk gruptaki tavşanlara kilosuna göre hedef derişimi 15µg/mL olması için gereken doz geliştirilen programa hesaplatılarak uygulandı ve eliminasyon hız sabitini (ke) hesap edecek şekilde belli zamanlarda alınan kan örnekleri valide edilen HPLC metodu ile analizlendi. ke için çizilen eğimin r^2 değerleri 0.86 ve 0.95 bulundu. Revize edilen FK bulguları ile gereken bireysel doz hesaplanarak 2.doz uygulaması yapılıp kan örnekleri alındı. Analizlenen sonuçlar ile teorik sonuçlar kıyaslandığında %sapma %5.53 ve %8.795 bulundu. 1. gruptan elde edilen FK bulguları, popülasyon FK'sı olarak alınarak diğer uygulamalarda kullanıldı.

Ikinci gruba iv çok doz bolus, üçüncü gruba ise iv hızlı-yavaş kombine infüzyon uygulaması yapıldı. Uygulamaya göre belirlenen zamanlarda alınan kan örneklerinin analizinden elde edilen sonuçlar teorik sonuçlarla kıyaslandı.

Sonuç olarak düşük derişimlerde teorik ile pratik arasında yüksek farklılık görülmek ile birlikte yüksek derişimlerde farklılanma çok azdır. Bu programı kullanarak teofilinin minimum toksik derişimine erişmeden ve minimum etkin derişiminin altına düşmeden istenilen düzeyde tutulması başarılmıştır. Daha büyük örneklemler ile sapmaların azaltılacağı düşünülmektedir.

Anahtar Kelimeler: TDM, teofilin, farmakokinetik yazılım programı

1 Introduction

Due to the individual variability of some drugs, not every patient can be treated with the standard drug method. Individual dose application is difficult for drugs whose clinical efficacy is unknown or that do not respond clinically until they have an irreversible toxic effect on the patient. In such cases, the therapy can be maintenaned through therapeutic drug monitoring (TDM). TDM can be defined as individual therapy to each patient for specific drugs (Freedman & Marshall, 1993a; Kang & Lee, 2009; Marks, 1985; Touw, Neef, Thomson, & Vinks, 2005). That's to adjust the dose needed to the patient and treated the disease. There is no certain solution for dose adjustment, but TDM especially utilizes if the relationship between plasma level and response can be computed mathematically (Touw et al., 2005). The aim of this strategy is to stay within the therapeutic index (TI, therapeutic window, or therapeutic range) and to continue the steady state concentration. TI encompasses the interval between a minimum level that causes the therapeutic effect (minimum effective concentration, MEC) and a minimum level that causes the toxicity (minimum toxic concentration, MTC) of a drug (Birkett, 1997; Marks, 1985; Whiting et al., 1984). This is especially important for drugs that have a narrow TI (NTI), such as theophylline. Theophylline has a dose-response relationship. It is used in asthma and chronic obstructive disease as a bronchodilator. Its NTI for adults is 10–20 µg/mL or 5–15 µg/mL depending on the source and changes according to the age of the patient (Hallworth & Watson, 2017; Hardman, Limbird, Gilman, Molinoff, & Ruddon, 1996; Pesce, Rashkin, & Kotagal, 1998). It is metabolized in the liver mostly by especially CYP1A2 and

CYP3A4. The clearance shows an alteration due to a variation in the rate of metabolism (Freedman & Marshall, 1993b; Hardman et al., 1996). The half-life is approximately 9 hours. However, it decreases in cigarette smokers because it induces the hepatic metabolism (Freedman & Marshall, 1993b; Jenne, Nagasawa, McHugh, Macdonald, & Wyse, 1975). The other pharmacokinetic (PK) parameters of theophylline are shown in Table 1 (Hardman et al., 1996).

Table 1. The pharmacokinetic parameters of theophylline

BA (oral) %	**Excretion by urine %**	**Plasma protein binding %**	**Cl (mL/min/kg)**	**Vd (L/kg)**	**$t_{1/2}$ (hour)**	**TI (μg/mL)**	**MTC (μg/mL)**
96±8	18±3	56±4	0.65±0.20	0.50±0.16	9.0±2.1	5-15	20

BA: Bioavailability, Cl: clearance, Vd: Volume of distribution, $t_{1/2}$: half-life of drug, TI: Therapeutic window, MTC: minimum toxic concentration; (±SD)

An important point for TDM is when and how much sample is collected from the patient. Many samples are required to create a PK profile. However, the patient's comfort requires medication monitoring with at least a few samples (Ghiculescu, 2008).

If area under the curve (AUC) and dose are correlated with each other, to determine the AUC, at least three blood samples are necessary. Taking more blood samples from patients is practically impossible.

Also, if there is a correlation between Ctrough (trough serum concentration is the pre-dose concentration) or Ct (the concentration of a determined time) and dose, a single sampling strategy is preferable and applicable for drug monitoring. If there is no relationship between Ctrough/Ct and dose, there is no other way except to determine AUC (Touw et al., 2005). Especially for drugs with NTI, peak concentration (Cmax) is an important parameter.

The analysis method is the most important step. It has to be safe and easy. To be cheap, fast, and available in laboratory environments is preferable in terms of application in practice. A kit may be preferable for this area in terms of ease of use, but there isn't any kit for theophylline.

Chromatographic methods are the best option because the simple sample preparation and small volume requirements make them especially suitable for monitoring theophylline therapy in a pediatric population (Freedman & Marshall, 1993c; Hendeles, Weinberger, & Johnson, 1978). In addition to chromatographic methods for the theophylline assay, electrochemical techniques with a faster response perspective can also be evaluated(Koçak, Nas, Kantekin, & Dursun, 2018; Wagnew et al., 2022). However, attention should be paid to the applicability of this method in the hospital. The analysis method must be validated according to guidelines set by the authorities. (Fda & Cder, 2018).

With a user-friendly program, monitoring as many drugs as possible is possible. For this reason, we aimed to develop a new software program for adjusting and individualizing the dose of

theophylline. *In vivo* studies on the rabbits were conducted under multiple bolus dose and IV infusion administration conditions to test the validity of the software program.

Currently, there are documents in the form of SOPs or online/setup programs that indicate what needs to be done for TDM, but there is no proven program with Turkish software (Fuchs, Csajka, Thoma, Buclin, & Widmer, 2013). In this way, theophylline will be a model substance for other IV drugs that will need to be followed. For this purpose, firstly, a Turkish program including PK algorithms was developed. Then, theophylline was analyzed by HPLC after the administration of an IV bolus, an IV multiple dose bolus, and an IV infusion to rabbits. Individual dose calculations were performed from the program developed using theophylline results obtained from the analysis. The accuracy and validity of the program were proved by comparing the theoretical results with plasma samples after the application of the calculated doses to rabbits.

2 Materials and Methods

2.1 Standards and Reagents

Neofleks 5% Dextrose Solution (Türktıpsan A.Ş., Turkey) and Teobag-200 (Eczacıbaşı-Baxter, Turkey) were purchased from the Drug Company. Teophylline (Cipla, India) and caffein (Cipla, India) were used for the analytical method as standards and internal standards, respectively. Heparin Sodium (Panpharma S.A., Turkey) was used as an anticoagulant agent in the cannula. All other chemicals and reagents were of analytical grade.

2.2 Execution of Software Program

The programming language C# was used as the host language for the software program in the Visiual Studio environment. For the data visualization, Component One Studio was used to make it convenient to prepare tables, and graphic procedures, and input media.

Firstly, the algorithms for PK calculations and the interface of the software program were prepared. Three screens, including patient, active substance, and administration route, were designed.

Patient screening involves the following parameters: that are name, surname, personal ID number, height, weight, sex, age, and blood group of the patient. For adjusting the dosage of theophylline, weight was used as a covariate.

Active substance screening involves the theoretical values of PK parameters obtained from references and pharmaceutical IV preparations on the market for the active substance. Beside the constant data, there is a numerical box to input the desired plasma concentration.

The administration route screen has five sub-screens: individual dose, IV bolus, IV multiple dose bolus, IV infusion, and IV combined with IV bolus and infusion. At first, a program user has to calculate the dose from the desired plasma concentration at the individual dose screen.

A patient, an active substance and its pharmaceutical form, and an administration route of drug are chosen, respectively, from the program. After the data of patient weight inputs into the patient screen, the desired plasma concentration to reach the target therapeutic level is written at the active substance screen. When the “Calculate the dose” button is pressed at the individual dose screen, the program gives the calculated dose on same screen in the related place. Following the drug administration to patients, three blood samples are taken at different times, and the drug concentrations in the blood samples analyzed by HPLC are inputted into interested text boxes at "calculating of individual dose screen" for estimating the elimination rate constant (ke), volume of distribution (Vd), and clearance (Cl) (Dhillon & Gill, 2006). While ke is calculated, it takes care of the coefficient of determination (r^2). Afterwards, the maintenance dose is calculated to reach the steady-state concentration.

2.3 *In vivo* Animal Study Design

Six white male rabbits weighing between 1.5 and 2 kg were used for this study. The drug was given at a calculated dose according to its weight by IV administration to the rabbit marginal vein of the left ear. The blood samples were taken from the rabbit marginal vein of the right ear by the 24G branule, and plasma was separated from whole blood by a vacutainer containing EDTA. After each blood sample was taken, 0.5 mL of the 1% heparin solution was injected into the branule. The investigations were performed after approval by the Animal Ethics Committee at the Faculty of Medicine of Ege University (No. 2007-37).

The study was designed as three groups with two rabbits in each group. The first group was used to find mean of their ke, Vd, and Cl parameters by administration of one dose bolus, and these results was considered the population PK.

For finding the population PK, the first bolus dose was calculated taking into account the weight of the rabbits and was administered to both rabbits in the first group. After injection, three blood samples taken at certain intervals from the rabbits were analyzed. The analyzing results were put in a concerned place in the program, and the second dose was calculated for each rabbit separately. After second dose administration, a last blood sample for measuring Ctrough was taken and analyzed to compare this analysis result with the corresponding to theoretical value for each rabbit.

The first doses for the second group used for examination of multiple dose bolus administration were calculated according to population PK, and the results from plasma samples were compared with theoretical values. The continuous infusion was applied to the third group. For the first infusion rate of the third group, the population PK was assumed to be their PK parameters.

As an expression of the closeness to the therapeutic target, deviation from the theoretical value of the practical value obtained was used. The practical values were compared with theoretical values on a deviation% from the theoretical to practical value by using Equation 1.

$$\text{Deviation\%} = \frac{\text{PC} - \text{TC}}{\text{TC}} \times 100$$

Equation 1- Calculation of deviation% from theoretical value to practical value. PC: The Practical Concentration Value Obtained; TC: The Theoretical Concentration Value calculated by the program.

2.4 The Strategy of Multiple Bolus Doses Administration

The bolus doses to be given to rabbits in the second group were separately calculated from the program using their weights. After being injected, three blood samples were taken at different hours and analyzed. The maintenance dose, Ctrough, and dose interval were estimated by the program for each rabbit, and the calculated maintenance dose was administrated. A last blood sample was taken to compare practical and theoretical values.

2.5 The Strategy of Continuous Infusion Administration

The infusion flow rate was determined by inputting the preferred time to reach the target concentration. After starting the infusion, three blood samples taken at different hours were analyzed. Then, when the preferred time was over, second infusion rates were adjusted to maintain steady-state concentrations. Before and after the second infusion rate administration, three blood samples were taken, and this study was completed by stopping the administration of drugs.

2.6 The Validation of Analytical Method of Theophylline

The analytical method was modified from Karasulu E. et al. (Karasulu, Apaydin, & Tuglular, 2006). An Agilent 1100 series HPLC was used at isocratic conditions. It was equipped with an injection valve of 20 µL, a UV detector set at 273 nm, and a C_{18}, 5 µm x 4.6 mm x 150 mm analytical column. The mobile phase composition was a mixture of acetonitrile, tetrahydrofuran, acetic acid, and distilled water (20: 20: 5: 955) (v/v/v/v) at a flow rate of 1.0 ml/min. The overall analysis time was 10 minutes.

The method validation was performed using the following parameters: selectivity, accuracy, precision and recovery, sensitivity, reproducibility, and stability of standard and test solution (Hendeles et al., 1978). The linearity of the method involved six points: 1, 4, 8, 12, 16, and 20 µg/mL.

Each sample (200 µL) was mixed with caffeine solution as an internal standard and shaken by vortex for 10 sec. 600 µL of methanol was added to it and shaken by vortex for 10 sec. After centrifuging at 10,000 rpm at 4 °C for 15 min, the supernatant was removed under the vacuum concentrator with nitrogen. The remainder was solved with 0.5 µL of mobile phase and injected into HPLC.

3 Results and Discussion

3.1 Execution of Software Program

The program has two parts: the source code, including the algorithms of PK, and the execution area for users. The source codes for the PK module of software were prepared in C#. The image of administration route screens is presented in Figure 1.

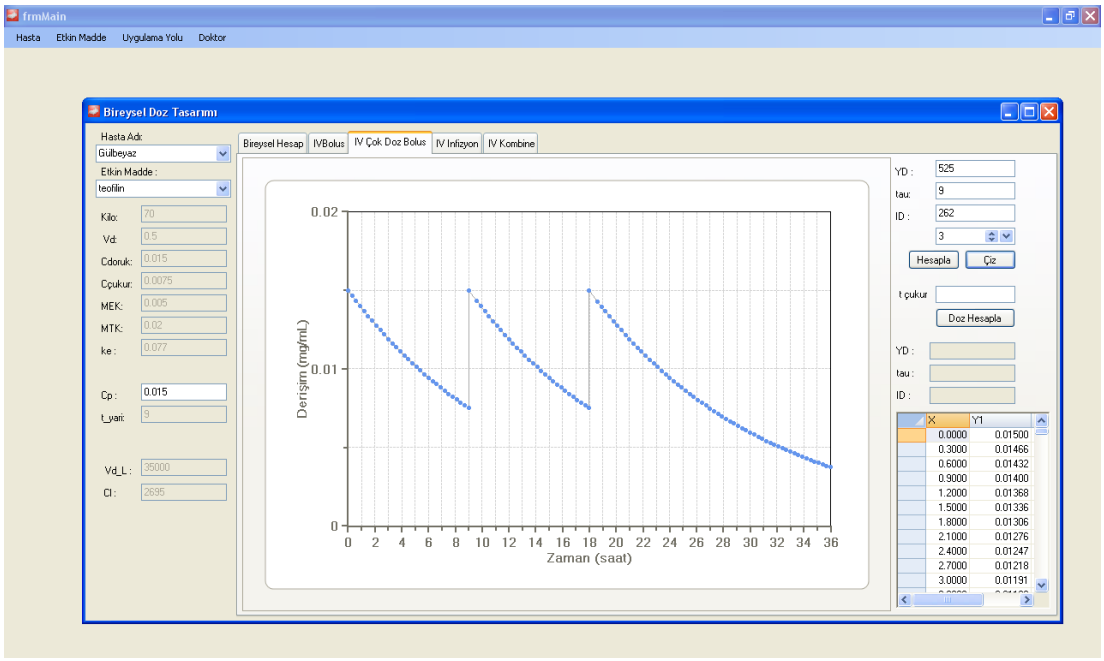

Figure 1- The administration route screen

3.2 The Strategy of Multiple Bolus Dose Administration

Three blood samples were taken after the first group received a bolus IV dose of the dose that was calculated from the source data. Vd and ke changed from 0.77 h-1 to 0.188 h-1 and 500 mL to 1242 mL, respectively (Table 2); r^2 was 0.86 and 0.95 for each rabbit. A blood sample was also taken immediately before the second dose. The deviation of the result from the theoretical result was -89.799% and 18.385% for each rabbit. The second dose was determined to reach the target concentration according to these values, which vary for each rabbit separately. When the theoretical results are compared with the sample results taken at a given time after the second dose, the deviation value was found to be 5.53% and 8.795%, respectively.

Table 2- Pharmacokinetic parameters of the rabbits at multiple bolus dose administration

	Accepted values in common**	1st rabbit	2nd rabbit	The parameter of Population PK	3th rabbit	4th rabbit
1. dose		14 mg / 7 mL	20 mg / 10 mL	-	20 mg / 10 mL	20 mg / 10 mL
ke (h^{-1})	0.077	0.252	0.124	0.188	-	-
Vd (mL)	500	1439	1045	1242	-	-
2. dose* theoretically		20 mg	11.652 mg	-	-	-
2. dose practically		20 mg / 10 mL	11 mg / 5.5 mL	-	20 mg / 10 mL	20 mg / 10 mL

* The second dose was given at 400 min and 340 min for the first and second rabbits, respectively.

** According to Hardman et al.(Hardman et al., 1996)

The values obtained from the first group were accepted as population PK. According to these values, the IV bolus dose of the second group, the time of administration of the second dose, the Ctrough before the administration of the second dose, and the maintenance dose were calculated according to their weight. The deviations from the theoretical results of the blood concentrations of rabbits before and after the second dose were 11.546% and -8.751% for the first rabbit, and 50.114% and 4.851% for the second, respectively.

The times of dose administrations, the time of Ctrough, and the deviation% of all samples belonging to the multiple bolus doses administration are presented in Table 3. The profiles of the plasma concentration time for practical and theoretical values at multiple bolus doses are presented as graphical in Figure 2.

Table 3- The deviation % from the theoretical value to the practical value at multiple bolus dose administration

First Group				**Second Group**			
1st rabbit		**2nd rabbit**		**3th rabbit**		**4th rabbit**	
t (min)	**Deviation%**	**t (min)**	**Deviation%**	**t (min)**	**Deviation%**	**t (min)**	**Deviation%**
0	First dose time	**0**	First dose time	**0**	First dose time	**0**	First dose time
5		**3**		**6**	-5.672	**10**	-0.473
30		**38**		**21**	-24.137	**20**	-21.564
60		**53**		**40**	-25.579	**50**	-18.945
385 (Ctrough)	-89.799	**360 (Ctrough)**	18.385	**416 (Ctrough)**	11.546	**340 (C_{trough})**	50.114
400	Second dose time	**360**	Second dose time	**416**	Second dose time	**340**	Second dose time
600	5.530	**365**	8.795	**425**	-8.751	**350**	4.851

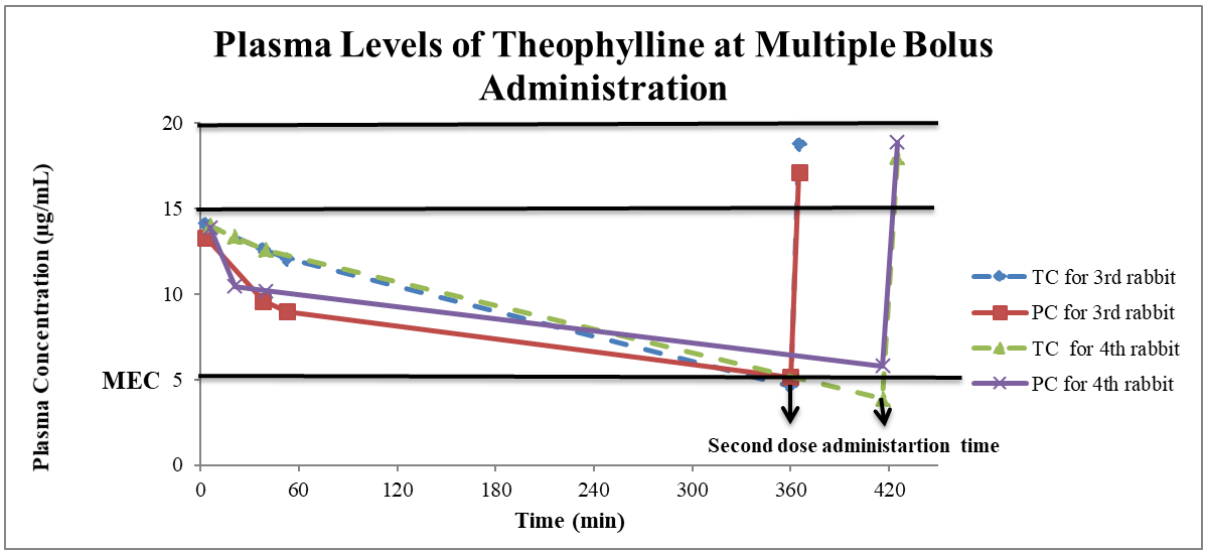

Figure 2- The plasma levels of theophylline at multiple bolus doses administration with practical and theoretical results of 3rd and 4th rabbits

3.3 The Strategy of Continuous Infusion Administration

The infusion rate required to reach the target level within 1 hour was calculated as 10 mL/hour (20 mg) based on the population PK parameters determined from the program, and three blood samples were taken after IV infusion administration. The first infusion was terminated with a blood sample taken at 60 minutes and the second infusion rate was calculated as 3.3 mL/hour (6.6 mg) from the program and administered for 30 minutes. Two blood samples were taken throughout the second infusion, and a final blood sample after the end of the second infusion was taken and analyzed. Theophylline level in the last blood sample of the first infusion was 15.718 µg/mL for the first rabbit and deviated from the theoretically calculated value by 2.331%. In the second rabbit, it was found to be 15.245 µg/mL and deviated from the theoretical calculated value by 17.269%. The deviations in the samples after the second infusion for both rabbits were between -0.846% and 18.664%.

The starting times of IV infusions, the time of C_{target}, and the deviation% of all samples are presented in Table 4. The deviations from the desired concentration of theophylline of results of samples taken during the second continuous infusion rate are shown in Table 5.

The profiles of the plasma concentration time of practical and theoretical values at IV infusion administration are presented as graphical in Figure 3.

Table 4- The Deviation % from the theoretical value to practical value at IV infusion administration

Third Group			
5th rabbit		**6th rabbit**	
t (min)	**Deviation%**	**t (min)**	**Deviation%**
0	First infusion rate time	**0**	First infusion rate time
15	73.947	**7**	96.280
30	30.807	**18**	47.300
45	16.480	**28**	17.269
60	2.331	**30**	Second infusion rate time
60	Second infusion rate time	**40**	-0.593
75	16.724	**60**	-0.846
90	18.664	**60**	The ended of infusion
90	The ended of infusion		

Table 5- The deviation from the desired concentration of theophylline in the results of samples taken during the second continuous infusion rate

5th rabbit		**6th rabbit**	
t (min)	**Deviation% (PC-15)/15x100***	**t (min)**	**Deviation% (PC-15)/15x100***
60	4.786	28	3.633
75	5.386	40	-14.460
90	11.306	60	-12.860

* 15 value is the therapeutic target or TC

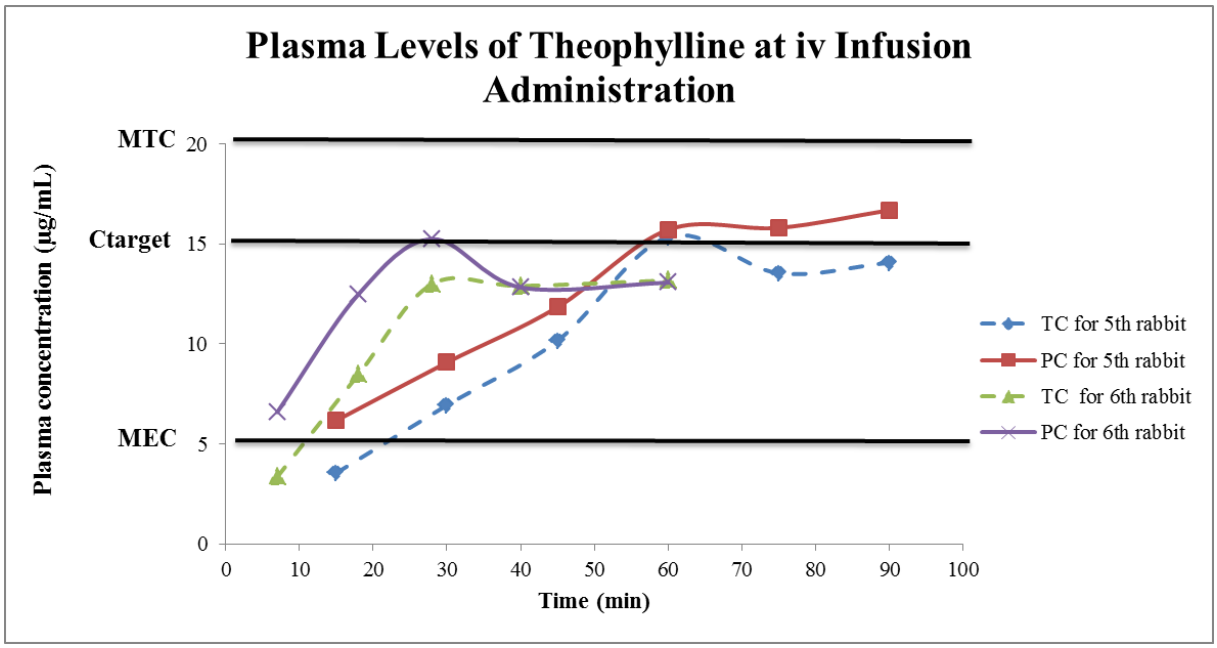

Figure 3- The plasma levels of theophylline at IV infusion administration with practical and theoretical results of 5th and 6th rabbits

3.4 The Validation of Analysis Method of Theophylline

In analytical validation, selectivity, determination of LOQ and LOD, repeatability of injection and extraction repeatability as precision criteria, solution stability, recovery studies, accuracy, and linearity studies were performed. The chromatogram with the blank plasma and matrix sample together is presented in Figure 4. The results of analytical method validation and specification limits according to CDER, FDA guidance (Fda & Cder, 2018) are shown comparatively in Table 6.

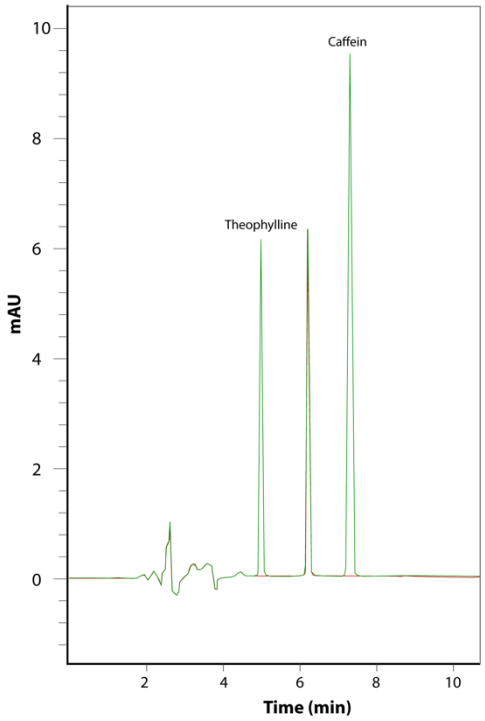

Figure 4- The chromatogram with the blank plasma (red line) and matrix sample (green line)

Table 6- The results of the theophylline's analytical validation

Validation Parameters		**Specification limits** (Hata! Başvuru kaynağı bulunamadı.)		**Results**
Selectivity	**RT of Theophylline**	-		5.086 min
	RT of Caffeine	-		7.554 min
Sensitivity	**LOD**	-		0.043 µg/mL
	LOQ	-		0.026 µg/mL
r ²		≥ 0.95		0.999
Calibration Curve		± 20% for the LLOQ (1µg/mL); ± 15% for the other points (4, 8, 12, 16, 20 µg/mL)		-13.6% - -0.1% for LLOQ 2.1% – 4.27 % for the other points
Precision (Repeatability)		RSD% ≤ 2%		0.206%
Reproducibility		Low concentration (1µg/mL)	RSD% ≤ 20%	6.524%
		Medium concentration (8µg/mL)	RSD% ≤ 15%	0.895%
		High concentration (20µg/mL)		1.095%
Recovery		Low concentration (1µg/mL)		94.6%
		Medium concentration (8µg/mL)		100.2%
		High concentration (20µg/mL)		97.3%
Stability of solutions at room temperature		Not more than 15% differences (during the 12 hours)		0.8% for lowest and highest concentrations

Following FDA guidelines(Fda & Cder, 2018) the method validation of theophylline was checked and found to be correct within the limits of the validation parameters (Table 6). The analysis time of one sample, including the sample preparation, is approximately 30 min with this method. In terms of chromatographic analysis, the method is simple and fast.

The appropriateness of the Ctrough or AUC data calculated from the samples taken is evaluated with the correlation coefficient. In the sources where the AUC calculation was made based on at least 3 samples, correlation coefficient values varied between 0.54 and 0.96 and were accepted (Erdman, Rodvold, & Pryka, 1991; Kuypers et al., 2010). In this study, the high correlation (the coefficients of determination of the first and second rabbit samples were 0.86 and 0.95, respectively) between the analysis results of the three blood samples after the dose determined by the two rabbits in the first group shows the accuracy and reliability of the sampling time and measurement method.

In line with the results obtained with high correlation, a dose adjustment was made to the first group, and a second dose was administered. The deviations % of Ctrough and Ct after the second dose decreased from %-89.799 to %5.53 and from %18.385 to %8.795 for each rabbit, respectively (Table 2). The decrease in the deviation values, which is close to the therapeutic target, shows the applicability of the program.

When McClain et al. interpreted the results of the critical values of therapeutic drugs obtained from 36 laboratories without any standardization, they showed that the relative coefficient of variation was large (> 88%) for Ctrough and less (> 19%) for Cpeak (McClain, Owings, & Bornhorst, 2011). The relative coefficient variation for the Cpeak value of theophylline obtained from 33 laboratories was 19%. It has been shown that theophylline can maintain its effectiveness in a narrow therapeutic range by reducing the deviation from the theoretical value in the Ctrough values obtained from this program for IV bolus application (Table 2). In this way, the monitoring of theophylline could be standardized.

When the population PK was compared to the other rabbits in the second group, the deviation% in Ctrough was observed as 11.546 and 50.114, but it was observed that the elevation of deviations at low concentrations did not affect MTC, and also that the practical concentration remained above TI at 5 μg/mL.

In the second post-dose measurement, deviation% values were found to be -8.751 to 4.851, and the target concentration was reached. The program has also been shown to work reliably for multiple dose administration (Table 3).

The third application, infusion, showed that the target concentration was reached in a certain time and the theophylline plasma levels of each rabbit covered the therapeutic range of theophylline (theophylline concentration range of blood samples taken between 15 and 90 minutes between 6.175 and 16.696 μg/mL). The measurement results at the time of reaching the target concentration were 15.718 and 15.245 μg/mL, and the deviations of these values from the theoretical calculation were found to be 2.331% and 17.269%. Also, deviations after the

second infusion rate ranged from -0.846 to 18.664 (Table 4). The program worked successfully in infusion administration.

4 Conclusion

Thanks to this program, it has been shown that theophylline, which has a NTI, can be used safely by achieving values close to the therapeutic target. And thanks to this clinical benefit, a cost-effectiveness program was designed.

In the implementation of the program, it is seen that it is a user-friendly program in order to clearly indicate the location of the data to be entered and to guide the user. In addition to the mathematical results, the graphical presentation of the results has made the program more visually understandable and interpretable by the expert.

The software program is in operation and will be developed in the future. TDM is not just a program; it is a whole, from the selection of the sampling time to the analytical method. Developing faster analytical methods will increase the applicability of TDM. For now, the program is practicable for the TDM of theophylline.

Acknowledgements: The study was conducted at ARGEFAR.

Conflict of interest statement: The authors declared no conflict of interest

References

Birkett, D. J. (1997). Pharmacokinetics made easy: therapeutic drug monitoring. *Australian Prescriber*, *20*, 9–11.

Dhillon, S., & Gill, K. (2006). Basic pharmacokinetics. In S. Dhillon & A. Kostrzewski (Eds.), *Clinical Pharmacokinetics* (1st ed., pp. 1–44). London and Chicago: Pharmaceutical Press.

Erdman, S. M., Rodvold, K. A., & Pryka, R. D. (1991). An Updated Comparison of Drug Dosing Methods Part III: Aminoglycoside Antibiotics. *Drug Disposition*, *20*(5), 374–388.

Fda, & Cder. (2018). *Bioanalytical Method Validation Guidance for Industry Biopharmaceutics Bioanalytical Method Validation Guidance for Industry Biopharmaceutics Contains Nonbinding Recommendations*. Retrieved from http://www.fda.gov/Drugs/GuidanceComplianceRegulatoryInformation/Guidances/default.htmand/

Freedman, D. B., & Marshall, W. (1993a). Theoretical Considerations. In D. B. Freedman & W. Marshall (Eds.), *Therapeutic Drug Monitoring and Clinical Biochemistry*. London: ACB Venture Publications.

Freedman, D. B., & Marshall, W. (1993b). Individual Drugs. In D. B. Freedman & W. Marshall (Eds.), *Therapeutic Drug Monitoring and Clinical Biochemistry*. London: ACB Venture Publications.

Freedman, D. B., & Marshall, W. (1993c). Analytical Aspects. In D. B. Freedman & W. Marshall (Eds.), *Therapeutic Drug Monitoring and Clinical Biochemistry*. London: ACB

Venture Publications.

Fuchs, A., Csajka, C., Thoma, Y., Buclin, T., & Widmer, N. (2013). Benchmarking therapeutic drug monitoring software: A review of available computer tools. *Clinical Pharmacokinetics*, *52*(1), 9–22.

Ghiculescu, R. A. (2008). Therapeutic drug monitoring: which drugs, why, when and how to do it. *Australian Prescriber*, *31*(2), 42–44.

Hallworth, M., & Watson, I. (2017). *Therapeutic drug monitoring clinical guide*. (D. Holt, S. Tett, & S. H. Wong, Eds.)*Abbott* (4th ed., Vol. 4). Retrieved from www.abbottdiagnostics.com.

Hardman, J. G., Limbird, L. E., Gilman, A. G., Molinoff, P. B., & Ruddon, R. W. (1996). *Goodman & Gilman's The Pharmacological Basis of Therapeutics*. (J. G. Hardman, L. E. Limbird, A. G. Gilman, P. B. Molinoff, & R. W. Ruddon, Eds.) (9th ed.). New York: McGraw-Hill: International Edition.

Hendeles, L., Weinberger, M., & Johnson, G. (1978). Monitoring Serum Theophylline levels. *Clinical Pharmacokinetics*, *3*, 294–312.

Jenne, J., Nagasawa, H., McHugh, R., Macdonald, F., & Wyse, E. (1975). Decreased theophylline half-life in cigarette smokers. *Life Sciences*, *17*, 195–198.

Kang, J. S., & Lee, M. H. (2009). Overview of therapeutic drug monitoring. *Korean Journal of Internal Medicine*, *24*(1), 1–10.

Karasulu, E., Apaydin, S., & Tuglular, I. (2006). Theophylline granule formulation prepared by the wet granulation method: comparison of in vitro dissolution profiles and estimation of in vivo plasma concentrations. *ID PHARMACOKINETICS*, *31*(4), 291–298.

Koçak, Ç. C., Nas, A., Kantekin, H., & Dursun, Z. (2018). Simultaneous determination of theophylline and caffeine on novel [Tetra-(5-chloroquinolin-8-yloxy) phthalocyanato] manganese(III)-Carbon nanotubes composite electrode. *Talanta*, *184*(December 2017), 452–460.

Kuypers, D. R. J., Le Meur, Y., Cantarovich, M., Tredger, M. J., Tett, S. E., Cattaneo, D., Tönshoff, B., et al. (2010). Consensus report on therapeutic drug monitoring of mycophenolic acid in solid organ transplantation. *Clinical Journal of the American Society of Nephrology*, *5*(2), 341–358.

Marks, V. (1985). A historical introduction. In B. Widdop (Ed.), *A historical introduction. In: Widdop B, (ed.) Therapeutic Drug Monitoring* (pp. 3–15). Edinburgh: Churchill Livingstone.

McClain, C. M., Owings, R., & Bornhorst, J. A. (2011). Heterogeneity of publicly accessible online critical values for therapeutic drugs. *Journal of Pathology Informatics*, *2*(1), 53. Elsevier BV.

Pesce, A. J., Rashkin, M., & Kotagal, U. (1998). Standards of laboratory practice: theophylline and caffeine monitoring. *Clinical Chemistry*, *44*(5), 1124–1128.

Touw, D. J., Neef, C., Thomson, A. H., & Vinks, A. A. (2005). Cost-Effectiveness of Therapeutic Drug Monitoring A Systematic Review. *Ther Dryg Monit*, *27*(1), 10–17. Retrieved from http://ctfphc.org/methods.htm.

Wagnew, A., Kassa, A., Abebe, A., Asmellash, T., Beyene, Y., Tesfaye, A., & Amare, M. (2022). Poly(aquachlorobis(1,10–phenanthroline)copper(II)iodidemonohydrate)/GCE for

simultaneous determination of caffeine and theophylline in human serum, tea, and tablet samples. *Arabian Journal of Chemistry*, *15*(1), 103458. The Author(s). Retrieved from https://doi.org/10.1016/j.arabjc.2021.103458

Whiting, B., Kelman, A. W., Bryson, S. M., Derkx, M., Thomson, A. H., Fotheringham, G. H., & Joel, S. E. (1984). Clinical pharmacokinetics: a comprehensive system for therapeutic drug monitoring and prescribing. *BRITISH MEDICAL JOURNAL*, *288*, 541–545.

Erzincan Üniversitesi
Fen Bilimleri Enstitüsü Dergisi
2024,17(1), 129-136
ISSN: 1307-9085, e-ISSN: 2149-4584
Araştırma Makalesi

Erzincan University
Journal of Science and Technology
2024,17(1), 129-136
DOI: 10.18185/erzifbed.1351751
Research Article

Does Articular Pressure Change Vital Signs During Temporomandibular Joint Arthrocentesis?

Fatih ÇELİK[1*], Samih DİYARBAKIR[2], Murat KAYA[1], Elif ÇELİK[3]

[1]Erzincan Ağız ve Diş Sağlığı Eğitim ve Araştırma Hastanesi: Erzincan, TR
[2]Erzincan Binali Yıldırım Üniversitesi Tıp Fakültesi: Erzincan, TR
[3]Erzincan Binali Yıldırım Üniversitesi Sağlik Hizmetleri Meslek Yüksekokulu: Erzincan, TR

Received: 29/08/2023, **Revised:** 27/09/2023, **Accepted:** 27/09/2023, **Published:** 28/03/2024

Abstract

Objective: The objective of this study was to evaluate and compare vital signs, especially mean blood pressure and heart rate, in patients treated with two techniques of arthrocentesis of the temporomandibular joint.
Methods: Thirty patients received TMJ arthrocentesis with either two needle arthrocentesis (TNA) or single needle arthrocentesis (SNA). Heart rate and arterial pressure measurements were recorded at six different stages of the procedure and these values were compared between the two techniques.
Results: Heart rate and mean blood pressure recorded their peak values during needle insertion for both local anesthesia and arthrocentesis administration (P<0.05). Heart rate and mean blood pressure scores were significantly higher in the SNA group.
Conclusion: It is necessary to be more cautious in patients receiving SNA as blood pressure and heart rate may increase.

Keywords: arthrocentesis, temporomandibular joint, blood pressure, heart rate

Temporomandibular Eklem Artrosentezinde Eklem Basıncı Yaşamsal Bulguları Değiştirir mi?

Öz

Amaç: Bu çalışmanın amacı, iki farklı temporomandibular eklem (TME) artrosentez tekniği uygulanan hastaların ortalama arter basıncı ve kalp hızı gibi yaşamsal bulgularını karşılaştırmaktır.

Yöntemler: Otuz hastaya; çift iğne girişli artrosentez veya tek iğne girişli artrosentez yöntemleri ile TME artrosentezi uygulandı. Kalp hızı ve arteriyel basınç ölçümleri işlemin altı farklı aşamasında kaydedilerek bu değerler iki teknik arasında karşılaştırılmıştır.

Sonuçlar: Ortalama kan basıncı ve nabız; anestezi ve iğne girişi sırasında en yüksekti (P<0.05). Kalp hızı ve ortalama arter basıncı skorları tek iğne girişli artrosentez yapılan hasta grubunda istatistiksel olarak daha yüksekti. Tek iğne girişi ile artrosentez yapılan hastalarda kan basıncı ve kalp hızı artabileceğinden daha dikkatli olmak gerekir.

Anahtar Kelimeler: artrosentez, temporomandibular eklem, kan basıncı, nabız

*Corresponding Author: fatihcelik@gmail.com
Fatih ÇELİK, https://orcid.org/0000-0001-6806-8480
Samih DİYARBAKIR, https://orcid.org/0000-0001-6755-7741
Murat KAYA, https://orcid.org/0000-0001-8269-930X
Elif ÇELİK, https://orcid.org/0000-0002-5059-9432

1. Introduction

Lysis and lavage of the Temporomandibular Joint(TMJ) were first applied using arthroscopy by Onishi [1]. In 1991, Nitzan first introduced the technique of TMJ arthrocentesis, which involves flushing the joint cavity by injector pressure with two needles inserted into the upper compartment of the joint [2]. This technique later became known as a double needle or two needle arthrocentesis (TNA) technique.

The joint irrigation procedure can be conducted either at a lower pressure using a suspended infusion bag or at a higher pressure with the use of a syringe [3].

Multiple adjustments have been recorded in the literature to address the challenges associated with the use of dual needles in the classical arthrocentesis technique. The single needle arthrocentesis technique was introduced by Guarda-Nardini in 2008 [4].

The single needle method includes flushing the upper joint compartment by allowing both the liquid inlet and outlet through the same cannula [5].

In SNA the fluid flow persists within the same cannula and lumen; therefore, arthrocentesis takes more time than TNA and SNA technique [6]. In addition, patients undergoing the SNA technique may find the arthrocentesis procedure more difficult to tolerate due to the higher intra-articular pressure compared to other techniques [7].

Several studies have compared the efficacy of TMJ arthrocentesis techniques [6,8,9] However, only one study has assessed patient comfort with these techniques about anxiety levels [10].

This study aimed to investigate patient HA and MBP values in the SNA technique compared to the TNA technique.

2. Material and Methods

This study received approval from the Erzincan Binali Yildirim University Clinical Research Ethics Committee. (2020/03-16). The study included 30 patients who were examined in Erzincan Oral and Dental Health Training and Research Hospital between 2019 and 2020 and diagnosed with disc displacement and underwent arthrocentesis with this diagnosis. Patients signed written informed consent before each procedure. This study included patients who were diagnosed according to the current diagnostic criteria and who also exhibited unilateral joint involvement, which was confirmed by magnetic resonance imaging (MRI) findings. All patients were adults, aged 18 years or older, and had been experiencing TMJ pain for a minimum of 6 months. Patients with systemic diseases affecting TMJ, previous TMJ surgical operations, and patients with incomplete clinical records were excluded from the study.

The patients were randomly allocated into two treatment groups based on the treatment they received. (SNA or TNA).

Arthrocentesis Techniques:

The TNA procedure used was described by Nitzan [2]. For this technique, a direct line was established from tragus to the lateral eye cantus, referred to as the Holmlund-Helsing line. The initial puncture point was designated as 20 mm in front and 10 mm below the tragus, while the second point was marked as 10 mm in front and 2 mm below the tragus. The superior joint compartment was washed up with 150 mL Lactated Ringer's fluid after preauricular local anesthesia infiltration. Two 21-gauge needles were used for irrigation, and upon completion of the procedure, following the removal of one of the needles, a 1 mL injection of hyaluronic acid was administered into the superior TMJ cavity via the remaining needle.

In the SNA technique, only a single needle entry point was used and both fluid entry and fluid exit were managed with the same cannula and lumen of a single 21-gauge needle as described by Guarda-Nardini et al. [4] The joint was irrigated with 150 mL RL solution. At the end of the procedure, 1 mL of hyaluronic acid was injected via needle.

Measurement Time Points:

MBP and HR of each patient were measured the operation (T0), during the needle insertion for local anesthesia (T1), during needle insertion(s) to the superior joint compartment (T2), during the arthrocentesis procedure at the fifth minute (T3) during the arthrocentesis procedure at the tenth minute (T4), and at the at the conclusion of the arthrocentesis procedure (T5).

Statistical Analysis:

Statistical analysis was carried out with IBM SPSS 22. The data were presented as mean ± standard deviation and median (minimum–maximum). The normality of variable distributions was assessed using the Kolmogorov-Smirnov test, and the Mann–Whitney U test was employed to compare values between the two groups due to the non-normal distribution of variables. Statistical significance was defined as a p-value less than 0.05.

3. Results and Discussion

There were no significant differences observed between the groups concerning age and sex. (Table 1). HR and MBP values were higher at all stages in the SNA group compared to the conventional arthrocentesis group. (Figure 1,Figure 2) however, there were no statistically significant differences between the two groups in all periods except at T4. (Table 2).

Table 1: Age and Sex Distribution of Patients in the Study

	SNA (n: 15)	TNA (n: 15)
Age (years)		
Mean ± SD	31.53 ± 10.76	27.33 ± 7.91
Median (min. – max.)	32 (17 – 53)	23 (19 – 42)
Sex		
Female	9/15 (60%)	10/15 (67%)
Male	6/15 (40%)	5/15 (33%)

SD: standard deviation; min: minimum; max: maximum

SNA: single needle Arthrocentesis, TNA: Two Needle Arthrocentesis

Table 2: Comparison of MBP and HR values according to process stages

	HR			**MBP**		
	SNA	**TNA**	**P**	**SNA**	**TNA**	**P**
T0	85.07 ± 12.78	87.07 ± 14.11	0.870	94.13 ± 8.10	90.00 ± 11.56	0.285
T1	89.07 ± 13.26	92.07 ± 14.98	0.744	100.60 ± 7.94	94.13 ± 12.11	0.148
T2	88.20 ± 13.24	94.20 ± 15.21	0.389	98.27 ± 8.51	94.27 ± 11.69	0.250
T3	84.07 ± 12.78	84.93 ± 13.85	0.967	95.33 ± 8.07	87.80 ± 11.37	0.056
T4	82.13 ± 12.41	83.93 ± 13.70	0.902	97.00 ± 7.91	86.67 ± 11.10	0.013*
T5	79.40 ± 11.84	82.07 ± 13.24	0.775	90.53 ± 7,85	83.33 ± 10.73	0.067

SNA: single needle Arthrocentesis, TNA: Two Needle Arthrocentesis

HR: Heart Rate, MBP: The Mean Blood Pressure

T0: Preoperative, T1: during the needle insertion for local anesthesia, T2: during needle insertion(s) to the superior joint compartment, T3: Fifth minute, T4: Tenth Minute, T5: At the conclusion of the arthrocentesis procedure

Figure 1: Change in HR Values According to Process Stage

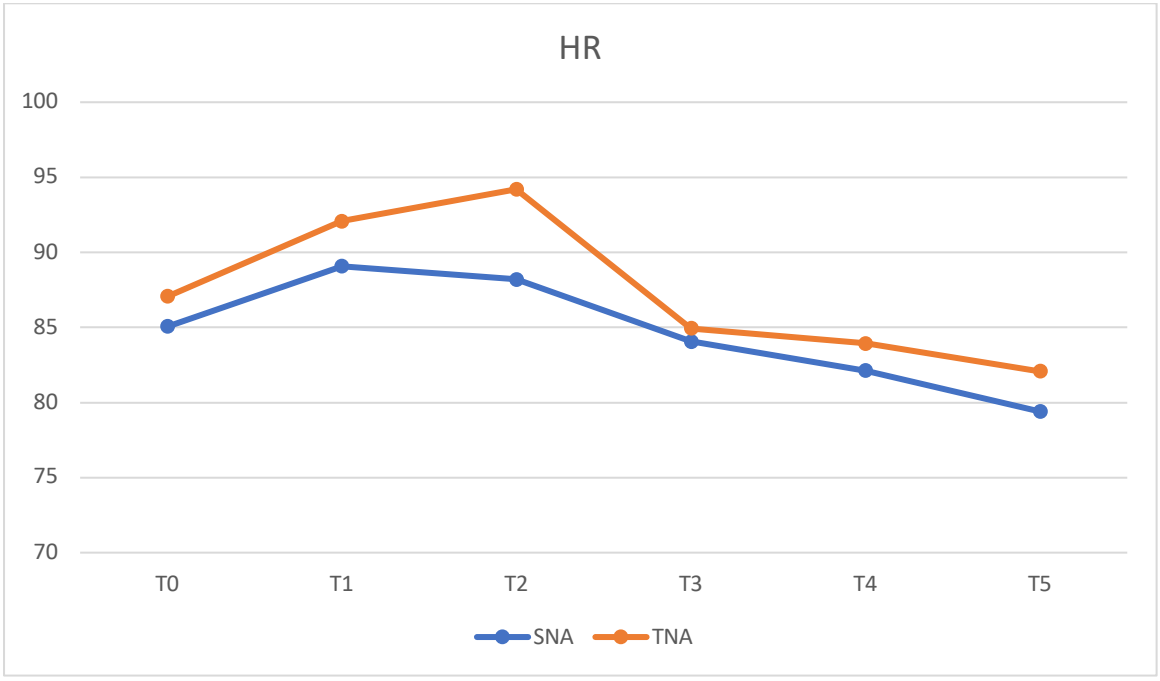

SNA: Single Needle Arthrocentesis, TNA: Two Needle Arthrocentesis
HR: Heart Rate, MBP: Mean blood Pressure

Figure 2: Change in MBP Values According to Process Stages

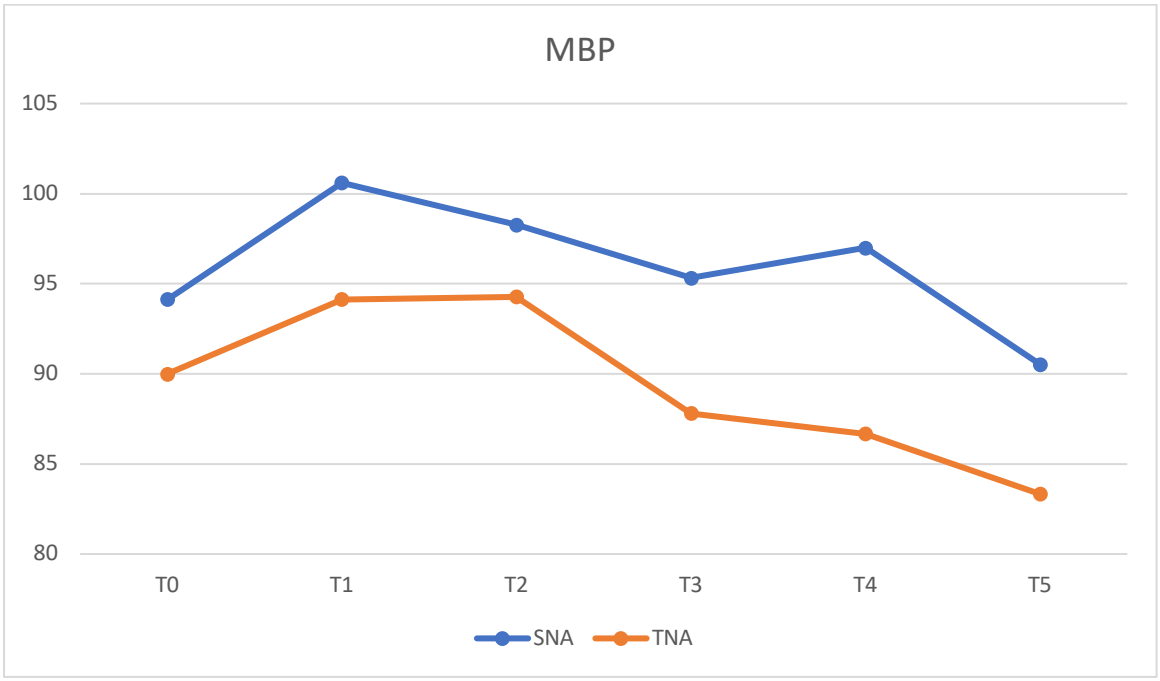

SNA: single needle Arthrocentesis, TNA: two needle Arthrocentesis
HR: Heart Rate, MBP: Mean Blood Pressure

Discussion:

The effect of maxillofacial surgical interventions on heart rate and mean blood pressure values has been frequently presented in the literature [11]. Many publications have shown increases in these two values during surgical procedures performed under local anesthesia [12]. Changes in blood pressure and heart rate are often attributed to dental anxiety and fear [13,14]. Patients not only have a fear of dental surgical procedures but also develop anxiety about the needle used for local anesthesia administered before surgery [15]. In the arthrocentesis procedure, in addition to the needle used for local anesthesia, the procedure itself involves separate needle entries, which can further increase anxiety. With the increase in anxiety and fear, an increase in heart rate and average blood pressure is an expected outcome [16].

Various studies published to compare the effectiveness of SNA and TNA techniques [6,8,9,17–21]. Two of them additionally focused on the ease of procedure [6,8]. They studied the ease of procedure by using subjective feedback from the operator performing arthrocentesis. Only one study investigated the comfort of patients observing vital signs [10]. In the SNA technique, it was presumed that the intraarticular pressure would be greater than in the TNA technique because both the liquid inlet and outlet were managed through the same cannula [22]. The higher pressure can be useful in TMJs presenting intraarticular adhesions as in disc displacement without reduction cases. However, this higher pressure can be assumed more uncomfortable for patients. Additionally using the same cannula takes longer time in the SNA technique [21]. Longer operation time can be an irritating factor for patients and thus the HR and MBP values would be expected higher compared to the TNA technique. Taskesen et al. studied HR and MBP and the Stait-Trait Anxiety Inventory Scale (STAI-S) to compare patient comfort and anxiety levels in TNA and SNA techniques [10]. They revealed no statistically significant differences in HR and MBP values in any period between SNA and TNA groups although they expected the HR and MBP values would be higher in SNA than in TNA because of the higher intraarticular pressure. Unlike their study, we found the statistically significant difference only at point T4 marking the tenth minute of the procedure. The difference at this time point may be due to the pressure and this difference may be explained by the fact that the longer the duration of the procedure, the less the patient tolerates the pressure.

Limited sample size and retrospective study design are two major limitations of our study. However, using objective parameters such as HR and MBP values may be considered pro of the present study.

4. Conclusion

This study revealed that the SNA technique may reduce HR and MBP values therefore patient tolerability of the SNA may need to be considered in the SNA technique. Further studies using similar objective parameters in larger patient groups are needed

Ethics in Publishing

This study was approved by the Erzincan Binali Yildirim University Clinical Research Ethics Committee (2020/03-16)

Acknowledgements

The authors would like to thank Dr. Fatih TAŞKESEN for his contribution to the planning and writing of this study.

References

[1] M. Onishi, *Arthroscopy of the temporomandibular joint (author's transl)*, Kokubyo Gakkai Zasshi **42**, 207 (1975).
[2] D. W. Nitzan, M. F. Dolwick, and G. A. Martinez, *Temporomandibular Joint Arthrocentesis: A Simplified Treatment for Severe, Limited Mouth Opening*, J Oral Maxillofac Surg **49**, 1163 (1991).
[3] A. R. Öreroğlu, Ö. Özkaya, M. B. Öztürk, D. Bingöl, and M. Akan, *Concentric-Needle Cannula Method for Single-Puncture Arthrocentesis in Temporomandibular Joint Disease: An Inexpensive and Feasible Technique*, Journal of Oral and Maxillofacial Surgery **69**, 2334 (2011).
[4] L. Guarda-Nardini, D. Manfredini, and G. Ferronato, *Arthrocentesis of the Temporomandibular Joint: A Proposal for a Single-Needle Technique*, Oral Surgery, Oral Medicine, Oral Pathology, Oral Radiology, and Endodontology **106**, 483 (2008).
[5] S. Tozoglu, F. A. Al-Belasy, and M. F. Dolwick, *A Review of Techniques of Lysis and Lavage of the TMJ*, British Journal of Oral and Maxillofacial Surgery **49**, 302 (2011).
[6] M. F. Şentürk, T. Yazıcı, Y. Fındık, and T. Baykul, *Intraoperative Comparison of Single- and Double-Puncture Techniques in Temporomandibular Joint Arthrocentesis*, International Journal of Oral and Maxillofacial Surgery **47**, 1060 (2018).
[7] F. Taşkesen and B. Cezairli, *Is Single Puncture Arthrocentesis Type-1 Superior to Double Puncture Arthrocentesis in Temporomandibular Joint Disc Displacement Without Reduction?*, Ahi Evran Med J **6**, 1 (2022).
[8] W. Talaat, M. M. Ghoneim, and M. Elsholkamy, *Single-Needle Arthrocentesis (Shepard Cannula) vs. Double-Needle Arthrocentesis for Treating Disc Displacement without Reduction*, CRANIO® **34**, 296 (2016).
[9] E. Grossmann, P. Guilherme Vargas Pasqual, R. L. Poluha, L. C. V. Iwaki, L. Iwaki Filho, and Ê. T. Setogutti, *Single-Needle Arthrocentesis with Upper Compartment Distension versus Conventional Two-Needle Arthrocentesis: Randomized Clinical Trial*, Pain Research and Management **2017**, e2435263 (2017).
[10] F. Taşkesen and B. Cezairli, *Comparing Anxiety Levels and Patient Comfort during Single- and Double-Puncture Arthrocentesis*, CRANIO® **0**, 1 (2021).
[11] M. H. J. Hollander, J. Schortinghuis, and A. Vissink, *Changes in Heart Rate during Third Molar Surgery*, International Journal of Oral and Maxillofacial Surgery **45**, 1652 (2016).
[12] Z. Qin, C. Zhou, Y. Zhu, Y. Wang, H. Cao, W. Li, and Z. Huang, *Virtual Reality for Hypertension in Tooth Extraction: A Randomized Trial*, J Dent Res **101**, 400 (2022).
[13] Y. Chen and J. Hawkins, *Effects of Music Listening to Reduce Preprocedural Dental Anxiety in Special Needs Patients*, Complement Ther Clin Pract **42**, 101279 (2021).
[14] J. Fernandez-Aguilar, I. Guillén, M. T. Sanz, and M. Jovani-Sancho, *Patient's Pre-Operative Dental Anxiety Is Related to Diastolic Blood Pressure and the Need for Post-Surgical Analgesia*, Sci Rep **10**, 9170 (2020).

[15] R. O. Abu Hantash, M. H. Abu Younis, and M. M. Aker, *Dental Anxiety and Fear among Medical Field Students at Al Quds University*, (2014).

[16] H. Erten, Z. Z. Akarslan, and E. Bodrumlu, *Dental Fear and Anxiety Levels of Patients Attending a Dental Clinic*, Quintessence Int **37**, 304 (2006).

[17] S. A. Nagori, S. K. Roy Chowdhury, H. Thukral, A. Jose, and A. Roychoudhury, *Single Puncture versus Standard Double Needle Arthrocentesis for the Management of Temporomandibular Joint Disorders: A Systematic Review*, Journal of Oral Rehabilitation **45**, 810 (2018).

[18] A. Sindel, F. Uzuner, M. Sindel, and S. Tozoğlu, *Comparison of the Efficiency of Irrigation of Single and Double-Needle Techniques of Temporomandibular Joint Arthrocentesis: A Cadaver Study*, CRANIO® **35**, 405 (2017).

[19] L. Guarda-Nardini, G. Ferronato, and D. Manfredini, *Two-Needle vs. Single-Needle Technique for TMJ Arthrocentesis plus Hyaluronic Acid Injections: A Comparative Trial over a Six-Month Follow Up*, International Journal of Oral and Maxillofacial Surgery **41**, 506 (2012).

[20] F. S. Folle, R. L. Poluha, E. T. Setogutti, and E. Grossmann, *Double Puncture versus Single Puncture Arthrocentesis for the Management of Unilateral Temporomandibular Joint Disc Displacement without Reduction: A Randomized Controlled Trial*, Journal of Cranio-Maxillofacial Surgery **46**, 2003 (2018).

[21] Z. Bayramoğlu and S. Tozoğlu, *Comparison of Single- and Double-Puncture Arthrocentesis for the Treatment of Temporomandibular Joint Disorders: A Six-Month, Prospective Study*, CRANIO® **39**, 151 (2021).

[22] J. Torres-Gaya, A. Boscà-Ramón, M. Marqués-Mateo, A. Valverde-Navarro, M. M. García-San Segundo, and M. Puche-Torres, *Temporomandibular Joint Arthrocentesis Guided by Ultrasonography: An Anatomical Study*, Journal of Stomatology, Oral and Maxillofacial Surgery **122**, e27 (2021).

Erzincan Üniversitesi
Fen Bilimleri Enstitüsü Dergisi
2024,17(1), 137-146
ISSN: 1307-9085, e-ISSN: 2149-4584
Araştırma Makalesi

Erzincan University
Journal of Science and Technology
2024,17(1), 137-146
DOI: 10.18185/erzifbed.1360145
Research Article

Examining Tongue Size in OSA Patients with Lateral Cephalometric Radiography

Elif ÇELİK [1]*, Samih DİYARBAKIR [2], Edhem ÜNVER [2], Fatih ÇELİK [3]

[1]Erzincan Binali Yildirim University School of Health Services: Erzincan, TR
[2]Erzincan Binali Yildirim University Faculty of Medicine: Erzincan, TR
[3]Erzincan Oral and Dental Health Training and Research Hospital: Erzincan, TR

Received: 14/09/2023, **Revised:** 09/10/2023, **Accepted:** 09/10/2023, **Published:** 28/03/2024

Abstract

Aim: This article aims to investigate tongue dimensions in patients using lateral cephalometric radiography, examining the potential impact of differences in tongue size on Obstructive Sleep Apnea Syndrome (OSAS).

Methods: This study included 80 patients, with 34 females and 46 males. Among these patients, 48 were in the patient group with OSA, and 32 were in the control group Apne-Hypopnea Index (AHI)<5. Tongue dimensions were measured in lateral cephalometric radiographs of the patients, and these measurements were compared between the groups.

Results: In our study, a statistically significant increase was observed in tongue length and tongue area in OSA patients ($p < 0.05$). However, the increase in tongue thickness was not statistically significant.

Conclusion: Our study shows that obstructive sleep apnea (OSA) patients tend to have larger tongues. A larger tongue may contribute to airway obstruction during sleep, leading to increased OSA severity. This information could aid clinicians in tailoring treatment strategies for OSA patients, potentially improving therapeutic outcomes.

Keywords: obstructive sleep apnea syndrome, tongue, fat, soft tissue

OUAS'lı Hastalarda Dil Boyutlarının Lateral Kafa Grafisi ile İncelenmesi

Öz

Amaç: Bu makalede, lateral sefalometrik radyografi kullanarak hastalarda dil boyutlarını inceleyerek, dil boyutlarındaki farklılıkların Obstrüktif Uyku Apnesi Sendromuna (OUAS) potansiyel etkisini araştırmak amaçlanmıştır.

Yöntemler: Bu çalışmaya 34 kadın 46 erkekten oluşan 80 hasta dahil edildi. Bu hastalardan OUAS'ı olan 48'i hasta grubunu, 32' si ise apne hipopne indeksi (AHİ)<5 olan kontrol grubunu oluşturmaktaydı. Hastalara ait lateral sefalometrik radyografilerde dil boyutları ölçüldü ve gruplar arasında bu değerler karşılaştırıldı.

Bulgular: Çalışmamızda obstrüktif uyku apnesi (OUA) hastalarında dil boyunda ve dil alanında istatistiksel olarak anlamlı bir artış gözlenmiştir ($p <0.05$). Fakat dil kalınlığındaki artış anlamlı derecede değildir.

Sonuç: Çalışmamız, OUA hastalarının genellikle daha büyük bir dile sahip olduğunu göstermektedir. Daha büyük bir dil, uyku sırasında hava yolunun tıkanmasına katkıda bulunabilir, bu da OUAS şiddetinin artmasına yol açabilir. Bu bilgi, klinisyenlere OUA hastaları için tedavi stratejilerini uyarlamada yardımcı olabilir ve tedavi sonuçlarını potansiyel olarak iyileştirebilir.

Anahtar Kelimeler: obstrüktif uyku apnesi sendromu, dil, yağ, yumuşak doku

*Corresponding Author: elif.celik@erzincan.edu.tr
Elif ÇELİK, https://orcid.org/0000-0002-5059-9432
Samih DİYARBAKIR, https://orcid.org/0000-0001-6755-7741
Edhem ÜNVER, https://orcid.org/ 0000-0002-0322-8102
Fatih ÇELİK, https://orcid.org/0000-0001-6806-8480

1. Introduction

Obstructive Sleep Apnea Syndrome (OSAS) is a sleep disorder with a high prevalence that continues to increase [1], characterized by repeated interruptions of breathing and/or a significant reduction in airflow during sleep [2]. The prevalence of OSA is increasing in the population, making it a significant public health issue that adversely affects both individuals' and society's well-being and increases susceptibility to many serious diseases [3]. Complications such as obesity and smoking ,hypertension, hyperlipidemia, metabolic syndrome, diabetes mellitus and insulin resistance are more common in OSAS patients compared with the general population [4].

The etiology of OSA is complex, involving the interplay of numerous factors. These factors include genetic predisposition, age, gender, obesity, and anatomical features such as neck circumference [5]. The upper airway consists of structures such as the nose, mouth, throat, and pharynx, and the anatomical characteristics of this region can influence the risk of OSA [6].

Untreated or poorly managed obstructive sleep apnea (OSA) can lead to serious consequences, including cardiovascular diseases, hearing loss, diabetes, mental and emotional problems, as well as accidents and injuries [7]. Therefore, it is crucial to seek professional medical evaluation and appropriate treatment when OSA is diagnosed, or its symptoms are recognized. Treatment options may include lifestyle modifications, positive airway pressure devices (such as continuous positive airway pressure), oral appliances, and, in some cases, surgical interventions. With proper treatment, the adverse effects of OSA can be reduced or prevented [8–10].

The role of soft tissues is more significant than that of hard tissues in shaping the upper airway. Among these soft tissues, the importance of the tongue and soft palate is greater. OSAS is a disease that generally occurs more frequently in the supine position. Probable factors contributing to increased obstruction in the supine position include the gravitational pull and changes in muscle tone leading to the repositioning of the soft palate or tongue backward. Therefore, the most common sites of obstruction are the retroglossal and retropalatal areas. Surgical procedures commonly used in the treatment of OSAS are also typically performed in these areas [11]. In addition to positional changes in soft tissues, volumetric increases, particularly in the tongue and other soft tissues due to fat accumulation, also play a significant role in upper airway obstruction [12]. Because of the importance of the role of tongue size in obstruction, it has been frequently studied by researchers. Lateral cephalometric radiography allows for an objective measurement of tongue size and offers the opportunity to investigate its relationship with the severity of OSA [13].

This article aims to investigate tongue size in OSA patients using lateral cephalometric radiography and evaluate the potential impact of these measurements on the severity of OSA. The results of our study may contribute to a deeper understanding of the pathophysiology and risk factors associated with OSA, potentially leading to improved treatment strategies.

2. Material and Methods

This study included 80 patients aged 18-65 years who presented to the Chest Diseases Clinic of Erzincan Binali Yildirim University Mengucek Gazi Training and Research Hospital between 2021 and 2022 with complaints of sleep-disordered breathing. Patients with craniofacial abnormalities, a history of tongue surgery, or any medical conditions affecting tongue size were excluded from the study.

Polysomnography

All patients were evaluated with nocturnal polysomnography (PSG) in the clinic's sleep department (55-channel polysomnography-Alice Sleepware; Philips Respironics, Pennsylvania, USA), and 48 of them were diagnosed with OSA according to the American Academy of Sleep Medicine (AASM) criteria. In 32 patients, the AHI value was below 5 according to PSG evaluation, and simple snoring was diagnosed. Apnea is defined as a reduction of at least 90% in airflow amplitude lasting less than 10 seconds and hypopnea is defined as a reduction of at least 30% in airflow amplitude lasting at least 10 seconds and associated with a 4% or greater oxygen desaturation. In patients with OSAS, the number of AHI episodes, including apnea and hypopnea episodes per hour of sleep, was calculated.

Cephalometric analysis

All X-rays were obtained with the DRGEM Diamond-6A (Korea) X-ray machine in a repeatable natural head position, where all teeth were in centric occlusion, with slight contact or at rest without contraction of the upper and lower lips. During the acquisition of lateral cephalograms, the patient-source distance was standardized at 152 cm, and the mid-sagittal plane film cassette distance was 13 cm (80 kV, 320 mA, 51.2 mAs). All X-ray films were taken by the radiologic technician.

While the radiographic images were captured by technicians, cephalometric images were transferred to the Corel-Draw program, and measurements were performed by our team. In terms of reliability, the measurements were repeated 25 days later.

Cephalometric Landmarks

TT: The most anterior point of the tongue seen in cephalometry.

Eb: The deepest point in front of the epiglottis.

Hy: anterosuperior point of the hyoid bone.

G: genial tubercle

Tongue Size Measurements:

TA, Tongue Area: A line connecting the Eb, Hy, and G points, along with a line drawn from the G point to the TT point following the inner contour of the mandible and continuing along the dorsum of the tongue back to the Eb point, defines the area referred to as the tongue area.

TL, Tongue length: The distance between Eb and TT.

TH, tongue height: The length of the line perpendicular to the line between Eb and TT from the top of the curvature of the tongue dorsum.

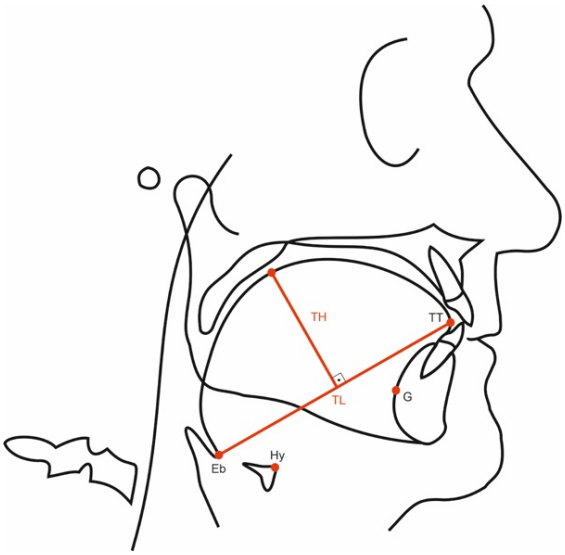

Figure 1: Anatomic Landmarks and Measurements

TL: Tongue length, TH: tongue height, Eb: Base of epiglottis, Hy: Hyoid bone, G: Genial tubercle, TT: Tip of tongue

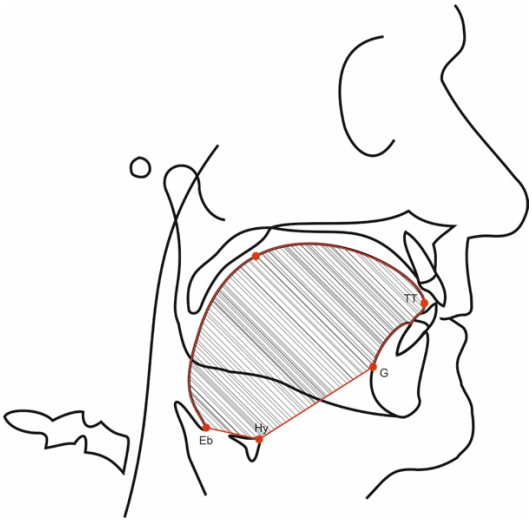

Figure 2: Borders of the Area of the Tongue

Eb: Base of the epiglottis, Hy: Hyoid bone, G: Genial tubercle, TT: Tip of tongue

Patients' cephalometric records and clinical data, including age, sex, and AHI values were collected from the hospital's medical records.

Statistical Analysis:

Statistical analysis was conducted using SPSS-22 software. The normal distribution of the data was assessed using the Kolmogorov-Smirnov test. Since the data followed a normal

distribution, they were compared using the T-test, and values with $P<0.05$ were considered statistically significant.

3. Results and Discussion

In a study conducted by Horner et al. tongue sizes were compared between patients with OSAS (AHI>5) and a control group (AHI<5) using magnetic resonance imaging (MRI). The study found that OSAS patients had a higher prevalence of tongue enlargement due to fat deposition in comparison to the control group [14].

In an MRI study conducted by Kim et al., they measured tongue volume and fat volume in apneic and non-apneic patients. They observed a statistically significant increase in both tongue and fat volumes in apnea patients compared to the control group ($P < 0.05$) [12].

In a study conducted by Wang et al. investigating the impact of weight factors on OSAS, they compared certain anatomical structures affecting upper airway dimensions between patients who lost weight and those who could not lose weight. In their research, they noted a statistically significant reduction in AHI values among patients who experienced weight loss ($P=0.0004$). The point of interest highlighted in their study was the significant reduction in tongue fat content observed in the group of patients who lost weight ($P<0.0001$) [15].

Kim TH et al. conducted a study using cephalograms obtained from obese and non-obese OSA patients. In their study, they attributed increased tongue volume in obese patients to the accumulation of fat and soft tissue in the tongue and pointed to the downward displacement of the hyoid bone as the cause of this condition [16].

Schwab and colleagues confirmed increased tongue volume in patients with OSA through their MRI study [17].

Lu et al. conducted a prospective study on patients with severe sleep apnea who underwent multilevel surgery, comparing their AHI values and tongue dimensions based on head and neck computerized tomography (CT) scans. As a result, it was determined that tongue length is associated with disease severity, and tongue volume significantly decreased after surgery [18].

In a magnetic resonance imaging study conducted by Do et al. and a CT scan study conducted by Ogawa et al., increased tongue sizes were observed in OSA patients compared to control groups, supporting findings from other studies [19,20]. Similarly, in MRI studies by Kando et al. and CT studies by Shigeta et al., the volumetric calculations of the tongue and oral cavity were performed, and in OSA patients, this ratio was found to be larger. These studies concluded that the increase in tongue size was negatively correlated with airway volume [20,21].

In a study conducted by Johal et al., they highlighted a significantly reduced intermaxillary space in patients with OSAS. This implies a restriction in the area where the tongue is positioned in individuals with OSAS [22].

Stipa et al. conducted a retrospective study on the cephalometric images of 253 OSA patients and evaluated tongue size and tongue length parameters about AHI values. However, no statistically significant relationship was found between disease severity and these parameters [23].

In a study conducted by Battagel et al. on cephalograms of 35 OSA patients and 24 healthy individuals from a total of 59 patients, they did not observe any difference in the tongue area among OSA patients [24].

Various advanced technologies such as CT and MRI are used to assess the anatomical characteristics of the upper airway and craniofacial structures and to identify areas of obstruction. However, the traditional cephalometric method has remained the most practical and widely used approach. Although cephalometry provides a static, two-dimensional assessment of the dynamic three-dimensional anatomical structures of the head and neck, it has proven to be useful because it reveals significant differences between asymptomatic controls and OSA patients. The main advantages of cephalometry include easy accessibility, low cost, and minimal radiation exposure [25].

We studied cephalograms from a group of 46 OSA patients and a control group consisting of 34 simple snoring patients (AHİ<5). 34 of the patients were female, and 46 were male. In our study, no significant differences were noted between the groups in terms of age and gender (Table 1).

Table 1: The Distribution of Age and Gender in the Groups

	OSA Positive (n: 48)	Control Group (n: 32)
Age (years)		
Mean ± SD	46.78 ± 13.30	45.94 ± 11.31
Median (minimum-maximum)	47 (20 – 73)	48 (20 – 67)
Sex		
Female	18/48 (37.5%)	16/32 (50%)
Male	30/48 (62.5%)	16/32 (50%)

This study demonstrates the presence of tongue enlargement in OSA patients. We observed a significant difference in tongue length between the two groups ($p=0.01$). The tongue area also showed a significant difference between the two groups ($p<0.01$). However, despite a slight increase in tongue height, this increase was not statistically significant (Table 2).

Despite the tongue being surrounded by hard tissues in the intermaxillary area, there is no limiting hard tissue in the oropharyngeal direction. Therefore, tongue enlargement may manifest as an increase in length rather than an increase in height, possibly leading to narrowing of the pharyngeal airway at the retroglossal level and exacerbating OSAS.

Table 2: Comparison of Data Between the Groups

	OSA Positive	Control Group	P
Tongue Length(mm)	81.11 ± 8.35	76.96 ± 7.52	0.01*
Tongue Height(mm)	32.56 ± 4.09	31.48 ± 6.99	0.436
Tongue Area(cm^2)	34.29 ± 3.74	31.92 ± 4.05	0.009*

Cephalometric examination is the most preferred method for evaluating the soft tissues in the upper airway in patients with OSA due to its cost-effectiveness and ease of application. However, like any procedure, there are certain limitations associated with cephalometric analysis. These limitations include the inability to obtain three-dimensional images, challenges in standardizing patient positioning, and the inability to assess the fat content in the tongue.

4. Conclusion

The increase in tongue size in OSA patients is believed to be due to fat accumulation in the tongue, which is associated with obesity, the primary etiological factor of OSA [12,15]. Studies can be supported by the STOP-Bang questionnaire [26], which includes questions about the patient's snoring habits and frequency, how tired they feel in daily life, whether they have experienced breathing pauses during sleep, the presence of hypertension, their age, gender, as well as the calculation of the patient's body mass index (BMI) and measurement of neck circumference. Furthermore, to determine the localization of fat accumulation in the tongue, it would be more accurate to supplement the study with an MRI investigation.

In patients with OSA, the role of the tongue is crucial in the detection and treatment of upper airway obstruction. Guidance results for clinicians can be obtained in future studies by implementing recommended practices and utilizing a broader patient population.

Ethics in Publishing

The ethical approval has been obtained with decision number 15/04 at the meeting of the Erzincan Binali Yıldırım University Clinical Research Ethics Committee on February 21, 2022, and documented as the 15th decision.

References

[1] N. M. Punjabi, *The Epidemiology of Adult Obstructive Sleep Apnea*, Proc Am Thorac Soc **5**, 136 (2008).

[2] J. A. Dempsey, S. C. Veasey, B. J. Morgan, and C. P. O'Donnell, *Pathophysiology of Sleep Apnea*, Physiological Reviews **90**, 47 (2010).

[3] J. L. Hossain and C. M. Shapiro, *The Prevalence, Cost Implications, and Management of Sleep Disorders: An Overview*, Sleep Breath **06**, 85 (2002).

[4] H. Ölmez, M. Tosun, E. Ünver, R. Çoşkun, G. S. Yalçın, M. Doğan, and Y. K. Arslan, *Can Biomarkers Predict the Risk of Cardiovascular Disease in Patients with Obstructive Sleep Apnea Syndrome? Biomarkers in Obstructive Sleep Apnea Syndrome*, Journal of Surgery and Medicine **7**, 2 (2023).

[5] F. Xia and M. Sawan, *Clinical and Research Solutions to Manage Obstructive Sleep Apnea: A Review*, Sensors **21**, 5 (2021).

[6] J. B. Schellenberg, G. Maislin, and R. J. Schwab, *Physical Findings and the Risk for Obstructive Sleep Apnea*, Am J Respir Crit Care Med **162**, 740 (2000).

[7] K. Bagai, *Obstructive Sleep Apnea, Stroke, and Cardiovascular Diseases*, The Neurologist **16**, 329 (2010).

[8] M. Barnes, R. D. McEvoy, S. Banks, N. Tarquinio, C. G. Murray, N. Vowles, and R. J. Pierce, *Efficacy of Positive Airway Pressure and Oral Appliance in Mild to Moderate Obstructive Sleep Apnea*, Am J Respir Crit Care Med **170**, 656 (2004).

[9] I. Bouloukaki, E. Daskalaki, E. Mavroudi, V. Moniaki, S. E. Schiza, and I. Tsiligianni, *A Dietary and Lifestyle Intervention Improves Treatment Adherence and Clinical Outcomes in Overweight and Obese Patients with Obstructive Sleep Apnea: A Randomized, Controlled Trial*, Life **13**, 8 (2023).

[10] H.-P. Chang, Y.-F. Chen, and J.-K. Du, *Obstructive Sleep Apnea Treatment in Adults*, The Kaohsiung Journal of Medical Sciences **36**, 7 (2020).

[11] R. W. Riley, N. B. Powell, K. K. Li, R. J. Troell, and C. Guilleminault, *Surgery and Obstructive Sleep Apnea: Long-Term Clinical Outcomes*, Otolaryngol Head Neck Surg **122**, 415 (2000).

[12] A. M. Kim, B. T. Keenan, N. Jackson, E. L. Chan, B. Staley, H. Poptani, D. A. Torigian, A. I. Pack, and R. J. Schwab, *Tongue Fat and Its Relationship to Obstructive Sleep Apnea*, Sleep **37**, 1639 (2014).

[13] B. C. Neelapu, O. P. Kharbanda, H. K. Sardana, R. Balachandran, V. Sardana, P. Kapoor, A. Gupta, and S. Vasamsetti, *Craniofacial and Upper Airway Morphology in Adult*

Obstructive Sleep Apnea Patients: A Systematic Review and Meta-Analysis of Cephalometric Studies, Sleep Medicine Reviews **31**, 79 (2017).

[14] R. L. Horner, R. H. Mohiaddin, D. G. Lowell, S. A. Shea, E. D. Burman, D. B. Longmore, and A. Guz, *Sites and Sizes of Fat Deposits around the Pharynx in Obese Patients with Obstructive Sleep Apnoea and Weight Matched Controls*, European Respiratory Journal **2**, 613 (1989).

[15] S. H. Wang, B. T. Keenan, A. Wiemken, Y. Zang, B. Staley, D. B. Sarwer, D. A. Torigian, N. Williams, A. I. Pack, and R. J. Schwab, *Effect of Weight Loss on Upper Airway Anatomy and the Apnea–Hypopnea Index. The Importance of Tongue Fat*, Am J Respir Crit Care Med **201**, 718 (2020).

[16] T. H. Kim, B. S. Chun, H. W. Lee, and J. S. Kim, *Differences of Upper Airway Morphology According to Obesity: Study with Cephalometry and Dynamic MD-CT*, Clin Exp Otorhinolaryngol **3**, 147 (2010).

[17] R. J. Schwab, M. Pasirstein, R. Pierson, A. Mackley, R. Hachadoorian, R. Arens, G. Maislin, and A. I. Pack, *Identification of Upper Airway Anatomic Risk Factors for Obstructive Sleep Apnea with Volumetric Magnetic Resonance Imaging*, Am J Respir Crit Care Med **168**, 522 (2003).

[18] Y.-A. Lu, C.-J. Wang, Y.-T. Chiang, and H.-Y. Li, *Volumetric Changes after Coblation Ablation Tongue (CAT) in Obstructive Sleep Apnea Patients*, Journal of Clinical Medicine **11**, 14 (2022).

[19] K. L. Do, H. Ferreyra, J. F. Healy, and T. M. Davidson, *Does Tongue Size Differ Between Patients With and Without Sleep-Disordered Breathing?*, The Laryngoscope **110**, 1552 (2000).

[20] Y. Shigeta, T. Ogawa, E. Ando, G. T. Clark, and R. Enciso, *Influence of Tongue/Mandible Volume Ratio on Oropharyngeal Airway in Japanese Male Patients with Obstructive Sleep Apnea*, Oral Surgery, Oral Medicine, Oral Pathology, Oral Radiology, and Endodontology **111**, 239 (2011).

[21] C. Iida-Kondo, N. Yoshino, T. Kurabayashi, S. Mataki, M. Hasegawa, and N. Kurosaki, *Comparison of Tongue Volume/Oral Cavity Volume Ratio between Obstructive Sleep Apnea Syndrome Patients and Normal Adults Using Magnetic Resonance Imaging*, Journal of Medical and Dental Sciences **53**, 119 (2006).

[22] A. Johal, S. I. Pa$^{\text{TEL}}$, and J. M. Battagel, *The Relationship between Craniofacial Anatomy and Obstructive Sleep Apnoea: A Case-Controlled Study*, Journal of Sleep Research **16**, 319 (2007).

[23] C. Stipa, M. Cameli, G. Sorrenti, D. R. Ippolito, I. Pelligra, and G. Alessandri-Bonetti, *Relationship between Cephalometric Parameters and the Apnoea–Hypopnoea Index in OSA*

Patients: A Retrospective Cohort Study, European Journal of Orthodontics **42**, 101 (2020).

[24] J. M. Battagel and P. R. L'Estrange, *The Cephalometric Morphology of Patients with Obstructive Sleep Apnoea (OSA)*, European Journal of Orthodontics **18**, 557 (1996).

[25] R. Bharadwaj, A. Ravikumar, and N. R. Krishnaswamy, *Evaluation of Craniofacial Morphology in Patients with Obstructive Sleep Apnea Using Lateral Cephalometry and Dynamic MRI*, Indian Journal of Dental Research **22**, 739 (2011).

[26] Y. Wang, I. Fietze, M. Salanitro, and T. Penzel, *Comparison of the Value of the STOP-BANG Questionnaire with Oxygen Desaturation Index in Screening Obstructive Sleep Apnea in Germany*, Sleep Breath **27**, 1315 (2023).

Erzincan Üniversitesi
Fen Bilimleri Enstitüsü Dergisi
2024,17(1), 259-267
ISSN: 1307-9085, e-ISSN: 2149-4584
Araştırma Makalesi

Erzincan University
Journal of Science and Technology
2024,17(1), 259-267
DOI: 10.18185/erzifbed.1362369
Research Article

Reconstruction of a Ruled Surface in 3-dimensional Euclidean Space

Mustafa Dede[1*], Cumali Ekici[2*], Mahmut Koçak[2*]

[1]Kilis 7 Aralık University, Department of Mathematics, Turkey

[2]Eskişehir Osmangazi University, Department of Mathematics and Computer Science, Turkey

Received: 18/09/2023, **Revised:** 15/11/2023, **Accepted:** 15/11/2023, **Published:** 28/03/2024

Abstract

In this paper, firstly, a summary of certain results related to the differential geometry of ruled surfaces is provided. Subsequently, the signature curve for ruled surfaces in Euclidean 3-space is introduced. Additionally, a simple algorithm for the reconstruction of a ruled surface, which is both efficient and entirely local, requiring only the initial motion direction and starting point, is presented. Finally, the efficiency and accuracy of the algorithm are demonstrated through several examples.

Keywords: Ruled surface, Signature curve, Curvature, Reconstruction

3-boyutlu Öklid Uzayında bir Regle Yüzeyin Yeniden Yapılandırılması

Öz

Bu makalede, öncelikle regle yüzeylerin diferesiyel geometrisi ile ilgili bazı sonuçların bir özeti sunulmuştur. Daha sonra, Öklid 3-uzayında regle yüzeyler için işaret eğrisi tanıtılmıştır. Ek olarak, bir regle yüzeyin yeniden yapılandırılması için hem verimli hem de tamamen yerel olan, yalnızca ilk hareket yönü ve başlangıç noktası gerektiren basit bir algoritma sunulmuştur. Son olarak, algoritmanın verimliliği ve doğruluğu birkaç örnekle gösterilmiştir.

Anahtar Kelimeler: Regle yüzey, İşaret eğrisi, Eğrilik, Yeniden yapılanma

*Corresponding Author: cekici@ogu.edu.tr
Mustafa DEDE, https://orcid.org/0000-0003-2652-637X
Cumali EKİCİ, https://orcid.org/0000-0002-3247-5727
Mahmut KOÇAK, https://orcid.org/0000-0001-7774-0144

1. Introduction

In the Euclidean plane, the parametric representation of a curve $\alpha(t)$ yields its signature curve $S(t) = \big(\kappa(t), \kappa_s(t)\big)$, where $\kappa(t)$ signifies the curvature and $\kappa_s(t)$ is the rate of change with respect to the arc length t. Calabi et al. used the signature curves to recognize invariant properties of visual objects in the Euclidean plane [1,2]. They also introduced a new method for invariant recognition of visual objects that involves numerical approximation of $\kappa(t)$ and $\kappa_s(t)$ to a differential invariant signature curve. Surazhsky and Elber explored the process of uniquely deriving a planar curve's curvature signature and, more importantly, the methodology for reconstructing the curve from its curvature signature [3]. Numerous geometers have examined these inquiries and extended the scope. In 2012, Hickman demonstrated a method for generating all planar curves that exhibit a specific signature curve [4]. In 2000, Boutin introduced a 3-dimensional adaptation of the Euclidean signature curve, encompassing curvature, torsion, and their respective derivatives concerning arc length [5]. In more recent times, Wu and Li introduced an algorithm for replicating a motion trajectory through the utilization of the signature curve within the Euclidean space [6,7,8]. The exploration of ruled surfaces represents an intriguing research domain within surface theory, with applications spanning various areas in CAD and CAGD [9]. Peternell delved into the reconstruction of developable surfaces from scattered data points, while Ryuh et al. harnessed ruled surfaces for robot motion planning [10, 11]. Pottmann et al. explored offsets of rational ruled surfaces [12]. Furthermore, the geometry of ruled surfaces plays a crucial role in the study of kinematic and positional mechanisms, as demonstrated by Kühnel, Abdel Baky, Ekici and Çöken, Zhang, Ünlütürk et al. and Ekici et al. [13,14,15,16,17,18]. Similar to the fundamental theorem of curves, which facilitates the determination of a curve based on curvature and torsion, a similar structure can be recognized in the field of reconstruction of a ruled surface. In this context, the signature curve plays a crucial role. The basic rationale behind the inclusion of a signature curve in a ruled surface reconstruction algorithm stems from the inherent independence of signature curves with respect to the choice of coordinate systems. As a result, the freedom to add segments of constant curvature at critical points of the curve is allowed. However, this freedom, together with an Euclidean transformation, constitutes the only freedom available to preserve the integrity of the signature curve. Moreover, these curves provide an accurate representation of the shape of the ruled surface and rigorously capture all its critical geometric features. The organization of this paper proceeds as follows: Section 2 describes the basic properties inherent to ruled surfaces. The following section briefly summarises the algorithmic concept governing the reconstruction of ruled surfaces. Finally, Section 4 analyses the pragmatic applications of the proposed algorithm, providing several illustrative examples for extensive discussion.

2. Ruled Surfaces

This section is devoted to the so-called ruled surfaces. A ruled surface in Euclidean 3-space $\mathbb{R}^3$ is a (smooth or discrete) one-parameter family of straight lines [9]. We briefly recall some

basic facts on ruled surfaces. Recall that, using standard parameters u and v, a ruled surface can be parameterized by

$$\varphi(u,v) = \alpha(u) + vX(u) \tag{1}$$

where $\|X(u)\| = \|X'(u)\| = 1$ and $\langle \alpha'(u), X'(u) \rangle = 0$.

Here $\alpha(u)$ is the striction line, the parameter u is the arc length of the spherical curve $X(u)$.

A ruled surface is, up to Euclidean motions, uniquely determined by the following quantities:

$$\begin{aligned} F &= \langle \alpha', X \rangle \\ Q &= \det(\alpha', X, X') \\ J &= \det(X, X', X'') \end{aligned} \tag{2}$$

each of which is a function of u. Conversely, every choice of these quantities uniquely determines a ruled surface.

Furthermore, the derivative of the striction line is completely determined by F and Q using the equation

$$\alpha' = FX + QX \wedge X' \tag{3}$$

where Q is the parameter of the distribution.

In the moving frame, $\{X, X', X \wedge X'\}$ we have the Frenet type matrix

$$\frac{d}{du}\begin{bmatrix} X \\ X' \\ X \wedge X' \end{bmatrix} = \begin{bmatrix} 0 & 1 & 0 \\ -1 & 0 & J \\ 0 & -J & 0 \end{bmatrix}\begin{bmatrix} X \\ X' \\ X \wedge X' \end{bmatrix}. \tag{4}$$

3. Reconstruction of a Ruled Surface from its Signature

As in the basic known theorem for curves; given curvature and torsion, the curve can be found by the difference in position. Similar to this structure, the reconstructed regular surface can be found using the signature curve. Recalling the fact that the ruled surfaces can be completely determined by F, Q and J we have the following definition.

Definition 2.1 Let φ be ruled surface in Euclidean space $\mathbb{R}^3$. The signature curve of the ruled surface is defined by

$$S(u) = \{F(u), Q(u), J(u)\}. \tag{5}$$

We can easily see that the signature curve of ruled surface is invariant under translations and rotation.

This paper aims to formulate an algorithm for the reproduction of the ruled surface based on its signature, denoted as *S*. Initially, the reproduction process involves the generation of the ruling and the striction line. Then, the reproduced ruling and the striction line are combined to reconstruct the ruled surface.

Firstly, to reproduce the moving frame of ruled surface we use the so called finite difference. Let u_i and $u_i + \Delta u_i$ be two consecutive points. The derivatives of moving frame vectors $M = \{X, X', X \wedge X'\}$ can be obtained by

$$\begin{aligned}\frac{d}{du}X(u_i) &= \frac{X(u_i+\Delta u_i)-X(u_i)}{\Delta u_i}\\ \frac{d}{du}X'(u_i) &= \frac{X'(u_i+\Delta u_i)-X'(u_i)}{\Delta u_i}\\ \frac{d}{du}(X\wedge X')(u_i) &= \frac{(X\wedge X')(u_i+\Delta u_i)-(X\wedge X')(u_i)}{\Delta u_i}.\end{aligned} \tag{6}$$

From Eq. (4) and (6) we can derive the following iteration equation expressed in matrix form as

$$\begin{bmatrix} X(u_i+\Delta u_i)\\ X'(u_i+\Delta u_i)\\ (X\wedge X')(u_i+\Delta u_i)\end{bmatrix}=\begin{bmatrix}1 & \Delta u_i & 0\\ -\Delta u_i & 1 & J\Delta u_i\\ 0 & -J\Delta u_i & 1\end{bmatrix}\begin{bmatrix} X(u_i)\\ X'(u_i)\\ (X\wedge X')(u_i)\end{bmatrix}. \tag{7}$$

We use this matrix to compute new vectors from old ones.

Since the moving frame vectors are unit vectors, we need to normalize the vectors, then we have the reproduced moving frame vectors obtained by

$$\begin{aligned}\tilde{X}(u_i+\Delta u_i) &= \frac{X(u_i+\Delta u_i)}{\|X(u_i+\Delta u_i)\|}\\ \widetilde{X'}(u_i+\Delta u_i) &= \frac{X'(u_i+\Delta u_i)}{\|X'(u_i+\Delta u_i)\|}\\ (\widetilde{X\wedge X'})(u_i+\Delta u_i) &= \frac{(X\wedge X')(u_i+\Delta u_i)}{\|(X\wedge X')(u_i+\Delta u_i)\|}\end{aligned} \tag{8}$$

where $\|.\|$ indicates the Euclidean norm of a vector.

The reproduced moving frame $M(u_i+\Delta u_i)$ at the point $u_i+\Delta u_i$ from $M(u_i)$ denoted by

$$M(u_i+\Delta u_i)=\{\tilde{X}(u_i+\Delta u_i),\widetilde{X'}(u_i+\Delta u_i),(\widetilde{X\wedge X'})(u_i+\Delta u_i)\}. \tag{9}$$

To the reproduce the moving frame vectors we need the initial motion direction given by

$$\Theta(u_0)=\{\tilde{X}(u_0),\widetilde{X'}(u_0),(\widetilde{X\wedge X'})(u_0)\}$$

where we set the initial point as u_0. Starting from the initial motion direction $\Theta(u_0)$ and the provided signature S of the ruled surface, by iteratively applying equations (7) and (8), we can compute the moving frame $M(u_i+\Delta u_i)$ for all points on the reconstructed ruled surface.

It is no surprise that the reproduced vector $X(u_i+\Delta u_i)$ can be considered to be the ruling of the reproduced ruled surface.

Next, we turn our attention to the reproduction of the striction line. To reproduce the striction line we use again finite difference method. Then, the derivative of the striction line of the ruled surface is obtained by

$$\frac{d}{du}\alpha(u_i)=\frac{\alpha(u_i+\Delta u_i)-\alpha(u_i)}{\Delta u_i}. \tag{10}$$

Substituting (3) into (10) gives

$$\alpha(u_i+\Delta u_i)=\alpha(u_i)+\Delta u_i[F(u_i)X(u_i)+Q(u_i)(X\wedge X')(u_i)]. \tag{11}$$

Using the initial starting point $\alpha(u_0)$ and (11) we can easily reproduce all the points of the striction line.

As the final step, combining iteration equations (8) and (11), the reproduced ruled surface $\varphi(u_i+\Delta u_i,v)$ can be easily constructed in the following form:

$$\varphi(u_i+\Delta u_i,v)=\alpha(u_i+\Delta u_i)+v\tilde{X}(u_i+\Delta u_i)\,. \tag{12}$$

To summarize, once the signature data is available, the above equation can be used to

reproduce all the points of the ruled surface. Therefore, given the initial starting point $\alpha(u_0)$ of the striction line, the initial motion direction $\Theta(u_0)$ of the moving frame, and iterate equation (12), we can reproduce all the points of the ruled surface.

4. Examples

In this section, we tested the performance of our algorithm. We give some examples as follows:

Example 3.1 Let us consider the well-known ruled surface helicoid parametrized by

$$\varphi(u,v) = (vcosu, vsinu, u). \tag{13}$$

We have the moving frame as

$$\begin{aligned} X(u) &= (cosu, sinu, 0) \\ X'(u) &= (-sinu, cosu, 0) \\ (X \wedge X')(u) &= (0,0,1). \end{aligned} \tag{14}$$

F, J and Q are obtained by

$$F = J = 0, \quad Q = 1. \tag{15}$$

In this example, we can simply set the initial motion direction $\Theta(1)$ in the following form:

$$\begin{aligned} X(1) &= (1,0,0) \\ X'(1) &= (0,1,0) \\ (X \wedge X')(1) &= (0,0,1). \end{aligned} \tag{16}$$

The initial point of origin is selected as

$$\alpha(1) = (10,5,0). \tag{17}$$

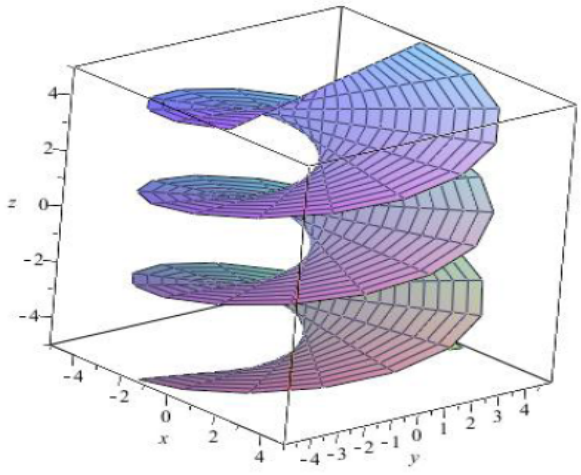

Figure 1. (a) The original ruled surfaces

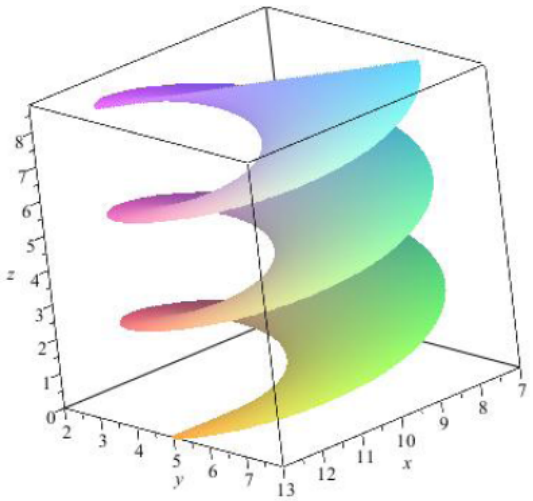

Figure 1. (b) The reproduced ruled surfaces

Now, consider the reconstruction of the ruled surface. At the initial starting point $\alpha(1)$ of the striction line, the initial motion direction $\Theta(1)$ of the moving frame of the ruled surface and signature curve $S(u)$ respectively, are firstly given as input data. Then, we reproduced the ruled surface with points $v \in (-3,3)$ and $u_i \in (1,10)$ with $\Delta u = u_{i+1} - \Delta u_i$ for $\Delta u = 0.01$. The ruled surface, which was produced by the signature of the original ruled surface, is shown in Figure 1(b). The original ruled surface is illustrated in Figure

1(a). Figure 1(a) and Figure 1(b) show that the original and reproduced ruled surfaces are similar. They have the same shape (signature curve) but they are not identical in space position.

Example 3.2 The Wallis' conical edge represents a ruled surface defined by the parametric equation:

$$\varphi(u,v) = \left(vcosu, vsinu, \sqrt{4 - 3cos^2u}\right).$$

The derived calculations yield the expression $S(u)$ as follows:

$$S(u) = \left(0, \frac{3cosusinu}{\sqrt{4 - 3cos^2u}}, 0\right).$$

Assuming that the initial direction of motion $\Theta(-3)$ and the initial starting point $\alpha(-3)$ are given by:

$$\begin{aligned} \tilde{X}(-3) &= (-0.989, -0.141, 0) \\ \tilde{X'}(-3) &= (-0.141, -0.989, 0) \\ (\widetilde{X \wedge X'})(-3) &= (0,0,1) \end{aligned}$$

and

$$\alpha(-3) = (0,0,1.02) \tag{18}$$

respectively.

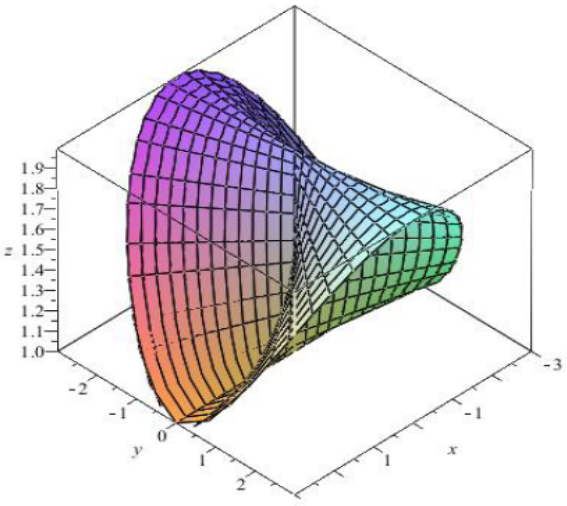

Figure 2. (a) The original ruled surfaces

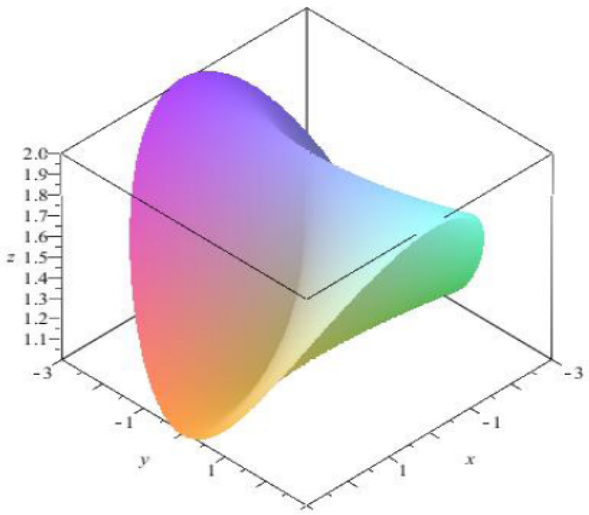

Figure 2. (b) The reproduced ruled surfaces

The ruled surface is then reproduced with points $v \in (-3,3)$ and $u_i \in (1,10)$ such that $\Delta u = u_{i+1} - \Delta u_i$ for $\Delta u = 0.01$. Figure 2(a) and Figure 2(b) show that if we choose the initial motion direction and the initial starting point identical to the original ruled surface then the original and reproduced ruled surfaces are completely identical.

Example 3.3 Assume that the signature curve is given as input data in the following form:

$$S(u) = \left(-2u, 0, \frac{u}{2}\right).$$

We start at an arbitrary initial motion direction $\Theta(-4)$ given by

$$\begin{aligned} \tilde{X}(-4) &= (1,0,0) \\ \widetilde{X'}(-4) &= (0,1,0) \\ (\widetilde{X \wedge X'})(-4) &= (0,0,1). \end{aligned} \tag{19}$$

In addition, assume we are given the initial starting point of the striction line of the ruled surface in the following form:

$$\alpha(-4) = (5,4,3). \tag{20}$$

Now using $\alpha(-4)$, $\Theta(-4)$, and $S(u)$, we can produce a ruled surface, illustrated in Figure 3. In Figure 3(a) and Figure 3(b), the appearance of the reconstructed ruled surface is plotted by rotating it in two different directions. We, here, computed the ruled surface with points $v \in (-3,3)$, $u_i \in (-4,4)$, and $\Delta u = u_{i+1} - \Delta u_i$ for $\Delta u = 0.01$.

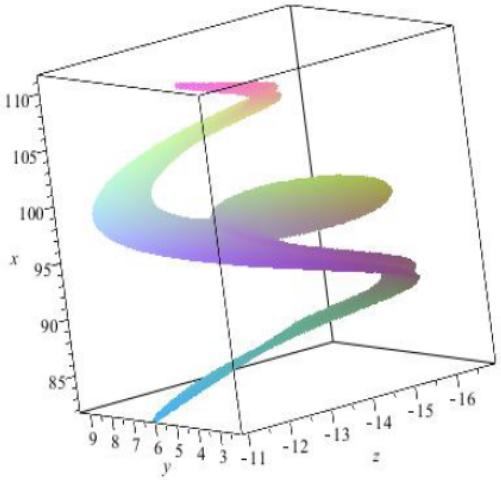

Figure 3. (a) The produced ruled surface

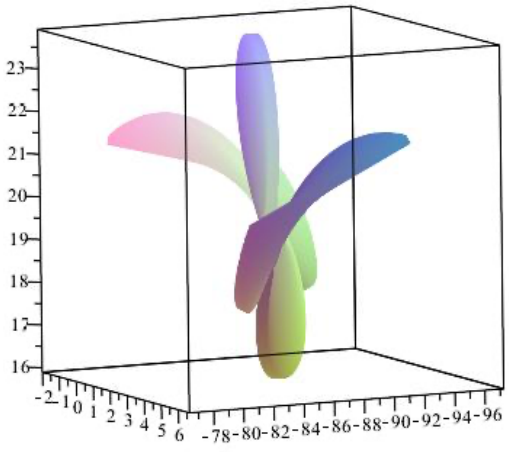

Figure 3. (b) The reproduced ruled surfaces

Conclusion

This article is devoted to the reproduction of ruled surfaces in Euclidean space. Examples are reported to show the reproduction algorithm for ruled surfacesis flexible and easy. The validity and effectiveness of the formulation are checked through several examples. According to our experiments, the accuracy of the ruled surface reproduction will be sufficient in most applications. If necessary, it can be improved by reducing the mesh size Δu. For future research our algorithm can be applied to Lorentz space as well. Furthermore, we will apply this method for surface reconstruction.

Ethics in Publishing

There are no ethical issues regarding the publication of this study.

Author Contributions

The authors contributed equally.

Acknowledgments

We would like to thank the referees for guiding us to provide important this publication and for the stimulating questions.

References

[1] Calabi, E., Olver, P. J., Shakiban, C., Tannenbaum, A., Haker, S. (1998). Differential and numerically invariant signature curves applied to object recognition, Int. J. Computer Vision, 26, 107-135.

[2] Calabi, E., Olver, P. J., Tannenbaum, A. (1996). Affine geometry, curve flows, and invariant numerical approximations, Adv. Math., 124, 154-196.

[3] Surazhsky, T., Elber, G. (2002). Metamorphosis of planar parametric curves via curvature interpolation, International Journal of Shape Modeling, 8, 201-216.

[4] Hickman, M. S. (2012). Euclidean signature curves, J. Math. Imaging. Vis., 43, 206-213.

[5] Boutin, M. (2000). Numerically invarint signature curves , Int. J. Comput. Vision, 40(3), 235-248.

[6] Wu, S., Li, Y. F., Zhang, J.W. (2007). Signature descriptor for free form trajectory modeling, in Proc. IEEE International Conference on Integration Technology, Shenzhen, China, 167-172.

[7] Wu, S., Li, Y. F. (2010). Motion trajectory reproduction from generalized signature description, Pattern Recognition, 43, 204-221.

[8] Wu, S., Li, Y. F. (2008). On signature invariants for effective motion trajectory recognition, The International Journal of Robotics Research, 27, 895-917.

[9] Chen, H. Y., Pottmann H. (1974). Approximation by ruled surfaces. J. Comput. Appl. Math. 102, 143-156.

[10] Ryuh, B. S., Pennock, G.R. (1988). Accurate motion of a robot end-effector using the curvature theory of ruled surfaces, Journal of Mechanisms, Transmissions, and Automation in Design, 110, 383-388.

[11] Peternell, M. (2004). Developable surface fitting to point clouds. Comp. Aided Geom. Design, 21, 785-803.

[12] Pottmann, H., Lüa, W., Ravani, B. (1996). Rational ruled surfaces and their Offsets, Graphical Models and Image Processing, 58, 544-552.

[13] Kühnel, W. (1994). Ruled W-surfaces, Arch. Math., 62, 475-480.

[14] Ekici, C., Çöken, A. C. (2012). The integral invariants of parallel timelike ruled surfaces, J. Math. Anal. Appl. 393, 97-107.

[15] Zhang, X.M., Zhu, L.M., Ding, H., Xiong, Y.L. (2012). Kinematic generation of ruled surface based on rational motion of point-line, Science China Technological Sciences, 55, 62-71.

[16] Abdel Baky, R. A. (2003). On the Blaschke approach of ruled surfaces, Tamkang J. Math., 34, 107-116.

[17] Ünlütürk, Y., Çimdiker, M., Ekici, C. (2016). Characteristic properties of the parallel ruled surfaces with Darboux frame in Euclidean 3-space, Communication in Mathematical Modeling and Applications. 1(1), 26-43.

[18] Ekici, C., Kaymanlı U.,G., Okur, S. (2021). A new characterization of ruled surfaces according to q-frame vectors in Euclidean 3-space, International Journal of Mathematical Combinatorics, 3, 20-31.

Erzincan Üniversitesi
Fen Bilimleri Enstitüsü Dergisi
2024,17(1), 268-278
ISSN: 1307-9085, e-ISSN: 2149-4584
Araştırma Makalesi

Erzincan University
Journal of Science and Technology
2024,17(1), 268-278
DOI: 10.18185/erzifbed.1371910
Research Article

A Research on the Generalizations of Modules Whose Submodules are Isomorphic to a Direct Summand

Fatih Karabacak[1], Özgür Taşdemir[2*]

[1]Anadolu University, UYEP Research and Practice Center, Eskisehir, Türkiye.
[2]Trakya University, Department of Business Administration, Faculty of Economics and Administrative Sciences, Balkan Campus, Edirne, Türkiye.

Received: 05/09/2023, **Revised:** 15/12/2023, **Accepted:** 15/12/2023, **Published:** 28/03/2024

Abstract

A module M is called $virtually\ semisimple$ (resp. $virtually\ extending$) if every submodule (resp. complement submodule) of M is isomorphic to a direct summand of M. It is known that virtually extending modules is a generalization of virtually semisimple modules. In this paper, the relationships between virtually extending modules and other generalizations of virtually semisimple modules are examined. Moreover, we introduce a new generalization of virtually semisimple modules; namely *CH* modules: We say a module M is a *c-epi-retractable* (or briefly *CH module*) if any complement submodule of M is a homomorphic image of M. *CH* modules contains the class of virtually extending modules and the class of epi-retractable modules. We also give some basic properties of this new module class.

Keywords: virtually semisimple module, virtually extending module, epi-retractable module, *CH* module

Her Alt Modülü Bir Diktoplanana İzomorf Olan Modüllerin Genellemeleri Üzerine Bir Araştırma

Öz

Eğer bir M modülünün her alt modülü (sırasıyla tamamlayıcı alt modülü), M modülünün bir dik toplananına izomorfik ise, M modülüne *sanal yarı basit (sırasıyla sanal genişleyen) modül* denir. Sanal genişleyen modüllerin, sanal yarı basit modüllerin bir genellemesi olduğu bilinmektedir. Bu yazıda, sanal genişleyen modüller ile sanal yarı basit modüllerin diğer genellemeleri arasındaki ilişkiler incelenmektedir. Ayrıca, sanal yarı basit modüllerin yeni bir genellemesini de tanıtıyoruz; yani CH modülleri: Bir M modülünün herhangi bir tamamlayıcı alt modülü, M modülünün bir homomorfik görüntüsü ise, M modülüne bir *epi-c-geri-çekilebilir modül* (ya da kısaca *CH modül*) olarak adlandırıyoruz. CH modüllerin sınıfı, sanal genişleyen modüllerin sınıfını ve epi-geri-çekilebilir modüllerin sınıfını içerir. Ayrıca bu yeni modül sınıfının bazı temel özelliklerini de veriyoruz.

Anahtar Kelimeler: sanal yarı-basit modül, sanal genişleyen modül, epi-geri-çekilebilir modül, CH modül.

*Corresponding Author: ozgurtasdemir@trakya.edu.tr
Fatih KARABACAK, https://orcid.org/0000-0003-4925-512X
Özgür TAŞDEMİR, https://orcid.org/0000-0003-2500-8255

1. Introduction

Throughout this note, any ring is associative with unity and is denoted by R, any module is unital right module. Some notations, which we will use in this paper, are listed below:

$A \leq M$	: A is a submodule of M.
$A \leq^{c} M$	: A is a complement (closed) submodule of M.
$A \leq^{ess} M$	: A is an essential submodule of M.
$A \leq^{\oplus} M$	: A is a direct summand of M.
$A \lesssim^{\oplus} M$	: A is isomorphic to a direct summand of M.
$A \cong B$	: A is isomorphic to B.
$E(M)$	: The injective hull of M.
$Hom_R(M,N)$	: The set of all R-homomorphisms from M to N.
$End_R(M)$	: The endomorphism ring of M.

We recall some of the definitions we used throughout the article: A submodule C of M is called *closed* if for any $A \leq M$ such that $C \leq^{ess} A$ in M, we have $C = A$. A submodule C of M is called *complement of a submodule* A of M if C is maximal with respect to the property that $C \cap A = 0$. In modules, being a closed submodule is equivalent to being a complement submodule [1, 1.10].

A module M is called *semisimple* if for any $X \leq M$, we have $X \leq^{\oplus} M$ (see [1, 1.15]). Semisimple modules and rings has significant role in module and ring theory. In 2018, the authors [2] introduced and investigated a new module class, namely virtually semisimple modules: A module M is called *virtually semisimple* if for any $X \leq M$, we have $X \lesssim^{\oplus} M$. For virtually semisimple rings, they proved a generalization of the reowned Weddernburn-Artin theorem (which characterize semisimple rings). Later, this interesting module family and related concepts were studied by many algebraist. Karabacak and his co-author(s) introduced several generalizations of virtually semisimple modules: Generalized SIP and SSP modules, and virtually extending modules [3,4,5]. Virtually extending modules is a generalization of both virtually semisimple modules and extending modules: A module M is called *extending* or CS (resp. *virtually extending*) if for any $X \leq^{c} M$, we have $X \leq^{\oplus} M$ ($X \lesssim^{\oplus} M$). The authors proved a generalization of the Osofsky-Smith Theorem in [3].

At the beginning of the study, we provide some equivalent definitions for virtually extending modules (Theorem 2). Then the relationships among the generalizations of virtually semisimple modules are examined. We proved in Propositions 3 and 4 that any virtually extending UC module has *GSIP*, any virtually extending module with *CSP* has *GSSP*. Then, a new module class, which are called CH modules, is introduced and its basic properties are examined. A module M is called CH if any complement submodule of M is a homomorphic image of M. An example is given in Example 9 that the CH condition is not inherited by direct

summands. After giving this example, we ensure some results on the CH condition to be inherited by direct summands and direct sums (Propositions 10, 11 and 12). We also give some results about that when CS, virtually extending and CH modules coincide (Proposition 13, 14 and 15). In Theorem 17, a characterization of quasi-projective virtually extending modules is given by using CH modules: A module M is virtually extending and quasi-projective if and only if it is a CH module and all of its complement submodules are M-projective. In Theorem 18, it is proved that if a module M is morphic and CH, then M is finitely generated if and only if M is CF (i.e., any closed submodule is finitely generated).

2. Results

We begin the paper by giving some equivalent definitions for virtually extending modules.

Theorem 2. The next statements are equivalent for a module M:

a. M is virtually extending.
b. For any $X \leq M$, there exists a $Z \leq^{c} M$ such that $X \leq^{ess} Z$ and $Z \lesssim^{\oplus} M$.
c. For any $X, Y \leq M$ with $X \cap Y = 0$, there exists a $Z \leq^{c} M$ such that $Y \leq Z$, $X \cap Z = 0$ and $Z \lesssim^{\oplus} M$.
d. For given $e^2 = e \in End(E(M))$, there exists $d^2 = d \in End(M)$ such that $eE(M) \cap M \cong dM$.

Proof. $(a) \Rightarrow (c)$ Let M be virtually extending, $X, Y \leq M$ with $X \cap Y = 0$. There exists a $Z \leq M$ satisfying that $Y \leq Z$ and Z is complement of X in M. By (a), $Z \lesssim^{\oplus} M$.

$(c) \Rightarrow (a)$ Let $Y \leq^{c} M$. There exists a $X \leq M$ satisfying that Y is complement of X in M. By (c), there exists a $Z \leq^{c} M$ satisfying that $Y \leq Z$, $X \cap Z = 0$ and $Z \lesssim^{\oplus} M$. Since $Y \leq^{c} M$, then $Y = Z$.

$(a) \Rightarrow (b)$ Let $X \leq M$. There exists a $Z \leq^{c} M$ satisfying that $X \leq^{ess} Z$. By (a), $Z \lesssim^{\oplus} M$.

$(b) \Rightarrow (d)$ Suppose (b) holds. Then $eE(M) \cap M \leq^{ess} C \leq^{c} M$ such that $C \cong D \leq^{\oplus} M$. It implies that $eE(M) = E(C)$ and so, $C \leq eE(M) \cap M$. Thus $C = eE(M) \cap M$. Now, by (b), there exists a $d^2 = d \in End(M)$ satisfying that $C = eE(M) \cap M \cong dM = D$.

$(d) \Rightarrow (a)$ Let $A \leq M$. There exists a $N \leq M$ such that $A \leq^{ess} N \leq^{c} M$. Then, we have

$$A \leq^{ess} N \leq^{ess} E(N) \leq^{\oplus} E(M).$$

Then, there exists a $e^2 = e \in End(E(M))$ satisfying that $eE(M) = E(N)$. Since $N \leq^{ess} E(N)$ and $M \leq^{ess} M$ and by [6, Lemma 1.1(2)], we have $N \cap M = N \leq^{ess} E(N) \cap M$. Now

$$N \leq^{ess} E(N) \cap M \leq M.$$

Since $N \leq^{c} M$, we have $N = E(N) \cap M$, and hence $N = eE(M) \cap M$. By (d), there exist $d^2 = d \in End(M)$ satisfying that $eE(M) \cap M \cong dM$. Therefore, M is virtually extending.

A module M is said to have *GSIP* if for any $X, Y \leq^{\oplus} M$, we have $X \cap Y \lesssim^{\oplus} M$ [4]. M is called UC if and only if for any $X, Y \leq^{c} M$, we have $X \cap Y \leq^{c} M$ [7].

Now, we give a result showing that virtually extending modules are related to modules having *GSIP*.

Proposition 3. If a module M is both virtually extending and UC, then M has *GSIP*.

Proof. Let $X, Y \leq^{\oplus} M$. Clearly, $X, Y \leq^{c} M$. Since M is *UC*, we have $X \cap Y \leq^{c} M$. Now, $X \cap Y \lesssim^{\oplus} M$ because M is virtually extending. It means that M has *GSIP*.

A module M is said to have *GSSP* if for any pair of $X, Y \leq^{\oplus} M$, we have $X + Y \lesssim^{\oplus} M$ [5]. M is said to have *closed sum property (CSP)* if for any $X, Y \leq^{c} M$, we have $X + Y \leq^{c} M$ [8].

Now, we give a result showing that virtually extending modules are related to modules having *GSSP*.

Proposition 4. If a module M is virtually extending and has *CSP*, then M has *GSSP*.

Proof. Let $X, Y \leq^{\oplus} M$. Clearly, $X, Y \leq^{c} M$. Since M has *CSP*, we have $X + Y \leq^{c} M$. Now, $X + Y \lesssim^{\oplus} M$ because M is virtually extending. It means that M has *GSSP*.

In the next section, we introduce a new generalization of virtually semisimple modules.

Khuri [9] calls a module M *retractable* if for every $X \leq M$, there exists a $\tau \in End_R(M)$ satisfying that $\tau(M) \subseteq X$ (i.e., $Hom(M, X) \neq 0$).

Ghorbani and Vedadi [10] call a module M *epi-retractable* if for every $X \leq M$, there exists a $\tau \in End_R(M)$ satisfying that $\tau(M) = X$.

Chatters and Khuri [11] call a module M *c-retractable* if for every $X \leq^{c} M$, there exists a $\tau \in End_R(M)$ satisfying that $\tau(M) \subseteq X$ (i.e., $Hom(M, X) \neq 0$).

Now, we introduce c-epi-retractable modules which is a generalization of epi-retractable modules:

Definition 5. We call a module M *c-epi-retractable* if for any $X \leq^{c} M$, there exists a $\tau \in End_R(M)$ satisfying that $\tau(M) = X$.

As it can be seen from the definition, since the complement submodules are the homomorphic image of the module M, we will briefly call this module class as CH *modules*, where, "C" is the first letter of the word "complement" and "H" is the first letter of the word "homomorphic".

First, we should state that any CS module is a CH module. More generally we have the following hierarchy:

$$CS \xrightarrow[\text{I}]{} \text{c-epi-retractable } (CH) \xrightarrow[\text{II}]{} \text{c-retractable}$$

IV

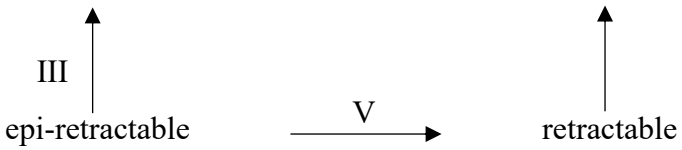

In the next theorem, we give some equivalent conditions for CH modules:

Theorem 6. The next statements are equivalent for a module M:

a. M is a CH module.
b. For any $X \leq M$, there exists a $Z \leq^{c} M$ such that $X \leq^{ess} Z$ and Z is homomorphic image of M.
c. For any $X, Y \leq M$ with $X \cap Y = 0$, there exists a $Z \leq^{c} M$ such that $Y \leq Z$, $X \cap Z = 0$ and Z is homomorphic image of M.
d. There exist epimorphisms $M \to N$ and $N \to M$ for some CH module N.
e. There exists an epimorphism $M/X \to M$ for some CH factor module M/X.

Proof. $(a) \Rightarrow (b)$ Let $X \leq M$. There exists a $Z \leq^{c} M$ satisfying that $X \leq^{ess} Z$. By (a), Z is homomorphic image of M.

$(b) \Rightarrow (a)$ Let $X \leq^{c} M$. By (b), there exists a $Z \leq^{c} M$ satisfying that $X \leq^{ess} Z$ and Z is homomorphic image of M. Thus $X = Z$, and hence M is CH.

$(a) \Rightarrow (c)$ Assume M is CH. Let $X, Y \leq M$ with $X \cap Y = 0$. There exists a complement Z of X in M satisfying that $Y \leq Z$. Then Z is homomorphic image of M by the hypothesis.

$(c) \Rightarrow (a)$ Let $Y \leq^{c} M$. There exists $X \leq M$ such that Y is complement of X in M. By the hypothesis, there exists a $Z \leq^{c} M$ satisfying that $Y \leq Z$, $X \cap Z = 0$ and Z is homomorphic image of M. Then $Y = Z$, and M is CH.

$(a) \Rightarrow (d)$ Clear.

$(d) \Rightarrow (e)$ Suppose that there exists a CH module N and epimorphisms $f: M \to N$, $g: N \to M$. Say $X = Ker(f)$. Then, f induces an isomorphism $\bar{f}: M/X \to N$. Thus, M/X is a CH module.

$(e) \Rightarrow (a)$ Let $C \leq^{c} M$. By our assumption, there exists an isomorphism $\bar{f}: M/Y \to M$ for some submodule Y of M with $X \subseteq Y$. Let $\bar{f}(A/Y) = C$ for some $A \leq^{c} M$. Since $A \leq^{c} M$ and by [7, Corollary 2(ii)], we have $A/X \leq^{c} M/X$. Since M/X is CH, then there exists an epimorphism $h: M/X \to A/X$. Consider $g: A/X \to A/Y$ with $g(a + X) = a + Y$, and the canonical epimorphism $\pi: M \to M/X$. Then, the map $\bar{f}gh\pi: M \to C$ is an epimorphism, and hence M is CH.

Example 7. Let M be an R-module as in [12, Example 2.6 or 2.7]. The authors show that M is CS (and hence CH) but not retractable (and hence not epi-retractable). Thus the reverse implication of (III) in above diagram doesn't hold, in general. Another example can also be given: the $\mathbb{Z}$-module $\mathbb{Q}$ which is CH but not retractable (see [10, Remark 2.12]).

As prior studies have indicated that the direct sum of CS (uniform) modules need not to be a CS module [13]. The next is a well-known example of this. In addition, the next example is a CH module.

Example 8. Let p be a prime number. The $\mathbb{Z}$-module $\mathbb{Z}_p \oplus \mathbb{Z}_{p^3}$ is a CH module because every finitely generated module over a PID is epi-retractable (see [10, Example 2.4(3)]). But it is not CS (see [13, p. 56]). Hence the reverse implication of (I) in above diagram doesn't hold, in general.

As prior studies have indicated that the CS property is inherited by direct summands [13], but the next example shows that the CH condition is not inherited by direct summands.

Example 9. [10, Remark 2.12] Let $\mathbb{F}$ be a free $\mathbb{Z}$-module with an infinite countable basic set and A be any countable $\mathbb{Z}$-module which is not CH. Then $M_{\mathbb{Z}} = \mathbb{F} \oplus A$ is epi-retractable by [10, Remark 2.12], and hence it is CH.

In the next results, we give some conditions which ensure that direct summands of CH modules are again CH.

Proposition 10. Let M be a CH module. Then

a. M/F is a CH module for any fully invariant complement submodule F of M.
b. If $M = M_1 \oplus M_2$ such that $Hom_R(M_1, M_2) = 0$, then M_2 is CH.

Proof. (a) Let F be a fully invariant complement submodule of M, and C/F be any complement submodule of M/F. Since $F \leq^c M$ and $C/F \leq^c M/F$, we have $C \leq^c M$ by [7, Corollary 2(iii)]. Then there is an epimorphism $\epsilon: M \to C$. Now, $\epsilon(F) \subseteq F$ by our assumption, and hence $\bar{\epsilon}: M/F \to C/F$ with $\bar{\epsilon}(m + F) = \epsilon(m) + F$ is an epimorphism. It means that M/F is CH.

(b) Note that $End_R(M) = \begin{bmatrix} End_R(M_1) & Hom_R(M_2, M_1) \\ 0 & End_R(M_2) \end{bmatrix}$. Thus $End_R(M) \begin{bmatrix} M_1 \\ 0 \end{bmatrix} \subseteq \begin{bmatrix} M_1 \\ 0 \end{bmatrix}$.
It implies that $M_1 \oplus 0$ is a fully invariant submodule of M. Now, we get result applying (a).

More generally, we can give the following result.

Proposition 11. Let $M = \oplus_{i \in I} M_i$ be an R-module with $End_R(M)$ is abelian. Then M is CH if and only if each M_i is CH.

Proof. First we note that $End_R(M)$ is abelian if and only if any direct summand of M is fully invariant in M (see [14, Theorem 4.4]).

($\Rightarrow$:) It is immediate by Proposition 10(b).

($\Leftarrow$:) Assume each M_i is CH and let $C \leq^c M$. Then by [15, Lemma 2.1], $C = \oplus_{i \in I}(C \cap M_i)$. Clearly, $C \cap M_i \leq^c M_i$ for each $i \in I$. Since each M_i is CH, for any $i \in I$ there exists $f_i \in End_R(M_i)$ such that $f_i(M_i) = C \cap M_i$. Now we can define the epimorphism

$$f \coloneqq \bigoplus_{i\in I} f_i : \bigoplus_{i\in I} M_i \ \rightarrow \ \bigoplus_{i\in I} (C \cap M_i)$$

Consequently,

$$f(M) = \bigoplus_{i\in I} f_i(M) = \bigoplus_{i\in I} f_i\left(\bigoplus_{i\in I} M_i\right) = \bigoplus_{i\in I} (C \cap M_i) = C,$$

as desired.

Proposition 12. Let $M = \oplus_{i\in I} M_i$ be a *UC* R-module. Then M is CH if and only if each M_i is CH.

Proof. ($\Rightarrow$:) Let M be both CH and UC. Suppose $D \leq^{\oplus} M$ and $A \leq D$. Since M is CH, by Theorem 6, there exists a $C \leq^{c} M$ such that $A \leq^{ess} C$ and C is homomorphic image of M. On the other hand, there exists a $K \leq^{c} D$ such that $A \leq^{ess} K$. Then, clearly, $C, K \leq^{c} D$. Since M is UC, we have $C = K$. It means that D is CH.

($\Leftarrow$:) Assume each M_i is CH and let $C \leq^{c} M$. Then, by [6, Lemma 6], $C \cap M_i \leq^{c} M_i$ for all $i \in I$. Since each M_i is CH, for any $i \in I$ there exists $f_i \in End_R(M_i)$ such that $f_i(M_i) = C \cap M_i$. Now we can define the epimorphism

$$f \coloneqq \bigoplus_{i\in I} f_i : \bigoplus_{i\in I} M_i \ \rightarrow \ \bigoplus_{i\in I} (C \cap M_i)$$

The proof follows by the argument which we use in the proof of Proposition 11.

Now, in the next three results, we show the relationship between CH modules and some other known module classes.

The authors [16] call a module M is *Rickart* if $Ker(\epsilon) \leq^{\oplus} M$ for every $\epsilon \in End_R(M)$. Clearly, the following implications is true for an R-module M:

$$M \text{ is } CS \Rightarrow M \text{ is virtually extending} \Rightarrow M \text{ is } CH.$$

The module in Example 8 is a CH module but not virtually extending. On the other hand an example of virtually extending module which is not CS is given in [3, Example 2.1].

The next result illustrates that the class of virtually extending modules and the class of *CH* modules coincide when the module is Rickart:

Proposition 13. Let M be a Rickart module. Then M is virtually extending if and only if M is CH.

Proof. ($\Rightarrow$:) Clear.

($\Leftarrow$:) Let $X \leq^{c} M$. Since M is CH, there exists an epimorphism $\epsilon: M \rightarrow X$. Let $i: X \rightarrow M$ be the inclusion map. We have, $Ker(i\epsilon) = Ker(\epsilon) \leq^{\oplus} M$ because of Rickartness. Then $M/Ker(\epsilon) \cong Im(\epsilon)$. Therefore, $Im(\epsilon) = X \lesssim^{\oplus} M$, as desired.

Corollary 14. Let R be right hereditary ring. Then every projective CH right R-module M is virtually extending.

Proof. Let $X \leq^c M$. Since M is CH, there exists an epimorphism $\epsilon: M \to X$. Since R is right hereditary, X is projective, and hence $Ker(\epsilon) \leq^{\oplus} M$. Therefore, $Im(\epsilon) = X \lesssim^{\oplus} M$, as desired.

The authors [17] call a module M is *dual Rickart* if $Im(\epsilon) \leq^{\oplus} M$ for every $\epsilon \in End_R(M)$.

Proposition 15. The next statements are equivalent for a dual Rickart module M:

a. M is CS.
b. M is virtually extending.
c. M is CH.

Proof. $(\boldsymbol{a}) \Rightarrow (\boldsymbol{b}) \Rightarrow (\boldsymbol{c})$ Clear.

$(\boldsymbol{c}) \Rightarrow (\boldsymbol{a})$ Let $X \leq^c M$. Since M is CH, there exists an epimorphism $\epsilon: M \to X$. We have $Im(\epsilon) = X \leq^{\oplus} M$ because of dual Rickartness. Hence, M is CS.

M is called $C2$ if for any $X \leq M$ with $X \lesssim^{\oplus} M$, we have $X \leq^{\oplus} M$. M is called *continuous* if it is CS and $C2$ [18].

Corollary 16. Any dual Rickart CH module is continuous.

Proof. By [17, Proposition 2.21], M is $C2$. Now, it is clear by Proposition 15.

Let M and P be R-modules. P is M-projective if and only if $Hom_R(P, -)$ is exact with respect to all exact sequences $0 \to K \to M \to N \to 0$. If P is P-projective, then P is also called *quasi-projective* (see [19, p.148]).

In the next theorem, we give a characterization of quasi-projective virtually extending modules with using CH modules.

Theorem 17. A module M is virtually extending and quasi-projective if and only if it is a CH module and all of its complement submodules are M-projective.

Proof. $(\Rightarrow:)$ M is CH because any virtually extending module is CH. Since M is virtually extending then any complement submodule of M is isomorphic to a direct summand of M. Thus by [19, Proposition 18.1], all complements submodules of M are M-projective.

$(\Leftarrow:)$ Let $X \leq^c M$. Since M is CH, there exists an epimorphism $\epsilon: M \to X$. Since X is M-projective, we have $Ker(\epsilon) \leq^{\oplus} M$ by [18, Lemma 4.30]. For some $K \leq M$, $M = Ker(\epsilon) \oplus K$. Then $K \cong M/Ker(\epsilon) \cong Im(\epsilon) = X$, i.e, $X \lesssim^{\oplus} M$. Thus, M is virtually extending. Again by [19, Proposition 18.1], M is quasi-projective.

The authors [20] call a module M *morphic* if for any $\epsilon \in End_R(M)$, $M/Im(\epsilon) \cong Ker(\epsilon)$; or equivalently, if for any $X, Y \leq M$ with $M/X \cong Y$ then $M/Y \cong X$.

Nguyen V. Dung [21] call a module M CF if any closed (complement) submodule is finitely generated. Now, it is proved that if a module M is morphic and CH then M is finitely generated if and only if M is CF.

Theorem 18. The next statements are equivalent for a morphic module M:

1) Every closed submodule of M is isomorphic to an image of M (i.e, M is CH).
2) For any $X \leq^c M$, M/X is isomorphic to a submodule of M.

In this case, the next statements hold:

a) If $X, Y \leq^c M$ then $M/X \cong M/Y$ if and only if $X \cong Y$.
b) M is finitely generated if and only if M is CF.

Proof. $(1) \Rightarrow (2)$: Let $X \leq^c M$. By (1), there is a $Z \leq M$ satisfying that $M/Z \cong X$. Since M is morphic, we have $M/X \cong Z$. So, (2) holds.

$(2) \Rightarrow (1)$: Let $X \leq^c M$. By (2), there is a $Z \leq M$ satisfying that $M/X \cong Z$. Since M is morphic, we have $M/Z \cong X$. So, (1) holds.

(a) $(\Rightarrow:)$ Let $X, Y \leq^c M$ with $M/X \cong M/Y$. By (2), there exists a $Z \leq M$ such that $M/X \cong M/Y \cong Z$. Since M is morphic, we have $X \cong Y \cong M/Z$.

$(\Leftarrow:)$ Let $X, Y \leq^c M$ with $X \cong Y$. By (2), there is a $Z \leq M$ such that $M/X \cong Z$, and there is a $T \leq M$ such that $M/Y \cong T$. Since M is morphic, we have $M/Z \cong X \cong Y \cong M/T$. Now, we have $M/Z \cong Y$. Now again, since M is morphic, $M/Y \cong Z$. On the other hand, we have just said above that $M/X \cong Z$. Thus, $M/Y \cong Z \cong M/X$.

(b) $(\Rightarrow:)$ Let $X \leq^c M$. By (1), there is a $Z \leq M$ such that $M/Z \cong X$. Thus, X is finitely generated because M is finitely generated. Hence M is CF.

$(\Leftarrow:)$ Clear.

Ethics in Publishing

There are no ethical issues regarding the publication of this study.

Acknowledgements

We express our gratitude to the referee(s) for thoroughly reviewing our paper and offering valuable advice that significantly enhanced its presentation. This study is supported by Anadolu University Scientific Research Projects Commission under the grant no: 2210E164.

References

[1] Clark J., Lomp C., Vanaja N., Wisbauer R., (2008) Lifting modules: supplements and projectivity in module theory. Springer Science & Business Media.

[2] Behboodi M., Daneshvar A., Vedadi M. R., (2018) Virtually semisimple modules and a generalization of the Wedderburn-Artin theorem, Comm. Algebra, 46(6), 2384-239.

[3] Karabacak F., Koşan M. T., Quynh T. C., Taşdemir Ö., (2022) On modules and rings in which complements are isomorphic to direct summands. Comm. Algebra, 50(3), 1154-1168.

[4] Taşdemir Ö., Karabacak F., (2019) Generalized SIP-modules, Hacettepe J. Math. Stat. 48(4), 1137-1145.

[5] Taşdemir Ö., Karabacak F., (2020) Generalized SSP-modules, Comm. Algebra, 48(3), 1068-1078.

[6] Nicholson W. K., Yousif M. F., (2003) Quasi-Frobenius Rings. Cambridge Univ. Press.

[7] Smith P. F., (1992) Modules for which every submodule has unique closure. Proceedings of the Biennial Ohio-Denison Conference 302-313.

[8] Hadi, I.M-I., Ghawi, Th.Y., (2014) Modules with the closed sum property, International Mathematical Forum, 9(32), 1539-1551.

[9] Khuri S. M., (1979) Endomorphism rings and lattice isomorphisms, Journal of Algebra 56(2), 401-408, 1979.

[10] Ghorbani A., Vedadi M. R., (2009) Epi-retractable modules and some applications, Bull. Iran. Math. Soc., 35(1), 155-166.

[11] Chatters A. W., Khuri S. M., (1980) Endomorphism rings of modules over non-singular CS rings. Journal of the London Mathematical Society, 2(3), 434-444.

[12] Rizvi S. T., Roman C. S., (2009) On direct sums of Baer modules, Journal of Algebra, 321(2), 682-696.

[13] Dung N. V., Huynh D. V., Smith P. F., Wisbauer R., (1994) Extending Modules, Pitman RN Mathematics, (Vol. 313). Harlow: Longman., Scientific & Technical.

[14] Călugăreanu G., Schultz P. (2010) Modules with Abelian endomorphism rings. Bull. Aust. Math. Soc. 82(1), 99-112.

[15] Özcan A. C., Harmanci A., Smith P. F., (2006) Duo modules, Glasg. Math. J. 48, 533-545.

[16] Lee G., Rizvi S. T., Roman C. S., (2010) Rickart Modules. Commun. Algebra, 38(11), 4005-4027.

[17] Lee G., Rizvi S. T., Roman C. S., (2011) Dual Rickart modules, Commun. Algebra, 39(11), 4036-4058.

[18] Mohamed S. H., Müller B. J., (1990) Continuous and Discrete Modules, London Math. Soc. Lecture Note Series, 147, Cambridge: Cambridge University Press.

[19] Wisbauer R., (1991) Foundations of Module and Ring Theory, Gordon and Breach, Reading.

[20] Nicholson W. K., Campos E. S., (2005) Morphic modules, Comm. Algebra, 33(8), 2629-2647.

[21] Dung N. V., (1991) Modules whose closed submodules are finitely generated. Proc. Edinb. Math. Soc. 34, 161–166.

Erzincan Üniversitesi
Fen Bilimleri Enstitüsü Dergisi
2024,17(1), 147-163
ISSN: 1307-9085, e-ISSN: 2149-4584
Araştırma Makalesi

Erzincan University
Journal of Science and Technology
2024,17(1), 147-163
DOI: 10.18185/erzifbed.1375233
Research Article

Genome-Wide Analysis and Characterization of the *AHL* Gene Family in Common Beans (*Phaseolus vulgaris* L.)

Yaren Bozkurt[1], Merve Yüce[2], Esra Yaprak[1], Ayşe Gül Kasapoğlu[1], Emre İlhan[1], Murat Turan[1], Murat Aydın[3], Ertan Yıldırım[2*]

[1]Erzurum Technical University, Faculty of Science, Department of Molecular Biology and Genetics, Erzurum/Türkiye
[2]Ataturk University, Faculty of Agriculture, Department of Horticulture, Erzurum/Türkiye
[3]Ataturk University, Faculty of Agriculture, Department of Agricultural Biotechnology, Erzurum/Türkiye

Received: 12/10/2023, **Revised:** 18/11/2023, **Accepted:** 18/11/2023, **Published:** 28/03/2024

Abstract

The AT-hook motif nuclear localized family (*AHL*) is defined as a small DNA-binding protein motif, functioning as a transcription factor. This transcription factor family plays a significant role in influencing plant growth, development processes, and the response mechanism to environmental stresses. In *Phaseolus vulgaris* (common bean) genome, 41 *AHL* genes have been identified. Using in silico bioinformatics tools, the characteristic features of AHL genes, their exon-intron structures, chromosomal locations of *AHL* genes, conserved motifs, promoter regions, duplication relationships, protein features of AHL proteins, protein-protein interactions, and the expression levels of *AHL* genes against drought and salinity stresses have been studied. Additionally, a phylogenetic comparison of *P. vulgaris* with *Arabidopsis thaliana* and *Glycine max* has been conducted. The amino acid lengths of these proteins vary between 167 and 422, with the molecular weights of the gene family ranging from 18.19 kDa to 45.13 kDa. The isoelectric points (pI) of the AHL proteins vary between 4.5 and 10.3. *AHL* genes are dispersed across all chromosomes of the bean, with the highest number of genes found on chromosomes 6 and 8. In *P. vulgaris*, 14 duplicated genes have been identified, and subsequent Ka/Ks analysis has revealed that all are subject to purifying selection. The findings from this research will aid future functional studies in better understanding the functions of *AHL* genes in beans.

Keywords: *AHL* motif, DNA-binding protein, PPC/DUF296, Genome-Wide Analysis

*Corresponding Author: ertanyil@atauni.edu.tr
Yaren BOZKURT, https://orcid.org/0009-0003-0213-5398
Merve YÜCE, https://orcid.org/0000-0003-1091-0609
Esra YAPRAK, https://orcid.org/0000-0002-8753-494X
Ayşe Gül KASAPOĞLU, https://orcid.org/0000-0002-6447-4921
Emre İLHAN, https://orcid.org/00000-0002-8404-7900
Murat TURAN, https://orcid.org/0000-0003-2900-1755
Murat AYDIN, https://orcid.org/0000-0003-1091-0609
Ertan YILDIRIM, https://orcid.org/0000-0003-3369-0645

Fasulye'de (*Phaseolus vulgaris* L.) *AHL* Gen Ailesinin Genom Çaplı Analizi ve Karakterizasyonu

Öz

AT-hook motifi nükleer lokalize ailesi (*AHL*), küçük bir DNA bağlayıcı protein motifi olarak tanımlanmış ve bir transkripsiyon faktörü olarak görev yapmaktadır. Bu transkripsiyon faktörü ailesi, bitki büyüme ve gelişme süreçlerini ve çevresel streslere verilen yanıt mekanizmasını etkilemede önemli bir rol oynamaktadır. *Phaseolus vulgaris* (fasulye) genomunda 41 *AHL* geni tanımlanmıştır. İn silico biyoinformatik araçlar kullanılarak, AHL genlerinin karakteristik özellikleri, ekzon-intron yapıları, *AHL* genlerinin kromozomlardaki yerleşimleri, korunmuş motifleri, promotor bölgeleri, duplikasyon ilişkileri, AHL proteinlerinin protein özellikleri, protein-protein etkileşimleri ve kuraklık ile tuzluluk streslerine karşı *AHL* genlerinin ifade düzeyleri incelenmiştir. Ayrıca, *P. vulgaris*'in *Arabidopsis thaliana* ve *Glycine max* ile filogenetik ilişkisi belirlenmiştir. Bu proteinlerin amino asit uzunlukları 167 ile 422 ve moleküler ağırlıkları ise 18.19 kDa ile 45.13 kDa arasında değişmektedir. AHL proteinlerinin izoelektrik noktaları (pI) 4,5 ile 10,3 arasında değişmektedir. Pvul-*AHL* genleri fasulyenin bütün kromozomlarına yayılmış olup, en fazla gen 6 ve 8 numaralı kromozomlarda bulunmaktadır. *P. vulgaris*'te 14 duplike olmuş gen tespit edilmiş ve ardından yapılan Ka/Ks analizi, tümünün arındırıcı seleksiyona tabi olduğunu göstermiştir. Bu araştırmadan elde edilen bulgular, gelecekte yapılacak fonksiyonel çalışmaların fasulyedeki *AHL* genlerinin işlevlerini daha iyi anlamamıza yardımcı olacaktır.

Anahtar Kelimeler: *AHL* motif, DNA bağlanma proteini, PPC/DUF296, Genome-Wide Analysis

1. Introduction

P. vulgaris are acknowledged as the primary food supply for millions of people in underdeveloped nations and a significant source of total protein, nutrients, and energy on a global scale. 100 grams of *P. vulgaris* provide 60 grams of carbs, 20 to 25 grams of protein, and 0.7 to 1.5 grams of fat. The *P. vulgaris* structure also includes these macromolecules as well as varying levels of other vitamins, minerals, and phytochemicals [1, 2].

Plant genomes have expanded and diversified rapidly from their common ancestor throughout the evolutionary process, beginning with the colonization of land plants. In this process, some genes that regulate important growth and development processes of plant species increased in number and gradually became multi-member gene families [3, 4, 5]. One of these gene families, the AT-hook motif nuclear localized (*AHL*) family, a small DNA binding protein motif, serves as a transcription factor and is found in all ordered dicot and monocot land plants. AT-hook motif and the plants and Prokaryotes Conserved Domain (*PPC/DUF296*) found in *AHL* proteins are two highly conserved domains [5].

The DNA-binding protein AHL was first discovered in the high mobility group (HMG-I/Y) of mammalian nonhistone chromosomes, and later discovered in prokaryotes and plants [5, 6, 7]. According to conserved amino acid sequences, AHL falls into two main categories: Type-I motifs with the consensus sequences Gly-Ser-Lys-Asn-Lys and Type-II motifs with the Arg-Lys-Tyr. The Arg-Gly-Arg-Pro sequence is preserved in both type 1 and type 2 motifs. The primary distinction between the conserved Arg-Gly-Arg sequence and other transcription factors is its ability to bind to the AT-rich minor groove of B-form DNA. About 120 amino acids make up the PPC domain, which is found at the carboxyl terminus of the AT-hook motif and is in charge of the nucleus localization of the AHL protein [8]. Their nuclear localization and interactions with other proteins are controlled by the PPC domain. They can also interact with some transcription factors and form homo- or hetero-oligomers with other AHLs [9].

AHL gene family members play important roles in different growth and development processes such as pollen development [10], flower development [11], regulation of flowering time [12], hypocotyl elongation [5], leaf aging [13], differentiation of vascular tissues [5], homeostasis of gibberellins [14], and regulation of auxin-related gene expression with jasmonic acid [15]. In addition, *AHL*s are involved in the response to biotic and abiotic stress [16]. In a study conducted in rice, the OsAHL1 gene was reported to positively regulate drought-affected genes to increase tolerance and resistance to abiotic stimuli such as salt and cold [17]. The AHL genes are known to have significant implications in several aspects of plant growth and development, as well as in the plant's ability to respond to both biotic and abiotic stressors. These genes achieve this by modulating the expression of target genes or by engaging in protein-protein interactions with other molecules [18].

So far, varying numbers of AHL gene family members have been identified in different plants: 29 in *Arabidopsis thaliana* (L.) Heynh. [14], 20 in *Oryza sativa* L. [18], 22 in *Sorghum bicolor* (L.) Moench [5], 37 in *Zea mays* L. [16], 48 in *Gossypium raimondii* Ulbr., 51 in *Gossypium arboreum* L., 99 in *Gossypium hirsutum* L. [20], 47 in cultivated carrot (*Daucus carota* subsp. *sativus*) [21], 63 in *Glycine max* L. Merr [22], 37 in *Populus trichocarpa* [8], 14 in *Vitis vinifera* L. [23] and 122 in *Brassica napus* L. [24], 42 in *Brassica rapa* L. [25] and 22 genes in *peach (Prunus persica)* [26]. However, the *AHL* gene family has not been characterized in the *Phaseolus vulgaris*. Thus, the aim of this study was to determine the *AHL* gene family in *P. vulgaris* and to characterize it genome-wide by in silico methods. This study possesses a high level of originality as it is the first in the literature to focus on the *AHL* genes of *P. vulgaris*.

2. Material and Method

Determination of *AHL* Genes

The sequences of the *AHL* gene family in *P. vulgaris* [27], *A. thaliana* [28] and *G. max* [29] genomes were obtained from the Phytozome database v13 [30] using the Pfam Accession Number (PF02178) [31]. In addition, The SMART database (Simple Modular Architecture Research Tool) was used to confirm the presence of AHL proteins [32].

Sequence Alignment and Phylogenetic Analyses

The protein sequences of the members of the *AHL* gene family in the genomes of *P. vulgaris*, *A. thaliana* and *G. max* species were aligned using the Multiple Sequence Alignment by CLUSTALW tool [33] and the phylogenetic tree was constructed using MEGA 11 program by the neighbor-joining (NJ) method with 1000 bootstrap replicates. Subsequently, the aligned protein sequences were used to construct a phylogenetic tree using the ITOL (Interactive Tree of Life) tool [34].

Identification of AHL Proteins in the *P. vulgaris* Genome

The amino acid count, molecular weight (kDa), theoretical isoelectric point (pI), and stability of AHL proteins in *P. vulgaris* were determined using the "ProtParam tool" [35].

Determination of the structure and chromosome location and promoter region analysis

The exon and intron regions of the *P. vulgaris* AHL proteins were determined using the GSDS (Gene Structure Display Server v2.0) [36]. The chromosomal locations and sizes of *P. vulgaris AHL* genes were determined via the Phytozome database v13 and mapped with the MapChart program [37]. Each member of the *P. vulgaris AHL* gene family had roughly 2000 bp of DNA extracted from the 5` upstream region, and cis acting element analysis was done using the PlantCARE database [38].

Gene duplications of *AHL* genes and identification of conserved motifs

Multiple EM for Motif Elimination (MEME) tool [39] was used to detect conserved motifs of *P. vulgaris AHL* genes. The maximum number of motifs was determined as 10 and the width range was at least 2 and maximum 50. Gene duplications were determined using the MCScanX (The Multiple Collinearity Scan Toolkit) tool in TBtools program. Synonym ratios (Ks), nonsynonymous ratios (Ka), and evolutionary strains (Ka/Ks) between binary pairs of genes were calculated using the TBtools program [40].

Synteny analysis

The duplications of *AHL* genes in *P. vulgaris*, *A. thaliana*, and *G. max* were identified using the MCScanX tool (The Multiple Collinearity Scan Toolkit) and were visualized using the TBtools program [40].

Protein-protein interactions (PPI)

Pvul-AHL protein-protein interactions (PPI) were identified at the physical, functional, and experimental levels using the STRING database [41].

In silico gene expression analysis

Illumina RNA-seq data were obtained from the Sequence Read Archive (SRA) data bank in the National Center for Biotechnology Information (NCBI) database. We used accession numbers for salt and drought conditions to locate pertinent RNA-seq data. The following leaf types were used: leaf under salt stress (SRR957668), leaf under drought stress (SRR8284481), and leaf under drought control (SRR8284480) [42]. Gene expression levels were normalized using the Read per Kilobase (RPKM) technique [43]. The CIMMiner tool was used to create a heatmap [44].

3. Results and Discussion

Determination and Characteristics of *AHL* Genes

AHL genes corresponding to *P. vulgaris*, *A. thaliana*, and *G. max* were extracted from the Phytozome database using the Pfam Accession Number. In this process, 41 genes from *P. vulgaris*, 32 genes from *A. thaliana*, and 65 genes from *G. max* were identified. These genes were then systematically numbered based on their chromosomal sequences. To enhance clarity in the manuscript, abbreviations were used for the nomenclature of the *AHL* genes specific to *P. vulgaris*. The details of these genes, including their abbreviations, Phytozome Transcript IDs, chromosomal locations, start and end points, and strand orientations, have been presented in Table 1. Upon examining the AHL proteins of *P. vulgaris*, it was observed that the amino acid counts of the genes ranged from 167 to 422. The protein with the shortest amino acid sequence was identified as *Pvul-AHL*-19 (167 amino acids), while the one with the longest sequence was *Pvul-AHL*-15 (422 amino acids). A correlation was noted between their molecular weights and amino acid lengths. Among these proteins, 21 were found to exhibit acidic or near-neutral acidic characteristics, and 22 proteins exhibited basic or near-neutral basic characteristics. In the analysis of the 41 AHL proteins, 6 were determined to be stable, while the remaining were identified as unstable (Table 1).

Table 1. Information about *Pvul-AHL* genes

Gene ID	Phytozome Transcript ID	Chr	Start	End	Strand	aa	MW (kDa)	pI	Stabitily
Pvul-AHL-1	Phvul.001G081632.1	Chr01	12159318	12160837	reverse	278	28.80	5.54	unstable
Pvul-AHL-2	Phvul.001G234600.1	Chr01	48832896	48834455	reverse	287	30.43	5.55	unstable
Pvul-AHL-3	Phvul.002G006700.1	Chr02	698485	703324	forward	351	36.74	8.34	unstable
Pvul-AHL-4	Phvul.002G006900.1	Chr02	722290	723601	reverse	272	28.61	5.8	unstable
Pvul-AHL-5	Phvul.002G118500.1	Chr02	25245881	25247521	reverse	208	23.14	4.86	unstable
Pvul-AHL-6	Phvul.002G151600.1	Chr02	30512278	30513948	forward	299	31.19	6.63	unstable
Pvul-AHL-7	Phvul.002G157300.1	Chr02	31183111	31187446	reverse	355	36.29	9.94	unstable
Pvul-AHL-8	Phvul.002G288900.1	Chr02	45766457	45770953	reverse	358	36.51	9.71	unstable
Pvul-AHL-9	Phvul.003G195100.1	Chr03	41924534	41925104	forward	189	20.24	5.61	unstable
Pvul-AHL-10	Phvul.003G216000.1	Chr03	44318578	44323527	reverse	326	33.28	9.08	unstable
Pvul-AHL-11	Phvul.003G216200.1	Chr03	44377183	44379047	forward	284	29.84	6.11	unstable
Pvul-AHL-12	Phvul.003G230500.1	Chr03	46212036	46217232	forward	368	37.36	9.24	unstable
Pvul-AHL-13	Phvul.003G230600.1	Chr03	46229664	46230522	reverse	285	30.07	5.87	unstable
Pvul-AHL-14	Phvul.004G127200.1	Chr04	42321598	42327649	forward	334	34.77	5.87	unstable
Pvul-AHL-15	Phvul.005G127900.1	Chr05	36564911	36567434	reverse	422	45.13	4.87	unstable
Pvul-AHL-16	Phvul.006G007200.1	Chr06	1056593	1057256	reverse	220	23.49	7.13	unstable
Pvul-AHL-17	Phvul.006G007300.1	Chr06	782344	782962	forward	205	22.76	4.5	unstable
Pvul-AHL-18	Phvul.006G013800.1	Chr06	6443800	6444580	reverse	259	28.12	8.9	unstable
Pvul-AHL-19	Phvul.006G016300.1	Chr06	7617513	7620976	reverse	167	18.19	10.3	stable
Pvul-AHL-20	Phvul.006G031000.1	Chr06	11868121	11868781	forward	219	23.69	7.71	stable
Pvul-AHL-21	Phvul.006G031100.1	Chr06	11882688	11883287	forward	188	20.22	5.67	stable
Pvul-AHL-22	Phvul.006G031200.1	Chr06	11927780	11928392	forward	203	21.90	9.75	stable
Pvul-AHL-23	Phvul.006G106500.2	Chr06	21587154	21592842	reverse	363	38.46	9.34	unstable
Pvul-AHL-24	Phvul.007G129400.1	Chr07	14122140	14123194	reverse	310	31.76	6.26	unstable
Pvul-AHL-25	Phvul.007G111600.1	Chr07	20569440	20576763	reverse	331	34.96	8.37	unstable
Pvul-AHL-26	Phvul.007G223900.1	Chr07	34761172	34765536	forward	377	39.11	6.85	stable
Pvul-AHL-27	Phvul.007G271800.1	Chr07	39308747	39309554	reverse	268	27.17	5.3	unstable
Pvul-AHL-28	Phvul.008G050100.1	Chr08	4352524	4353889	forward	271	27.99	5.83	unstable
Pvul-AHL-29	Phvul.008G065900.1	Chr08	6037682	6044398	forward	341	35.16	9.86	unstable
Pvul-AHL-30	Phvul.008G076100.1	Chr08	7332658	7337374	forward	332	34.47	9.4	unstable
Pvul-AHL-31	Phvul.008G181100.1	Chr08	51225879	51226665	reverse	261	27.29	7.72	unstable
Pvul-AHL-32	Phvul.008G192600.1	Chr08	53291708	53292560	reverse	283	29.51	4.79	unstable
Pvul-AHL-33	Phvul.008G231500.1	Chr08	53537135	53538349	reverse	248	26.45	9.14	unstable
Pvul-AHL-34	Phvul.008G200900.1	Chr08	54741078	54741993	forward	253	27.48	5.1	unstable
Pvul-AHL-35	Phvul.008G264600.1	Chr08	61064853	61065423	reverse	189	20.39	5.86	unstable
Pvul-AHL-36	Phvul.009G008300.1	Chr09	1270665	1274490	reverse	369	37.70	10	unstable

Pvul-AHL-37	Phvul.009G144300.1	Chr09	21607296	21608142	reverse	281	29.32	6.79	unstable
Pvul-AHL-38	Phvul.010G085300.1	Chr10	23954897	23956568	reverse	310	31.92	7.2	unstable
Pvul-AHL-39	Phvul.010G084600.1	Chr10	24191274	24197814	forward	356	36.56	9.08	unstable
Pvul-AHL-40	Phvul.010G097000.1	Chr10	36212885	36218337	reverse	340	34.87	9.87	unstable
Pvul-AHL-41	Phvul.011G089400.1	Chr11	8654261	8657512	forward	373	38.93	5.74	stable

*:aa: aminoacid length, pI: theoretical isoelectric points, Chr: Chromosome.

Phylogenetic Analysis of AHL Genes

The AHL genes' protein sequences from *P. vulgaris*, *A. thaliana*, and *G. max* were aligned in ClustalW, and a phylogenetic tree was constructed using the Mega11 program. The ITOL online tool was used to colorize the phylogenetic tree branching. According to this analysis, AHL proteins are basically divided into two classes: Clade A and Clade B. Clade A contains Type I AHL proteins, while Clade B contains Type II and Type III AHL proteins. There are 16 bean, 16 *A. thaliana*, and 31 soybean AHL proteins in the Clade A group. In the Clade B group, there are 25 bean, 16 *A. thaliana*, and 34 soybean AHL proteins. When the phylogenetic tree was examined, Type I *AHL*s were clearly separated from the others, while Type II and Type III *AHL*s showed mixed branching (Figure 1). A similar branching pattern was observed in the phylogenetic trees generated from maize, rice, sorghum, and *A. thaliana* [45] and *P. trichocarpa*, *A. thaliana*, and *O. sativa* [8].

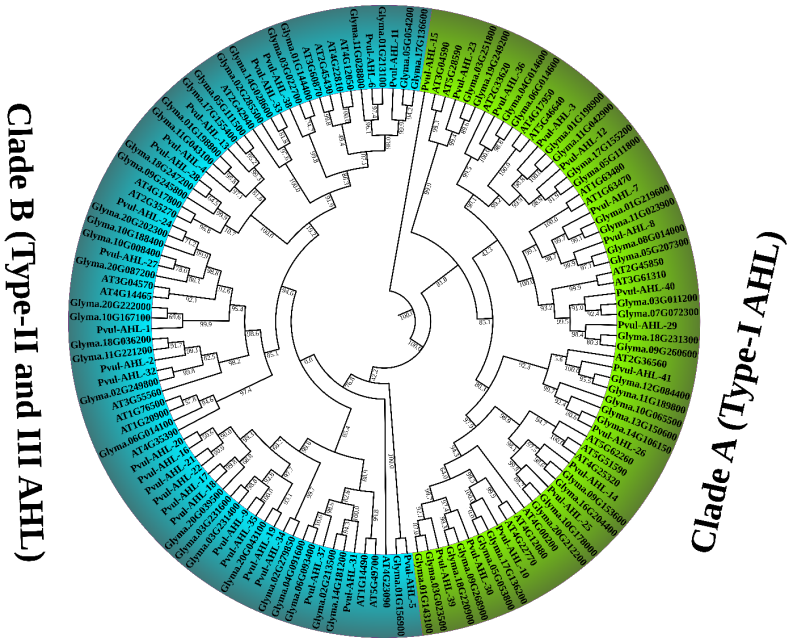

Figure 1. Phylogenetic tree illustrating the relationship of *AHL* family in *P. vulgaris*, *A. thaliana* and *G. max*. The phylogenetic tree was drawn with AHL proteins from P. vulgaris, A. thaliana and G. max. AHL full-length amino acid sequences from P. vulgaris and 2 other species are aligned by ClustalW and the phylogenetic tree was constructed using MEGA 11 program by the neighbor-joining (NJ) method with 1000 bootstrap replicates. AHL proteins are basically divided into two classes: Clade A (green) and Clade B (blue).

Structure of *AHL* Genes

The similarity in the intron/exon structures of homologous and paralogous genes across different species can be utilized as an indicator to assess the evolutionary proximity or distance between these species [46]. It has been discovered that some genes of *P. vulgaris* contain only one exon region, while others have multiple. The highest number of exons (6) and introns (5) were observed in the *Pvul-AHL-23* gene. Variability in the structures and numbers of exon and intron regions was observed to be dependent on the branches in the phylogenetic tree of *P. vulgaris*. In 19 genes, no intron regions were present, containing only a single exon region. Additionally, 16 genes were found to have 5 exon regions and 4 intron regions. It was determined that the identified *Pvul-AHL* genes are located on all chromosomes of *P. vulgaris* (Figure 2). The 6th and 8th chromosomes were found to have the highest number of *AHL* genes, with 8 each (Figure 3).

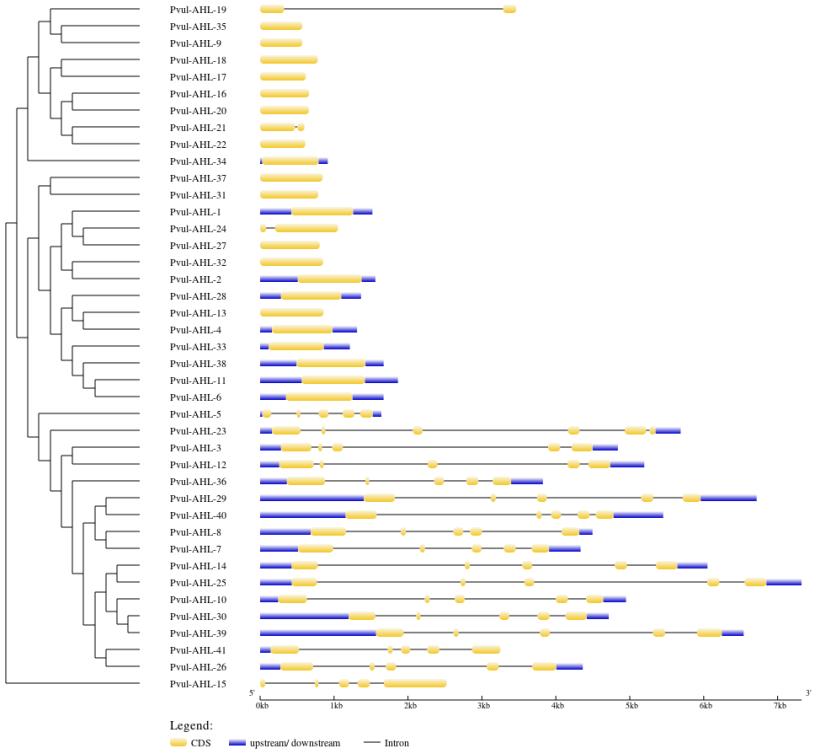

Figure 2. The length and position of exons and introns in the Pvul-AHL genes. The blue lines represent 5′-UTR or 3′-UTR, yellow boxes indicate exons, and black lines exhibit introns.

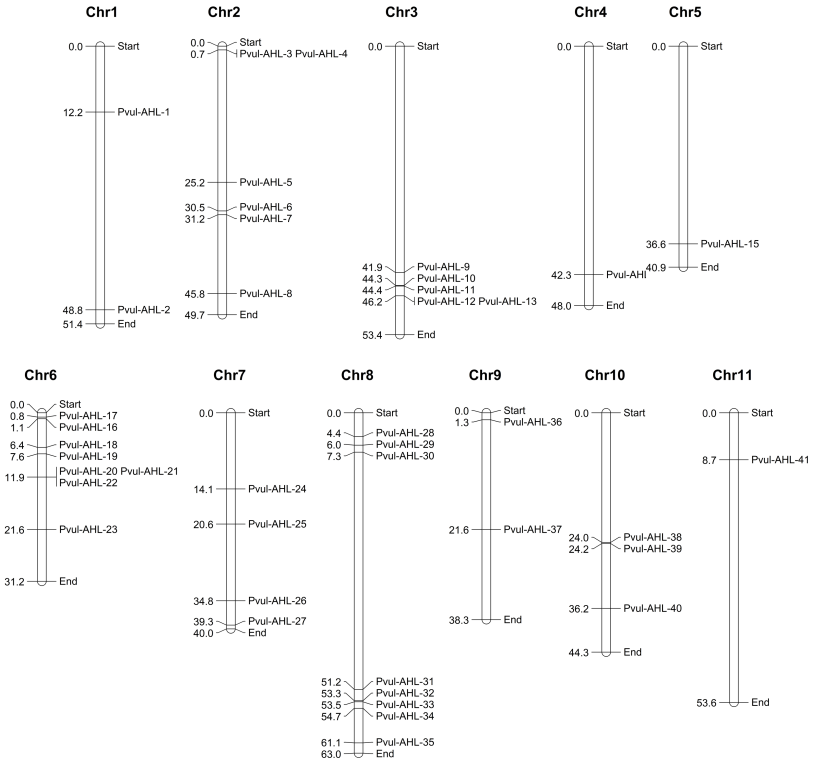

Figure 3. Chromosomal locations of *P. vulgaris* AHL genes. Distribution of the AHL genes on *P. vulgaris* chromosomes according to the linkage map.

Conserved Motifs of *AHL* Genes

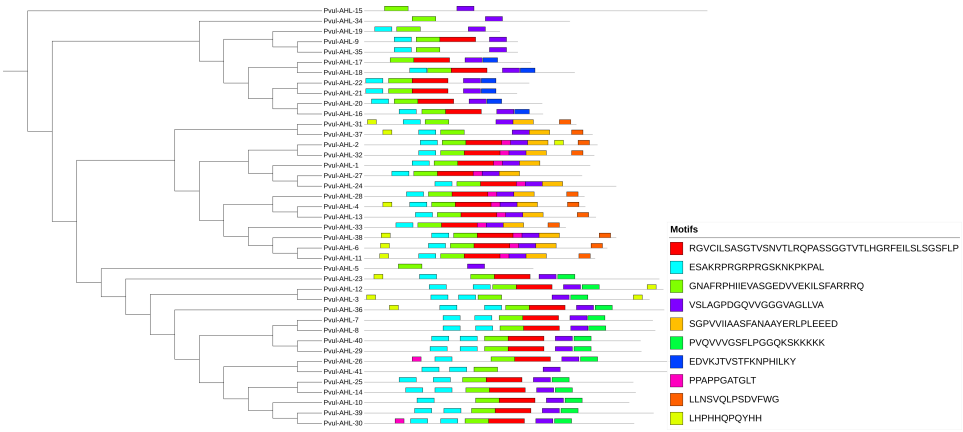

Figure 4. Distribution of predicted motifs in *AHL* genes in *P. vulgaris.* Predicted motif distribution in Pvul-AHL proteins identified MEME suite program. The motifs are exhibited with a specific color.

The conserved motifs within the *AHL* gene family were delineated using MEME-Suite. In the course of this analysis, a total of ten distinct conserved motif patterns were successfully identified, facilitating further examination and review of the *AHL* gene family. The range of

identified motifs varied between 2 and 8. It was noted that *Pvul-AHL-15* and *Pvul-AHL-34* exhibited the least number of conserved motifs, with only 2 each, whereas *Pvul-AHL-2*, *Pvul-AHL-4*, *Pvul-AHL-6* and *Pvul-AHL-11* were characterized by the highest number, each containing 8 conserved motifs. Motif 3 and Motif 7 were detected in all *Pvul-AHL* proteins. Motif 1, which was determined to be *AHL* domain, was detected in all other genes except *Pvul-AHL-5* gene (Figure 4).

Promoter region analysis of *AHL* Genes

Sequences retrieved from 2000 bp upstream in the 5′ upstream region of *AHL* genes have been examined, and it has been determined that promoter regions in these genes are influential in plant development, molecular response to abiotic stresses, and adaptation to environmental factors. Cis-acting elements found in sequences of *Pvul-AHL* genes have been identified through analyses in the PlantCARE database and visualized using the TBTools program. A comprehensive identification of cis-acting elements has been achieved across all Pvul-*AHL* genes. Key elements associated with abiotic and biotic stresses, such as MYB (in all except *Pvul-AHL-12*), TC-rich repeats (in *Pvul-AHL-2, Pvul-AHL-6, Pvul-AHL-8, Pvul-AHL-10, Pvul-AHL-13, Pvul-AHL-15, Pvul-AHL-16, Pvul-AHL-21, Pvul-AHL-24, Pvul-AHL-26, Pvul-AHL-29, Pvul-AHL-30, Pvul-AHL-36, Pvul-AHL-38, Pvul-AHL-41*), LTR (in *Pvul-AHL-2, Pvul-AHL-20, Pvul-AHL-21, Pvul-AHL-24, Pvul-AHL-29, Pvul-AHL-30, Pvul-AHL-31, Pvul-AHL-33*), W box (in *Pvul-AHL-1, Pvul-AHL-4, Pvul-AHL-5, Pvul-AHL-11, Pvul-AHL-12, Pvul-AHL-14, Pvul-AHL-16, Pvul-AHL-19, Pvul-AHL-20, Pvul-AHL-21, Pvul-AHL-22, Pvul-AHL-25, Pvul-AHL-27, Pvul-AHL-31, Pvul-AHL-38, Pvul-AHL-41*) have been observed in *Pvul-AHL* genes (Figure 5).

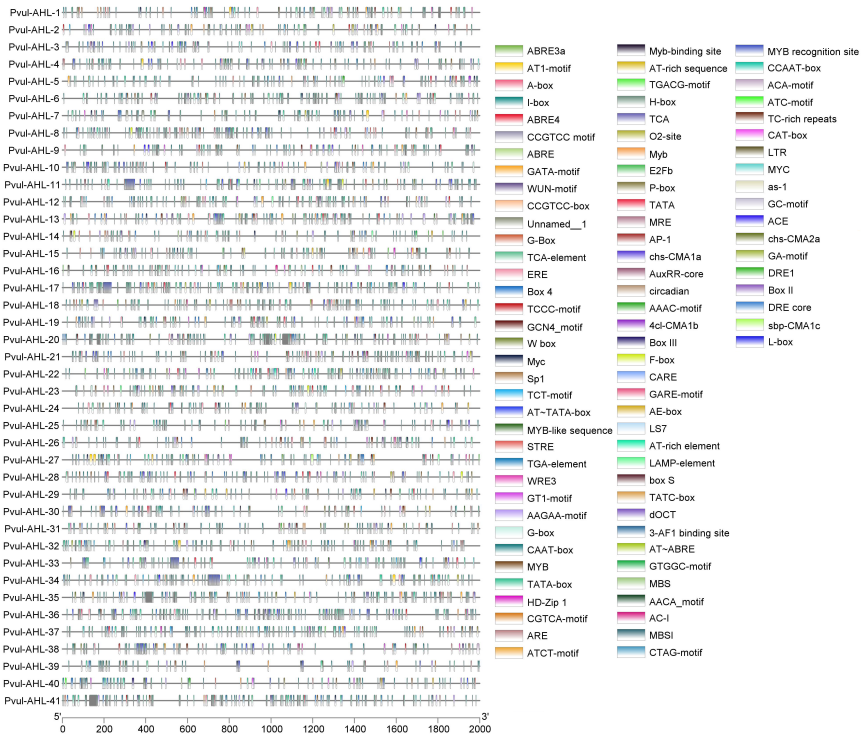

Figure 5. Promoter regions of *Pvul-AHL* genes. PlantCARE analyzed promoter sequences (−2000 bp) of 41 *Pvul-AHL* genes. The scale indicates the upstream length through the translation codon. Different color rectangles indicate different cis elements.

Synteny Analysis of *AHL* Genes

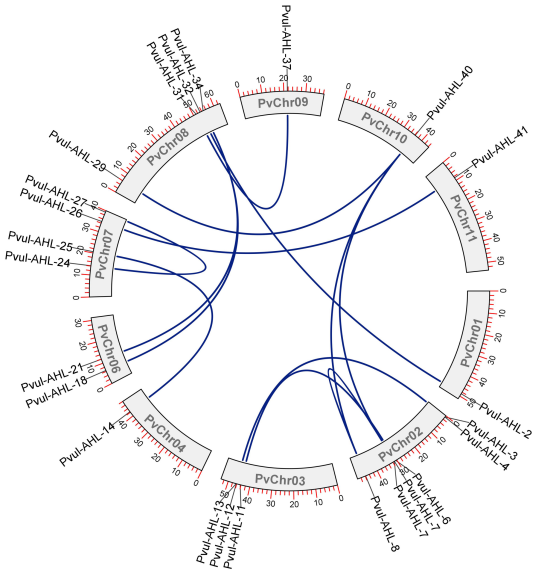

Figure 6. Self-synteny of the AHL genes in the *P. vulgaris* genome. The AHL genes in *P. vulgaris* were mapped to different chromosomes. Gene pairs of the AHL with a syntenic relationship are joined by a blue line.

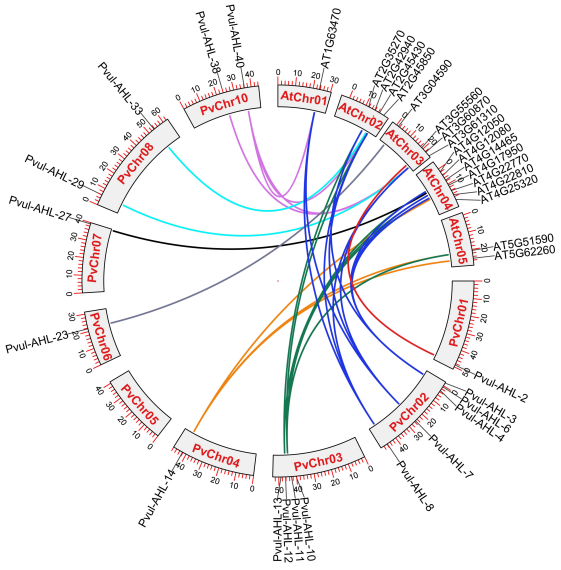

Figure 7. Gene duplication and synteny analysis of AHL genes between *P. vulgaris* and *A. thaliana.* It has been indicated that arrows originating from all chromosomes of *P. vulgaris* are represented in different colors.

In the synteny analysis conducted using MCScanX, duplicated genes among *P. vulgaris* genes, their interconnections, and the resulting selection types have been examined. Additionally, duplicated genes between *P. vulgaris* and *A. thaliana* have been studied. Within *P. vulgaris*, 14 duplicated genes have been identified, and subsequent Ka/Ks analysis has revealed that all are subject to purifying selection (Table 2). In the synteny analysis of *AHL* genes within *P. vulgaris*, it has been determined that duplicated genes exist in all chromosomes except for *Pvul-AHL-5* (Figure 6). When examining duplicated genes between *P. vulgaris* and *A. thaliana*, duplicated genes have been found in all chromosomes of *A. thaliana* (Figure 7).

Table 2. Gene duplications of the *Pvul-AHL* genes

Gene 1	Gene 2	Ka/Ks	Selection Type
Pvul-AHL-2	*Pvul-AHL-32*	0.22	Purifying selection
Pvul-AHL-3	*Pvul-AHL-12*	0.24	Purifying selection
Pvul-AHL-4	*Pvul-AHL-13*	0.11	Purifying selection
Pvul-AHL-6	*Pvul-AHL-11*	0.07	Purifying selection
Pvul-AHL-7	*Pvul-AHL-40*	0.17	Purifying selection
Pvul-AHL-7	*Pvul-AHL-8*	0.30	Purifying selection
Pvul-AHL-8	*Pvul-AHL-40*	0.20	Purifying selection
Pvul-AHL-14	*Pvul-AHL-25*	0.28	Purifying selection
Pvul-AHL-18	*Pvul-AHL-34*	0.34	Purifying selection
Pvul-AHL-21	*Pvul-AHL-34*	0.38	Purifying selection
Pvul-AHL-24	*Pvul-AHL-27*	0.07	Purifying selection
Pvul-AHL-26	*Pvul-AHL-41*	0.31	Purifying selection
Pvul-AHL-29	*Pvul-AHL-40*	0.15	Purifying selection
Pvul-AHL-31	*Pvul-AHL-37*	0.22	Purifying selection

Protein-protein interaction (PPI) Analysis of *AHL* Genes

The protein-protein interactions of *Pvul-AHL* proteins have been analyzed and visualized using the STRING database. It was found that *Pvul-AHL*-9, *Pvul-AHL*-17, *Pvul-AHL*-20, *Pvul-AHL*-34 are interrelated, as are *Pvul-AHL*-15, *Pvul-AHL*-21, *Pvul-AHL*-39 with each other. No relationships have been found among all the other genes (Figure 8).

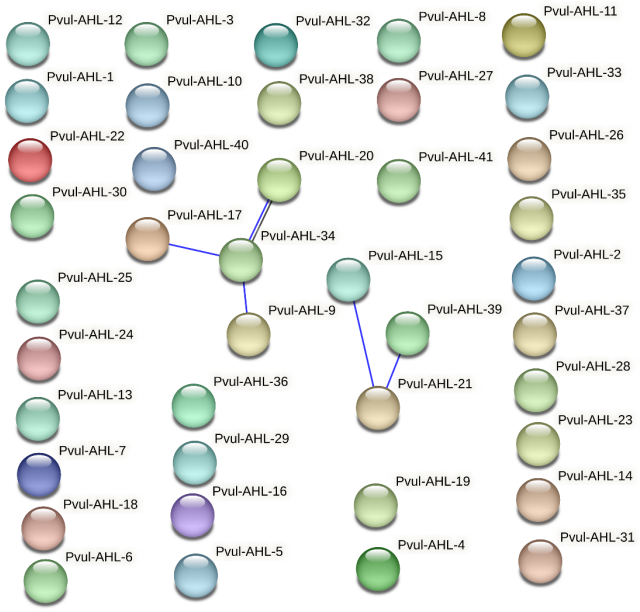

Figure 8. Protein–protein interactions of identified AHL proteins. Protein-protein interactions of *Pvul-AHL* proteins have been analyzed and visualized using the STRING database. Related genes are shown with blue line.

Expression Analysis of *AHL* Genes

The expression profiles of *AHL* genes in leaf tissues of *P. vulgaris* under salt and drought stress were examined using information from the NCBI SRA repository. In drought stress, the expression levels of *Pvul-AHL-19*, *Pvul-AHL-22*, *Pvul-AHL-34* and *Pvul-AHL-40* genes increased compared to the control. In salt stress, the expression levels of *Pvul-AHL-23*, *Pvul-AHL-29*, *Pvul-AHL-36*, *Pvul-AHL-40* and *Pvul-AHL-41* genes increased compared to the control. No change was observed in the expression levels of *Pvul-AHL-5*, *Pvul-AHL-17*, *Pvul-AHL-18*, *Pvul-AHL-19*, *Pvul-AHL-20*, *Pvul-AHL-21*, *Pvul-AHL-22*, *Pvul-AHL-34* and *Pvul-AHL-35* genes under salt stress (Figure 9).

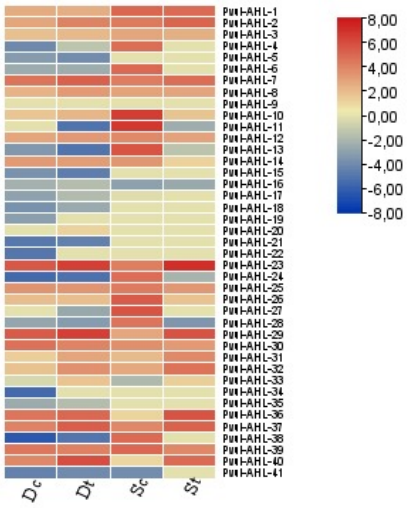

Figure 9. Heat map of the *Pvul-AHL* genes that are differentially expressed in leaf tissue under salt and drought stress. C: control, T: treatment, S: salt, D: drought. The expression levels are represented according to the color bar.

4. Conclusions

An essential transcription factor in plants, the AHL protein controls a variety of biological processes. *AHL* have been the subject of ongoing research into their evolution and role ever since their discovery. The expression differences of *Pvul-AHL* genes were determined in the gene expression analyzes performed in silico in leaf tissues under salt and drought stress. This evaluation will serve as a starting point for additional functional research and crop breeding. The results of this study will shed light on future studies with *P. vulgaris*.

Author Contributions

All authors contributed equally to the writing of this manuscript.

Acknowledgements

This study was presented at the "The 6th Symposium on EuroAsian Biodiversity (SEAB) 2023" and published in the Symposium Book as an abstract.

References

[1] Petry, N., Boy, E., Wirth, J.P., and Hurrell, R.F., (2015) Review: The potential of the common bean (*Phaseolus vulgaris*) as a vehicle for iron biofortification, *Nutrients*, 7, 1144–1173. doi: 10.3390/nu7021144. Physiol., 129, 500–15.

[2] Pereira, W. J., Melo, A. T. D. O., Coelho, A. S. G., Rodrigues, F. A., Mamidi, S., Alencar, S. A. D., Vianello, R. P., (2020) Genome-wide analysis of the transcriptional response to drought stress in root and leaf of common bean, *Genetics and Molecular Biology*, *43*.

[3] Lynch, M., Conery, J. S., (2003) The origins of genome complexity, *Science*, *302*(5649), 1401-1404.

[4] Bowman, J. L., Floyd, S. K., Sakakibara, K., (2007) Green genes—comparative genomics of the green branch of life, *Cell*, *129*(2), 229-234.

[5] Zhao, J., Favero, D. S., Peng, H., Neff, M. M., (2013) Arabidopsis thaliana AHL family modulates hypocotyl growth redundantly by interacting with each other via the PPC/DUF296 domain, *Proceedings of the National Academy of Sciences*, *110*(48), E4688-E4697.

[6] Goodwin, G. H., Sanders, C., Johns, E. W., (1973) A new group of chromatin-associated proteins with a high content of acidic and basic amino acids, *European Journal of Biochemistry*, *38*(1), 14-19.

[7] Eckner, R., Birnstiel, M. L., (1989) Cloning of cDNAs coding for human HMG I and HMG Y proteins: both are capable of binding to the octamer sequence motif, *Nucleic acids research*, *17*(15), 5947-5959.

[8] Wang, H., Leng, X., Yang, J., Zhang, M., Zeng, M., Xu, X., Li, C., (2021) Comprehensive analysis of AHL gene family and their expression under drought stress and ABA treatment in *Populus trichocarpa*, *PeerJ*, *9*, e10932.

[9] Širl, M., Šnajdrová, T., Gutiérrez-Alanís, D., Dubrovsky, J. G., Vielle-Calzada, J. P., Kulich, I., Soukup, A., (2020) At-hook motif nuclear localised protein 18 as a novel modulator of root system architecture, *International journal of molecular sciences*, *21*(5), 1886.

[10] Lou, Y., Xu, X. F., Zhu, J., Gu, J. N., Blackmore, S., Yang, Z. N., (2014) The tapetal AHL family protein TEK determines nexine formation in the pollen wall, *Nature Communications*, *5*(1), 1-9.

[11] Jin, Y., Luo, Q., Tong, H., Wang, A., Cheng, Z., Tang, J., Zhu, L., (2011) An AT-hook gene is required for palea formation and floral organ number control in rice, *Developmental biology*, *359*(2), 277-288.

[12] Xu, Y., Gan, E. S., Ito, T., (2013) The AT-hook/PPC domain protein TEK negatively regulates floral repressors including MAF4 and MAF5, *Plant signaling & behavior*, *8*(8), e25006.

[13] Lim, P. O., Kim, Y., Breeze, E., Koo, J. C., Woo, H. R., Ryu, J. S., Nam, H. G., (2007) Overexpression of a chromatin architecture-controlling AT-hook protein extends leaf longevity and increases the post-harvest storage life of plants, *The Plant Journal, 52*(6), 1140-1153.

[14] Matsushita, A., Furumoto, T., Ishida, S., Takahashi, Y., (2007) AGF1, an AT-hook protein, is necessary for the negative feedback of AtGA3ox1 encoding GA 3-oxidase, *Plant physiology*, *143*(3), 1152-1162.

[15] Rashotte, A. M., Carson, S. D., To, J. P., Kieber, J. J., (2003) Expression profiling of cytokinin action in *Arabidopsis*, *Plant Physiology*, *132*(4), 1998-2011.

[16] Bishop, E. H., Kumar, R., Luo, F., Saski, C., Sekhon, R. S., (2020) Genome-wide identification, expression profiling, and network analysis of AT-hook gene family in maize, *Genomics*, *112*(2), 1233-1244.

[17] Zhou, L., Liu, Z., Liu, Y., Kong, D., Li, T., Yu, S., Mei, H., Xu, X., Liu, H., Chen, L., & Luo, L. (2016). A novel gene OsAHL1 improves both drought avoidance and drought tolerance in rice. Scientific reports, 6, 30264. https://doi.org/10.1038/srep30264.

[18] Zhou, J., Wang, X., Lee, J. Y., Lee, J. Y., (2013) Cell-to-cell movement of two interacting AT-hook factors in Arabidopsis root vascular tissue patterning, *The Plant Cell*, *25*(1), 187-201.

[19] Kumar, A., Singh, S., Mishra, A., (2023) Genome-wide identification and analyses of the AHL gene family in rice (*Oryza sativa*), *3 Biotech*, *13*(7), 248.

[20] Zhao, L., Lü, Y., Chen, W., Yao, J., Li, Y., Li, Q., Zhang, Y., (2020) Genome-wide identification and analyses of the AHL gene family in cotton (*Gossypium*), *BMC genomics*, *21*(1), 1-14.

[21] Machaj, G., Grzebelus, D., (2021) Characteristics of the AT-hook motif containing nuclear localized (AHL) genes in carrot provides insight into their role in plant growth and storage root development, *Genes*, *12*(5), 764.

[22] Wang, M., Chen, B., Zhou, W., Xie, L., Wang, L., Zhang, Y., Zhang, Q. (2021). Genome-wide identification and expression analysis of the AT-hook Motif Nuclear Localized gene family in soybean. *BMC Genomics, 22*(1), 361.

[23] Li, X., He, H., Wang, H., Wu, X., Wang, H., Mao, J., (2021) Identification and expression analysis of the AHL gene family in grape (*Vitis vinifera*), *Plant Gene*, *26*, 100285.

[24] Zhang, W. M., Fang, D., Cheng, X. Z., Cao, J., Tan, X. L., (2021) Insights Into the Molecular Evolution of AT-Hook Motif Nuclear Localization Genes in *Brassica napus, Frontiers in Plant Science*, *12*.

[25] Zhang, X., Li, J., Cao, Y., Huang, J., Duan, Q., (2023) Genome-Wide Identification and Expression Analysis under Abiotic Stress of BrAHL Genes in *Brassica rapa*, *International Journal of Molecular Sciences*, *24*(15), 12447.

[26] Zhao, J., Xu, E., Wang, Q., (2023) Dissection of AT-Hook Motif Nuclear-Localized Genes and Their Potential Functions in Peach Growth and Development, *Forests*, *14*(7), 1404.

[27] Schmutz, J., McClean, P. E., Mamidi, S., Wu, G. A., Cannon, S. B., Grimwood, J., Jackson, S. A., (2014) A reference genome for common bean and genome-wide analysis of dual domestications, Nature genetics, 46(7), 707-713.

[28] Lamesch, P., Berardini, T. Z., Li, D., Swarbreck, D., Wilks, C., Sasidharan, R., Huala, E. (2012) The Arabidopsis Information Resource (TAIR): improved gene annotation and new tools, *Nucleic Acids Research*, *40*(D1), D1202-D1210.

[29] Zhao, J., Favero, D. S., Qiu, J., Roalson, E. H., Neff, M. M., (2014) Insights into the evolution and diversification of the AT-hook Motif Nuclear Localized gene family in land plants, *BMC plant biology*, *14*(1), 1-19.

[30] Goodstein, D.M., Shu S., Howson, R., Neupane, R., Hayes, R.D., Fazo, J., Mitros, T., Dirks, W., Hellsten, U., Putnam, N., Rokhsar, D.S. (2012) Phytozome: a comparative platform for green plant genomics, *Nucleic Acids Research*. *40*(D1), D1178-D1186.

[31] Mistry, J., Chuguransky, S., Williams, L., Qureshi, M., Salazar, G.A., Sonnhammer, E.L.L., Tosatto, S.C.E., Paladin, L., Raj, S., Richardson, L.J., Finn, R.D., Bateman A. (2020) Pfam: The protein families database in 2021, *Nucleic Acids Research*, *49,* D412-D419.

[32] Letunic, I., Khedkar, S., Bork, P. (2021) SMART: recent updates, new developments and status in 2020", *Nucleic Acids Research*, *49*, D458–D460.

[33] Thompson, J.D., Gibson, T.J., Plewniak, F., Jeanmougin, F., Higgins, D.G. (1997) The CLUSTAL_X windows interface: flexible strategies for multiple sequence alignment aided by quality analysis tools, *Nucleic Acids Research*, *25*, 4876-4882.

[34] Letunic, I., Bork, P. (2021) Interactive Tree of Life (iTOL) v5: an online tool for phylogenetic tree display and annotation, *Nucleic Acids Research*, *49*, W293–W296.

[35] Gasteiger, E., Hoogland, C., Gattiker, A., Duvaud, S., Wilkins, M.R., Appel, R.D., Bairoch, A. (2005) Protein Identification and Analysis Tools on the Expasy Server, The Proteomics Protocols Handbook, Humana Press.

[36] Hu, B., Jin, J.¸ Guo, A.Y., Zhang, H., Luo, J., Gao, G. (2015) GSDS 2.0: an upgraded gene feature visualization server, *Bioinformatics*, *31*, 1296-1297.

[37] Voorrips, R.E. (2002) MapChart: Software for the Graphical Presentation of Linkage Maps and QTLs. *Journal of Heredity*, *93*(1), 77–78.

[38] Lescot, M., Déhais, P., Thijs, G., Marchal, K., Moreau, Y., Van de Peer, Y., Rombauts, S. (2002) PlantCARE, a database of plant cis-acting regulatory elements and a portal to tools for in silico analysis of promoter sequences, Nucleic acids research, 30(1), 325-327.

[39] Bailey, T.L., Williams, N., Misleh, C., Li, W.W. (2006) MEME: discovering and analyzing DNA and protein sequence motifs, *Nucleic Acids Research*, *34*, W369-W373.

[40] Chen, C., Chen, H.¸ Zhang, Y., Thomas, H.R., Frank, M.H., He, Y.¸ Xia, R. TBtools: An Integrative Toolkit Developed for Interactive Analyses of Big Biological Data, *Molecular Plant*, *13*(8), 1194-1202, 2020.

[41] Szklarczyk, D., Gable, A.L., Lyon, D., Junge, A., Wyder, S., Huerta-Cepas, J., Simonovic, M., Doncheva, N.T., Morris, J.H., Bork, P., Jensen, L.J., Mering, C.V. (2019) STRING v11: protein-protein association networks with increased coverage, supporting functional discovery in genome-wide experimental datasets, *Nucleic Acids Research*, *47*(D1), D607–D613.

[42] Hiz, M. C., Canher, B., Niron, H., Turet, M., (2014) Transcriptome analysis of salt tolerant common bean (*Phaseolus vulgaris* L.) under saline conditions, *PloS one*, *9*(3), e92598.

[43] Mortazavi, A., Williams, B. A., McCue, K., Schaeffer, L., Wold, B., (2008) Mapping and quantifying mammalian transcriptomes by RNA-Seq, Nature methods, 5(7), 621-628.

[44] Luna, A., Elloumi, F., Varma, S., Wang, Y., Rajapakse, V.N., Aladjem, M.I., Robert, J., Sander, C., Pommier, Y., Reinhold, W.C. (2021) CellMiner Cross-Database (CellMinerCDB) version 1.2: Exploration of patient-derived cancer cell line pharmacogenomics. *Nucleic Acids Research*, *49*(D1), D1083-D1093.

[45] Bishop, E. H., Kumar, R., Luo, F., Saski, C., & Sekhon, R. S. (2020) Genome-wide identification, expression profiling, and network analysis of AT-hook gene family in maize. *Genomics*, *112*(2), 1233-1244.

[46] Rakhimzhanova, A., Kasapoğlu, A.G., Sapakova, A., İlhan, E., Zharmukhametova, R., Turan, M., Zekenova, L., Muslu, S., Kazhygeldiyeva, L., Aydın, M., Çiltaş, A. (2023) Expression analysis and characterization of the CPP gene family of Melatonin-treated common bean cultivars under different abiotic stresses, *South African Journal of Botany*, *160*, 282-294.

Erzincan Üniversitesi
Fen Bilimleri Enstitüsü Dergisi
2024,17(1), 164-173
ISSN: 1307-9085, e-ISSN: 2149-4584
Araştırma Makalesi

Erzincan University
Journal of Science and Technology
2024,17(1), 164-173
DOI: 10.18185/erzifbed.1376859
Research Article

The Combined Effect of Vulpinic Acid and Doxorubicin in Breast Cancer MCF-7 Cells

Esma Kübra KAĞAN YENİÇERİ [1], Ahmet ALTAY [2*]

[1] Institute of Science and Technology, Erzincan Binali Yıldırım University, 24030, Erzincan, Turkey
[2]Department of Chemistry, Faculty of Arts and Science, Erzincan Binali Yıldırım University, 24100, Erzincan, Turkey

Received: 16/10/2023, **Revised:** 11/12/2023, **Accepted:** 11/12/2023, **Published:** 28/03/2024

Abstract

Breast cancer is a major global health problem that imposes a significant social and economic burden on individuals and societies. Chemotherapy, a common treatment approach, often leads to resistance and unwanted side effects, especially in the advanced stages of the disease. This has led to a search for more effective and less toxic anticancer agents. Lichens, associations of fungi and algae, are gaining attention for their potential in cancer therapy. Lichens are rich sources of secondary metabolites with diverse biological effects, including anti-tumor properties. In this study, we summarise the combined effects of vulpinic acid a lichen acid, with doxorubicin, a chemotherapeutic drug, on breast cancer MCF-7 cells. The results of the XTT assay and subsequent Compusyn analysis showed that VA and doxorubicin, a chemotherapeutic drug, alone exhibited potent anti-proliferative effects in a dose- and time-dependent manner, and interestingly, when used in combination, they produced an antagonistic effect in the same cancer line. These results provide the first example of a study to show what effect the combination of VA and Dox will have on other breast cancer cell lines.
Keywords: breast cancer, vulpinic acid, doxorubicin, combination effect.

Vulpinik Asit ve Doksorubisinin Meme Kanseri MCF-7 Hücrelerinde Kombine Etkisi

Öz

Meme kanseri bireylere ve toplumlara önemli sosyal ve ekonomik yük getiren önemli bir küresel sağlık sorunudur. Yaygın bir tedavi yaklaşımı olan kemoterapi, özellikle hastalığın ileri evrelerinde sıklıkla direnç ve istenmeyen yan etkilere yol açmaktadır. Bu durum daha etkili ve daha az toksik antikanser ajanlarının araştırılmasına yol açmıştır. Mantar ve alglerin birleşimi olan likenler, kanser tedavisindeki potansiyelleri nedeniyle dikkat çekmektedir. Likenler, anti-tümör özellikleri de dahil olmak üzere çeşitli biyolojik etkilere sahip, zengin ikincil metabolit kaynaklarıdır. Bu çalışmada, bir liken asit olan vulpinik asidin kemoterapötik bir ilaç olan doksorubisin ile meme kanseri MCF-7 hücreleri üzerindeki kombine etkileri araştırıldı. XTT testinin sonuçları ve ardından Compusyn analizleri, VA ve kemoterapötik bir ilaç olan doksorubisinin, yalnız hallerinde doz ve zaman bağımlı olarak güçlü anti-proliferatif etkiler sergilediğini, öte yandan ilginç bir şekilde, kombine halinde kullanıldıklarında aynı kanser hattında antagonistik bir etki sergiledikleri belirlendi. Bu sonuçlar, VA ve Dox kombinasyonunun diğer meme kanseri hücre hatları üzerinde nasıl bir etki yaratacağını gösteren bir çalışmanın ilk örneğini sağlamıştır.
Anahtar Kelimeler: meme kanseri, vulpinik asit, doksorubisin, kombine etki

*Corresponding Author: aaltay2013@gmail.com
Esma Kübra KAĞAN YENİÇERİ, https://orcid.org/0000-0001-8120-8900
Ahmet ALTAY, https://orcid.org/0000-0001-8120-8900

1. Introduction

Cancers are malignant tumors that result from the uncontrolled growth of cells in tissues or organs [1]. Cancer is not only a growing public health problem but also a social and economic burden for societies. Breast cancer is the most commonly diagnosed cancer and the second most common cause of cancer-related death in women after lung cancer [2, 3]. Today, the most common treatments for breast cancer are surgery, radiotherapy, and chemotherapy. Depending on the type and stage of cancer, chemotherapy is used to treat the disease, prevent the spread of the tumor, slow its growth, and improve some symptoms of cancer, and in some cases, chemotherapy is the only treatment option. Some of the chemotherapeutic drugs commonly used for breast cancer treatment are cisplatin, docetaxel, and doxorubicin [4]. The mechanism of action of each chemotherapy drug may be the same and/or different. Doxorubicin (DOX), for example, interacts with DNA to provide its most effective mechanism of action against cancer. Doxorubicin stabilizes the topoisomerase-DNA complex that forms after topoisomerase II cuts the DNA during DNA transcription. This prevents the DNA double helix from recombining, thus preventing DNA from pairing [5]. Although these synthetic drugs, including Dox, are used in the treatment of cancer, they have many undesirable side effects in patients undergoing treatment [6]. For instance, nausea, vomiting, irregular heartbeat, neutropenia, baldness, heart failure, and cardiomyopathy are some of the side effects of doxorubicin [4]. As cancer is one of the most common diseases of our time, and the number of cancer diagnoses is increasing every day, scientists are working hard to discover and develop new drugs with fewer side effects [7]. More than 60% of cancer drugs in use today are developed from natural sources such as plants, bacteria, fungi, and marine organisms [8]. Medically important plants with pharmaceutical properties have been used for centuries by the general public in all developing and developed countries for the treatment of a wide range of diseases [9].

Many of the therapeutic properties of these medicinal plants are due to the secondary metabolites that they contain. Secondary metabolites have many biological effects including antiviral, antibacterial, antifungal, antiprotozoal, anti-herbicidal, mutagenic, antioxidative, antiulcer, antipyretic, anti-inflammatory, and anti-tumor [10]. Besides medicinal plants, there are still many natural resources that have not been adequately explored, including lichens formed by the symbiotic association of fungi and algae [11]. Similar to medicinal plants, lichens have many biological properties, including anti-cancer effects, thanks to the lichen secondary metabolites. Vulpinic acid (VA), one of the lichens' secondary metabolites, is known to have many biological properties including antimicrobial [12], antidiabetic [13], and anticancer activities [14]. Even, our previous study found that VA has significant anti-cancer potential in many cancers, including breast cancer [11]. The drugs used in chemotherapy either become less effective during treatment or cancer cells can develop resistance to these drugs. For this reason, several drugs may be given in combination to make the treatment more effective [15, 16]. Indeed, studies of the combined effects of currently used chemotherapeutic drugs and secondary metabolites with anticancer potential have gained momentum over recent years. While the literature contains studies on the anti-cancer effects of the chemotherapy agents DOX and VA

on breast cancer alone, no data exist on the effect of these two compounds on cancer cells when used together [11]. In this regard, the dose- and time-dependent anticancer effects of the two aforementioned compounds, both alone and in combination at different doses, were comparatively investigated on the breast cancer cell line MCF-7.

2. Material and Methods

2.1. Cell lines and culture

The breast cancer MCF-7 cell line was purchased from the ATCC (American Type Culture Collection, LGC Promochem, UK). The MCF-7 cell line was cultured in Dulbecco's Modified Eagle Medium (DMEM, Sigma-Aldrich). Basal mediums were supplemented with 10% (v/v) heat-inactivated fetal bovine serum (FBS) (HyClone), 1% l-glutamine (Thermo Fisher Scientific), 1% penicillin, and streptomycin (Sigma-Aldrich). Cells were maintained in a 5% CO_2 incubator at 37 °C. All the studies were carried out in the biosafety -II cabine (Nuve, Turkey).

2.2. Preparation of chemicals doxorubicin and vulpinic acid.

Vulpinic Acid (VA) was purchased from Cayman Chemicals Company. Doxorubicin (DOX) was purchased from Cell Signaling Technology. The chemicals were dissolved in dimethyl sulfoxide (DMSO, Sigma-Aldrich) as a stock solution and stored at −20 °C until usage. The various concentrations of VA ranging from 5 to 150 µM were performed with the culture mediums. Similarly, the different concentrations of DOX were prepared ranging from 0.05-100 µM with the complete culture medium.

2.3. Cell proliferation assay

The dose- and time-dependent antiproliferative effects of vulpinic acid (VA) and doxorubicin (DOX), alone and in combination, on breast cancer cell lines were investigated using 2,3-bis(2-methoxy-4-nitro-5-sulfophenyl)-2H-tetrazolium-5-carboxanilide (XTT) assay. The principle underlying the assay is that only living cells have an active metabolism and can convert XTT to purple formazan, which has a maximum absorbance of 490 nm [17, 18]. Firstly, the dose- and time-dependent antiproliferative effects of DOX and VA alone on MCF-7 cell was investigated. For this purpose, both cell lines were plated in 96-well plates with 7500 cells per well in 150 µL of medium and kept overnight in a 5% CO_2 incubator at 37°C. This process was performed separately for each time point (24, 48, and 72h). The following day, different doses (0.1, 1, 10, 50, and 100 µM) obtained from the stock solution of Dox were applied to the cell line, and the plates were kept in the 5% CO_2 incubator for each period. The same procedure was performed for VA at varying concentrations depending on the cell type (10, 25, 50, 75, 100, and 150 µM). At the end of each incubation period, the old medium in the wells was removed and the wells were washed with PBS. Subsequently, 50 µL of XTT solution was added to the wells together with 100 µL of fresh medium, and after incubation in the 5% CO_2 incubator for 5 hours, the absorbances were measured at 490 nm. The cells containing only fresh medium were used as vehicle control. The cell proliferation was calculated with the help of the following equation;

Proliferation % = [Abs $_{(extract\text{-}treated\ cells)}$ - Abs $_{(extract\ in\ cell\text{-}free\ medium)}$] / [Abs $_{(control\ group\ cells)}$ - Abs $_{(cell\text{-}free\ medium)}$].

Considering the data obtained from XTT assays, different concentrations of DOX and VA were combined (VA+DOX), and XTT experiments were performed similarly. The absorbances obtained here and in the previous step were entered into the Compusyn program and CI Combinational Index (CI) values were calculated. CI is the value indicating the effect on the cell of combining two or more drugs. The CI value obtained from combination studies between 1 and 10 means that the effect is antagonistic, equal to 1 means that the effect is additive, and between 0.9 and 0 means that the effect is synergistic [19].

2.4. Statistical analysis

The results of the XTT assay were analyzed using the unpaired t-test with the GraphPad Prism software version 6.0. The COMPUSYN program was used to calculate the Combination Index (CI) results. Three independent experiments were conducted in every group, and all measurements were performed three times. $p < 0.05$ was considered statistically significant.

3. Results and Discussion

To determine the antiproliferative effects of DOX and VA alone against MCF-7 cancer cells, different concentrations of DOX ranging from 0.1 to 100 µM and various concentrations of VA ranging from 10 to 150 µM were applied to the MCF-7 cells for three different periods (24, 48, and 72 h). The results of the XTT experiments were presented in Table 1.

Table 1. Dose- and time-dependent inhibitory effects of DOX and VA on MCF-7 cells.

24 h			
Doxorubicin (µM)	**%inhibition**	**Vulpinic Acid (µM)**	**%inhibition**
0.1	46.24	10	10.29
1	57.74	25	25.82
10	86.31	50	30.21
50	≥100	75	37.60
100	≥100	100	56.25
48 h			
Doxorubicin (µM)	**%inhibition**	**Vulpinic Acid (µM)**	**%inhibition**
0.1	83.01	10	52.48
1	85.90	25	58.69
10	97.25	50	59.86
50	≥100	75	71.88
100	≥100	100	73.03
72 h			
Doxorubicin (µM)	**%inhibition**	**Vulpinic Acid (µM)**	**%inhibition**
0.1	94.81	10	78.72
1	94.55	25	88.35
10	97.51	50	89.79
50	≥100	75	≥100
100	≥100	100	≥100

Examining the dose-dependent inhibitory effects of DOX on MCF-7 cells at the end of each period individually from Table 1, it can be seen that DOX inhibited 46.24% cell proliferation at 0.1 µM, and this inhibition increased to 86 % at 10 µM after 24 h. At a concentration of 50 µM, DOX almost completely stopped cell proliferation. The 48 h results showed that DOX inhibited cell proliferation by 86.3 % at a concentration of 0.1 µM, and by increasing the concentration to 10 µM, inhibition increased to 97.2 %. At the end of 72 h, even the lowest dose of DOX increased cell proliferation inhibition to around 95%. These data reveal that DOX has a strong anticancer effect on MCF-7 cells in a dose- and time-dependent manner.

Similarly, when the antiproliferative activity of VA, one of the lichen metabolites, was tested against MCF-7 cells after 24 h, it was found to have a significant dose-dependent antiproliferative effect between 10 and 100 µM. While VA showed 10.29 % inhibition at the lowest dose of 10 µM, the inhibition rate reached 50 % at the highest dose of 100 µM. A dose-dependent inhibition was observed with increasing incubation time. VA, for instance, was found to inhibit cell proliferation by 52.4 % and 78.7 % at the lowest concentration of 10 µM after 48 and 72 h, respectively.

Detailed information on the anti-cancer mechanism of DOX, which is commercially used as a chemotherapeutic agent, is available in the literature. The number of studies on the biological activity of VA, a natural product, including its anti-cancer activity, is increasing day by day. In addition, it has been reported in several studies on the mechanism of action of VA in cancer. Kilic et al. (2018) reported the antiproliferative and apoptotic effects of VA on human breast cancer MCF-7 and non-cancerous MCF-12A cell lines. The results showed that VA significantly inhibited cell viability and induced apoptosis of human breast cancer cells while While it has no significant cytotoxic or apoptotic effects on non-cancerous cells [14]. Cansaran-Duman et al. (2021) investigated the role of vulpinic acid (VA) on the progression of breast cancer and reported that VA could downregulate the expression of 12 miRNAs by silencing the FOXO-3 gene [20]. Another study reported that VA exhibited anti-cancer activity in the breast cancer cell lines MCF-7 and MDA-MB-453 by inhibiting Thioredoxin reductases-1 (TRXR1) enzyme, which is recognized as a cancer marker, preventing migration and inducing apoptosis [11].

Recently, as cancer tumors develop resistance to the drugs used in chemotherapy over time, and the effects of these drugs are not sufficient, there has been an increase in the use of combinations of different drugs to treat patients. For example, Jin et al (2021) applied the combination of platycodin and docetaxel to prostate cancer DU-145 cells and reported that it synergistically inhibited cell growth, upregulated the Bax/Bcl-2 ratio, increased apoptosis, and ROS production, and suppressed the AKT/mTOR and ERK signaling pathways. [15]. Shokrzadeh et al (2021) applied the combination of Dox with lutein to the MCF-7 cells and reported that the result was a significant decrease in antioxidant enzymes while a significant increase in ROS levels, with a synergistic anticancer mechanism. [16].

In this regard, at this stage of the study, the aim was to apply different doses of combinations of VA, which is a natural compound and may have much fewer side effects in living organisms compared to synthetic drugs, and DOX, a drug widely used in chemotherapy, to MCF-7 cancer cells and then determine whether this situation is synergistic or antagonistic in the cell. The period over which the results of VA and DOX would be used to decide on combination studies was evaluated by looking at Table 1. For each dose of DOX, from lowest to highest, similar doses of VA were combined and applied to the cells, taking into account the data at 48 hours, which is the most effective period. For this, each combined dose of DOX + VA was prepared and applied to MCF-7 cells for 48 h and subjected to antiproliferative activity tests using XTT assay. The absorbance values obtained from the XTT tests were processed in the Compusyn program and CI values were calculated (Figure. 1).

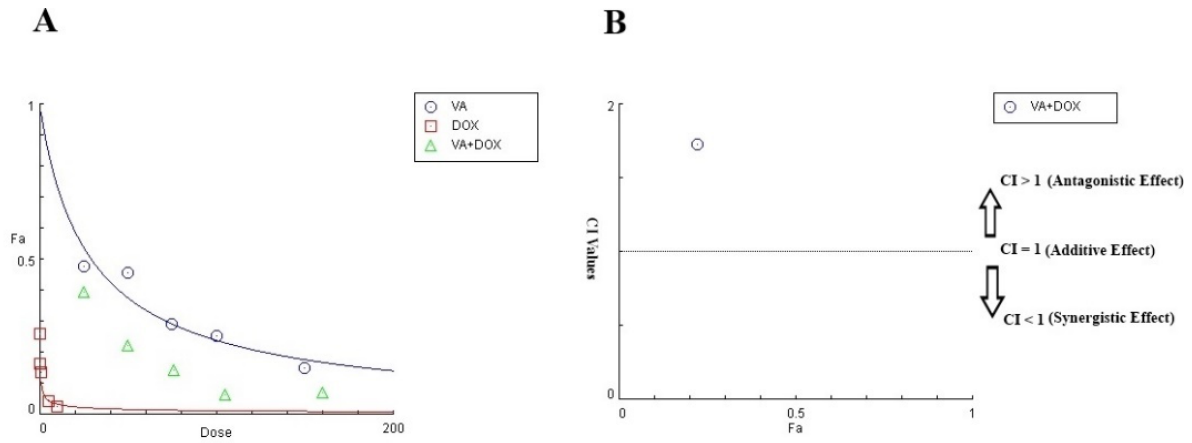

Figure 1. Compusyn results of vulpinic acid (VA) and Doxorubicin (DOX) in MCF-7 cells. **A)** Dose effect curves for VA, DOX, and VA+ DOX combination, **B)** Combination Index Value – Fa (Fraction Affected Level) for VA+ DOX. The value obtained in the combination index indicates a mild antagonism when 1.1 - 1.2, a moderate antagonism when 1.2 - 1.45, 1.45 - 3.3 antagonism, 3.3 - 10 strong antagonism, > 10 very strong antagonism, 0.85 - 0.9 mild synergy, 0.7 - 0.85 moderate synergy, 0.3 - 0.7 synergy, 0.1 - 0.3 strong synergy, < 0.1 very strong synergy.

Table 2. Combined effects and CI values of VA+DOX in MCF-7 cells

VA+DOX (µM)	Absorbance	CI
25-0.05	0.394	4.73265
50-0.1	0.222	1.72574
75-1	0.144	4.19017
100-5	0.064	2.62389
150-10	0.070	6.37395

CI: Combination Index

Looking at the data in Table 2, although each combined version of VA and DOX reduces the proliferation of MCF-7 cancer cells, each of the CI values is greater than 1. This indicates that the two compounds used in combination produced an antagonistic effect in this cell line, weakening each other to some extent, rather than having a synergistic effect. MCF-7 cells are known to be estrogen receptor-positive (ER+). Therefore, anti-cancer agents that act on this cell line bind to these receptors and exert their effects on the cell. While both compounds studied here showed a strong antiproliferative effect alone, presumably by binding to these receptors, when combined they showed an antagonistic situation, reducing the rate or ability to bind to this receptor and some extent preventing each other from binding. Although the combined use

of VA+ DOX has an antagonistic effect on MCF-7 cells in this study, further studies are needed to determine the effect of the combination on MDA-MB-453, MDA-MB-231, and other similar breast cancer cell lines.

4. Conclusion

As a result, this study showed that VA and DOX alone exerted a dose- and time-dependent anticancer effect on MCF-7 cells, whereas it was expected that they would exert a stronger anticancer effect when combined, but they weakened each other's effect by showing an antagonistic effect.

Ethics in Publishing

There are no ethical issues regarding the publication of this study.

Author Contributions

Conceived and designed the experiments: Dr. Ahmet Altay (AA), and Esma Kübra KAĞAN YENİÇERİ (EKKY). Performed the experiments: AA, and EKKY. Analyzed the data: AA, and EKKY. Contributed reagents/materials/analysis tools: AA, and EKKY. Wrote the paper: AA, and EKKY. The final version of the manuscript was read and approved by all authors.

Acknowledgments

I would like to thank the 100/2000 YÖK Doctoral Project, which financially supported my doctoral thesis in the field of "Natural and Herbal Products/Cosmetics". This study is part of the doctoral thesis. I would also like to thank the Erzincan Binali Yıldırım University Basic Sciences Application and Research Center and, Medicinal Aromatic Plants Application and Research Center for all the experiments that were carried out.

References

[1] Hausman, D. M. (2019). What is cancer?. Perspectives in biology and medicine, 62(4), 778-784.

[2] DeSantis, C. E., Ma, J., Gaudet, M. M., Newman, L. A., Miller, K. D., Goding Sauer, A., Siegel, R. L. (2019). Breast cancer statistics, 2019. CA: a cancer journal for clinicians, 69(6), 438-451.

[3] Sung, H., Ferlay, J., Siegel, R. L., Laversanne, M., Soerjomataram, I., Jemal, A., & Bray, F. (2021). Global cancer statistics 2020: GLOBOCAN estimates of incidence and mortality worldwide for 36 cancers in 185 countries. CA: a cancer journal for clinicians, 71(3), 209-249.

[4] Nicoletto, R. E., & Ofner III, C. M. (2022). Cytotoxic mechanisms of doxorubicin at clinically relevant concentrations in breast cancer cells. Cancer Chemotherapy and Pharmacology, 89(3), 285-311.

[5] Thorn, C. F., Oshiro, C., Marsh, S., Hernandez-Boussard, T., McLeod, H., Klein, T. E., & Altman, R. B. (2011). Doxorubicin pathways: pharmacodynamics and adverse effects. Pharmacogenetics and genomics, 21(7), 440.

[6] Epstein, J. B. (2007). Mucositis in the cancer patient and immunosuppressed host. Infectious disease clinics of North America, 21(2), 503-522.

[7] Temel, Y., Kucukler, S., Yıldırım, S., Caglayan, C., & Kandemir, F. M. (2020). Protective effect of chrysin on cyclophosphamide-induced hepatotoxicity and nephrotoxicity via the inhibition of oxidative stress, inflammation, and apoptosis. Naunyn-Schmiedeberg's archives of pharmacology, 393, 325-337.

[8] Mondal, S., Bandyopadhyay, S., K Ghosh, M., Mukhopadhyay, S., Roy, S., & Mandal, C. (2012). Natural products: promising resources for cancer drug discovery. Anti-Cancer Agents in Medicinal Chemistry (Formerly Current Medicinal Chemistry-Anti-Cancer Agents), 12(1), 49-75.

[9] Baytop, T. (1999). Therapy with medicinal plants in Turkey (past and present). Publication of the istanbul University, 312, 2-3.

[10] Mitrović, T., Stamenković, S., Cvetković, V., Nikolić, M., Tošić, S., & Stojičić, D. (2011). Lichens as source of versatile bioactive compounds. Biologica Nyssana, 2(1), 1-6.

[11] Kalın, Ş. N., Altay, A., & Budak, H. (2022). Inhibition of thioredoxin reductase 1 by vulpinic acid suppresses the proliferation and migration of human breast carcinoma. Life Sciences, 310, 121093.

[12] Lauterwein, M., Oethinger, M., Belsner, K., Peters, T., & Marre, R. (1995). In vitro activities of the lichen secondary metabolites vulpinic acid,(+)-usnic acid, and (-)-usnic acid against aerobic and anaerobic microorganisms. Antimicrobial agents and chemotherapy, 39(11), 2541-2543.

[13] Demir, Y., Ceylan, H., Türkeş, C., & Beydemir, Ş. (2022). Molecular docking and inhibition studies of vulpinic, carnosic and usnic acids on polyol pathway enzymes. Journal of Biomolecular Structure and Dynamics, 40(22), 12008-12021.

[14] Kılıç, N., Aras, S., & Cansaran-Duman, D. (2018). Determination of vulpinic acid effect on apoptosis and mRNA expression levels in breast cancer cell lines. Anti-Cancer Agents in Medicinal Chemistry (Formerly Current Medicinal Chemistry-Anti-Cancer Agents), 18(14), 2032-2041.

[15] Jin, Y. Y., Li, Y. J., Ge, D. S., Zhu, L. L., Wang, Y. Y., Luo, J., ... & Chen, Y. Q. (2021). Combination of Platycodin D with docetaxel synergistically suppressed cell growth in DU-145 by enhancing apoptosis and alleviating autophagy. European Journal of Integrative Medicine, 42, 101302.

[16] Shokrzadeh, M., Mortazavi, P., Moghadami, A., Khayambashi, B., & Motafeghi, F. (2021). Synergistic antiproliferative and anticancer activity of carotenoid lutein or coenzyme Q10 in combination with doxorubicin on the MCF7 cell line. Applied In Vitro Toxicology, 7(4), 167-174.

[17] De Logu, A., Pellerano, M. L., Sanna, A., Pusceddu, M. C., Uda, P., & Saddi, B. (2003). Comparison of the susceptibility testing of clinical isolates of Mycobacterium tuberculosis by the XTT colorimetric method and the NCCLS standards method. International journal of antimicrobial agents, 21(3), 244-250.

[18] Altay, A., & Budak, H. (2023). Diffractaic acid exhibits thioredoxin reductase 1 inhibition in lung cancer A549 cells.

[19] Sever, A. (2018). Mcf-7 hücrelerinde oksidatif hasara karşı cisplatin ile kombinasyonda resveratrolün sinerjik etkisi ve oksidatif stres indeksi (Doctoral dissertation, Anadolu University (Turkey)).

[20] Cansaran-Duman, D., Yangin, S., & Çolak, B. (2021). The role of vulpinic acid as a natural compound in the regulation of breast cancer-associated miRNAs. Biological Research, 54.

Erzincan Üniversitesi
Fen Bilimleri Enstitüsü Dergisi
2024,17(1), 174-195
ISSN: 1307-9085, e-ISSN: 2149-4584
Araştırma Makalesi

Erzincan University
Journal of Science and Technology
2024,17(1), 174-195
DOI: 10.18185/erzifbed.1377310
Research Article

Exploring Novel Schiff Base Compounds Derived from Benzothiophene-3-carboxaldehyde Hydrazones: In vitro and In silico Evaluation as Potential Inhibitors of Cholinesterases and Carbonic Anhydrases I-II

Şule GÜRSOY[1], Zeynep ÇAKA[2], Nagihan FAYDALI[3,4], Hanif ŞIRINZADE[3], Esra DILEK[1*]

[1]Department of Biohemistry, Faculty of Pharmacy, Erzincan Binali Yıldırım University, 24030, Erzincan, Turkey.
[2]Faculty of Pharmacy, Erzincan Binali Yıldırım University, 24030, Erzincan, Turkey.
[3]Department of Pharmaceutical Chemistry, Faculty of Pharmacy, Selcuk University, 42130, Konya, Turkey.
[4]Graduate School of Health Sciences, Ankara University, Ankara, Turkey

Received: 17/10/2023, **Revised:** 07/03/2024, **Accepted:** 07/03/2024, **Published:** 28/03/2024

Abstract

In this study, we evaluated the inhibition of several cytosolic enzymes, aiming to shed light on and potentially treat various associated diseases such as Alzheimer's, Parkinson's, and Glaucoma. Our goal is to minimize drug side effects by combining multiple effects in a single molecule. To achieve this, we investigated the *in vitro* effects of two new benzothiophene Schiff bases on cholinesterases (AChE and BuChE) as well as human carbonic anhydrase isoforms (CAI and CAII). Molecular modeling studies were also conducted to elucidate the inhibition mechanism of these two compounds on these enzymes. Subsequently, both compounds (1a and 1b) were tested *in vitro* on the aforementioned enzymes. Furthermore, the *in vitro* results were supported by data obtained from in silico studies. Our findings indicate that benzothiophene derivatives significantly inhibited these enzymes. Compound 1b exhibited a stronger inhibitory effect against CAI and CAII compared to the AZA control compound. Additionally, both compounds demonstrated more potent inhibitory effects on cholinesterases (AChE and BuChE) compared to the control compound Tacrine.

Keywords: Benzothiophene, Schiff bases, cholinesterases, carbonic anhydrase, inhibition.

Schiff Baz Bileşikleri olarak yeni benzotiyofen-3-karboksaldehid hidrazon türevleri: Potansiyel kolinesteraz (AChE-BuChE) ve karbonik anhidraz (CAI-CAII) inhibitörleri olarak *in vitro* ve *in silico* değerlendirmesi

Öz

Bu çalışmada, birçok sitozolik enzimin inhibisyonunu değerlendirdi ve Alzheimer, Parkinson ve Glokom gibi çeşitli ilişkili hastalıkları aydınlatılması ve potansiyel olarak tedavi edilmesi amaçlanmıştır. Amacımız, tek bir molekülde birden fazla etkiyi birleştirerek ilaç yan etkilerini en aza indirmektir. Bunun için, iki yeni benzotiyofen Schiff bazının kolinesterazlar (AChE ve BuChE) ile insan karbonik anhidraz izoformları (CAI ve CAII) üzerindeki *in vitro* etkileri araştırılmıştır. Bu iki bileşiğin enzimler üzerindeki inhibisyon mekanizmasını aydınlatmak için moleküler modelleme çalışmaları da yürütülmüştür. Daha sonra, her iki bileşiği (1a ve 1b) söz konusu enzimler üzerinde *in vitro* olarak test edildi. Ayrıca, *in vitro* sonuçlarımızı in silico çalışmalardan elde edilen verilerle desteklendi. Bulgular, benzotiyofen türevlerinin bu enzimleri önemli ölçüde inhibe ettiğini göstermektedir. Bileşik 1b, AZA kontrol bileşiğine kıyasla CAI ve CAII üzerinde daha güçlü bir inhibisyon etkisi sergiledi. Ayrıca, her iki bileşiğin de kolinesterazlar (AChE ve BuChE) üzerinde kontrol bileşiği takrin'e kıyasla daha güçlü inhibisyon etkileri gösterdiği belirlenmiştir.

Anahtar Kelimeler: Benzotiyofen, Schiff Bazı, kolinesteraz, karbonik anhidraz, inhibisyon.

*Corresponding Author: edilek@erzincan.edu.tr
Şule GÜRSOY, https://orcid.org/0000-0001-5236-5974
Zeynep ÇAKA, https://orcid.org/0000-0002-3629-5168
Nagihan FAYDALI, https://orcid.org/0000-0002-8895-1825
Hanif SİRİNZADE, https://orcid.org/0000-0001-9663-9199
Esra DİLEK, https://orcid.org/0000-0002-3629-5168

1. Introductıon

Different derivatives of benzothiophenes has been reported as compounds which demonastrate various biolgical and pharmacological activities like anti-inflammatory (1), antibacterial (2-4), antiviral (5) and anticancer agents (6, 7). Also, Schiff bases are an important class of organic compounds that have antifungal and antimalarial activity, among others, and are widely used and researched for their numerous applications in many fields including analytical, biological and inorganic chemistry (8-16). The synthesis of benzothiophene-derived Schiff bases has been made by some researchers and antimicrobial, antioxidant, antileishmanial activities of them have been examined. (17-20). Activity studies of such compounds, especially against cholinesterase and carbonic anhydrase enzymes, have not been found more in the literature. Therefore, ~~in silico~~ molecular docking studies of new synthesized compounds and enzymes were carried out to gain an idea about the possible interaction between enzymes and synthesized compounds. Data obtained as a result of molecular docking motivated us to make this study about the preparation and characterization of Schiff base with benzothiophene derivatives and also their anti-cholinesterase and anti-carbonicanhydrase activities.

Enzymes act as catalysts in many biochemical reactions and are important in regulating, controlling and accelerating these reactions. In the drug development process, the inhibition of enzymes plays an important role in the development of drugs used for the treatment of many diseases. Acetylcholine esterase (AChE) and butyrylcholinesterase (BuChE), which are enzymes that terminate the effects of molecules known as neurotransmitters on the nervous system, are used as targets in the treatment of nervous system disorders such as Alzheimer's disease. In addition, this enzyme, which has effects on its functions in the respiratory muscles, has an important place in the treatment of diseases such as myasthenia gravis (21). Another group of enzymes associated with the respiratory system are the carbonicanhydrases (CAs). CAs are also responsible for respiration and CO_2/(HCO_3^-) transport, pH and CO_2 homeostasis, electrolyte release in various organs and tissues, biosynthesis reactions (such as gluconeogenesis, lipogenesis, and ureagenesis), bone resorption, calcification and tumorigenesis. Additionally they also play an important role in many physiological and pathological processes in different organisms(22). Therefore, enzyme inhibition is an important strategy to be selected as a target in the drug development process.

Alzheimer's disease (AD) is a progressive, irreversible, incurable, neurodegenerative disease and is the most common form of dementia. In addition, AD is a problematic and expensive disease for humanity, and it is also known as a 'silent threat' (23,24). Acetylcholine esterase inhibitors are drugs used to increase acetylcholine (ACh) levels in the brain. Alzheimer's disease causes a decrease in the level of acetylcholine in the brain, and as a result, neural transmission processes are disrupted (25). Acetylcholine esterase inhibitors can help relieve the symptoms of this disease by increasing the levels of acetylcholine in the brain.

On the other hand, carbonic anhydrase (CA) plays a crucial role in signal processing, long-term synaptic conversion, and the careful overhaul of memory storage. Abnormalities in carbonic anhydrase enzyme activity impair cognition and are associated with mental retardation,

Alzheimer's disease, and aging (26). CA function has been associated with AD pathology as well as stroke. CAs are important potential mediators and inhibition of CA is essential in AD. The aim of several recent studies is to further elucidate the association of CAs with both AD and stroke (27).

In this study, the in vitro activity of synthesized new benzothiophene rings against AChE, BuChE, hCAI and hCAII enzymes was evaluated and molecular docking studies were carried out.

2. Material and Methods

2.1 Chemicals

The Stuart melting point SMP30 apparatus was employed for determining uncorrected melting points, while ^{1}H and ^{13}C NMR spectra were recorded using a Varian 400 MHz spectrometer located in Palo Alto, CA. TMS served as the internal standard, and DMSO-d6 was utilized as the solvent during this process. ESI mass spectra were generated using a Waters Micromass ZQ device, and elemental analyses were conducted using the CHNS-932 instrument from Leco Corporation in St. Joseph, MI. Merck silica gel 60 (230–400 mesh ASTM) was employed for chromatography procedures. All spectral analyses were carried out at the Central Laboratory of the Faculty of Pharmacy at Ankara University. With the exception of L-tyrosine (E.Merck), Sepharose-4B, indazole molecules, and chemicals for electrophoresis, all other chemical reagents used in synthesis and other procedures were obtained from Sigma (Germany) and Aldrich (USA). Furthermore, AChE (CAS no. 9000-81-1) and BuChE (CAS no. 9001-08-5) were procured from Sigma-Aldrich.

2.2 Synthesis of compounds 1a and 1b

The general procedure for synthesizing compounds 1a and 1b involved the condensation of bromo-substituted phenylhydrazine hydrochloride with benzothiaphene-3-carboxaldehyde (Fig. 1). The new imines were obtained using a methodology adapted from Kidwai (28).

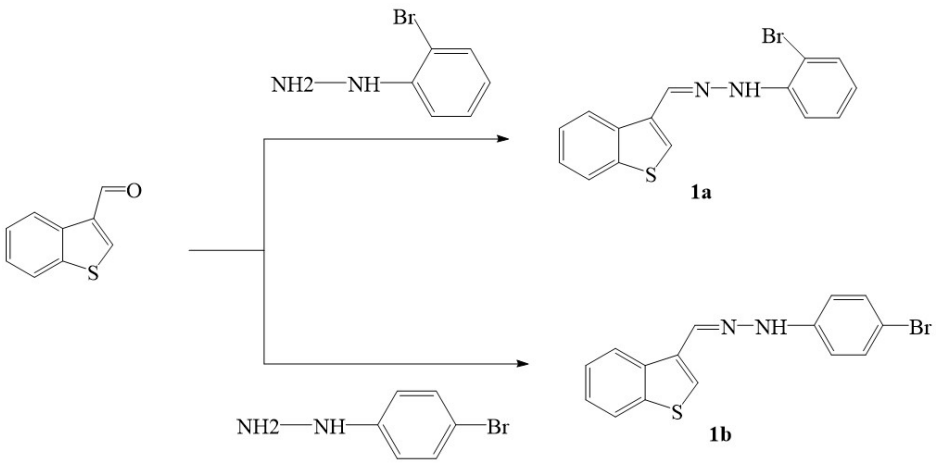

Figure 1. Synthesis of benzothiophene-3-carboxaldehyde hydrazones

2.3 Synthesis of 1-(benzo[b]thiophen-3-ylmethylene)-2-(2-bromophenyl)hydrazine (1a)

Benzothiophene-3-carboxaldehyde (1 mmol) was reacted with 2-bromophenyl hydrazine hydrochloride (1.2 mmol) in 20 ml of absolute ethanol in the presence of 0.4 g CH_3COONa for 2 hours on a hot water bath. Upon completion of the reaction, the mixture was cooled to room temperature. The resulting precipitate was collected, washed with cold water, and recrystallized from EtOH to obtain compound 1a. Yield 70%; m.p. 129–131°C; ^{1}H-NMR: 6.76(td, 1H, J=8 & 1.6 Hz), 7.37(td, 1H, J=8 & 1.6 Hz), 8.01(s, 1H), 7.44-8.72(m, 6H, Ar-H) 8.66(s, 1H, azomethine-CH), 9.61(s, 1H, hydrazon-NH); ^{13}C-NMR: 106.13; 114.10; 120.23; 123.05; 124.46; 125.12; 125.16; 128.79; 129.24; 131.66; 132.68; 135.67; 137.89; 140.18; 142.44 (azomethine C); ESI MS m/z 331(M+,%100),333(M+2, %90).

2.4 Synthesis of 1-(benzo[b]thiophen-3-ylmethylene)-2-(4-bromophenyl)hydrazine (1b)

Benzothiophene-3-carboxaldehyde (1 mmol) was reacted with 4-bromophenyl hydrazine hydrochloride (1.2 mmol) in 20 ml of absolute ethanol in the presence of 0.4 g CH_3COONa for 2 hours on a hot water bath. Upon completion of the reaction, the mixture was cooled to room temperature. The resulting precipitate was collected, washed with cold water, and recrystallized from EtOH to obtain compound 1b. Yield 84%; m.p. 133–135°C; ^{1}H-NMR: 7.05(d, 2H, J=11.8 Hz), 7.41(d, 2H, J=8.8 Hz), 7.43-8.73-8.7(m, 4H), 7.99(s, 1H) 8.22(s, 1H, azomethine-CH), 10.44(s, 1H, hydrazon-NH); ^{13}C-NMR: 109.38; 113.78; 123.00; 124.61; 125.05; 125.12; 128.53; 131.79; 131.87; 134.90; 135.62; 140.17; 144.63 (azomethine C); ESI MS m/z 331(M+,%100),333(M+2, %90).

2.5 Molecular docking studies

In the molecular docking study, hCA I (PDB: 2FOY) (29) and hCA II (PDB: 1IF7) (29), as well as AChE and BChE (30), were retrieved from the Protein Data Bank in pdb format. Ions, water molecules, and ligands were removed from the downloaded proteins, and polar hydrogens and Gasteiger charges were added to the proteins. The proteins were saved in pdbqt format using AutoDockTools 1.5.6 (31). Ligands were drawn in ChemDraw3D 19.0, minimized, and saved in pdb format. After conversion to pdbqt format using AutoDockTools 1.5.6, molecular docking was carried out using the latest AutoDock Vina program (32). The results were visualized in 2D and 3D using PyMOL (33) and the Discovery Studio Visualizer (34).

2.6 Biological activity studies

Inhibition Studies of Cholinesterase Enzymes

AChE (CAS no. 9000-81-1) and BuChE (CAS no. 9001-08-5) used in the study were purchased from Sigma-Aldrich. The inhibitory effects of, two benzothiophene Schiff bases (1a and 1b compounds) on AChE and BuChE activities were determined by IC_{50} and Ki values under *in vitro* conditions, following the methodology outlined by Ellman et al. (35). IC_{50} means the

inhibitor concentration that reduces the enzyme activity by half, and a low IC_{50} value indicates high inhibition power. To determine the IC_{50} values of (**1a and 1b**) compounds, AChE and BChE activities were measured at least five different concentrations of each molecule and %Activities were calculated. The activity of the enzymes without inhibitor was accepted as 100%. %Activity versus inhibitor concentrations were then plotted for each molecule. From these graphs, the IC_{50} values of each molecule for AChE and BChE were determined. Lineweaver–Burk graphs were drawn using three different concentrations of 1a and 1b compounds and six different concentrations of substrate (Acetylthiocholine iodide: ACh and Butyrylthiocholine iodide: BuCh) for the calculation of K_i values. The same procedures were done for tacrine, the standard inhibitor of AChE and BChE enzymes, and both IC_{50} and K_i values were calculated. The enzyme unit was calculated using the molar absorption coefficient (13.600 $M^{-1}.cm^{-1}$) of 5-thio-2-nitrobenzoic acid (DTNB) at 412 nm (36).

Carbonic Anhydrase Isoenzymes Inhibition Studies

All purification procedures were conducted following protocols outlined in our previous studies (37-40). Protein quantification at each purification step was performed spectrophotometrically at 595 nm using the Bradford method (41). Carbonic anhydrase (CA) isoenzyme activities were determined according to the method described by Verpoorte et al. (42). Enzyme activities were assessed by measuring the increase in absorbance spectrophotometrically at 348 nm. A concentration-response curve of inhibitor concentration versus percentage activity was generated to assess the inhibitory potency of each benzothiophene-derived Schiff base compound (1a-1b) against both hCA isoenzymes. IC50 values were derived from these curves. Ki values were calculated using three different concentrations of the tested compounds and five different concentrations of substrate. Additionally, inhibition curves of the most potent compounds were plotted and presented. Both IC50 and Ki values were determined using the same procedures applied to AZA, which served as the standard inhibitor of CA isoenzymes.

3. Results and Discussion

In this study, first, in silico studies of novel benzothiophene derived Schiff bases compounds and then in vitro effects were studied on hCAI, hCAII isoenzymes, and cholinesterases (AChE and BuChE) activities.

After CAI and CAII isoenzymes were purified by CNBr-activated Sepharose-4B-L-tyrosine sulfanilamide affinity chromatography method, the effects of novel benzothiophene derived Schiff bases compounds on these isoenzymes were examined. 1a and 1b showed strong inhibitiory effects at very low concentrations on hCAI and hCAII isoenzymes. Inhibitor concentration versus %Activity for 1a and 1b compounds showing inhibition effect on hCAI and hCAII isoenzymes were graphed (Fig.2). Ki values were determined by three different concentrations of each compound. The compounds were found to showed inhibitory effects at all three different concentrations. Lineweaver-Burk curves was drawn for identifying of Ki values and inhibition type. For hCAI and hCAII, the obtained IC_{50} and Ki values were given in Table 1. Ki values were determined to be in the range of 58.82 ± 7.96-126.28 ± 26.22 nM for

hCAI and 27.86 ± 3.76-74.30 ± 7.89 nM for hCAII. Compared to the control compound AZA, both 1a and 1b represent potent inhibitory effect on carbonicanhydrase isoenzymes (Fig 1.) while 1b demonstrated more strong inhibition effect on these isoenzymes (Fig 2.) (Table 1).

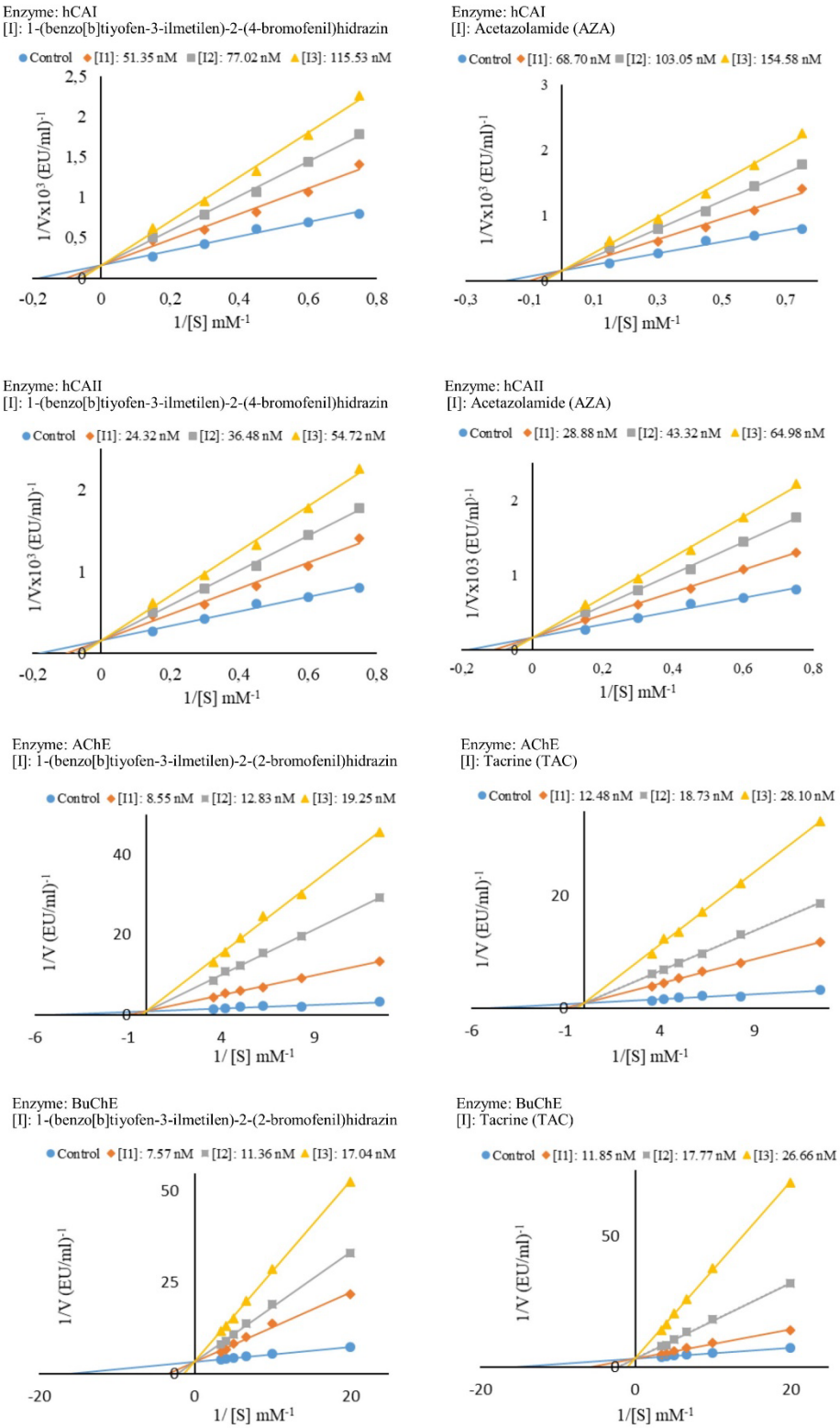

Figure 2. Ki constants and inhibition types were determined by using Lineweaver-Burk graphs for

excellent inhibitors of hCAI, hCAII, AChE and BuChE enzymes. (Each enzyme was given in comparison with its specific inhibitor.)

Table 1. Experimental IC_{50} and Ki values of hCAI and hCAII for thiophene derivative schiff bases (1a-1b) and AZA as standard inhibitors.

	IC_{50} (nM)				K_i (nM)	
Compounds	**hCA I**	**R^2**	**hCA II**	**R^2**	**hCA I**	**hCA II**
1a	86.64	0.9970	38.51	0.9960	126.28 ± 26.22	74.30 ± 7.89
1b	77.02	0.9968	36.48	0.9959	58.82 ± 7.96	27.86 ± 3.76
Acetazolamide (AZA)	103.05	0.9979	43.32	0.9937	78.70 ± 10.64	33.63 ± 5.41

On the other hand, the in vitro effects of 1a and 1b compounds on AChE and BuChE activity were investigated. Compared with the control compound Tacrine, both compounds showed the best inhibitory effect for cholinesterases (AChE and BuChE). Ki values were determined to be in the range of 1.31 ± 0.39-2.16 ± 1.01 nM for acetylcholinesterase; in the range of 1.80 ± 0.27-2.01 ± 1.67 nM for butyrylcholinesterase. In addition, to explain the inhibition mechanism Ki values and inhibition types were determined for 1a and 1b compounds on whole enzymes. Except that 1a non-competitively inhibited CAI, other enzymes were competitively inhibited by the all compounds. (Table 2, Fig.1).

Table 2. Experimental IC_{50} and Ki values of AChE and BuChE for thiophene derivative schiff bases (1a-1b) and Tacrine as standard inhibitors.

	IC_{50} (nM)				K_i (nM)	
Compounds	**AChE**	**R^2**	**BuChE**	**R^2**	**AChE**	**BuChE**
1a	12.83	0.9977	11.36	0.9951	1.31 ± 0.39	1.80 ± 0.27
1b	13.86	0.9909	13.08	0.9916	2.16 ± 1.01	2.01 ± 1.67
Tacrine (TAC)	18.73	0.9974	17.77	0.9908	2.57 ± 0.39	3.92 ± 2.76

Selectivity index values of the compounds were calculated to assess their preference for targeting specific enzymes. According to these values, compound 1b, which exhibited higher potency compared to AAZ, reduced hCAI activity approximately 1.34-fold and hCAII activity approximately 1.21-fold, with a higher affinity towards hCAII (Ki (hCAI)/ Ki (hCAII): 2.11). Conversely, compound 1a, with greater potency compared to TAC, decreased AChE activity approximately 2.17-fold. Compound 1b, surpassing TAC in potency, reduced BuChE activity approximately 1.07-fold. Moreover, compound 1a, which outperformed BuChE, reduced AChE activity approximately 1.96-fold (Table 3).

Table 3. Selectivity index values of the compounds (1a-1b).

Compounds	Ki (hCAI)/ Ki (hCAII)	Ki(AAZ)/ Ki (hCAI)	Ki (AAZ)/ Ki(hCAII)	Ki(AChE)/ Ki (BuChE)	Ki(TAC)/ Ki (AChE)	Ki(TAC)/ Ki (BuChE)
1a	1.68	0.62	0.45	1.96	2.17	0.73
1b	2.11	1.34	1.21	1.19	1.95	1.07

In molecular docking studies, it was observed that the binding energies of 1a and 1b to hCA-I and hCA-II enzymes were lower than the reference drug acetazolmide. Likewise, compounds 1a and 1b were found to bind to AChE and BChE enzymes with lower binding energies than the reference drug tacrine (Table 4).

Table 4. Enzyme binding energies of compounds and reference drugs

Bileşik Adı	Binding energy for hCA-I (kcal/mol)	Binding energy for hCA-II (kcal/mol)	Binding energy for AChE (kcal/mol)	Binding energy for BChE (kcal/mol)
1a	-6.5	-7.1	-9.7	-8.6
1b	-6.9	-7.1	-9.6	-8.1
Asetazolamide	-5.7	-6.1	-	-
Tacrine	-	-	-8.5	-8.0

When the 2D images are examined, it is seen that the benzothiophene rings of the compounds make a pi-sulfur bond with the asparagine amino acid, The nitrogen atom in the schiff base is connected to the serine amino acid in compound 1a, while it is connected to the lysine amino acid in compound 1b. The reference drug, acetazolamide, binds with threonine, histamine and glycine amino acids (Fig 3.).

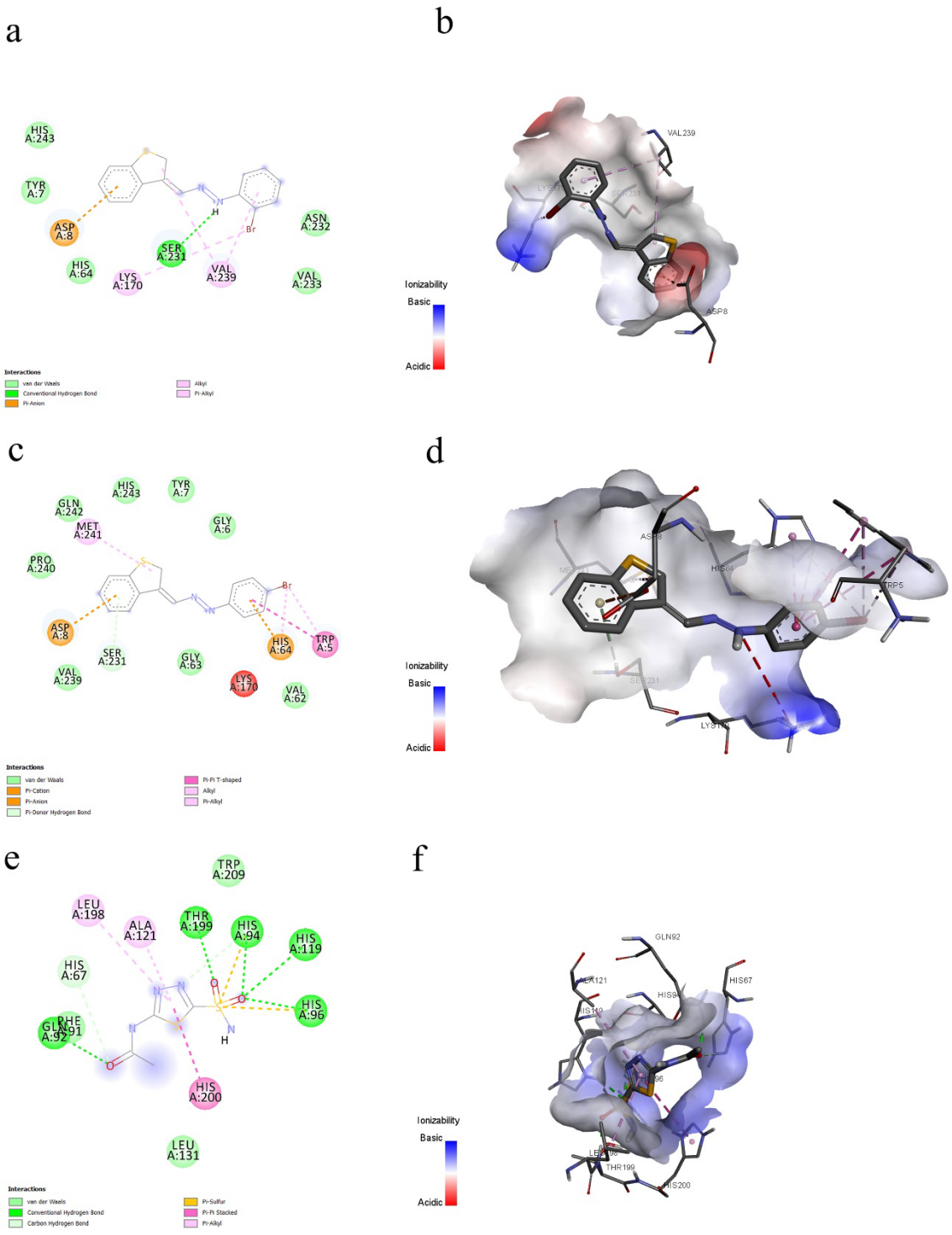

Figure 3. 2D molecular docking images of 1a (a), compound 1b (c) and reference drug acetazolamide (e) located in the active site of the hCA I enzyme and 3D molecular docking images of 1a (b), compound 1b (d) and reference drug acetazolamide (f) located in the active site of the hCA I enzyme

In compounds 1a and 1b the benzothiophene ring, makes pi-pi bonds with tryptophan and phenylalanine amino acids. In addition, the N atom in the Schiff base is also bonded with the amino acids glutamine and phenylalanine. Moreover in both compounds, it is seen that the phenyl group attached to the Schiff base is bonded with glutamine in compound 1a and tyrosine in compound 1b. The reference drug acetazolamide binds with tyrosine, histamine, gultamine and glycine amino acids (Fig 4.).

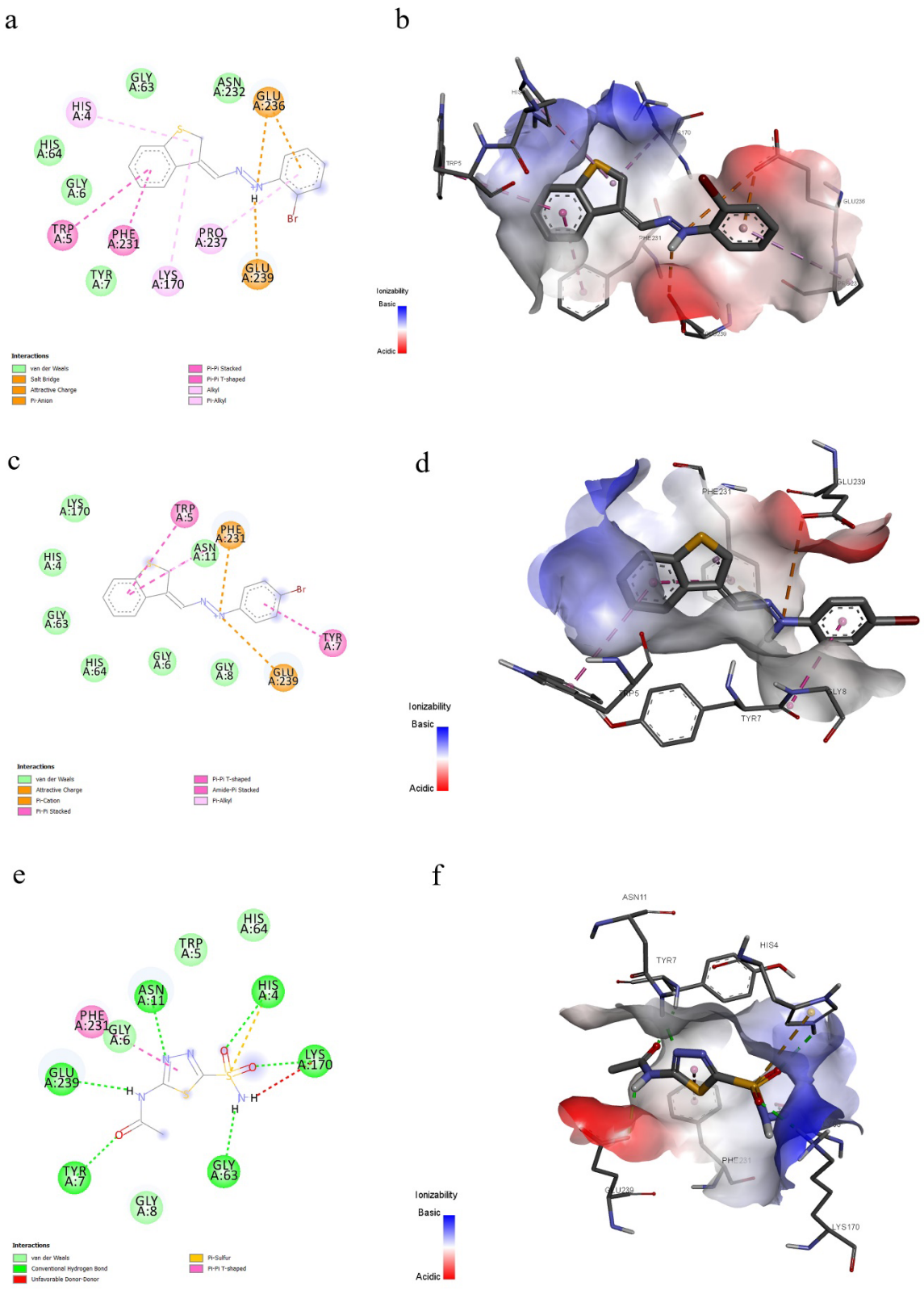

Figure 4. 2D molecular docking images of 1a (a), compound 1b (c) and reference drug acetazolamide (e) located in the active site of the hCA II enzyme and 3D molecular docking images of 1a (b), compound 1b (d) and reference drug acetazolamide (f) located in the active site of the hCA II enzyme

When the 2D molecular docking images of the 1a compound bound to the AChE enzyme are examined, it is observed that the benzothiophene ring in the compound makes a pi-pi bond with the tryptophan, phenylalanine and tyrosine amino acids in the enzyme.

Also, it has been revealed that the bromine atom in the 2nd position and the phenyl ring attached to the schiff base form pi-sigma, pi-pi bonds with the tyrosine amino acid. The reference drug, tacrine, was observed to bind only to tryptophan and tyrosine amino acids via pi-pi bonds (Fig 5.).

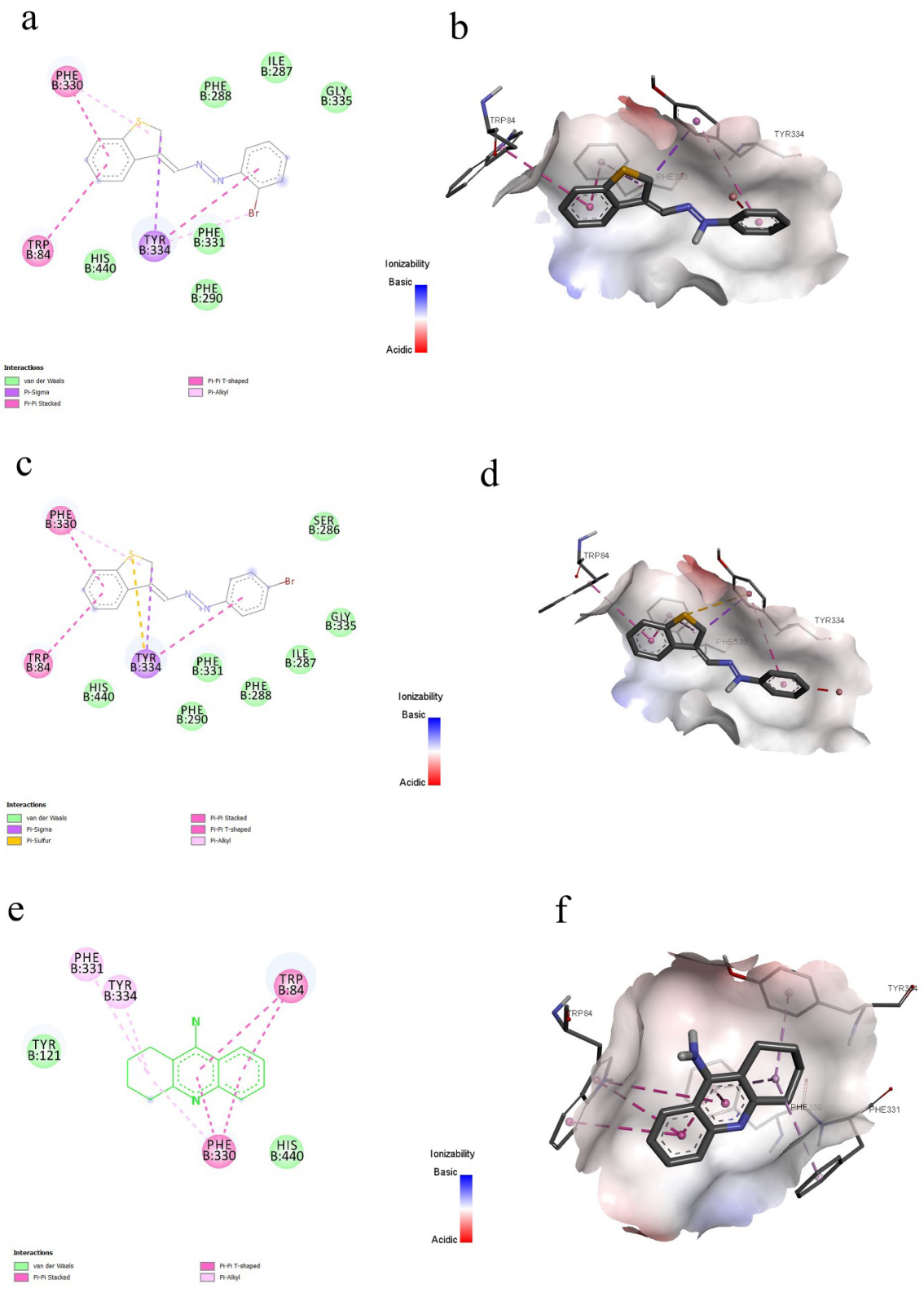

Figure 5. 2D molecular docking images of 1a (a), compound 1b (c) and reference drug tacrine (e) located in the active site of the AChE enzyme and 3D molecular docking images of 1a (b), compound 1b (d) and reference drug tacrine (f) located in the active site of the AChE enzyme

Considering the interactions present in the regions where the compounds bind to the BChE enzyme; It was determined that the benzothiophene ring in compound 1a makes a pi-pi bond with the tryptophan amino acid and the S atom makes a pi-sulfur bond with the phenylalanine amino acid. However, the same benzothiophene ring in compound 1b was found to form a pi-sulfur bond with phenylalanine and a pi-pi bond with tryptophan.

Nitrogen atoms contained in the schiff base in both compounds were observed to interact with histamine in compound 1a, while it was observed to interact with serine in compound 1b. It is detected that the reference drug tacrine molecule interacts with tryptophan and histamine amino acids (Fig.6.)

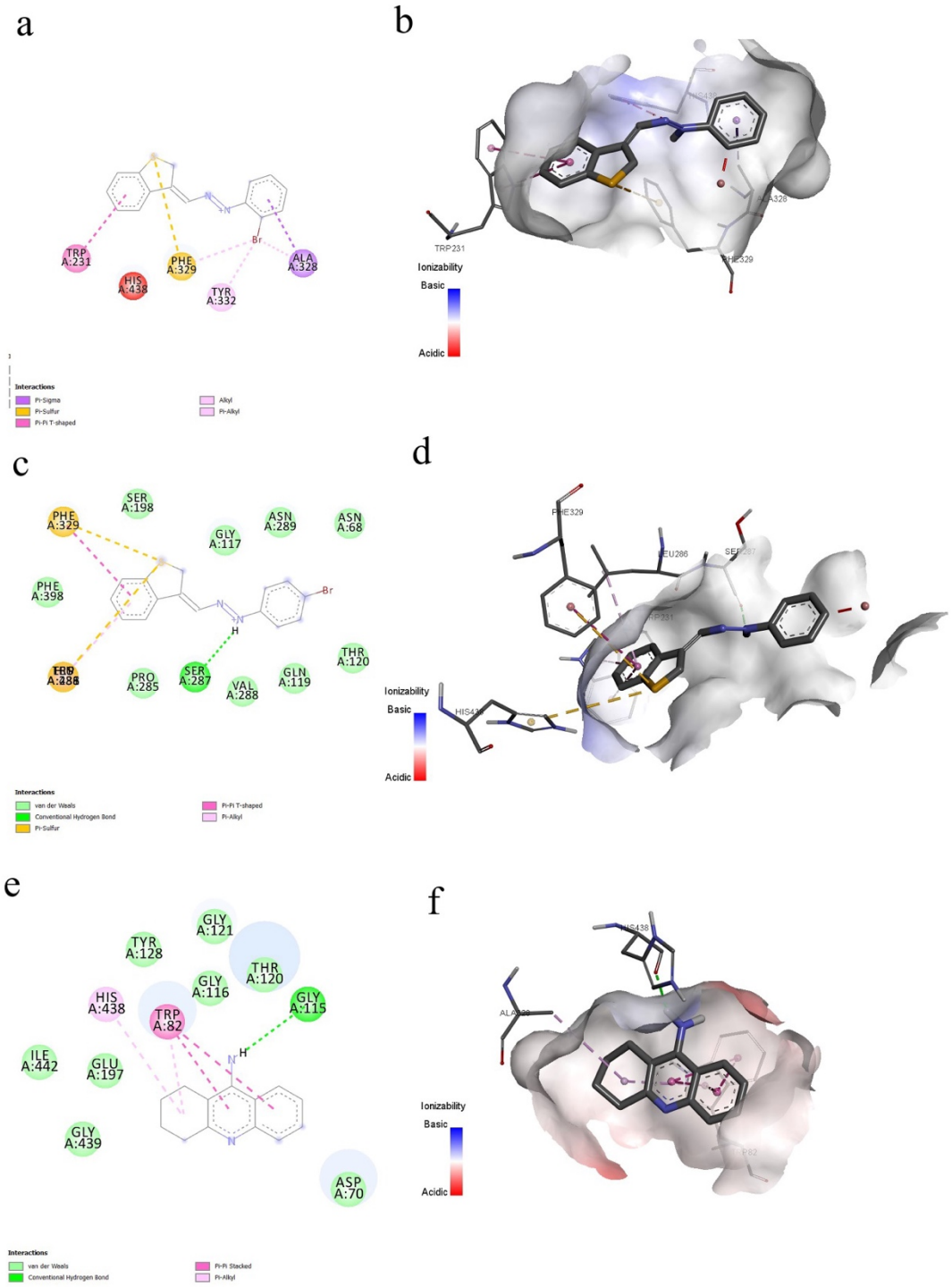

Figure 6. 2D molecular docking images of 1a (a), compound 1b (c) and reference drug tacrine (e) located in the active site of the BChE enzyme and 3D molecular docking images of 1a (b), compound 1b (d) and reference drug tacrine (f) located in the active site of the BChE enzyme

Schiff base compounds are both stable and easily synthesized compounds. Because of these features they have wide usage areas in many fields of chemistry (43), industry (44,45), medicine and pharmacy (46) has increased the interest in these compounds and made them widely used in different fields. In addition, some activities of schiff bases like anti-inflammatory,

antimicrobial, anticancer, antioxidant, antimalarial, antifungal, antiviral, analgesic, anticonvulsant, antituberculous, anthelmintic (17-20, 47,48) have been studied by many researchers. The fact that Schiff bases and derivatives can be used especially as drugs (49) has inspired many researches working in the field of health. It has been reported that different derivatives of benzothiophenes have biological and pharmacological activities, used as anti-inflammatory (1), antibacterial (2-4), antiviral (5) and anticancer agents (6, 7).

In the light of this information, benzothiophene derivative Schiff bases were designed, synthesized and characterized by spectroscopic methods such as ^{1}H-NMR, ^{13}C-NMR, LC-MS/MS. Molecular docking of the compounds into active site of AChE, BuChE, hCAI and hCAII was performed in order to understand ligand–protein interactions and calculate to bindng energy. Compounds 1a and 1b bind to the hCA I, hCAII, AChE, BuChE isoenzyms with a lower binding energy than the reference drug acetazolamide.

To understand ligand-protein interactions, molecular docking studies of compounds into the active site of AChE, BuChE, hCAI and hCAII was evaluated.

It has been observed in our data that the benzothiophene rings of the compounds interact with the Asparagine amino acid in the active site of the AchE enzyme and the tryptophan, phenylalanine and histidine amino acids in the BuChE enzyme.

Phenylalanine and tryptophan amino acids which have exist in the different active site of the hCA I and hCA II enzymes have been interacted with benzothiophene ring. Moreover, the bromine atom in the ortho position contributed to the interaction.

Inhibition of enzymatic activity, besides creating a control mechanism in biological systems, various drugs and toxic compounds exert their effects by enzyme inhibition. Many drugs that are widely used today also act as enzyme inhibitors. In order to determine how inhibitory substances interact with enzymes, IC_{50} values are determined first. Then Ki values are calculated by using the IC_{50} values. Inhibition types can also be determined from Lineweaver Burk graphs drawn for calculating K_i values. To determine the interaction of our synthesized benzothiophene derivative schiff bases with these enzymes, Lineweaver Burk graphs were drawn and K_i values were calculated. According to our results, compound 1b demonstrated excelent inhibition effect on hCAI and hCAII isoenzymes. Compound 1a inhibited both enzymes non-competitively, whereas compound 1b competitively inhibited both isoenzymes. Compared to the control compound AZA, the compound with small Ki value shows strong inhibitor feature (Table 1, Fig.2). On the other hand, compounds 1a and 1b demonstrated excelent inhibition effect on on AChE and BuChE activity. Compared with the control compound Tacrine, both compounds showed the best inhibitory effect for cholinesterases (AChE and BuChE). Both compounds competitively inhibited cholinesterase enzymes (Table 2., Fig.2). Competitive inhibition indicates that the inhibitor acts as a substrate and binds to the active site of the enzyme. It also means that the inhibition effect can be eliminated when the amount of substrate is increased.

4. Conclusion

In conclusion, inhibition of both carbonicanhydrase isoenzymes (hCAI and CAII) and cholinesterases (AChE and BuChE) is important in the treatment of Alzheimer's disease. This study aimed to design and synthesize benzothiophene derivative Schiff bases and test their inhibition activities against AChE and BuChE, hCAI and hCAII. Compounds 1a and 1b demonstrate perfect inhibition activities against to AChE, BChE, hCAI and hCAII. It has been seen at in silico studies that 1a and lb compounds can bind to the active site of the enzyme in a similar way and at appropriate positions, and these results are also supported by in vitro studies. The presence of the bromine atom in the 4th position in the 1b compound caused it to interact more with the active site of the hCAI enzyme. This situation is also confirmed by in-vitro activity results.The position of the bromine atom did not contribute to its interaction with the hCA II enzyme, however, it showed different interactions with the enzyme by affecting the conformations of the molecule.The bromine atom attached to the 2nd position in compound 1a interacted only with tyrosine in the AChE enzyme While it interacted with phenylalanine, tyrosine and alanine amino acides in the BuChE enzyme.In conclusion to evaluate all obtained data, has been considered that these compounds can be evaluated as lead compounds for the development of new drugs for neurodegenerative disorders and may be suitable for further studies.

Acknowledgments

This study received support from project number 1919B012109379 under the auspices of the 2209-A University Students Research Projects Support Program 2021, spanning 2 semesters, administered by the TÜBITAK Scientist Support Programs Presidency (BIDEB). We extend our gratitude to TUBITAK for their financial assistance.

Conflicts of Interest

The authors declare no conflict of interest.

Ethics in Publishing

There are no ethical issues regarding the publication of this study.

Author Contributions

Dilek E. written manuscript; Gürsoy Ş., Dilek E. and Şirinzade H. designed the study, prepared protocols, analyzed the data; Gürsoy Ş., Dilek E., Çaka Z., Faydalı N., and Şirinzade H.; performed the experiments and participated in discussions. All the authors were responsible for the data acquisition, review and editing of the paper.

References

[1]. Deka S, Mohan S, Saravanan J, Kakati M, Talukdar A, Sahariah BJ, Dey BK and Sarma RK (2012) Syntheses, characterization and in-vitro anti-Inflammatory activity of some novel thiophenes, Maced. J. Med. Sci. 5:159–163 DOI: org/10.3889/MJMS.1957-5773.2012.0225.

[2]. Abbas S, Hussain M, Ali S, Parvez M, Raza A, Haider A and Iqbal J (2013) Structural, enzyme inhibition, antibacterial and DNA protection studies of organotin (IV) derivatives of thiophene-2-carboxylic acid, J. Organometallic Chem. 724:255–261 https://doi.org/10.1016/j.jorganchem.2012.11.033

[3]. Asiri AM and Khan SA (2011) Synthesis and antibacterial activities of a bis-chalcone derived fromthiophene and its bis-cyclized products, Molecules 16:523–531. https://doi.org/10.3390/molecules16010523

[4]. Khalil AM, Berghot MA and Gouda MA (2009) Synthesis and antibacterial activity of some newthiazole and thiophene derivatives, Eur. J. Med. Chem. 44:4434–4440 https://doi.org/10.1016/j.ejmech.2009.06.002

[5]. Rashad AE, Shamroukh AH, Abdel-Megeid RE, Mostafa A, El-Shesheny R, Kandeil A, Ali MA and Banert K (2010) Synthesis and screening of some novel fused thiophene and thienopyrimidine derivatives for anti-avian influenza virus (H5N1) activity, Eur. J. Med.Chem. 45:5251–5257. https://doi.org/10.1016/j.ejmech.2010.08.044

[6]. Forsch RA, Wright JE and Rosowsky A (2002) Synthesis and in vitro antitumor activity of thiopheneanalogues of 5-chloro-5,8-dideazafolic acid and 2-methyl-2-desamino-5-chloro- 5,8-dideazafolicacid, Bioorg. Med. Chem. 10:2067–2076 https://doi.org/10.1016/S0968-0896(02)00018-4

[7]. Saad HA, Youssef MM and Mosselhi MA (2011) Microwave assisted synthesis of some new fused1,2,4-triazines bearing thiophene moieties with expected pharmacological activity, Molecules, 16:4937–4957 https://doi.org/10.3390/molecules16064937

[8]. Aziz A, Salem AE, Sayed MA, Aboaly MM (2012). Synthesis, structural characterization, thermal studies, catalytic efficiency and antimicrobial activity of some M(II) complexes with ONO tridentate Schiff base N-salicylidene-o-aminophenol (saphH2). Journal of Molecular Structure, 1010:130-138. https://doi.org/10.1016/j.molstruc.2011.11.043

[9]. Sujarani A and Ramu A (2013) Synthesis, characterization, antimicrobial and DNA interaction studies of benzophenone - ethanamine schiff base with transition metal (II) [Cu(II), Co(II), Mn(II) and Ni(II)] complexes. Journal of Chemical and Pharmaceutical Research 5(4):347-358

[10]. Lam PL, Lee KKH, Kok SHL, Gambari R, Lam KH, Ho CL, Ma X, Lo YH, Wong WY, Dong QC, Bian ZX, Chui CH (2016), Antifungal study of substituted 4-pyridylmethylene-4'-aniline Schiff bases, RSC Adv., 106:104575-104581. https://doi.org/10.1039/C6RA20186E

[11]. Chopde HN, Meshram JS, Pandhurnekar CP, Pagadala R, Jonnalagadda SB (2016) Efficient Synthesis, Characterization, In Vitro Antibacterial and Antifungal Activity Study and Computational Tool for Prediction of Molecular Properties of Some Novel Schiff's Base via Betti's Protocol and Azetidinones,Journal of Heterocyclic Chemistry, 53(3):824-831. https://doi.org/10.1002/jhet.2349.

[12]. Kgokong JL, Smith PP, Matsabisa GM. (2005) 1,2,4-Triazino-[5,6b]indole derivatives: effects of the trifluoromethyl group on in vitro antimalarial activity. Bioorg Med Chem. Apr 15;13(8):2935-42. https://doi.org/10.1016/j.bmc.2005.02.017

[13]. Rathelot P, Vanelle P, Gasquet M, Delmas F, Crozet MP, Timon-David P, Maldonado J (1995) Synthesis of novel functionalized 5-nitroisoquinolines and evaluation of in vitro antimalarial activity, European Journal of Medicinal Chemistry, 30(6):503-508. https://doi.org/10.1016/0223-5234(96)88261-4

[14]. Kumar G, Devi S, Kumar D (2016) Synthesis of Schiff base 24-membered trivalent transition metal derivatives with their anti-inflammation and antimicrobial evaluation, J. Mole. Str., 1108:680-688. https://doi.org/10.1016/j.molstruc.2015.12.059

[15]. Alam MS, Choi JH, Lee DU. (2012) Synthesis of novel Schiff base analogues of 4-amino-1,5-dimethyl-2-phenylpyrazol-3-one and their evaluation for antioxidant and anti-inflammatory activity. Bioorg Med Chem. 20(13):4103-8. https://doi.org/10.1016/j.bmc.2012.04.058

[16]. Jarrahpour A, Khalili D, De Clercq E, Salmi C, Brunel JM. (2007) Synthesis, antibacterial, antifungal and antiviral activity evaluation of some new bis-Schiff bases of isatin and their derivatives. Molecules. 12(8):1720-30. https://doi.org/10.3390/12081720

[17]. Nayab S, Alam A, Ahmad N, Khan SW, Khan W, Shams DF, Shah MIA, Ateeq M, Shah SK, and Hyosun Lee. (2023) Thiophene-Derived Schiff Base Complexes: Synthesis,

Characterization, Antimicrobial Properties, and Molecular Docking. ACS Omega, 8 (20):17620-17633 https://doi.org/10.1021/acsomega.2c01981

[18]. Bingöl M, Turan N (2020) Schiff base and metal(II) complexes containing thiophene-3-carboxylate: Synthesis, characterization and antioxidant activities. Journal of Molecular Structure 1205(5):127542. https://doi.org/10.1016/j.molstruc.2019.127542

[19]. Unver Y, Unlüer D, Direkel S, Durdağı S. (2020) Bis benzothiophene Schiff bases: synthesis and in silico-guided biological activity studies. Turk J Chem. 44(4):1164-1176. https://doi.org/10.3906/kim-2004-78

[20]. Puthran D, Poojary B, Nayak SG, Purushotham N, Bhat M, Hedge H (2020) Novel Schiff bases–based thiophenes: Design, synthesisand biological evaluation. J Chin Chem Soc. 67:1278–1288. https://doi.org/10.1002/jccs.201900388

[21]. Langerman et al. (2020) Recent Advances in Acetylcholinesterase Inhibitors and Their Potential Applications in Central Nervous System Disorders. ACS Chemical Neuroscience 11(13): 1825-1836. https://doi.org/10.1021/acschemneuro.0c00029

[22]. Supuran CT (2010). Carbonic anhydrase inhibitors. Bioorganic & Medicinal Chemistry Letters, 20(12): 3467-3474. https://doi.org/10.1016/j.bmcl.2010.05.009

[23]. Zverova M. (2018) Alzheimer's disease and blood-based biomarkers–potential contexts of use. Neuropsychiatric disease and treatment. 14:1877-1882. https://doi.org/10.2147/NDT.S172285

[24]. Zverova M. (2019) Clinical aspects of Alzheimer's disease. Clinical biochemistry. 72:3-6 https://doi.org/10.1016/j.clinbiochem.2019.04.015

[25]. Rezazadeh et al. (2020) A Review of Acetylcholinesterase Inhibitors as Alzheimer's Disease Therapeutics. Neurotherapeutics 17(1): 53-77. https://doi.org/10.1007/s13311-019-00781-6

[26]. Sun MK and Alkon DL (2002) Carbonic anhydrase gating of attention: memory therapy and enhancement Trends Pharmacol. Sci., 23, 83-89. https://doi.org/10.1016/S0165-6147(02)01899-0

[27]. Lemon N, Canepa E, Ilies MA, Fossati S. (2021) Carbonic Anhydrases as Potential Targets Against Neurovascular Unit Dysfunction in Alzheimer's Disease and Stroke. Front Aging Neurosci. 13:772278. https://doi.org/10.3389/fnagi.2021.772278

[28]. Kidwai M, Negı N, Gupta S.D. (1994) Synthesis and antifertility activity of 1,5-diaryl-3(3'indolyl) formazans. Chem Pharm Bull (Tokyo) 42(11): 2363-64. https://doi.org/10.1248/cpb.42.2363

[29]. Xiang F, Xiang J, Fang Y, Zhang M, Li M. (2014) Discovering isozyme-selective inhibitor scaffolds of human carbonic anhydrases using structural alignment and de novo drug design approaches. Chem Biol Drug Des. 83(2):247-58. https://doi.org/10.1111/cbdd.12234

[30]. Gao H, Jiang Y, Zhan J, Sun Y. (2021) Pharmacophore-based drug design of AChE and BChE dual inhibitors as potential anti-Alzheimer's disease agents. Bioorg Chem.114:105149. https://doi.org/10.1016/j.bioorg.2021.105149

[31]. Huey R and Morris GM. (2008) Using AutoDock 4 with AutoDocktools: a tutorial. The Scripps Research Institute, USA. 54-56.

[32]. Trott O, Olson AJ. (2010) AutoDock Vina: improving the speed and accuracy of docking with a new scoring function, efficient optimization, and multithreading. J Comput Chem. 31(2): 455-461. https://doi.org/10.1002/jcc.21334

[33]. Lill MA, Danielson ML. (2011) Computer-aided drug design platform using PyMOL. J Comput Aided Mol Des. 25(1): 13-19. https://doi.org/10.1007/s10822-010-9395-8

[34]. Biovia DS. (2017) Discovery studio visualizer. San Diego, CA, USA. 936.

[35]. Ellman GL, Courtney KD, Andres V, Featherstone RM (1961) A new and rapid colorimetric determination of acetylcholinesterase activity, Biochemical Pharmacology, 7(2): 88-95. https://doi.org/10.1016/0006-2952(61)90145-9

[36]. Gocer H, Akıncıoğlu A, Oztaşkın N, Göksu S, Gulcin I (2013) Synthesis, antioxidant and antiacetylcholinesterase activities of sulfonamide derivatives of dopamine related compounds. Arch Pharm 346(11): 783–792. https://doi.org/10.1002/ardp.201300228

[37]. Bayram E, Senturk M, Kufrevioglu OI, Supuran CT (2008) In vitro inhibition of salicylic acid derivatives on human cytosolic carbonic anhydrase isozymes I and II. Bioorg. Med. Chem., 6, 9101-9105. https://doi.org/10.1016/j.bmc.2008.09.028

[38]. Burmaoğlu S, Dilek E, Yılmaz AO, Supuran CT (2016) Synthesis of two phloroglucinol derivatives with cinnamyl moieties as inhibitors of the carbonic anhydrase isozymes I and II: an in vitro study. J. Enzyme Inhib. Med. Chem., 31(sup2):208-212. https://doi.org/10.1080/14756366.2016.1181626

[39]. Caglar S, Dilek E, Caglar B, Adigüzel E, Temel E, Buyukgungor O (2016) New metal complexes with diclofenac containing 2-pyridineethanol or 2-pyridinepropanol: synthesis, structural, spectroscopic, thermalproperties, catechol oxidase and carbonic anhydrase activities. J. Coord. Chem., 69:3321-3335. https://doi.org/10.1080/00958972.2016.1227802

[40]. Shirinzadeh H and Dilek E (2020) Synthesis, characterization and biological activity evaluation of novel naphthalenylmethylen hydrazine derivatives as carbonic anhydrase

inhibitors. J. Mol. Struct., 1220: Article 128657. https://doi.org/10.1016/j.molstruc.2020.128657

[41]. Bradford MM (1976) A rapid and sensitive method for the quantitation of microgram quantities of protein utilizing the principle of protein-dye binding. Anal. Biochem. 72:248-254. https://doi.org/10.1016/0003-2697(76)90527-3

[42]. Verpoorte J, Mehta S, Edsall JT (1967) Esterase activities of human carbonic anhydrases B and C. J. Biol. Chem. 242(18), 4221-4229. https://doi.org/10.1016/S0021-9258(18)95800-X

[43]. Redshaw C (2017) Use of Metal Catalysts Bearing Schiff Base Macrocycles for the Ring Opening Polymerization (ROP) of Cyclic Esters, Catalysts, 7(5): 165-176. https://doi.org/10.3390/catal7050165

[44]. DiRisio RJ, Armstrong JE, Frank MA, Lake WR, McNamara WR (2017) Cobalt Schiff-base complexes for electrocatalytic hydrogen generation, Dalton Trans., 46: 10418-10425. https://doi.org/10.1039/C7DT01750B

[45]. Upadhyay KK, Kumar A, Upadhyay S, Mishra PC (2008) Synthesis, characterization, structural optimization using density functional theory and superoxide ion scavenging activity of some Schiff bases, J. Mol. Struct., 873: 5-16. https://doi.org/10.1016/j.molstruc.2007.02.031

[46]. Roberts DW, Schultz TW, Api AM, (2017) Skin Sensitization QMM for HRIPT NOEL Data: Aldehyde Schiff-Base Domain, Chem. Res. Toxicol., 30(6): 1309- 1316. https://doi.org/10.1021/acs.chemrestox.7b00050

[47]. Shokrollahi S, Amiri A, Fadaei-Tirani F, Schank-Job K (2020) Promising anti-cancer potency of 4,5,6,7-tetrahydrobenzo[*d*]thiazole-based Schiff-bases J. Mol. Liq. 2020, 300:122262. https://doi.org/10.1016/j.molliq.2019.112262

[48]. Shukla , Singh AP, Sonar P, Mishra M, Saraf K. (2016). Schiff bases of benzothiazol-2-ylamine and thiazolo[5,4-b] pyridin-2-ylamine as anticonvulsants: synthesis, characterization and toxicity profiling. Cent. Nerv. Syst. Agents Med. Chem. 16(3):240–248. DOI: 10.2174/1871524916666160428110728

Zoubi WA (2013) Biological Activities of Schiff Bases and Their Complexes: A Review of Recent Works. Int. J. Org. Chem., 3:73-95. DOI: 10.4236/ijoc.2013.33A008

Erzincan Üniversitesi
Fen Bilimleri Enstitüsü Dergisi
2024,17(1), 210-229
ISSN: 1307-9085, e-ISSN: 2149-4584
Araştırma Makalesi

Erzincan University
Journal of Science and Technology
2024,17(1), 210-229
DOI: 10.18185/erzifbed.1390920
Research Article

First Description of Deutonymph Male of *Eustigmaeus anauniensis* (Canestrini) (Trombidiformes: Stigmaeidae)

Salih Doğan[1*], Sibel Doğan[2], Şifanur Uğurlu[3], Nisanur Polat[1]

[1]Department of Biology, Faculty of Arts and Sciences, Erzincan Binali Yıldırım University, Erzincan, Türkiye
[2]Vocational School of Health Services, Erzincan Binali Yıldırım University, Erzincan, Türkiye
[3]Department of Biology, Graduate School of Natural and Applied Sciences, Erzincan Binali Yıldırım University, Erzincan, Türkiye

Received: 14/11/2023, **Revised:** 21/02/2024, **Accepted:** 21/02/2024, **Published:** 28/03/2024

Abstract

With more than 130 species, *Eustigmaeus* Berlese is one of the most diverse genera in the family of Stigmaeidae. The genus has a worldwide distribution and is found in all zoogeographic regions with the exception of Antarctica. The adult female, adult male, deutonymph, protonymph, and larva of *Eustigmaeus anauniensis* (Canestrini) are known till now, but the immature male stage is unknown. In this study, five deutonymph male specimens of *E. anauniensis* were found in Türkiye. The description, illustrations of deutonymph males of *E. anauniensis*, and its measurements of some body parts were made. This is the first record of deutonymph male of *E. anauniensis*.

Keywords: Acari, first record, immature, mite, Türkiye

Eustigmaeus anauniensis'in (Canestrini) (Trombidiformes: Stigmaeidae) Erkek Deutonimfinin İlk Tanımı

Öz

Eustigmaeus Berlese, 130'dan daha fazla türle Stigmaeidae familyasının en çeşitli cinslerinden biridir. Bu cins, tüm dünyada geniş bir dağılıma sahip olup, Antarktika hariç bütün zoocoğrafik bölgelerde bulunur. Şu ana kadar *Eustigmaeus anauniensis* (Canestrini) türünün ergin dişi, erkek, deutonimf, protonimf ve larvası bilinmekte; ancak ergin olmayan erkek bireyleri bilinmemektedir. Bu çalışmada, *E. anauniensis*'in beş deutonimf erkek örneği Türkiye'den bulunmuştur. *E. anauniensis*'in deutonimf erkeklerinin tanımı yapılarak görüntüleri verilmiş ayrıca vücut parçalarının ölçümleri alınmıştır. *E. anauniensis*'in deutonimf erkekleri ilk defa bu çalışmada kaydedilmiştir.

Anahtar Kelimeler: Acari, ilk kayıt, olgunlaşmamış, akar, Türkiye

*Corresponding Author: salihdogan@erzincan.edu.tr
Salih DOĞAN, https://orcid.org/0000-0001-5030-0544
Sibel DOĞAN, https://orcid.org/0000-0002-0644-0280
Şifanur UĞURLU, https://orcid.org/0000-0002-7128-1861
Nisanur POLAT, https://orcid.org/0009-0007-7095-1855

1. Introduction

Members of the family Stigmaeidae live on plants, in soil, plant litter, mosses and lichens, feeding on a variety of small arthropods, and some of which have long been considered economically important predators of plant feeding mites [1-6]. The family Stigmaeidae currently contains more than 640 species within 33 valid genera [3, 4, 6, 7].

Mites of the genus *Eustigmaeus* Berlese are generally free-living but a few are parasitic on sand flies [8, 9]. *Eustigmaeus* is one of the largest genera of the Stigmaeidae. This genus comprises more than 130 species worldwide [3, 4, 6, 7], 28 of which have been reported from Türkiye [9, 10].

Eustigmaeus anauniensis was originally described by Canestrini (1889). Summers (1957) synonymised *Eustigmaeus granulosus* Wilmann, 1951 with *Raphygnathus pectinatus* (*sic*) Ewing, 1917. Afterwards, Wood in 1973, synonymised *Raphignathus pectinatus* Ewing, 1917 with *E. anauniensis* (Canestrini, 1889), and he stated that the specimens named as *Ledermuelleria pectinata* (Ewing) by Marshall and Kevan (1964) belonged a separate species and described them as *Ledermuelleria collegiensis* Wood, 1972 [11-15]. Faraji et al. (2007) and Dönel and Doğan (2011) suggested that *E. kentingensis* Tseng, 1982 to be a synonym of *E. anauniensis* (Canestrini, 1889); however, this possibility was not supported by Fan et al. (2016) [3, 16-18].

Eustigmaeus anauniensis (Canestrini) is widely distributed and has been recorded from many countries including Türkiye [3, 4, 10]. This species can be recognized by having eyes, dorsal dimples with punctuations, dorsal body setae bushy, not bearing hyaline sheaths, setae c_2 similar other dorsal body setae, endopodal shields fused, femur II with four setae, three pairs of aggenital setae in female.

Undescribed deutonymph males of *E. anauniensis* were collected from Türkiye. The aim of this study is to describe deutonymph male of *E. anauniensis*.

2. Materials and Methods

The mite specimens were extracted by using Berlese-Tullgren funnels, cleaned in 60% lactic acid, mounted on microscope slides in Hoyer's medium, and viewed with a Leica DM 4000B microscope [1, 19]. The designations for idiosoma, palp and leg setae follow those of Grandjean (1944, 1946) and Kethley (1990) [20-22]. Leica Application Suite (LAS) Software Version 4.8 was used to take in micrometers (μm) the measurements, which were provided as a range. Setal formulae of leg segments are given with solenidia in parentheses. The examined specimens were deposited in EBYU (Acarology Laboratory of Erzincan Binali Yıldırım University, Erzincan, Türkiye).

3. Results

***Eustigmaeus anauniensis* (Canestrini, 1889)** (Figures 1-12)

Raphignathus anauniensis Canestrini, 1889: 511.

Description of the deutonymph male (n=5) (Figures 7, 8)

Length of body: 233-320. Width of body: 165-210.

Gnathosoma. Gnathosoma 49-58, chelicerae 61-69, palp 74-79 long. Subcapitulum with two pairs of adoral setae ($or_{1,2}$) and two pairs of subcapitular setae (*m, n*). Dimensions and distance between subcapitular setae, *m* 7-10, *n* 6-8, *m–m* 16-19, *n–n* 18-21, *m–n* 6-10. Number of setae on palp segments: Tr 0, Fe 3, Ge 2, Ti 2 +1 claw, Ta 5 (+ 3 fused eupathidia, + 1 ω).

Dorsum. Dorsal shields slightly dimpled and punctuated. Eyes present, post-ocular bodies absent. Eyes 7-9 in diameter. Dorsal setae barbed. Lengths and distances of dorsal idiosomal setae as follows: *vi* 15-23, *ve* 16-20, *sci* 12-17, *sce* 14-22, c_1 13-18, c_2 18-33, d_1 14-19, d_2 12-19, e_1 18-24, e_2 18-27, f_1 36-40, h_1 22-25, h_2 22-28, *vi–vi* 24-32, *ve–ve* 65-72, *vi–ve* 23-35, *sci–sci* 109-127, *ve–sci* 26-31, *sce–sce* 136–156, *sci–sce* 29-34, c_1–c_1 52-67, c_2–c_2 141-177, d_2–d_2 132-154, c_1–d_1 38-42, c_1–d_2 48-52, d_1–d_1 36-45, d_2–d_1 46-51, e_2–e_2 93-110, d_2–e_2 42-48, d_1–e_1 41-45, d_1–e_2 40-47, e_1–e_1 39-48, e_2–e_1 24-27, f_1–f_1 40-49, e_1–f_1 23-26, e_2–f_1 42-45, h_1–h_1 14-19, h_2–h_2 35-46, h_1–h_2 10-11.

Venter. Coxisternal shields divided in midline and bearing setae *la*, *3a* and *4a*. Dimensions of the setae and distances between them as follows: *la* 8-10, *3a* 10-12, *4a* 6-9, *1a–1a* 20-26, *3a–3a* 20-26, *4a–4a* 14-29. Aggenital shield with two pairs of setae. Three pairs of pseudanal setae present. Aggenital setae ag_1 6-8, ag_2 7-9. Pseudanal setae ps_1 4-7, ps_2 6-10, ps_3 9-10.

Legs. Formulae of setae and solenidia on legs I–IV: coxae 2–2–2–2, trochanters 1–1–2–0, femora 6–4–3–2, genua 3(+1κ)–2(+1κ)–0–0, tibiae 5(+1φ+1φρ)–5(+1φρ)–5(+1φρ)–5(+1φρ), tarsi 13(+1ω)–9(+1ω)–7(+1ω)–7. Measurements of legs I-IV 114-119, 94-121, 100-119, 110-124 respectively.

Materials examined

232 ♀♀, 17♂♂, 18 deutonymphs, 5 deutonymph males, 22 protonymphs, 17 larvae.

1♀ from litter under oak, 39°36'06.0"N 39°08'58.5"E, 1376 m a.s.l., 26 April 2022; 1♀ from litter under oak, 39°36'34.31"N 39°9'18.62"E, 1138 m a.s.l., 29 October 2022; 3 protonymphs, 3 larvae from litter under oak, 39°36'08.4"N 38°39'30.4"E, 1624 m a.s.l., 25 June 2022; 2♀♀, 1 deutonymph and 1 protonymph from same habitat, 31 July 2022; 6♀♀ from same habitat, 28 October 2022; 1♀ from same habitat, 24 December 2022; 4♀♀ and 1 deutonymph from same habitat, 28 January 2023; 9♀♀ from same habitat, 26 March 2023; 28♀♀ from litter under oak, 39°36'45.2"N 38°39'59.7"E, 1715 m a.s.l., 26 April 2022; 2♀♀ from same habitat, 29 May 2022; 1♀, 1 deutonymph male, 4 protonymphs and 7 larvae from same habitat, 26 June 2022;

1 deutonymph and 1 larva from same habitat, 31 July 2022; 17♀♀, 2♂♂ and 2 larvae from same habitat, 27 September 2022; 4♀♀ from same habitat, 28 October 2022; 3♀♀ from same habitat, 28 November 2022; 22♀♀ from litter under oak, 39°36'16.1"N 38°39'54.3"E, 1693 m a.s.l., 26 April 2022; 31♀♀ from same habitat, 29 May 2022; 4♀♀, 1 protonymph from same habitat, 26 June 2022; 16♀♀ 1♂, 1 deutonymph, 1 deutonymph male and 4 protonymphs from same habitat, 31 July 2022; 1♀, 1♂, 6 deutonymphs, 1 deutonymph male, 2 protonymphs and 3 larvae from same habitat, 27 August 2022; 21♀♀, 8♂♂, 4 deutonymphs and 4 protonymphs from same habitat, 28 September 2022; 2♀♀, 2♂♂ and 1 deutonymph from same habitat, 29 October 2022; 2♀♀ from same habitat, 25 December 2022; 1♀ from litter under oak, 39°12'31.84"N 38°34'36.21"E, 922 m a.s.l., 28 October 2022; 1♀ from soil, 39°36'34.31"N 39°9'18.62"E, 1138 m a.s.l., 29 May 2022; 21♀♀ from same habitat, 27 January 2023; 1♀ from soil, 39°36'45.2"N 38°39'59.7"E, 1715 m a.s.l., 27 August 2022; 1♀ from same habitat, 24 December 2022; 2♀♀ from soil, 39°36'16.1"N 38°39'54.3"E, 1693 m a.s.l., 26 April 2022; 1♀ from moss, 39°36'18.9"N 39°09'20.7"E, 1176 m a.s.l., 28 January 2023; 1♀ from moss, 39°36'34.31"N 39°9'18.62"E, 1138 m a.s.l., 25 March 2023; 1♀ from moss, 39°36'08.4"N 38°39'30.4"E, 1624 m a.s.l., 28 October 2022; 1 deutonymph from same habitat, 26 March 2023; 8♀♀, 2♂♂, 1protonymph from moss, 39°36'45.2"N 38°39'59.7"E, 1715 m a.s.l., 27 September 2022; 2♀♀ from same habitat, 24 December 2022; 10♀♀, 1 deutonymph from same habitat, 26 March 2023; 3♀♀ from moss, 39°36'16.1"N 38°39'54.3"E, 1693 m a.s.l., 26 June 2022; 1♂ from same habitat, 28 September 2022; 1♀ from grassy and mossy soil, 39°36'18.9"N 39°09'20.7"E, 1162 m a.s.l., 26 June 2022—the Karasu Valley, Erzincan, Türkiye. 1 deutonymph from moss, 39°35'08.7"N 39°52'12.4"E, 1357 m a.s.l., 13 October 2018; 1 deutonymph male from soil and litter under oak, 39°31'43.3"N 39°54'21.7'E, 1719 m a.s.l., 22 June 2019; 1 larva and 1 protonymph from moss, same habitat, 22 June 2019; 1 protonymph from soil and litter under oak, 39°23'51.4"N 39°46'50.3"E, 1508 m a.s.l., 22 June 2019; 1 deutonymph male from moss, 39°23'32.2"N 39°47'05.7"E, 1534 m a.s.l., 18 August 2019—Tunceli, Türkiye.

Distribution

Austria, Azerbaijan, Canada, China, Crimea, Holland, Hungary, Iran, Israel, Italy, Japan, Latvia, Lithuania, Poland, Russia, Slovakia, Taiwan, Türkiye, Ukraine and USA [3, 4, 13 ,15].

4. Discussion and Conclusion

Four active postembryonic developmental stages are typically present in members of the family Stigmaeidae: the six-legged larva, the eight-legged protonymph, the deutonymph, and the adult. The lack of genital setae allows the protonymph and deutonymph stages to be clearly distinguished from adult stages; the genitalia of the larva are absent [23].

During the nymphal examination, we noticed that five specimens of *Eustigmaeus anauniensis* are different from the other deutonymphs. They are identified as deutonymph males. In general, the male deutonymphs, are similar to female deutonymphs except for the numbers of aggenital

setae (Table 1). Male deutonymphs resemble adult males in having two pairs of aggenital setae (Table 1).

Table 1. Distinguishing features of mature and immature stages of *Eustigmaeus anauniensis*.

Characters	Larva	Protonymph	Deutonymph female	Deutonymph male	Adult female	Adult male
Number of setae on coxae I-IV	1–0–0	2–2–2–0	2–2–2–2	2–2–2–2	2–2–2–2	2–2–2–2
Number of setae on trochanters I-IV	0–0–0	0–0–1–0	1–1–2–0	1–1–2–0	1–1–2–1	1–1–2–1
Number of setae on femora I-IV	4–4–3	4–4–3–1	6–4–3–2	6–4–3–2	6–4–3–2	6–4–3–2
Number of setae on genua I-IV	2(+1κ)–2(+1κ)–0	3(+1κ)–2(+1κ)–0–0	3(+1κ)–2(+1κ)–0–0	3(+1κ)–2(+1κ)–0–0	3(+1κ)–3(+1κ)–1–1	3(+1κ) –3(+1κ)–1–1
Ventral setae *4a*	–	–	+	+	+	+
Number of pairs of subcapitular setae	0	1	2	2	2	2
Number of pairs of aggenital setae	0	1	3	2	3	2

+ present, – absent

Although all life stages of this species have been recorded, deutonymph males have not been identified yet. With this study, this life stage is described and illustrated for the first time. To the best of knowledge, this stage in the genus has only been detected in *Eustigmaeus bochkovi* by Khaustov (2019) [24].

Ethics in Publishing

There are no ethical issues regarding the publication of this study.

Author Contributions

Salih Doğan: Conceptualization, investigation, methodology, resources, funding acquisition, supervision, visualisation, validation, writing – original draft, writing – review & editing. Sibel Doğan: Investigation, methodology, data curation, writing – original draft. Şifanur Uğurlu & Nisanur Polat: Investigation, methodology, data curation.

Acknowledgements

The mite materials from the Karasu Valley were collected from a project (121Z986) that was supported by the Scientific and Technological Research Council of Türkiye (TÜBİTAK). We appreciate the financial support of TÜBİTAK. For granting the legal approvals (E-21264211-288.04-4255389 and E-50411936-903.07.02-4372543) for the field surveys, we are grateful to Republic of Türkiye Ministry of Agriculture and Forestry.

References

[1] Fan Q.-H., Zhang, Z.-Q. (2005) Raphignathoidea (Acari: Prostigmata). Fauna of New Zealand, 52, 1-400.
https://doi.org/10.7931/J2/FNZ.52

[2] Fan Q.-H., Flechtmann C.H.W. (2015) Chapter 7. Stigmaeidae. *In*: Carrillo, D., Moraes, G.J. de & Peña, J. (Eds), *Prospects for Biological Control of Plant Feeding Mites and Other Harmful Organisms*. Springer, New York, USA 185-206.
http://dx.doi.org/10.1007/978-3-319-15042-0_7

[3] Fan Q.-H., Flechtmann C.H.W., De Moraes, G.J. (2016) Annotated catalogue of Stigmaeidae (Acari: Prostigmata), with a pictorial key to genera, Zootaxa, 4176, 1-199.
https://doi.org/10.11646/zootaxa.4176.1.1

[4] Beron P. (2020) *Acarorum Catalogus VII. Trombidiformes, Prostigmata, Raphignathoidea. Fam. Barbutiidae, Caligonellidae, Camerobiidae, Cryptognathidae, Dasythyreidae, Dytiscacaridae, Eupalopsellidae, Homocaligidae, Mecognathidae, Raphignathidae, Stigmaeidae, Xenocaligonellididae.* Pensoft & National Museum of Natural History & Bulgarian Academy of Sciences, Sofia, 306 pp.
https://doi.org/10.3897/ab.e55087

[5] Khaustov A.A. (2023) Review of *Cheylostigmaeus* (Acari: Stigmaeidae) of Russia, Acarina, 31(1), 31-75.
https://doi.org/10.21684/0132-8077-2023-31-1-31-75

[6] Khaustov A.A., Kravchenko S.V., Kazakov D.V. (2023) Two new species and a new synonym of *Eustigmaeus* (Acari: Stigmaeidae) from Russia with COI barcode, Acarina, 31(1), 77-99.
https://doi.org/10.21684/0132-8077-2023-31-1-77-99

[7] Fan Q.-H., Flechtmann C.H.W., De Moraes, G.J. (2019) Emendations and updates to "Annotated catalogue of Stigmaeidae (Acari: Prostigmata), with a pictorial key to genera", Zootaxa, 4647, 88-103.
https://doi.org/10.11646/zootaxa.4647.1.9

[8] Stathakis T.I., Kapaxidi E.V., Papadoulis G.Th. (2016) The genus *Eustigmaeus* Berlese (Acari: Stigmaeidae) from Greece, Zootaxa, 4191(1), 1-102.
https://doi.org/10.11646/zootaxa.4191.1.1

[9] Pekağırbaş M., Karakuş M., Yılmaz A., Erişöz Kasap Ö., Sevsay S., Özbel Y., Töz S., Doğan, S. (2023) Two parasitic mite species on Phlebotominae sand flies (Diptera: Psychodidae) from Türkiye: *Biskratrombium persicum* (Microtrombidiidae) and *Eustigmaeus johnstoni* (Stigmaeidae), Acarological Studies, 5(1), 11-16.
https://doi.org/10.47121/acarolstud.1209774

[10] Doğan S. (2019) Raphignathoidea (Acari: Trombidiformes) of Turkey: A review of progress on the systematics, with an updated checklist, Acarological Studies, 1, 129-151.

[11] Ewing H.E. (1917) New Acarina. Part II. Descriptions of new species and varieties from Iowa, Missouri, Illinois, Indiana, and Ohio, Bulletin of the American Museum of Natural History, 37, 149-172.

[12] Willmann C. (1951) Untersuchungen über die terrestrische Milbenfauna im pannonischen Klimagebiet Österreichs. *Sitzungsberichte österreichische Akademie der Wissenschaften, Mathematisch-naturwissenschafiliche, Klasse*, Abtheilung 1, 160(1-2), 91-176. (in German)

[13] Summers F.M. (1957) American species of *Ledermuelleria* and *Ledermuelleriopsis*, with a note on new synonymy in *Neognathus* (Acarina, Stigmaeidae, Caligonellidae), Proceedings of the Entomological Society of Washington, 59(2), 49-60.

[14] Wood T.G. (1972) New and redescribed species of *Ledermuelleria* Oudms. and *Villersia* Oudms. (Acari: Stigmaeidae) from Canada, Acarologia, 13(2), 301-318.

[15] Wood T.G. (1973) Revision of Stigmaeidae (Acari: Prostigmata) in the Berlese collection, Acarologia, 15, 76-95.

[16] Tseng Y.-H. (1982) Mites of the family Stigmaeidae of Taiwan with key to genera of the world (Acarina: Prostigmata), Phytopathologist and Entomologist of the National Taiwan University, 9, 1-52.

[17] Faraji F., Ueckermann E.A., Bakker F. (2007) First record of *Eustigmaeus jiangxiensis* Hu, Chen and Huang (Acari: Stigmaeidae) from France with a key to the European species of *Eustigmaeus* Berlese, 1910, International Journal of Acarology, 33(2), 145-151. http://dx.doi.org/10.1080/01647950708684515

[18] Dönel G., Doğan S. (2011) The stigmaeid mites (Acari: Stigmaeidae) of Kelkit Valley (Turkey), Zootaxa, 2942, 1-56. https://doi.org/10.11646/zootaxa.2942.1.1

[19] Walter D.E., Krantz G.W. (2009) Collecting, rearing and preparing specimens. *In*: Krantz, G.W. and Walter, D.E. (Eds), *A Manual of Acarology*. The third edition. Texas Tech University Press, Lubbock, Texas, USA, pp. 83-96.

[20] Grandjean F. (1944) Observations sur les acariens de la famille des Stigmaeidae, Archives des Sciences Physiques et Naturelles, 26, 103-131. (in French)

[21] Grandjean F. (1946) Au sujet de l'organe de Claparède, des eupathides multiples et des taenidies mandibulaires chez les Acariens actinochitineux, Archives des Sciences Physiques et Naturelles, 28, 63-87. (in French)

[22] Kethley J. (1990) Acariformes, Prostigmata. *In*: Dindal, D.L. (Ed.), *Soil Biology Guide*, New York, USA, Wiley, pp. 667-756.

[23] Doğan S., Doğan S., Zeytun E. (2019) Existence of tritonymphal stage of *Stigmaeus elongatus* Berlese (Acari: Stigmaeidae), with numerical variations in some body setae in its adult stage, Systematic and Applied Acarology, 24(5), 711-730. https://doi.org/10.11158/saa.24.5.1

[24] Khaustov A.A. (2019) Contribution to systematics of the genus *Eustigmaeus* (Acari: Stigmaeidae) of Russia, Acarologia, 59(1), 152-173. https://doi.org/10.24349/acarologia/20194320

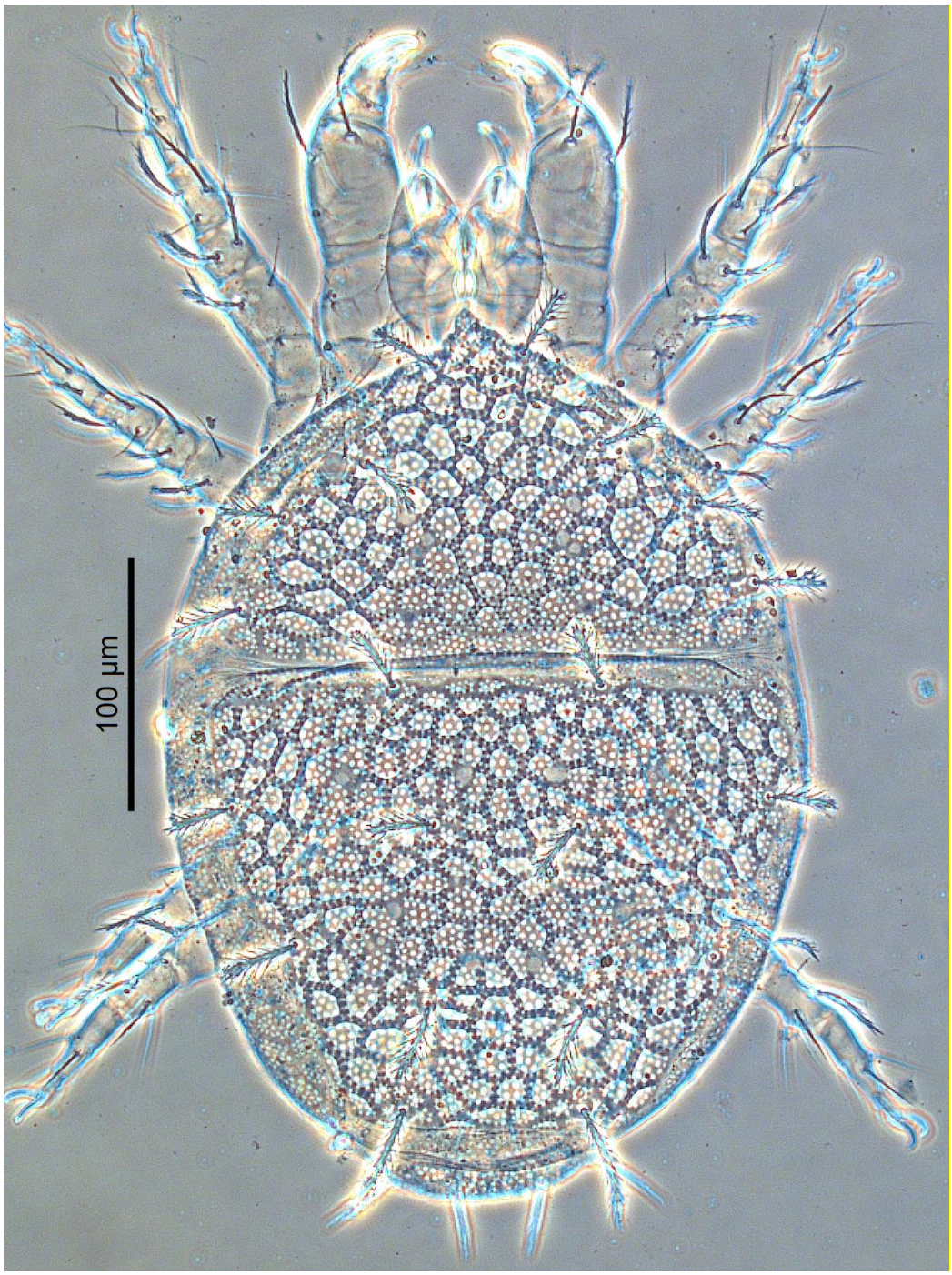

Figure 1. *Eustigmaeus anauniensis* (Canestrini) (female). Dorsal view.

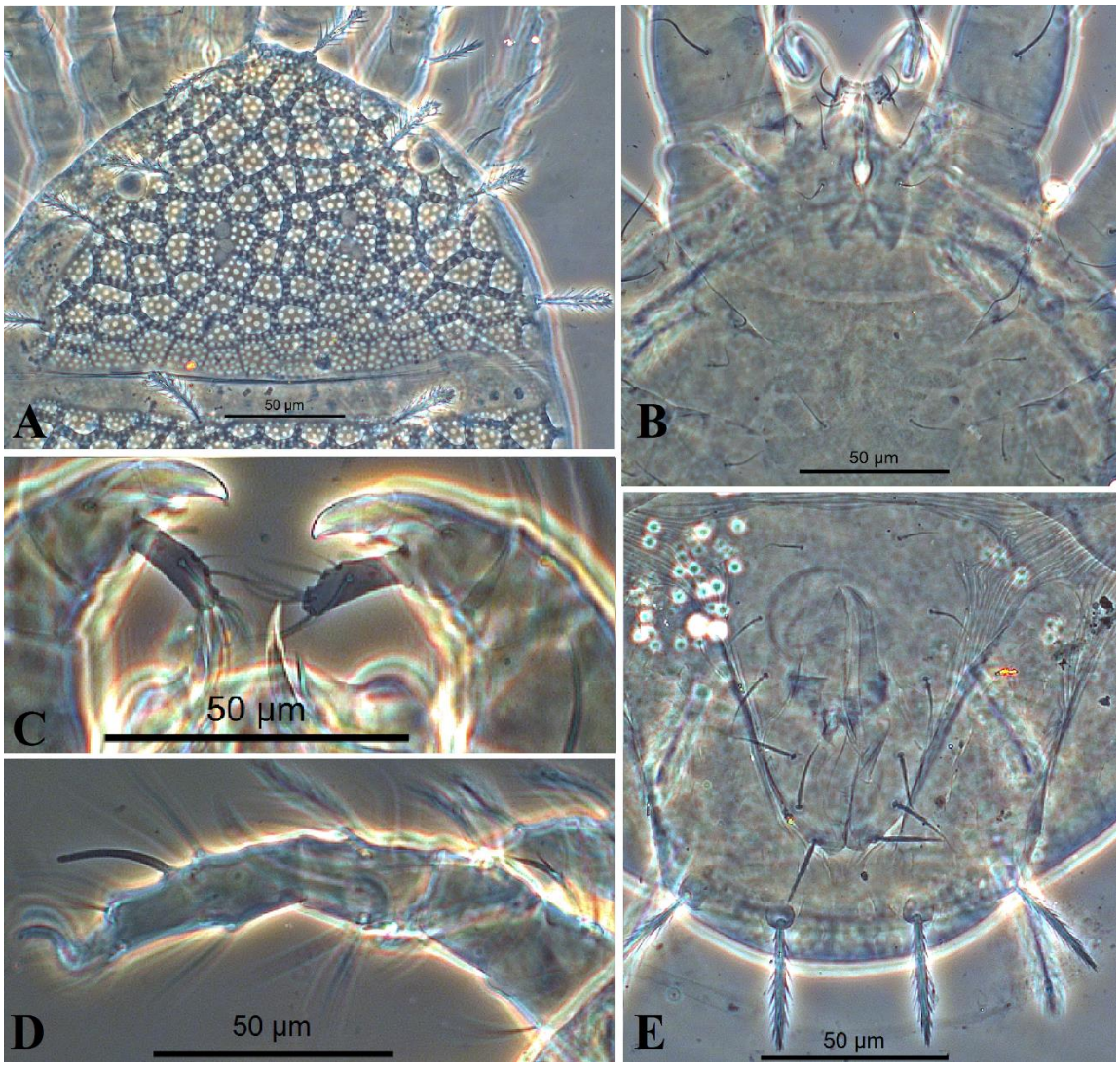

Figure 2. *Eustigmaeus anauniensis* (Canestrini) (female). A) Prodorsum, B) Coxisternal region, C) Palp, D) Leg I, E) Anogenital region.

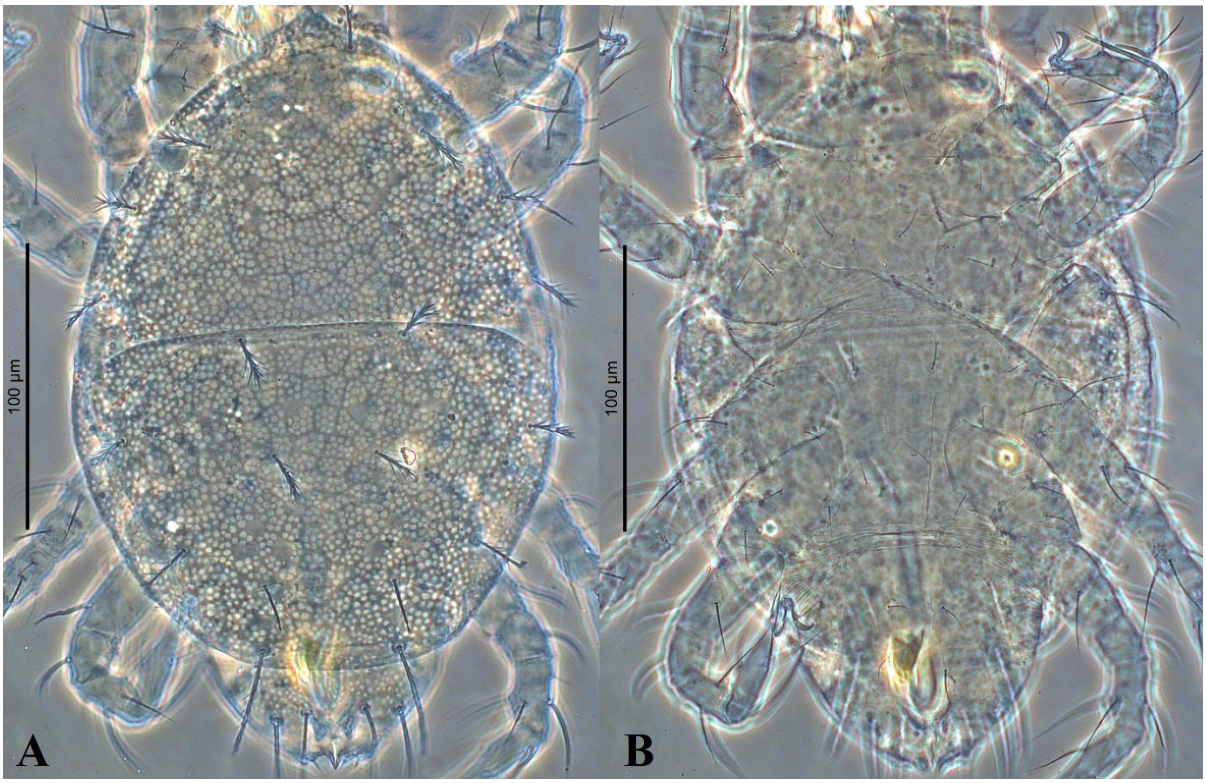

Figure 3. *Eustigmaeus anauniensis* (Canestrini) (male). A) Dorsal view, B) Ventral view.

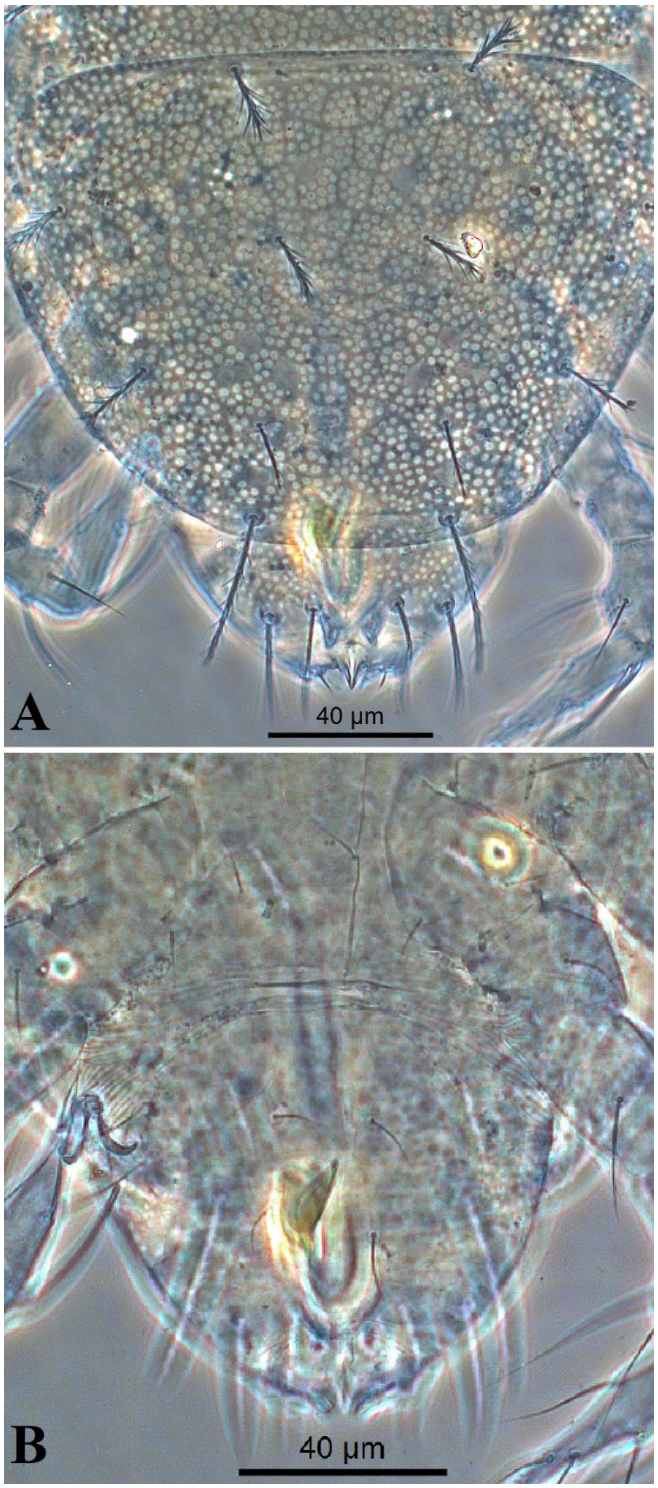

Figure 4. *Eustigmaeus anauniensis* (Canestrini) (male). A) Dorsal hysterosoma, B) Ventral hysterosoma.

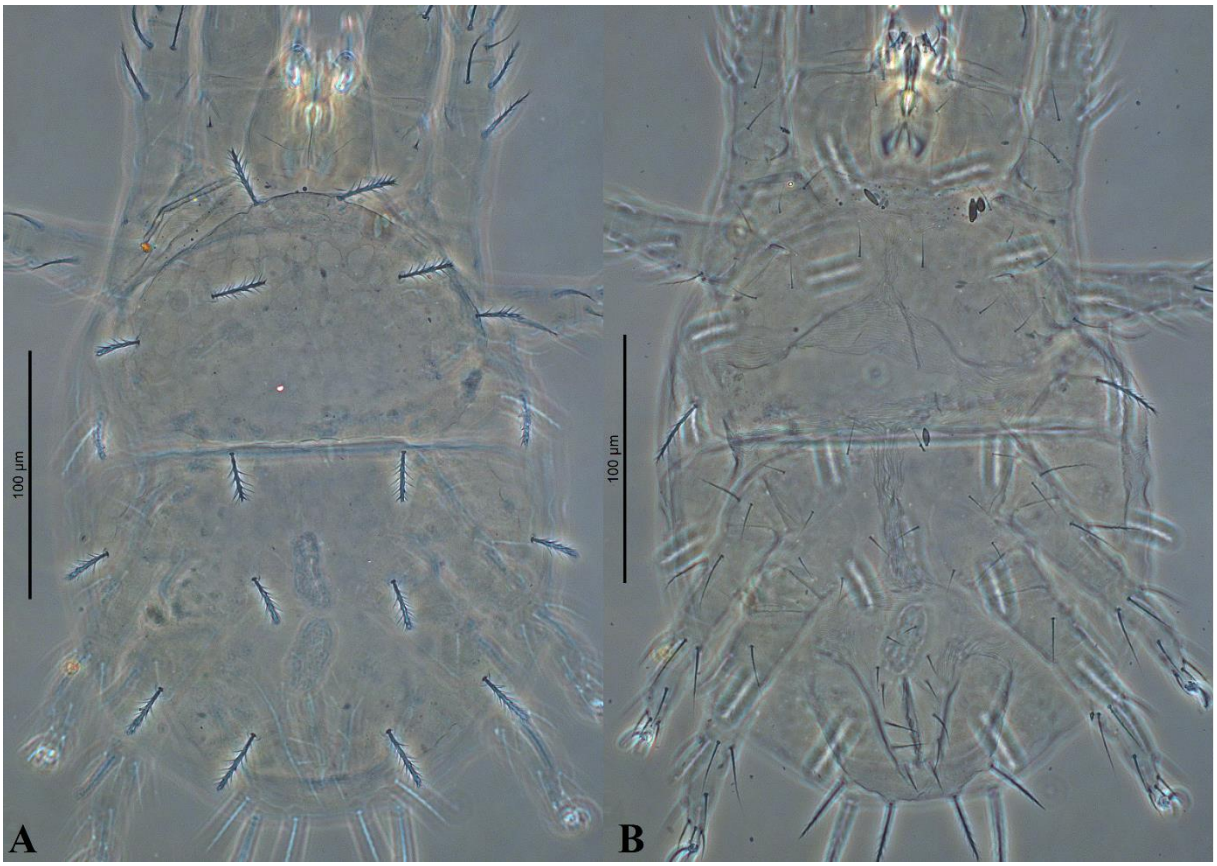

Figure 5. *Eustigmaeus anauniensis* (Canestrini) (deutonymph female). A) Dorsal view, B) Ventral view.

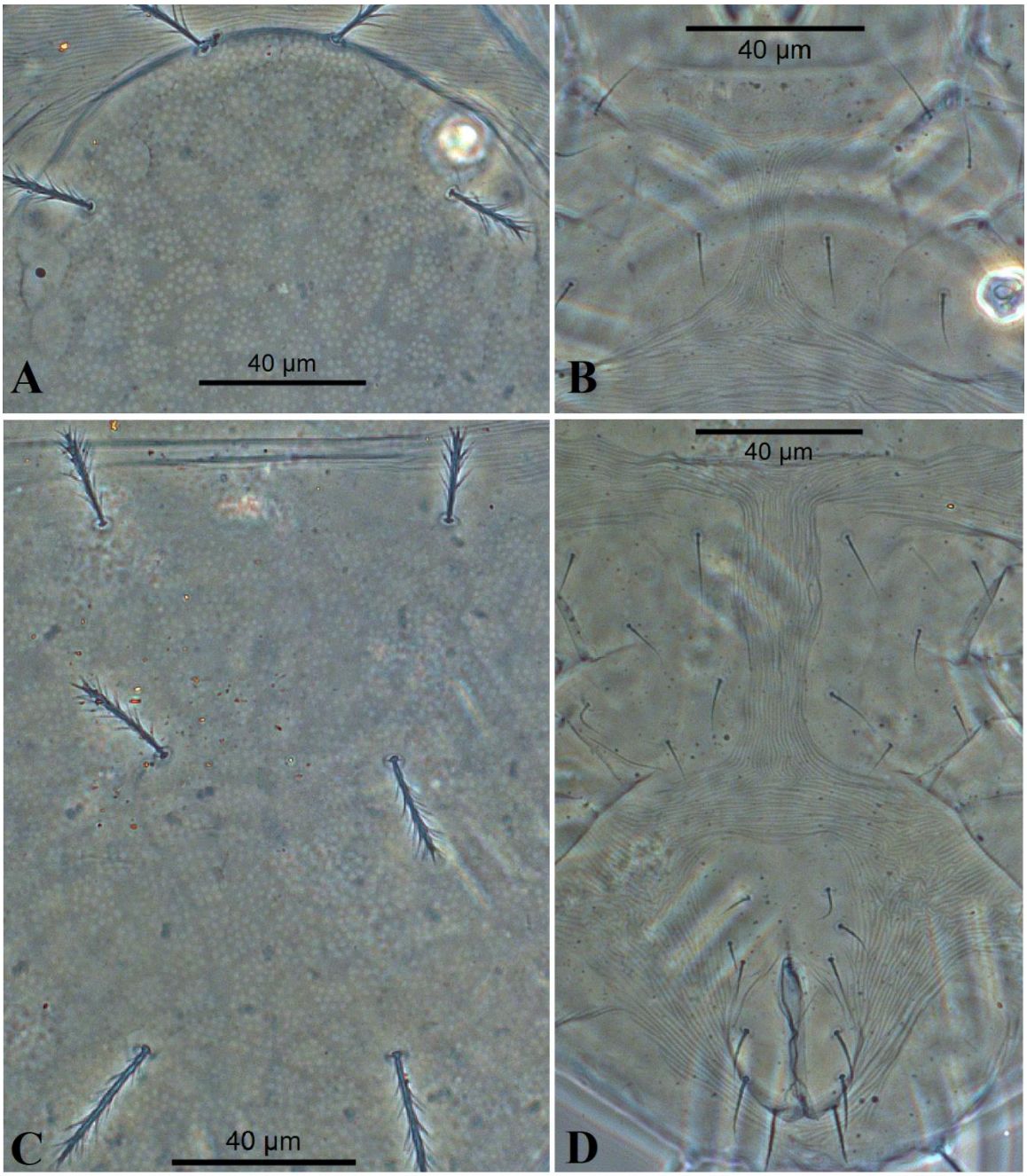

Figure 6. *Eustigmaeus anauniensis* (Canestrini) (deutonymph female). A) Prodorsum, B) Coxisternal region, C) Dorsal hysterosoma, D) Ventral hysterosoma.

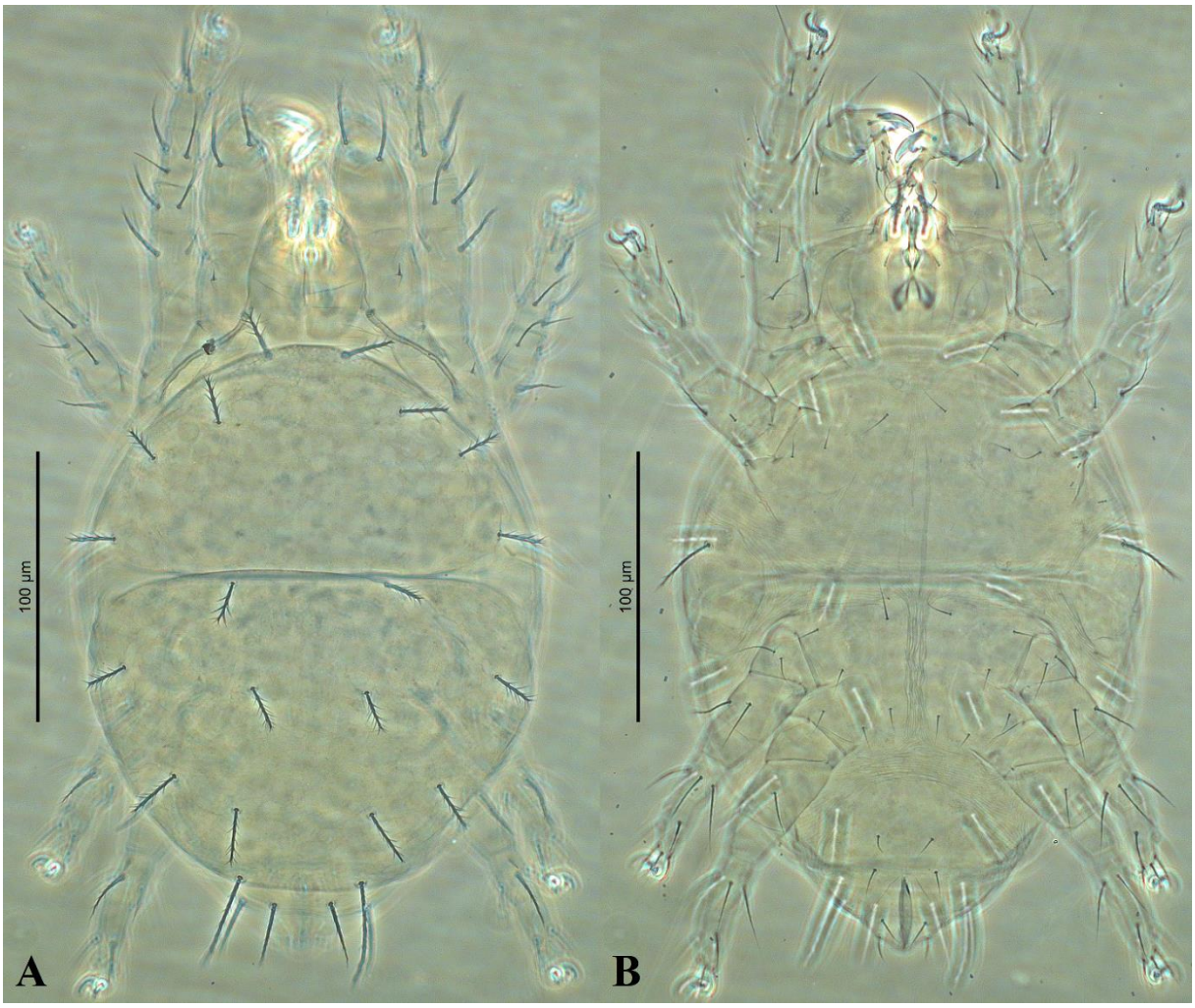

Figure 7. *Eustigmaeus anauniensis* (Canestrini) (deutonymph male). A) Dorsal view, B) Ventral view.

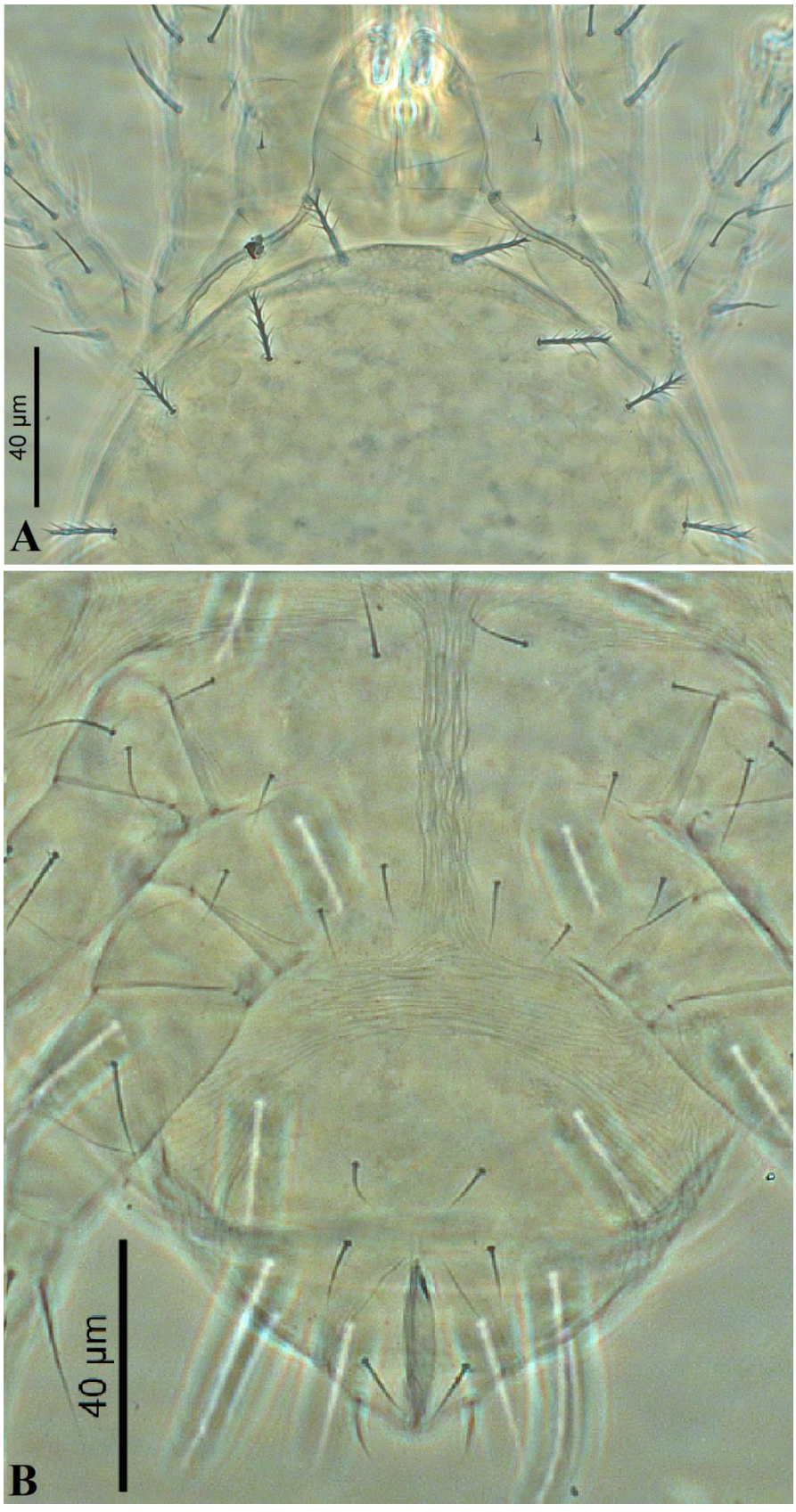

Figure 8. *Eustigmaeus anauniensis* (Canestrini) (deutonymph male). A) Prodorsum, B) Ventral hysterosoma.

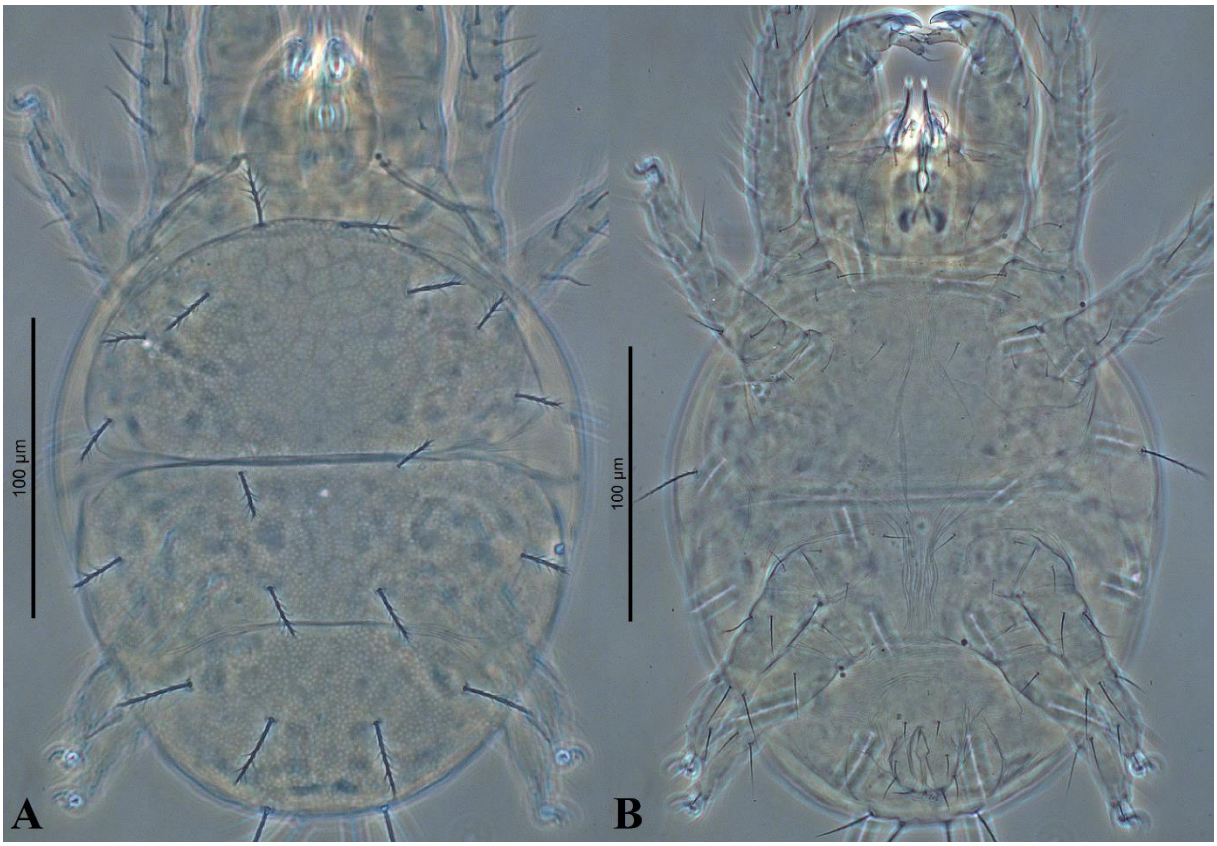

Figure 9. *Eustigmaeus anauniensis* (Canestrini) (protonymph). A) Dorsal view, B) Ventral view.

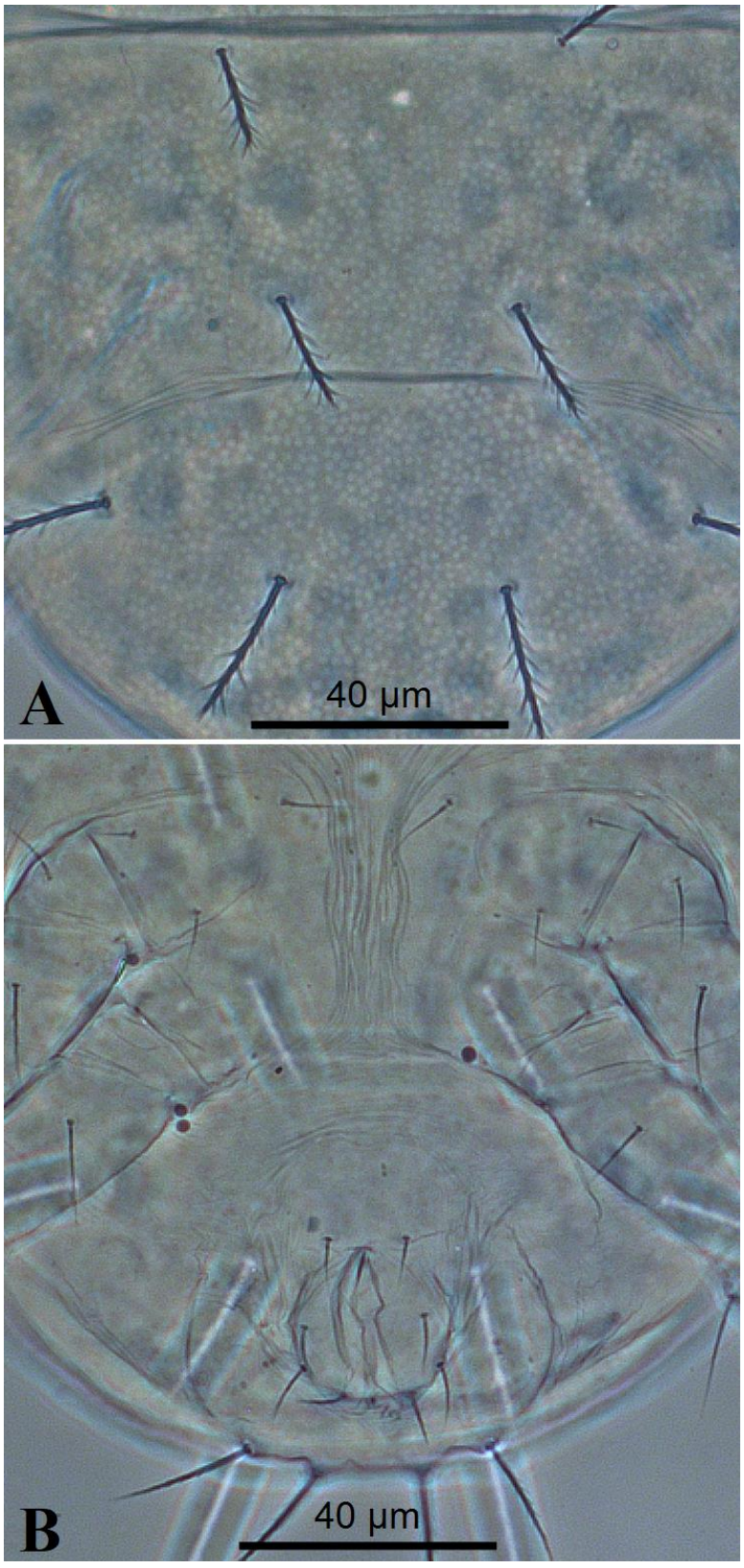

Figure 10. *Eustigmaeus anauniensis* (Canestrini) (protonymph). A) Dorsal hysterosoma, B) Ventral hysterosoma.

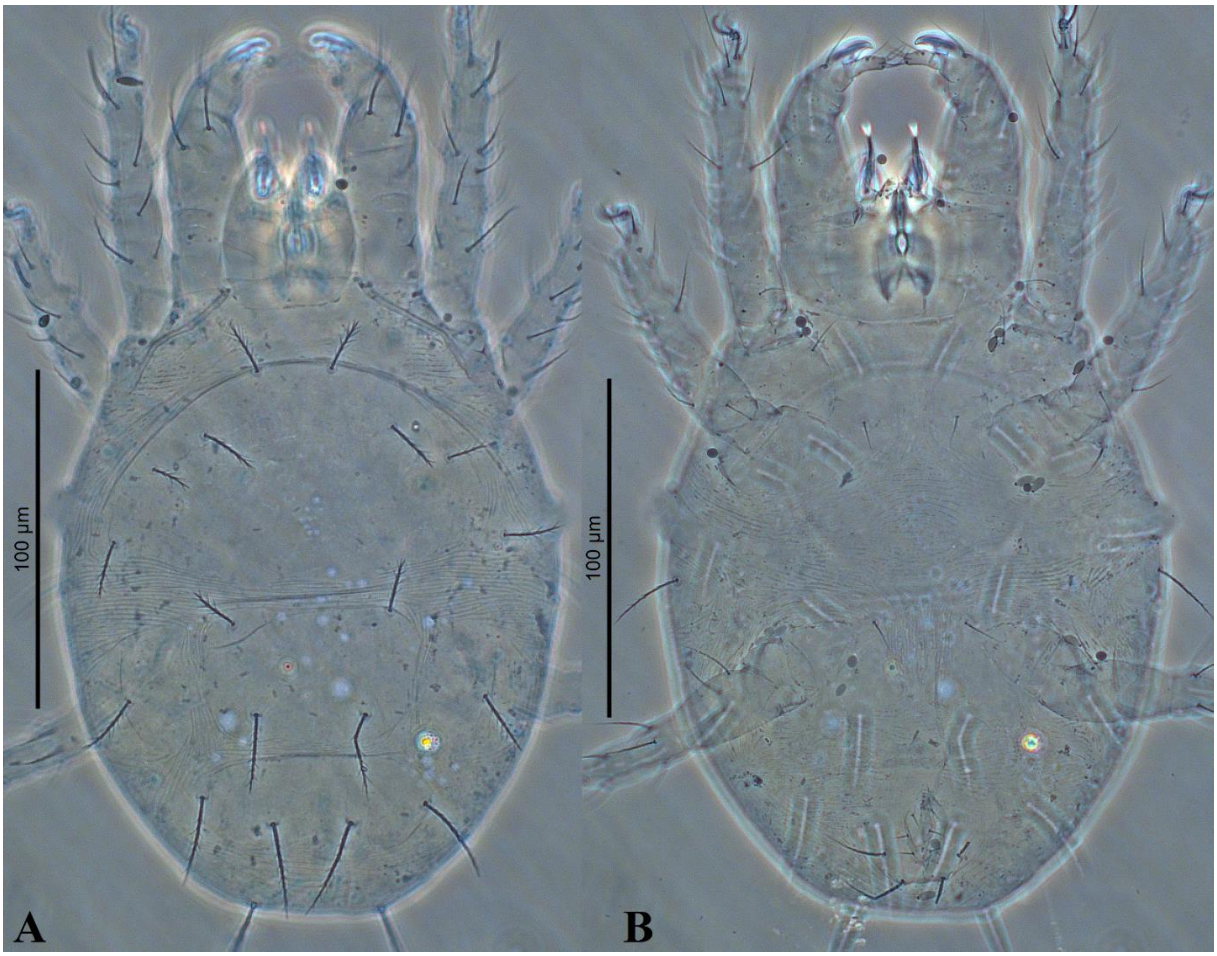

Figure 11. *Eustigmaeus anauniensis* (Canestrini) (larva). A) Dorsal view, B) Ventral view.

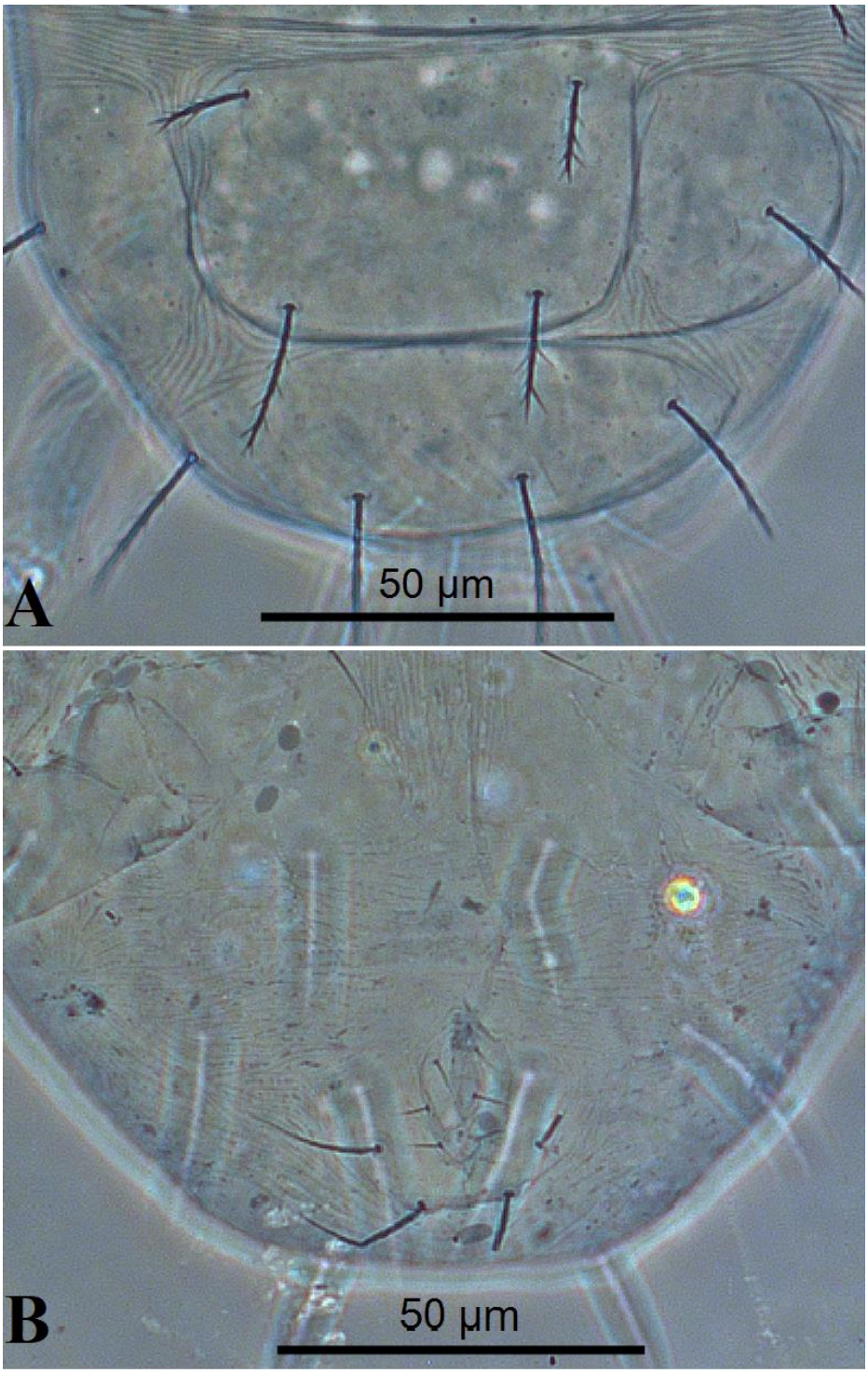

Figure 12. *Eustigmaeus anauniensis* (Canestrini) (larva). A) Dorsal hysterosoma, B) Ventral hysterosoma.

Erzincan Üniversitesi
Fen Bilimleri Enstitüsü Dergisi
2024,17(1), 196-209
ISSN: 1307-9085, e-ISSN: 2149-4584
Araştırma Makalesi

Erzincan University
Journal of Science and Technology
2024,17(1), 196-209
DOI: 10.18185/erzifbed.1392027
Research Article

Effect of Hydrothermal Reaction Temperature on the Structural and Optical Properties of CuO Thin Films

Aykut ASTAM[1*], Ömer KAYA[2]

[1] Department of Physics, Faculty of Art and Science, Erzincan Binali Yıldırım University, Erzincan, Turkey
[2] Institute of Science and Technology, Erzincan Binali Yıldırım University, Erzincan, Turkey

Received: 16/11/20.23, **Revised:** 04/12/2023, **Accepted:** 18/12/2023, **Published:** 28/03/2024

Abstract

Copper oxides are one of the first semiconductors studied for device applications. In the present work, CuO thin films were deposited on fluorine-doped tin oxide (FTO) substrates via hydrothermal method without using any surfactant and the effects of reaction temperature on the properties of the films were studied. CuO thin films deposited at different reaction temperatures were characterized for their structural and optical properties using X-ray diffraction (XRD), scanning electron microscopy (SEM), energy dispersive X-ray analysis (EDAX), Raman spectroscopy, and optical absorption measurements. XRD results revealed that all the films consisted of polycrystalline CuO with a monoclinic crystal structure without any impurity phase. SEM images showed that chrysanthemum-like structures were formed, the number of which increased with increasing hydrothermal reaction temperature. EDAX measurements proved the existence of Cu and O elements and showed that all the films have Cu/O ratios close to unity. The Raman spectra confirmed the formation of crystalline CuO in all the films. From the optical absorption measurements, the direct forbidden energy gap values of the CuO thin films were found to be between 1.34 eV and 1.41 eV, depending on the hydrothermal reaction temperature.
Keywords: CuO thin films, hydrothermal method, reaction temperature.

Hidrotermal Reaksiyon Sıcaklığının CuO İnce Filmlerin Yapısal ve Optik Özelliklerine Etkisi

Öz

Bakır oksitler cihaz uygulamaları için incelenen ilk yarı iletkenlerden biridir. Bu çalışmada, CuO ince filmler, herhangi bir yüzey aktif madde kullanılmadan, hidrotermal yöntemle flor katkılı kalay oksit (FTO) altlıklar üzerine büyütülmüş ve reaksiyon sıcaklığının filmlerin özellikleri üzerine etkisi araştırılmıştır. Farklı reaksiyon sıcaklıklarında büyütülen CuO ince filmler, X-ışını kırınımı (XRD), taramalı elektron mikroskobu (SEM), enerji dağılımlı X-ışını analizi (EDAX), Raman spektroskopisi ve optik soğurma ölçümleri kullanılarak yapısal ve optik özellikleri açısından karakterize edilmiştir. XRD sonuçları, tüm filmlerin herhangi bir safsızlık fazı içermeyen, monoklinik kristal yapıya sahip, polikristal CuO'dan oluştuğunu ortaya çıkarmıştır. SEM görüntüleri, krizantem benzeri yapıların oluştuğunu ve hidrotermal reaksiyon sıcaklığının artmasıyla bu yapıların sayısının arttığını göstermiştir. EDAX ölçümleri Cu ve O elementlerinin varlığını kanıtlamış ve tüm filmlerin Cu/O oranlarının bire yakın olduğunu göstermiştir. Raman spektrumları tüm filmlerde kristal CuO oluşumunu doğrulamıştır. Optik soğurma ölçümlerinden CuO ince filmlerinin doğrudan yasak enerji aralığı değerlerinin hidrotermal reaksiyon sıcaklığına bağlı olarak 1,34 eV ile 1,41 eV arasında olduğu bulunmuştur.
Anahtar Kelimeler: CuO ince filmler, hidrotermal method, reaksiyon sıcaklığı.

*Corresponding Author: aastam@erzincan.edu.tr
Aykut ASTAM, https://orcid.org/0000-0002-4321-3626
Ömer KAYA, https://orcid.org/0000-0002-5019-3109

1. Introduction

Metal oxides are important materials for engineering and scientific applications due to their distinctive physical and chemical properties. Among various metal oxides, copper oxides are one of the first semiconductors studied for device applications and widely used in a range of fields, such as solar cell technology [1, 2], electrochromic devices [3], gas and humidity sensing applications [4, 5], electrochemical energy storage devices [6], and photocatalytic degradation of biological pollutants and organic dyes [7, 8]. In addition, copper oxides are of interest because of their chemical stability, low production cost, and non-toxic nature. Copper oxides are known to have p-type conductivity and two familiar forms of copper oxides are cupric oxide or tenorite (CuO) with the reported direct optical band gap ranging from 1.0 eV to 2.1 eV and cuprous oxide or cuptite (Cu_2O) with the reported direct optical band gap ranging from 2.0 eV to 2.6 eV [7, 9]. Specifically, relatively narrow optical band gap of the CuO makes it an important material for the absorption of ultraviolet–visible to near-infrared radiation. For the deposition of copper oxide thin films, a variety of physical and chemical processes have been proposed including sputtering [8, 9], chemical-thermal oxidation [7], electrodeposition [2], chemical vapor deposition [10], chemical bath deposition [6, 11], spin coating [12], successive ionic layer adsorption and reaction [13, 14] and hydrothermal method [15], etc. Among these processes, the hydrothermal method attracts intensive attention because of its low cost, simple operating procedure, and low process temperatures, which improves surface coverage on the substrates and reduces the possibility of film cracking [16, 17]. Therefore, this method is known to be one of the most important soft solutions chemical processes and suitable for large-scale production. Because the process is controlled by dissolution / precipitation of reactants in an aqueous solution, the nature and properties of the product can be controlled by different process parameters such as reaction temperature and time, properties of precursor solution, and the types of additives such as surfactants, templates, or mineralizers used [15, 16]. Although the use of surfactant has some advantages such as controlling particle size, morphology and size distribution of the final product, the introduction of surfactant means a more complicated reaction process and can cause an increase of impurity concentration in the final product.

In this paper, we report the synthesis of CuO thin films via hydrothermal method without using any surfactant. To evaluate the effect of reaction temperature on the structural and optical properties of the films, CuO thin films were synthesized by varying the reaction temperature while keeping the reaction time constant.

2. Material and Methods

The copper (II) sulfate pentahydrate ($CuSO_4.5H_2O$) and ammonia solution (NH_4OH) 32% were used as precursor materials for deposition of CuO thin films using hydrothermal route. All raw materials were analytical grade and purchased from Sigma-Aldrich Company. Deionized water was used as a solvent. Fluorine-doped tin oxide (FTO) glass slides (20 mm × 10 mm × 3 mm) were chosen as substrate material. Prior to the deposition process, FTO substrates were cleaned ultrasonically in the commercial detergent, acetone, 1:1 ethanol-water solutions, and finally deionized water for 15 min sequentially. To obtain the precursor solution, first 50 mM $CuSO_4.5H_2O$ solution was prepared by dissolving a proper amount of material in 30 ml deionized water under magnetic stirring for 15 min at room temperature. Then NH_4OH was slowly added dropwise to the above solution under constant stirring. Initially a pale blue and then a clear, dark blue solution was obtained. At this point, the pH of the solution reached 10.5. The solution was stirred for a further 30 min, then transferred into a teflon-lined stainless-steel autoclave with 50 ml capacity. FTO substrates were vertically dipped into the precursor solution and the autoclave was sealed and placed in a hot oven for 24 h at different reaction temperatures (120ºC, 140ºC, 160ºC, and 180ºC). At the end of the growth process, the autoclave was cooled to room temperature naturally. The coated substrates were removed, washed with deionized water several times, and dried in air overnight. The films on the non-conductive sides of the FTO substrates peeled off during washing, but the films obtained on the conductive sides were well adherent, nearly uniform and, dark brown in color.

Structural, morphological, compositional, and optical properties of the CuO thin films deposited at different reaction temperatures were analyzed. The determination of the crystal structure and phase was carried out using Panalytical Empyrean X-ray diffractometer using Cu-Kα radiation with the wavelength λ=1.5405 Å at 45 kV and 40 mA. The diffraction patterns were recorded in the 2θ range 20°–80° at a scanning rate of 1.50° min^{-1}. The surface morphology and elemental compositional analysis of the films were investigated with FEI Quanta FEG 450 scanning electron microscopy (SEM) coupled with Amatek energy dispersive X-ray analysis (EDAX) attachment. Raman spectroscopy was further used as a supplementary method to prove the phase purity of the CuO thin films, and the spectra were obtained using Witec alpha 300R Raman module in the spectrum range 200–800 cm^{-1}. Optical absorption spectra of the CuO thin films were obtained with UV-1810 DASPC UV-VIS double beam spectrophotometer. The spectra were recorded in the wavelength range of 500–1100 nm at room temperature. Optical band gap energies of the films were estimated through the Tauc method.

3. Results and Disscussion

A series of CuO thin films were obtained on FTO substrates using hydrothermal method for 24 h by varying the reaction temperature from 120ºC to 180ºC with 20ºC steps. The formation mechanism of CuO thin films can be explained as follows. When NH_4OH is added into the $CuSO_4.5H_2O$ solution, initially $Cu(OH)_2$ occurs according to the following reaction:

$$\mathrm{CuSO_4 + 2NH_4OH \rightarrow Cu(OH)_2 + (NH_4)_2SO_4} \quad (1)$$

Addition of excess NH_4OH dissolves $Cu(OH)_2$:

$$\mathrm{Cu(OH)_2} + NH_4\mathrm{OH} \rightarrow (NH_4)CuO_2^- + H_2O + H^+ \quad (2)$$

Under hydrothermal conditions, the ionic product exceeds the solubility product and CuO film forms on the FTO substrate by the following reaction [6]:

$$(NH_4)CuO_2^- + H^+ \rightarrow \mathrm{CuO} + NH_4OH \quad (3)$$

XRD method was used to analyze the phase composition and crystallographic structure of the CuO thin films, and Figure 1 shows the diffraction patterns of the films deposited at different hydrothermal reaction temperatures. The patterns revealed that all the films had a polycrystalline nature and observed diffraction peaks were in closely match with the standard pattern of monoclinic CuO (JCPDS No.:45-0937) along with the diffractions from the FTO substrate which were marked with *. Two characteristic peaks of CuO corresponding to reflections from (11-1) and (111) planes were clearly observed in all the patterns, and no peaks from impurities such as Cu_2O or $Cu(OH)_2$ were seen.

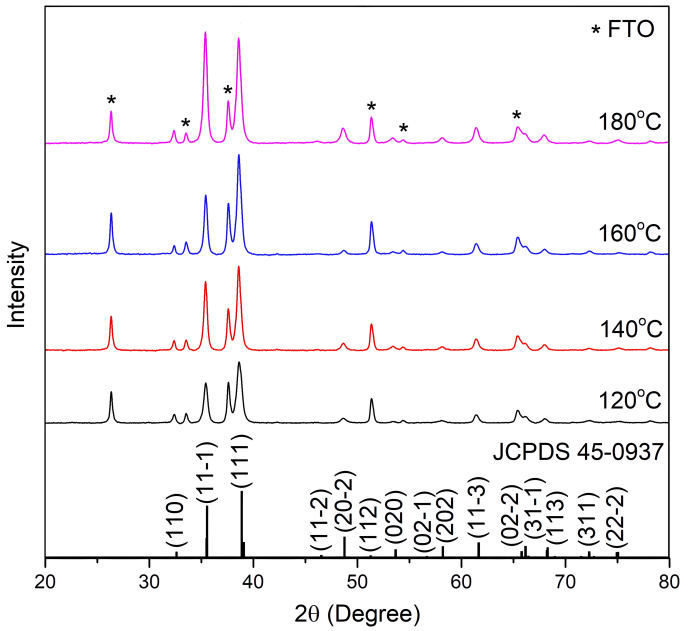

Figure 1. XRD patterns of CuO thin films deposited at different hydrothermal reaction temperatures

XRD analysis also showed no remarkable changes in the crystallographic structure and phase composition of the films depending on hydrothermal reaction temperature. Increasing hydrothermal reaction temperature generally increased the intensity and sharpening of the observed peaks, which means the crystallinity increases with the increasing reaction temperature.

With the help of XRD measurements, interplanar distances (d) of the planes and average grain size values (D) of CuO thin films were calculated for prominent (11-1) and (111) planes, using Bragg's diffraction condition [18] and Scherrer Equation [19]:

$$D = \frac{K\lambda}{\beta Cos\theta} \tag{4}$$

where K is a constant which is referred as the shape factor (K=0.9 was used), λ is the wavelength of the X-ray, β is the full width at half maximum of the peak in radian, and θ is the Bragg angle that corresponds to the peak analyzed. Obtained results are shown in Table 1 along with the standard values of the interplanar distances. It can be seen from the table that the calculated d values are compatible with the standard values and increasing the hydrothermal reaction temperature from 120ºC to 160ºC increased the grain size from 15.2 nm to 18.7 nm, while further increasing the reaction temperature to 180ºC caused a slight decrease in grain size. Differences between the relative X-ray diffraction intensities of the samples and the standard

JCPDS data indicate that a preferential orientation is present, and the preferential orientation can be determined considering the texture coefficient (T_c). T_c values for all planes of randomly oriented materials are approximately 1. Values of T_c greater than 1 indicate preferential orientation, while values less than 1 indicate the absence of grains oriented in that direction [20]. The T_c values of the CuO thin films were calculated using the equation [19]:

$$T_c(hkl) = \frac{I(hkl)/I_0(hkl)}{\frac{1}{N}\sum I(hkl)/I_0(hkl)} \quad (5)$$

where I is measured X-ray diffraction intensity, I_0 is standard JCPDS intensity and N is the reflection number. Calculated T_c values of CuO thin films deposited under different hydrothermal reaction temperatures are shown in Table 1. As can be clearly seen from the table, increasing reaction temperature caused a periodic change in preferential orientation.

Table 1. Standard and calculated interplanar distances with average grain size and texture coefficient values

Reaction Temperature	2θ (observed)	hkl	d(Å) (standard)	d(Å) (calculated)	D (nm)	T_c
120ºC	35.49	11-1	2.529	2,527	15.2	0.91
	38.69	111	2.322	2.325		1.09
140ºC	35.46	11-1	2.529	2.529	18.4	1.03
	38.64	111	2.322	2.328		0.97
160ºC	35.49	11-1	2.529	2.527	18.7	0.87
	38.67	111	2.322	2.326		1.13
180ºC	35.44	11-1	2.529	2.531	16.8	1.15
	38.64	111	2.322	2.328		0.85

The film's surface morphology was studied by SEM and the images of the films deposited at different hydrothermal reaction temperatures are shown in Figure 2. To illustrate the shape of CuO structures distinctly, higher magnification (30000×) images are displayed in inset of all the SEM images. Close examination of the SEM image reveals that, in the early stage of the hydrothermal process, randomly oriented rod-like nanostructures completely cover the surface of the FTO substrates without any voids, pinhole or cracks and numerous CuO nanostructures assemble together possibly to reduce the excess interfacial energy and form the micrometer-sized spherical, chrysanthemum-like structures [21]. As the reaction temperature increases, chrysanthemum-like structures become more compact, and the number of these structures increases.

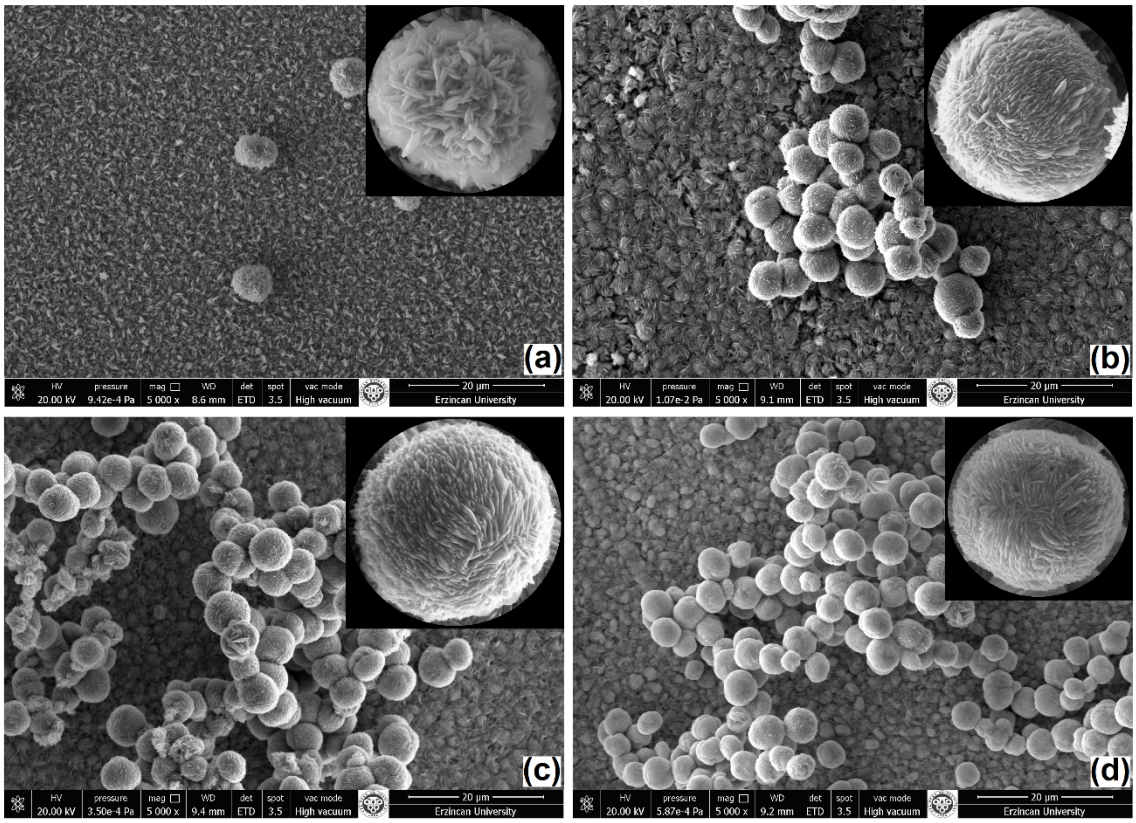

Figure 2. SEM images of CuO thin films deposited at different hydrothermal reaction temperatures, (a) 120ºC, (b) 140ºC, (c) 160ºC, (d) 180ºC.

The elemental compositional analysis of the CuO thin films were estimated by EDAX and the spectra are given in Figure 3. All EDAX spectra show the existence of Cu, O, and Sn elements. The Cu/O ratios of the films were determined from the spectra and found to be 0.95, 1.07, 1.02, and 1.04 for hydrothermal reaction temperatures of 120ºC, 140ºC, 160ºC, and 180ºC respectively. Although Cu/O ratios change in a non-regular manner with increasing hydrothermal reaction temperature, the variations are very small and all the films have Cu/O ratios of unity, which is in agreement with the XRD results. The appearance of weak Sn peaks in the EDAX spectra is due to the FTO substrate and the spectra show that increasing reaction temperature resulted in a decrease in relative Sn content, which may be due to the increasing film thickness.

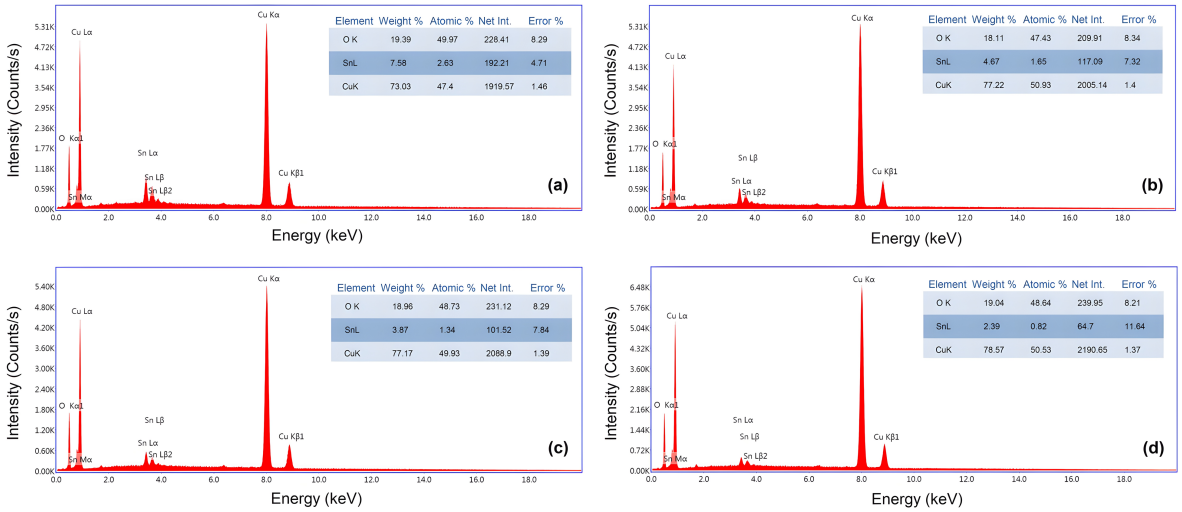

Figure 3. EDAX spectra of CuO thin films deposited at different hydrothermal reaction temperatures, (a) 120ºC, (b) 140ºC, (c) 160ºC, (d) 180ºC.

For the structural analysis of materials, Raman scattering has proven to be an appropriate alternative and/or complementary method to XRD studies [22]. The films were further analyzed using Raman analysis and Figure 4 shows the Raman scattering spectra of the CuO thin films, obtained at different reaction temperatures. All films are characterized by an intense peak at 274 cm^{-1}, a less intense peak at 323 cm^{-1}, and a rather weak and broad peak at about 605 cm^{-1}. These three Raman peaks can be assigned to A_g and the two B_g modes of CuO respectively, and are comparable with the reported values [11, 23]. The trend in intensity of the prominent Raman peak at 274 cm^{-1} is consistent with the XRD results. Furthermore, all three peaks are red shifted as compared to reported values for the CuO single crystal [24]. This relative shift to lower frequencies can be attributed to size effects [25]. The weak peak observed at 249 cm^{-1} may be caused by FTO substrate [26]. Due to the relatively low thickness of the films, this peak is more clearly observed in the Raman spectra of the films obtained at reaction temperatures of 120ºC and 140ºC that is agreement with the EDAX results. No vibrational mode belonging to any impurity phase was identified in all Raman spectra, which indicates the purity of the CuO thin films and is consistent with XRD results.

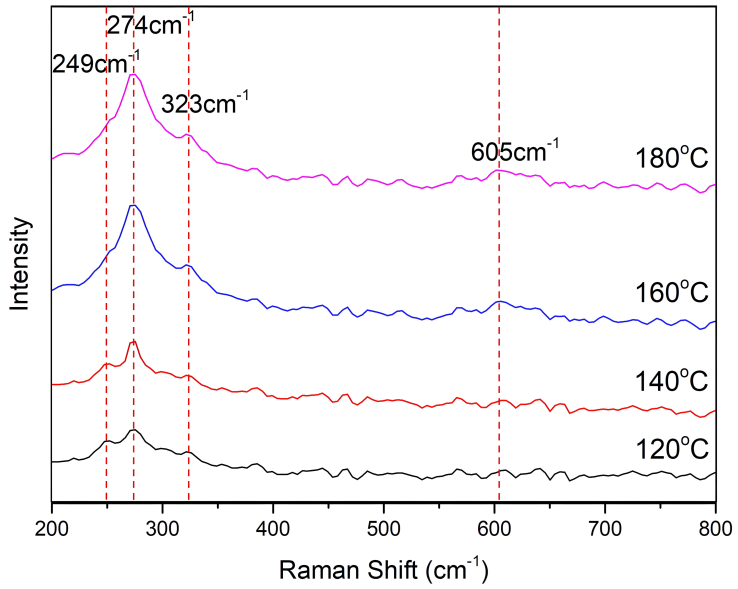

Figure 4. Raman scattering spectra of CuO thin films deposited at different hydrothermal reaction temperatures.

The equation between the absorption coefficient (α) and the optical band gap energy (E_g) is given by;

$$\alpha = \frac{A(h\upsilon - E_g)^n}{h\upsilon} \quad (6)$$

where A is a constant dependent on the effective masses associated with the valence and conduction bands and $h\upsilon$ is the photon energy. The value of n is related to the type of the transition (n=2 for indirect allowed, n=½ for direct allowed transition). According to equation 6, the direct band gap energy values of the materials are determined by extrapolating the linear part of the $(\alpha h\upsilon)^2$ versus $h\upsilon$ graphs onto the horizontal axis. Figure 5 shows the optical absorption spectra and variations of $(\alpha h\upsilon)^2$ as a function of photon energy for CuO thin films deposited at different hydrothermal reaction temperatures. From the absorption spectra, it can be seen that all the films exhibit high absorbance at wavelengths < 750 nm, which is very useful for applications of solar cell devices. The linear nature of the all $(\alpha h\upsilon)^2$ - Energy plots confirm the direct optical transition in CuO thin films. It is clear from the figure that optical band gap values were all found to be similar and 1.34 eV, 1.41 eV, 1.37 eV, and 1.40 eV for hydrothermal reaction temperatures of 120ºC, 140ºC, 160ºC, and 180ºC respectively. The obtained direct band gap values are in the good agreement with the literature values [27, 28].

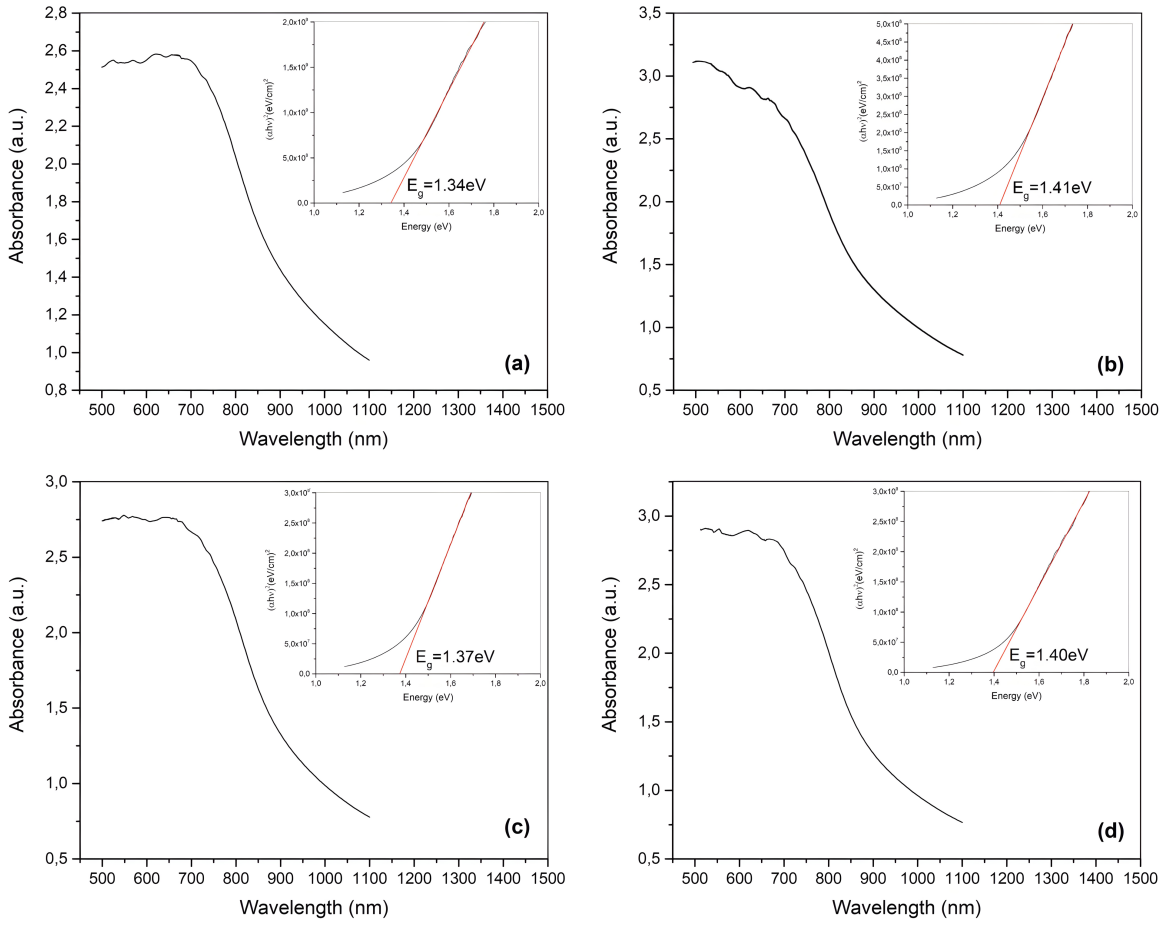

Figure 5. Optical absorption spectra with the variations of $(\alpha hv)^2$ as a function of photon energy for CuO thin films deposited at different hydrothermal reaction temperatures, (a) 120ºC, (b) 140ºC, (c) 160ºC, (d) 180ºC.

4. Conclusion

In the present study, CuO thin films were deposited on FTO substrates via hydrothermal method and the effect of reaction temperature on some structural and optical properties of the films were reported. XRD results showed that all the films had a polycrystalline nature with monoclinic symmetry and revealed no significant variations in the crystallographic structure and phase composition of the films deposited at different reaction temperatures. Increasing hydrothermal reaction temperature generally improved the crystallinity and caused a change in the texture coefficient of the films. The films deposited at 160ºC hydrothermal reaction temperature showed better crystallinity with a grain size of 18.7 nm. SEM images revealed the formation of micrometer-sized chrysanthemum-like structures, the number of which increased with increasing hydrothermal reaction temperature. It was confirmed with the help of EDX measurements that all films had stoichiometric ratios very close to CuO. Phase purity and crystalline nature of the films were further proved through the Raman scattering measurements. The estimated direct optical band gap energies of the films were in the range of 1.34 eV-1.41

eV, depending on reaction temperature. Obtained results demonstrated that CuO thin film, which has been considered as a potential absorber material for low-cost photovoltaic applications, could be successfully deposited using facile hydrothermal method under mild conditions without using any surfactant.

Ethics in Publishing

There are no ethical issues regarding the publication of this study.

Acknowledgements

Bu kısımda makalede belirtilmek istenen; tez çalışması/ proje ismi ve numarası/ finansman sağlayıcılar gibi verilebilir.

References

[1] T.K.S. Wong, S. Zhuk, S. Masudy-Panah, G.K. Dalapati, "Current Status and Future Prospects of Copper Oxide Heterojunction Solar Cells", Materials 9 (2016) 271–292.

[2] G.G. Welegergs, Z.M. Mehabaw, H.G. Gebretinsae, M.G. Tsegay, L. Kotsedi, Z. Khumalo, N. Matinisie, Z.T. Aytuna, S. Mathur, Z.Y. Nuru, S. Dube, M. Maaza, "Electrodeposition of nanostructured copper oxide (CuO) coatings as spectrally solar selective absorber: Structural, optical and electrical properties", Infrared Physics and Technology 133 (2023) 104820.

[3] N. Ozer, C.M. Lampert, "Electrochromic characterization of sol—gel deposited coatings", Solar Energy Materials and Solar Cells 54 (1998) 147–156.

[4] S. Keerthana, M.B. Arthina Titlin, C. Ravi Dhas, R. Venkatesh, S. Esther Santhoshi Monica, "Unraveling the role of solvent type in the physical and chemiresistive gas sensing properties of nebulizer-sprayed CuO films", Materials Science and Engineering B 297 (2023) 116821.

[5] S.B. Wang, C.H. Hsiao, S.J. Chang, K.T. Lam, K.H. Wen, S.J. Young, S.C. Hung, B.R. Huang, "CuO nanowire-based humidity sensor", IEEE Sensors Journal 12 (2012) 1884–1888.

[6] D.P. Dubal, D.S. Dhawale, R.R. Salunkhe, V.S. Jamdade, C.D. Lokhande, "Fabrication of copper oxide multilayer nanosheets for supercapacitor application", Journal of Alloys and Compounds 492 (2010) 26–30.

[7] F. Ansari, S. Sheibani, M. Fernandez-Garcia, "Surface modification of Cu_2O-CuO photocatalyst on Cu wire through decorating with TiO_2 nanoparticles for enhanced visible light photocatalytic activity", Journal of Alloys and Compounds 919 (2022) 165864.

[8] N.J. Karazmoudeh, M. Soltanieh, M. Hasheminiasari, "Structural and photocatalytic properties of undoped and Zn-doped CuO thin films deposited by reactive magnetron sputtering", Journal of Alloys and Compounds 947 (2023) 169564.

[9] E.M. Alkoy, P.J. Kelly, "The structure and properties of copper oxide and copper aluminium oxide coatings prepared by pulsed magnetron sputtering of powder targets", Vacuum 79 (2005) 221–230.

[10] D. Chua, S.B. Kim, K. Li, R. Gordon, "Low Temperature Chemical Vapor Deposition of Cuprous Oxide Thin Films Using a Copper(I) Amidinate Precursor", ACS Applied Energy Materials 2 (2019) 7750–7756.

[11] C.M. Muiva, A.O. Juma, L.M. Lepodise, K. Maabong, D. Letsholathebe, "Surfactant assisted chemical bath deposition based synthesis of 1-D nanostructured CuO thin films from alkaline baths", Materials Science in Semiconductor Processing 67 (2017) 69–74.

[12] S. Baturay, "Structural and Optical Properties of Sb Doped CuO Films", Academic Platform Journal of Engineering and Science 8 (2020) 84–90.

[13] Y. Akaltun., "Effect of thickness on the structural and optical properties of CuO thin films grown by successive ionic layer adsorption and reaction", Thin Solid Films 594 (2015) 30–34.

[14] O. Gençyılmaz, T. Taşköprü, "Effect of pH on the synthesis of CuO films by SILAR method", Journal of Alloys and Compounds 695 (2017) 1205–1212.

[15] Y. Liu, Y. Chu, M. Li, L. Li, L. Dong, "In situ synthesis and assembly of copper oxide nanocrystals on copper foil via a mild hydrothermal process", Journal of Materials Chemistry 16 (2006) 192–198.

[16] J. Wu, B. Yan, "Photoluminescence intensity of $Y_xGd_{1-x}VO_4:Eu^{3+}$ dependence on hydrothermal synthesis time and variable ratio of Y/Gd", Journal of Alloys and Compounds 455 (2008) 485–488.

[17] A.M. Holi, Z. Zainal, Z.A. Talib, H.N. Lim, C.C. Yap, S.K. Chang, A.K. Ayal, "Effect of hydrothermal growth time on ZnO nanorod arrays photoelectrode performance", Optik 127 (2016) 11111–11118.

[18] W.L. Bragg, "The diffraction of short electromagnetic waves by a crystal", Proceedings - Cambridge Philosophical Society 17 (1913) 43–57.

[19] C. Barrett, T.B. Massalski, Structure of Metals, Pergamon, Oxford, 1980.

[20] R. Mariappan, V. Ponnuswamy, S.M. Mohan, P. Suresh, R. Suresh, "The effect of potential on electrodeposited CdSe thin films", Materials Science in Semiconductor Processing 15 (2012) 174–180.

[21] N. Zhao, H. Fan, M. Zhang, X. Ren, C. Wang, H. Peng, H. Li, X. Jiang, X. Cao, "Facile preparation of Ni-doped $MnCO_3$ materials with controlled morphology for high-performance supercapacitor electrodes", Ceramic International 45 (2019) 5266–5275.

[22] T. Gao, H. Fjellvag, P. Norby, "Structural and morphological evolution of β-MnO_2 nanorods during hydrothermal synthesis", Nanotechnology 20 (2009) 055610.

[23] H. Siddiqui, M.S. Qureshi, F.Z. Haque, "Surfactant assisted wet chemical synthesis of copper oxide (CuO) nanostructures and their spectroscopic analysis", Optik 127 (2016) 2740–2747.

[24] H.F. Goldstein, D. Kim, P.Y. Yu, L.C. Bourne, "Raman study of CuO single crystals", Physical Review B 41 (1990) 7192–7194.

[25] J.F. Xu, W. Ji, Z.X. Shen, W.S. Li, S.H. Tang, X.R. Ye, D.Z. Jia, X.Q. Xin, "Raman Spectra of CuO Nanocrystals", Journal of Raman Spectroscopy 30 (1999) 413–415.

[26] C.Y. Kim, D.H. Riu, "Raman scattering, electrical and optical properties of fluorine-doped tin oxide thin films with (200) and (301) preferred orientation", Materials Chemistry and Physics 148 (2014) 810–817.

[27] F. Bayansal, H.A. Çetinkara, S. Kahraman, H.M. Çakmak, H.S. Güder, "Nano-structured CuO films prepared by simple solution methods: Plate-like, needle-like and network-like architectures", Ceramics International 38 (2012) 1859–1866.

[28] G.G. Welegergs, H.G. Gebretnisae, M.G. Tsegay, Z.Y. Nuru, S. Dube, M. Mazaa, "Thickness dependent morphological, structural and optical properties of SS/CuO nanocoatings as selective solar absorber", Infrared Physics and Technology 113 (2021) 103619.

Erzincan Üniversitesi
Fen Bilimleri Enstitüsü Dergisi
2024,17(1), 230-240
ISSN: 1307-9085, e-ISSN: 2149-4584
Araştırma Makalesi

Erzincan University
Journal of Science and Technology
2024,17(1), 230-240
DOI: 10.18185/erzifbed.1407972
Research Article

Benzimidazole-Platinum Complex and Its Cytotoxic activity on U87 Cell Lines

Aydan Arı[1], Salih Günnaz[1], Sevil İrişli[1*]

[1]Department of Chemistry, Ege University, Bornova, İzmir, Türkiye

Received: 21/12/2023, **Revised:** 12/02/2024, **Accepted:** 21/02/2024, **Published:** 28/03/2024

Abstract

The aim of the study is to evaluate the synthesis, characterization and cytotoxic activities of a novel benzimidazole-platinum(II) complex that may have strong cytotoxic activity and low side effects. A benzimidazole ligand, 2-(3-phenoxyphenyl)-1-phenyl-1H-benzimidazole (L) and its novel platinum complex (Pt-L) was synthesized and characterized by different spectroscopic methods. In the study, firstly the activity of the synthesized complex in the U87 cancer line was examined and then it has been studied on healthy Vero lines.

Keywords: Benzimidazole, Benzimidazole-Platinum complexes, glioblastoma, cytotoxic activity.

Benzimidazol-Platin Kompleksi ve U87 Hücre Hatları Üzerindeki Sitotoksik Aktivitesi

Öz

Çalışmanın amacı, güçlü sitotoksik aktiviteye ve düşük yan etkilere sahip olabilen yeni bir benzimidazol-platin(II) kompleksinin sentezi, karakterizasyonu ve sitotoksik aktivitelerinin değerlendirilmesidir. Bir benzimidazol ligandı, 2-(3-fenoksifenil)-1-fenil-1H-benzimidazol (L) ve bunun yeni platin kompleksi (Pt-L), sentezlenmiş yapıları farklı spektroskopik yöntemlerle karakterize edilmiştir. Çalışmada, sentezlenen kompleksin öncelikle U87 kanser hattındaki aktivitesi incelenmiş, daha sonra sağlıklı Vero hatları üzerinde çalışılmıştır.

Anahtar Kelimeler: Benzimidazol, Benzimidazol-Platin kompleksleri, glioblastoma,sitotoksik aktivite.

1. Introduction

The imidazole nucleus, especially benzimidazole, and related structures are molecules whose structure and function are very important from a biological perspective. Benzimidazoles may be considered as structural isosters of nucleotides owing to the fused heterocyclic nuclei in their structures and potential activity for chemotherapeutic applications [1]. The benzimidazole moiety itself is a crucial pharmacophore in modern drug discovery [2]. It is common in drugs that show various pharmacological activities such as anti-inflammatory [3], histamine-H3 antagonist [4], antioxidant [5], gastroprotective [6], antitumoral [7], antiparasitic [8],

*Corresponding Author: sevil.irisli@ege.edu.tr
Aydan ARI, https://orcid.org/0009-0004-0768-2232
Salih GÜNNAZ, https://orcid.org/0000-0002-7422-6593
Sevil İRİŞLİ, https://orcid.org/0000-0002-3727-2216

antimicrobial [9], anthelmintic [10]. They are also found in insecticidal and herbicidal [11] drugs.

The importance of Pt(II) complexes increased with the discovery of cis platinum by Rosenberg in 1965 and its clinical use in the treatment of tumors with cytotoxic effects. For this reason, researchers have focused on the synthesis of new analogous platinum(II) coordination compounds.

Platinum complexes containing imidazolic/benzimidazolic ligands [12, 13] have drawn attention of several research groups, since imidazole/benzimidazole and their derivatives are important class of organic compounds. In the last decade, a lof of benzimidazol – platinum complexes synthesized and reported their antineoplastic activities on different cancer cell lines [14, 15, 16]. Brain tumors are an aggressive type of cancer seen in all age groups, including infants. Commonly known brain tumors are neuroblastoma and glioma. Central nervous system tumors occupy a larger place among childhood cancers and constitute approximately 20% of all tumors. One of the therapeutic applications is drug therapy and it is inevitable to develop agents with antiproliferative effects. One of the main topics of these studies is that they focus on the effect of substituents attached to the C-2 carbon atom on cytotoxic activity [17, 18, 19]. The limited number of coordination compounds effective on neuroblastoma and glioblastoma [20, 21, 22] in the literature has guided us in the synthesis of new compounds that can be used for this purpose, elucidating their structures and determining their biological activities.

In this study; A new benzimidazole ligand containing a 3-phenoxy group at the C-2 position and its platinum(II) complex with and cytotoxic effect on glioblastoma cancer cell line, U87 cell, was evaluated.

2. Materials and Methods

2.1. Chemicals

The reagents 3-phenoxybenzaldehyde, N-phenyl-o-phenylene diamine, sodium metabisulfite ($Na_2S_2O_5$), dimethylformamide (DMF), acetone, chloroform, dichloromethane (DCM), diethylether used in the synthesis were commercially purchased from Sigma, Merck, and Aldrich. *cis*-dichlorobis(dimethyl sulfoxide)platinum(II) [$Pt(DMSO)_2Cl_2$], used as starting complex, was synthesized according to literature data [23]. However, the following synthesis methods were used to increase the yield and can be synthesized according to literature.

2.2. Instrumentations

Melting points were obtained using an Electrothermal Melting Point detection apparatus. Elemental analysis were performed by the Scientific Resarch and Analysis Laboratories of Inönü University. Infrared spectra were recorded on a Perkin Elmer FT-IR spectrophotometer in the range of 4000- 400 for ligand, 4000- 200 cm^{-1} for complex. ^1H and ^{13}C NMR spectra were measured at Varian AS 400 MHz spectrometer. $CDCl_3$ and DMSO-d_6, were used as the solvents and TMS was used as the internal standard. In thin layer chromatography (TLC) studies, ready-made plates coated with Kieselgel 60 F254 with a thickness of 0.2 mm were

used. Stains were detected using a UV lamp. The LC/Q-TOF/MS measurements in the compound were recorded using the Agilent 6550 QTOF LC/MS device at the Ege University MATAL center.

2.3. Synthesis of Ligand and its Platinum Complex

2.3.1. 2-(3-phenoxyphenyl)-1-phenyl-1H-benzimidazole (L)

3-phenoxybenzaldehyde (0.1075 g, 0.542 mmol) was kept in 2 ml DMF medium in a schlenk. Then, N-phenyl-ortho-phenylenediamine (0.998 g, 0.542 mmol) was added dropwise in 1 ml DMF medium and $Na_2S_2O_5$ was added. The reflux temperature was stirred for 6 hours. As a result of the reaction, cold water was added. The precipitated cream-colored solid was filtered with the aid of a nuclei funnel. This solid was crystallized from DCM/diethyl ether to give the pure product. Yield: 60%, Melting point: 141-142 ºC. FT-IR (KBr disk, cm^{-1}): υ Ar-H –C=N: 3398-2915. ^{1}H-NMR (400 MHz, $CDCl_3$) δ ppm:7.87 (dt, 1H, J_1=8.4Hz, J_2=0.8 Hz, Ar-*H*), 7.49-7.00 (m,15H, Ar-*H*), 6.86 (d, 2H, *J*=7.6 Hz, Ar-*H*). ^{13}C -NMR (100 MHz, $CDCl_3$) δ (ppm):157.2, 156.5, 151.8, 142.9, 137.2, 136.8, 131.6, 129.9, 129.8, 128.6, 127.3, 124.3, 123.5, 123.1, 119.9, 119.3, 119.1, 110.5. Elemental analysis (%) = ($C_{25}H_{18}N_2O$) (m.w.= 362,43); calculated; C, 82.85; H, 5.01; N, 7.73; found; C,81.80; H, 4.71; N,7.52.

2.3.2. Synthesis of Complex (Pt-L)

L ligand (0.03 g, 0.082 mmol) was dissolved in 2 ml chloroform medium in a schlenk. Then, the suspension of $Pt(DMSO)_2Cl_2$ (0.03 g, 0.082 mmol) prepared in 1ml chloroform medium in a test tube was added dropwise onto L. The mixture was then stirred at room conditions for 4 days. After the reaction, the solvent was dried under vacuum. The resulting solid was first washed with acetone. The insoluble portion was separated. The solvent was evaporated in vacuo and washed with diethyl ether. Yield: 72% Melting Point: 232^{0}C.

FT-IR (CsI disk, cm^{-1}): υ Ar-H = 3398-2915, υ S-O =1121, υ Pt-CI =319.13

^{1}H-NMR (400 MHz, $CDCl_3$) δ (ppm): 8.41(d, 1H, *J*=8.4 Hz, Ar-*H*), 8.03 (d, 1H, *J*=7.6 Hz, Ar-*H*), 7.56-7.45 (m, 5H, Ar-*H*), 7.37 (t, 2H, *J*=7.8 Hz, Ar-*H*), 7.31-7.20 (m, 7H, Ar-*H*), 7.11(t, 1H, *J*=6.8 Hz, Ar-*H*), 6.83 (d, 2H, *J*=8.8 Hz, Ar-*H*), 3.34 (s, 3H, O-S-CH_3), 2.70 (s, 3H, O-S-CH_3). ^{13}C-NMR (100MHz, $CDCl_3$) δ (ppm): 157.0, 155.7,151.6, 139.5, 134.5, 130.2,130.1,130.0, 129.5,129.0, 127.2, 126.3, 125.6, 125.1, 124.0, 121.5, 120.7, 119.4,119.0, 111.3, 77.0, 76.6, 44.5, 43.8. Elemental analysis (%)= ($C_{27}H_{24}Cl_2N_2O_2PtS$) (706.53); calculated; C, 45.90; H, 3.42; N, 3.96; found; C, 45.73; H, 3.48; N, 4.02.

2.4. Cytotocxicity

Cytotocxicity tests were obtained by using U87 and Vero cells. Cells were purchased from ATCC, USA. Cells were seeded 96-well plate $1x10^5$ cell/mL concentration. They were grown in culture media (MEM Earle's FG0325-BC, Merck, Germany,10% Fetal Bovine Serum FBS, A0500-3010, Cegrogen Biotech, Germany, 1% Gentamicine A2712, Merck, Germany). The complex was added at different concentrations (0.1-0.5-1.0- 10- 100 µM) of this media and

incubated for 72 hours. Growth inhibitions of cells were measured spectrophotometrically using a standard method (MTT) at 570 nm.

3.Results and Discussion

3.1. Synthesis and spectroscopic studies

Benzimidazole derived from N-phenyl-ortho-phenylenediamine were synthesized. 2-(3-phenoxyphenyl)-1-phenyl-1H-benzo[d]imidazole(L)) ligand and Benzimidazole-Pt complex derived from this ligand were synthesized. The structures of the ligand and metal complex were elucidated using various spectroscopic methods (FT-IR, ^{1}H-NMR, ^{13}C-NMR) and elemental analysis. The general synthesis route of ligand is given in Figure 1.

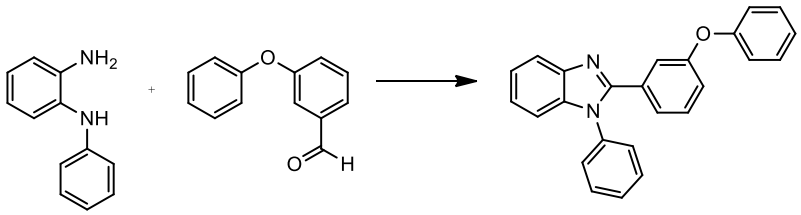

Figure 1. Synthetic pathway of Ligand L.

FT-IR spectrum of L (Figure 2) was obtained by preparing KBr pellets. Only aromatic groups are present in the L ligand, the ring bodies appear in the 700-800 cm^{-1} region. The disappearance of the peak of secondary N-H stretching vibrations, which are seen as a double peak in the 3300-3400 cm^{-1} region, indicates that the reaction has occurred to form a ligand L. Peaks related to aromatic C-H stretching vibrations appear in the spectrum above 3000 cm^{-1}. ^{1}H-NMR spectrum of L ligand was obtained by dissolving in $CDCl_3$ medium. In the ^{1}H-NMR spectrum (Figure 3), the peak of N-C=CH is observed at 7.88 ppm, while peaks corresponding to all other protons are observed at 7.49-6.85 ppm. Again, in the ^{13}C-NMR spectrum (Figure 4), there are peak groups depending on the structures of different C atoms. The C2 carbon (between two nitrogen atoms) of the imidazole ring is observed at 142.87 ppm. The carbons to which the oxygen atom of the functional group attached to the C2 carbon is attached were observed at 156.48 and 157.20 ppm.

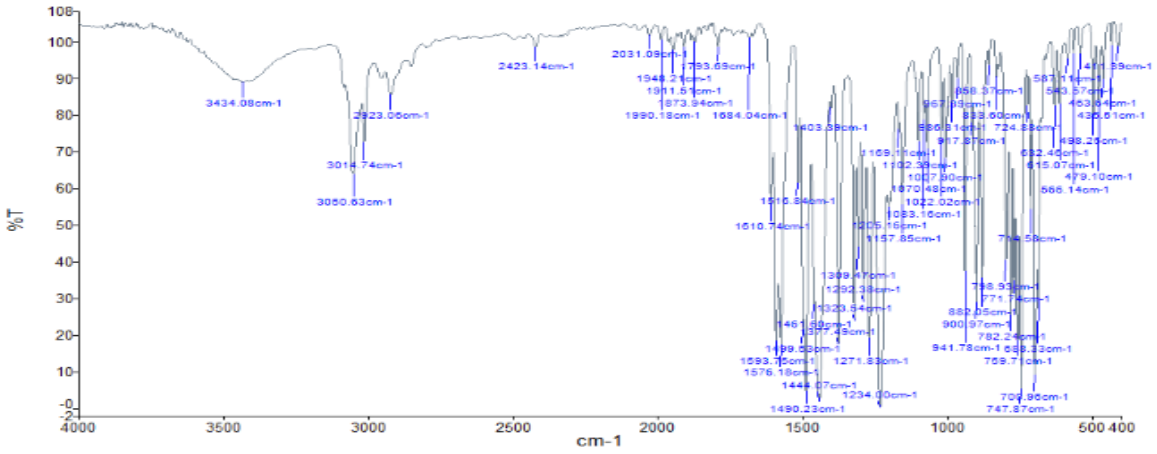

Figure 2. FT-IR Spectrum of the Ligand L.

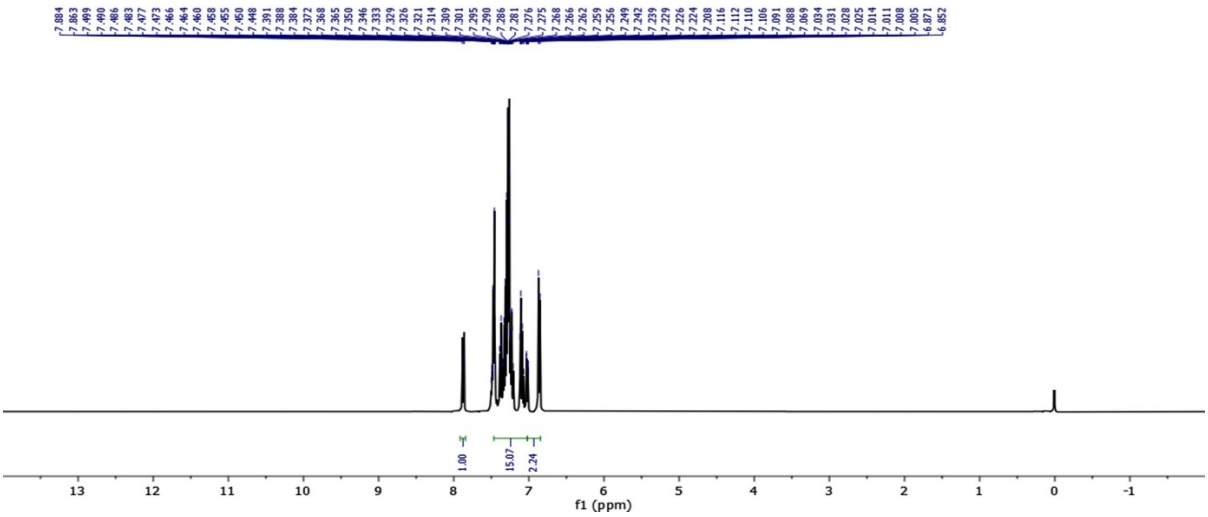

Figure 3. ^{1}H NMR Spectrum of the Ligand L.

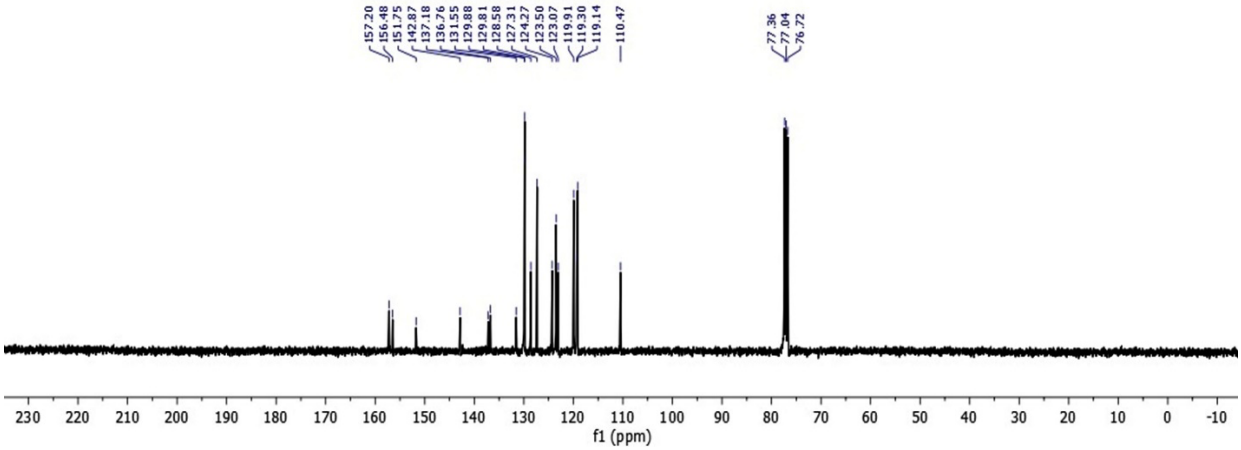

Figure 4. ^{13}C NMR Spectrum of the Ligand L.

[$PtCl_2$(DMSO)(L)] complex were prepared by treating [$PtCl_2(DMSO)_2$] with benzimidazole (L) in chloroform in a 1:1 molar ratio. Ligand and complex have been isolated as stable solids in air. Complex syntheses is given in Figure 5.

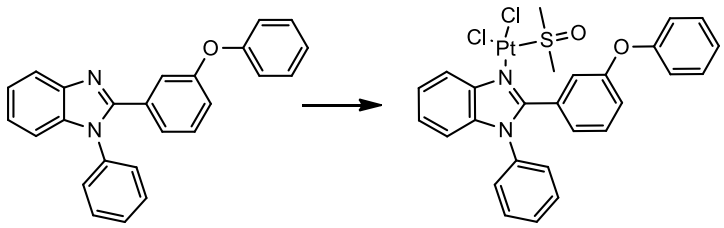

Figure 5. Synthetic pathway of complex (Pt-L).

FT-IR spectrum (Figure 6) of the complex was taken by creating a CsI pellet. Pt-Cl stretching vibrations appear to be shifted to the weak area compared to the initial complex. The S-O stretching vibration of the DMSO group bonded via S is observed at 1121 cm^{-1} [23]. The *cis* Pt-Cl stretching vibrations shifted according to the initial complex and, as expected, a peak containing a shoulder was observed at 319.13 cm^{-1}. The ^{1}H-NMR spectrum of the complex is given in Figure 7. In the spectrum, the defining peak is the methyl protons of the dmso group. These peaks are located at 2.70 ppm and 3.34 ppm as supporting the cis structure of complex. Again, in the ^{13}C-NMR spectrum (Figure 8), carbons of this group are observed in the range of 44.6-43.8 ppm. No significant shift is observed in the peaks of the carbon atoms of the ligand in the complex, as expected. The result of the elemental analyses is suitable with the theoretical value [24].

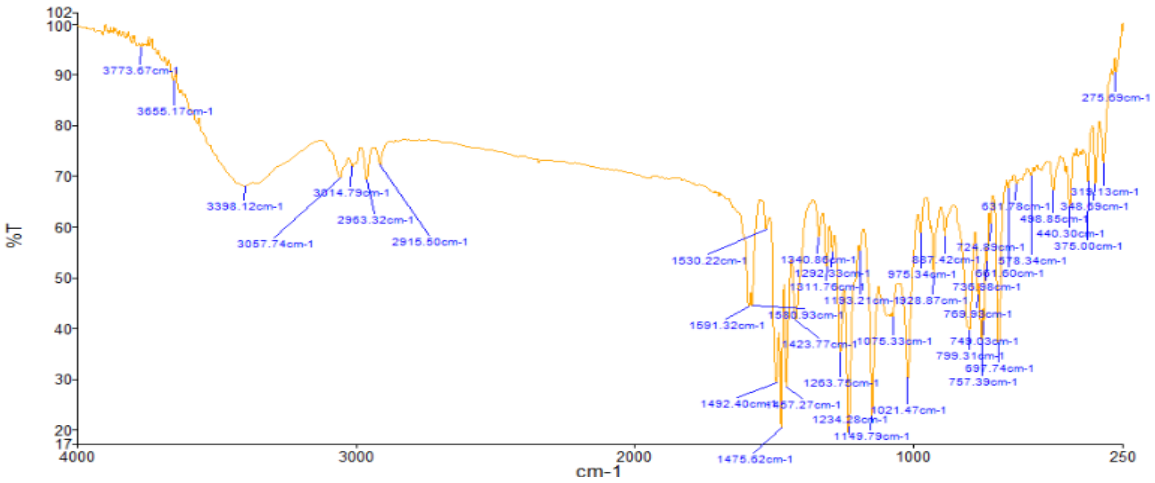

Figure 6. FT-IR Spectrum of the complex (Pt-L)

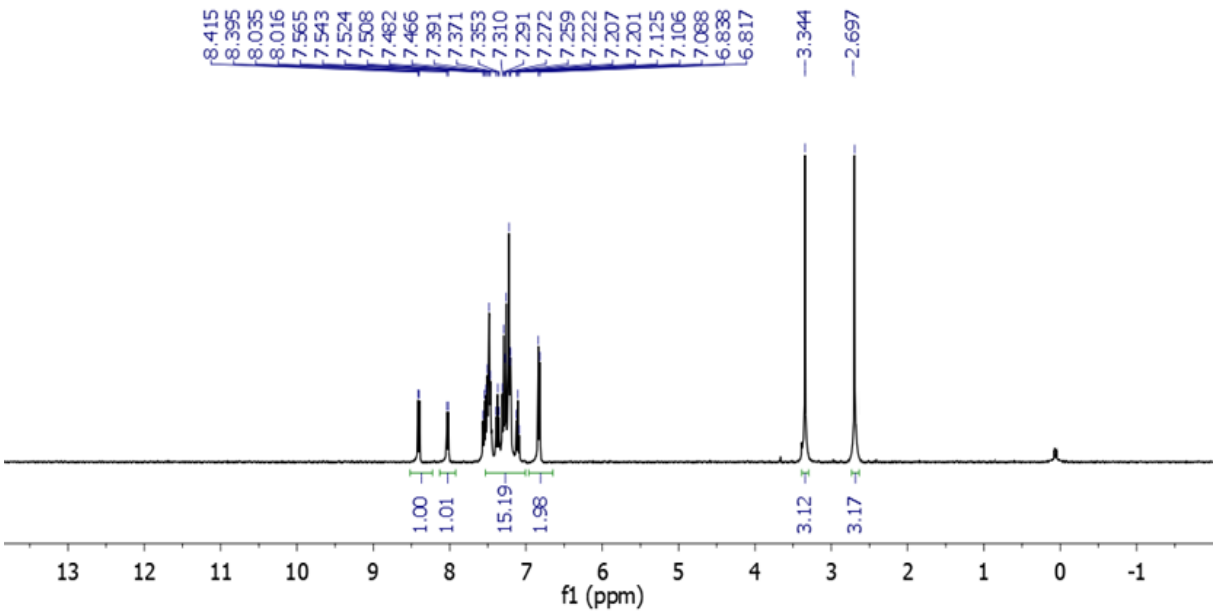

Figure 7. ^{1}H NMR Spectrum of the complex (Pt-L)

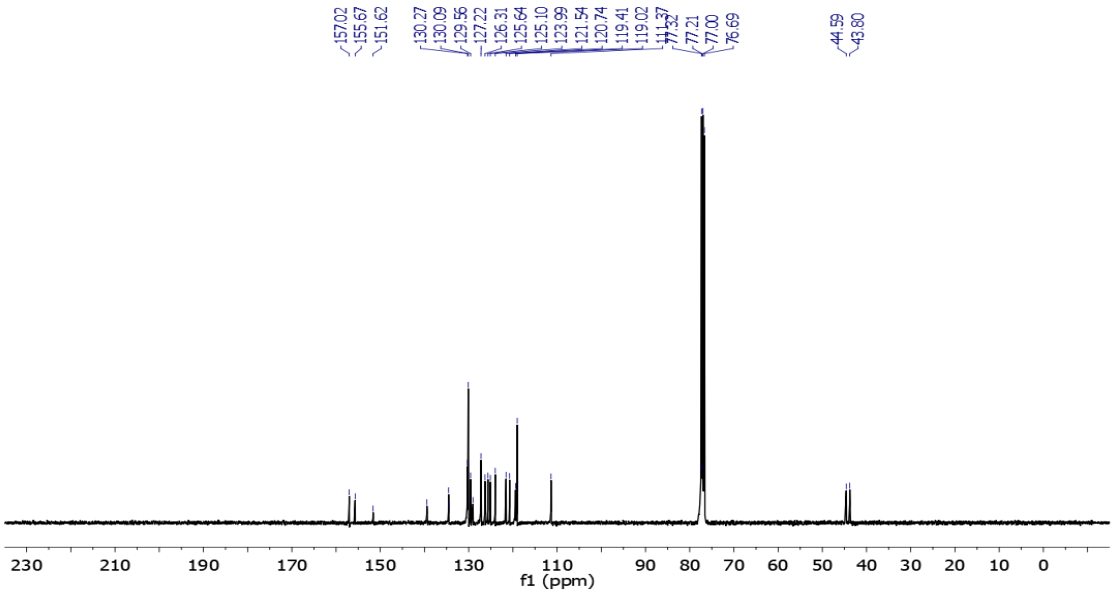

Figure 8. ^{13}C NMR Spectrum of the complex (Pt-L).

3.3 Biological Activity

The results of the cytotoxicity of complex Pt-L on U87 and healthy Vero cells are given in Figure 9. Five different concentrations were tried for all measurements. Toxicity measurements of the complex (Pt-L) on Cancer cell U87 show an IC_{50} value of 31.45 µM. For healthy Vero cells, this value is 9.43 µM (Table 1). Considering the cytotoxic activity of the complex synthesized in the U87 cell line, it is important to calculate selectivity index (SI) values to determine its selectivity and potential inducing anticancer agent compared to the complexes and the cancer drug cis-platinum. These two results show that the complex has no effect on the

cancerous cell. For cis-Pt, which is also widely used in cancer chemotherapy, the IC_{50} values for its effect on these two cell lines are 5.70 and 5.11 µM respectively [25, 26, 27].

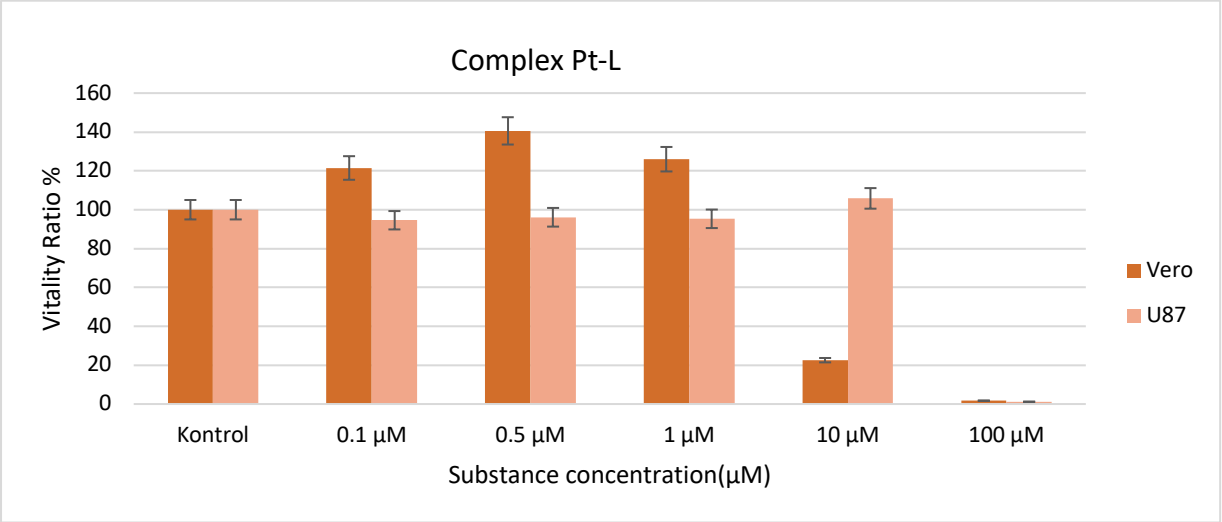

Figure 9. Cytotoxicity control of complex Pt-L on U87 and healthy Vero cells

Table 1. IC_{50} (µM) and Selectivity (SI) Values of Complex (Pt-L)

	IC_{50} (µM) (SI)	
	Complex (Pt-L)	**Cis platin**
U87	31.45**(0.29)**	5.70 (0.90) [25, 26]
VERO	9.43	5.11[27]

(SI = Healthy cell IC_{50} / Diseased cell IC_{50})

The fact that the complex had no activity on the cancer cell showed that the presence of the aromatic group at the C2 carbon did not make a special contribution.

4. Conclusion

In this study, a new benzimidazole ligand and metal complex were synthesized, and their structures were elucidated using spectroscopic methods. The aim of the study was to determine the cytotoxic activity of the synthesized complex on the U87 cell line, a type of glioblastoma cell. This is particularly important as there are limited studies on the activity of complexes against glioblastomas, which are aggressive brain tumor cells, especially prevalent in children. In this context, the activity of the complex on healthy Vero cells was also compared. The cytotoxicity of the synthesized Pt-L complex was found to be low for U87 cells and high for Vero cells. Therefore, the complex was not found to be promising for brain tumor Glioblastoma cancer chemotherapy.

Ethics in Publishing

There are no ethical issues regarding the publication of this study.

Author Contributions

Aydan Arı: Conducted the experiment.

Salih Günnaz: Interpreting spectroscopic studies, writing publication.

Sevil İrişli: Determining the topic, managing the study, interpreting, and writing publication.

Acknowledgement

We thank to Ege University Scientific Research Project (No: FYL-2019-21012). We also give thanks to MATAL Center, Ege University, for cytotoxicity activities.

References

[1] Zhong, H., Bowen J.P. (2006) Antiangiogenesis drug design: multiple pathways targeting tumor vasculature, Curr. Med. Chem., 13, 849-862.

[2] Han, J., Gao X., Liu R., Yang J., Zhang M., Mi Y., Shi Y., Gao Q. (2016) Design, Synthesis of Novel Platinum(II) Glycoconjugates, and Evaluation of Their Antitumor Effects, Chem. Biol. Drug. Des., 87, 867-877.

[3] Wang, D., Lippard S. J. (2005) Cellular Processıng of Platınum Antıcancer Drugs, Nat. Rev. Drug. Discov., 4, 307-20.

[4] Ören, I., Temiz, Ö., Yalçin, I., Sener, E., Altanlar, N. (1999) Synthesis and antimicrobial activity of some novel 2,5- and/or 6-substituted benzoxazole and benzimidazole derivatives, Eur. J. Pharm. Sci., 7, 153-60.

[5] Townsend, L. B., Revankar, G. R. (1970) Benzimidazole nucleosides, nucleotides, and related derivatives, Chem. Rev., 70, 389-438.

[6] Tebbe, M. J., Spitzer, W. A., Victor, F., Miller, S. C., Lee, C. C., Sattelberg, T. R., Mckinney, E., Tang, C. J. (1997) Antirhino/Enteroviral Vinylacetylene Benzimidazoles: A Study of Their Activity and Oral Plasma Levels in Mice , J. Med. Chem., 40, 3937-3946.

[7] Spasov, A. A., Yozhitsa, I. N., Bugaeva, L. I., Anisimova, V. A. (1999) Benzimidazole derivatives: Spectrum of pharmacological activity and toxicological properties, Khim.-Farm. Zhurn., 33, 6-17.

[8] Labanauskas, L.K., Brukstus, A.B., Gaidelis, P.G., Buchinskaite, V.A., Udrenaite E.B., Dauksas, V. K. (2000) Synthesis and antiinflammatory activity of some new 1-acyl derivatives of 2-methylthio-5,6- diethoxybenzimidazole, Pharm. Chem. J., 34, 353-355.

[9] Graßmann, S., Sadek, B., Ligneau, X., Elz, S., Ganellin, C.R., Arrang, J.M., Schwartz, J.C., Stark, H., Schunack, W. **(**2002) Progress in the proxifan class: heterocyclic congeners as novel potent and selective histamine H3-receptor antagonists, Eur. J. Pharm. Sci., 15, 367-378.

[10] Can-Eke, B., Puskullu, M. O., Buyukbingol, E., Iscan, M. (1998) A study on the antioxidant capacities of some benzimidazoles in rat tissues, Chem. Biol. Interact*.,* 113*,* 65-77.

[11] Sevak, R., Paul, A., Goswami S., Santini, D. (2002) Gastroprotective effect of beta3 adrenoreceptor agonists ZD 7114 and CGP 12177A in rats, Pharmacol. Res., 46*,* 351-356.

[12] Ozden, S., Atabey, D., Yildiz, S., Goker, H. (2005), Synthesis and potent antimicrobial activity of some novel methyl or ethyl 1-*H*-benzimidazole-5-carboxylates derivatives carrying amide or amidine groups, Bioorg. Med. Che*m.,* 13(5), 1587-1597.

[13] Valdez, J., Cedillo, R., Hernandez-Campos, A., Yepez, L., Hernandez- Luis, F., Navarrete-Vazquez, G., Tapia, A., Cortes, R., Hernandez, M., Castillo, R. (2002) Synthesis and antiparasitic activity of 1-*H*-benzimidazole derivatives. Bioorg. Med. Chem. Lett., 12, 2221-2224.

[14] Mock, C., Puscasu, I., Rauterkus, M.J., Tallen, G., Wolff, J.E.A., Krebs B. (2001) Novel Pt(II) anticancer agents and their Pd(II) analogues: syntheses, crystal structures, reactions with nucleobases and cytotoxicities, Inorganica Chimica Acta, 319, 109-116.

[15] Eren, G., Emerce E., Acik, L., Aydin, B., Gumus, F. (2019) A novel Trans-Pt(II) complex bearing 2-acetoxymethylbenzimidazole as a non-leaving ligand (trans-[$Pt(AMBi)_2Cl_2$]): Synthesis, antiproliferative activity, DNA interaction and molecular docking studies compared with its cis isomer (cis-[$Pt(AMBi)_2Cl_2$]), Journal of Molecular Structure, 1184, 512-518.

[16] Garnuszek, P., Liciánska, I., Skierski, J. S., Koronkiewicz, M., Mirowski, M., Wiercioch, R., Mazurek, A. P. (2002) Biological investigation of the platinum(II)-[∗I]iodohistamine complexes of potential synergistic anti-cancer activity, Nuclear Medicine and Biology, 29 (2), 169-175.

[17] Tarı, Ö., Gümüs, F., Açık, L., Aydın, B. (2017) Synthesis, characterization and DNA binding studies of platinum(II) complexes with benzimidazole derivative ligands, Bioorganic Chemistry, 74, 272-283.

[18] Mitra, I., Mukherjee, S., Venkata P. Reddy B., Dasgupta, S., Bose K, J. C., Mukherjee, S., Linertd, W. and Ch. Moi, S. (2016) Benzimidazole based Pt(II) complexes with better normal cell viability than cisplatin: synthesis, substitution behavior, cytotoxicity, DNA binding and DFT study, RSC Adv., 6, 76600-76613.

[19] Nicasio-Collazo, J., Ramirez-Garcia, G., Flores-´ Alamo, M., Gutierrez-Granados, S. Peralta-Hernandez, J. M., Luis Maldonado, J., J., Jimenez-Halla, O. C. and Serrano, O. (2019) A novel coordination mode of k1-N-Br pyridylbenz-(imida, oxa or othia)-zole to Pt(II): synthesis, characterization, electrochemical and structural analysis, RSC Adv., 9, 14033-14039.

[20] Gerth, H.U.V., Rompel, A., Krebs, B., Boos, J., Lanvers-Kaminsky, C. (2005) Cytotoxic effects of novel polyoxotungstates and a platinum compound on human cancer cell lines, Anti-Cancer Drugs, 16, 101-106.

[21] Tundo, G.R., Sbardella, D., De Pascali, S.A., Ciaccio, C., Coletta, M., Fanizzi, F.P., Marini, S. (2015) Effect of Cisplatin on Proteasome Activity, J. Biol. Inorg. Chem., 20,101-108.

[22] Doğan, U., Özcan, Ö., Alaca, G., Arı, A., Günnaz, S., Yalçın, H. T. Şahin, O., İrişli, S. (2021) Novel Benzimidazole- Platinum(II) Complexes: Synthesis, Characterization, Antimicrobial and Anticancer Activity, Journal of Molecular Structure, 1229, 129785.

[23] Price, J.H., Williamson, A.N., Schramm, R.F., Wayland, B.B. (1972) Palladium(II) and platinum(II) alkyl sulfoxide complexes. Examples of sulfur-bonded, mixed sulfur- and oxygen-bonded, and totally oxygen-bonded complexes, Inorg. Chem., 11 (6), 1280-1284.

[24] Al-Allaf, T. A. K, Sheet, A. Z. M. (1995) Platinum Group Metal Schiff Base Complexes, Polyhedron, 14, (2), 239-248.

[25] Wang, Q., Wang, Z., Chu, L., LI, X., Kan, P., Xin, X., Zhu, Y., Yang, P. (2015) The Effects and Molecular Mechanisms of MiR-106a in Multidrug Resistance Reversal in Human Glioma U87/DDP and U251/G Cell Lines, PLoS One, 10 (5), e0125473.

[26] Gao, J., Wang, W. Chem. (2019) Knockdown of galectin-1 facilitated cisplatin sensitivity by inhibiting autophagy in neuroblastoma cells, Biol. Interac., 297, 50-56.

[27] Cabrera, A.R., Espinosa-Bustos, C., Faundez, M., Melendez, J., Jaque, P., Danil- iuc, C.G., Aguirre, A., Rojas, R.S., Salas, C.O. (2017) New imidoyl-indazole platinum (II) complexes as potential anticancer agents: Synthesis, evaluation of cytotoxicity, cell death and experimental-theoretical DNA interaction studies, J. Inorg. Biochem., 174, 90-101.

Erzincan Üniversitesi
Fen Bilimleri Enstitüsü Dergisi
2024,17(1), 241-258
ISSN: 1307-9085, e-ISSN: 2149-4584
Araştırma Makalesi

Erzincan University
Journal of Science and Technology
2024,17(1), 241-258
DOI: 10.18185/erzifbed.1408702
Research Article

Trichomes on Vegetative and Reproductive Organs of Endemic *Ballota macrodonta* (Lamiaceae)

Nezahat KANDEMİR[1*]

[1]Amasya University, Faculty of Education, Department of Mathematics and Science Education, Türkiye.

Received: 22/12/2023, **Revised:** 08/03/2024, **Accepted:** 08/03/2024, **Published:** 28/03/2024

Abstract

The morphological features and distributions of trichomes on both vegetative and reproductive organs of endemic *Ballota macrodonta* were examined in this study. The species has limited distrubution in Türkiye and is endemic Iranian Turanian element. In this taxon, different trichome types were seen and these trichomes were divided into two main groups. The first group forms eglandular trichomes, the other group forms glandular trichomes. Two types of eglandular trichomes were obtained on the vegetative and reproductive organs of the taxon: simple unbranched and branched. Stellate type of branched eglandular trichomes were seen more frequently on the lower surface, margins, veins of leaves, corolla, and outer part of calyx, while long unicellular, bicellular, tricellular and multicellular types of simple unbranched eglandular trichomes were seen more frequently on all the organs of this taxon. Glandular trichomes were categorized as capitate with different stalk lengths and one–two head cells and peltate with four–eight secretory cells. According to number of stalk cells, capitate trichomes were grouped into as unicellular, bicellular, tricellular and multicellular trichomes. The capitate ones were seen nearly on all organs of *B. macrodonta*. Peltate trichomes were rarely found on the stem, upper surface of leaf and corolla, while these trichomes were densely found on the surface of the calyx. It was emphasized that both simple unbranched and stellate eglandular trichomes could be used as valuable characters in the classification of this species.

Keywords: *Ballota macrodonta*, endemic, trichome morphology, Türkiye.

Endemik *Ballota macrodonta*'nın (Lamiaceae) Vejetatif ve Üreme Organları Üzerindeki Tüyler

Öz

Bu çalışmada, endemik *Ballota macrodonta*'nın hem vejetatif hem de üreme organları üzerindeki tüylerin morfolojik özellikleri ve dağılımları incelendi. Tür, Türkiye de limitli yayılışa sahiptir ve endemik Iran-Turan elementidir. Bu taksonda, farklı tüy tipleri görüldü ve bu tüyler iki ana gruba ayrıldı. Birinci grup örtü tüylerini oluşturur, diğer grup salgı tüylerini oluşturmaktadır. Taksonun vejetatif ve üreme organları üzerinde örtü tüylerinin iki tipi bulundu: basit dallanmamış ve dallanmış. Basit dallanmamış örtü tüylerinin uzun bir hücreli, iki hücreli, üç hücreli ve çok hücreli tipleri bu taksonun bütün organları üzerinde daha sık görülürken, dallanmış örtü tüylerin yıldızsı tipine yaprakların alt yüzeyinde, yaprakların damarları ve kenarlarında, korolla ve kaliks'in dış yüzeyinde daha sık görüldü. Salgı tüyleri farklı sap uzunluklarına ve bir-iki baş hücreye sahip kapitat ve dört-sekiz salgı hücresine sahip peltat olarak kategorize edildi. Sap hücre sayılarına göre, kapitat tüyler bir hücreli, iki hücreli, üç hücreli ve çok hücreli olarak gruplandırıldı. Kapitat olanlar *B. macrodonta*'nın hemen hemen bütün organlarında görüldü. Peltat tüyler nadir olarak gövdede, yaprağın üst yüzeyinde ve korolla da nadir olarak bulunurken, bu tüyler kaliks yüzeyinde yoğun olarak bulundu. Bu türün sınıflandırılmasında hem basit dallanmamış hem de yıldız şeklindeki örtü tüylerinin değerli karakterler olarak kullanılabileceği vurgulandı.

Anahtar Kelimeler: *Bollata macrodonta*, endemik, tüy morfolojisi, Türkiye

*Corresponding Author: nezahatkndmr@gmail.com
Nezahat KANDEMİR, https://orcid.org/0000-0002-5428-4139

1. Introduction

Lamiaceae family is recognized as a medicinal aromatic plant family due to its high chemical compounds [1]. Türkiye is an important gene center of the Lamiaceae family and this family is represented by 45 genera, 581 species and 751 taxa [2].

Ballota L. genus is known to be important medicinal plants belonging to the Lamiaceae family. Specially, the aerial parts of taxa are widely used in traditional medicine. *Ballota* genus is represented by 35 species and 14 subspecies in the temperate regions of Europe, North Africa and West Asia in the world. 12 species and 8 subspecies of this genus are distributed in Türkiye [2-4]. This genus is rich in endemic species (72.7%) and has a high diversity, especially in the Mediterranean Basin. In Türkiye, *Ballota* species are known with names such as shalba, calba, balotu, honeygrass, nemnem grass, nettle, aerobatic grass, dog grass, black ground leek, hand-saving, smack grass, leylim kara, somruk and ant worm. Some species of the genus are used by the public for cough, asthma, diuretic, headache, nausea, hemorrhoids, wound and burns treatment [4-8]. *B. macrodonta* Boiss. et Balansa is a medicinal plant and reported to have strong antioxidant activity due to its rich phenolic content [9].

Trichomes can develop on the surface of all plant organs. The micromorphology of their provides significant information in the separation of species and subspecies of the Lamiaceae family [10-12]. Also, the importance of trichomes in taxonomy was emphasized by many researchers [12-16]. They are widely obtained on the vegetative and generative organs of taxa of the Lamiaceae family. According to different characteristics and functions, trichomes are grouped into single-celled or multicellular, branched or unbranched, and glandular or eglandular [17]. The glandular trichomes were recorded in four types; subsessile glandular, clavate glandular, branched glandular and capitate glandular trichomes [18]. The eglandular ones were identified with four types; simple unicellular, simple multicellular, branched unuicellular and branched multicellular [19]. The trichomes are known to act as a protective barrier in plant defense against abiotic and biotic stress, such as herbivores, parhogen attacks, seed spread, seed protection, ultraviolet (UV) irradiation, excessive transpiration, drought, salinity and he the presence of heavy metals [20, 21]. They play an important role in many plant-environment interactions, since they are at the outermost boundary between plant and environment. The morphology and distribution of trichomes are related to many factors and even the density distribution of trichomes can show changes in different organs of plants. Namely, the density of trichomes on the lower surface of the same leaf was significantly higher than that of the upper surface [22].

The micromorphology of trichomes is used as important taxonomic characters in distinguishing the species and genera of the Lamiaceae family, which includes the *Ballota* genus. The aim of this study is to emphasize the importance of the availability of trichomes as taxonomic

characters. In addition, *Ballota marodonta* is distinguished from other taxa of the *Ballota* genus according to its trichome morphology.

2. Materials and Methods

The plant materials were collected during the flowering period. Flora of Turkey was used for taxonomic description of the plant materials [2]. For the light microscopy observations (LM), some of fresh materials were fixed in 70 % alcohol solution. The ten different plant samples were used for trichome examinations. The cross and surface-sections of the vegetative (stem, leaf and petiole) and reproductive organs (flowers) were taken by hand using commercial razor blades. Preparations were prepared by taking fifteen surface and fifteen cross-sections from each of the vegetative and reproductive organs of different plant samples. Sartur reagent was applied to the cross and surface-sections [23]. For the stereo microscopy investigations, surface sections were taken from fresh samples and in 70 % alcohol solution samples. Temporary preparations were made and preparations were photographed with a binocular light microscope, with equiped camera and 40X objectives (Leica ICC50 HD). The classification of trichome types were identified according to Cantino [19] and Navarro and El Oualidi [18]. Trichome types and their distribution on the organs of the studied taxon were shown in Tables 1-3. The locality where plant materials were collected was given below;

C5 Kayseri: Yahyalı, Çamlıca-Ulupınar vicinity, sparse *Pinus brutia* forests, serpentine areas, 1112 m., 27. 07. 2021, N. Kandemir.

3. Results and Discussion

In the members of the Lamiaceae family, the presence of trichomes (especially glandular ones, but also eglandular ones) is significant characteristic features [24]. In this study, the types of glandular and eglandular trichomes and their distribution on the vegetative and reproductive organs of *B. macrodonta* were investigated for systematic purposes. Different types of both glandular and eglandular trichomes were identified on the vegetative and reproductive organs of the studied taxon. The two types of glandular trichomes were recorded; peltate and capitate glandular trichomes. The eglandular trichomes were identified with two types; branched (stellate) and simple unbranched trichomes.

3.1. Morphology and distribution of eglandular trichomes

3.1.1. Simple unbranced eglandular trichomes

The simple unbranched eglandular trichomes were again divided into four subtypes (unicellular, bicellular, tricellular, multicellular trichomes) based on the number cell of stalk in this study. The multicellular trichomes were rarely observed on the leaf, calyx teeth, outside part of the calyx of *B. macrodonta*. However, the multicellular trichomes were densely observed on the stem, petiole and corolla of the taxon (Fig. 1 G; Fig. 2 F). This type of trichomes was detected on the petiole of *B. pseudodictamnus* (L.) Benth. subsp. *lycia* Hub.-Mor. [25], organs of *B. undulata* (Sieber ex Fresen.) Benth. [14] and the vegetative and reproductive organs of *B. glandulosisssima* Hub.-Mor & Patzak [12]. The long unicellular, bicellular and tricellular

trichomes were densely found on all organs of *B. macrodonta* (Figs. 1 A, C, D, F, H and M; Figs. 2 A, C, E, F, H, L, M and P). The long unicellular and bicellular trichomes were abundance seen on the calyx teeth of *B. macrodonta*, while long unicellular trichomes were adundance seen on the calyx surface (Table 1). Similar eglandular trichome types were also reported in some Türkiye species of the genus *Teucrium* L. [15], on the organs of *B. pseudodictamnus* (L.) Benth. subsp. *lycia* Hub.-Mor. in Türkiye [25], in *Phlomoides* taxa [26], *B. acetabulosa* (L.) Benth. [27], on the organs of *B. glandulosisssima* [12], on the leaves of *Phlomis herba-venti* subsp. *pungens* (Willd.) Maire ex DeFilipps. [28] and on the stem and leaves of *B. nigra* L. subsp. *nigra* [29]. Moreover, these trichomes were seen in *B. kaiseri* Tachk., *B. undulata B. saxatilis* Sieber ex J. Et C. Presl and *B. pseudodictamnus* [14].

3.1.2. Branched eglandular trichomes

Stellate trichomes are multicellular and branched structure. They are called as star-shaped trichomes [30]. The stellate trichomes have with 3–8 equal branches and surface of their can be smooth or rough. These trichomes were abudantly seen on the lower surface, margins and veins of leaves, outside part of the calyx and corolla of *B. macrodonta* (Figs. 2 D, G, K) (Table 1). Especially, this type of trichomes was highly dense on the lower surface of leaf of the studied taxon. The dense, short stellate trichomes are seen only in the ridge parts of corolla upper lip of *B. macrodonta*. On the petiole, stem and upper surface of leaf of the taxon, stellate trichomes were not observed. In addition, *B. macrodonta* has two different leaf colors depending on the presence and density of stellate trichomes on the upper and lower surfaces of the leaf. The upper surface of the leaf is not stellate trichomes and green in coloured, while the lower surface is densely stellate trichomes and white in coloured. The stellate trichomes were a common feature of *Ballota* taxa. El-Deen Osman [14] and Kandemir [12] reported presence of stellate trichomes in other *Ballota* taxa (*B. kaiseri, B. saxatilis, B. undulata* and *B. glandulosissima*), respectively. Also, this type of trichomes were recorded in *Phlomoides* taxa [26] and *Marrubium astracanicum* subsp. *astracanicum* Jacq. [16].

In the Lamiaceae family and the *Ballota* genus are mostly known for its stellate and dendroid trichomes. In the studied taxon, dendroid trichomes were seen neither on the vegetative nor reproductive organs of this taxa. Also, this kind of trichomes was not found in some *Ballota* species (*B. kaiseri, B. saxatilis, B. undulata*) growing in Egypt [14]. The dendroid ones were found in *B. acetabulosa* (L.) Bentham., *B. pseudodictamnus* subsp. *lycia* and *B. cristata* P.H. Davis distributed in Türkiye [25,31] and *B. damascens* Boiss., and *B. pseudodictamnus* distributed in Egypt [14]. On the other hand, Giuliani et al. [27] and Kandemir [12] did not detect the dendroid trichomes on the organs of *B. acetabulosa* and *B. glandulosissima*, respectively. Since the presence of dendroid and stellate trichomes had systematic value for taxa division, some *Ballota* taxa (*B. kaiseri, B. saxatilis, B. undulata and B. pseudodictamnus*) in Egypt were distinguished according to the presence or absence of stellate and dendroid trichomes by El Deen Osman [14].

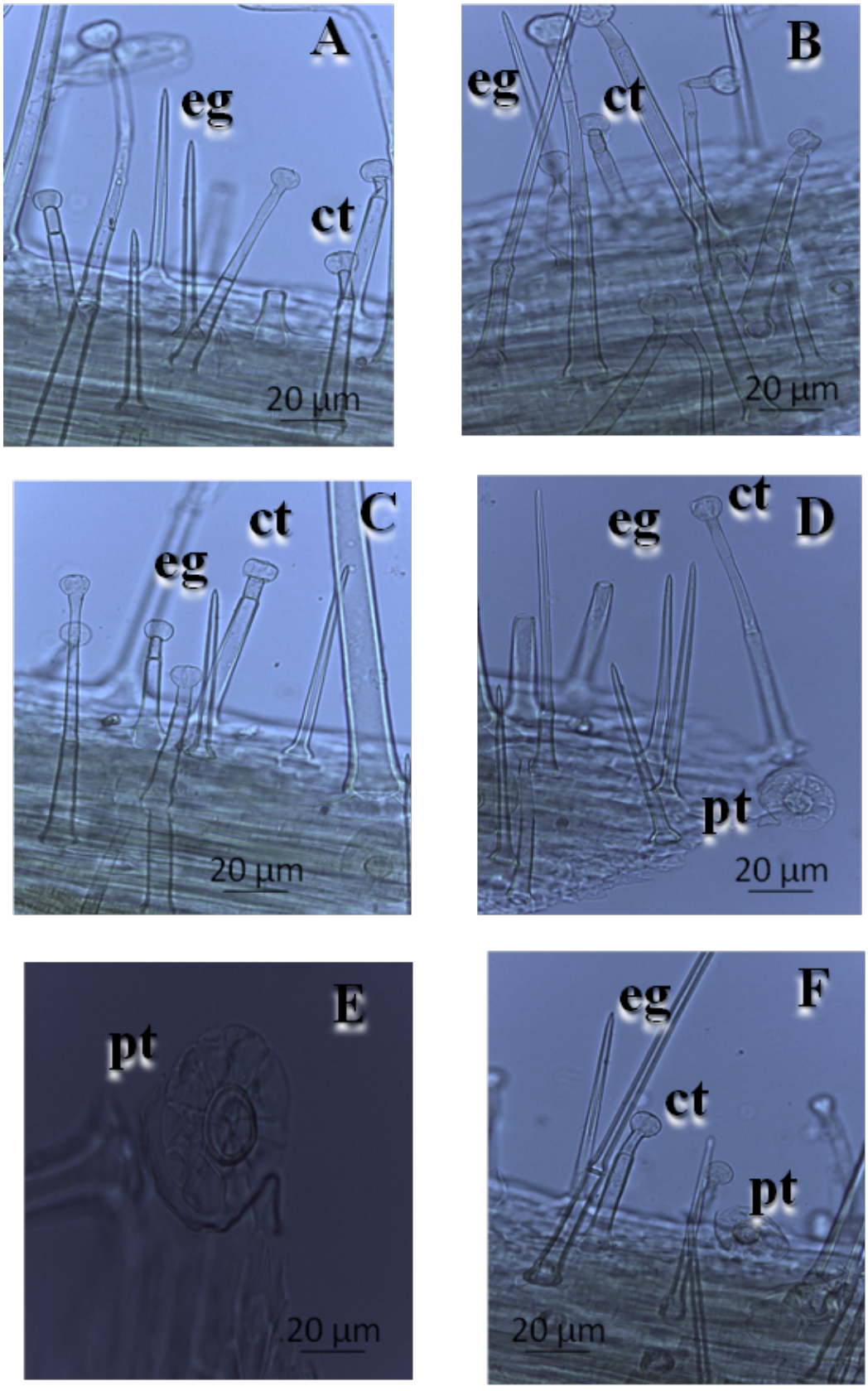

Figure 1. Continues

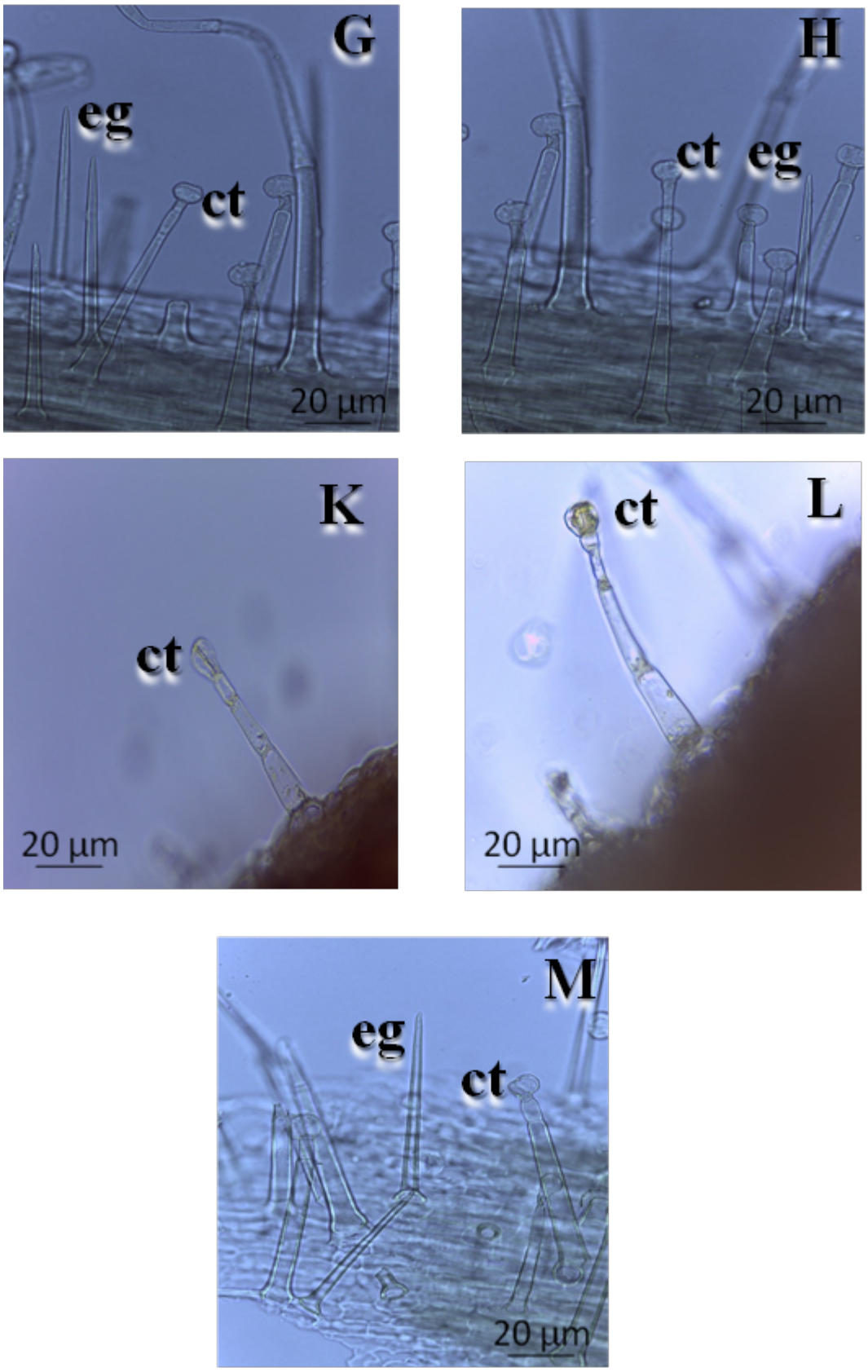

Figure 1. Glandular and eglandular trichome types on the stem and petiole. (A) Unicellular eglandular and bicellular, tricellular stalked with unicellular head capitate trichomes on the stem, (B) Unicellular, bicellular

eglandular and bicellular, tricellular, multicellular stalked with unicellular head capitate trichomes on the petiole, (C) Unicellular eglandular and unicellular, tricellular stalked with unicellular head capitate trichomes on the stem, (D) Unicellular eglandular and unicellular, multicellular stalked with unicellular head capitate and peltate trichomes on the stem, (E) Peltate trichomes on the stem, (F) Bicellular, unicellular eglandular and bicellular stalked with unicellular head capitate and peltate trichomes on the stem, (G) Unicellular, multicellular eglandular and bicellular, multicellular stalked with unicellular, bicellular head capitate trichomes on the stem, (H). Multicellular, bicellular stalked with unicellular, bicellular head capitate and unicellular eglandular trichomes on the stem, (K) Tricellular swollen stalked with bicellular head capitate trichomes on the petiole, (L) Multicellular swollen stalked with bicellular head capitate trichomes on the stem, (M) Unicellular eglandular and bicellular and multicellular stalked with unicellular head capitate trichome on the petiole, (eg) Eglandular trichomes, (ct) Capitate trichomes, (pt) Peltate trichomes.

Table 1. Eglandular trichome types and distribution on the vegetative and reproductive organs of *Ballota macrodonta*.

Organs of *Ballota macrodonta*	**Unbranched unicellular**	**Unbranched bicellular**	**Unbranched tricellular**	**Unbranched multicellular**	**Stellate trichomes**	**Dendroid trichomes**
Stem	++	++	++	++	_	_
Petiole	++	++	++	++	_	_
Margin and veins of leaf	++	++	++	+	+++	_
Lamina of leaf (upper surface)	++	++	++	+	_	
Lamina of leaf (lower surface)	++	++	++	+	+++	_
Calyx teeth	+++	+++	++	+	_	_
Outer surface of calyx	+++	++	++	+	+++	_
Corolla	++	++	++	++	+++	_

-: absent; **+:** scarce; **++:** dense; **+++:** abundant

3.2. Morphology and distribution of glandular trichomes

The two different types of glandular trichomes were detected on vegetative and reproductive organs of *B. macrodonta*–capitate and peltate trichomes. These trichomes were sessile, short stalked or long stalked. The glandular ones and their distribution, morphological shapes and frequency provide valuable characters at subfamily level in the Lamiaceae family [22].

3.2.1. Capitate glandular trichomes

The capitate glandular trichomes are the most common in the Lamiaceae family and they can be used for taxonomic identification of taxa in this family. However, the stalk length and head shape of these trichomes are very variable. This kind of trichomes were reported on the vegetative and reproductive organs of some Lamiaceae taxa [12, 16, 26, 28, 32]. In the present

study, capitate glandular trichomes in *B. macrodonta* were divided into four subtypes which were unicellular long or short stalked (subtype I), bicellular (subtype II), tricellular (subtype III) and multicellular (subtype IV) stalked.

3.2.1.1. Unicellular stalked capitate glandular trichomes (Subtype I)

These trichomes have a stalk cell and unicellular, bicellular, tricellular and multicellular head. Therefore, this type of capitate trichomes is classified as unicellular, bicellular, tricellular and multicellular headed trichomes, according to number of head cells. In the present study, two form of these trichomes were recognized (Table 3). The first form was unicellular headed and was seen on the stem, petiole, upper and lower surface of leaf, outside part of the calyx, calyx teeth and corolla of this taxon (Figs. 1 C, D). The second form had bicellular head and was rarely observed on the petiole, stem, calyx teeth, lower surface of leaf of *B. macrodonta* (Table 2). The unicellular stalked capitate trichomes were found on the stem and leaves of *B. nigra* subsp. *nigra* [29], the vegetative and reproductive of *B. glandulosissima* [12], in *B. kaiseri, B. undulata, B. damascens, B. saxatilis, B. pseudodictamnus* [14], in some Turkish species of *Teucrium* [15], the organs of *B. pseudodictamnus* subsp. *lycia* [25] and the organs of *Phlomis herba-venti* subsp. *pungens* [28]. Also, these trichomes were seen especially on the leaf and corolla abaxial sides, on the vein system of the whole plant, of *B. acetabulosa* [27]. On the other hand, the unicellular stalked capitate ones were quite widespread in all taxa of the Lamiaceae family [33, 12, 16, 22, 28, 33].

3.2.1.2. Bicellular stalked capitate trichomes (Subtype II)

The stalk was two celled, head had one or two cells (Table 3). These trichomes had also a long or short neck cell. On the leaves, stem, petiole, calyx and calyx teeth of *B. macrodonta*, unicellular and bicellular headed of these capitate trichomes were found (Figs. 1 A, B, F, G, H and M; Figs. 2 B, C, F, H, L, M and P) (Table 2). This kind of trichomes was quite dense on the stem. These capitate trichomes were determined in some members of the genera *Salvia* L., *Stachys* L., *Sideritis* L., *Scutellaria* L., and *Ballota* [12, 29, 33-35]. Moreover, bicellular stalked capitate ones were detected in *B. kaiseri, B. undulata, B. damascens, B. saxatilis,* and *B. pseudodictamnus*) [14] and on leaves and the calyx abaxial side of *B. acetabulosa* [27], on the leaves of some Turkish species of *Teucrium* [15] and on the organs of *B. pseudodictamnus* subsp *lycia* [25].

3.2.1.3. Tricellular stalked capitate trichomes (Subtype III)

In the subtype III capitate trichomes, there are three celled long stalk, unicellular, bicellular head and a long or short neck cell. This type of capitate trichomes was obtained on the petiole, stem, lower surface of leaf, calyx and calyx teeth of *B. macrodonta* (Figs. 1 A-C; Figs. 2 B, F,). Stalk cells of this type trichome were swollen (Fig. 1 K). Although the tricellular stalked and unicellular, bicellular headed capitate trichomes were rarely seen on the stem, petiole, outside part of the calyx and calyx teeth of *B. macrodonta*, these trichomes were densely seen on the lower surface of leaf. This type of trichomes were observed on the leaf adaxial side, on the sepal abaxial side and on the floral peduncle of *B. acetabulosa* [27], the organs of some *Ballota* taxa

(*B. nigra subsp. nigra*, *B. kaiseri, B. undulata, B. damascens, B. saxatilis, B. pseudodictamnus, B. glandulosissima*) [29, 14, 12], respectively.

3.2.1.4. Multicellular stalked capitate trichomes (Subtype IV)

The stalk in this type of trichomes had multicellular (four, five and six celled). The head part of this trichome was one or two celled. In this study, the stalk part of this kind of capitate trichomes was four-celled and head was one-celled. Multicellular stalked (subtype IV) trichomes were recorded on the stem, petiole, leaf and calyx of *B. macrodonta* (Figs. 1 B, D, G, H; Figs. 2 E, L, N). Stalk cells of multicellular trichomes were swollen (Fig. 1 L). Multicellular stalked capitate ones were found in only *B. saxatilis* and *B. kaiseri* [14], on the leaf adaxial side, the sepal abaxial side and the floral peduncle *B. acetabulosa* [27], the vegetative and reproductive organs *B. glandulosissima* [12], the stem and leaves of *B. nigra* subsp. *nigra* [29] and the reproductive organs of other Lamiaceae taxa [33], the leaves of *Teucrium* taxa [15] and in *Phlomoides* taxa [26].

3.2.2. Peltate glandular trichomes

The peltate trichomes in the Lamiaceae consist of a basal cell, a short stalk, and a large head of several secretory cells (up to 16) [36]. In this study, peltate trichomes were seven and eight celled (Table 3). The peltate ones were rarely seen on the stem, upper surface of leaf and outer surface of the calyx and corolla of *B. macrodonta* (Figs. 1 D-F). These trichomes were dense on the outer surface of the calyx. Such trichomes (peltate) were observed on the leaves, sepals and petals of *B. acetabulosa* [27], both vegetative and reproduvtive organs of *B. glandulosissima* [12], the stem and leaves of *B. nigra* subsp. *nigra* [29]. The presence of peltate trichomes was reported on organs of *B. pseudodictamnus* subsp *lycia* and the organs of *Scutellaria brevibracteata* subsp. *subvelutina* (Rech. f.) Greuter & Burdet [25, 27]. But, peltate trichomes were not found on the leaves of *P. herba-venti* subsp. *pungens* [28].

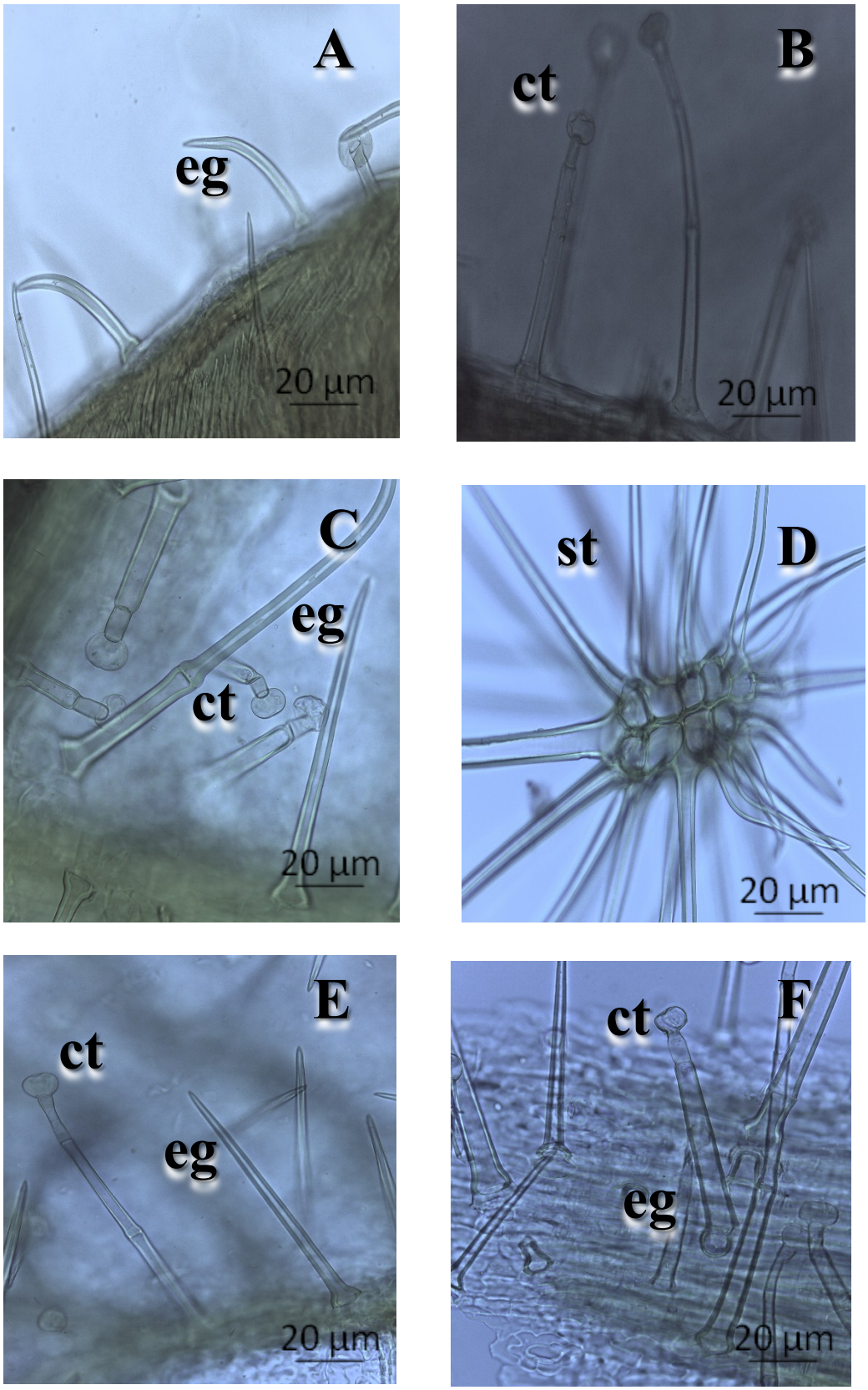

Figure 2. Continues

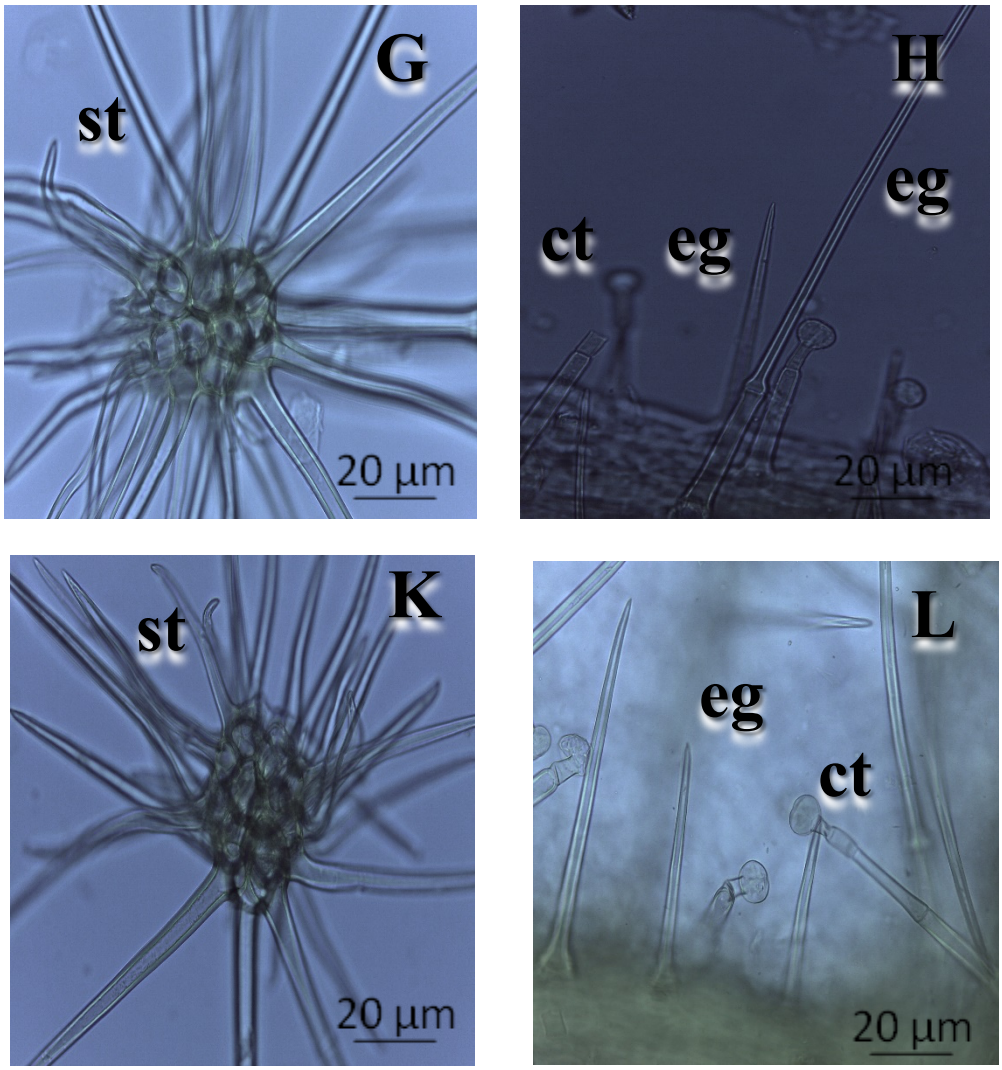

Figure 2. Continues

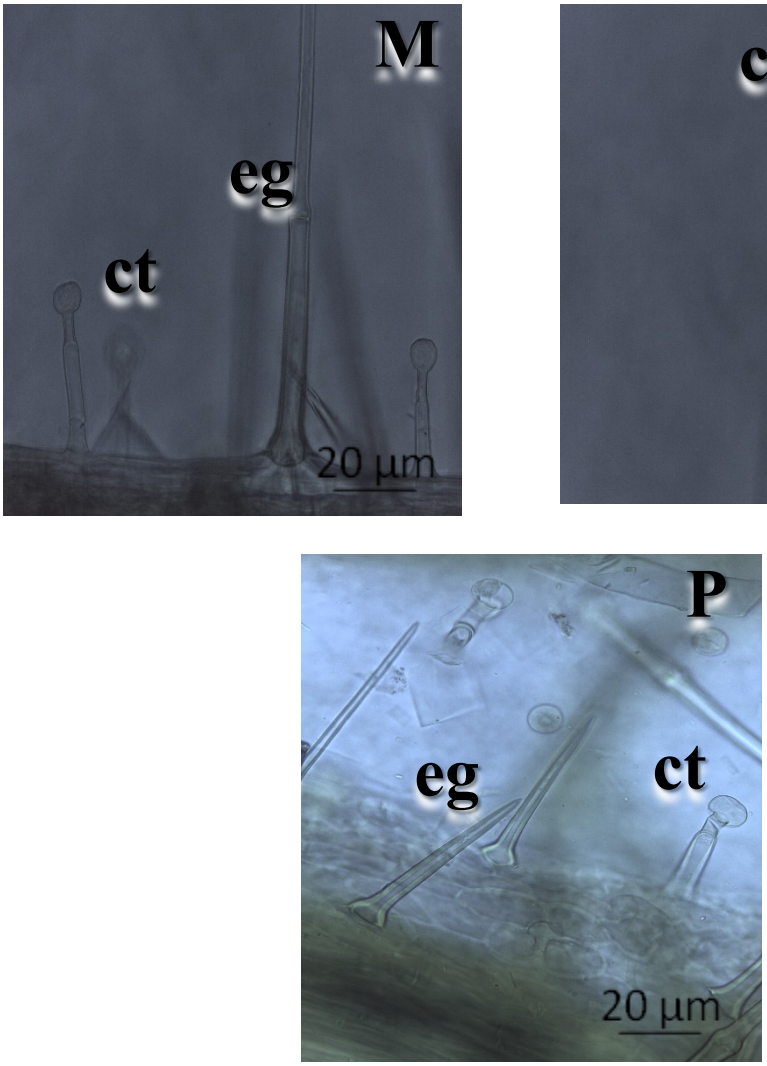

Figure 2. Glandular and eglandular trichome types on the leaf, calyx and corolla. (A) Unicellular eglandular trichomes on the calyx, (B) Bicellular and tricellular stalked with unicellular head capitate trichomes on the calyx, (C) Unicellular, bicellular eglandular and bicellular stalked with unicellular head capitate trichomes on the calyx, (D) Stellate trichomes on the calyx, (E) Unicellular eglandular and multicellular stalked with unicellular head capitate trichomes on the calyx, (F) Unicellular, multicellular eglandular and bicellular, tricellular stalked with unicellular head capitate trichomes on the calyx, (G) Stellate trichomes on the corolla, (H) Bicellular stalked with bicellular head capitate and unicellular, bicellular eglandular trichomes on the corolla, (K) Stellate trichomes on the leaf, (L) Unicellular, bicellular eglandular and bicellular, multicellular stalked with unicellular head capitate trichomes on the leaf, (M) Bicellular eglandular and bicellular stalked with unicellular head capitate trichomes on the leaf, (N) Multicellular stalked with unicellular head capitate trichome on the leaf, (P) Unicellular eglandular and bicellular stalked with unicellular head capitate trichomes on the leaf, (eg) Eglandular trichomes, (st) Stellate trichomes, (ct) Capitate trichomes.

Table 2. Glandular trichome types and distribution on the vegetative and reproductive organs of *Ballota macrodonta*

Organs of *Ballota macrodonta*	**Subtype I capitate**	**Subtype II capitate**	**Subtype III capitate**	**Subtype IV capitate**	**Peltate trichomes**
Stem	+	++	+	+	+
Petiole	+	+	+	+	_
Margin and veins of leaf	+	+	+	+	_
Lamina of leaf (upper surface)	+	+	_	_	+
Lamina of leaf (lower surface	+	+	++	_	_
Calyx teeth	+	+	+	_	_
Outer surface of calyx	+	+	+	+	++
Corolla	+	_	_	_	+

-: absent; **+:** scarce; **++:** dense; **+++:** abundant

Table 3. The stalk and head cell numbers of glandular trichomes on the vegetative and reproductive organs of *Ballota macrodonta*

	Capitate trichomes								**Peltate trichomes**	
Plant part	Subtype I		Subtype II		Subtype III		Subtype IV			
	Head cell	Stalk cell	Head cell	Stalk cell	Head cell	Stalk cell	Head cell	Stalk cell	Center cell	Periphery cell
Stem	1	1	1	2	1	3	1	4	1	7
	2	1	_	_	_	_	2	4	_	_
Petiole	1	1	1	2	1	3	1	4	_	_
	2	1	_	_	2	3	_	_	_	_
Leaf (upper surface)	1	1	1	2	_	_	1	4	1	8
Leaf (lower surface)	1	1	1	2	1	3	1	4	_	_
	2	1	_	_	_	_	1	4	_	_
Calyx	1	1	1	2	1					
						3	_	_	1	8
Corolla	1	1	_	_	_	_	_	_	1	8
	_	_	2	2	_	_	_	_	_	_

4. Conclusions

Trichomes are commonly used as value taxonomic characters in taxonomy of plants, since the distribution, density and types of trichomes show significant variability among different taxa. Also, Kandemir [12] and Gurdal [25] reported that trichome micromorphology can be useful in the taxonomy of the genus *Ballota.* On both the vegetative and reproductive organs of this taxon, four main trichome types (peltate glandular, capitate glandular, simple unbranched eglandular and branched eglandular) were seen. The unicellular, bicellular, tricellular and multicellular simple unbranced eglandular and stellate trichomes were densely observed on the vegetative and reproductive organs of this taxon. Specially, the densest trichome type was stellate ones and these trichomes were abundance seen on the lower surface and veins, leaf margins, corolla and outer part of calyx of the studied taxon. But, such trichomes did not observe on the upper surface of leaf, petiole and stem of this taxon. The simple unbranched eglandular and stellate trichomes were detected to having significant taxonomic characteristics in distinguishing from other *Ballota* taxa of *B. macrodonta*. On the other hand, *Ballota* taxa were characterized by the presence of stellate trichomes. Also, *B. macrodonta* can be easily distinguished from other species in *Ballota* genus by the presence of dense stellate trichomes on the lower surface of leaf. The capitate glandular trichomes were seen nearly all organs of the taxon, while peltate glandular trichomes were seen on the stem, upper surface of leaf and outer surface of the calyx and corolla. Especially the subtype II and subtype III types of capitate feathers were found more frequently on the organs of this taxon.

Ethics in Publishing

There are no ethical issues regarding the publication of this study.

Author Contributions

Designing the study, collecting data; evaluating the results, writing the article, etc. transactions were made by Nezahat Kandemir

References

[1] Hashemi, M., Kharazian, N., (2021) Identification of flavonoids from *Marrubium* and *Ballota* species (Lamiaceae) and determination of chemotaxonomic markers using high performance liquid chromatography mass spectrometer, Journal of Sciences Islamic Republic of Iran, 32 (4):305-320.

[2] Davis, P.H., Doroszenko, A., (1982) Flora of Turkey and The East Aegean Islands. In: Davis, P.H., Edmondson, R., Mill, R.R., Tan, Kit. (Eds.), *Ballota* L. (pp.156-160). Edinburg University Press. Edinburg.

[3] Güner, A., (2012) Turkey Plants List (Vascular Plants). In: Güner, A., Aslan, S., Ekim, T., Vural, M., Babaç, M.T. (Eds.), *Ballota* L. (pp. 548-550). Nezahat Gökyiğit Botanical Garden and Flora Research Association Publication, İstanbul-Türkiye.

[4] Morteza-Semnani, K., Ghanbarimasir, Z., (2019) A review on traditional use phytochemical and pharmacological activities of the genus *Ballota*, Journal of Ethnopharmacolgy, 233:197-217.

[5] Yazgan, A.N., Yılmaz, G., Sever, Y.B., (2010) Anatomical studies on *Ballota acetabulosa* (L.) Benth., Ankara Eczacılık Fakültesi Dergisi, 39:265–274.

[6] Dulger, B., Dulger, G., (2012) Antimicrobial activity of the leaves of *Ballota acetabulosa* on microorganisms isolated from urinary tract infections, Turkish Journal of Pharmaceutical Sciences, 9 (3): 257-262.

[7] Dulger, G., Dulger, B., (2017) Antibacterial activity of endemic *Ballota nigra subsp. anatolica* against some human eye pathogens from Turkey, Innovare Journal of Life Sciences, 5 (2): 1-3.

[8] Agca Can, A., Yılmaz Sarıaltın, S., Yazgan Ekici, A. N., Çoban, T., Saltan Iscan, G., Sever Yılmaz, B., (2021) Anti-inflammatory and anti-diabetic activity of *Ballota* L. species grown in Turkey. Istanbul Journal Pharmacy, 51 (3): 326-332.

[9] Uysal, S., Aumeeruddy-Elafi, Z., Zengin, G., Aktumsek, A., Mocan, A., Custodio, L., Neng, N.R., Nogueria, J.M.F., Ciric, A., Glamoclija, J., Sokovic, M., Mahomoodally, F., (2018) Insight into the biological properties and phytochemical composition of *Ballota macrodonta* Boiss. Et Balansa,-an endemic medicinal plant from Turkey. Industrial. Crops and Products, 133: 422-428.

[10] Salmaki, Y., Zarre, S., Jamzad, Z., Bräuchler, C., (2009**)** Trichome micromorphology of Iranian *Stachys* (Lamiaceae) with emphasis on its systematic implication, Flora, 204: 371–381.

[11] Eiji, S., Salmaki, Y., (2016) Evolution of trichomes and its systematic significance in *Salvia* (Mentheae; Nepetoideae; Lamiaceae), Botanical Journal of the Linnean Society, 180 (2): 241-257.

[12] Kandemir, N., (2023) Glandular and eglandular trichomes of endemic *Ballota glandulosissima* (Lamiaceae). Türler ve Habitatlar, 4 (2): 110-124.

[13] Beyrouthy, E.M., Arnold-Apostolides, N., Dupont, F., (2009) Trichomes morphology of six Lebanese species of *Stachys* (Lamiaceae), Flora Mediterranea, 19: 129-139.

[14] El-Deen Osman, A.K., (2012) Trichome micromorphology of Egyptian *Ballota* L. (Lamiaceae) with emphasis on its systematic implication, Pakistan Journal of Botany, 44(1): 33-46.

[15] Ecevit-Genç, G., Özcan, T., Dirmenci, T., (2018) Leaf indumentum in some Turkish species of *Teucrium* (Lamiaceae), Istanbul Journal of Pharmacy, 48 (1): 6-11.

[16] Koçak, K.V., Kandemir, N., (2023) Taxonomic importance of anatomical, ecological andtrichome features of *Marrubium astracanicum* subsp. *astracanicum* Jacq. (Lamiaceae), Black Sea Journal of Engineering and Science, 6 (3):199-209.

[17] Wang, X., Shen, C., Meng, P., Tan, G., Lv, L., (2021) Analysis and Review of Trichomes in Plants, BMC Plant Biology, 21(70): 1-11.

[18] Navarro, T., El Oualidi, J., (2000) Trichome morphology in *Teucrium* L. (Labiatae). A taxonomic review, Anales del Jardin Botanico de Madrid, 57 (2): 277-297.

[19] Cantino, P.D., (1990) The phylogenetic significance of stomata and trichomes in the Labiatae and Verbenaceae, Journal of the Arnold Arboretum, 71(3):323-370.

[20] Xiao, K., Mao, X., Lin, Y., Xu, H., Zhu, Y., Cai, Q., Xie, H., Zhang, J., (2017) Trichome, a functional diversity phenotype in plant, Molecular Biology:Open Access, 6 (1):1–6.

[21] Karabourniotis, G., Liakopoulos, G., Nikolopoulos, D., Bresta, P., (2020) Protective and defensive roles of non-glandular trichomes against multiple stresses: structure–function coordination, Journal of Forestry Research, 31:1–12.

[22] Ascensão, L., Marques, N., Pais, M.S., (1995) Glandular trichomes on vegetative and reproductive organs of *Leonotis leonurus* (Lamiacea), Annals of Botany, 75(6): 619–626.

[23] Çelebioğlu, S., Baytop, T., (1949) A New Reagent for Microscopical Investigation of Plant Publication of the Institute of Pharmacognosy. İstanbul.

[24] Santos Tozin, L.R.D., De Melo Silva, S.C., Rodrigues, T.M., (2016) Non-Glandular Trichomes in Lamiaceae and Verbenaceae Species: Morphological and Histochemical Features Indicate More than Physical Protection, New Zealand Journal of Botany, 54(4):446–457.

[25] Gurdal, B., (2021) Anatomy and trichome micromorphology of endemic *Ballota pseudodictamnus* subsp. *lycia* (Lamiaceae), Düzce University Journal of Science & Technology, 9(4):1078-1085.

[26] Khosroshahi, E.E., Salmaki, Y., (2019) Evolution of trichome types and its systematic significance in the genus *Phlomoides* (Lamioideae–Lamiaceae), Nordic Journal of Botany, 37 (5):1-14.

[27] Giuliani, C., Bottoni, M., Ascrizzi, R., Milani, F., Falsini, S., Papini, A., Flamini, G., Fico, G., (2021) Micromorphological and phytochemical survey of *Ballota acetabulosa* (L.) Benth., Plant Biology (Stuttgart), 23(4):643-652.

[28] Gostin, I.N., (2023) Glandular and non-glandular trichomes from *Phlomis herba-venti* subsp. *pungens* leaves: light, confocal, and scanning electron microscopy and histochemistry of the secretory products, Plants,(Basel) 12(13):2423.

[29] Şahin, F.P., Toker, M.C., Ezer, N., (2005) Botanical Properties of a Mild Sedative: *Ballota nigra* L. subsp. *nigra*, FABAD Journal of Pharmaceutical Sciences, 30: 94-99.

[30] Xiang, C., Dong, Z., Peng, H., Lui, Z., (2010) Trichome micromorphology of the East Asiatic genus *Chelonopsis* (Lamiaceae) and its systematic implications, Flora, 205(7):434-441

[31] Tezcan, F., (2001) Revision of Türkiye *Ballota* L. (Labiatae) Genus. Doctoral Thesis, Gazi University, Graduate School of Natural and Applied Sciences, Department of Biology.

[32] Kandemir, N., (2011) Trichomes on *Salvia pomifera* (Lamiaceae) in Turkey, *Botanica* Lithuanica, 17(1):3-11.

[33] Giuliani, C., Maleci, B.L., (2008) Insight into the structure and chemistry of glandular trichomes of Labiatae, with emphasis on subfamily Lamioideae, Plant Systematics and Evolution, 276(3):199-208.

[34] Giuliani, C., Bottoni, M., Ascrizzi, R., Santagostini, L., Papini, A., Flamini, G., Fico, G., (2020) A novel study approach on *Scutellaria altissima* L. cultivated at the Ghirardi Botanic Garden (Lombardy, Italy), Plant Biology (Stuttgart), 22(6):1013–1021.

[35] Giuliani, C., Bottoni, M., Ascrizzi, R., Santagostini, L., Papini, A., Flamini, G., Fico, G., (2022) *Scutellaria brevibracteata* subsp. *subvelutina* (Rech.f.) Greuter & Burdet: morphological and phytochemical characterization, Natural Product Research, 36(1):54-62.

[36] Hallahan, L.D., (2000) Monoterpenoid biosynthesis in glandular trichomes of Labiatae plants. In: Hallahan, D.L., Gray, J.C. (Eds.), Advances in botanical research. Incorporating advances in plant pathology (pp. 77-120). *Plant trichomes* London: Academic Press. London.

Erzincan Üniversitesi
Fen Bilimleri Enstitüsü Dergisi
20.., ..(..), **??-??**
ISSN: 1307-9085, e-ISSN: 2149-4584
Araştırma Makalesi

Erzincan University
Journal of Science and Technology
20.., ..(.), **??-??**
DOI: 10.18185/erzifbed. . . . . .
Research Article

A Note On ϕ- Strongly Quasi Primary Ideals

Rabia Nagehan Uregen[1*]

Department of Mathematics and Science Education, Erzincan Binali Yildirim University, Erzincan, Turkey

GeliÅŸ / Received: ../../20.., Kabul / Accepted: ../../20..

Abstract

Our aim in this study is to define the ϕ-sq primary ideal, which is a prime ideal generalization, and investigate some of its fundamental characteristics. Given a commutative ring R that has an identity, $L(R)$ denotes the set of all ideals of R. Assume that $\phi : L(R) \to L(R) \cup \{\emptyset\}$ a function. A proper ideal I of R is called ϕ-sq primary ideal if $ab \in I - \phi(I)$ implies $a^2 \in I$ or $b \in \sqrt{I}$ for each $a, b \in R$. Afterwards, the basic features of this new structure were determined and its relationship with other ideals such as ϕ-2 prime ideal, strongly quasi primary ideal and ϕ-semiprimary ideal was examined.

Keywords: prime ideal, ϕ-sq primary ideal, ϕ-2 prime ideal, strongly quasi primary ideal, ϕ-semiprimary ideal

ϕ-kuvvetli Yarı Asalımsı İdealler Üzerine Bir Not

Öz

Bu çalışmanın amacı asal ideallerin bir genelleştirmesi olan ϕ-kuvvetli yarı asalımsı idealleri tanımlamak ve bu ideallerin bazı temel özelliklerini incelemektir. R birimli ve değişmeli bir halka ve $L(R)$, R nin tüm ideallerinin kümesi olsun. $\phi : L(R) \to L(R) \cup \{\emptyset\}$ olduğunu kabul edelim. Her $a, b \in R$ olmak üzere $ab \in I - \phi(I)$ iken $a^2 \in I$ veya $b \in \sqrt{I}$ ise R nin I has idealine ϕ-kuvvetli yarı asalımsı ideal denir. Tanımın ardından bu yeni yapının temel özellikleri belirlenerek ϕ-2 asal, kuvvetli yarı asalımsı ideal ve ϕ-yarıasal ideal gibi ideallerle olan ilişkisi incelenmiştir.

Anahtar Kelimeler: asal ideal, ϕ-kuvvetli yarı asalımsı ideal, ϕ-2 asal, kuvvetli yarı asalımsı ideal ve ϕ-yarıasal ideal

*Rabia Nagehan Üregen:rabia.uregen@erzincan.edu.tr

1. Introduction

Prime ideals and their extensions play a significant role in the field of commutative algebra. A large number of authors have conducted research on prime ideals for this reason. The purpose of this investigation is to precisely outline the concept of the ϕ-sq primary ideal, which is a broader category of prime ideals, and thoroughly analyze its fundamental characteristics. The recently developed framework has been thoroughly analyzed and its associations with several significant ideals have been examined and determined. It is assumed that R is a commutative ring with identity throughout the paper. Let I be a proper ideal of R. $\sqrt{I} = \{a \in R : a^n \in I for some n \in \mathbb{N}\}$ denotes the radical of R. And also $(I : a) = \{r \in R : ra \in I\}$. Recall that weakly prime ideals were examined by Anderson and Smith in 2003 [2]. A proper ideal P of R is classified as a weakly prime ideal if, given that $0 \neq ab \in P$, it follows that either a belongs to P or b belongs to P. Anderson and Bataineh researched a type of ideal called ϕ-prime ideals, which combine prime ideals and weakly prime ideals[1]. A proper ideal Q of R is a ϕ-prime ideal if for $ab \in Q - \phi(Q)$ implies $a \in Q$ or $b \in Q$ for some $a, b \in R$. In a recent study [6] Koç and others defined the concept of a strongly quasi-primary ideal and provided a characterization of divided domains. They defined as follows: A proper ideal I of R is a strongly quasi-primary ideal if whenever $ab \in R$ provides $a^2 \in I$ or $b^n \in I$ for some $a, b \in I$ and $n \in \mathbb{N}$. In [3], researchers introduced the concept of wsq-primary ideals. A proper ideal I of R is said to be a wsq primary ideal if $0 \neq ab \in I$ implies that $a^2 \in I$ or $b \in \sqrt{I}$. Our goal in this article is to extend the concept of strongly quasi-primary and weakly prime ideals by introducing the notion of a ϕ-strongly quasi-primary ideal (abbreviated as ϕ-sq primary ideal). Additionally, Von Neumann regular rings, an important ring class, can be characterized using these ideals.

2. Preliminaries

Definition 1. *A proper ideal I of R is called ϕ-sq primary ideal if $ab \in I - \phi(I)$ implies $a^2 \in I$ or $b \in \sqrt{I}$ for each $a, b \in R$.*

Remark 1. *(1) If $\phi(I) = \emptyset$, then I is sq primary ideal if and only if I is ϕ-sq primary ideal.*

(2) If $\phi(I) = \{0\}$, then I is wsq primary ideal if and only if I is ϕ-sq primary ideal.

Recall that an ideal I of R is called ϕ-primary ideal if $ab \in I - \phi(I)$ implies $a \in I$ or $b \in \sqrt{I}$ [1]. Recall from [4] that a proper ideal I of R is said to be a ϕ-2-absorbing primary ideal if whenever $abc \in I - \phi(I)$ then $ab \in I$ or $ac \in \sqrt{I}$ or $bc \in \sqrt{I}$. A proper ideal I of R is said to be ϕ-2 prime ideal if $ab \in I - \phi(I)$ implies $a^2 \in I$ or $b^2 \in I$.

Proposition 1. *Let I be a proper ideal of R. The following statements are satisfied.*

(i) Every ϕ-primary ideal is also ϕ-sq primary ideal.

(ii) Every ϕ-2 prime ideal is also ϕ-sq primary ideal.

(iii) Every sq primary ideal is also ϕ-sq primary ideal.

(iv) Every ϕ-sq primary ideal is ϕ-semiprimary ideal. In particular every ϕ-sq primary ideal is also ϕ-2-absorbing primary ideal.

Proof. (i), (ii): It is clear.

(iii): Let I be a sq primary ideal. Now we will show that I is ϕ-sq primary ideal. Let $ab \in I - \phi(I)$ for some $a, b \in R$. Then $ab \in I$ implies $a^2 \in I$ or $b \in \sqrt{I}$, which completes the proof.

(iv): Let I be ϕ-sq primary ideal and $ab \in I - \phi(I)$. Then we have $a^2 \in I$ or $b \in \sqrt{I}$. If $a^2 \in I$, then $a \in \sqrt{I}$. Thus, I is a ϕ-semiprimary ideal. Now we will show that I is ϕ-2-absorbing primary ideal. Let $a(bc) \in I - \phi(I)$ for some $a, b, c \in R$. Since I is ϕ-sq primary ideal, we have $a^2 \in I$ or $bc \in \sqrt{I}$. If $a^2 \in I$, then $a \in \sqrt{I}$ which implies $ac \in \sqrt{I}$. Hence I is ϕ-2-absorbing primary ideal. □

In Proposition 1, the converses of (i), (ii) and (iii) are not true in general (Take $\phi(I) = 0$ and see Example 1, Example 2, Example 3 of [6]).

Proposition 2. *Let I be an ideal of R such that $\sqrt{I}^2 \subseteq I$. Then I is ϕ-2-prime ideal if and only if I is ϕ-sq primary ideal if and only if I is ϕ-semiprimary ideal.*

Proof. The implication "I is ϕ-2-prime ideal $\Rightarrow$ I is ϕ-sq primary ideal$\Rightarrow$ I is ϕ-semiprimary ideal" follows from Proposition 1. Let I be a ϕ-semiprimary ideal and $ab \in I - \phi(I)$ for some $a, b \in R$. Then $a \in \sqrt{I}$ or $b \in \sqrt{I}$ which implies that $a^2 \in \sqrt{I}^2 \subseteq I$ or $b^2 \in \sqrt{I}^2 \subseteq I$. So I is ϕ-2-prime ideal. □

Proposition 3. *Let I be a ϕ-sq primary ideal which is not sq primary ideal. Then $I^2 \subseteq \phi(I)$. In this case $\sqrt{I} \subseteq \sqrt{\phi(I)}$.*

Proof. Suppose that $I^2 \nsubseteq \phi(I)$. Now, we will show that I is sq primary ideal. Let $xy \in I$ for some $x, y \in R$. Assume that $x^2 \notin I$. If $xy \notin \phi(I)$, then $xy \in I - \phi(I)$ which implies that $y \in \sqrt{I}$ that completes the proof. Thus, we assume that $xy \in \phi(I)$. If $xI \nsubseteq \phi(I)$, then there exists $c \in I$ such that $xc \notin \phi(I)$. This implies that $x(y+c) \in I - \phi(I)$. Since I is ϕ-sq primary ideal, we have $(y+c) \in \sqrt{I}$. Thus we may assume that $xI \subseteq \phi(I)$. Now we will show that $yI \subseteq \phi(I)$. If $yI \nsubseteq \phi(I)$, then we can choose $d \in I$ such that $yd \notin \phi(I)$. Then $y(x+d) \in I - \phi(I)$ which implies that $(x+d)^2 = x^2 + 2xd + d^2 \in I$ or $y \in \sqrt{I}$. If $y \in \sqrt{I}$, then we're through. If $(x+d)^2 = x^2 + 2xd + d^2 \in I$, then $x^2 \in I$ which is a contradiction. Thus, we have $yI \subseteq \phi(I)$. Since $I^2 \nsubseteq \phi(I)$, we have $p, q \in I$ such that $pq \notin \phi(I)$. Then $(x+p)(y+q) = xy + xq + yp + pq \in I - \phi(I)$. This gives $(x+p)^2 = x^2 + 2xp + p^2 \in I$ or $y + q \in \sqrt{I}$. Thus $x^2 \in I$ or $y \in \sqrt{I}$ which completes the proof. □

Proposition 4. *Let R be a ring and I be a proper ideal of R. Then I is a ϕ-sq primary ideal if and only if $I/\phi(I)$ is a wsq primary ideal of $R/\phi(I)$.*

Proof. Let I be a ϕ-sq primary ideal of R and choose $a, b \in R$ such that $0_{R/\phi(I)} \neq (a+\phi(I))(b+\phi(I)) \in I/\phi(I)$. Then we conclude that $ab \in I - \phi(I)$. Since I is a ϕ-sq primary ideal, we obtain $a^2 \in I$ or $b \in \sqrt{I}$. This implies that $(a+\phi(I))^2 = a^2 + \phi(I) \in I/\phi(I)$ or $b + \phi(I) \in \sqrt{I}/\phi(I) = \sqrt{I/\phi(I)}$. Thus, $I/\phi(I)$ is a wsq primary ideal of $R/\phi(I)$. Contrarily, assume that $I/\phi(I)$ is a wsq primary ideal of $R/\phi(I)$. Now, we will show that I is a ϕ-sq primary ideal. Let $ab \in I - \phi(I)$ for some $a, b \in R$. Then we have $0_{R/\phi(I)} \neq (a+\phi(I))(b+\phi(I)) \in I/\phi(I)$. As $I/\phi(I)$ is a wsq primary ideal of $R/\phi(I)$, we conclude that $(a+\phi(I))^2 = a^2 + \phi(I) \in I/\phi(I)$ or $b + \phi(I) \in \sqrt{I}/\phi(I) = \sqrt{I/\phi(I)}$. Then we get $a^2 \in I$ or $b \in \sqrt{I}$ which completes the proof. □

Theorem 1. *The followings are equivalent for a proper ideal I of R :*

(i) I is a ϕ-sq primary ideal.

(ii) $(a) \subseteq (I : a)$ or $(I : a) \subseteq \sqrt{I}$ or $(I : a) \subseteq (\phi(I) : a)$ for every $a \in R$.

(iii) $aJ \subseteq I$ and $aJ \nsubseteq \phi(I)$ implies $a^2 \in I$ or $J \subseteq \sqrt{I}$ for every $a \in R$ and ideal J of R.

Proof. $(i) \Rightarrow (ii)$: Suppose that I is a ϕ-sq primary ideal. Choose an element $a \in R$. If $a^2 \in I$, then one can easily see that $(a) \subseteq (I : a)$. So, assuming that $a^2 \notin I$. Let $x \in (I : a)$. Then we have $ax \in I$. If $ax \in \phi(I)$, then we have $x \in (\phi(I) : a)$. If $ax \notin \phi(I)$, then we conclude that $x \in \sqrt{I}$ since I is a ϕ-sq primary ideal and $ax \in I - \phi(I)$. Thus we conclude that $(I : a) \subseteq \sqrt{I} \cup (\phi(I) : a)$. The rest follows from the fact that if an ideal is contained in the union of two ideals, then it must be contained in one of them.

$(ii) \Rightarrow (iii)$: Let $aJ \subseteq I$ and $aJ \nsubseteq \phi(I)$ for some $a \in R$ and ideal J of R. It is possible to make a general assumption without any loss of relevance that $a^2 \notin I$. Since $J \subseteq (I : a)$ and $J \nsubseteq (\phi(I) : a)$, by (ii), we have $J \subseteq (I : a) \subseteq \sqrt{I}$, as needed.

$(iii) \Rightarrow (i)$: It is straightforward. □

Definition 2. *Let R, S be two commutative rings with unity, $\phi : L(R) \to L(R) \cup \{\emptyset\}$ and $\psi : L(S) \to L(S) \cup \{\emptyset\}$ be two functions. A ring homomorphism $f : R \to S$ is said to be a (ψ, ϕ)-homomorphism if $f^{-1}(\psi(J)) = \phi(f^{-1}(J))$ for every $J \in L(S)$.*

Theorem 2. *Let R, S be two commutative rings with unity, $\phi : L(R) \to L(R) \cup \{\emptyset\}$ and $\psi : L(S) \to L(S) \cup \{\emptyset\}$ be two functions. Assume that $f : R \to S$ is a (ψ, ϕ)-homomorphism of rings. The following expressions are provided.*

(i) If J is a ψ-sq primary ideal of S, then $f^{-1}(J)$ is a ϕ-sq primary ideal of R.

(ii) If I is a ϕ-sq primary ideal of R containing $Ker(f)$ and f is surjective, then $f(I)$ is a ψ-sq primary ideal of S.

Proof. (i) : Let J be a ψ-sq primary ideal of S and $ab \in f^{-1}(J) - \phi(f^{-1}(J))$ for some $a, b \in R$. Since $\phi(f^{-1}(J)) = f^{-1}(\psi(J))$, we conclude that $f(ab) = f(a)f(b) \in J - \psi(J)$. As J is a ψ-sq primary ideal of S, we get $f(a)^2 = f(a^2) \in J$ or $f(b)^n = f(b^n) \in J$ for some $n \in \mathbb{N}$. This gives that $a^2 \in f^{-1}(J)$ or $b^n \in f^{-1}(J)$. Thus, $f^{-1}(J)$ is a ϕ-sq primary ideal of R.

(ii) : Suppose that I is a ϕ-sq primary ideal of R containing $Ker(f)$ and f is surjective. Let $yz \in f(I) - \psi(f(I))$ for some $y, z \in S$. Since f is surjective, $f(a) = y$ and $f(b) = z$ for some $a, b \in R$. This implies that $f(ab) = yz \in f(I)$, and this yields $ab \in I$. Now, first note that $I = f^{-1}(f(I))$ since I contains

$Ker(f)$. Put $J = f(I)$, then by (ψ, ϕ)-homomorphism, we have $f^{-1}(\psi(J)) = f^{-1}(\psi(f(I))) = \phi(f^{-1}(f(I)))$. Then we get $f^{-1}(\psi(f(I))) = \phi(I)$. Since f is surjective, we conclude that $\psi(f(I)) = f(\phi(I))$. If $ab \in \phi(I)$, then we have $f(ab) = yz \in f(\phi(I)) = \psi(f(I))$ which is a contradiction. Thus we have $ab \in I - \phi(I)$. Since I is a ϕ-sq primary ideal of R, we get $a^2 \in I$ or $b \in \sqrt{I}$ which implies that $y^2 = f(a^2) \in f(I)$ or $z = f(b) \in f(\sqrt{I}) = \sqrt{f(I)}$. Consequently, $f(I)$ is a ψ-sq primary ideal of S. □

Theorem 3. *Let S be a multiplicative closed subset of R and $\phi_q : L(S^{-1}R) \to L(S^{-1}R) \cup \{\emptyset\}$, defined by $\phi_q(S^{-1}I) = S^{-1}(\phi(I))$ for each ideal I of R, be a function. Then the statements below are true.:*

(i) If I is a ϕ-sq primary ideal of R with $S \cap I = \emptyset$, then $S^{-1}I$ is a ϕ_q-sq primary ideal of $S^{-1}R$.

(ii) Let I be an ideal of R such that $Z_{\phi(I)}(R) \cap S = \emptyset$ and $Z_I(R) \cap S = \emptyset$. If $S^{-1}I$ is a ϕ_q-sq primary ideal of $S^{-1}R$, then I is a ϕ-sq primary ideal of R.

Proof. *(i)* Let $\frac{a}{s}\frac{b}{t} \in S^{-1}I - \phi_q(S^{-1}I)$ for any $a, b \in R$ and $s, t \in S$. Since $\phi_q(S^{-1}I) = S^{-1}(\phi(I))$, we have $uab = (ua)b \in I - \phi(I)$ for some $u \in S$. As I is a ϕ-sq primary ideal of R, we get $(ua)^2 \in I$ or $b \in \sqrt{I}$. This implies that $\frac{u^2a^2}{u^2s^2} = \frac{a^2}{s^2} \in S^{-1}I$ or $\frac{ub}{ut} = \frac{b}{t} \in S^{-1}\sqrt{I} = \sqrt{S^{-1}I}$. Therefore $S^{-1}I$ is a ϕ_q-sq primary ideal of $S^{-1}R$.

(ii) Let $ab \in I - \phi(I)$ for some $a, b \in R$. Then $\frac{a}{1}\frac{b}{1} \in S^{-1}I$. As $Z_{\phi(I)}(R) \cap S = \emptyset$, it is obvious that $\frac{a}{1}\frac{b}{1} \notin S^{-1}(\phi(I)) = \phi_q(S^{-1}I)$. Since $S^{-1}I$ is a ϕ_q-sq primary ideal of $S^{-1}R$, we have $\frac{a^2}{1} \in S^{-1}I$ or $\frac{b}{1} \in S^{-1}\sqrt{I}$. If $\frac{a^2}{1} \in S^{-1}I$, then $ua^2 \in I$ for some $u \in S$. Since $Z_I(R) \cap S = \emptyset$, we get $a^2 \in I$ and so I is a ϕ-sq primary ideal of R. If $\frac{b}{1} \in S^{-1}\sqrt{I}$, then $ub \in \sqrt{I}$ and hence $u^n b^n \in I$ for some $n \in \mathbb{N}$. Since $Z_I(R) \cap S = \emptyset$, we have $b^n \in I$ and so I is a ϕ-sq primary ideal of R. □

Theorem 4. *Let R_1, R_2 be two commutative rings and $\psi_i : \mathfrak{I}(R_i) \to \mathfrak{I}(R_i) \cup \{\emptyset\}$ be function for $i = 1, 2$. Let $\phi_\times = \psi_1 \times \psi_2$. Then $\phi_\times$-sq primary ideals of $R_1 \times R_2$ have exactly one of the following three forms:*

(i) $I_1 \times I_2$ where I_i is a proper ideal of R_i with $\psi_i(I_i) = I_i$.

(ii) $I_1 \times R_2$ where I_1 is a ψ_1-sq primary ideal of R_1 which must be strongly quasi primary ideal if $\psi_2(R_2) \neq R_2$.

(iii) $R_1 \times I_2$ where I_2 is a ψ_2-sq primary ideal of R_2 which must be strongly quasi primary ideal if $\psi_1(R_1) \neq R_1$.

Proof. Suppose that $I = I_1 \times I_2$ is a $\phi_\times$-sq primary ideal of $R_1 \times R_2$. Without loss of generality, we may assume that $I_1 \times I_2 \neq \psi_1(I_1) \times \psi_2(I_2)$. We first demonstrate that I_1 is a ψ_1-sq primary ideal of R_1. Let $xy \in I_1 - \psi_1(I_1)$ for some $x, y \in R_1$. Then we have $(x,0)(y,0) = (xy,0) \in I - \phi_\times(I)$. By assumption, we conclude that $(x,0)^2 \in I$ or $(y,0) \in \sqrt{I}$. Then we have $x^2 \in I_1$ or $y \in \sqrt{I_1}$. Thus, I_1 is a ψ_1-sq primary ideal of R_1. Similar argument shows that I_2 is a ψ_2-sq primary ideal of R_2. Since $I_1 \times I_2 \neq \psi_1(I_1) \times \psi_2(I_2)$, we may assume that $I_1 \neq \psi_1(I_1)$. Then there exists $a \in I_1 - \psi_1(I_1)$. Choose $b \in I_2$. Then we have $(a,1)(1,b) = (a,b) \in I - \phi_\times(I)$ which implies that $(a,1)^2 \in I$ or $(1,b) \in \sqrt{I}$. This gives $I_1 = R_1$ or $I_2 = R_2$. Assume that $I_2 = R_2$. Now, we will show that I_1 is quasi primary if $\psi_2(R_2) \neq R_2$. Now, choose $c \in R_2 - \psi_2(R_2)$ and $xy \in I_1$. Then $(x,c)(y,1) = (xy,c) \in I - \phi_\times(I)$ which implies that $(x,c)^2 \in I$ or $(y,1) \in \sqrt{I}$. Thus we have $x^2 \in I_1$ or $y \in \sqrt{I_1}$ which completes the proof. Conversely, nothing needs to be proven if (i) is satisfied. We may presume that without losing generality (ii) is satisfied. If $\psi_2(R_2) \neq R_2$, then I_1 is strongly quasi primary ideal of R_1. Then by [6, Lemma 2.1], $I = I_1 \times R_2$ is a strongly quasi primary ideal of $R_1 \times R_2$. The rest follows from Proposition 1. Now, assume that $\psi_2(R_2) = R_2$ and I_1 is a ψ_1-sq primary ideal of R_1. Let $(a,b)(x,y) \in I - \phi_\times(I)$. Then we have $ax \in I_1 - \psi_1(I_1)$. Since I_1 is a ψ_1-sq primary ideal of R_1, we have $a^2 \in I_1$ or $x \in \sqrt{I_1}$. Then we obtain $(a,b)^2 \in I$ or $(x,y) \in \sqrt{I}$. Hence, I is a $\phi_\times$-sq primary ideal. In the other case, it is evident that I is a $\phi_\times$-sq primary ideal □

Let $\phi_n : \mathfrak{I}(R) \to \mathfrak{I}(R) \cup \{\emptyset\}$ be a function defined by $\phi_n(I) = I^n$ for a fixed natural number $n \in \mathbb{N}$. Then we say that I is an n-almost sq primary ideal if I is a ϕ_n-sq primary ideal of R. Recall from [7] that a ring R is said to be a von Neumann regular ring if $I = I^2$ for every ideal I of R. In this case, $I = I^n$ for all $n \in \mathbb{N}$. By [5, Theorem 1], a ring R is a von Neumann regular ring if and only if $I = \sqrt{I}$ for every ideal I of R if and only if $IJ = I \cap J$ for every ideals I, J of R. Now, we will give a new characterization of von Neumann regular rings in terms of n-almost sq primary ideals of R.

Theorem 5. *Let $R_1, R_2, \ldots, R_m$ be commutative rings and $R = R_1 \times R_2 \times \cdots \times R_m$, where $3 \leq m < \infty$. Suppose that $n \geq 2$. Then the following expressions are equivalent.*

(i) Every proper ideal of R is an n-almost sq primary ideal.

(ii) $R_1, R_2, \ldots, R_m$ are von Neumann regular rings.

Proof. $(i) \Rightarrow (ii)$: Suppose that every proper ideal of R is an n-almost sq primary ideal. Now, we will show that $R_1, R_2, \ldots, R_m$ are von Neumann regular rings.Without loss of generality R_1 is not von Neumann regular. Then there exists a proper ideal I_1 of R_1 such that $I_1^n \neq I_1$. Then there exists $x \in I_1 - I_1^n$. Let $I = I_1 \times 0 \times 0 \times R_4 \times R_5 \times \cdots \times R_m$. Now, put $a = (x, 0, 1, 1, \ldots, 1)$ and $b = (1, 1, 0, 1, \ldots, 1)$. Then note that $ab = (x, 0, 0, 1, \ldots, 1) \in I - I^n$. However, $a^2 = (x^2, 0, 1, \ldots, 1) \notin I$ and $b = (1, 1, 0, 1, \ldots, 1) \notin \sqrt{I}$. Thus, we have a non n-almost sq primary ideal I of R which is a contradiction. Hence, $R_1, R_2, \ldots, R_m$ are von Neumann regular rings.

$(ii) \Rightarrow (i)$: Let $R_1, R_2, \ldots, R_m$ be von Neumann regular rings. Then by [5, Proposition 4] $R = R_1 \times R_2 \times \cdots \times R_m$ is a von Neumann regular ring. In this case, $I = I^n = \phi_n(I)$ for every ideal I of R. Thus, every every proper ideal of R is trivially an n-almost sq primary ideal. □

Theorem 6. *Let $f : Y \to Z$ be a ring homomorphism. Assume that δ is an ideal expansion of $I(Y)$, φ is a reduction function of $I(Y)$ and also γ is an ideal expansion of $I(Z)$, ψ is a reduction function of $I(Z)$. Then f is said to be $(\delta, \varphi) - (\gamma, \psi)$ homomorphism if $\varphi(f^{-1}(J)) = f^{-1}(\psi(J))$ for every $J \in I(Z)$. Let $f : Y \to Z$ be a (γ, ψ) homomorphism.*

(i) If J is a ϕ-sq primary ideal of Z, then $f^{-1}(J)$ is a ϕ-sq primary ideal of Y.

(ii) If I is ϕ-sq primary ideal of Y containing $Ker(f)$ and f is a surjective, then $f(I)$ is a ϕ-sq primary ideal of Z.

Proof. (i) : Let J be a ϕ-sq primary ideal of Z. Take $a, b \in Y$ such that $ab \in f^{-1}(J) - \phi(f^{-1}(J))$. Then we have $f(a)f(b) \in J - \psi(J)$. Since is a ϕ-sq primary ideal, $(f(a))^2 \in J$ or $(f(b))^n \in J$ which implies that $a^2 \in f^{-1}(J)$ or $b^n \in f^{-1}(J)$. So $f^{-1}(J)$ is a ϕ-sq primary ideal of Y.

(ii) : Suppose that I is a ϕ-sq primary ideal of R containing $Ker(f)$ and f is surjective. Let $mn \in f(I) - \psi(f(I))$ for some $m, n \in S$. Since f is surjective, $f(a) = m$ and $f(b) = n$ for some $a, b \in R$. This implies that $f(ab) = mn \in f(I)$, and this yields $ab \in I$. Now, first note that $I = f^{-1}(f(I))$ since I contains

$Ker(f)$. Set $J = f(I)$, then by (ψ, ϕ)-homomorphism, we have $f^{-1}(\psi(J)) = f^{-1}(\psi(f(I))) = \phi(f^{-1}(f(I)))$. Then we get $f^{-1}(\psi(f(I))) = \phi(I)$. Since f is surjective, we conclude that $\psi(f(I)) = f(\phi(I))$. If $ab \in \phi(I)$, then we have $f(ab) = mn \in f(\phi(I)) = \psi(f(I))$ which is a contradiction. Thus we have $ab \in I - \phi(I)$. Since I is a ϕ-sq primary ideal of R, we get $a^2 \in I$ or $b \in \sqrt{I}$ which implies that $m^2 = f(a^2) \in f(I)$ or $n = f(b) \in f(\sqrt{I}) = \sqrt{f(I)}$. Consequently, $f(I)$ is a ψ-sq primary ideal of S. □

References

[1] Anderson, D. D., Bataineh, M. (2008) Generalizations of prime ideals, Communications in Algebra, 36(2) 686-696.

[2] Anderson, D. D., Smith, E. (2003) Weakly prime ideals, Houston Journal of Mathematics, 29(4) 831-840.

[3] Aslankarayiğit Uğurlu, E., Bouba, E. M., Tekir, Ü., Koç, S. (2023) On wsq-primary ideals, Czechoslovak Mathematical Journal, 73(2) 415-429.

[4] Badawi, A., Tekir, Ü., Uğurlu, E. A., Ulucak, G.,Celikel, E. Y. (2016) Generalizations of 2-absorbing primary ideals of commutative rings, Turkish Journal of Mathematics, 40(3) 703-717.

[5] Jayaram, C., Tekir, Ü. (2018) von Neumann regular modules, Communications in Algebra, 46(5) 2205-2217.

[6] Koc, S., Tekir, U., Ulucak, G. (2019) On sq primary ideals, Bulletin of the Korean Mathematical Society, 56(3) 729-743.

[7] Von Neumann, J. (1936) On regular rings, Proceedings of the National Academy of Sciences, 22(12) 707-713.